

Atlas**Coordinating Lead Authors:**

José Manuel Gutiérrez (Spain), Richard Graham Jones (UK), Gemma Teresa Narisma (Philippines)

Lead Authors:

Muhammad Amjad (Pakistan), Nana Ama Browne Klutse (Ghana), Svitlana Krakovska (Ukraine), Jian Li (China), Daniel Martínez-Castro (Cuba), Sebastian H. Mernild (Denmark/Norway, Denmark), Lincoln Muniz Alves (Brazil), Bart van den Hurk (Netherlands), Jin-Ho Yoon (South Korea)

Contributing Authors:

Joaquín Bedia (Spain), Tereza Cavazos (Mexico), Abel Centella-Artola (Cuba), Haoming Chen (China), Antonio S. Cofiño (Spain), Erika Coppola (Italy), Joseph Daron (UK), Alessandro Dosio (Italy), Natalia Gnatiuk (Russia, Ukraine), Irina V. Gorodetskaya (Portugal, Belgium/Russia), Patrick Grenier (Canada), David S. Gutzler (USA), Cédric Hananel (Belgium, France), Sixto Herrera (Spain), Maialen Iturbide (Spain), Sanjay Jayanarayanan (India), Eleni Katragkou (Greece), Erik Kjellström (Sweden), Marta Pereira Llopart (Brazil), Douglas Maraun (Austria, Germany), Linda Mearns (USA), Liew Ju Neng (Malaysia), Thanh Ngo-Duc (Vietnam), Gregory Nikulin (Sweden, Russia/Sweden), Andrew Orr (UK), Ma. Laurice Preciado Jamero (Philippines), Mehwish Ramzan (Pakistan), Annette Rinke (Germany), Daniel San Martín (Spain), Chris Shaw (UK), Stefan Sobolowski (Norway, USA), Samuel Somot (France), Anna Amelia Sorensson (Argentina), Francis Nkrumah (Ghana), Christopher Lennard (South Africa), Sarah Osima (Tanzania), Fredolin Tangang (Malaysia), Claas Teichmann (Germany), Emilie Vanvyve (UK, Belgium), Geert-Jan van Oldenborgh (Netherlands)

Review Editors:

Ines Camilloni (Argentina), Jens Hesselbjerg Christensen (Denmark), Fatima Driouech (Morocco)

Chapter Scientists:

Ma. Laurice Preciado Jamero (Philippines), Emilie Vanvyve (United Kingdom, Belgium)

Date of Draft:

29/04/2019

Note:

TSU Compiled Version

Do not forget to review the AR6 WGI Interactive Atlas Mock up.

To access the Interactive Atlas, please copy 'ipcc-atlas.ifca.es' in any web browser. You will be asked for your credential login details:

user: reviewer

password: internalreview

When navigating through the Interactive Atlas, you will find a "Get a review code (for this page)" button at the bottom right-hand corner. By clicking on it, you will get a code (which uniquely identifies the page that is being shown), together with some brief instructions on how to use this code to make comments using the Review Form provided.

1 Executive Summary..... 6

2 Atlas.1 Introduction 10

3 Atlas.1.1 Purpose..... 10

4 Atlas.1.2 Context and framing..... 10

5 Atlas.2 Defining temporal, spatial and typological domains and scales 11

6 Atlas.2.1 Baseline and future time slice periods and temporal scales of analysis 11

7 Atlas.2.2 Spatial domains and scales of analysis..... 13

8 Atlas.2.3 Typological domains 14

9 Atlas.3 Combining multiple sources of information for regions 15

10 Atlas.3.1 Observations..... 15

11 Atlas.3.1.1 Consistency and differences in observational data 17

12 Atlas.3.2 Reanalysis 19

13 Atlas.3.3 Global Model Data (CMIP5 and CMIP6) 19

14 Atlas.3.4 Regional Model Data (CORDEX) 21

15 Atlas.4 Global synthesis..... 24

16 Atlas.4.1 Global atmosphere and land surface 24

17 Atlas.4.2 Global oceans 26

18 Atlas.4.3 Extremes..... 27

19 Atlas.5 Regional syntheses and case studies..... 28

20 Atlas.5.1 Information sources for regional synthesis 28

21 Atlas.5.2 Africa 28

22 Atlas.5.2.1 Observations, trends and attribution..... 29

23 Atlas.5.2.1.1 Observed trends and extremes..... 29

24 Atlas.5.2.1.2 Attribution of trends and extremes 30

25 Atlas.5.2.2 Assessment of model performance 30

26 Atlas.5.2.3 Assessment of projections..... 31

27 Atlas.5.3 Asia 33

28 Atlas.5.3.1 East Asia 33

29 Atlas.5.3.1.1 Observations, trends and attribution..... 33

30 Atlas.5.3.1.2 Assessment of model performance 35

31 Atlas.5.3.1.3 Assessment of projections..... 37

32 Atlas.5.3.2 Southeast Asia..... 41

33 Atlas.5.3.2.1 Observations, trends and attribution..... 41

34 Atlas.5.3.2.2 Assessment of model performance 43

35 Atlas.5.3.2.3 Assessment of projections..... 44

36 Atlas.5.3.3 South Asia 46

37 Atlas.5.3.3.1 Observations, trends and attribution..... 46

38 Atlas.5.3.3.2 Assessment of model performance 47

39 Atlas.5.3.3.3 Assessment of projections..... 48

40 Atlas.5.3.4 Central Asia..... 50

1	Atlas.5.3.4.1	Observations, trends and attribution.....	50
2	Atlas.5.3.4.2	Assessment of model performance	51
3	Atlas.5.3.4.3	Assessment of projections.....	51
4	Atlas.5.4	Australasia.....	53
5	Atlas.5.4.1	Observations, trends and attribution.....	53
6	Atlas.5.4.1.1	Previous findings from WGII AR5	53
7	Atlas.5.4.2	Assessment of model performance	53
8	Atlas.5.4.3	Assessment of projections.....	53
9	Atlas.5.4.3.1	Previous findings from WGII AR5	53
10	Atlas.5.5	Central and South America	54
11	Atlas.5.5.1	Central America	54
12	Atlas.5.5.1.1	Observations, trends and attribution.....	55
13	Atlas.5.5.1.2	Assessment of model performance	57
14	Atlas.5.5.1.3	Assessment of projections.....	59
15	Atlas.5.5.2	South America.....	61
16	Atlas.5.5.2.1	Observations, trends and attribution.....	62
17	Atlas.5.5.2.2	Assessment of model performance	64
18	Atlas.5.5.2.3	Assessment of projections.....	66
19	Atlas.5.6	Europe	74
20	Atlas.5.6.1	Observations, trends and attribution.....	74
21	Atlas.5.6.1.1	Summary of findings from AR5 and SR1.5.....	74
22	Atlas.5.6.1.2	Assessment of observed trends, particularly on extremes.....	75
23	Atlas.5.6.1.3	Attribution of observed trends and extremes	76
24	Atlas.5.6.1.4	Availability of observation and reanalysis datasets containing information on higher resolution and/or sub-daily climate metrics.....	76
25			
26	Atlas.5.6.2	Assessment of model performance	77
27	Atlas.5.6.2.1	Summary of findings from AR5.....	77
28	Atlas.5.6.2.2	Assessments of modelled climatology of mean annual cycle and extremes in relation to observations.....	78
29			
30	Atlas.5.6.2.3	Assessments of modelled trends and variability	79
31	Atlas.5.6.2.4	Added value of RCMs and convection permitting models (CPMs).....	79
32	Atlas.5.6.2.5	Assessment of coupled regional climate system models.....	80
33	Atlas.5.6.3	Assessment of projections.....	81
34	Atlas.5.6.3.1	Summary of findings from AR5 and SR1.5	81
35	Atlas.5.6.3.2	Assessment of regional projections, and the uncertainty cascade for future projections	82
36			
37	Atlas.5.6.3.3	New experimental designs, particularly those involving CPMs: time slice simulations, surrogate warming experiments	84
38			
39	Atlas.5.6.3.4	National climate change scenario's, their method of aggregating climate projections, and the fit-for-purpose to assess climate change impacts.....	84
40			
41	Atlas.5.7	North America.....	86

1	Atlas.5.7.1	Observations, trends and attribution.....	86
2	Atlas.5.7.2	Assessment of model performance	87
3	Atlas.5.7.3	Assessment of projections.....	88
4	Atlas.5.8	Small Islands	89
5	Atlas.5.8.1	Observations, trends and attribution.....	89
6	Atlas.5.8.2	Assessment of model performance	89
7	Atlas.5.8.3	Assessment of projections.....	90
8	Atlas.5.9	Oceans.....	90
9	Atlas.5.9.1	Observations, trends and attribution.....	90
10	Atlas.5.9.2	Assessment of model performance	90
11	Atlas.5.9.3	Assessment of projections.....	90
12	Atlas.5.10	Polar regions	90
13	Atlas.5.10.1	Arctic.....	90
14	Atlas.5.10.1.1	Assessment of observations, trends and attribution	90
15	Atlas.5.10.1.2	Assessments of model performance	91
16	Atlas.5.10.1.3	Assessment of projections.....	93
17	Atlas.5.10.2	Antarctic.....	94
18	Atlas.5.10.2.1	Assessment of observations, trends and attribution	94
19	Atlas.5.10.2.2	Assessment of model performance	96
20	Atlas.5.10.2.3	Assessment of projections.....	97
21	Atlas.5.11	Typological Domains	99
22	Atlas.5.11.1	Mountains.....	99
23	Atlas.5.11.1.1	Observations, trends and attribution.....	100
24	Atlas.5.11.1.2	Assessment of model performance	100
25	Atlas.5.11.1.3	Assessment of projections.....	101
26	Atlas.6	Assessment of communication approaches with case studies/narratives and guidance on how to	
27		interpret these	102
28	Key messages:	102
29	Atlas.6.1	Approaches to communicating uncertainty and confidence.....	103
30	Atlas.6.1.1	Communicating uncertainty information using ensembles of models and scenarios...	103
31	Atlas.6.1.2	Event attribution.....	103
32	Atlas.6.1.3	Narratives and storylines to communicate climate change impacts.....	104
33	Atlas.6.1.4	Climate services portals and national and regional climate assessments	104
34	Atlas.6.2	Effectiveness of climate information communication	104
35	Atlas.7	Description of the online “Interactive Atlas”	107
36	Atlas.7.1	Why an interactive online Atlas in AR6?.....	107
37	Atlas.7.2	Description of the interactive Atlas: Functionalities and datasets	108
38	Atlas.7.3	Accessibility and reproducibility	110
39	Atlas.7.4	Exporting products (including metadata) in different formats	111
40	Atlas.7.5	Provenance for the full chain from the data source to the final product	111

1 Atlas.8 Knowledge gaps 112

2 Frequently Asked Questions..... 114

3 FAQ ATLAS.1: If results from models are uncertain, how can we trust them? 114

4 References 129

5 Figures 159

6

1 **Executive Summary**

2

3 ***Regional statements***

4

5 **Africa**

6

7 **Future temperature increases over most of Africa are *likely* to increase more than the global mean.**

8

9 **Projected changes in average precipitation are *uncertain* across many parts of the African continent.**

10

11 Most areas of Africa lack sufficient observational data to draw conclusions about long-term precipitation trends and in many regions there are discrepancies between observed datasets.

13

14 **There has been a significant increase in research on climate change over Africa and by African scientists.**

16

17 **East Asia**

18

19 **There is *low confidence* that the East Asian monsoon has weakened** given the nature and quality of the evidence.

21

22 **Consistent model projections of a warming trend for both mean temperature and extreme events indicate it is *likely* that these will continue over East Asia** although the magnitude of projected changes is largely model dependent.

25

26 **Climate projections show more increased severe precipitation extreme events and more long-duration drought events with the increase in temperature in East Asia,** although internal variability and model uncertainties cause large differences among different simulations, especially at regional and seasonal scales

29

30 **Regional climate models (RCMs) simulate patterns and magnitude of temperature and precipitation extremes over East Asia reasonably well,** although RCMs still show some large biases in simulating East Asian climatology and variability and the performance is largely model dependent.

33

34 **CORDEX-EA models reasonably capture the observed climatological spatial distribution and interannual variability of tropical cyclone over the western North Pacific.**

36

37 **Regional climate models over East Asia can reproduce more realistic regional climate characteristics,** but they do not always show added value compared to their driving GCMs.

39

40 **Southeast Asia**

41

42 **There is an increasing trend in mean temperature and extreme maximum and minimum temperatures and an overall increase in the frequency of warm nights and a decrease in the frequency of cold days and nights over Southeast Asia,** which is consistent with AR5 findings.

45

46 **There is a decreasing trend in seasonal and mean annual rainfall** although changes in mean precipitation is less spatially coherent over Southeast Asia.

48

49 **While annual precipitation and precipitation events in general have declined in Southeast Asia, there is an increasing trend in extremes and annual total wet-day rainfall.**

51

52 **Temperature projections show a *likely* increase of more than 3.5°C across Southeast Asia by the end of the century under RCP8.5 and maximum increase of 2°C under RCP4.5.**

54

55

South Asia

Minimum and maximum daily temperatures in South Asia are increasing and winters are getting warmer faster than summer.

The frequency of heavy precipitation events have increased over India while light rain events have decreased, although there is no clear evidence of changes in the seasonal mean monsoon rainfall trends and the inter-annual variability over the whole of India under a warmer climate.

Summer monsoon precipitation in South Asia is likely to increase by the end of the 21st century while winter monsoons are projected to be drier.

River systems are likely to experience an increase in temperatures but with greater warming in the upper basins than the lower basins and mean annual runoff is also projected to increase over South Asian rivers but with different spatial trends.

Model projections all agree that temperature are expected to increase in the future over South Asia.

South America

There has been an increase in mean temperature (*medium confidence*) and increase in frequency of extreme rainfall events (*medium confidence*) in many areas of South America during the last decades.

The ability of climate models to simulate important regional aspects has improved in many areas, such as Amazonia, and there has been substantial additional regional analysis done using regional climate models allowing for better details of future changes in climate and extremes in South America.

Climate projections suggest an increase in temperature across South America and both increases and decreases in precipitation for South America by 2100 (*medium confidence*).

Europe

In most European areas it is very likely that positive trends in extreme precipitation and warm temperatures are persistent. This is documented using new datasets with homogenized observations at higher spatial and temporal resolution.

Over Europe, improved observational spatial and temporal coverage allows detection of trends in additional climate variables such as oceanic temperature and salinity, radiation and winds.

It is very likely that a substantial number of weather events involving extreme temperatures in Europe can be attributed to human contributions to climate change following the application of a range of method (*high confidence*) .

[Placeholder to include headline statements on projected trends on precipitation/temperature, and on region-specific events such as Mediterranean/mountainous/oceanic features]

Model representation of the climatology of European mean and extreme temperature and precipitation has improved compared to AR5 (*likely*), and this is aided by continuous model development, the existence of new coordinated modelling initiatives dedicated to Europe such as Euro-CORDEX and Med-CORDEX, and the release of new (high-resolution) observational data sets and reanalysis data.

There is low confidence that current models are able to reproduce the trends and decadal variability of climate characteristics in Europe. Large biases still exist and, for some of these, the reasons for the differences between model and observations are well understood, while for others this is not the case.

There is high confidence that state-of-the-art coupled atmosphere-ocean Regional Climate System

1 **Models exhibit skill similar to non-coupled atmosphere-only Regional Climate Models (RCMs) in**
2 **reproducing the European climate over land when driven by reanalyses.** They show overall good skills
3 to reproduce sea-surface temperature and salinity, and for some models also temperature and salinity deeper
4 in the ocean.

5
6 **It is *very likely* that strong winter warming in Northern Europe and strong summer warming in**
7 **Southern Europe will continue,** also when global mean temperature increase remains limited.

8
9 **It is *likely* that the associated northern European increase in seasonal mean precipitation and reduced**
10 **summer mean precipitation in southern Europe will continue.**

11
12 **There is *limited evidence* that for some specific climate phenomena, high resolution, convection**
13 **permitting RCMs show climate change signals that differ significantly from their driving coarser-**
14 **resolution GCMs and RCMs.** Projections of large-scale features, for example, such as heatwaves are not
15 changed significantly when applying convection-permitting models.

16
17 **An increasing number of national climate change projection programs is being carried out** and these
18 use a range of methodologies and resources to generate local-scale scenarios, making the comparison or
19 aggregation of these national scenarios difficult due to this variety in approaches and scope.

20 North America

21
22
23 **In most North America, it is *very likely* that positive trends in extreme precipitation and warm**
24 **temperatures are persistent.** This is documented using new datasets with homogenized observations at
25 higher spatial and temporal resolution.

26
27 **Detection of trends in additional climate variables such as oceanic temperature and salinity, radiation**
28 **and winds is possible over North America** due to improved observational spatial and temporal coverage.

29
30 **It is *very likely* that a substantial number of weather events involving extreme precipitation and**
31 **temperatures in North America has been increasing** but human contribution to such events is diverse and
32 more uncertain.

33
34 **Model representation of the climatology of North American mean and extreme climate condition has**
35 **improved compared to AR5 (*likely*).** This is aided by continuous model development and the existence of
36 new coordinated modelling initiatives.

37 Typological

38
39
40 **The Hindu Kush Himalayan mountains have shown a rising trend of extreme warm events; a falling**
41 **trend of extreme cold events; and a rising trend in extreme values and frequencies of temperature-**
42 **based indices (both minimum and maximum)** based on a 55-year period (1961–2015) global land surface
43 daily air temperature dataset.

44
45 **There is a statistically significant strong rate of warming (0.03–0.09 °C yr⁻¹) across all the seasons and**
46 **RCPs projected over the Indian Himalayan region** by the CORDEX South Asia regional climate models.

47
48 **CORDEX South Asia multi-RCMs RCP8.5 scenario climate projections over the Hindu Kush**
49 **Himalayan region showed seasonal warming for the hilly sub-region within the Karakoram and north-**
50 **western Himalaya, with higher projected change during winter (5.4°C) than during summer monsoon**
51 **season (4.9°C) by the end of 21st century** although there is less agreement among RCMs on the magnitude
52 of the projected warming over the hilly sub-regions within the central Himalaya and the south-eastern
53 Himalaya and Tibetan Plateau.

54
55 **CORDEX South Asia downscaled CMIP5 experiments project in general wetter/drier conditions in**

1 **near future for western/eastern Himalayan region, except for a part of the Hindu-Kush area in**
2 **western Himalayan region** and this scenario gets further intensified in the far future.

3 4 **General statements**

5
6 **There has been an explosion in the quantity and availability of regional climate data** though with
7 significant regional variations and without corresponding efforts to develop comprehensive guidance on their
8 quality and applicability.

9
10 **There is significantly enhanced evaluation of downscaled climate data over multiple regions** but with
11 regional variations in the level of this activity and there being insufficient results available to do a globally
12 comprehensive assessment.

13
14 **There are many good examples of integration of physical climate science information into adaptation**
15 **policy and action** as demonstrated by the case studies, taken from the broad range of those available.

16
17 **There has been a significant increase in the range of, especially regional, scientists, engaged in the**
18 **understanding of regional climate and developing and assessing regional climate information across**
19 **multiple regions** often through the formation of regional teams and with significant representation from
20 developing countries

21
22 **Significant improvements in technical infrastructure and open source tools and methodologies for**
23 **accessing and analysing observed and simulated climate data** have broadened the community able to
24 interact with these data with a wide range of activities involved from fundamental climate research to
25 providing inputs into assessing impacts, building resilience and developing adaptations.

26
27 **Tools to analyse and assess climate information have improved to allow development of information**
28 **beyond averages (e.g. on future climate thresholds and extremes) and which is relevant for regional**
29 **climate risk assessments**

30
31 **Significant advances in technological tools and social methodologies in communicating science**
32 **information** means that scientific findings are now reaching a much broader audience, and this demands
33 new skills of scientists to use and interact with these new opportunities for communication of their results.

34
35 **Whilst there have been significant increases in the range of data available and their ease of access,**
36 **often there are still significant gaps in understanding the context in which they are to be used** so more
37 effort is required to develop multidisciplinary teams in relevant areas of research and practice.

38
39 **Calculating observed climate changes, evaluation of models and developing bias correction and**
40 **downscaling is hampered by uneven distribution of observations, monitoring and poor data**
41 **availability.**

1 **Atlas.1 Introduction**

2

3 *Atlas.1.1 Purpose*

4

5 The Atlas serves several purposes. It expands on and integrates results from other WGI chapters and recent
6 literature to provide summaries of observed and relevant regional/local climate phenomena, historical
7 simulations and projected future climate change across different scales. It includes the description of an
8 online interactive tool (the Interactive Atlas), which allows for a flexible spatial and temporal analyses of
9 these results. One specific focus for the summaries is providing hazard information relevant to sectoral and
10 regional chapters of the WGII report, being informed by and complementing the work of Chapter 12 in
11 creating a bridge to Working Group II (WGII). Similarly, a specific aim of the integration is synthesising
12 information drawn from across multiple chapters that is relevant to the WGII report and the mitigation and
13 sectoral chapters of the Working Group III (WGIII) report. Finally, the Atlas also assesses approaches to
14 communication of climate information, illustrated with case studies and guidance on how to interpret them.

15

16

17 *Atlas.1.2 Context and framing*

18

19 Information on global and regional climate change in the form of maps, tables, graphs and infographics has
20 always been a key output of IPCC reports. With the consensus that climate has changed and will continue to
21 do so, policy-makers are focusing more on understanding the implications which often requires an increase
22 in regional and temporal details of observed and future climate. In response, the AR5 included in the WGI
23 contribution a globally comprehensive coverage of land regions and some oceanic regions in the Atlas of
24 Global and Regional Climate Projections (Annex I), focusing on projected changes in temperature and
25 precipitation. In the WGII contribution, the Regional Context Chapter (21) included continental scale maps
26 of observed and future temperature and precipitation changes, subcontinental changes in high percentiles of
27 daily temperature and precipitation, and a table of changes in extremes over subcontinental regions (updating
28 an assessment in the SREX report). However, there was only limited coordination between these two
29 contributions despite the largely common data sources and their relevance across the two working groups
30 and to wider communities of climate change-related policy and practice. This resulted in inefficiencies and
31 the potential for confusing or inconsistent messages which the Atlas, with its links with other WGI/II/III
32 chapters, is designed to address.

33

34 Given the aims of the Atlas, there are several important factors to consider. There is a clear requirement for
35 climate change information over a wide range of ‘regions’, and classes thereof, and temporal scales. There is
36 also often the need for integrated information relevant for policy, practice and awareness raising. However,
37 most other chapters in WGI are disciplinary, focusing on specific processes in the climate system or on its
38 past or future behaviour, and have limited space to be spatially and temporally comprehensive. The Atlas
39 provides an opportunity to facilitate this integration and exploration of information.

40

41 Developing this information often requires a broad range of data sources (various observations, global and
42 regionally downscaled baselines and projections) to be analysed and combined and, where appropriate,
43 reconciled. This is a topic which is assessed from a methodological perspective in Chapter 10 using a limited
44 set of examples. The Atlas then builds on this work with a more comprehensive treatment of the available
45 results, including (but not exclusively) CMIP5, CMIP6 and CORDEX, to provide wider coverage and to
46 further demonstrate techniques and issues.

47

48 Generating information relevant to policy or practice requires understanding the context of the systems that
49 they focus on. In addition to the hazards these systems face, their vulnerability and exposure, and the related
50 socio-economic and other physical drivers, also needs to be understood. To ensure this relevance, the Atlas is
51 informed by the assessments in Chapter 12 and the regional and thematic chapters and cross-chapter papers
52 of WG II. It will thus focus on generating messages and information on hazards applicable to assessing risks
53 on human and ecological systems whilst noting the potential relevance of these to related contexts such as
54 the Sustainable Development Goals and the Sendai Framework for Disaster Risk Reduction.

55

1 Finally, developing and synthesising all of this information, whilst understanding the context in which it is or
2 could be usefully applied, draws on and further develops methods for communicating climate information. It
3 also provides a series of best practise examples on constructing clear and credible messages. This is used to
4 provide an assessment of communication methods, with accompanying guidelines on generating relevant
5 climate information and a final section describing the online Interactive Atlas and how to interpret the
6 information it displays.

9 **Atlas.2 Defining temporal, spatial and typological domains and scales**

11 Over the past decades scientists have engaged in a wide array of investigations aimed at quantifying and
12 understanding the state of the components of the land surface–ocean–atmosphere system, the complex nature
13 of their interactions and impacts over different temporal and spatial scales. Through these studies a great deal
14 has been learned about the importance of treating the appropriate temporal and spatial scale when estimating
15 changes due to internal climate variability, trends, characterization of the spatiotemporal variability and
16 quantifying the range and establishing confidence in climate projections. It is therefore important to be able
17 to explore a whole range of spatial and temporal scales and the Atlas will complement other chapters by
18 facilitating this exploration of their assessments. This section presents the basic definitions of temporal
19 scales of analysis and domains used by Atlas accounting for potential synergies between WGs I and II. Also,
20 noting the recent IPCC special report on the impacts of global warming of 1.5°C above pre-industrial levels
21 (IPCC, 2018a), the Atlas will also include its approach of presenting key global and regional climate changes
22 at different warming levels.

25 *Atlas.2.1 Baseline and future time slice periods and temporal scales of analysis*

27 Chapter 1 has extensively explored this topic in Section 1.5.3 and Cross-Chapter Box 1.3 and a summary of
28 the main points as relevant to the Atlas are provided here. There is no standard baseline in literature although
29 the WMO recommends the approach to the 30-year baselines and the current official climate normal period
30 is 1981–2010. However, it will retain 1961–1990 as the historical base period for the sake of supporting
31 long-term climate change assessments (WMO, 2017). The AR6 WGI has established the period 1995–2014
32 as modern reference period (for similar reasons to the 1986–2005 period used in AR5 WGI) since 2014
33 (2005) is the final year of the historical simulations (see more details in Cross-Chapter Box 1.2).

35 Choosing a different baseline and averaging period can significantly influence the results of analysing
36 changes in mean climate (Hawkins and Sutton, 2016) and its variability and extremes. Thus, assessing the
37 sensitivity of results to the reference period is important and can be achieved using figures or tables
38 comparing different climate baseline periods. The Interactive Atlas (see Section Atlas.7) allows users to test
39 the implications of a wide range of different baselines, including:

- 41 • the AR6 standard 1995–2014 period (20 years),
- 42 • the AR5 standard 1986–2005 period (20 years),
- 43 • WMO climate normal periods such as 1981–2010 (30 years).

45 The use of the WMO standards conforms to the convention of 30-year climatological periods and provides
46 sample sizes relevant to calculating changes in statistics other than the mean. Moreover, these baselines are
47 relevant to work on impacts and thus would help to promote cross-working group consistency.

49 Also, using the WMO 1971–2000 standard baseline facilitates comparison between CMIP5 (and CORDEX)
50 and CMIP6 simulations since there exist ‘current climate’ simulations for all these datasets and thus can act
51 as a common baseline for comparing results from AR5 with AR6. Applying the more modern WMO 1981–
52 2010 or (particularly) the AR6 standard baseline would introduce an inconsistency as anthropogenic
53 emissions in the CMIP5 and CORDEX models do not follow the observed trajectory from 2006. To an
54 extent this can be circumvented by adopting the pragmatic choice of using scenario data to fill the missing
55 segments (2006–2010 and 2006–2014, respectively) using the first years of RCP8.5-driven transient

1 projections, in which the emissions are close to those observed. This is the approach that is used here and in
 2 Chapter 12. Also, on a more practical level, this helped to demonstrate how climate scientists can analyse
 3 and interpret outputs of simulations relevant to international standards and applications.
 4

5 Regarding the future reference periods, for consistency with previous reports, the Interactive Atlas First
 6 Order Draft (FOD) considers the future periods used in AR5: near-term, mid-term and long-term (referring
 7 to 2016–2035, 2046–2065 and 2081–2100 respectively). These are three important timescales to provide
 8 assessments for, so the same convention is used in AR6, with updated periods 2021–2040, 2041–2060, and
 9 2081–2100, respectively. *[For consistency with the 30-year WMO periods, the Interactive Atlas will also
 10 consider alternative timescales, such as 30-year near-term (2021–2050), mid-term (2046–2075) and long-
 11 term (2071–2100) periods].*
 12

13 Moreover, from the SR1.5 report global warming is defined as ‘The estimated increase in global mean
 14 surface temperature (GMST) averaged over a 30-year period, or the 30-year period centred on a particular
 15 year or decade, expressed relative to preindustrial levels unless otherwise specified. For 30-year periods that
 16 span past and future years, the current multi-decadal warming trend is assumed to continue.’ Therefore, we
 17 also consider different global warming levels (GWLs) to support future climate assessment, in particular
 18 +1.5, +2 in the Interactive Atlas FOD. *[To be extended to include +3 and +4°C.]*
 19

20 To calculate GWLs for the preliminary datasets used in the Atlas FOD (using a subset of nine CMIP5 ESMs
 21 and CORDEX RCMs; see Section Atlas.3), we quantify the global near-surface air temperature change for
 22 the 30-year period centred at the year when each model reaches the defined warming level (+1.5, +2, +3 and
 23 +4°C) for future projection assuming RCP 4.5 and 8.5 emissions, relative to preindustrial levels as simulated
 24 by the historical run. Here, we take the period 1861–1890 to define the pre-industrial (PI) period, as it is
 25 available across all CMIP5 historical simulations (Nikulin et al., 2018), and compute the mean PI
 26 temperature as baseline. Then, 30-year running mean timeseries are computed for each RCP, starting from
 27 the base period 1971–2000, and for each ESM (the running mean is centred around each year of the inter-
 28 annual time series). As a result, the GWLs are determined by the year when the running mean crosses the
 29 GWL threshold (see Figure Atlas.1:). When the projections stabilize before reaching the threshold and the
 30 warming period extends beyond year 2100, it is discarded (this is indicated by the asterisks in Table
 31 Atlas.1:). For CORDEX simulations, the periods of the driving ESM are used as in Nikulin et al. (2018).
 32 Note that this procedure will be updated in subsequent drafts when an adoption is made for AR6 WGI.
 33
 34

35 **[START FIGURE ATLAS.1: HERE]**
 36

37 **Figure Atlas.1:** Global mean temperature (30-year running mean) for the selected CMIP5 ensemble, considering
 38 RCPs 4.5 and 8.5. The reference GWLs are indicated by the horizontal grey lines. Preindustrial
 39 (1861–1890) and reference (1971–2000) periods are also delimited by the dashed vertical lines.
 40

41 **[END FIGURE ATLAS.1: HERE]**
 42
 43

44 **[START TABLE ATLAS.1: HERE]**
 45

46 **Table Atlas.1:** Time periods for which the +1.5, +2, +3 and +4°C Global Warming Levels (compared to pre-
 47 industrial times) were reached in the given list of CMIP5 global climate projections. Values
 48 correspond to the central year (n) of the 30-year window (the GWL period is thus calculated as [$n -$
 49 14, $n + 15$]). Asterisks indicate that the GWL was not reached before 2100.

	RCP 4.5				RCP 8.5			
	+1.5°C	+2°C	+3°C	+4°C	+1.5°C	+2°C	+3°C	+4°C
CanESM2_r1i1p1	2016	2031	2073	*	2013	2026	2049	2067
CNRM-CM5_r1i1p1	2035	2056	*	*	2029	2043	2066	*
CSIRO-Mk3-6-0_r1i1p1	2034	2047	*	*	2032	2044	2064	2082
EC-EARTH_r12i1p1	2023	2044	*	*	2020	2036	2059	2081

Do Not Cite, Quote or Distribute

Atlas-12

Total pages: 242

EC-EARTH_rli1p1	2021	2043	*	*	2017	2035	2060	2082
GFDL-ESM2M_rli1p1	2044	*	*	*	2034	2051	2080	*
HadGEM2-ES_rli1p1	2029	2045	*	*	2023	2036	2055	2071
IPSL-CM5A-MR_rli1p1	2016	2035	2080	*	2016	2030	2050	2067
MIROC5_rli1p1	2040	2072	*	*	2033	2048	2071	*
MIROC-ESM_rli1p1	2020	2034	2071	*	2020	2030	2052	2069
MPI-ESM-LR_rli1p1	2020	2043	*	*	2018	2035	2060	2080
NorESM1-M_rli1p1	2041	2076	*	*	2033	2048	2073	*

1
2 **[END TABLE ATLAS.1: HERE]**
3
4

5 Climate information over many temporal scales and a wide range of temporal averaging periods is required
6 for the assessment of climate change and its implications. These range from annual to multi-decadal averages
7 required to characterise low-frequency variability and trends in climate to hourly or instantaneous maximum
8 or minimum values of impactful climate variables. In between, information on seasonal averages of, for
9 example, rainfall is important with the definition of relevant averaging periods being geographically-
10 dependent. As a result, the Atlas presents results over wide range of timescales and averaging periods with
11 the Interactive Atlas enabling the choice of user-defined seasons and choices from a range of predefined
12 daily to multi-day climate indices.
13

14 For the sake of simplicity, only illustrative time slices will be shown in the Atlas text (warming levels will be
15 included in the Interactive Atlas).
16

17 *Atlas.2.2 Spatial domains and scales of analysis*

18
19 Many factors influence the spatial domains and scales over which climate information can be credibly
20 generated and is required. Despite all efforts in researching, analysing, and understanding climate change, a
21 key factor in the spatial scales at which analysis can be undertaken is directly related to the availability and
22 reliability of data, both observational and from model simulations. In addition, information is required over a
23 wide range of spatial domains, defined either from a climatological or geographical perspective (e.g. a
24 monsoon rainfall region or a river basin) or from a socio-economic or political perspective (e.g. least
25 developed countries or nation states). Chapter 1 provides an overview of these topics in Section 1.5.2 and
26 this subsection discusses some relevant issues, summarizes recent advances in defining domains and spatial
27 scales used by AR6 analyses and how these can be explored within the Interactive Atlas.
28
29

30 Recent IPCC reports (AR5, Chapter 14 and SR1.5, Chapter 3) have summarized information on projected
31 future climate changes over subcontinental regions defined in the IPCC SREX report and later extended in
32 AR5 from the 26 regions in SREX including polar and Caribbean, two Indian Ocean, and three Pacific
33 Ocean regions (hereafter known as the AR5 WGI reference regions) (Figure Atlas.2:a). More recently, new
34 subregions have been used in recent literature, for example, for South America, Africa and Central America,
35 together with the new definition of reference oceanic regions. As a result, an updated version of the reference
36 regions has been considered for AR6 (hereafter known as AR6 WGI land/ocean reference regions) as shown
37 in Figure Atlas.2:b. [AR6 WGI reference regions are currently used in the Interactive Atlas FOD as the
38 default regionalization for atmospheric variables]. These new regions build from a scientific reason as
39 described below for South America (SA) and Central America Caribbean (CAMC).
40
41

42 **[START FIGURE ATLAS.2: HERE]**
43

44 **Figure Atlas.2:** Reference AR5 (a) and AR6 (b) WGI regions. The latter includes both land and ocean regions and it
45 is used as the standard for the regional analysis of atmospheric variables in the Interactive Atlas.
46

1 **[END FIGURE ATLAS.2: HERE]**

2
3
4 In the case of South America the new regions were selected based on them having a consistent climate
5 change response signals and that they are climatically consistent regions (Barros et al., 2015; Neukom et al.,
6 2010; Nobre et al., 2016; Solman et al., 2008). Also, several studies have used those regions for analysis and
7 impact studies (Alves et al., 2013; Cabré et al., 2016; Fu et al., 2013).

8
9 In the case of the Central America and Caribbean Region, the AR5 WGI reference domains are considered
10 acceptable as large subcontinental regions assuming some minor modifications. These are important for
11 geographic homogeneity, and considering political and coastal boundaries. For Central America this involves
12 moving the eastern boundary west to exclude parts of Cuba and Jamaica, the northern boundary further
13 north, to include the northern border of Mexico (and particularly all of the Baja California Peninsula) and the
14 southern boundary northwest to exclude part of the South American continent. Similarly, small
15 enhancements to the Caribbean domain are proposed by shifting its northern boundary northward to include
16 the Bahamas and its eastern boundary eastward to include Barbados. To provide more details, subdivisions
17 of these domains are used to resolve the different particular features of Mexico and the Central American
18 isthmus and to separate Greater Antilles (including Bahamas) and Lesser Antilles (Figure Atlas.2:b). As the
19 CA region is very complex it could also justifiably be further subdivided for the projections of particular
20 features, as the diurnal and annual precipitation cycles, which differ between southern, central and northern
21 parts of Mexico and between the two coasts of the central American Isthmus (Angeles et al., 2007; Campbell
22 et al., 2011; Centella-Artola et al., 2015; Karmalkar et al., 2011, 2013; Martínez-Castro et al., 2018; McLean
23 et al., 2015; Taylor and Alfaro, 2005).

24
25 Besides the definition of generic reference/typological regions, there are further regionalisations that have
26 been used by the regional modelling communities, which might be relevant for model evaluation purposes
27 and AR6 WGII. As an illustrative example, in Southeast Asia, CORDEX simulation results are validated for
28 the whole region and for the subregions shown in Figure Atlas.3: (Cruz and Sasaki, 2017; Juneng et al.,
29 2016; Ngo-Duc et al., 2017). These subregions are based on the historical behaviour of rainfall from
30 previous studies on Southeast Asia. For example, there are two subregions over the Philippines, which are
31 based on two dominant climate types that are strongly influenced by the synoptic scale southwest and
32 northeast monsoon systems (Manzanas et al., 2015). Over Vietnam, there is a north-south division of
33 subregions as rainfall is highest in the north during summer while rainfall peaks during winter in Southern
34 Vietnam. More information on the climatic subregions over Southeast Asia can be found in Juneng et al.,
35 (2016).

36
37
38 **[START FIGURE ATLAS.3: HERE]**

39
40 **Figure Atlas.3:** CORDEX-SEA subregions based on historical rainfall climatology and variability (Juneng et al.,
41 2016)

42
43 **[END FIGURE ATLAS.3: HERE]**

44 45 46 *Atlas.2.3 Typological domains*

47
48 In addition to contiguous spatial domains discussed in the previous subsection, there are domains that are
49 defined by specific climatological, geographical, ecological or socio-economic domains where climate is
50 either an important determinant or influencer. Thus, the domain will be subject to specified physical
51 processes that are important for its climatology or involve systems which are affected by the climate in a way
52 that observations and climate model simulations can be used to understand. Many of these are the basis of
53 the cross-chapter working papers to be developed in the WGII report, namely biodiversity hotspots, tropical
54 forests, cities, coastal settlements, deserts and semi-arid areas, the Mediterranean, mountains and Polar
55 regions. It is therefore important to generate climate information relevant to these typological domains and

1 summary information is provided in Section Atlas.5.11 and expanded on in the Interactive Atlas. Figure
2 Atlas.4: shows some examples of typological domains that can be used in the Atlas, such as Monsoon region
3 and ocean biomes. [*Ocean biomes are currently used in the Interactive Atlas FOD as the default*
4 *regionalization for oceanic variables*].

5
6
7 **[START FIGURE ATLAS.4: HERE]**

8
9 **Figure Atlas.4:** Land monsoon regions (top) and ocean biomes (bottom).

10
11 **[END FIGURE ATLAS.4: HERE]**

12
13
14 [*Placeholder: Example of material on climate information relevant to WGI and II cross-chapter papers*]

15
16 Finally, due to the many potential definitions of the regions relevant for WGI and WGII, it is important to
17 keep some flexibility in the definition of regions in the Interactive Atlas (including the possibility of 'nested'
18 regions). However, the Atlas should be a useful instrument for AR6, and not necessarily cover all particular
19 regions relevant to specific chapters.

20 21 22 **Atlas.3 Combining multiple sources of information for regions**

23
24 This section introduces the observational data sources and reanalyses that are used in the assessment of
25 regional climate change and evaluating and bias-correcting the results of models (see Annex I). Also, it
26 introduces the different global and regional climate model output that are used for regional climate
27 assessment considering both historical and future climate projections (see Annex III). Many of these models
28 are run as part of coordinated Model Intercomparison Projects (MIPs), including the global Coupled Model
29 Intercomparison Projects (CMIP5 and CMIP6) and the COordinated Regional Downscaling EXperiment
30 (CORDEX), which are also described below. Combining information from these multiple data sources is a
31 significant challenge (see Chapter 10 for an in-depth treatment of the problem) though if clear messages on
32 regional climate change can be generated then they can be used to guide policy and support decisions
33 responding to these changes. An important and necessary part of this process is to check for consistency
34 amongst the data sources which is discussed in the final section.

35 36 37 **Atlas.3.1 Observations**

38
39 There are various sources of observational information available with disparity, inadequacy and
40 contradictions in these as well as applications of observations being assessed in Chapter 10. Observational
41 uncertainty is a key factor when assessing and attributing historical trends, so assessment should build on
42 integrated analysis from different datasets. The Atlas can supplement and complement Chapter 10 by
43 providing the opportunity to visualise and expand on its assessment. This includes displaying maps of
44 density of stations observations (including those that are used in the different datasets) and illustrating the
45 number of observational datasets for different regions (e.g. CORDEX, SREX or other defined regions).

46
47 Two of the most commonly used variables in climate studies are gridded monthly surface air temperature
48 and precipitation. There are many datasets available, commonly used ones including CRU, GISTEMP and
49 HadSST3 for temperature and GPCC and CRU for precipitation. Although the ultimate source of these
50 datasets is surface station reported values, each has access to different numbers of stations and lengths of
51 records and employs different ways of creating the gridded product and ensuring quality control.

52
53 For example, Figure Atlas.5: shows the long-term change in number of stations reported and illustrates the
54 declining number of observations used, especially for precipitation, in the CRU data.

1 **[START FIGURE ATLAS.5: HERE]**

2
3 **Figure Atlas.5:** Number of stations reported over the entire globe for surface air temperature (above) and precipitation
4 (below) for CRU TS4.0 dataset.

5
6 **[END FIGURE ATLAS.5: HERE]**

7
8
9 Figure Atlas.6: shows the spatial coverage of the total number of observation stations for surface air
10 temperature and precipitation, respectively, for 1901–1910, 1971–1980, and 2001–2010 and illustrates
11 spatially the declining trend of observation station data used in the precipitation dataset for certain regions
12 (South America, Africa) after the 1990s (both figures generated from contextual data available with the CRU
13 TS4.0 dataset). This demonstrates the regional inhomogeneity in station density.

14
15
16 **[START FIGURE ATLAS.6: HERE]**

17
18 **Figure Atlas.6:** Number of stations per 0.5 x 0.5 grid cell reported over the period of 1901–1910, 1971–1980, and
19 2001–2010 for surface air temperature for CRU TS4.0 dataset.

20
21 **[END FIGURE ATLAS.6: HERE]**

22
23
24 In addition to surface observation, satellites have been widely used to produce rainfall estimates. The
25 advantage of satellite-based rainfall products is their globally uniform coverage including remote areas.
26 However, there have been reported inconsistencies among different satellite-based rainfall products over
27 complex terrain (Rahmawati and Lubczynski, 2018; Satgé et al., 2019).

28
29 The Atlas can also cover other observation data, e.g. sea surface temperature. The most widely used SST
30 datasets are HadSST3, ERSST, and KaplanSST. The largest difference among the three datasets lie in how
31 inconsistency in number of observations during early and recent years is treated. Figure Atlas.7: shows the
32 change in the number of observations that is used in HadSST3 (Kennedy et al., 2011b, 2011a). There is a
33 limited number of observations available at the beginning of the period covered by the data set.

34
35
36 **[START FIGURE ATLAS.7 HERE]**

37
38 **Figure Atlas.7:** Same as Figure Atlas.5.; but for number of observations in the HadSST3 dataset.

39
40 **[END FIGURE ATLAS.7 HERE]**

41
42
43 Figure Atlas.8: shows that the contrast in the available observations used in HadSST3 in different time
44 periods become much clearer when shown in terms spatial maps distribution.

45
46
47 **[START FIGURE ATLAS.8 HERE]**

48
49 **Figure Atlas.8:** Same as Figure Atlas.6.; but for number of observations in the HadSST3 dataset.

50
51 **[END FIGURE ATLAS.8 HERE]**

52
53
54 Figure Atlas.9: provides an example of the discrepancies in different SST datasets from (Rupa Kumar et al.,
55 2006). The difference in number of observations and irregular distribution in space and time introduces
56 different ways of treating uncertainty and temporal/spatial gaps, resulting in difference in long-term trends.

Do Not Cite, Quote or Distribute

1
2
3 **[START FIGURE ATLAS.9 HERE]**
4

5 **Figure Atlas.9:** Global (excluding the Southern Ocean) annual average SST anomaly (relative to 1971–1990), for the
6 period 1871–2000. Annual averages smoothed using a 21-pt binomial filter (from Rayner et al., 2003).
7

8 **[END FIGURE ATLAS.9 HERE]**
9

10
11 *Atlas.3.1.1 Consistency and differences in observational data*
12

13 There are some recent studies assessing observational datasets globally (Beck et al., 2017; Sun et al., 2018)
14 that report large differences among them. Regional studies have also been undertaken on comparing and
15 assessing observational datasets with similar results (Manzanas et al., 2014; Prakash, 2019; Salio et al.,
16 2015), thus stressing the importance of considering observational uncertainty in regional climate assessment
17 studies. For example, Indasi (2019) assessed rainfall characteristics of ten gridded precipitation datasets over
18 Southern Africa (Table Atlas.2:). They demonstrated that those sharing similar source data displayed similar
19 rainfall characteristics while station-based datasets showed the least similarities. No single dataset was found
20 to capture the rainfall characteristics across the entire Southern Africa region, and each performed better or
21 worse depending on location. They also noted the decline in the number of stations available, mainly due to
22 insufficient resources but also a tendency by country meteorological services to restrict free access,
23 increasing relevance of satellite data and significant relationships between some of the datasets (Figure
24 Atlas.10:). Another important aspect is that many stations do not report to the WMO networks, with their
25 data being kept domestically or regionally, which has made regional datasets become more important in the
26 recent years.
27
28

29 **[START TABLE ATLAS.2: HERE]**
30

31
32 **Table Atlas.2:** Gridded precipitation datasets assessed in Indasi (2019) over South Africa, indicating the different
33 data sources used in each case.

Dataset	GHCN stations	WMO GTS stations	FAO station data	Other station data	CFS	NCEP/ NCAR Reanalysis	ERA- Interim	TRMM	Thermal IR satellite
CRU	X	X		X					
GPCC	X	X	X	X					
UDEL	X			X					
ARC		X							X
CHIRP					X			X	X
CHIRPS		X		X	X			X	X
CMAP	X	X	X	X		X			X
GPCP	X	X	X	X					X
WFDEI_CRU	X	X		X			X		
WFDEI_GPCC	X	X	X	X			X		

34
35 **[END TABLE ATLAS.2: HERE]**
36
37

1 **[START FIGURE ATLAS.10: HERE]**

2
3 **Figure Atlas.10:** Relationship between gridded precipitation dataset and three classes of input data; station, satellite
4 and reanalysis. Input datasets are shown in green, blue shows gridded datasets that are used as input to
5 others shown in orange. (Indasi, 2019)

6
7 **[END FIGURE ATLAS.10: HERE]**

8
9
10 This section describes the disparities and inconsistencies in observations at different regions, especially
11 rainfall and temperature data. Conflicts in observation data are a concern when producing reliable results for
12 any region, with greater confidence in findings if observation products are consistent. For example,
13 observations agree on increases in the number of heavy precipitation events (e.g., 95th percentile) within
14 many land regions (Trenberth and Josey, 2007) including over China (Ma et al., 2009) and Europe.

15
16 Uncertainty in observations is a key factor preventing a rigorous evaluation of climate models over most
17 regions. Scientists publish varying results because of uncertainty in the temporal and spatial characteristics
18 of observations over certain regions. This is highlighted in various other chapters and the Atlas expands on
19 the treatment of this, especially based on CORDEX literature, complementing the discussions on
20 discrepancies/conflicts in observations presented in Chapter 10 and expanding on and replicating their results
21 for other regions. For example, Figure Atlas.11: show a sample figure from Juneng et al., (2016) on the
22 differences in precipitation values in the observation data in Southeast Asia. Figure Atlas.12: replicates this
23 for Africa.

24
25
26 **[START FIGURE ATLAS.11: HERE]**

27
28 **Figure Atlas.11:** Differences in precipitation values in the different observation datasets in Southeast Asia (from
29 Juneng et al., 2016)

30
31 **[END FIGURE ATLAS.11: HERE]**

32
33
34 **[START FIGURE ATLAS.12: HERE]**

35
36 **Figure Atlas.12:** Similar to Figure Atlas.11 but for Africa.

37
38 **[END FIGURE ATLAS.12: HERE]**

39
40
41 The Atlas also discusses differences in surface and satellite observations. Sylla et al. (2013) assessed
42 uncertainties in climate observation products by intercomparing three gridded observed daily rainfall datasets
43 over Africa – FEWS (Famine Early Warning System), GPCP (Global Precipitation Climatology Project) and
44 TRMM (Tropical Rainfall Measuring Mission). Different observation products were shown to exhibit
45 differences in mean rainfall, higher order daily precipitation statistics, such as frequency of wet days,
46 precipitation intensity and extremes as well as maximum length of wet and dry spells. FEWS showed mostly
47 higher frequency and lower intensity events than TRMM and GPCP.

48
49 *[Placeholder: Figure from Sylla et al., 2013]*

50
51 Finally, some research is currently focusing on the distillation and consistency of climate change projections
52 from multi-MIP global and regional projects (Fernández et al., 2018). These studies will be assessed in
53 Chapter 10 and will inform on the methods to be implemented in the Interactive Atlas in order to synthesize
54 multi-MIP projections.

55
56 *[Placeholder: Cross chapter box with Chapter 10 on distillation and synthesis of multi-MIP projections]*

Atlas.3.2 Reanalysis

There are currently many atmospheric reanalysis datasets with different spatial resolution and assimilation algorithms (see Annex I, Observations). There are also substantial differences among those datasets and the Atlas will show and intercompare those that are used in the report. These differences are due to the types of observations assimilated into these reanalyses, the assimilation techniques that are used, and the resolution of the outputs amongst other reasons. For example, 20CR only assimilates surface pressure and sea surface temperature to achieve the longest record but at relatively low resolution. At the other extreme, very sophisticated assimilation systems using multiple surface, upper air and earth observation data sources are employed, e.g. for ERA5, ERA-Interim and JRA-55, which also have much higher resolutions. Most of reanalysis dataset covers the entire globe. However, there are also high-resolution regional reanalysis datasets (see, e.g. Section Atlas.5.6.1.4 for the case of Europe).

In principle, inconsistency among different ocean reanalysis datasets will be primarily treated in Chapter 9 but expanded in the Atlas.

Atlas.3.3 Global Model Data (CMIP5 and CMIP6)

The Atlas uses global model simulations from both CMIP5 and CMIP6 (the latter only partially since this dataset is not entirely available yet). This facilitates comparison of the assessments from two IPCC cycles and thus the detection of new features and findings coming from recent science and the latest CMIP6 ensemble.

The Interactive Atlas FOD is based on a subset of nine CMIP5 models (focusing on the more recent Earth System Models) shown in Table Atlas.3.; in future drafts, the full CMIP5 curated dataset will be used for consistency with the results of the AR5 Atlas. Building on this information, the Interactive Atlas displays a number of (mean and extreme) indices considering both atmospheric and oceanic variables. Some of these indices have been selected in coordination with Chapter 12, in order to support and extend the assessment performed in this Chapter (see Annex VII Hazards and Extreme Indices for details on the indices). Other indices have been included to support the regional assessment made in the Section Atlas.5. The set of indices will be further coordinated with other Chapters in future drafts, building on the experience gained (and tools developed) in this collaboration.

[START TABLE ATLAS.3: HERE]

Table Atlas.3: Data availability for the subset of CMIP5 models used in the Interactive Atlas FOD for the historical period and the RCP4.5 and RCP8.5 emissions-driven future projections: For the atmospheric – mean (tas, in °C), maximum (tx, in °C) and minimum (tn, in °C) temperatures, precipitation (pr, in mm/day) – and oceanic – sea surface temperature (tos, °C), PH (PH) and oxygen (O₂, in mol m³) – variables. Salient features of these models are described in IPCC AR5 Appendix 9.A (model names are taken from Table 9.A.1).

	Atmospheric				Oceanic	
	tas	tx	tn	pr	tos	pH O2
CMIP5_CanESM2_r1i1p1_historical	yes	yes	yes	yes	yes	yes
CMIP5_CanESM2_r1i1p1_rcp45	yes	yes	yes	yes	yes	yes
CMIP5_CanESM2_r1i1p1_rcp85	yes	yes	yes	yes	yes	yes
CMIP5_CNRM-CM5_r1i1p1_historical	yes	yes	yes	yes	yes	yes
CMIP5_CNRM-CM5_r1i1p1_rcp45	yes	yes	yes	yes	yes	yes
CMIP5_CNRM-CM5_r1i1p1_rcp85	yes	yes	yes	yes	yes	yes

CMIP5_IPSL-CM5A-MR_r1i1p1_historical	yes						
CMIP5_IPSL-CM5A-MR_r1i1p1_rcp45	yes						
CMIP5_IPSL-CM5A-MR_r1i1p1_rcp85	yes						
CMIP5_MIROC-ESM_r1i1p1_historical	yes	yes	yes	yes			
CMIP5_MIROC-ESM_r1i1p1_rcp45	yes	yes	yes	yes			
CMIP5_MIROC-ESM_r1i1p1_rcp85	yes	yes	yes	yes			
CMIP5_GFDL-ESM2M_r1i1p1_historical	yes						
CMIP5_GFDL-ESM2M_r1i1p1_rcp45	yes						
CMIP5_GFDL-ESM2M_r1i1p1_rcp85	yes						
CMIP5_MPI-ESM-LR_r1i1p1_historical	yes						
CMIP5_MPI-ESM-LR_r1i1p1_rcp45	yes						
CMIP5_MPI-ESM-LR_r1i1p1_rcp85	yes						
CMIP5_HadGEM2-ES_r1i1p1_historical	yes						
CMIP5_HadGEM2-ES_r1i1p1_rcp45	yes						
CMIP5_HadGEM2-ES_r1i1p1_rcp85	yes						
CMIP5_EC-EARTH_r12i1p1_historical	yes	yes	yes	yes	yes		
CMIP5_EC-EARTH_r12i1p1_rcp45	yes	-	yes	yes	yes		
CMIP5_EC-EARTH_r12i1p1_rcp85	yes	yes	yes	yes	yes		
CMIP5_NorESM1-M_r1i1p1_historical	yes	yes	yes	yes	yes		
CMIP5_NorESM1-M_r1i1p1_rcp45	yes	yes	yes	yes	yes		
CMIP5_NorESM1-M_r1i1p1_rcp85	yes	yes	yes	yes	yes		

1
2 [END TABLE ATLAS.3 HERE]
3
4

5 As of September 2018, there are 23 CMIP6-endorsed MIPs. Each has a specific purpose listed in Table
6 Atlas.4:. Besides CMIP5 (and CORDEX, see below), the Atlas will use information based on some multi-
7 MIPs (including ScenarioMIP and HighResMIP) when available, in order to produce indices to support and
8 extend the assessment of the different chapters, and to allow intercomparability with the previous AR5.
9

10
11 [START TABLE ATLAS.4 HERE]
12

13 **Table Atlas.4:** The 23 CMIP6-endorsed (from www.wcrp-climate.org/modelling-wgcm-mip-catalogue/modelling-wgcm-cmip6-endorsed-mips) MIPs.
14

1	AerChemMIP	Aerosols and Chemistry Model Intercomparison Project
2	C4MIP	Coupled Climate Carbon Cycle Model Intercomparison Project
3	CDRMIP	The Carbon Dioxide Removal Model Intercomparison Project
4	CFMIP	Cloud Feedback Model Intercomparison Project
5	DAMIP	Detection and Attribution Model Intercomparison Project
6	DCPP	Decadal Climate Projection Project
7	FAFMIP	Flux-Anomaly-Forced Model Intercomparison Project
8	GeoMIP	Geoengineering Model Intercomparison Project

9	GMMIP	Global Monsoons Model Intercomparison Project
10	HighResMIP	High-Resolution Model Intercomparison Project
11	ISMIP6	Ice Sheet Model Intercomparison Project for CMIP6
12	LS3MIP	Land Surface, Snow and Soil Moisture
13	LUMIP	Land-Use Model Intercomparison Project
14	OMIP	Ocean Model Intercomparison Project
15	PAMIP	Polar Amplification Model Intercomparison Project
16	PMIP	Paleoclimate Modeling Intercomparison Project
17	RFMIP	Radiative Forcing Model Intercomparison Project
18	ScenarioMIP	Scenario Model Intercomparison Project
19	VolMIP	Volcanic forcing Model Intercomparison Project
20	CORDEX	Coordinated Regional Climate Downscaling Project
21	DynVarMIP	Dynamics and Variability Model Intercomparison Project
22	SIMIP	Sea Ice Model Intercomparison Project
23	VIACS AB	Vulnerability, Impacts, Adaptation, and Climate Services Advisory Board

1
2 **[END TABLE ATLAS.4: HERE]**
3
4

5 The Atlas also aims to cover as much information on regional climate changes as possible, so information
6 from the existing CMIP5 as well as the CMIP6 datasets is supplemented with downscaled regional climate
7 simulations from CORDEX. This facilitates an assessment of the effects from higher resolution including
8 whether this modifies the projected climate change signals compared to global models and adds any value,
9 especially in terms of high-resolution features and extremes.

10
11
12 ***Atlas.3.4 Regional Model Data (CORDEX)***
13

14 Global model data, as generated by the CMIP ensembles, are available everywhere, but their spatial
15 resolution is limited for reproducing certain processes and phenomena relevant for regional analysis. The
16 Coordinated Regional Climate Downscaling Experiment – CORDEX (Gutowski et al., 2016) – coordinates
17 regional downscaling experiments worldwide over a number of domains (example domains are presented in
18 Figure Atlas.13.; more details are provided in Annex III; Table AIII.1). However, in some domains only a
19 few simulations have been performed and in others it is not easy to access data (see the list of contributing
20 models in Table AIII.2 and the data inventory in Table AIII.3). Moreover, there are regions of overlapping
21 simulation domains, e.g. the Mediterranean or Central Asia, and guidance on the synthesis and use of this
22 information is needed for scientifically rigorous analysis and generation of defensible climate information
23 for stakeholder use. This limits the level of analysis and assessment that can be done in some regions.
24 Ongoing efforts, such as the multi-domain CORE simulations (Gutowski et al., 2016), are promoting more
25 homogeneous coverage thus allowing more systematic treatment of CORDEX domains in the Interactive
26 Atlas. Data from both the individual CORDEX domains and from CORDEX CORE will be used in future
27 versions of the Atlas. Finally, the amount, quality and resolution of observational data available in some
28 regions can limit the ability to validate and establish confidence in the model simulations of recent past,
29 current and projected future climate changes.

30
31
32 **[START FIGURE ATLAS.13: HERE]**
33

34 **Figure Atlas.13:** Major non-polar CORDEX domains and topography. [This figure includes incomplete information.
35 To be updated.]
36

37 **[END FIGURE ATLAS.13: HERE]**
38

1
2 A lot of progress has been made in the different CORDEX domains in order to produce and analyse
3 downscaled climate information for evaluation (driven by ERA-Interim) and historical and future climate
4 scenarios (under a range of future emissions, i.e. RCP2.6, RCP4.5 and RCP8.5). As a result, datasets
5 obtained with ensembles of RCMs are now available on the Earth System Grid Federation (ESGF), for a
6 number of domains (see Annex III; Tables AIII.2 and AIII.3). However, the available information is not yet
7 comprehensive in most of the domains (either scarce RCMs or GCMs used as boundary conditions), so in the
8 Interactive Atlas FOD we have focused on the two most populated domains (Africa-AFR44, and Europe-
9 EUR44) and have selected the common sub-ensemble for these two regions, for the common 0.44° resolution
10 (see Table Atlas.5:). This is done to guarantee the consistency of results and to limit misleading conflicts in
11 overlapping regions (the Mediterranean in this case). This gives the opportunity to identify conflicts and
12 applying methods for distilling synthesis regional information; this is currently an active area of research
13 which is expected to produce some results soon to be adopted in future drafts.

14
15
16 **[START TABLE ATLAS.5: HERE]**

17
18 **Table Atlas.5:** GCM/RCM simulations available for both Africa (ARF-44) and Europe (EUR-44) domains for the
19 historical and RCP45 and RCP85 scenarios (as from ESGF at March 2019). Note that the model
20 versions are different for both domains for some particular models. For details on the GCMs see Table
21 Atlas.3: for details on the RCMs see Annex III models; Table AIII.2).
22

GCM_run	RCM
CanESM2_r1i1p1	RCA4_v1
CNRM-CM5_r1i1p1	RCA4_v1
CSIRO-Mk3-6-0_r1i1p1	RCA4_v1
EC-EARTH_r1i1p1	RACMO22E_v1 (RACMO22T for AFR-44)
EC-EARTH_r3i1p1	HIRHAM5_v1 (HIRHAM5_v2 for AFR-44)
EC-EARTH_r12i1p1	RCA4_v1
GFDL-ESM2M_r1i1p1	RCA4_v1
HadGEM2-ES_r1i1p1	RCA4_v1 RACMO22E_v2 (RACMO22T for AFR-44)
IPSL-CM5A-MR_r1i1p1	RCA4_v1
MIROC5_r1i1p1	RCA4_v1
MPI-ESM-LR_r1i1p1	CCLM4-8-17_v1 REMO2009_v1 RCA4_v1
NorESM1-M_r1i1p1	RCA4_v1

23
24 **[END FIGURE ATLAS.5 HERE]**
25
26

27 Besides these two CORDEX domains we have also considered for illustrative purposes the data available
28 from one of the Polar domains (Antarctic, ANT-44) with only three simulations (i.e. ESM-RCM
29 combinations) available for the historical and RCP45 and RCP85 scenarios (see Table Atlas.6:; view also
30 www.climate-cryosphere.org/activities/targeted/polar-cordex for more information).
31

1
2 **[START TABLE ATLAS.6: HERE]**

3
4 **Table Atlas.6:** As Table Atlas.5., but for Antarctica (ANT-44).

5

GCM_run	RCM
EC-EARTH_r3i1p1	HIRHAM5_v1
EC-EARTH_r1i1p1	RACMO21P_v1
HadGEM2-ES_r1i1p1	RACMO21P_v2

6
7 **[END TABLE ATLAS.6: HERE]**

8
9
10 The Atlas assesses research on CORDEX simulations over different regions analysing past and current
11 climate, and future climate projections. It also focuses on model evaluation in order to complement the
12 evaluation of global models done in Chapter 4 extending it to regional climate models, taking into account
13 the specificity of these type of models, and building on existing initiatives and frameworks for evaluating
14 downscaling methods for climate research (Maraun et al., 2015a). The goal is characterizing the
15 heterogeneity of simulations available and validation studies across different domains in order to identify
16 where an assessment is feasible (to be done in collaboration with regional Chapters 10 to 12).

17
18 In order to provide some basic evaluation results for the CORDEX models (to be further developed in
19 collaboration with Regional Chapters 10 to 12), the validation approach proposed in the VALUE initiative
20 (Maraun et al., 2015a) was followed, using the same indices and diagnostic measures proposed in the
21 synthesis paper (Maraun et al., 2018), which are shown in Table Atlas.7.: The biases obtained for these
22 indices from the different RCMs shown in Table Atlas.5: have been computed for the EUR-44 and AFR-44
23 domains and are shown Section Atlas.5.2 (for Europe) and Atlas.5.6 (for Africa). Results are only shown for
24 precipitation.

25
26
27 **[START TABLE ATLAS.7: HERE]**

28
29 **Table Atlas.7:** Diagnostics considered for the evaluation of CORDEX data (see Maraun et al., 2018) . Relative biases
30 as considered as performance measure for all indices.

Code	Index/Diagnostic	Description
Mean	Mean	Mean precipitation
R01	Wet day frequency	Number of wet days in year/season
SDII	Wet day intensity	Mean on wet days (≥ 1 mm) only
Skewness	Skewness	Skewness of the wet-day distribution
WWProb	Wet–wet transition probability	Probability of a wet day, given that the previous was wet
DWProb	Dry–wet transition probability	Probability of a dry day, given that the previous was wet
WetAnnualMaxSpell	Longest wet spell	Median of the annual max. wet (≥ 1 mm) spell duration
DryAnnualMaxSpell	Longest dry spell	Median of the annual max. dry (< 1 mm) spell duration
AnnualCycleRelAmp	Relative Amplitude of the Annual Cycle	Difference between maximum and minimum value (30-day moving window over calendar days), relative to the mean of these two values.

31
32 **[END TABLE ATLAS.7: HERE]**

33
34 For illustrative purposes, Figure Atlas.14: shows the climatologies of the observational reference used for

35 **Do Not Cite, Quote or Distribute**

1 validation (the 0.5° EWEMBI gridded observational dataset; see Annex VII Hazards and Extreme Indices for
2 more details) for two particular indices, mean daily rainfall and relative amplitude of the annual cycle. This
3 figure shows the results on the different European and African AR6 WGI reference regions (see Section
4 Atlas.2 for details) to illustrate the overlap over the Mediterranean region (MED), where the observed
5 climatological (e.g. EWEMBI) values are identical, but where CORDEX EUR-44 and AFR-44 could
6 produce conflicting results.
7
8

9 **[START FIGURE ATLAS.14 HERE]**

10
11 **Figure Atlas.14:** (Left) Annual mean daily precipitation (mm/day) for the observational reference EWEMBI for the
12 different AR6 WGI reference regions over Europe and Africa used for spatial aggregation of regional
13 information in the Interactive Atlas (see Section Atlas.2 for more details). (Right) Relative Amplitude
14 of the Annual Cycle, defined as the difference between maximum and minimum value (30-day
15 moving window over calendar days), relative to the mean of these two values.
16

17 **[END FIGURE ATLAS.14 HERE]**

18 19 20 **Atlas.4 Global synthesis**

21
22 Most other chapters in WGI focus on past or future behaviour of the global climate system or specific
23 components within it. Noting the overall WGI contribution aims to have wide-ranging application that
24 frequently requires integration of information sources, this section combines findings from these other
25 chapters (2–9) with a focus on messages that are relevant to WGII and WGIII contexts. It also provides a
26 global overview assessment of findings from the CMIP5 and CMIP6 ensembles focusing on climate indices
27 underpinning the regional assessments in Section Atlas.5 and the results displayed in the Interactive Atlas.
28 Thus, its aim is not to provide information relevant to deriving messages about regional climate changes but
29 to provide the global context for such messages derived later in the Atlas. The first subsection (Atlas 4.1)
30 considers global atmospheric and land-surface results, with findings on the global oceans in the second
31 (Atlas 4.2) and the third (Atlas 4.3) focusing on extreme events.
32

33 *[Much of the material to be presented here depends on findings which are currently being developed in the*
34 *other chapters. Whilst these are maturing, examples are provided below of selected results from CMIP5*
35 *models. These partially act as placeholders demonstrating the type of information which will be included in*
36 *future but also provide global context for the regional-scale results presented in Atlas.5 and the Interactive*
37 *Atlas. These include results from CORDEX which are based on downscaling of CMIP5 models. The material*
38 *below consists of examples which are cross-cutting and of relevance to the handshake with WGII.]*
39
40

41 **Atlas.4.1 Global atmosphere and land surface**

42
43 The principle atmospheric quantities of interest for understanding how climate change may impact human
44 and ecological systems, as well as being key global indicators of change, are surface air temperature and
45 precipitation. They are therefore a significant focus of the regional climate assessments in Section Atlas.5
46 and of the Interactive Atlas. As described earlier, this information is required both at different time periods in
47 the future under a range of emissions scenarios but also for different global warming levels. Figure Atlas.15:
48 shows the global surface air temperature change projection calculated from the ensemble mean of nine
49 CMIP5 models for the middle of the century under the RCP 4.5 and 8.5 emissions scenarios compared to the
50 end of the century warming under RCP8.5 and for a global mean warming levels of 2°C.
51

52
53 **[START FIGURE ATLAS.15: HERE]**

54
55 **Figure Atlas.15:** Global temperature changes projected for mid-century (left column) under RCP4.5 (top) and 8.5
56 (bottom) compared to, in the right column, a global mean warming levels of 2°C (top) and at the end

1 of the century under RCP8.5 emissions (bottom) from an ensemble of nine CMIP5 GCMs. Note that
2 the future period warmings are calculated against a baseline period of 1986–2005 whereas the global
3 mean warming level is defined with respect to a ‘pre-industrial’ baseline of 1861–1890. Thus, the
4 other three maps would show greater warmings with respect to this earlier baseline.
5

6 **[END FIGURE ATLAS.15: HERE]**
7
8

9 Figure Atlas.15: presents a mean projection from averaging the changes from nine CMIP5 models but it is
10 also important to explore the full range of outcomes from the ensemble, for example when undertaking a
11 comprehensive risk assessment in which temperature is an important hazard. This is displayed in Figure
12 Atlas.16: for the global average surface air temperature increases projected by the models throughout the
13 century under the RCP 8.5 emissions scenario. Of course, information of this nature is also important
14 regionally and this can be explored within the Interactive Atlas over the AR6 reference regions defined by
15 the polygons on the maps in Figure Atlas.15: (and described in Section Atlas.2). These regional results
16 demonstrate how temperature is projected to increase for all regions, and at a greater rate than the global
17 average over many land regions and the North Pole.
18

19
20 **[START FIGURE ATLAS.16: HERE]**
21

22 **Figure Atlas.16:** Global average surface air temperature increases projected by nine CMIP5 models under the RCP8.5
23 emissions scenario from 2005 to 2100 relative to a 1986–2005 baseline.
24

25 **[END FIGURE ATLAS.16: HERE]**
26
27

28 Precipitation changes present a more complex picture with regions of decrease as well as increase as shown
29 in Figure Atlas.17: which displays the ensemble mean changes corresponding to the right-hand panels of
30 Figure Atlas.15: (projected changes at 2°C global mean warming compared to pre-industrial levels compared
31 with at the end of the century under RCP8.5 emissions compared to the recent past). The figure also shows
32 that at lower warming levels there are many land regions, especially in the southern hemisphere, where there
33 is no robust signal of change from the models (note that stippling indicates those gridboxes where less than
34 six out of the nine models do not agree on the sign of the projected change).
35

36
37 **[START FIGURE ATLAS.17: HERE]**
38
39

40 **Figure Atlas.17:** Global precipitation changes projected at 2°C global mean warming compared to pre-industrial levels
41 (left) and for 2081–2100 under RCP8.5 emissions compared to the 1986–2005 (right) from an
42 ensemble of nine CMIP5 GCMs. Regions are stippled where less than six out of the nine models do
43 not agree on the sign of the change (noting that this assessment does not take into account whether the
44 individual models’ projected changes are significant).
45

46 **[END FIGURE ATLAS.17: HERE]**
47
48

49 *[Later drafts will also include information on other important surface quantities such as soil moisture and*
50 *runoff and, if appropriate, derived quantities such as river flow and indices relevant to drought. Also, if*
51 *appropriate, atmospheric quantities, e.g. relating to global monsoons or atmospheric pollutants/air quality,*
52 *will also be included.]*
53

54 In addition to focusing on changes in individual climate variables it is also important to note that concurrent
55 extreme atmospheric hazards may also pose significant risks to human and ecological systems. Their
56 magnitude or likelihood are often influenced by global climate drivers and understanding these links can be

1 important in assessing risks from, and developing adaptations in response to, clear anthropogenic influences
2 on individual hazards. This will also support the related fields of disaster risk reduction and global
3 sustainable development efforts as noted by Steptoe et al., (2018). They demonstrated that 15 regional
4 hazards shared connections via the El Niño–Southern Oscillation, with the Indian Ocean Dipole, North
5 Atlantic Oscillation and the Southern Annular Mode being secondary sources of significant regional
6 interconnectivity (Figure Atlas.18:). Understanding these connections and quantifying the concurrence of
7 resulting hazards can support adaptation planning as well as multi-hazard resilience and disaster risk
8 reduction goals.

9
10
11 **[START FIGURE ATLAS.18: HERE]**

12
13 **Figure Atlas.18:** Influence of major modes of variability on regional extreme events relevant to assessing multi-hazard
14 resilience (Steptoe et al., 2018). Ribbon colours define the driver from which they originate and their
15 width is proportional to the correlation. Hatching represent where there is conflicting evidence for a
16 correlation or where the driver is not directly related to the hazard and dots represent drivers that have
17 both a positive and negative correlation with the hazard.

18
19 **[END FIGURE ATLAS.18 HERE]**

20
21
22 *[Placeholder: When material in other sections of the Atlas on observed changes regionally and the use of*
23 *observations in model evaluation has matured, along with the assessment in Chapter 2, material will also be*
24 *introduced into this section on observations and observed changes.]*

25 26 27 **Atlas.4.2 Global oceans**

28
29 As with the atmosphere, there are several key ocean-related quantities which are relevant for understanding
30 how climate change may impact human and ecological systems and/or key global indicators of change.
31 These include ocean surface temperature and heat content, sea ice cover and thickness, and certain chemical
32 properties such as ocean acidity and oxygen concentration. For example, there is growing awareness of the
33 threat presented by ocean acidification to ecosystem services and the socio-economic consequences are
34 becoming increasingly apparent and quantifiable (Hurd et al., 2018) and the IPCC Special Report Global
35 Warming of 1.5°C (IPCC, 2018b) noted a significant impact of low levels of global warming on the state of
36 the global oceanic ecosystems and food security. For instance, 70% of global coral reefs are expected to
37 disappear at a warming level of 1.5°, while no coral will be preserved when warming levels reach 2°C or
38 higher.

39
40 Thus, because of their importance to ocean ecosystems, the Atlas (and, in particular, the Interactive Atlas)
41 initially focuses on ocean temperature, pH and dissolved oxygen and projected changes in the subset of 9
42 CMIP5 models used to establish a reference for the CMIP6 and CORDEX results (to be) assessed in section
43 Atlas.5.9. Figure Atlas.19: shows projected changes in these variables at the end of the century under
44 RCP4.5 and 8.5 emissions, demonstrating the much larger changes seen with the higher emissions scenario.

45
46
47 **[START FIGURE ATLAS.19: HERE]**

48
49 **Figure Atlas.19:** Projected changes in sea-surface temperature (top), ocean pH (middle) and dissolved oxygen (bottom)
50 for 2081-2100 under the RCP4.5 (left column) and 8.5 (right column) emissions compared to a 1986–
51 2005 baseline period from an ensemble of nine CMIP5 GCMs. Regions are stippled where less than
52 six out of the nine models do not agree on the sign of the change (noting that this assessment does not
53 take into account whether the individual models' projected changes are significant)

54
55 **[END FIGURE ATLAS.19 HERE]**

1 [Placeholder: Later drafts will include findings selected from other chapters such as
2 • maps of historical temperature change, sea level rise, P-E, salinity, pH and dissolved oxygen
3 • projections of sea level rise, P-E, salinity
4 • regional displays of historical or projected changes in currents, storm frequency, sea ice cover, sea ice
5 thickness]
6
7

8 **Atlas.4.3 Extremes**

9
10 Many of the most severe impacts of climate are felt through extreme events and climate change has been
11 demonstrated to increase either the frequency or intensity of many types of such hazardous events. Thus, the
12 third important area of focus for this global synthesis section is on the implications of global warming for
13 high-impact extreme climate events. This topic is a focus for Chapter 12 in its treatment of hazards relevant
14 to risk assessment and Chapter 11 is devoted entirely to extreme events, so the results presented here are
15 intended to complement these more in-depth treatments whilst providing context for the regional
16 assessments presented in the following section (and expanded on in the Interactive Atlas) and synthesis
17 material relevant to the WGII assessment.
18

19 As an example, Figure Atlas.20: shows the projected increase in the number of days in which maximum
20 temperature exceeds a high absolute threshold of 35°C, a hazard relevant to risks to human well-being, as
21 derived from the ensemble mean of nine CMIP5 GCMs. The two rows show results for 2046-65 compared to
22 1986–2005 under the RCP4.5 and 8.5 emissions scenarios respectively, with those in the left column derived
23 from raw output from the models and the right when a bias correction has been applied to these model
24 outputs. This figure demonstrates that significant increases are *likely* to occur in many areas of all inhabited
25 continents.
26
27

28 **[START FIGURE ATLAS.20: HERE]**

29
30 **Figure Atlas.20:** Projected changes in the number of days per year in which the maximum temperature exceeds 35°C
31 from an ensemble of nine CMIP5 GCMs (the ensemble mean is considered in all cases). The
32 top/bottom rows correspond to a future mid-term period 2046–2065 (compared to 1986–2005) under
33 the RCP4.5/8.5 emissions scenarios respectively considering the raw model data (left column) and
34 bias corrected (EQM method) data (right column). Regions are stippled where less than six out of the
35 nine models do not agree on the sign of the change (noting that this assessment does not take into
36 account whether the individual models' projected changes are significant). [*The Interactive Atlas*
37 *shows the results for two alternative bias correction methods; see Annex VII for more details.*]
38

39 **[END FIGURE ATLAS.20: HERE]**

40
41
42 The reason for using bias correction for some of the results displayed in Figure Atlas.20: is that the historical
43 simulations of the climate models used to generate these projected changes often validate poorly when
44 compared with observations. If the mean of the distribution of daily maximum temperatures is shifted by a
45 few °C then even if the shape of the distribution is well captured the frequency of exceedance of a high
46 threshold event will be significantly biased. In order to generate realistic results from the models and to
47 provide a basis for a reasonable comparison between them, this issue is generally addressed by applying bias
48 correction to the model data based on comparing distributions from the historical simulations with
49 observations. As there are several approaches to bias correction and no clearly preferred method (see Chapter
50 10) the results in Figure Atlas.20: should be taken as indicative of the direction of change and the relative
51 impact of different future scenarios with *low confidence* in the absolute values. In order to provide an idea of
52 the implications of using different bias correction approaches, the Interactive Atlas displays the results
53 obtained for this index from raw and bias corrected model data, using two different bias correction
54 techniques (see Annex VII). *Future drafts will expand on this for a wider range of hazard indices assessed*
55 *in Chapter 12.*

1
2 *[Placeholder: Further material on a wider range of extremes over land and in the atmosphere and oceans*
3 *will be added in later drafts in collaboration with other chapters in the WGI report and following*
4 *consultation with authors in WGII and WGIII on material that would be particularly relevant to their*
5 *assessments.]*
6
7

8 **Atlas.5 Regional syntheses and case studies**

9

10 This section aims to synthesise information enabling an understanding of the climate change context across
11 all regions, documenting findings that are relevant to applications of regional information in WGII and III
12 contexts and providing examples of best practice and information that can be explored further in the
13 Interactive Atlas. In particular, changes in mean and extreme temperatures and precipitation are displayed in
14 the Interactive Atlas in terms of a number of illustrative indices (including some of the indices assessed in
15 Chapter 12, thus supporting and extending the assessment performed in this chapter) and allowing for a
16 regional analysis of the results. This also builds and expands on and complements the assessment of
17 extremes in Chapter 11. The Interactive Atlas then presents the different regional information that has been
18 assessed in these chapters and in the CORDEX literature assessed in the Atlas, including the different
19 climate variables and indices as well as relevant climate processes.
20
21

22 **Atlas.5.1 Information sources for regional synthesis**

23

24 In the following regional sub-sections, the Atlas presents information on observations (station data, gridded
25 data sets, reanalysis, and satellite based) and observed trends, extremes and variability and also how they are
26 applied in the literature in validating CORDEX output (drawing on the assessment of methodologies in
27 Chapter 10, section 10.6). It also expands on regional information based on the assessments in Chapters 11
28 and 12 and provides some examples of attribution of regional climate changes. Datasets and issues related to
29 availability and integrity of observational data are described in Section Atlas.3.
30

31 For illustrative purposes, in the following region by region synthesis sections, we include some reference
32 plots for three of those indices based on percentiles, so they can be representative around the world. In
33 particular we consider 90th percentiles for daily minimum and maximum temperatures and 95th percentiles
34 for daily precipitation as thresholds in order to define the frequencies of "warm nights", "warm days", and
35 "very wet days" (as the number of days above the thresholds). We have used a simple definition here
36 computing the percentiles using all available data for a specified time period (month, season, or year) in the
37 baseline period, and obtaining the frequency of exceeding these thresholds in the different future periods
38 (either time-slices or warming levels). Therefore, note that these indices do not correspond to the standard
39 ETCCDI definition. The results displayed below in the region by region synthesis correspond to the annual
40 indices whereas the Interactive Atlas allows for a flexible season definition (including monthly values).
41
42

43 **Atlas.5.2 Africa**

44

45 **Climate of Africa**

46

47 Africa has many varied climates: equatorial, tropical (wet, dry, monsoon), semi-arid, arid, subtropical
48 highland, and each climate region has its local variations. Rainfall amount varies within each climate region.
49 Temperatures are hottest in the north and coolest across the south and at elevation within the topography
50 across the continent.
51
52

53 **[START FIGURE ATLAS.21: HERE]**
54

55 **Figure Atlas.21:** Koppen-Geiger climate type map of Africa (Peel et al., 2007).

Do Not Cite, Quote or Distribute

1
2 **[END FIGURE ATLAS.21: HERE]**

3
4
5 The assessment in this subsection of the Atlas focuses on regional climate variability features and is
6 complemented by a display of projected trends of temperature and precipitation in the Interactive Atlas [*with*
7 *the observations to be included in a later draft*]. The results are [*currently*] based on the evaluation of
8 CMIP5 and CORDEX multi-model projections.

9
10
11 *Atlas.5.2.1 Observations, trends and attribution*

12
13 The findings of the most recent IPCC reports, AR5 and SR1.5, state that over most parts of Africa, minimum
14 temperatures are warming more rapidly than maximum temperatures, and both have increased by 0.5°C or
15 more during the last 50 to 100 years. An increase in the frequency of extreme warm events has been
16 observed for countries bordering the western Indian Ocean. There has been an increase in seasonal mean
17 temperature in many areas of East Africa. In addition, an increase in frequency of extreme rainfall events has
18 been observed over the past 50 years.

19
20 Temperature increases have been attributed to anthropogenic activities in the 20th century. For example,
21 Figure Atlas.22: shows observed annual trends (°C/century) and indicates that temperatures have been rising
22 rapidly over Africa over the last five decades and at most locations the increases are statistically significant.
23 This is attributed in a limited amount of literature to SST, modes of variability of large scale forcing and
24 GHG forcing (Richard et al., 2001; Sylla et al., 2016; Williams and Funk, 2011; Yang et al., 2015).

25
26
27 **[START FIGURE ATLAS.22: HERE]**

28
29 **Figure Atlas.22:** Observed trends in annual-average near-surface temperatures (°C/century) over Africa for the period
30 1961–2010, calculated using the method of pairwise-slopes applied to the 5° longitude × 5° latitude
31 gridded CRUTEM4v data of CRU. The grid boxes where the trends are statistically significant
32 according to the Spearman rank correlation test are indicated by crosses (Engelbrecht et al., 2015).

33
34 **[END FIGURE ATLAS.22: HERE]**

35
36
37 A companion figure for Figure Atlas.22 is Figure Atlas.23, which shows the time-series of West African
38 land area averaged seasonal temperature anomalies between 1963 and 2012, as obtained from the CRU
39 TS3.22 dataset (Daron, 2014a). The increasing trends are evident from 1980 onwards.

40
41
42 **[START FIGURE ATLAS.23: HERE]**

43
44 **Figure Atlas.23:** Time series of West Africa land area averaged seasonal temperature anomalies between 1963 and
45 2012. Data taken from CRU TS3.22 dataset (Daron, 2014a).

46
47 **[END FIGURE ATLAS.23: HERE]**

48
49
50 *Atlas.5.2.1.1 Observed trends and extremes*

51
52 Temperatures over West Africa have increased over the last 50 years (Mouhamed et al., 2013; Niang et al.,
53 2014) with a spatially variable gradual warming reaching 0.5°C per decade from 1961 to present (Sylla et al.,
54 2016). Mouhamed et al. (2013) have also reported a negative trend in the number of cool nights, more
55 frequent warm days and warm spells. They also reported a general tendency of decreased annual total

1 rainfall, and maximum number of consecutive wet days. Figure Atlas.24: shows the 90th percentiles for
2 maximum and minimum temperatures. Extreme rainfall events have become more frequent in the West
3 African Sahel during the last decade, compared to the 1961–1990 period (Mouhamed et al., 2013) with
4 significant increases in Sahelian storms seen in satellite observations since 1982 (Taylor et al., 2017).
5
6

7 **[START FIGURE ATLAS.24: HERE]**

8
9 **Figure Atlas.24:** 90th percentiles for maximum and minimum temperatures during 1986-2005 from EWEMBI, the
10 reference dataset for ISI-MIP, which is a calibrated version of ERA-Interim (Engelbrecht et al., 2015).
11

12 **[END FIGURE ATLAS.24: HERE]**

13
14
15 For South Africa, over the period studied, warm extremes increased and cold extremes decreased since the
16 mid-1960s (Kruger and Sekele, 2013). MacKellar et al. (2014) reported a statistically significant (95%
17 confidence level) decreases in rainfall and the number of rainy days in autumn over central and north-eastern
18 part of South Africa but significant increases in the number of rain days around the southern Drakensberg in
19 spring and summer during the period of 1960–2010. They also reported a significant increase in maximum
20 temperatures and minimum temperatures in all seasons except for the central interior, where minimum
21 temperatures have decreased significantly. Jury (2013) found a poleward drift of the southern hemisphere
22 sub-tropical anticyclones and a +1.5 mm/year rise in sea surface height along the coast.
23

24 Over East Africa, the highest temperatures are experienced in the drier regions towards the north and east
25 with Eritrea and Djibouti having an average summer high temperatures exceed 30°C and Ethiopia, Kenya
26 and Tanzania in the East African Rift Valley having the lowest temperatures (Daron, 2014b). He also
27 reported with *medium confidence* a spatially varying minimum temperature trends and increases in warm
28 nights in Southern tip but spatially varying dryness with *low confidence* over East Africa.
29

30 Most areas of the African continent lack sufficient observational data to draw conclusions about trends in
31 annual precipitation over the past century. In addition, according to Sylla et al. (2013) many regions of
32 Africa have discrepancies between different observed precipitation data sets.
33
34

35 *Atlas.5.2.1.2 Attribution of trends and extremes*

36
37 Hoerling et al. (2006) asserted that the drying trends in Africa during each monsoon season is attributable to
38 oceanic influences where air-sea interactions have been most relevant. In particular, they demonstrated that
39 the drying over the Sahel can be attributed to warming of the South Atlantic SST and southern African
40 drying as a response to Indian Ocean warming (Dai, 2011; Hoerling et al., 2006). Meque and Abiodun
41 (2015) showed a strong link between ENSO and droughts over Southern Africa. Over East Africa, drying
42 trend is associated with an anthropogenic-forced relatively rapid warming of Indian Ocean SSTs (Williams
43 and Funk, 2011). However, Lyon and Dewitt (2012) associated the decline in the East African long rains
44 with a shift to warmer SSTs over the western tropical Pacific and cooler SSTs over the central and eastern
45 tropical Pacific. Similarly, Lyon (2014) attributed the increase in drought frequency to multidecadal
46 variability of SSTs in the tropical Pacific, with cooling in the east and warming in the west. Wang et al.
47 (2014) also showed that the drying trend of the East Africa long rains is associated with decadal natural
48 variability from SST variations over the Pacific Ocean. Also, Intensified climate extremes climate over West
49 Africa have been attributed to mid-level GHG forcing (Sylla et al., 2016).
50

51 *Atlas.5.2.2 Assessment of model performance*

52
53
54 Gbobaniyi et al. (2014) found that the RCMs show acceptable performance in simulating the spatial
55 distribution of the main precipitation and temperature features. In particular, Gbobaniyi et al. (2014) reported

1 that the CORDEX models simulate the occurrence of the West African Monsoon jump and the
2 intensification and northward shift of the Saharan Heat Low (SHL). The models also capture the timing and
3 amplitude of mean annual cycle of precipitation and temperature over the homogeneous subregions of West
4 Africa. Endris et al. (2013) reported that CORDEX RCMs reasonably simulate eastern Africa rainfall
5 adequately. Over Southern Africa, Pinto et al. (2016) showed that CORDEX models are able to capture the
6 observed climatological spatial patterns of the extreme precipitation. Shongwe et al. (2015) also reported that
7 CORDEX models simulate the phasing and amplitude of monthly rainfall evolution and the spatial
8 progression of the wet season onset are well over Southern Africa. Jury (2013) found the southern African
9 rainfall trend to have a significant downtrend of -0.013 mm/day per year and -0.003 mm/day per year for
10 longer periods over the 20th century. Kisembe et al. (2018) also reported discrepancies and biases in present-
11 day rainfall over Uganda from the RCM-simulated rainfall compared to three gridded observational datasets.
12 Specifically, they reported that the CORDEX models underestimate annual rainfall of Uganda and also
13 struggle to reproduce the variability of the long and short rains seasons.

14
15 An evaluation of the CORDEX-Africa models has been carried out using the data included in the Interactive
16 Atlas portal (Section Atlas.7) with results for precipitation displayed in Figure Atlas.25:. Section Atlas.3.4
17 gives a detailed description of the reference data, metrics and models being evaluated.

18
19
20 **[START FIGURE ATLAS.25: HERE]**

21
22 **Figure Atlas.25:** Evaluation of precipitation-based indices for five RCMs driven by ERA-Interim (rows 2-6), in terms
23 of relative bias with respect to the observational reference (EWEMBI) over the eight AR6 African
24 regions. For comparison purposes, results are also shown for the driving dataset, ERA-Interim (first
25 row). Section Atlas.3.4 provides details about the RCMs, observations and indices used.

26
27 **[END FIGURE ATLAS.25: HERE]**

28 29 30 *Atlas.5.2.3 Assessment of projections*

31
32 Projected rainfall changes over sub-Saharan Africa in the mid and late 21st century is uncertain. The findings
33 of the most recent IPCC reports, AR5 and SR1.5, state that based on the Coupled Model Intercomparison
34 Project Phase 5 (CMIP5) ensemble, temperatures in Africa are projected to rise faster than the global average
35 increase during the 21st century. Specifically, over tropical West Africa, temperature increases of a certain
36 magnitude are projected to occur one to two decades earlier than when the global average reaches that level.
37 Over the North of Africa, faster increase in minimum temperature is consistent with greater warming at
38 night, resulting in a decrease in the future diurnal temperature range. Higher temperature increases are
39 projected during boreal summer. Southern Africa is *likely* to exceed the global mean land surface
40 temperature increase in all seasons. Temperature projections for east Africa indicate considerable warming
41 from RCPs. In particular, under RCP 8.5, the average warming across all models shows temperature
42 increment of approximately 4°C by the end of the century for East Africa.

43
44 Some uncertainties are reported over parts Africa from CORDEX projections. Over Central Africa, Mba et
45 al. (2018a) found large uncertainties associated with projections at 1.5°C and 2°C. Over West Africa,
46 Diedhiou et al. (2018) reported uncertainties exhibited in total precipitation and Sylla et al. (2016) also found
47 large uncertainty range in Sahel. Gbobaniyi et al. (2014) emphasized that RCMs from CORDEX exhibit
48 some biases, which vary in both magnitude and spatial extent from model to model. Similarly, Dosio and
49 Panitz (2016), Endris et al. (2016) and Klutse et al. (2016) reported large uncertainties in rainfall
50 characteristics simulated by CORDEX RCMs.

51
52 Research over Africa has improved since AR5 although there is still not enough information on specific
53 areas for assessment. Towards, the special report on the impact of 1.5°C and 2°C of global warming, a good
54 effort has been made on the African continent. Klutse et al. (2018), Lennard et al. (2018), Maure et al.
55 (2018), Mba et al. (2018b), Nikulin et al. (2018), and Osima et al. (2018) used a large ensemble of CORDEX

1 Africa simulations, to present the impact of 1.5°C and 2°C global warming levels (GWLs). While Lennard et
2 al. (2018) and Nikulin et al. (2018) worked over the whole African continent, Diedhiou et al. (2018), Klutse
3 et al. (2018), Kumi and Abiodun (2018), Maure et al. (2018) and Mba et al. (2018b) focused on specific
4 regions of Africa.

5
6 Lennard et al. (2018) and Nikulin et al. (2018) reported that the CORDEX simulations give a robust
7 warming over Africa to exceed the mean global warming. A further warming of 0.5°C from 1.5°C can
8 produce a robust change in some aspects of the African climate and its extremes (Nikulin et al., 2018).
9 Klutse et al. (2018) and Sylla et al. (2016) also reported continuous stronger warming over West Africa.
10 Osima et al. (2018) projected temperature increases reaching 0.8°C over Sudan and northern Ethiopia
11 implying that the Greater Horn of Africa would warm faster than the global mean. Over southern Africa,
12 areas in the south-western region of the subcontinent, covering South Africa and parts of Namibia and
13 Botswana are projected to experience the largest increase in temperature, which are expected to be greater
14 than the global mean warming (Maure et al., 2018).

15
16 A consistent increase in daily precipitation intensity of wet days is reported over a large fraction of Africa at
17 1.5°C GWL and strengthening at 2°C (Lennard et al., 2018; Nikulin et al., 2018). Nikulin et al. (2018)
18 projected wetter conditions over eastern Africa at both 1.5°C and 2°C GWLs. Sylla et al. (2016) projected
19 increase in intensity of very wet events over West Africa. Pinto et al. (2016) projected that rainfall intensity
20 is *likely* to increase and magnified under the RCP8.5 compared with the RCP4.5. Osima et al. (2018)
21 projected the length of dry spells to increase and wet spells to decrease over East Africa. This agrees with
22 Maure et al. (2018) over southern Africa, Klutse et al. (2018) over West Africa, Mba et al. (2018a) over
23 Central Africa that the number of consecutive dry days are projected to increase and the number of
24 consecutive wet days are projected to decrease.

25
26
27 **[START FIGURE ATLAS.26: HERE]**

28
29 **Figure Atlas.26:** Time series of the change in West Africa annual average temperatures from three CORDEX models
30 analysed (see the legend). The model changes are relative to the average of the models from 1963 to
31 2000, while the CRU TS3.22 observational data (from 1963 to 2012) are relative to the observed 1963
32 to 2000 average (Daron, 2014a).

33
34 **[END FIGURE ATLAS.26: HERE]**

35
36
37 Over Southern Africa, enhanced warming is projected to result in a reduction in mean rainfall across the
38 region (Maure et al., 2018) and in particular up to 0.4 mm/day over the Limpopo Basin and smaller areas of
39 the Zambezi Basin in Zambia, and also parts of Western Cape, South Africa. West African river basins
40 would also decline in the basin-scale irrigation potential under 2°C global warming (Sylla et al., 2018). Kumi
41 and Abiodun (2018) projected the western and eastern Sahel as the hotspots for a delayed rainfall onset dates
42 and reduced length of rainy season (LRS) in the 1.5°C to 2°C warmer climates under RCP4.5 and RCP8.5
43 scenarios. They also projected a delay in rainfall cessation dates and longer LRS over the western part of the
44 Guinea coast in West Africa.

45
46 *[Placeholder: Example of material on climate information providing a summary of WGI assessments of
47 observed and projected climate change and relevant to WGII regional chapters]*

48
49 *[Placeholder: Figure Atlas.27, taken from the AR5 WGII Chapter 22 (Africa, Figure 22-1) shows observed
50 and projected temperature and precipitation change and an updated version consistent with assessments in
51 the other WGI chapters could be presented here as a summary with sub-continental maps and other figures
52 made available in the Interactive Atlas. For example, the observed trend maps could be reproduced in the
53 Interactive Atlas with the facility to plot the associated timeseries and trends over predefined subregions
54 allowing closer inspection of analysed gridded observations underpinning the continental scale maps.]*
55

1 **[START FIGURE ATLAS.27: HERE]**

2
3 **Figure Atlas.27:** Observed and projected temperature and precipitation change in Africa (from the AR5 WGII Chapter
4 22 (Africa, Figure 22-1)).

5
6 **[END FIGURE ATLAS.27: HERE]**

7
8
9 **[START FIGURE ATLAS.28: HERE]**

10
11 **Figure Atlas.28:** Daily rainfall amount corresponding to the 95th percentile (P95, in mm/day) defining ‘very wet days’
12 for (a) the observational reference (EWEMBI) and (b) the CMIP5_subset of nine GCMs, for the
13 reference period 1986–2005. (c) Change in frequency of very wet days for the future 2081–2100
14 period (RCP8.5) defined as exceeding the historical P95 threshold (results shown as relative change,
15 %). Results are shown model by model in the bottom panels, with the ensemble means shown in the
16 upper panels.

17
18 **[END FIGURE ATLAS.28: HERE]**

19
20
21 The ensemble of CMIP5 model generally performs well for R95 rainfall intensity but overestimates the
22 highlands of the continent (Figure Atlas.53:). It also projects an increase in frequency of very wet days over
23 the equatorial region in the future, which is larger in the east, and a decrease to the north and south. These
24 features are seen in most of the ensemble members though there are some regional variations where some
25 models do not agree with the sign of the change (Figure Atlas.53:). In particular, MIROC projects a band of
26 100% increase at most regions north of the equator. CNRM on the other hand, projects a general increase (at
27 different percentage changes) in frequency across Africa as does CanESM1 except for most western regions.

28 29 30 *Atlas.5.3 Asia*

31 32 **Climate of Asia**

33
34 The climate over Asia, which has profound societal and economic impacts, has multiple time-scale
35 variabilities and exhibited some clear trends in recent decades. Climate models play an irreplaceable role in
36 understanding the past changes and projecting future changes in climate. However, current state of the art
37 climate models still shows evident biases in their simulations over Asia, including where: a) complex
38 topography exists in East Asia; b) the archipelagic nature of most of Southeast Asia pose complex
39 interactions between land, sea, and mountain dynamics; c) and regions such as Central Asia where there are
40 limited observations and limited work on evaluating the models. These model deficiencies have limited our
41 understanding of the mechanisms responsible for climate variability and change based on numerical model
42 experiments and reduced the reliability of long-term climate change projections. In this section, the Atlas
43 specifically focuses on assessing findings from recent literature on observed changes and global and regional
44 modelling, including those from CMIP5/CMIP6 and CORDEX, for East, Southeast, South and Central Asia.

45 46 47 *Atlas.5.3.1 East Asia*

48 49 *Atlas.5.3.1.1 Observations, trends and attribution*

50
51 The findings of the most recent IPCC reports, AR5 and SR1.5, state that since the middle of the 20th
52 century, it is *likely* that there has been an increasing trend in winter temperatures, the frequency of
53 heatwaves, the numbers of warm days and nights, and the length of drought and/or extreme precipitation
54 events across much of Asia. Finally, it is *likely* that surface ozone has strongly increased in East Asia since
55 the 1990s.

1 Much of East Asia also experiences monsoons, characterized by a wet season and southerly flow in summer
2 and by dry cold northerly flow in winter. The East Asian summer (EAS) monsoon circulation has
3 experienced an inter-decadal weakening from the 1960s to the 1980s (Hori et al., 2008; Li et al., 2010a),
4 associated with deficient rainfall in North China and excessive rainfall in central East China along 30°N
5 (Gong and Ho, 2002a; Hu, 1997; Wang and An, 2001; Yu et al., 2004). The summer monsoon circulation
6 has begun to recover in recent decades (Liu et al., 2012; Zhu et al., 2012). The summer rainfall amount over
7 East Asia shows no clear trend during the 20th century (Zhang and Zhou, 2011), although significant trends
8 may be found in local station records (Wang et al., 2006). The winter monsoon circulation weakened
9 significantly after the 1980s (Wang et al., 2009a; Wang and Chen, 2010). The observed monsoon circulation
10 changes are partly reproduced by GCMs driven by PDO-related SST patterns (Li et al., 2010b; Zhou and
11 Zou, 2010).

12
13 Also, a year-round decrease has been reported for wind speeds over China at the surface and in the lower
14 troposphere based on surface observations and radiosonde data (Guo et al., 2011; Jiang et al., 2010; Vautard
15 et al., 2010; Xu et al., 2010). The changes in wind speed are concomitant with changes in pressure centres
16 such as a westward extension of the Western Pacific Subtropical High (Gong and Ho, 2002b; Zhou et al.,
17 2009b). A weakening of the East Asian summer monsoon since the 1920s has been also found in SLP
18 gradients (Zhou et al., 2009a). However, trends derived from wind observations and circulation trends from
19 reanalysis data carry large uncertainties, and monsoon rainfall trends depend, for example, on the definition
20 of the monsoon area (Hsu et al., 2011). The suggested weakening of the East Asian monsoon has *low*
21 *confidence*, given the nature and quality of the evidence.

22
23 In an attribution study on the effect of anthropogenic climate change on the intensity of tropical cyclones,
24 Takayabu et al. (2015) showed that simulations of super typhoon Haiyan using a hypothetical natural
25 condition without anthropogenic climate change results in higher minimum central pressure and lower
26 maximum wind speeds that consequently leads to lower storm surge heights than in simulations with the
27 observed climate (Figure Atlas.29:).

28

29
30 **[START FIGURE ATLAS.29: HERE]**

31

32 **Figure Atlas.29:** Maximum surface water elevation from storm surge simulations driven by Supertyphoon Haiyan in a
33 hypothetical natural climate without anthropogenic influence (top) compared to in the current climate
34 (bottom). The coloured dots show inundation data collected by a field study. (Takayabu et al., 2015).

35

36 **[END FIGURE ATLAS.29: HERE]**

37

38

39 Attribution studies have also assessed if climate change played a role in the frequency or magnitude of the
40 record breaking 5-day heatwave in Central Eastern China in July 2017 that affected much of the population
41 and caused severe impacts on public health, agriculture and infrastructure. Using extreme event attribution
42 techniques where large ensembles of models are run for present day and pre-industrial conditions and their
43 results compared, Sparrow et al. (2018) simulated a present day climatology over China (Figure Atlas.30:a),
44 and simulations of the year 2017 with and without anthropogenic effects (with two atmospheric models, a
45 global climate model, HadGEM3-GA6, and a global and regional modelling system, weather@home). The
46 study showed that both modelling systems were reasonably close to and captured the range of the observed
47 distribution (Figure Atlas.30:b). HadGEM3-GA6 suggested that a pre-industrial 2017-like event would never
48 attain the magnitude of events in its simulation of present day climate (Figure Atlas.31:a) whereas in the
49 weather@home simulations (Figure Atlas.31:b) the frequency of such an event has increased by a factor of
50 ~5 (Sparrow et al., 2018). Both results suggest that climate change would have significantly increased the
51 magnitude and such an extreme event and the associated risks for human systems and ecosystems.

52

1 **[START FIGURE ATLAS.30: HERE]**

2
3 **Figure Atlas.30:** (a) Weather@home East Asia 50-km regional boundary (purple, with shading indicating the regional
4 model sponge layer). The study area for the analysis is shown in green. (b) Distributions of the
5 fractional occurrence of July Tx5x for 1987–2013 from the station data observations (Li et al., 2016)
6 (red), HadGEM3-GA6 (blue) and weather@home (yellow). For the observations and HadGEM3-GA6
7 a GEV fit is shown. For weather@home a normal fit is shown.

8
9 **[END FIGURE ATLAS.30: HERE]**

10
11
12 **[START FIGURE ATLAS.31: HERE]**

13
14 **Figure Atlas.31:** Return times from Historical (yellow), Historical2017 (red) and Natural2017 (green) simulations for
15 Tx5x from (a) HadGEM3-GA6 and (b) CPDN weather@home ensemble. Both normal (dashed black)
16 and GEV (solid black) fits are shown with the exception of ‘CPDN Historical’ where the GEV fit is
17 poor and thus omitted from the figure.

18
19 **[END FIGURE ATLAS.31: HERE]**

20 21 22 *Atlas.5.3.1.2 Assessment of model performance*

23
24 The findings of the most recent IPCC reports, AR5 and SR1.5, state that the simulation of interannual
25 variability of the EAS monsoon circulation has improved in CMIP5 models (Sperber et al., 2013).

26
27 Evaluation of CORDEX-EA models in simulating the climatology of summer extremes in East Asia shows
28 that the models simulate temperature means more accurately compared to extremes, while precipitation
29 extremes are simulated better than their means (Park et al., 2016). Estimations of the spatial extent of
30 drought events using the RCMs are generally accurate in wet regions but inaccurate in dry regions (Um et
31 al., 2017).

32
33 Topography has a strong effect on the precipitation patterns, and the simulation of precipitation over regions
34 with complicated topography is a major challenge from scientific viewpoint. RCMs were found to have large
35 biases in simulating temperature and precipitation over regions characterized by complex topography, such
36 as the Tibetan Plateau (Guo et al., 2018; Zhou et al., 2016a) and Loess Plateau in northern China (Wang et
37 al., 2018).

38
39 Figure Atlas.32: and Figure Atlas.33: show an example of climatological rainfall and extreme rainfall in East
40 Asia, respectively, with maps of accumulated precipitation and the maximum total precipitation in five
41 consecutive days in observations, two RCMs (RegCM3 and FROALS) and their driving GCM (FGOALS)
42 (Zou et al., (2016)). These show that the RCMs simulations are more realistic than their driving model in
43 terms of spatial patterns and magnitudes of the extremes.

44
45
46 **[START FIGURE ATLAS.32: HERE]**

47
48 **Figure Atlas.32:** The spatial distribution of the JJA total rainfall (shading) averaged over 1981–2005 derived from (a)
49 the APHRO data set, (b) the FGOALS model (GCM), (c) the RegCM3, and (d) the FROALS model.
50 Figure from Zou et al. (2016).

51
52 **[END FIGURE ATLAS.32: HERE]**

1 **[START FIGURE ATLAS.33: HERE]**

2
3 **Figure Atlas.33:** As in Figure Atlas.32: but for the maximum consecutive 5-day precipitation (R5d). Figure from Zou
4 et al. (2016).

5
6 **[END FIGURE ATLAS.33: HERE]**

7
8
9 Figure Atlas.34: shows the spatial distribution of 22-year averaged surface temperature extreme indices from
10 observation and the biases between observation and simulation. The model generally well reproduces the
11 spatial pattern of the temperature extreme indices.

12
13
14 **[START FIGURE ATLAS.34: HERE]**

15
16 **Figure Atlas.34:** Extreme temperature indices for the period 1989–2010, as given by the CN051 observations (left
17 column), the CCLM RCM (middle column), and the corresponding (CCLM-CN051) biases (right
18 column): TNn (minimum daily Tmin), Txx (maximum daily Tmax), GSL (annual count between first
19 span of mean temperature > 5°C and first span after < 5°C), FD (annual count when the daily
20 minimum temperature < 0°C), and SU (annual count when daily maximum temperature > 25°C) from
21 top to bottom rows. Figure from Zhou et al. (2016b).

22
23 **[END FIGURE ATLAS.34: HERE]**

24
25
26 Another example of showing and validating climate variability is given in Figure Atlas.35:, which shows
27 seasonal variation of the simulated summer rainfall in East Asia. Significant seasonal variation in rainfall is
28 the most distinguishing feature of the monsoonal regions of East Asia. The ability to simulate precipitation in
29 various seasons is an important aspect in model evaluation. Figure Atlas.35: shows the time-latitude cross
30 section of precipitation over East Asia, which is a good metric to evaluate the key features of the northward
31 movement of the major rainfall belt in summer. Models with different horizontal resolutions reproduce the
32 key features of the northward movement of the major rainfall belt in summer. As the resolution increases, the
33 whole process of the migration tends to be earlier (Li et al., 2015).

34
35
36 **[START FIGURE ATLAS.35: HERE]**

37
38 **Figure Atlas.35:** Time-latitude cross section of precipitation averaged between 110°E and 120°E from (a) TRMM
39 observed estimates and simulated by CAM5 at (b) T42, (c) T106, and (d) T266. The bottom x axis
40 represents the pentad number. Figure from Li et al. (2015).

41
42 **[END FIGURE ATLAS.35: HERE]**

43
44
45 Figure Atlas.36: shows an example of validating the general ability of the regional model to reproduce the
46 seasonal surface temperature climatology by comparing the CORDEX-EA model simulations with the
47 observations during the period of 1989–2010. In winter, CCLM has large warm biases over most of the high
48 latitude region above 40°N and the Indian Peninsula. On the other hand, cold biases occur over the Tibetan
49 Plateau and Indochina Peninsula. In summer, the model tends to overestimate the surface temperature over
50 most of China.

51
52
53 **[START FIGURE ATLAS.36: HERE]**

54
55 **Figure Atlas.36:** Observed and simulated seasonal mean 2-m temperatures for the period 1989–2010, for 0.22 CCLM
56 simulations (CCLM, top row), CCLM bias against CRU (CCLM-CRU, second row), CCLM bias

1 against CN051 (CCLM-CN051, third row) and 0.22 CCLM simulations difference against 0.44
2 CCLM simulations (CCLM-CCLM44, bottom row). The columns from left to right are for winter
3 (DJF), spring (MAM), summer (JJA), and autumn (SON). Figure from Zhou et al. (2016b).
4

5 **[END FIGURE ATLAS.36: HERE]**
6

7
8 *[Placeholder: Many more examples of assessing how well model simulations simulate historical climate will
9 be made available in the Interactive Atlas in future drafts.]*
10

11 Evaluation of the ability of CORDEX-EA models in simulating tropical cyclone (TC) activity over the
12 western North Pacific indicates that models reasonably capture the observed climatological spatial
13 distribution and interannual variability of TC activity. But due to the low horizontal resolutions (~50 km),
14 RCMs tend to underestimate TC intensity (Jin et al., 2016).
15

16 *Atlas.5.3.1.3 Assessment of projections*

17
18 The findings of the most recent IPCC reports, AR5 and SR1.5, state that future increase in precipitation
19 extremes related to the monsoon is *very likely* in East Asia, South Asia, Southeast Asia and Australia. Lesser
20 model agreement results in *medium confidence* that monsoon-related interannual precipitation variability will
21 increase in the future. Model skill in representing regional monsoons is lower compared to the global
22 monsoon and varies across different monsoon systems. For the East Asian summer monsoon, both monsoon
23 circulation and precipitation are projected to increase. More than 85% of CMIP5 models show an increase in
24 mean precipitation of the East Asian summer (EAS) monsoon, while more than 95% of models project an
25 increase in heavy precipitation events. A slight increase in the East Asian monsoon circulation is projected.
26
27

28 In summary, based on CMIP5 model projections, there is *medium confidence* that with an intensified East
29 Asian summer monsoon, summer precipitation over East Asia will increase (AR5). Under RCP4.5 scenario,
30 precipitation increase is *likely* over East Asia during the Meiyu-Changma-Baiu season in May to July, and
31 precipitation extremes are *very likely* to increase over the eastern Asian continent in all seasons and over
32 Japan in summer. However, there is only *low confidence* in more specific details of the projected changes
33 due to the limited skill of CMIP5 models in simulating monsoon features such as the East Asian monsoon
34 rainband.
35

36 Figure Atlas.37: shows an example of projected changes in summer rainfall in East Asia by looking at
37 several widely used rainfall indices. The accumulated precipitation amount is defined as the total
38 precipitation of days with daily precipitation greater than or equal to 1 mm (PRCPTOT). Consecutive dry
39 days (CDD) are defined as the greatest number of consecutive days with daily precipitation below 1 mm.
40 R5d is defined as the maximum consecutive 5-day total precipitation. R95p is defined as the accumulated
41 precipitation amounts of daily precipitation greater than the 95th percentile of wet days. These show the
42 potential for significant changes in the hydrological cycle to result from global warming but also differences
43 in spatial details from the various model projections (see Chapter 10 for a discussion of the implications of
44 such findings).
45

46 *[Placeholder: Similar results from the analysis of CORDEX E Asia, see Technical Annex X, and CMIP6
47 simulations will be provided in subsequent Atlas drafts and included in the Interactive Atlas.]*
48
49

50 **[START FIGURE ATLAS.37: HERE]**
51

52 **Figure Atlas.37:** Spatial distributions of the projected changes to the June-July-August (JJA) mean total rainfall
53 (PRCPTOT, mm), extreme rainfall amount indices (R5d and R95p, mm) and maximum number of
54 consecutive dry days (CDDs, day) for the period of 2051–2070 under the RCP 8.5 scenario relative to
55 the period of 1986–2005. Results for FGOALS-g2, RegCM3 and FROALS are shown in the left,

1 middle and right column, respectively. Dotted areas are statistically significant at the 5% level,
2 according to Student's t test. Figure from Zou and Zhou (2016).
3

4 **[END FIGURE ATLAS.37: HERE]**
5
6

7 Projections using the HadGEM2-ES and the Providing Regional Climate Impacts for Studies (PRECIS)
8 model under RCP4.5 and RCP8.5 suggest that there would be an increase in the days with precipitation
9 higher than 15 mm and a decrease in the days with precipitation less than 5 mm. Under both RCPs, there
10 would be an increasing trend in the magnitude of changes in precipitation extremes indices (R95p, R99p, and
11 simple daily intensity index) over China, while an opposite trend is projected for consecutive wet days
12 (CWD) and no apparent trend is projected for wet-day frequency (WDF) from 2036–2065 to 2070–2099.
13

14 Figure Atlas.38: shows the annual very wet days, warm nights and warm days over East Asia for an
15 ensemble of nine CMIP5 models in historical period of 1986–2005 and changes in future period of 2081–
16 2100. Ensemble results indicates that models generally well reproduce the spatial distribution and magnitude
17 of 'warm nights' and 'warm days', but show relative large uncertainty in simulating 'very wet days', e.g., the
18 models tends to overestimate (underestimate) the P95 intensity over the southwestern China leeside of the
19 Tibetan Plateau (southern coastal areas). The change of 'very wet days' frequency in CMIP5 models over
20 central eastern China is relative small, while it is larger over eastern Tibetan Plateau and northern China. The
21 changes of 'warm nights' and 'warm days' in RCP8.5 is similar, i.e., a large (small) increase over the regions
22 south (north) of Yangtze river valley.
23

24
25 **[START FIGURE ATLAS.38: HERE]**
26

27 **Figure Atlas.38:** (a-c) Daily rainfall amount corresponding to the 95th percentile (P95, in mm/day) defining 'very wet
28 days' for (a) the observational reference (EWEMBI) and (b) the CMIP5_subset (ensemble mean of
29 nine GCMs), for the reference period 1986–2005. (c) Change in frequency of very wet days for the
30 future 2081–2100 period (RCP8.5) defined as exceeding the historical P95 threshold (results shown as
31 relative change, %). Similar results in (d–f) and (g–i) for absolute daily minimum and maximum
32 temperature amounts corresponding to the 90th percentile (P90, defining 'warm nights' and 'warm
33 days', respectively) and the corresponding changes in frequency for the future 2081–2100 period
34 (RCP8.5) defined as exceeding the historical P90 threshold (results shown as relative change, %).
35 Similar analysis for other indices and scenarios (including warming levels) are available at the
36 Interactive Atlas (<http://ipcc-atlas.ifca.es>).
37

38 **[END FIGURE ATLAS.38: HERE]**
39
40

41 Increased extreme precipitation amounts accompanied with decreased frequencies of extreme precipitation
42 suggest that the future daily extreme precipitation intensity will likely increase in northeast China and south
43 China (Zhu et al., 2018). The future projected change in annual and seasonal mean temperature by RCMs
44 is consistent with the results from the driving GCM. However, changes in annual and seasonal mean
45 precipitation exhibit significant inter-RCM differences, which implies that there is still large uncertainty in
46 the projection of precipitation (Gu et al., 2018).
47

48 *[Placeholder: Example of a summary of the range of projected changes in an index of heavy daily*
49 *precipitation in the CMIP ensemble of potential relevance to WGII regional chapters]*
50

51 *[Placeholder: Figure Atlas.39:, which is taken from the AR5 WGII Chapter 21 (Regional Context, Figure*
52 *21-8), shows projected changes in heavy rainfall days in the CMIP5 ensemble for two future time periods*
53 *and two emissions scenarios (RCP4.5 and 8.5) relative to a 1961–1990 baseline. Summary figures of this*
54 *nature will be provided in the Atlas once CMIP6 and CORDEX data have been analysed with related figures*
55 *for other indices, references periods and scenarios available in the Interactive Atlas.]*
56

1
2
3
4
5
6
7
8
9
10
11
12
13
14
15
16
17
18
19
20

[START FIGURE ATLAS.39: HERE]

Figure Atlas.39: Projected changes in heavy rainfall days (defined as events above the 90% percentile of daily rainfall in the model baseline simulation) in the CMIP5 ensemble for two future time periods and two emissions scenarios (RCP4.5 and 8.5) relative to a 1961–1990 baseline (Figure 21-8 in the AR5 WGII Chapter 21 Regional Context)

[END FIGURE ATLAS.39: HERE]

[Placeholder: In future drafts the Atlas will synthesize the different sets of information available over Asia in terms of in terms of time period, temporal resolution, spatial resolution, climate variables analysed, see Table Atlas.8:]

[START TABLE ATLAS.8: HERE]

Table Atlas.8: Table of CORDEX runs over East Asia region.

Cordex Runs' Serial Number	GCM	RCM	Resolution	Baseline Period	Projections Period	RCP	Observation Data Used	Historical Variables Validated	Climate Variables Analyzed in The Projections	Institutes
EA 1	HadGEM2-AO	RSM	50 km	1980–2005	2006–2050	RCP4.5 RCP8.5				
EA 2	HadGEM2-AO	RegCM4	50 km	1979–2005	2006–2050	RCP4.5 RCP8.5				
EA 3	HadGEM2-AO	SNURCM	50 km	1980–2005	2006–2049	RCP4.5 RCP8.5				
EA 4	HadGEM2-AO	WRF3.2	50 km	1980–2005	2006–2049	RCP4.5 RCP8.5				
EA 5	HadGEM2-AO	HadGEM3-RA	12.5 km	1950–2005	2006–2100	RCP4.5 RCP8.5 RCP85				
EA 6	EC-EARTH	RegCM4				RCP26 RCP45 RCP85				
EA 7	MPI-ESM-MR	RegCM4	25 km 25 km			RCP26 RCP45 RCP85				
EA 8	CSIRO-MK3.6	RegCM4				RCP45 RCP85				
EA 9	HadGEM2-ES	RegCM4	25 km 25 km			RCP26 RCP45 RCP85				
EA 10	ERA-Int			1980–2010	2075–2095	RCP8.5				
EA 11	MRI-AGCM			1980–2010	2075–2095	RCP8.5				
EA 12	ERA-Int	WRF	25 km							
EA 13	ERA-Int	RegCM4.3	25 km							

EA 14	ERA-Int	RegCM4.4	25 km	
EA 15	ERA-Int	CCLM5.0	0.22°	
EA 16	EC-EARTH	WRF	25 km	RCP8.5
EA 17	EC-EARTH	RegCM4.3	25 km	RCP8.5
EA 18	EC-EARTH	RegCM4.4	25 km	RCP4.5 RCP8.5
EA 19	MPI-ESM-MR	RegCM4.4	25 km	RCP2.6 RCP4.5 RCP8.5
EA 20	MPI-ESM-LRr1	WRF	25 km	RCP4.5 RCP8.5
EA 21	MPI-ESM-LRr1	RegCM4.3	25 km	RCP4.5 RCP8.5
EA 22	CNRM-CM5	RegCM4.3	25 km	RCP8.5
EA 23	CNRM-CM5	WRF	25 km	RCP8.5
EA 24	NorESM1-M	RegCM4.3	25 km	RCP2.6 RCP4.5 RCP8.5

1
2
3
4
5
6
7
8
9
10
11
12
13
14
15
16
17
18
19
20
21
22
23
24
25
26
27

[END TABLE ATLAS.8: HERE]]

[Placeholder: A synthesis of this information can also be illustrated, e.g. in Figure Atlas.40:, which shows the different climate change projections simulations from CORDEX-EA in terms of RCP scenarios, GCM forcing data, and regional climate models used.]

[START FIGURE ATLAS.40: HERE]

Figure Atlas.40: Different climate change projections simulations from CORDEX-EA in terms of RCP scenarios, GCM forcing data, and regional climate models used.

[END FIGURE ATLAS.40: HERE]]

[Placeholder: Table on other additional information to be added in the SOD]

[Placeholder: In future drafts the Atlas will also include tables or figures on the density of literature on regional climate modelling data, including CORDEX, in Asia, e.g. Table Atlas.9:]

[START TABLE ATLAS.9: HERE]

Table Atlas.9: Scientific literature on regional climate modelling data in Asia

Literature on climate modelling datasets in Asia	Southeast Asia	Central Asia	East Asia	South Asia
Type of Data				
Total number of literature				
Number of academic refereed publications				
Number of grey literature				
Type of Data				
Total number of literature				
Number of academic refereed publications				
Number of grey literature				

28

1 **[END TABLE ATLAS.9: HERE]**

2
3 *Atlas.5.3.2 Southeast Asia*

4
5 The Southeast Asia region is composed of countries that are part of Indochina (or Mainland Southeast Asia)
6 and countries that are very archipelagic in nature and have strong interactions between land and ocean,
7 including those that are part of the maritime continent. Rainfall seasonal variability in the region is affected
8 by tropical cyclones from the Northwest Pacific and the synoptic scale monsoon systems (northeast and
9 southwest) while intraseasonal variability can be influenced by the Madden-Julian Oscillation (MJO).
10 Temperature and especially rainfall are also affected by the El Niño-Southern Oscillation (ENSO). Southeast
11 Asia can be further divided into subregions because of the different ways these atmospheric systems affect
12 the region. In particular, CORDEX simulation results are validated for the whole region and for the
13 subregions shown in Figure Atlas.41: (Cruz and Sasaki, 2017; Juneng et al., 2016; Ngo-Duc et al., 2017).
14 These subregions are based on the historical behaviour of rainfall from previous studies on Southeast Asia.
15 For example, there are two subregions over the Philippines, which are based on two dominant climate types
16 that are strongly influenced by the synoptic scale monsoon systems (the southwest and northeast monsoons).
17 Over Vietnam, there is a north-south division of subregions as rainfall is highest in the north during summer
18 while rainfall peaks during winter in Southern Vietnam. More information on the climatic subregions over
19 Southeast Asia can be found in Juneng et al. (2016).

20
21
22 **[START FIGURE ATLAS.41: HERE]**

23
24 **Figure Atlas.41:** CORDEX-SEA subregions based on historical rainfall climatology and variability (Juneng et al.,
25 2016)

26
27 **[END FIGURE ATLAS.41: HERE]**

28
29
30 *Atlas.5.3.2.1 Observations, trends and attribution*

31
32 Within the last decade, there has been an increasing number of studies on climatic trends over the Southeast
33 Asia region. These studies were either carried out on regional basis (Cheong et al., 2018; Thirumalai et al.,
34 2017) or focused on specific countries (Cinco et al., 2014; Guo et al., 2017; Mayowa et al., 2015; Sa'adi et
35 al., 2017; Supari et al., 2017; Villafuerte et al., 2014; Villafuerte and Matsumoto, 2015). In general, these
36 studies have indicated an increasing trend in the mean temperature as well as the extreme maximum and
37 minimum temperature. Cheong et al. (2018) analysed stations data from 1972-2010 over Southeast Asia and
38 reported faster increment rate in the minimum temperature related extremes, and suggested a reduction in the
39 daily temperature range. The increment rate of the annual minimum of daily minimum temperature was
40 reported to be 0.6°C/decade averaged over the entire region. There would correspond to an overall increase
41 in the frequency of warm nights, coupled with a decrease in the frequency of cold days and nights, with the
42 largest increment of warm nights and warm days occurring in DJF at 4.8% and 8.8% of day/decade,
43 respectively. The increase in hot days and decrease in cold nights are evident and significant over the
44 Philippines (Cinco et al., 2014), Thailand (Limjikanan and Limsakul, 2012; Sharma and Babel, 2014) and
45 Indonesia (Siswanto et al., 2016; Supari et al., 2017), with both the highest and lowest values of daily
46 minimum temperatures also increasing over Thailand, the decline in the frequency of cold nights occurring at
47 a relatively faster rate over Indonesia. Over Jakarta (Indonesia), the daily maximum temperature has
48 increased relatively faster than mean and minimum temperatures. These results are consistent with the
49 findings of the AR5, which showed that the mean annual temperature of Southeast Asia (SEA) has been
50 increasing at a rate of 0.14°C to 0.20°C per decade since the 1960s, along with an increasing number of
51 warm days and nights, and a decreasing number of cold days and nights.

52
53 Extreme temperatures are also strongly influenced by ENSO. Thirumalai et al. (2017) reported that almost
54 all April extreme temperature occur in El Niño years and that global warming contributed to about half of the
55 warming observed in 2016. In most of Southeast Asia (except for the north-eastern areas), Cheong, et al

1 (2018) detected an increase in the number of warm nights with El Niño episodes within the period of 1972–
2 2010. Over the Philippines, the largest positive anomaly in mean temperatures since the 1960s occurred in
3 1998 at the end of a strong El Niño event (Cinco et al., 2014)

4
5 Changes of mean precipitation is less spatially coherent over Southeast Asia. There have been observed
6 decreasing long term trends in annual and seasonal rainfall, with a decline in Southwest monsoon rainfall
7 during the months of June to September in the Philippines, a declining trend especially in dry season rainfall
8 in Indonesia that is correlated with ENSO, and a decrease in the annual and seasonal maximum daily rainfall
9 in most parts of the Maritime Continent (Cruz et al., 2013; Kirono et al., 2015; Supari et al., 2017;
10 Villafuerte and Matsumoto, 2015). While annual precipitation and precipitation events in general have
11 declined, there have been an increase in the contribution of very wet days to annual total precipitation in the
12 north-western and southwestern areas of the region and a significant increase in the annual total wet-day
13 precipitation and in the numbers of heavy and extremely heavy precipitation days in the equatorial
14 subregions in the south-eastern and southwestern areas (Cheong et al., 2018; Limsakul and Singhruck, 2016;
15 Sharma and Babel, 2014; Siswanto et al., 2016). Country specific studies have shown similar increasing
16 trends on extreme rainfall related indices. Supari et al. (2017) analysed observation station data over
17 Indonesia and reported a tendency of increment in rainfall related extreme, with a simple daily rainfall
18 intensity rate of 0.21 mm/day per decade and an annual highest daily amount rate of 1.65 mm/decade. Over
19 the Philippines, Cinco et al. (2014) reported a weak increasing trend of extreme rainfall event intensity and
20 frequency. Over Malaysia, Sa'adi et al. (2017) and Syafrina (2015) also reported an increment of hourly
21 rainfall extreme over the east and the Peninsular of Malaysia respectively. Over Thailand, Limsakul and
22 Singhruck (2016) analysed station data and concluded that on the average, rain day events have decrease by
23 a rate of –.99 days/decade while simple daily intensity has increased by 0.17mm/day per decade. The
24 increase in rainfall extremes and annual total wet-day rainfall are consistent with AR5 findings, which
25 showed that the annual total wet-day rainfall and rainfall from extreme rainy days have increased by 22 mm
26 and 10 mm per decade, respectively and that the ratio of rainfall in wet to dry season in SEA has also
27 increased between 1955 and 2005. Findings of AR5 also show that the frequency of extreme rainfall events
28 has been increasing in the northern parts of SEA, although it is decreasing in Myanmar.

29
30 As with temperature, precipitation is also affected by ENSO events in Southeast Asia. There has been a
31 significant increase in the amount of maximum daily precipitation with La Niña episodes in 1972-2010,
32 especially during the winter monsoon period between December and February (Cheong et al., 2018). Over
33 the Maritime Continent and Thailand, the likelihood of extreme rainfall events and greater amounts of
34 precipitation are higher during La Niña and lower during El Niño years (Limsakul and Singhruck, 2016;
35 Villafuerte and Matsumoto, 2015).

36
37 It is important to note that the availability, quality, and temporal and spatial density of observation data can
38 introduce uncertainties to the detected changes in historical climate. This may lead to varying results because
39 of the uncertainty in the temporal and spatial characteristics of observations in the region. Juneng et al.
40 (2016) showed root mean square differences (RMSD) in precipitation values of up to 8 mm/day when
41 comparing four different observation datasets available for Southeast Asia. Figure Atlas.42: shows the
42 differences in the precipitation values, density, and temporal coverage, of the various observation datasets
43 available for Southeast Asia. The lack of observation data was a key finding of AR5 where the report noted
44 that there is a lack of sufficient observational records to allow for full understanding of precipitation trends
45 over the past century in most of the Asian region and that precipitation trends that are available (e.g.
46 Southeast Asia) differ vastly across the region and between seasons.

47
48
49 **[START FIGURE ATLAS.42: HERE]**

50
51 **Figure Atlas.42:** [Placeholder: Differences in the precipitation values of the various observation datasets available for
52 Southeast Asia from Juneng et al. (2016). (Note that differences in density, and temporal coverage
53 will also be shown).]
54

1 **[END FIGURE ATLAS.42: HERE]**

2
3
4 *Atlas.5.3.2.2 Assessment of model performance*

5
6 Compared to AR5, the number of publications using climate model greatly increased for Southeast Asia.
7 However there are difficulties in validating high-resolution simulations due to the inadequacies of coarse-
8 scale observed gridded datasets (Van Khiem et al., 2014) or the uncertainties in the observations themselves
9 (Juneng et al., 2016). Some efforts have been done to produce better observationally-based gridded datasets
10 for the region (e.g. APHRODITE2; Nguyen-Xuan et al., 2016; SA-OBS; van den Besselaar et al., 2017).

11
12 Regional climate models (RCMs) have been intensively used over the regions in recent years. The RCMs
13 can reproduce reasonably well seasonal climate pattern of temperature, precipitation and large-scale
14 circulation over the different subregions of SEA (Cruz et al., 2017; Juneng et al., 2016; Katzfey et al., 2016;
15 Kwan et al., 2014; Loh et al., 2016; Ngo-Duc et al., 2014, 2017; Raghavan et al., 2016; Ratna et al., 2017;
16 Trinh-Tuan et al., 2018; Van Khiem et al., 2014). The performance of GCMs should be assessed before
17 being used as boundary conditions for the RCM experiments (Katzfey et al., 2016; Siew et al., 2013). Some
18 GCMs are capable of simulating the precipitation seasonal cycle reasonably well but with weaker interannual
19 variations (Siew et al., 2013). The CMIP5 models could simulate the spatial pattern of the winter monsoon
20 rainfall but with a large spread of wet bias magnitude (Siew et al., 2013). Raghavan et al. (2018b) analysed
21 randomly 10 CMIP5 models and revealed that no particular model performed well in simulating historical
22 rainfall over SEA. Katzfey et al. (2016) bias corrected the GCM SST before using it for downscaling.

23
24 Some RCMs generally showed a systematic cold bias for near surface temperature (Cruz et al., 2017; Cruz
25 and Sasaki, 2017; Kwan et al., 2014; Loh et al., 2016; Manomaiphiboon et al., 2013; Ngo-Duc et al., 2014).
26 Cold biases are mainly due to model physics (Kwan et al., 2014; Manomaiphiboon et al., 2013) and/or the
27 biases in the SST forcing (Ngo-Duc et al., 2014). Van Khiem et al. (2014) however showed a slight warm
28 bias of simulated temperature over some subregions of Vietnam. Temperature was shown to be strongly
29 influenced by the choice of cumulus scheme (Cruz et al., 2017). The biases for precipitation were found to
30 be greater and less systematic with wet or dry biases depending on the subregions (Juneng et al., 2016; Kwan
31 et al., 2014; Manomaiphiboon et al., 2013; Van Khiem et al., 2014). Systematic wet biases were found in
32 model simulations in both DJF and JJA (Juneng et al., 2016; Kirono et al., 2015; Kwan et al., 2014; Van
33 Khiem et al., 2014). The wet biases over mainland Indochina could be linked to the lack of summer air-sea
34 interactions in the RCM experiments (Juneng et al., 2016). Regional climate models differ in simulating
35 rainfall interannual variability. Juneng et al. (2016) found stronger interannual variability of rainfall
36 compared to observations while Kirono et al (2015) showed model underestimation of interannual
37 variability. Simulated rainfall amount is sensitive to the choice of convective scheme (Juneng et al., 2016;
38 Ngo-Duc et al., 2017) and the choice of land-surface scheme (Chung et al., 2018). Rainfall biases can be
39 greatly reduced if a bias correction method such as the quantile mapping is applied (Trinh-Tuan et al., 2018).

40
41 Extreme indices have been generally estimated using the core indices recommended by the joint WMO
42 Commission for Climatology (CCI)/World Climate Research Programme (WCRP) Climate Variability and
43 Predictability (CLIVAR) project's Expert Team on Climate Change Detection, Monitoring and Indices
44 (ETCCDMI) (Manomaiphiboon et al., 2013; Ngo-Duc et al., 2014, 2017). There is better coherence for
45 temperature extreme indices than for precipitation extreme indices. Over Thailand, the occurrence frequency
46 of dry days are under-predicted (Manomaiphiboon et al., 2013). Climatic heavy rainfall centres can be well
47 captured (Kieu-Thi et al., 2016). The pattern of tropical cyclone numbers can be reasonable represented by
48 RCM outputs (Kieu-Thi et al., 2016; Van Khiem et al., 2014).

49
50 Multi-model experiments have been conducted (Cruz et al., 2017; Juneng et al., 2016; Katzfey et al., 2016;
51 Ngo-Duc et al., 2014, 2017; Raghavan et al., 2018a; Van Khiem et al., 2014). Ngo-Duc et al. (2014) showed
52 that the ensemble mean product tends to outperform the individual model in representing the climatological
53 mean state. By examining the similarity index omega (Koster et al., 2000, 2002) to assess how model
54 simulations agree or disagree in simulating historical climate for temperature and precipitation extreme
55 indices, Ngo-Duc et al. (2017) found that there are relatively high similarities among the simulations over

1 mainland Asia compared to those over the Maritime Continent for both seasonal and inter-annual variability.
2 The extreme rainfall indices had a lower omega compared to that of temperature. Figure Atlas.43: and Figure
3 Atlas.44: show the similarity index omega for the different CORDEX-SEA historical simulations for
4 extreme indices of temperature and rainfall, respectively [*These are placeholder figures for summary model*
5 *evaluation figures using data available in the Interactive Atlas*].

6
7
8 **[START FIGURE ATLAS.43: HERE]**

9
10 **Figure Atlas.43:** Similarity index omega between the different CORDEX-SEA historical simulations for different
11 temperature-based extreme indices (from Ngo-Duc et al., 2017)

12
13 **[END FIGURE ATLAS.43: HERE]**

14
15
16 **[START FIGURE ATLAS.44: HERE]**

17
18 **Figure Atlas.44:** The same as Figure Atlas.43: but for precipitation (from Ngo-Duc et al., 2017)

19
20 **[END FIGURE ATLAS.44: HERE]**

21 22 23 *Atlas.5.3.2.3 Assessment of projections*

24
25 There has been limited published literature on future climate projections for Southeast Asia that are based on
26 multi-model regional climate simulations. Many of the previous works were country specific and were based
27 on either limited GCMs or RCMs or both. Ngo-Duc et al. (2014) used three RCMs for projecting future
28 climate in Vietnam and some extreme indices until 2050s for the SRES A1B scenario. The temperature trend
29 was found to be positive and significant over the study area and may increase up to 1.8°C in the boreal
30 summer (JJA). Loh et al. (2016) concluded that the projected temperature increments over Malaysia were
31 uniform, ranging from 2.7 to 4.2°C and 1.7 to 3.1°C for A2 and B2 scenarios, respectively.

32
33 More recent works that use the RCP scenarios over the region are consistent with previous results that used
34 the SRES scenarios. Temperature over Southeast Asia are projected to increase by more than 3.5°C across
35 the region by the end of the century under RCP 8.5, and a maximum increase of 2°C under RCP 4.5.
36 Furthermore, under RCP 8.5, daily maximum temperatures of more than 30°C could be expected more
37 frequently by the end of the century, although different areas and cities in the region could have higher
38 values (Raghavan et al., 2018a). Further, the completion of multi-model and high-resolution (25 km)
39 simulations under CORDEX Southeast Asia provided more opportunity for robust assessment of future
40 climate changes over SEA. Based on ten ensemble members, Tangang et al. (2018) showed that the
41 projected temperature increase over SEA ranges from 3.6 to 5.6°C by the end of 21st century under RCP8.5.
42 These findings on regional warming in Southeast Asia are consistent with WGII AR5 findings that showed
43 warming is *very likely* in the mid- and late 21st century over all land areas of Asia based on CMIP5
44 simulations under all four RCP scenarios. For SEA in particular, WGII AR5 assessed that, under the RCP8.5
45 scenario, the ensemble-mean changes in mean annual temperature over the region will likely exceed 3°C
46 above the late 20th century baseline in the late 21st century.

47
48 Data from CMIP5 models available in the Interactive Atlas show projected trends in temperature that are
49 consistent with current observation trends. There is a projected slight increase in the percentage of days
50 when the maximum temperature exceeds the 90% percentile (TX90p) under the RCP8.5 scenario (see Figure
51 Atlas.45:). Figure Atlas.46: shows the same but for the minimum temperature (TN90p).

1 [START FIGURE ATLAS.45: HERE]

2
3 **Figure Atlas.45:** An ensemble average of the CMIP5 models (available in the Interactive Atlas) for (a) the simulation
4 of the percentage of days when the maximum temperature exceeds 90th percentile values (TX90p) for
5 the historical baseline period (1986–2005) and (b) the projected mid-future (2041–2060) changes,
6 under RCP85, compared to the baseline values. Similar analysis for other indices and scenarios
7 (including warming levels) are available at the Interactive Atlas (<http://ipcc-atlas.ifca.es>).
8

9 [END FIGURE ATLAS.45: HERE]

10
11
12 [START FIGURE ATLAS.46: HERE]

13
14 **Figure Atlas.46:** The same as Figure Atlas.45: but for minimum temperature (TN90p).
15

16 [END FIGURE ATLAS.46: HERE]

17
18 Projections of future rainfall changes in terms of means and extremes are highly variable. Over the 2020–
19 2050 period, an increase in precipitation is projected over most of Southeast Asia, with the change being
20 more pronounced in the Maritime Continent under RCP4.5. However, towards the end of the century, high
21 increase in precipitation over the northern areas of Southeast Asia are projected under RCP8.5 (Raghavan et
22 al., 2018a). Over Vietnam, future changes in precipitation vary from –25% to +15% depending on regions
23 and seasons, with the most significant increasing trend over the coastal area during the rainy season,
24 suggesting more severe water-related disasters in this region in the future (Ngo-Duc et al., 2014). Over
25 Indonesia, *significant and robust increase* is projected for annual CDD, when global mean temperature
26 would reach 2°C and for RCPs 8.5 and 4.5 (Tangang et al., *in prep.*). Based on seven ensemble members,
27 Tangang et al. (*in prep.*) showed significant mean rainfall changes up to 15% over Thailand during dry
28 months (boreal winter) with a tendency of getting wetter and drier over northern-central-eastern parts and
29 southern parts, respectively. During wet months (boreal summer), reduction of rainfall is projected
30 throughout the country by as much as 10% in some areas. Recent work by Kang et al. (2019), which was
31 based on 3 GCMs and one RCM, projected significant decrease in rainfall, especially during the inter-
32 monsoon periods.
33

34 CORDEX simulations show that, for both 1.5°C and 2°C global warming levels, the projected precipitation
35 extremes are significantly amplified over Indochina Peninsula and the Maritime Continent, with the numbers
36 of wet and extremely wet days increasing more abruptly than the total and daily average precipitation of all
37 wet days. Overall, median changes of all precipitation indices, except for the number of CWD, are always
38 larger across Southeast Asia under a 2°C global warming scenario. In particular, the number of heavy
39 precipitation days would increase to 29.28% from 20.66% associated with a 1.5°C global warming level (Ge
40 et al., 2019). These confirm the findings of WGI AR5 on future increases in precipitation extremes related to
41 the monsoon that are *very likely* in SEA.
42

43 Consistent with literature, daily rainfall amount corresponding to the 95th percentile (very wet day) over
44 Southeast Asia are projected to increase under the RCP8.5 scenario, based on an ensemble mean of the
45 results from the CMIP5 models in the Interactive Atlas, by at least 20% in most regions and as much as 80%
46 over the maritime continent (see Figure Atlas.47). Projections from individual models are generally
47 consistent with this result though there are some models having reductions in some regions.
48
49

50 [START FIGURE ATLAS.47: HERE]

51
52 **Figure Atlas.47:** Daily rainfall amount corresponding to the 95th percentile (P95, in mm/day) defining “very wet days”
53 for (a) the observational reference (EWEMBI) and (b) the CMIP5_subset, for the reference period
54 1986–2005. (c) Change in frequency of very wet days for the future 2081–2100 period (RCP8.5)
55 defined as exceeding the historical P95 threshold (results shown as relative change, %). Results are
56 shown model by model in the bottom panels, with the ensemble means shown in the upper panels.

1 Similar analysis for other indices and scenarios (including warming levels) are available at the
2 Interactive Atlas (<http://ipcc-atlas.ifca.es>).

3
4 **[END FIGURE ATLAS.47: HERE]**

5
6
7 *Atlas.5.3.3 South Asia*

8
9 *Atlas.5.3.3.1 Observations, trends and attribution*

10
11 IPCC AR5 assessed that it is *very likely* that the mean annual temperature over South Asia has increased
12 during the past century (see Figure 2.21 in Hartmann et al., 2013 and Figure 24-2 in Hijioka et al. 2014), and
13 the frequency of cold (warm) days and nights have decreased (decreased) across most of Asia since about
14 1950 (based on Figure 2.32 in Hartmann et al., 2013). There is only *medium confidence* (due to the issues
15 with defining events) that globally the length and frequency of warm spells, including heat waves, has
16 increased since the middle of the 20th century although it is *likely* that heat wave frequency has increased
17 during this period in large parts of few continents including Asia (Hartmann et al., 2013).

18
19 Recent studies show that the Indian annual mean land temperatures have warmed at a rate by around
20 0.6°C/century during 1901–2010, which was primarily contributed by significant increase in annual
21 maximum temperature by 1.0°C/century, while the annual minimum temperature showed lesser increasing
22 trend of 0.18°C/century during this period, with significant rise only in the recent few decades (1981-2010)
23 at a rate of 0.17°C per decade (A.K. Srivastava, 2017). The observed frequency of total duration and
24 maximum duration of heat waves over central and north-western parts of India during April to June summer
25 months are increasing (Rohini et al., 2016). It was attributed that the anomalous persistent high with anti-
26 cyclonic flow, supplemented with clear skies and depleted soil moisture were primarily responsible for the
27 occurrence of heat waves over India. The increase in the number of intensive heat waves between March and
28 June in India over a recent-past decade was attributed to an upper level cyclonic anomaly over the west of
29 North Africa and a cooling anomaly in the Pacific (Ratnam et al., 2016). The surface air temperature changes
30 over India during 1956–2005 was attributed to anthropogenic forcing mostly by greenhouse gases and
31 partially offset by other anthropogenic forcing including aerosols and land use land cover change by a
32 detection and attribution study using observational datasets and the CMIP5 archive of multiple global
33 climate models with forced and unforced simulations (Dileepkumar et al., 2018). The observed changes in
34 maximum temperature during the post-monsoon and minimum temperature during the pre-monsoon and
35 monsoon seasons in South India during 1950–2005 were found to be detectably different from natural
36 variability, and these temperature changes were attributed to climate change induced by anthropogenic
37 effects (Sonali and RS, 2018).

38
39 On precipitation, IPCC AR5 reported that most areas of the Asian region lack sufficient observational
40 records to draw conclusions about trends in annual precipitation over the past century (Hartmann et al., 2013;
41 see Figure 24-2 in Hijioka, et al., 2014). In South Asia, seasonal mean rainfall showed inter-decadal
42 variability, noticeably a declining trend with more frequent deficit monsoons under regional
43 inhomogeneities. The frequency of heavy precipitation events have increased over India, while light rain
44 events have decreased (Christensen et al., 2013). However, literature based on observational records reported
45 *no clear evidence* in the seasonal mean monsoon (June–September) rainfall trends as well as the inter-annual
46 variability over the whole of India under warming climate e.g. (Mooley and Parthasarathy, 1984; Kripalani et
47 al., 2003; Guhathakurta and Rajeevan, 2008). Although, consistent with AR5 findings, several studies on the
48 variability and trends in the South Asian summer monsoon (SASM) rainfall using observational data agree
49 with the consensus that the mean monsoon rainfall over most parts of the eastern and central north regions of
50 India is decreasing significantly (Jin and Wang, 2017; Juneng et al., 2016; Latif et al., 2017; Pulak
51 Guhathakurta and Jayashree V Revadekar, 2017; Roxy et al., 2015; Sabin and Mujumdar, 2016; Singh et al.,
52 2014).

53
54 Several studies also report that the observed frequency of very heavy and extreme rainfall events over parts
55 of India has significantly increased (Goswami et al., 2006; Mukherjee et al., 2018; Pai et al., 2015; Paiva et

1 al., 2016; Pulak Guhathakurta and Jayashree V Revadekar, 2017; Rajeevan et al., 2008; Ratnam et al., 2016).
2 The scaling relationship between extreme precipitation and dew point temperature showed a super (more
3 than 7% increase per unit rise in dew point temperature) Clausius–Clapeyron (C–C) relationship during the
4 last few decades for the majority of south India (Ahmad et al., 2015; Ali et al., 2015; Latif et al., 2015;
5 Mukherjee et al., 2018; Serreze et al., 2000; Zahid and Rasul, 2012); based on observational data sets,
6 suggesting an increasing trend in the monsoon, pre-monsoon, and extreme rainfall events over Pakistan,
7 particularly over the core monsoon region of Pakistan.

8
9 Latif et al. (2017) identified dipole-like structure in the monsoon rainfall trends over north of the Indo-
10 Pakistan subcontinent on seasonal (June–September, JJAS) inter-annual timescales, where significant
11 increasing trends are observed over Pakistan and decreasing over central north India adjoining land regions.
12 Their results showed that the strengthening (weakening) of vertically integrated meridional moisture
13 transport (VIMMT) trends over the Arabian Sea (Bay of Bengal) is a likely reason for why the monsoon
14 rainfall is increasing (decreasing) over the Pakistan (India) region. However, many studies have shown that
15 there is a considerable spread in the seasonal and annual mean precipitation climatology and interannual
16 variability among the different observed precipitation data sets over India (Collins et al., 2013; Kim et al.,
17 2018; Prakash et al., 2014; Ramarao et al., 2018) by computing the signal-to-noise ratio (Fig. 1c in Ramarao
18 et al., 2018) as well as the ratio of multi-data ensemble mean to the multi-data standard deviation representing
19 the inter-data spread.

22 *Atlas.5.3.3.2 Assessment of model performance*

23
24 The IPCC AR5 assessed that there is *high confidence* that large-scale patterns of surface air temperature are
25 well simulated by the CMIP5 models, although in certain regions this agreement with observations is
26 limited, particularly at elevations over the Himalayas (Flato et al., 2013). The evaluation of four RCMs
27 (CLM, HadRM3, HIRAM5, and REMO) during the south Asian summer monsoon season found that most
28 models were too warm in the north of India compared to the various gridded observations (Lucas-Picher et
29 al., 2011). An assessment of the CORDEX South Asia RCM ensemble showed they followed their driving
30 GCMs in underestimating seasonal mean surface air temperature but overestimating its spatial variability
31 though they added value in the spatial patterns (Sanjay et al., 2017a). Most also improved the simulation of
32 the amplitude and phase of the annual cycle of monthly mean temperature over central India. The RCM
33 ensemble also captures the spatial patterns of temperature climatology over Himalayas though they have a
34 significant cold bias (Nengker et al., 2018). The range of biases in these RCMs, 1–3.6°C, over the
35 Himalayan water towers (e.g., Indus, Ganges, and Brahmaputra river basins) is larger than the observational
36 uncertainty (Mishra, 2015) and they have a relatively larger cold bias than their driving CMIP5 GCMs over
37 the hilly subregions within the Hindu Kush Himalayan (HKH) region (Sanjay et al., 2017a). Finally, both
38 RCMs and their CMIP5 GCMs do not reproduce well the observed climatology of temperature over the
39 Himalayan watersheds of the Indus Basin with substantial cold biases of 6–10 °C (Hasson et al., 2019).

40
41 IPCC AR5 assessed that the broad-scale features of precipitation as simulated by the CMIP5 models are in
42 modest agreement with observations, but there are systematic errors in the Tropics (Flato et al., 2013). The
43 evaluation of four RCMs (CLM, HadRM3, HIRAM5, and REMO) using various gridded observations found
44 that the spatial distribution of the south Asian summer monsoon precipitation with a maximum over the
45 central and west coast of India are found to be simulated well, but with important biases at the regional scale
46 on the east coast of India, in Bangladesh and Myanmar (Lucas-Picher et al., 2011). The amount of
47 precipitation and its distribution at regional scale differ substantially between a set of RCMs forced with
48 same lateral boundary conditions (Kumar et al., 2013; Lucas-Picher et al., 2011). The evaluation of RegCM4
49 RCM over South Asia showed that the model performs well in reproducing not only the mean climate and
50 seasonality but also most of the chosen indicators of climate extremes (Gu et al., 2012). The Indian summer
51 monsoon rainfall is significantly reduced when the RegCM4 RCM domain size for the integration is reduced
52 from South Asia to the Indian domain (Dash et al., 2015b).

53
54 The spatial variability of the Indian Summer Monsoon Rainfall (ISMR) was found to be relatively better in
55 the CORDEX South Asia RCM simulations with respect to their host CMIP5 GCMs, however the other

1 important characteristics of ISMR such as northward and eastward propagation, onset, seasonal rainfall
2 patterns, intra-seasonal oscillations and patterns of extremes did not show consistent improvement (Singh et
3 al. 2017). Also these RCM simulations did not indicate added value in capturing the observed changes in
4 ISMR characteristics over recent decades. The CORDEX South Asia RCMs showed added value relative to
5 their respective driving CMIP5 GCMs in simulating the spatial features of precipitation distribution that are
6 characteristically associated with the Indian summer monsoon (Choudhary and Dimri, 2018).

9 *Atlas.5.3.3.3 Assessment of projections*

11 IPCC AR5 assessed that there is *high confidence* in projected rise in temperature over South Asia. There is
12 *medium confidence* in summer monsoon precipitation increase in the future over South Asia. Model
13 projections diverge on smaller regional scales. CMIP5 models projected a clear increase in temperature over
14 South Asia, especially during winter season. Summer precipitation changes in South Asia were reported to
15 be consistent overall between CMIP3 and CMIP5 projections, but model scatter were large in winter
16 precipitation change. The changes in the summer monsoon dominated the annual rainfall over South Asia.
17 The studies using CMIP3 multi-model ensemble showed an increase in summer precipitation, although there
18 were wide variations among model projections. The spatial variation of rainfall increase was found to be
19 stronger over northern parts of South Asia, with a weak decrease over Pakistan. The CMIP5 projections of
20 the frequency of extreme precipitation days showed consistent increasing trends in 2060 and beyond under
21 RCP6.0 and RCP8.5 scenarios (see Christensen et al., 2013).

23 Projected warming over the region using SRES scenarios is consistent with AR5 findings. ECHAM5
24 downscaled by RegCM4 at 30 km resolution for South Asia shows steadily progressing warming, which
25 would be widespread across the region with increases of 4°C to 5°C by the 2080s for the A2 scenario
26 (Ahmed and Suphachalasai, 2014). The would be a similar warming of 2.5 to 5°C, with the largest values
27 over northern Pakistan and India sub- region, and a 30% increase in summer monsoon precipitation over
28 north eastern India, Bangladesh and Myanmar (Syed et al., 2014a). PRECIS RCM under A1B scenario over
29 the entire Indus river basin shows greater warming over the upper Indus basin than the lower Indus, with
30 greater warming in winter than in the other seasons (Rajbhandari et al., 2015). In the central and western
31 regions of Punjab province of Pakistan, robust changes in the temperature by the end of twenty-first century
32 are in the range of 3 to 4°C during the winter season and on an annual basis, especially in A2 and A1B
33 emission scenarios. Changes in both precipitation and temperature as expected to be larger in the summer
34 season (JAS) as compared to the winter season in the coming decades, relative to the baseline period (Saeed
35 and Athar, 2018). Using CORDEX South Asia RCM projections, consistent future increasing trends in the
36 occurrence of heat waves over Pakistan have been also found (Saeed et al., 2017). Further, CORDEX-South
37 Asia projections over northeast India under RCP4.5 scenario for time period of 2011-2060 shows increasing
38 trends for both seasonal maximum and minimum temperature over the northeast India. The frequency of
39 extreme monthly maximum and minimum temperature are projected to increase (Soraisam et al., 2018).
40 Under A1B scenario GCM20 mean DJF temperature change in 2008–2025 projection period suggests an up
41 to 5°C rise in the North–most region of the country. RegCM4.3 under RCP8.5 scenario suggests an up to
42 11°C rise in the mean temperature projection of 2008–2025 DJF season over the Northern region of the
43 country (Hussain, 2017). The projected robust changes in the temperature by the end of twenty-first century
44 are in the range of 3°C to 4°C during the winter season and on an annual basis, in the central and western
45 regions of Punjab province of Pakistan, especially in A2 and A1B emission scenarios. Changes in both
46 precipitation and temperature are likely to be larger in the summer season (JAS) as compared to the winter
47 season in the coming decades, relative to the baseline period (Saeed and Athar, 2018).

49 ECHAM5 downscaled by RegCM4 at 30 km resolution for South Asia shows an increased summer monsoon
50 precipitation, which is becoming an identified signal by the end of 21st century while winter monsoon is
51 getting drier (Ahmed and Suphachalasai, 2014). 23 CMIP5 GCMs under RCP8.5 scenario show an increase
52 in South Asian Monsoon precipitation due to anthropogenic climate change (Srivastava and Delsole, 2014).
53 30 CMIP5 GCMs under RCP8.5 scenario show a *moderate confidence* for increase in precipitation intensity
54 and frequent extreme precipitation for the Indian region due to increased atmospheric moisture content and
55 circulation (Freychet et al., 2015). Out of 20 CMIP5 GCMs, four showed increase in magnitude and

1 lengthening of all-India summer monsoon under the RCP85 scenario. Both strong and weak monsoon
2 intensity is expected to increase from 2051–2099. Heavy rainfall events (> 40 mm/day) are also likely to
3 increase while the low rain-rate events (< 10 mm/day) are expected to decrease (Sharmila et al., 2015).
4 CMIP5 GCMs show increasing moisture convergence and summer monsoon precipitation over South Asia
5 (Mei et al., 2015). CMIP5 GCMs for RCP4.5 and RCP8.5 scenarios show summer monsoon increase over
6 Himalayas (Palazzi et al., 2015). CMIP5 GCMs show unrealistic Indian Summer Monsoon precipitation due
7 to excessive convective precipitation rather than stratiform precipitation. They suggested using improved
8 model physics before conducting projection experiment (Suryachandra and Dhakate, 2015). 3 GCMs and 7
9 RCMs driven by ECHAM5 under A1B scenario project, higher Indian summer monsoon activity during
10 2041 to 2060 (Niu et al., 2015). Stretched-grid GCM (Sabin et al., 2013) downscaled by Land Surface Model
11 at 35 km resolution over the domain of South Asian Monsoon region and tropical Indian Ocean under
12 RCP4.5 scenario projects continuous decline in summer monsoon rainfall till the end of 21st century. The
13 zooming GCM model (Sabin et al., 2013) showed a persistent monsoonal decrease and soil drying over
14 South Asia (Krishnan et al., 2016). CMIP5 GCMs under transient warming of 0.5°C shows more frequent
15 and heavy precipitation over monsoon region (Lee et al., 2018). Canadian Centre for Climate Modeling
16 (CGCM3.1) is downscaled by Statistical Downscaling Model (SDSM) river basins in South Asia including
17 Ganges and the Brahmaputra under A1B and A2 scenario. The projections for precipitation show an increase
18 during and after the monsoon along with the shift of monsoon peak from July to August (Pervez and
19 Henebry, 2014a).

20
21 Forty-five CMIP5 GCMs at 0.5° resolution for South Asia under RCP8.5 scenario for 2046–2075, show an
22 increase in future runoff over most parts of the region except for far northeast and northwest. The mean
23 annual runoff will increase by 20-30% in the Indian sub-continent (Zheng et al., 2018). CMIP5 GCMs
24 (CanESM2, CNRM-CM5, GFDL-ESM2M, MIROC5 and MPI-ESM-LR) under RCP4.5 scenario (2080-
25 2099) shows strengthening of active spell over in northern Indian region making it wetter than the southern
26 peninsular region where it is weakening causing drying in future (Sudeepkumar et al., 2018). CMIP5 GCMs
27 under RCP4.5 and RCP8.5 scenario for time period of 2006–2050 shows a possible decline in JJAS rainfall
28 over India due to the anti-cyclonic circulation over Arabian Sea at 850 hPa and cyclonic circulation at 200
29 hPa (40° N and 70° E–90° E respectively) (Sarathi et al., 2015). CORDEX–South Asia projections over
30 northeast India under RCP4.5 scenario for time period of 2011–2060 shows decreasing seasonal precipitation
31 trend (Soraisam et al., 2018) but most of the literature does not agree with this finding. As CMIP5
32 projections under RCP8.5 scenario show an increase in frequency of precipitation extremes over southern
33 and central India in mid and end of 21st century (Mukherjee et al., 2018). AOGCMs for time period 2011–
34 2030, 2046–2065, and 2080–2099 under IPCC AR4 scenario shows a gradual increase in annual
35 precipitation in Azad Jammu and Kashmir, Khyber Pakhtunkhwa and Punjab regions of Pakistan, whereas an
36 increase and then decrease in Balochistan and Sindh. In humid and semi-arid climate areas, there is an
37 increase in annual precipitation in all three projected periods (Saeed and Athar, 2018). 22 AOGCMs under
38 A2, A1B, and B1 scenarios for the time periods 2025–2049, 2050–2074, and 2075–2099 show 66% of the
39 models exhibit robust projected increase of winter precipitation by about 10% relative to the baseline period,
40 irrespective of emission scenario and future period, in the upper northern subregion of Pakistan (latitude >
41 35° N) (Saeed and Athar, 2018). CMIP3 downscaled with PRECIS model, projects that 1-day duration of
42 rainstorm over Indus basin in India will increase in intensity but decrease in frequency (Deshpande and
43 Kulkarni, 2015). 1 GCM (GFDL–ESM2M) downscaled by RegCM4 under RCP4.5 and RCP8.5 scenario
44 shows a decreasing JJAS rainfall over central, eastern and peninsular India by 30-40% under RCP8.5
45 scenario. For RCP4.5 scenario, this decrease is observed from 15 to 25% respectively (Dash et al., 2015a).
46 PRECIS RCM under A1B scenario over the entire Indus river basin shows increase precipitation over upper
47 Indus basin and decrease over lower Indus basin. The winter precipitation would be also decreasing over the
48 southern part of basin. The numbers of rainy days are increasing over all basin area but the trend is different
49 for upper and lower border area of basin. There is a decreasing number of rainy days with increased intensity
50 (Rajbhandari et al., 2015). Figure Atlas.48: shows a projected increase in the number of very wet days in the
51 future (2081–2100) for RCP8.5 using the CMIP5 models in the interactive online Atlas. Table Atlas.10:
52 gives a summary of the projected climate changes over South Asia.
53

1 **[START FIGURE ATLAS.48: HERE]**

2
3 **Figure Atlas.48:** Daily rainfall amount corresponding to the 95th percentile (P95, in mm/day) defining “very wet days”
4 for (a) the observational reference (EWEMBI) and (b) the CMIP5_subset, for the reference period
5 1986–2005. (c) Change in frequency of very wet days for the future 2081–2100 period (RCP8.5)
6 defined as exceeding the historical P95 threshold (results shown as relative change, %). Results are
7 shown model by model in the bottom panels, with the ensemble means shown in the upper panels.
8 Similar analysis for other indices and scenarios (including warming levels) are available at the
9 Interactive Atlas (<http://ipcc-atlas.ifca.es>).

10
11 **[END FIGURE ATLAS.48: HERE]**

12
13
14 **[START TABLE ATLAS.10 HERE]**

15
16 **Table Atlas.10:** [Placeholder: Regional Scale Summary of Climate Change projections in South Asia.]

17
18 **[END TABLE ATLAS.10 HERE]**

19
20
21 *Atlas.5.3.4 Central Asia*

22
23 *Atlas.5.3.4.1 Observations, trends and attribution*

24
25 An overview of observational datasets for Northwest–Northeast Asia is given in Table Atlas.11: with the
26 corresponding domain covered, climate variable available, data type, spatial and temporal resolution and
27 period covered for each data set.

28
29
30 **[START TABLE ATLAS.11 HERE]**

31
32 **Table Atlas.11:** Overview of observational datasets for Northwest-Northeast Asia

33

Observed Datasets	Domain	pr	temp	Data type	Spatial Resolution	Temporal Resolution	Period	Reference
CLIMATER	Russia, Kazakhstan, Turkmenistan, Georgia, Armenia, Tajikistan and Uzbekistan.	x	mean, min, max	Station based	600 meteorological stations	DD, MM	from 1874 to the present, each station is available individually.	Russian Research Institute of Hydrometeorological Information - World Data Center (RIHMI-WDC) http://aisori.meteo.ru/climater (Булыгина et al., 2014)
HadGHCND	global	-	min, max	gridded	2.5° lat – 3.75° lon grid	DD	from 1950 to present	Met Office Hadley Centre observations datasets https://www.metoffice.gov.uk/hadobs/hadghcnd/ (Caesar et al., 2006)

HadAT2 gridded radiosonde temperature product: anomalies relative to the monthly 1966-95 climatology	global	-	min, max	gridded at pressure levels 850, 700, 500, 300, 200, 150, 100, 50, 30 hPa)	10° lon – 5° lat grid	MM	from 1950 to 2012	Met Office Hadley Centre observations datasets https://www.metoffice.gov.uk/hadobs/hadat/hadat2.html (Thorne et al., 2005)
CRUTE M4	global	-	min, max	gridded	5° grid	DD	from 1850 to present	Met Office Hadley Centre observations datasets https://www.metoffice.gov.uk/hadobs/crutem4/ (Jones et al., 2012)
CCU "IKI- Monitoring" satellite data archive	global	-	x	satellite images	full coverage with satellite images	DD	from 1984-03- 06 to 2019-03- 31	Center for collective use of satellite data (CCU "IKI- Monitoring"), Space Research Institute of the Russian Academy of Sciences (IKI RAS) ЦКП "ИКИ-Мониторинг" http://ckp.geosmis.ru/default.aspx?page=6 (Loupian et al., 2015)
CPC Merged Analysis of Precipitati on (CMAP)	global	x	-	gridded	2.5° lat – 2.5° lon grid	MM	from 1979-01 to 2019-02	NOAA/OAR/ESRL PSD, Boulder, Colorado, USA https://www.esrl.noaa.gov/psd/data/gridded/data.cmap.htm#detail (Xie et al., 2007)

Note: The symbols *x* and *-* in the precipitation (*pr*) and temperature (*temp*) columns indicate that data are available and unavailable, respectively. On the other hand, *mean*, *min* and *max* specify which type of temperature data is available.

[END TABLE ATLAS.11 HERE]

Atlas.5.3.4.2 Assessment of model performance
[Section to be completed.]

Atlas.5.3.4.3 Assessment of projections

Table Atlas.12: gives on overview of national and other climate change assessments for the countries in Central Asia. Country specific assessments have different reference periods and time horizons for projected climate change. These also vary in terms of the emissions scenarios used.

[START TABLE ATLAS.12 HERE]

Table Atlas.12: Overview of national and other climate change assessments

Country	Reference period	Time horizons	RCPs or emission scenarios	National / other	Reference
Armenia	1961–1990	2011–2040, 2041–2070, 2071–2100.	RCP6.0, RCP8.5	National; other	(Vermishev and Moir, 2015); (Gevorgyan, 2014; Gevorgyan et al., 2016)
Azerbaijan	1961–1990		1, 2, 3, 4, 5 °C 21 CMIP5 climate models	other	National average climate information from ClimGen, climate information for Azerbaijan https://crudata.uea.ac.uk/~timo/climgen/national/web/Azerbaijan/projs_seas.htm (Osborn et al., 2016)
Bahrain	1986–2005	2080–2099	RCP2.6, RCP4.5, RCP6.0, RCP8.5	other	Climate Change Knowledge Portal https://climateknowledgeportal.worldbank.org/country/bahrain/climate-data-projections (World Bank Climate Change Knowledge Portal)
Georgia	1986–2010	2021–2050, 2071–2100	A2, A1B, B1	national	Georgia's Third National Communication to the UNFCCC (Georgia's Third National Communication to the UNFCCC, 2015)
Iran	1982–2009	2016–2030	B1, A2, A1B	national	Iran's Third National Communication to the UNFCCC (Iran's third National Communication to UNFCCC, 2017)
Iraq	1961–2005		2070–2099	other	(Salman et al., 2018)
Kazakhstan	1986–2005	2016–2035; 2046–2065; 2081–2099	RCP 4.5, RCP 8.5 42 CMIP5 models	national	(Кожухметов and Никифорова, 2016)
Kyrgyzstan	1961–1990	2020, 2050, 2080, 2100	16 CMIP3 models, A2	national	(Ильясов et al., 2013)
Tajikistan	1961–1990	2011–2041, 2041–2070, 2071–2099	RCP2.6, RCP8.5	other	(Aalto et al., 2017)
Turkmenistan	1990	2020, 2040, 2060, 2080, 2100	A1FI и B1, a MAGICC/SCE NGEN	national	(Allaberdiyev, 2010)
Uzbekistan	1850–2005	2011–2100	RCP2.6, RCP4.5, RCP8.5	other	(Huang et al., 2014)
Russia	1981–2000	2011–2030, 2041–2060, 2080–2099	RCP4.5, RCP8.	national	Climate Center of Roshydromet http://cc.voeikovmgo.ru/ru/klimat/izmeneniye-klimata-rossii-v-21-veke (Frolov et al., 2014)

1 [ENDTABLE ATLAS.12 HERE]

2
3 *Atlas.5.4 Australasia*

4
5 *Atlas.5.4.1 Observations, trends and attribution*

6
7 *Atlas.5.4.1.1 Previous findings from WGII AR5*

8
9 WGII AR5 for Australasia reports that there is *very high confidence* that the mean air temperatures in
10 Australia and New Zealand have increased by $0.09 \pm 0.03^\circ\text{C}$ per decade since 1911 and by $0.09 \pm 0.03^\circ\text{C}$ per
11 decade since 1909, respectively. There is also *high confidence* that cool extremes have become rarer in
12 Australia and New Zealand since 1950, while hot extremes have become more frequent and intense. On the
13 other hand, precipitation trends are characterized by variabilities within the region. For example, while
14 annual rainfall has been increasing in north-western Australia since the 1950s (*very high confidence*), it has
15 been decreasing in the northeast of the South Island of New Zealand over 1950–2004 (*very high confidence*).

16
17 In terms of sea surface temperatures, WGII AR5 indicates that there is *very high confidence* that
18 measurements have increased by about 0.12°C per decade for north-western and north-eastern Australia, and
19 by about 0.2°C per decade for south-eastern Australia since 1950, as well as by about 0.07°C per decade for
20 New Zealand over 1909–2009. Mean sea levels have also increased in Australia and New Zealand at average
21 rates of relative sea-level rise of 1.4 ± 0.6 mm/yr from 1900 to 2011, and 1.7 ± 0.1 mm/yr from 1900 to
22 2009, respectively (*very high confidence*).

23
24 WGII AR5 also found that the volume of ice in New Zealand has declined by 36–61% from the mid-late
25 1800s to the late 1900s (*high confidence*), while late season significant snow depth has also declined in three
26 out of four Snow Mountain sites in Australia between 1957 and 2002 (*high confidence*).

27
28
29 *Atlas.5.4.2 Assessment of model performance*

30 [Section to be completed.]

31
32 *Atlas.5.4.3 Assessment of projections*

33
34 *Atlas.5.4.3.1 Previous findings from WGII AR5*

35
36 This section discusses the previous findings of WGII AR5 on projected climate change for the Australia
37 region. Most studies reviewed by WGII AR5 were based on Coupled Model Intercomparison Project Phase 3
38 (CMIP3) models and Special Report on Emission Scenarios (SRES) scenarios, as well as CMIP5 model
39 results whenever available.

40
41 According to WGII AR5, in the future, it is *virtually certain* that mean air temperatures will continue to
42 increase, with *very high confidence* that the greatest increase will be experienced by inland Australia and the
43 least increase by coastal areas and New Zealand. There is also a projected decrease in the number of cold
44 days and nights, and increase in the number of hot days and nights during the 21st century (*high confidence*).

45
46 Future projections for precipitation extremes indicate an increase in most of Australia and New Zealand, in
47 terms of rare daily rainfall extremes (i.e. current 20-year return period events) and of short duration (sub-
48 daily) extremes (*medium confidence*). Likewise, however, there is a projected increase the frequency of
49 drought in southern Australia (*medium confidence*) and in many parts of New Zealand (*medium confidence*).
50 Owing to hotter and drier conditions, there is *high confidence* that the fire weather will increase in most of
51 southern Australia, and *medium confidence* that the fire danger index will increase in many parts of New
52 Zealand.

53
54 In the future, sea surface temperatures (*very high confidence*) and mean sea levels (*very high confidence*) are
55 projected to continue to increase in both Australia and New Zealand. As mean sea-level rise is projected to
Do Not Cite, Quote or Distribute

1 continue for at least several more centuries, there is *very high confidence* that this will lead to large increases
2 in the frequency of extreme sea-level events in Australia and New Zealand.

3
4 On the other hand, the volume of winter snow and the number of days with low-elevation snow cover in
5 New Zealand are projected to decrease in the future (*very high confidence*), while both snow depth and area
6 are projected to decline in Australia (*very high confidence*).

7
8
9 **[START FIGURE ATLAS.49: HERE]**

10
11 **Figure Atlas.49:** Absolute daily maximum temperature amount corresponding to the 90th percentile (P90, in °C)
12 defining ‘warm days’ for (a) the observational reference (EWEMBI) and (b) the CMIP5_subset, for
13 the reference period 1986–2005. (c) Change in frequency of warm days for the future 2081–2100
14 period (RCP8.5) defined as exceeding the historical P90 threshold (results shown as relative change,
15 %). Results are shown model by model in the bottom panels, with the ensemble means shown in the
16 upper panels. Similar analysis for other indices and scenarios (including warming levels) are available
17 at the Interactive Atlas (<http://ipcc-atlas.ifca.es>).

18
19 **[END FIGURE ATLAS.49: HERE]**

20 21 22 *Atlas.5.5 Central and South America*

23
24 Summary features of climate change in Central and South America are described in Chapter 10. More
25 specific information is given in this section, utilizing the Interactive Atlas to display observed and projected
26 trends of temperature and precipitation. Results are based on evaluation of both CMIP5, CMIP6 and
27 CORDEX multi-model projections.

28 29 30 *Atlas.5.5.1 Central America*

31 32 **Climate of Central America, Mexico and the Caribbean**

33
34 A description of the observed climate and climate change in Central America and the Caribbean is
35 summarized by Taylor and Alfaro (2005).

36
37 The dominant annual cycle of the Central American region, except for the central part of its Atlantic coast, is
38 monsoonal, with highest temperatures in April, just before the summer rains, and minimum temperatures in
39 January, related with strong trade winds. Precipitation in most Central America is characterized by two
40 maxima in June and September, an extended dry season from November to May, and a shorter dry season in
41 July–August, known as the midsummer drought (MSD). The main dry season of winter and early spring is
42 more intense on the Pacific slopes of the isthmus, due to the seasonal reversal of the winds on the Pacific
43 side which blow offshore during winter and to the migration of the Intertropical convergence zone (ITCZ)
44 which shifts to its southernmost position from February to March.

45
46 The climate of Mexico is temperate to the north of the Tropic of Cancer, with marked difference between
47 winter and summer, modulated by the north American monsoon, and generally arid and tropical to the south,
48 with higher temperatures, even if modulated by height, with cooler temperatures in the mountains of the
49 central ridge, and a less pronounced annual cycle than in the North. The precipitation cycle in the southeast
50 presents a midsummer drought from July to August, as most of Central America.

51
52 The Caribbean islands have two main seasons characterized by differences in temperature and precipitation.
53 The wet or rainy season, with higher values of temperature and accumulated precipitation, occurs during the
54 boreal summer, including part of spring and autumn, although its limits depends on the subregion of the
55 Caribbean. The dry season occurs during boreal winter, with minimum temperatures above 18°C. Within this
56 general pattern, there are important differences for subregions. The annual range of average temperatures

1 varies between 2°C, for south western Lesser Antilles and to 7°C, for the Bahamas and the Greater Antilles.
2 The average temperatures, in the rainy season, are generally below 30°C, although they can reach 37°C. In
3 the small islands and coastal areas of the Greater Antilles, the sea breeze attenuates the diurnal temperature
4 cycle, limiting the temperature extremes.
5

6 In the Caribbean, precipitation during the rainy season (May to October-November) is largely controlled by
7 the position of the North Atlantic Subtropical High (NASH), the variable intensity of the trade winds and the
8 sea surface temperature (SST) of the Atlantic Ocean. Generally, in the first half of June there are easterly
9 waves, which migrate from the coasts of Africa, stimulating convection and occasionally creating
10 disturbances of low pressure. When arriving at the islands, these waves interact with the orography and its
11 effect is intensified by the diurnal heating, with heavy rainfall in the afternoon, particularly in the zones of
12 convergence of breezes on the islands and upstream of the mountain ranges. The direct influence of the ITCZ
13 on precipitation in the Caribbean islands is not significant. The MSD is present in most of the Caribbean,
14 particularly in the Greater Antilles.
15

16 A persistent climatological feature of the low level circulation in the Caribbean is the Caribbean low level jet
17 (CLLJ), which consists of a maximum in the vertical profile of wind speeds at 925 hPa (Amador, 1998;
18 Magaña et al., 1999). Its centre is located approximately in the region defined by (70–80°W, and 15°N) and
19 its maximum horizontal wind speed can reach 16 m/s at the 925 hPa level.
20

21 The whole Central America and Caribbean region is frequently affected by tropical cyclones (TC), which are
22 a characteristic feature of the region, generally forming between June and November in the cyclogenetic
23 regions of the Atlantic and Pacific Oceans and the Gulf of Mexico, and in some cases enter land, with strong
24 winds and high precipitation (Hobgood, 2005). An average of eight hurricanes pass near or through the
25 Caribbean region in a year, but this number can vary significantly from year to year.
26

27 It is likely that El Niño Southern Oscillation (ENSO) influences the frequency of TC developing and passing
28 over the Caribbean, so that during the warm phase their frequency decreases, because of an increase in wind
29 shear in the hurricane season. There is also evidence of decadal variation in storm activity (Taylor and
30 Alfaro, 2005).
31

32 33 *Atlas.5.5.1.1 Observations, trends and attribution* 34

35 It is *very likely* that average and minimum temperatures have increased in some areas of the Caribbean
36 during the second half of the 20th century, and it is likely that extreme rainfall increased during the same
37 period, while the maximum number of dry days showed a negative trend (Naranjo-Díaz and Centella, 1998;
38 Peterson et al., 2002). Other studies suggest it is *very likely* that surface air temperature have also increased
39 during the 1961–2010 and 1986–2010 intervals (Peterson et al., 2002; Stephenson et al., 2014) in the
40 Caribbean. Consistent with this observed warming, it is very likely that the frequency of warm days and
41 warm nights have also increased, while fewer cold days, and cold nights have been found in both periods
42 (Cueto et al., 2013). Changes in mean precipitation rates are less consistent and trends are generally weak.
43 Small positive trends were observed in the total annual precipitation, daily intensity, maximum number of
44 consecutive dry days, and episodes of heavy rains (Stephenson et al., 2014).
45

46 It is *very likely* that the frequency and intensification of heatwaves and other warming indexes has been
47 detected in the Caribbean and Central America regions since 1998 (Angeles-Malaspina et al., 2018). There is
48 also a *high confidence* that estimated trends of temperature and its extremes (heatwaves, hot days, tropical
49 nights, etc.) over parts of Mexico (Cueto et al., 2010, 2013; Martínez-Austria et al., 2016; Martínez-Austria
50 and Bandala, 2017; Navarro-Estupiñan et al., 2018) and the Caribbean (McLean et al., 2015) have increased
51 in the last 30–40 years. In north-western Mexico, Gutiérrez-Ruacho et al. (2010) also found significant
52 positive trends in annual maximum and minimum air temperatures and a strong correlation with inter-
53 decadal oscillations from 1922 to 2004. Navarro-Estupiñan et al. (2018) characterized the impacts of
54 increasing maximum air temperatures in Sonora, Mexico, using heat days (HDs) and heatwaves (Hws); they
55 obtained statistical evidence of an increasing frequency (62 to 205%) in HDs and Hws during the historical

1 period, and after 1986–1995 low elevation sites, around 30–320 m, showed a higher Hws/yr than
2 intermediate and high-elevation climate stations, which exhibit small changes or decreases in Hws. Cueto et
3 al. (2013) studied the annual temperatures trend from 1950 to 2010 for Mexicali, Mexico, finding
4 statistically significant trends in summer maximum temperature and winter minimum temperature.
5

6 A significant positive correlation between precipitation rates in the Caribbean and the Atlantic multidecadal
7 oscillation (AMO) index was found by Enfield et al. (2001) A similar result was found in southern Mexico in
8 the MSD region, while a positive AMO is negatively correlated with the summer NAM precipitation
9 (Cavazos et al., 2019; Méndez and Magaña, 2010). On the other hand, ENSO favours wet condition in
10 Mexico during summers of low Pacific Decadal Oscillation (PDO) and during winters of high PDO. Cooler
11 conditions are favoured during La Niña summers and El Niño winters, regardless of the PDO phase, while
12 summers with high PDO and El Niño condition favours warmer temperature (Pavia et al., 2006). For the
13 Caribbean, in particular.
14

15 **Mid-Summer-Drought**

16
17 South-eastern Mexico and most of Central America, the Greater Antilles and the Bahamas are characterized
18 by the MSD, which is not strictly a drought, but a relative minimum of precipitation at the height of the
19 boreal summer (mid-July to mid-August). Different hypotheses have been suggested to explain this
20 phenomenon, as the interaction between the migration of ITCZ, cloudiness and solar radiation (Magaña et
21 al., 1999) that partially explains the phenomenon in Central America and southern Mexico, the importance of
22 the proximity of the NASH wedge in the Atlantic side, which produces an increase in the speed of the
23 easterly winds at low levels and interacts with the northern edge of the ITCZ (Karnauskas et al., 2013;
24 Karnauskas and Busalacchi, 2009; Small et al., 2007). For the Caribbean in particular, the expansion of the
25 NASH and the subsequent intensification of the Caribbean Low Level Jet is *very likely* to inhibit convection,
26 favouring coastal cold waters in the Caribbean Sea west of Jamaica. combined with an increase in vertical
27 wind shear, and subsidence over the Caribbean which is a consequence of the intensified tropical convection
28 throughout the Caribbean side of Central America, modulated by the variability of aerosol concentrations
29 (Angeles et al., 2010; Gamble and Curtis, 2008).
30

31 **Caribbean Low level Jet (CLLJ)**

32
33 The CLLJ has a semiannual cycle with a maxima in February and July and can be observed throughout the
34 Caribbean during the summer coinciding with the MSD season, being considered by many authors as one of
35 the causes of the divergent flows associated with the MSD (Magaña et al., 1999; Whyte et al., 2008).
36 Hidalgo et al. (2015) introduced a new conceptual model, which relates the CLLJ with the position of the
37 ITCZ during the summer, and with certain mechanisms in the Eastern Pacific.
38 Martin and Schumacher (2011) highlighted the difficulty in reproducing the CLLJ summer maximum by
39 global models (GCMs), given the limitation of some of them in accurately representing the wedge of the
40 NASH; thus, an important goal of the application of regional climate models (RCMs) is to improve the
41 representation of this and other characteristic features of the regional climate. The ability of the RCMs to
42 reproduce the winter and summer core winds associated to the CLLJ is another reference test for climate
43 models that aim to reproduce the Caribbean climate.
44

45 **Tropical cyclones**

46
47 Among the most relevant meteorological phenomena in the Caribbean region, with more implications in its
48 economy are the Tropical Cyclones (TC). They consist of synoptic low-pressure centers, with a warm core,
49 that develop over the tropical oceans, although exceptionally they can arise in extratropical zones (Hobgood,
50 2005). Their formation environment is characterized by a disturbance with strong convective activity,
51 vorticity and convergence near the surface of the ocean, more than 500 km from the equator, the SST
52 exceeding 26°C and the warm water extending several tens of meters of depth, conditional instability in the
53 troposphere and sufficient humidity in the middle troposphere with relatively small vertical wind shear. One
54 of the main cyclogenetic areas is the Tropical North Atlantic (TNA) region, including the Caribbean Sea and
55 the Gulf of Mexico. In this zone, approximately 10 TCs per year are formed, with a wide variability,

1 concentrated in the period from June to November, although the highest frequency is observed from August
2 to October, with a relative minimum in July, coinciding with the MSD. At the beginning and end of the
3 hurricane season, TC formations are more frequent in the Western Caribbean and the Gulf of Mexico, while
4 in the rest of the season TCs that are formed by perturbations in the eastern flow are predominant between
5 the coasts of Africa and the Lesser Antilles.

6
7 There has been much debate on the possible existence of a relationship between the observed increase in the
8 frequency of occurrence of tropical cyclones in the last decades and a tendency to increase the SST due to
9 anthropogenic causes related to the emission of greenhouse gases into the atmosphere. As a conceptual basis
10 for these considerations, the works of Emanuel and Holland (Emanuel, 1995; Holland and Webster, 2007)
11 can be taken as a theoretical basis. Some authors (Holland and Webster, 2007; Hoyos et al., 2006; Mann et
12 al., 2007; Webster et al., 2005) have argued the tendency to increase SST detected during the last century is
13 due to anthropogenic causes and this is, in turn, the fundamental cause of the increase in the frequency of
14 occurrence of TC in general and, in particular, of major hurricanes. Other authors, however, have questioned
15 the reliability of the data sources or have presented other arguments to explain the climatic trends of TC
16 behaviour, based on natural climatic variability (Bell and Chelliah, 2006; Landsea, 2007; Pielke et al., 2005).

17
18 Regarding TCs originating in the Pacific Ocean, Martinez Sanchez and Cavazos (2014) hypothesized that a
19 larger size of the North Atlantic warm pool and a weaker CLLJ during ENSO Neutral years favour
20 cyclogenesis in the Eastern Tropical Pacific

21 22 23 *Atlas.5.5.1.2 Assessment of model performance*

24
25 The ability of climate models to simulate the climate in this region has improved in many key aspects
26 (Campbell et al., 2011; Diro et al., 2012a; Fuentes-Franco et al., 2014, 2015, 2017; Karmalkar et al., 2011,
27 2013; Martinez-Castro et al., 2017; Vichot-Llano, 2017; Vichot-Llano et al., 2014). Particularly relevant for
28 this region are increased model resolution and a better representation of the land surface processes.

29
30 The most frequently used regional climate models in the region are the PRECIS system (Taylor et al., 2013a)
31 and RegCM 3 and 4 (Giorgi et al., 2012; Pal et al., 2007). There is *very high confidence* in the PRECIS
32 performance that reproduces the maximum temperatures in summer and minimum temperatures in winter,
33 but with a bias of +1 to +1.7°C (Campbell et al., 2011; Centella-Artola et al., 2015; Karmalkar et al., 2013).
34 There is *very high confidence* in the ability of these models to reproduce the seasonal spatial patterns of
35 temperature, and the bimodal characteristics of the Caribbean rainfall. Similarly, the simulated rainfall
36 climatology of the central Caribbean basin captures the bimodal characteristics of Caribbean rainfall though
37 overestimating the late season peak rainfall and displacing the rainfall maximum to November. The
38 placement of the NDJ rainfall maximum south of Jamaica in NDJ is interesting and suggests that the model
39 may be over or underestimating the strength of the Caribbean low-level jet (CLLJ) It is *very likely* that the
40 PRECIS system simulations have not any improvement with the dimensions of the domain, as important
41 features of the regional circulation and key rainfall climate features, as the Caribbean low level jet (CLLJ)
42 and the mid-summer drought (MSD) are well represented for a variety of domains of different dimensions
43 (Centella-Artola et al., 2015); concluding that a reduction in domain size does not significantly affect the
44 reproduction of atmospheric circulation patterns, especially at low levels (Figure Atlas.50:). Using CORDEX
45 output, Cerezo-Mota et al. (2015) evaluated the capability of four RCMs – RCA 3.5 (Samuelsson et al.,
46 2011), HadGem3-RA (Hewitt et al., 2011), REMO (Jacob, 2001) and RegCM4 using ERA-Interim as
47 driving data to reproduce the climate of the North American Monsoon region, including the northern part of
48 Mexico. They especially analysed two years of extremely low and high precipitation within the period of
49 simulations, with good results in the reproduction of the key climatic features of the region. Recently Cabos
50 et al. (2018) applied the ROM oceanic model (Sein et al., 2015), coupled with the RCM REMO to the
51 Central America isthmus and Mexico to simulate the climate in the region, showing improvements in the
52 reproduction of the in-shore and off-shore precipitation and of regional climate features as MSD and CLLJ.
53

1 **[START FIGURE ATLAS.50: HERE]**

2
3 **Figure Atlas.50:** Domains D1 (red), D2 (green) and D3 (blue), defined in the work of Centella-Artola et al. (2015)
4 excluding the buffer zones.

5
6 **[END FIGURE ATLAS.50: HERE]**

7
8
9 There is *very high confidence* that PRECIS simulated well the observed negative trends in consecutive wet
10 days (CWD) and negative trends in extreme rainfall events (R95p) over the Caribbean. Also simulate the
11 observed positive trends in the consecutive dry days (CDD) over some locations in the Caribbean, showing
12 in general that the model displayed greater skill at representing CWD and extreme rainfall events than CDD,
13 wet days, and maximum 5-day precipitation over the region. In the case of temperature the model exhibits
14 skill in simulating decreases in the frequency of warm nights (TN90p) over most stations and decreases in
15 the number of cool days (TX10p) with increases observed over the eastern islands. Increases in the number
16 of warm days (TX90p) over some northern locations and decrease over the eastern Caribbean were also
17 observed suggesting warmer conditions over the north and cooler conditions over the eastern Caribbean.
18 (McLean et al., 2015)

19
20 About RegCM4, there is *sufficient evidence* to allow higher than *medium confidence* in use it, for horizontal
21 resolutions of 50 and 25 km and different combinations of physical parameterizations, getting consistent
22 reproductions of the main climate features of the region, as the diurnal and annual temperature and
23 precipitation cycles, and the wind circulation, reproducing particular features as the MSD and the CLLJ
24 (Figure Atlas.51:). (Diro et al., 2012b; Martínez-Castro et al., 2017; Martínez-Castro et al., 2006, 2016;
25 Vichot-Llano et al., 2014).

26
27
28 **[START FIGURE ATLAS.51: HERE]**

29
30 **Figure Atlas.51:** Averaged winds for January, February, June and July (in columns) for the different configurations of
31 the model tested in Martínez-Castro et al. (2016) (in rows) for the central region of the Caribbean
32 where the Caribbean low level jet is located. The isotach intervals with more than 10 m/s are shown
33 shaded.

34
35 **[END FIGURE ATLAS.51: HERE]**

36
37
38 Multi-model ensembles of 14 GCMs from CMIP5 were applied by Colorado et al. (2018) to scenarios
39 RCP4.5 and RCP8.5 for the 21st century for the North American Monsoon region (NAM) and the south-
40 eastern Mexican area known by the Mexican MSD region. The validation of the models showed that the
41 annual cycle of temperature is reproduced by part of them, but some models greatly overestimate mean
42 temperature especially during summer. However, all ensembles reproduce well the annual precipitation
43 cycle. They also found that all ensembles capture well the MSD's double peak of rainfall, but underestimate
44 summer precipitation.

45 **Representation of tropical cyclones in numerical models**

46
47
48 The representation of tropical cyclones (TCs) in numerical models (Diro et al., 2014; Fuentes-Franco et al.,
49 2014, 2017; Nguyen, 2001; Serreze et al., 2000; Walsh et al., 2004) is one of the most important challenges
50 in tropical regions. As these cannot be obtained directly from the wind fields, it is necessary to develop
51 algorithms for their detection, which identify in the fields the grid point structure that meet the characteristics
52 defining the TC.

53
54 In the work of Fuentes-Franco et al. (2014), the conditions imposed on each grid point are that at least once a
55 day, the wind speed is greater than or equal to 21 m/s, the pressure at sea level less than or equal to 1005 hPa
56 and the higher precipitation intensity or equal to 15 mm/day, being a very simple detection algorithm, which

1 allows to infer the capacity of the model to reproduce cyclones, estimating the possible days with cyclonic
2 vortices. In the same way, Diro et al. (2014) examined the characteristics of tropical cyclones in the
3 CORDEX Central America (CAM) domain of for present and future time, with the aim of reducing the scale
4 to 50 km and increasing the capacity of vortex detection. It is very likely that the regional climate model
5 RegCM4 adequately reproduces the cyclogenetic zones of the region (Diro et al., 2014; Fuentes-Franco et
6 al., 2014). The results showed good agreement with the observed climatology, with some overestimation in
7 the Tropical North Atlantic and the Caribbean, while an underestimation in the Tropical Eastern Pacific
8 could be seen.

9
10 Subsequently, Fuentes-Franco et al. (2017) used the same methodology of vortex occurrence detection of
11 Diro et al. (2014), but removing the precipitation threshold, to evaluate the occurrence of cyclonic vortices at
12 different grid intervals of 50 and 25 km (Figure Atlas.52:). In here, the model showed a response dependent
13 on the specific cyclogenetic zone, greater sensitivity to physics schemes was determined than resolution. The
14 parameterization of ocean flows strongly influenced the frequency of estimated vortices and their intensity.
15 However, the methodology applied to assess sensitivity to resolution could be questioned, since the same
16 detection thresholds are used for different resolutions, which does not take into account the experience of
17 previous investigations (Walsh et al., 2007).

18
19
20 **[START FIGURE ATLAS.52: HERE]**

21
22 **Figure Atlas.52:** Biases of the density of trajectories by grid points for the different model configurations used by
23 Fuentes-Franco et al. (2017).

24
25 **[END FIGURE ATLAS.52: HERE]**

26 27 *Atlas.5.5.1.3 Assessment of projections*

28
29 During the last decade, regional climate groups in the Central America and Caribbean area have produced
30 several regional projections using the PRECIS system, RegCM and other regional climate models,
31 downscaling CMIP3 and CMIP5 GCM output, using the CORDEX CAM domain or similar smaller domains
32 including the region. Statistical downscaling methods of CMIP5 projections have been also applied to obtain
33 bias-corrected regional projections (Colorado-Ruiz et al., 2018; Taylor et al., 2013a; Vichot-Llano et al.,
34 2019).

35 36 **Temperature and precipitation projections**

37
38 Twenty first century projections developed by applying bias correction methods to the output of six CMIP3
39 GCMs for the North American monsoon (NAM) region and north-western Mexico project larger interannual
40 variations for precipitation and larger uncertainties than temperature. The A2 scenarios show the largest
41 reductions of precipitation in the last 20 years of the 21st century and a decrease of 30% is projected for Baja
42 California mainly in winter and spring, while precipitation in the North America Monsoon region is
43 projected to decrease by 20% during winter, spring, and summer. After 2050, a significant reduction of
44 precipitation is expected in north-western Mexico and the south-western United States south of 35°N, and
45 temperature increase larger than 2°C could occur (Cavazos and Arriaga-Ramírez, 2012).

46
47 Cueto et al. (2013) applied the generalized extreme value (GEV) distribution to model the maximum air
48 temperatures in four cities in Baja California, finding that extreme temperature could increase to up to 5°C
49 by the end of this century.

50
51 In their study applying multi-model ensembles CMIP5 to the region of Mexico for scenarios RCP4.5 and
52 RCP8.5 for the 21st century, Colorado-Ruiz et al. (2018) found that, according to all ensembles, temperature
53 increases of 1.5–2°C may be reached between 2035 and 2055 relative to the baseline, and by 2070–2099
54 temperature in Mexico may increase between 2 and 5.8°C in the RCP4.5 and RCP8.5 scenarios; and
55 precipitation may decrease between 5 and 10%, respectively for the two scenarios. The largest impacts are

1 expected during summer with a possible decrease of ~13% (up to -1.5 mm/day), especially in southern
2 Mexico, Central America, and the Caribbean, while autumn precipitation may slightly increase.

3
4 According to dynamically downscaled GCM output, using the PRECIS regional climate modelling system,
5 Caribbean temperatures estimates show a *very likely* increase of around 1–4°C (Campbell et al., 2011).

6
7 In the same way, Karmalkar et al. (2011) found that the RCM projected warming for Mexico and Central
8 America was greater than the global temperature increase. Warming in the wet season (over 4°C) would be
9 higher than that in the dry season (3–4°C) in most of Central America except for the Caribbean coasts of
10 Costa Rica and Panama.

11
12 Statistical downscaling models applied by Stennett-Brown et al. (2017) showed good skill in reproducing the
13 monthly climatology of the mean daily temperatures and the frequencies of warm days, warm nights, cool
14 days and cool nights between 1961 and 2001. Even if models for rainfall were less effective, they showed
15 skill in simulating the monthly climatology of mean daily rainfall and the spatial distribution of the mean
16 annual maximum number of CDD, so as the mean annual number of days with daily rainfall above 10 mm
17 (R10). According to their projections, by the end of the century warm days and nights would increase and
18 cool days and nights would decrease, and CDD would increase for most of the Caribbean, but part of Eastern
19 Caribbean and the Bahamas. According to these analyses, the AMO, the Atlantic SST and the Caribbean low
20 level jet (CLLJ) could significant predictors for Caribbean temperature and rainfall extremes.

21
22 For the annual and seasonal projections under the A2 and B2 scenarios in the Caribbean region, there is *high*
23 *confidence* that for 2071–2100, the annual rainfall is projected to increase north of 22°N and decrease (25–
24 50%) south of this demarcation, during the dry season. Besides, there is a projected drying (up to 35% under
25 the A2 scenario) during MJJ and ASO, which is a basin-wide feature. It is noteworthy that the simulated
26 CLLJ index shows an increase in the phenomenon's strength between June and August by the end of the
27 century associated with a drier Caribbean basin partially due to the increased vertical wind shear. Regarding
28 precipitation, the Caribbean is projected to become significantly drier, even if this effect is not expected to
29 manifest in all the Caribbean area and not to be so large as to make the mean season outside the range of
30 conditions experienced in the past (Biasutti et al., 2012). According to McLean et al. (2015), there is *medium*
31 *confidence* that the pattern of future projections from PRECIS RCM for 2071–2099 under A2 and B2 show a
32 tendency towards more intense rainfall events over some part of the region and drier conditions over
33 Trinidad and northern Guyana via an increase in CDD and less intense rainfall events.

34
35 There is *very high confidence* in increased temperature projections on small islands, being virtually certain.
36 High-resolution models project a warming in the range 1.6°C and 3.0°C over land more than on sea
37 (1.2°C/2.3°C) under RCP4.5/RCP8.5. On the other hand, over sea, it is *very likely* that annual precipitation
38 decreases around 20%. Over land, RCM projections are moderate and can be different from one island to the
39 other, but it seems that the RCM response tends to have wetter wet-seasons and drier dry-seasons (Cantet et
40 al., 2014).

41
42 It is *virtually certain* that particularly for rainfall, the intensification of the dry anomalies is not proportional
43 to the temperature increment (Taylor et al., 2018). A 10-member ensemble from CMIP5 has been applied by
44 these authors to analyse the Caribbean's future climate when mean global surface air temperatures are 1.5,
45 2.0, and 2.5°C above preindustrial (1861–1900) values.

46
47 Most of the Caribbean region project smaller mean surface air temperature increases than the rest of the
48 world, even if the opposite is true for part of the region, which would get warmer than the global average.
49 Applying the 1971–2000 baseline, the Caribbean domain is projected to get 0.5 to 1.5°C warmer at the 1.5°C
50 target, which means 5–10% wetter, except for the northeast and southeast Caribbean, which would get drier.
51 Under the 1.5°C target, the region would undergo increases in annual warm spells of more than 100 days,
52 which would be significantly more at the 2°C target. A shift to a predominantly drier region (5–15% less than
53 present day), and a greater occurrence of droughts is also projected.

54
55 Future projections using a multi-model ensemble mean for five CMIP5 global circulation models were used

1 by Angeles-Malaspina et al. (2018) to project heatwaves in the future under scenarios RCP4.5 and RCP8.5.
2 According to these projections, a significant increase of heatwaves would occur at the end of the 21st
3 century, especially for the RCP8.5 scenario.

4
5 An ensemble of CMIP5 models was run for the present assessment, to estimate climate change at the end of
6 the century. Figure Atlas.53: shows the comparison of the precipitation index of 95th percentile of
7 precipitation intensity (P95, in mm/day) defining ‘very wet days’ and the percentage of ‘very wet days’ for a
8 ‘present’ (1986–2005) and future (2081–2100) time periods, under the RCP 8.5. It can be seen that P95 and
9 the percentage of wet days present a moderate positive bias in the Pacific ITCZ, and the frequency change in
10 very wet days increases to the south of the precipitation maximum in the ITCZ.

11
12
13 **[START FIGURE ATLAS.53: HERE]**

14
15 **Figure Atlas.53:** Daily rainfall amount corresponding to the 95th percentile (P95, in mm/day) defining ‘very wet days’
16 for (a) the observational reference (EWEMBI) and (b) the CMIP5 subset, for the reference period
17 1986–2005. (c) Change in frequency of very wet days for the future 2081–2100 period (RCP8.5)
18 defined as exceeding the historical P95 threshold (results shown as relative change, %). Results are
19 shown model by model in the bottom panels, with the ensemble means shown in the upper panels.
20 Similar analysis for other indices and scenarios (including warming levels) are available at the
21 Interactive Atlas (<http://ipcc-atlas.ifca.es>).

22
23 **[END FIGURE ATLAS.53: HERE]**

24 25 26 **Tropical cyclone projections**

27
28 The analysis of CMIP3 projections revealed that models did not show great changes in Atlantic tropical
29 cyclone tracks, projecting a decrease in the overall number of Atlantic TCs for the end of the present century,
30 with *high uncertainty*, but showing a significant increase in the frequency of very intense hurricanes,
31 duration and areas of impact (Bender et al., 2010; Knutson et al., 2008).

32
33 The application of the PRECIS regional climate modelling system to the evolution of the CLLJ in a future
34 climate (Taylor et al., 2013b) shows that it reproduces the present-day characteristics of this feature
35 reasonably well, simulating its winter and summer peaks. The projections to the end of the century show an
36 intensification of the CLLJ’s core strength and duration, particularly in the summer, extending from May to
37 November, and causing decrease in precipitation.

38
39 Jones et al. (2016) applied statistical downscaling of CMIP5 GCM output to the dependence of future
40 Atlantic TC activity with the projections of atmospheric circulation parameters. Their results suggest that
41 CLLJ summer variability is strongly associated with Atlantic TC frequency. According to Yang et al. (2007)
42 and Klotzbach (2011), the CLLJ is correlated with the vertical wind shear for the TC season and with the
43 size of the Atlantic Warm Pool (AWP). On the other hand, Wang (2009) observed correlation of between the
44 AWP and Atlantic tropical cyclones. Atlantic SST anomalies. Villarini and Vecchi (2013) found low
45 response of TC frequency with the difference between local and tropical mean SST. Consequently, Jones et
46 al. (2016) results suggest that in a warmer climate, zonal winds, and particularly the CLLJ become the main
47 indicator of TC frequency, as the SST thresholds to support convection are almost always met.

48 49 50 *Atlas.5.5.2 South America*

51 52 **Climate of South America**

53
54 The extent of the South America land area gives this region strongly varying characteristics, as much in its
55 physical aspects, as in its cultural conditions. Factors such as topography, particularly the Andes mountains,
56 vegetation – the Amazon rainforest – and the proximity of the Atlantic and Pacific oceans play a key role in

1 climatic patterns.

2
3 The South America region is also characterized by numerous regional and local climates, which are
4 influenced by multiple forcings. The main large-scale drivers include the ongoing, anthropogenically-driven
5 long-term changes in climatic conditions, the interdecadal modes of natural variability (the Atlantic Multi-
6 decadal Oscillation – AMO, the North Atlantic Oscillation – NAO, and the Pacific Decadal Oscillation –
7 PDO), the interannual to annual modes of natural variability (the El Niño-Southern Oscillation – ENSO and
8 the Quasi-Biennial Oscillation – QBO), the seasonal variability driven by the meridional migration of the
9 Intertropical Convergence Zone – ITCZ and the timing and intensity of the North American Monsoon
10 System, the Madden-Julian Oscillation – MJO subseasonal mode of natural variability, and the behaviour at
11 finer scales of the tropical easterly waves. At the subregion scale, several phenomena drive climate
12 variability. In the Amazon (AMZ), key drivers include the South-Atlantic Convergence Zone, the Bolivian
13 high, the 40- to 60-day intraseasonal oscillation, and the forcing of the high Andes Mountains to the west
14 (Almeida et al., 2017). In the south-western South America (SWS) stripe, climate is driven by seasonal
15 changes in the position of subtropical high-pressure air masses in the South Atlantic and South Pacific
16 oceans, the Antarctic Oscillation, the dynamics of the cold Humboldt ocean current, and the icy cold fronts
17 and mid-latitude westerlies (Valdés-Pineda et al., 2016). In the densely populated (Penalba and Robledo,
18 2010), highly productive subregion of south-eastern South America (SES), climatic conditions are strongly
19 tied to ENSO, whose influence is moderated by local air-sea thermodynamics in the South Atlantic
20 (Barreiro, 2010). Lastly, the climate of the southern tip of South America (SSA) is influenced by the
21 Southern Annular Mode, and the interaction between the wetter Pacific winds and the Andean Cordillera.

22
23 Figure Atlas.54:, taken from the Satyamurty et al., (1998), shows the schematic representation of
24 atmospheric systems in the lower troposphere over South America that were described above. A schematic
25 representation of physical processes, annual cycle, trends and information that can be accessed from wider
26 geographical or global coverage are important for stakeholder and users.

27
28 *[Placeholder: It would also be relevant contextual material for the corresponding WGI and WGII cross-*
29 *chapter paper to be presented here in summary and made available in the Interactive Atlas.]*

30
31
32 **[START FIGURE ATLAS.54: HERE]**

33
34 **Figure Atlas.54:** Schematic of lower tropospheric systems over South America (Satyamurty et al., 1998).

35
36 **[END FIGURE ATLAS.54: HERE]**

37
38
39 Given that climates and biomes transcend national political boundaries, new regions have been used for the
40 assessment (Section Atlas.2.2) that have a consistent climate change response signal and are climatically
41 consistent (Barros et al., 2015; Neukom et al., 2010; Nobre et al., 2016; Solman et al., 2008). Several studies
42 also have used those regions for analysis and impact studies (Alves et al., 2013; Cabré et al., 2016; Fu et al.,
43 2013).

44 45 46 *Atlas.5.5.2.1 Observations, trends and attribution*

47
48 Analyses of historical temperature time series strongly point to an increased warming trend across many
49 South America regions, except for a cooling off the Chilean coast (*high confidence*). Annual rainfall has
50 increased over south-eastern South America and decreased in most tropical land regions. The number and
51 strength of extreme events, such as extreme temperatures, droughts and floods, have already increased
52 (*medium confidence*). These are some of the main findings of the most recent IPCC assessment reports (AR5
53 and SR1.5), however, not all of these changes are attributed to human activities in the 20th century.

54
55 Taking into account these findings, it is still noted that the major barrier to the study of climate change in

1 many regions of South America is the absence or insufficiency of long time series of observational data.
2 Most national datasets were created in the 1970s and 1980s, preventing a more comprehensive long-term
3 trend analysis. To fulfil the users demand for climatological and meteorological data products covering the
4 whole region several interpolation techniques have been used, such as reanalysis and gridded gauge-analysis
5 products, and adds necessary spatial detail to the climate analyses over land and for climate variability and
6 trend studies, however subject to uncertainties (Skansi et al., 2013).

7
8 Historically many regions across the world have observations from the end of the 19th century and record
9 temperatures in these have been more intense in the 21st century (Fischer and Knutti, 2015a). In recent
10 decades, many studies have been done on climate trends in South America, which indicated that extremely
11 warm maximum and minimum temperatures have shown an increasing trend (de Barros Soares et al., 2017;
12 Skansi et al., 2013) as shown in Figure Atlas.55:a. Ceccherini et al., (2016) analysed the magnitude and
13 frequency of heat and cold waves for 254 stations in South America for the period 1980–2014 and showed
14 an increase in intensity and in frequency of these extreme events in an area covering most of South America.
15 Conversely, there has been no significant change for cold waves. They also showed that the trend of the
16 difference between the annual mean of the daily maximum temperature and the annual mean of the daily
17 minimum temperature is positive – up to 1°C per decade – over the extratropics and negative – up to 0.5°C
18 per decade – over the tropics.

19
20 Regionally, analyses of temperatures point to an increased warming trend over Amazonia over the last 40
21 years, which reached approximately 0.5°C, and with stronger warming during the dry season and over the
22 southeast. The analyses also showed that 2016 was the warmest year since at least 1950 (Marengo et al.,
23 2018). In many areas in Brazil the frequency and length of heatwaves has increased over the last five
24 decades (Bitencourt et al., 2016). Temperature extremes and heatwaves trends are also positive over most of
25 Argentina during the recent decades (Barros et al., 2015). In central Argentina, the trends of temperature
26 extremes show warming in several months with clear increases in heatwaves. However, in other parts of the
27 country, combinations of different trends and decadal variability resulted in some cases in a decrease of
28 extreme heatwaves (Rusticucci et al., 2016). In addition, Wu and Polvani, (2017) analysis of the Hadley
29 Centre extremes dataset, HadEX2 (Donat et al., 2013), found a decrease in maximum temperature extremes
30 over south-eastern South America (SESA) in the second half of the 20th century mostly caused by
31 stratospheric ozone depletion over the South Pole.

32
33 Andean temperatures showed significant warming trends, especially at inland and higher elevations sites,
34 while trends are non-significant or negative at coastal sites, as found in previous studies (Burger et al., 2018;
35 Vicente-Serrano et al., 2018; Vuille et al., 2015). The analysis over Chile and Peru also showed that the
36 positive trends are largely to austral spring, summer and autumn seasons (Burger et al., 2018; Vicente-
37 Serrano et al., 2018). Over Peru a general warming trend in surface air temperature was observed, albeit with
38 clear spatial and seasonal variation (Vicente-Serrano et al., 2018).

39
40 In general, the spatial patterns of observed trends in temperature are more consistent than for precipitation
41 across the whole South America. However, significant changes in the spatial and temporal rainfall variability
42 were observed over South America in recent decades (Figure Atlas.55:b). For Brazil, Awange et al., (2016)
43 studied droughts over a period of more than 100 years and observed *no evidence* of significant trend in
44 drought frequency, intensity and duration over the last 11 decades (since 1901), although the drought areal
45 extent show increasing trends of 3.4% per decade. The annual trends of dry days showed a significant
46 increase in south-eastern Amazon, Upper São Francisco, northern Paraná and throughout the Tocantins
47 basins and increasing annual trends in extreme rainfall events were detected in south-western Paraná,
48 northeast Amazon and north-western Tocantins basins (Valverde and Marengo, 2014). In southeast Brazil
49 there is a region of highly significant decrease of rainfall in both wet and dry seasons (Rao et al., 2016). In
50 contrast, Saurral et al., (2017) found that the Southern South America has experienced significant increase of
51 the annual precipitation mostly explained by positive trends in austral summer. They also found an increase
52 in precipitation in eastern Patagonia and a marked decrease in rainfall in Chile.

53
54 The Amazon biome is perhaps the most-studied in South America due to the important role it plays in the
55 global energy, hydrological cycle and carbon balance. The Amazon basin has experienced more frequent

1 floods and droughts over the past two decades (Espinoza et al., 2013; Gloor et al., 2015; Marengo and
2 Espinoza, 2016). Observational studies also show that the dry-season length over southern Amazonia has
3 increased significantly since 1979, and is accompanied by a prolonged fire season (Alves, 2016; Fu et al.,
4 2013). On the other hand, recent analyses of Amazon hydrological and precipitation data suggest an
5 intensification of the hydrological cycle over the past few decades (Gloor et al., 2015). In general, these
6 changes are attributed partly to decadal climate fluctuations, El Niño-Southern Oscillation (ENSO), the
7 Atlantic SST north-south gradient, feedbacks between fire and land-use change mainly across south south-
8 eastern Amazon and changes in the frequency of organized deep convection (Fernandes et al., 2015; Sánchez
9 et al., 2015a; Tan et al., 2015).

10
11 In the south-eastern South America, a positive significant increase of total annual precipitation and intensity
12 of rainfall events have been observed for several regions of Argentina (Barros et al., 2015; Cavalcanti et al.,
13 2015; Scian and Pierini, 2013; Wu and Polvani, 2017) from the late 1960s and increase the probability of
14 mean flows over the main rivers of the Plata Basin. In contrast, it was found that droughts were more
15 frequent in the western than in the eastern sector of Plata Basin and, over the Andes Mountains, reduced
16 rainfall and increased temperature have led to glaciers receding and reduced river flows.

17
18
19 **[START FIGURE ATLAS.55: HERE]**

20
21 **Figure Atlas.55:** Local robust trends estimated annually for the 1969–2009 period for (a) cold nights (upper left plot),
22 cold days (upper right panel), warm nights (bottom left panel) and warm days (bottom right panel), all
23 showing warming and (b) for annual total rainfall (upper left panel), very wet days (upper central
24 panel), extremely wet days (upper right panel), annual maximum consecutive 5-day precipitation
25 (bottom left panel), annual maximum 1-day precipitation (bottom central panel) and consecutive dry
26 days (bottom right panel). [*Note, here placeholder figure taken from Skansi et al. (2013). To be
27 updated to observational reference dataset (e.g. EWEMBI or other that will be used in the Atlas).*]

28
29 **[END FIGURE ATLAS.55: HERE]**

30
31
32 Since South America has already experienced an increase in extreme events a few studies have been
33 conducted in extreme-event attribution. Otto et al., (2015) showed that the human-induced greenhouse gas
34 emissions seems to not be a major influence on the 2014/2015 drought in southeast of Brazil, whereas
35 increasing population and water use changes increased vulnerability. On the other hand, Hannart et al. (2015)
36 and de Abreu et al. (2019) indicated that anthropogenic climate change has increased the chance of receiving
37 extreme events, such as the Argentinian heat wave of December 2013 and April–May 2017 extreme rainfall
38 in the Uruguay River basin, by at least twofold with a most likely increase of about fivefold.

40 41 *Atlas.5.5.2.2 Assessment of model performance*

42
43 As reported in Chapter 9 of the WGI AR5 the models are able to reproduce quite well the general features of
44 the regional-scale mean surface temperature. Despite of the simulation of regional-scale patterns of
45 precipitation has improved somewhat since the AR4, the models continue to perform less well for
46 precipitation than for surface temperature, and the assessment remains difficult owing to observational
47 uncertainties. In additional, the multi-model mean is closer to observations than most of the individual
48 models.

49
50 A review of the scientific literature of the most important issues related to the assessment of climate models
51 performance and their projections in South America reveals that since the AR5 the number of publications
52 has increased, particularly on regional climate modelling studies (Ambrizzi et al., 2019)

53
54 Although improvements in climate modelling capabilities in the past decades have advanced understanding
55 of climate variability in South America, significant biases still persist mainly at regional scales (Abadi et al.,
56 2018; Blázquez and Nuñez, 2013; Gulizia et al., 2013; Gulizia and Camilloni, 2015; Joetzjer et al., 2013;

1 Jones and Carvalho, 2013; Torres and Marengo, 2013; Zazulie et al., 2017). For example, the majority of
2 global and regional climate models are able to simulate reasonably well the current climatological features of
3 South America, such as seasonal mean and annual cycles, while underestimating rainfall over tropical South
4 America including the Amazon, Northeast Brazil and Andes (Fernandes et al., 2015; Joetzjer et al., 2013;
5 Torres and Marengo, 2013; Yin et al., 2013; Yoon, 2016). Yin et al., (2013) have showed that during the dry
6 season, both convective and large-scale precipitation are underestimated in most models over Amazonia.

7
8 The biases in seasonal precipitation, annual precipitation and climate extremes over several regions of South
9 America were reduced, including the Amazon, central South America, Bolivia, eastern Argentina and
10 Uruguay, in the CMIP5 models when compared to of CMIP3. In general, the multi-model ensemble results
11 have demonstrated better performance compared to individual models in most seasons and regions (Gulizia
12 and Camilloni, 2015; Sillmann et al., 2013a; Torres and Marengo, 2013). For instance, as shown in Figure
13 Atlas.56:, the CMIP5 ensemble mean showed simulations closer to observations than any of the individual
14 GCMs for warm nights (panel a) and very wet days (panel b).

15
16 Jones and Carvalho (2013) and de Carvalho and Cavalcanti (2016) so that some CMIP5 models exhibited a
17 significant improvement in the representation of the South America Monsoon System (SAMS) life cycle
18 compared to their versions in the CMIP3 whereas others continue to have problems in representing
19 accurately the main SAMS features, such as amplitude and length. Reboita et al. (2014) found similar results
20 using the RegCM3 RCM and also showed that the simulations overestimated the air temperature in northern
21 Argentina and underestimated it in the Amazon. A systematic temperature overestimation and precipitation
22 underestimation, with the warm bias amplified for austral summer and the dry bias amplified for rainy
23 season, over the La Plata Basin was also found by Solman (2016) using a suite of seven regional climate
24 model simulations.

25
26 De Jesus et al. (2016a) demonstrated that the dry bias shown by most RCMs in the La Plata Basin (Solman et
27 al., 2013) is due to errors in representing cold-front passages over southern Brazil. They found that in
28 summer the precipitation bias is explained by a too low frequency of passages of cold fronts, while in winter
29 it is explained by the fact that low pressure systems are not deep enough and that there is a lack of moisture
30 availability in low levels.

31
32 Over regions with complex orographic, such as the subtropical central Andes, the CMIP5 models were found
33 to reproduce adequately well the regional and seasonal surface temperature and precipitation, as well as sea-
34 level pressure and circulation Zazulie et al., (2017).

35
36 Overall, climate modelling has made some progress in the past decades, but the results reveals that there is
37 no model that performs well in simulating all aspects of the present climate over South America. The
38 performance of the models varies according to the region, time scale, and variables analysed (Abadi et al.,
39 2018). There is also a fairly narrow spread in the representation of temperature and precipitation over South
40 America by the CMIP5 GCMs and also the RCMs, with biases that can be associated with the
41 parametrizations and schemes of surface, boundary layer, microphysics and radiation used by the models.
42 Finally, observational reference datasets, such as reanalysis products, used in the validation of climate
43 models also can be quite uncertain and may explain part of the important biases present in climate models.
44 For example, ‘observed radiation’ like GEWEX-SRB is very uncertain over South America and in particular,
45 the use of GEWEX-SRB in satellite algorithms causes important biases in evapotranspiration (Sörensson and
46 Ruscica, 2018).

47
48
49 **[START FIGURE ATLAS.56: HERE]**

50
51 **Figure Atlas.56:** (a) Absolute daily minimum temperature amount corresponding to the 90th percentile (P90, in °C)
52 defining ‘warm nights’ for the observational reference (EWEMBI) and the CMIP5_subset, for the
53 reference period 1986–2005; (b) Daily rainfall amount corresponding to the 95th percentile (P95, in
54 mm/day) defining ‘very wet days’ for the observational reference (EWEMBI) and the CMIP5_subset,
55 for the reference period 1986–2005. Results are shown model by model in the bottom panels, with the

1 ensemble means shown in the upper panels. Similar analysis for other indices and scenarios (including
2 warming levels) are available at the Interactive Atlas (<http://ipcc-atlas.ifca.es>).

3
4 **[END FIGURE ATLAS.56: HERE]**

5
6
7 *Atlas.5.5.2.3 Assessment of projections*

8
9 According to the WGI Chapter 12, WGII Chapter 27 AR5 and SR1.5 Chapter 3 climate projections, derived
10 from CMIP5 models and regional climate models for various Representative Concentration Pathways
11 (RCPs), warming at the end of 21st century could reach 2°C to 6°C in a large portion of South America. For
12 extreme heat events, an additional 0.5°C of warming implies a shift from the upper bounds of observed
13 natural variability to a new global climate regime (Schleussner et al., 2016), with distinct implications for the
14 urban poor. Rainfall changes for South America vary geographically, most notably showing a reduction in
15 northeast Brazil, and an increase in southern South America. By 2100 projections show a substantial increase
16 in meteorological drought.

17
18 The most important anthropogenic influences on climate are the emission of greenhouse gases (GHG).
19 Anthropogenic GHG emissions are indeed expected to alter substantially the climate over South America
20 (SA) in the coming decades (Ambrizzi et al., 2019; Cabré et al., 2016; Coppola et al., 2014a; da Rocha et al.,
21 2014; Fernandez et al., 2017; Llopart et al., 2014, 2019; Menéndez et al., 2016; Reboita et al., 2018, 2014a,
22 2016; Ruscica et al., 2016a; Sánchez et al., 2015b; Solman, 2013a; Zaninelli et al., 2019). Increases in
23 extreme events, such as flood, drought, heatwaves and thermal comfort (Batista et al., 2016; Giorgi et al.,
24 2014; López-Franca et al., 2016; Marengo et al., 2017; Sillmann et al., 2013b) associated with climate
25 change may pose severe stresses on natural ecosystems and various sectors of society in the continent.

26
27 According to GCM and RCM projections, temperature may increase over South America (SA) by a wide
28 range, up to ~1.0°C to 6.0°C, by the end of the 21st century (Ambrizzi et al., 2019; Coppola et al., 2014b;
29 Llopart et al., 2019; Sánchez et al., 2015b), with the highest warming projected over the central SA (Cabré et
30 al., 2016; Chou et al., 2014a; Coppola et al., 2014b; Llopart et al., 2019; Menéndez et al., 2016; Ruscica et
31 al., 2016a). According to Torres and Marengo (2013), the temperature change is larger than the interannual
32 variability range for entire SA. The precipitation changes expected for the late 21st century are complex due
33 to the large spread exhibited by the future projections, but the ensemble average changes indicate a general
34 drying of northern and wetting of southern SA (e.g. Chou et al., 2014b; Llopart et al., 2014; Menéndez et al.,
35 2016; Reboita et al., 2014b; Ruscica et al., 2016a; Sánchez et al., 2015b; Solman, 2013b; Zaninelli et al.,
36 2019), though with a large inter-model spread (Coppola et al., 2014a; Llopart et al., 2014, 2019; Sánchez et
37 al., 2015b; Solman, 2013a). These changes will clearly impact natural and agricultural ecosystems (e.g.
38 Camilo et al., 2018). On the other hand, according to Torres and Marengo (2013) the projected changes of
39 precipitation have the same magnitude as the annual variability, however these results do not apply to the
40 climate projections of climate extremes.

41
42 To assess the future climate changes in precipitation (P), air temperature at to 2 m (T) and extreme events
43 due to the global warming, we will focus here on the extreme events shown in Table Atlas.13: to Table
44 Atlas.19: (Heat wave Day Index (HWD), Dry Spell Length Index (also known as Consecutive Dry Days
45 CDD), Heavy Precipitation Index (R95p), Hydroclimatic Intensity Index (HY-INT), Total Annual
46 Precipitation (PRCPTOT), Cold Nights (TN10p), Cold Days (TX10p), Warm Nights (TN90p), and Warm
47 Days (TX90p)) over seven key regions in SA (NWS, AMZ, SAM, NEB, SWS, SES and SSA; see Figure
48 Atlas.2:).

49
50 Table Atlas.13: to Table Atlas.19: summarize the projected change expected for the end of this century,
51 relative to the present day. The baseline depends on the reference article – for example, Coppola et al. (2014)
52 used 1975–2005 as reference period and Mourão et al. (2016) used 1961–1990.

1
2
3
4
5
6

7
8
9
10
11
12
13
14
15

[START TABLE ATLAS.13 HERE]

Table Atlas.13: South America NWS region. If both increase and decrease are indicated, papers have shown different change signal or the signal is mixed over the region, i.e. there are positive and negative changes in the same region and it is difficult to assess the climate signal.

Season	Climate variables changes				Extreme events ^e			
	P GCMs	P RCMs	T GCMs	T RCMs	P GCMs	P RCMs	T GCMs	T RCMs
DJF	Increase ^a	Increase ^a	Increase ^a	Increase ^a				
MAM		Decrease ^b						
JJA	Decrease or increase ^c	Decrease ^c	Increase ^c	Increase ^c				
SON								
Annual	Increase ^d	Decrease ^d	Increase ^d	Increase ^d	CDD: decrease or increase	PRCPTOT: increase	HWD: increase	HWD: increase
					R95p: increase	CDD: decrease	TN10p: decrease	TN10p: decrease
					HY-INT: increase	R95p: increase	TX10p: decrease	TX10p: decrease
					PRCPTOT: increase	HY-INT: increase	TN90p: increase	TN90p: increase
					R95p: increase		TX90p: increase	TX90p: increase

Notes:

(a) (Chou et al., 2014b; Coppola et al., 2014b; Giorgi et al., 2014; Llopart et al., 2019; LYRA et al., 2016; Reboita et al., 2014a)

(b) (Ruscica et al., 2016b)

(c) (Chou et al., 2014b; Coppola et al., 2014b; Giorgi et al., 2014; Llopart et al., 2019; LYRA et al., 2016; Reboita et al., 2014a)

(d) (Coppola et al., 2014b; LYRA et al., 2016)

(e) (Chou et al., 2014b; Giorgi et al., 2014; López-Franca et al., 2016; Sillmann et al., 2013b)

[END TABLE ATLAS.13 HERE]

[START TABLE ATLAS.14 HERE]

Table Atlas.14: As Table Atlas.13 but for the South America AMZ region.

Season	Climate variables changes				Extreme events ^f			
	P GCMs	P RCMs	T GCMs	T RCMs	P GCMs	P RCMs	T GCMs	T RCMs
DJF	Decrease ^a	Decrease ^a	Increase ^a	Increase ^a				
MAM		Decrease ^b		Increase ^b				
JJA	Decrease ^c	Decrease ^c	Increase ^c	Increase ^c				
SON		Decrease ^d		Increase ^d				
Annual	Decrease ^e	Decrease ^e	Increase ^e	Increase ^e	CDD: increase	PRCPTOT: increase	HWD: increase	HWD: increase
					R95p: increase	CDD: increase	TN10p: decrease	TN10p: decrease
					HY-INT: increase	R95p: increase or decrease	TX10p: decrease	TX10p: decrease
					PRCPTOT: decrease	HY-INT: increase	TN90p: increase	TN90p: increase
					R95p: increase		TX90p: increase	TX90p: increase

Notes:

(a) (Chou et al., 2014b; Coppola et al., 2014a; Llopart et al., 2014, 2019; LYRA et al., 2016; Reboita et al., 2014a)

(b) (Chou et al., 2014b; Ruscica et al., 2016b)

(c) (Chou et al., 2014; Llopart et al., 2014, 2019; LYRA et al., 2016; Reboita et al., 2014)

(d) (Chou et al., 2014b; Ruscica et al., 2016b)

(e) (Coppola et al., 2014a; LYRA et al., 2016)

(f) (Chou et al., 2014b; Giorgi et al., 2014; López-Franca et al., 2016; Sillmann et al., 2013b)

[END TABLE ATLAS.14 HERE]

1
2
3
4
5
6
7
8
9
10
11
12
13
14
15
16

[START TABLE ATLAS.15 HERE]

Table Atlas.15: As Table Atlas.13, but for the South America SAM region.

Season	Climate variables changes				Extreme events ^f			
	P GCMs	P RCMs	T GCMs	T RCMs	P GCMs	P RCMs	T GCMs	T RCMs
DJF	Increase ^a	Decrease or increase ^a	Increase ^a	Increase ^a				
MAM		Decrease ^b		Increase ^b				
JJA	Decrease ^c	Decrease or increase ^c	Increase ^c	Increase ^c				
SON		Decrease ^d		Increase ^d				
Annual	Decrease ^e	Decrease ^e	Increase ^e	Increase ^e	CDD: increase	PRCPTOT: increase	HWD: increase	HWD: increase
					R95p: increase	CDD: increase	TN10p: decrease	TN10p: decrease
					HY-INT: increase	R95p: increase	TX10p: decrease	TX10p: decrease
					PRCPTOT: decrease	HY-INT: increase	TN90p: increase	TN90p: increase
					R95p: increase		TX90p: increase	TX90p: increase

Notes:

(a) (Chou et al., 2014b; Coppola et al., 2014a; Llopart et al., 2014, 2019; LYRA et al., 2016; Marengo et al., 2016; Reboita et al., 2014a)

(b) (Chou et al., 2014b; Ruscica et al., 2016b)

(c) (Chou et al., 2014b; Coppola et al., 2014a; Llopart et al., 2014, 2019; LYRA et al., 2016; Marengo et al., 2016; Reboita et al., 2014a)

(d) (Chou et al., 2014b; Ruscica et al., 2016b)

(e) (Coppola et al., 2014a; LYRA et al., 2016)

(f) (Chou et al., 2014b; Giorgi et al., 2014; López-Franca et al., 2016; Sillmann et al., 2013b)

[END TABLE ATLAS.15 HERE]

[START TABLE ATLAS.16 HERE]

Table Atlas.16: As Table Atlas.13, but for the South America NEB region.

Season	Climate variables changes				Extreme events ^f			
	P GCMs	P RCMs	T GCMs	T RCMs	P GCMs	P RCMs	T GCMs	T RCMs
DJF	Increase ^a	Decrease or increase ^a	Increase ^a	Increase ^a				
MAM		Decrease or increase ^b		Increase ^b				
JJA	Decrease or increase ^c	Decrease or increase ^c	Increase ^c	Increase ^c				
SON		Decrease ^d		Increase ^d				
Annual	Increase ^e	Decrease ^e	Increase ^e	Increase ^e	CDD: increase	PRCPTOT: increase	HWD: increase	HWD: increase
					R95p: increase	CDD: increase	TN10p: decrease	TN10p: decrease
					HY-INT: increase	R95p: increase or decrease	TX10p: decrease	TX10p: decrease
					PRCPTOT: decrease	HY-INT: increase	TN90p: increase	TN90p: increase
					R95p: increase		TX90p: increase	TX90p: increase

Notes:

(a) (Chou et al., 2014; Coppola et al., 2014a; Llopart et al., 2014, 2019; LYRA et al., 2016; Marengo et al., 2017; Reboita et al., 2014)

(b) (Chou et al., 2014b; Marengo et al., 2017; Ruscica et al., 2016b)

(c) (Chou et al., 2014b; Coppola et al., 2014a; Llopart et al., 2014, 2019; LYRA et al., 2016; Marengo et al., 2017; Reboita et al., 2014a)

(d) (Chou et al., 2014b; Marengo et al., 2017; Ruscica et al., 2016a)

(e) (Coppola et al., 2014a; LYRA et al., 2016; Marengo et al., 2017; Zaninelli et al., 2019)

(f) (Chou et al., 2014b; Giorgi et al., 2014; López-Franca et al., 2016; Sillmann et al., 2013b)

[END TABLE ATLAS.16 HERE]

1
2
3
4

[START TABLE ATLAS.17 HERE]

Table Atlas.17: As Table Atlas.13, but for the South America SWS region.

Season	Climate variables changes				Extreme events ^f			
	P GCMs	P RCMs	T GCMs	T RCMs	P GCMs	P RCMs	T GCMs	T RCMs
DJF	Decrease or increase ^a	Decrease or increase ^a	Increase ^a	Increase ^a				
MAM		Decrease ^b		Increase ^b				
JJA	Decrease ^c	Decrease ^c	Increase ^c	Increase ^c				
SON		Decrease ^d		Increase ^d				
Annual	Decrease ^e	Decrease or increase ^e	Increase ^e	Increase ^e	CDD: increase	PRCPTOT: decrease	HWD: increase	HWD: increase
					R95p: increase	CDD: increase	TN10p: decrease	TN10p: decrease
					HY-INT: increase	R95p: increase	TX10p: decrease	TX10p: decrease
					PRCPTOT: decrease	HY-INT: increase	TN90p: increase	TN90p: increase
					R95p: decrease		TX90p: increase	TX90p: increase

Notes:

(a) (Cabré et al., 2016; Chou et al., 2014b; Coppola et al., 2014a; Llopart et al., 2014, 2019; Reboita et al., 2014a)

(b) (Cabré et al., 2016; Ruscica et al., 2016a)

(c) (Chou et al., 2014; Coppola et al., 2014a; Llopart et al., 2014, 2019; Reboita et al., 2014)

(d) (Cabré et al., 2016; Ruscica et al., 2016a)

(e) (Barros et al., 2015; Coppola et al., 2014a; LYRA et al., 2016)

(f) (Chou et al., 2014b; Giorgi et al., 2014; López-Franca et al., 2016; Sillmann et al., 2013b)

[END TABLE ATLAS.17 HERE]

5
6
7
8
9
10
11
12
13
14

1
2
3
4**[START TABLE ATLAS.18 HERE]****Table Atlas.18:** As Table Atlas.18, but for the South America SES region.

Season	Climate variables changes				Extreme events ^f			
	P GCMs	P RCMs	T GCMs	T RCMs	P GCMs	P RCMs	T GCMs	T RCMs
DJF	Decrease or increase ^a	Increase ^a	Increase ^a	Increase ^a				
MAM		Increase ^b		Increase ^b				
JJA	Decrease or increase ^c	Decrease or increase ^c	Increase ^c	Increase ^c				
SON		Decrease or increase ^d		Increase ^d				
Annual	Decrease or increase ^e	Decrease or increase ^e	Increase ^e	Increase ^e	CDD: increase	PRCPTOT: decrease or increase	HWD: increase	HWD: increase
					R95p: increase	CDD: increase or decrease	TN10p: decrease	TN10p: decrease
					HY-INT: increase	TX10p: decrease	TX10p: decrease	TX10p: decrease
					PRCPTOT: decrease	R95p: increase or decrease	TN90p: increase	TN90p: increase
					R95p: increase	HY-INT: increase	TX90p: increase	TX90p: increase
								TMINmean: increase
								TMAXmean: increase

5 Notes:
6 (a) (Chou et al., 2014b; Coppola et al., 2014a; Llopart et al., 2014, 2019; LYRA et al., 2016; Mourão et al., 2016;
7 Reboita et al., 2014a)
8 (b) (Chou et al., 2014b; Ruscica et al., 2016a)
9 (c) (Chou et al., 2014b; Coppola et al., 2014a; Llopart et al., 2014, 2019; LYRA et al., 2016; Mourão et al., 2016;
10 Reboita et al., 2014a)
11 (d) (Cabré et al., 2016; Chou et al., 2014b; Ruscica et al., 2016a)
12 (e) (Barros et al., 2015; Coppola et al., 2014a; LYRA et al., 2016)
13 (f) (Chou et al., 2014b; Giorgi et al., 2014; López-Franca et al., 2016; Sillmann et al., 2013b; Silva et al., 2014)

[END TABLE ATLAS.18 HERE]

16

1
2
3
4**[START TABLE ATLAS.19 HERE]****Table Atlas.19:** As Table Atlas.13, but for the South America SSA region.

Season	Climate variables changes				Extreme events ^f			
	P GCMs	P RCMs	T GCMs	T RCMs	P GCMs	P RCMs	T GCMs	T RCMs
DJF	Decrease ^a	Decrease or increase ^a	Increase ^a	Increase ^a				
MAM		Increase ^b		Increase ^b				
JJA	Decrease or increase ^c	Decrease or increase ^c	Increase ^c	Increase ^c				
SON		Decrease ^d		Increase ^d				
Annual	Decrease or increase ^e	Decrease or increase ^e	Increase ^e	Increase ^e	CDD: increase	PRCPTOT: increase	HWD: increase	HWD: increase
					R95p: increase	CDD: increase	TN10p: decrease	TN10p: decrease
					HY-INT: increase	R95p: increase	TX10p: decrease	TX10p: decrease
					PRCPTOT: decrease	HY-INT: increase	TN90p: increase	TN90p: increase
					R95p: increase		TX90p: increase	TX90p: increase

Notes:

(a) (Chou et al., 2014b; Coppola et al., 2014a; Llopart et al., 2014, 2019; Reboita et al., 2014a)

(b) (Cabr e et al., 2016)

(c) (Chou et al., 2014b; Coppola et al., 2014a; Llopart et al., 2014, 2019; Reboita et al., 2014a)

(d) (Cabr e et al., 2016)

(e) (Barros et al., 2015; Coppola et al., 2014a; Zaninelli et al., 2019)

(f) (Chou et al., 2014; Giorgi et al., 2014; L pez-Franca et al., 2016; Sillmann et al., 2013b)

[END TABLE ATLAS.19 HERE]

In general, the studies focusing on the climate change over South America (SA) have been done at the annual scale or for the austral summer; there is a lack of studies for the other seasons that are still of importance – for example during the austral spring the El Ni o–Southern Oscillation (ENSO) plays an important role in August–September. Concerning the temperature both GCM and RCM show the same signal positive change in the future over all SA, and this signal is independent of the climate model used (Chou et al., 2014b; Coppola et al., 2014a; Llopart et al., 2019). Regarding the precipitation change signal there is a large spread in the literature – for example for the regions analysed (NWS, NEB, WS, SES, SSA and SAM) some papers show an increase of precipitation and others a decrease which in turn makes it difficult to assess the precipitation signal in the future, while on the other hand for AMZ all studies agree in the signal of the changes. Regarding the extreme events over the continent in general, they focus on the annual scale and indicate that HWD, TNp10, TN90p will likely increase and TX10p and TX90p will likely decrease over all South America. On the other hand for the precipitation extremes the results show an increase in R95p and CDD.

In order to summarize what has been shown in Table Atlas.13: to Table Atlas.19; Figure Atlas.57: shows the climate change in frequency of warm night (left) and very wet days (right) computed with theCMIP5 for the future 2081–2100 under RCP8.5. It was noted that, in general, the frequency of warm night increases over the entire region. Regarding precipitation, Figure Atlas.57: shows the possible increase in the frequency of extremely wet days under future climate conditions mainly over La Plata basin, western Amazonia, Peru, Ecuador and Colombia (with large uncertainty depending on the choice of GCM).

1 **[START FIGURE ATLAS.57: HERE]**

2
3 **Figure Atlas.57:** (Left) Change in frequency of warm nights for the future 2081-2100 period (RCP8.5) defined as
4 exceeding the historical P90 threshold (results shown as relative change, %); (right) Change in
5 frequency of very wet days for the future 2081-2100 period (RCP8.5) defined as exceeding the
6 historical P95 threshold (results shown as relative change, %). Results are shown model by model in
7 the bottom panels, with the ensemble means shown in the upper panels. Similar analysis for other
8 indices and scenarios (including warming levels) are available at the Interactive Atlas ([http://ipcc-](http://ipcc-atlas.ifca.es)
9 [atlas.ifca.es](http://ipcc-atlas.ifca.es)).

10
11 **[END FIGURE ATLAS.57: HERE]**

12 13 14 *Atlas.5.6 Europe*

15
16 Summary features of climate change in Europe are described in Chapter 10. More specific information is
17 given in this section, utilizing the Interactive Atlas portal to display observed and projected trends of
18 temperature and precipitation. Results are based on evaluation of both CMIP5, CMIP6 and CORDEX multi-
19 model projections.

20 21 **Climate of Europe**

22
23 The regional European climate and main hazards were assessed in SREX, [SROCC], AR5 (WGII) and SR1.5
24 so only a brief overview of Europe's climate characteristics is provided here. In SREX, the European
25 continent was divided into three climate regions, one of which (Mediterranean) also included North Africa.
26 SREX mostly focused on changes in extreme events. SR1.5 is the most recent report available and is focused
27 on changes in mean and extreme climate, hazards and related sectorial impacts under a 1.5°C warming
28 compared to a 2°C warming above the pre-industrial era.

29
30 The climatic regions defined for Europe include (see Figure Atlas.58):

- 31 • [MED] The Mediterranean region in the south characterized by mild winters and hot and dry
32 summers (Mediterranean climate), and of which the climate is determined by sinking motion on the
33 eastern flank of the climatological high pressure in the Atlantic region in boreal summer and by a
34 part of the Atlantic storm track in boreal winter.
- 35 • [CEU] The more continental region in the northeast characterized by warm summers and cold
36 winters.
- 37 • [NEU] The north-western regions, close to the Atlantic Ocean, characterized by more humidity and
38 low temperatures in summers and by relatively mild winters.

39
40 The main climatic features that characterize daily- to inter-annual variability in the European region are
41 westerly winds and the accompanying Atlantic storm track with cyclones and anticyclones travelling mainly
42 from the Atlantic towards inland Europe. Intra-seasonal and inter-annual variations are driven by modes of
43 climate variability such as the North Atlantic Oscillation (Hurrell et al., 2003), and atmospheric flow patterns
44 characterized as “weather regimes” in winter or summer seasons (Cassou et al., 2005; Michelangeli et al.,
45 1995). Feedbacks may amplify climate variability, in particular those between soil moisture and temperature
46 in central Europe in summer (Boé and Terray, 2014) and those related to snow cover in winter (Henderson
47 and Leathers, 2009).

48 49 50 *Atlas.5.6.1 Observations, trends and attribution*

51 52 *Atlas.5.6.1.1 Summary of findings from AR5 and SR1.5*

53
54 Previous reports assessed several present-day hazards in Europe. AR5 WGI and SREX assessment reported
55 that it is *likely* that heatwave frequency has increased since 1950 in large parts of Europe and that there is

1 *high confidence* that the frequency and intensity of precipitation have increased. It is *very likely* that human
2 influence has contributed to the observed global-scale changes in the frequency and intensity of daily
3 temperature extremes since the mid 20th century. It is *likely* that human influence has more than doubled the
4 probability of occurrence of heatwaves in some locations. There is *medium confidence* that the observed
5 warming has increased heat-related human mortality and decreased cold-related human mortality in some
6 regions. Central and southern Europe, including the Mediterranean region, are highlighted as the regions
7 with the highest levels of warming for extreme hot days. These regions are characterized by a strong
8 coupling between soil moisture and temperature, and projected increased dryness.

9
10 It is *very likely* that the number of cold days and nights has decreased and the number of warm days and
11 nights has increased at both the European and global scales. In the Russian European north, a considerable
12 reduction in permafrost thickness and areal extent has been observed over the 1975–2005 period (*medium*
13 *confidence*).

14
15 For mean temperature and cold extremes, the strongest warming is found in the northern high-latitude
16 regions due to substantial ice-snow-albedo-temperature feedbacks. The annual Arctic sea-ice extent
17 decreased dramatically over the 1979–2012 period. The rate of this decrease was *very likely* between 3.5 and
18 4.1% per decade (0.45 to 0.51 million km² per decade). It is *likely* that there has been an anthropogenic
19 contribution to the substantial Arctic warming over the past 50 years.

20
21 Since the 1970s, it is *virtually certain* that the frequency and intensity of storms in the North Atlantic have
22 increased, although the reasons for this increase are debated. With *high confidence*, floods recorded in the
23 20th century have been larger than those occurring during the past five centuries in northern and central
24 Europe, and the western Mediterranean region. Thresholds used to assess the change in floods are 1:20 or
25 1:100 year return period.

26
27 It is *very likely* that aerosol column amounts have declined over Europe and the eastern USA since the mid-
28 1990s.

29 30 *Atlas.5.6.1.2 Assessment of observed trends, particularly on extremes*

31
32 An assessment of more recent literature largely confirms the findings of previous reports (both AR5 and
33 SREX) but with additional detail and higher confidence (for some measure) due to improvements in
34 observations and refinement in methods. Trends related to temperature and its extremes (heatwaves, hot
35 days, tropical nights, etc.) have been positive over Europe (Cardil et al., 2014; Scherrer et al., 2016; Vicente-
36 Serrano et al., 2014). There are no 30-year periods in the last two millennia in which the mean European
37 summer temperatures exceeded the temperature of the 1986–2015 period (Luterbacher et al., 2016).

38
39 In many regions and in country-specific studies, generally positive trends in precipitation extremes
40 (Casanueva et al., 2014; Madsen et al., 2014) as well as droughts (Gudmundsson and Seneviratne, 2015)
41 over the second half of the 20th century have been found. Northern Europe and Scandinavia have become
42 wetter with attendant increases in extreme precipitation (Fleig et al., 2015; Gregersen et al., 2015;
43 Irannezhad et al., 2017). Increasing trends in both heavy precipitation and extreme temperatures have been
44 reported at most Swiss meteorological stations (Scherrer et al., 2016).

45
46 It is *extremely likely* that daily precipitation extremes have increased since the 1960s over the French
47 Mediterranean area (Blanchet et al., 2018; Ribes et al., 2019; Vautard et al., 2015). Using a large collection
48 of quality-checked and homogenized station data, Ribes et al. (2019) have estimated the mean intensity
49 increase of the annual maximum rainfall amount at 22% (7–39% at the 90% confidence level) over the
50 1961–2015 period. It is suggested that intense precipitation increases faster with increasing temperature than
51 can be deduced from the Clausius-Clapeyron relationship (Drobinski et al., 2018), but contradicting results
52 are found due to lack of consistence in methodologies and observational characteristics.

53
54 In a recent analysis of snow conditions over Europe, Fontrodona Bach et al. (2018) showed that there is a
55 widespread and accelerated decrease of both mean and extreme snow depth in Europe. An exception to this

1 are areas with the coldest climates, including north-eastern Europe and high-altitude parts of Scandinavia.
2 For the Baltic Sea, the annual maximum sea-ice extent has decreased, the length of the ice season has
3 shortened and the occurrence of severe ice winters has decreased over the past decades (Haapala et al.,
4 2015).

5
6 For the Mediterranean Sea, duration, maximal surface, and intensity of surface and sub-surface marine
7 heatwaves have increased over the 1982–2017 period (Darmaraki S., Somot S., Sevault F., 2019) (*high*
8 *confidence*). This is confirmed by both a satellite-based SST product and a hindcast simulation using a
9 coupled Regional Climate System Model. Long-term and intercalibrated in-situ observations demonstrate
10 that with (*very*) *high confidence* that temperature, salinity and density of the deepest layers of the north-
11 western Mediterranean Sea have increased over the 1980–2013 period (Somot et al., 2018a).

12 13 14 *Atlas.5.6.1.3 Attribution of observed trends and extremes*

15
16 A substantial fraction of temperature extremes including Europe can be attributed to anthropogenic activity
17 (Coumou and Rahmstorf, 2012; Fischer and Knutti, 2015b). Examples include: the heatwave over large parts
18 of northern Europe in summer 2018 with exceptionally warm conditions over an extended period of time
19 (Kjellström et al. 2018, *in prep.*), the heatwave in southern Europe in summer 2017 with unusual hot
20 conditions (e.g. Kew et al., 2019), warm wintertime conditions in France in 2015 where global warming and
21 unusual atmospheric circulation jointly played a role (Jézéquel et al., 2018), and unusual large volumes of
22 precipitation over the British Isles in the winter of 2013/2014 (Christidis et al., 2015; Schaller et al., 2016).
23 However, for precipitation and at local to regional scales, this attribution is less straightforward (Stott, 2016).
24 During the northwest European dry and warm spell in the spring and summer of 2018, the temperature
25 extremes could be attributed to global warming, but the drought could not. Some approaches may lead to
26 overconfident statements on an attributable human influence on extreme events (Bellprat and Doblus-Reyes,
27 2016).

28
29 The increasing trend in surface shortwave radiation, documented in AR5 to occur since the 1980s and
30 referred to as a brightening effect, is substantiated over Europe and the Mediterranean region (Nabat et al.,
31 2014; Sanchez-Lorenzo et al., 2015). This increasing trend has been attributed to the decrease in
32 anthropogenic sulphate aerosols over the 1980–2012 period (Nabat et al., 2014). In model sensitivity
33 experiments, the aerosol trend has been quantified to explain $81 \pm 16\%$ of the European surface shortwave
34 trend and $23 \pm 5\%$ of the European surface temperature warming. Using cloud and radiation observations at
35 the CESAR observatory in the Netherlands, Boers et al. (2017) showed that decadal trends in cloud
36 characteristics also play a role. Assessing studies on the Baltic Sea area, Rutgersson et al. (2015) also found
37 a coincidence of negative trends in cloudiness with positive trends in solar radiation over recent decades
38 (*medium confidence*).

39 40 41 *Atlas.5.6.1.4 Availability of observation and reanalysis datasets containing information on higher* 42 *resolution and/or sub-daily climate metrics*

43
44 To support climatological analyses and model evaluation, national meteorological and hydrological services
45 are increasingly making available high spatial and temporal resolution gridded and in situ homogenized and
46 quality-checked datasets. The inclusion of additional station data lead to a better representation of extreme
47 precipitation statistics than the global-scale CRU or continental-scale E-OBS datasets. For example, in
48 Norway a 1km gridded daily precipitation and temperature dataset is available from 1957 to the present
49 (Lussana et al., 2018). Switzerland, Sweden, France, Germany, Poland, Spain and the Carpathians also boast
50 gridded observation-based datasets at resolution of 2 to 25 km (Berg et al., 2016; Déqué and Somot, 2008;
51 Herrera et al., 2016; Ivušić S., Somot S., Güttler I.; Noël et al., 2015; Rauthe et al., 2013; Ruti et al., 2016a;
52 Vidal et al., 2010). Recent gridded products merging radar and station data allow to reach higher resolution
53 such as 1 km × 1 hour – for instance COMEPHORE over France (Fumière et al., 2019; Tabary et al., 2011).

54
55 While the emergence of very high-resolution observation-based gridded datasets does provide additional

1 information for climate assessments and model evaluation, a number of caveats exists. The gridded datasets
 2 are unreliable over data-sparse regions. Also, many datasets employ different approaches to interpolation and
 3 gridding, which adds to their uncertainty and complicates comparative evaluations (Berthou et al., 2018;
 4 Fantini et al., 2018; Kotlarski et al., 2017). For example, differences between different precipitation datasets
 5 have been shown to be of the same magnitude as errors in regional climate models (Prein and Gobiet, 2017).
 6

7 A number of high-resolution reanalysis products exists (Table Atlas.20:). While these very high-resolution
 8 products show richer spatial structure and correct for unphysical features seen in coarser-resolution
 9 interpolation-based products, some of them tend to overestimate mean precipitation, frequency of wet days
 10 and underestimate the frequency of heavy precipitation (Isotta et al., 2015). HIRLAM reanalysis outperforms
 11 ERA-Interim at describing extreme values of 2-m temperature and 24-hour accumulated precipitation, but no
 12 added value could be quantified for the wind speed at 10 m over land (Dahlgren et al., 2016). In contrast,
 13 MÉRA is shown to improve the representation of wind and precipitation extremes (Whelan et al., 2018).
 14

15 Regional ocean reanalysis have been recently produced and evaluated for the European seas – such as the
 16 Mediterranean Sea (Hamon et al., 2016). They improve surface ocean characteristics (SST, circulation, eddy-
 17 kinetic energy) compared to hindcast simulations that do not include data assimilation.
 18

19
 20 **[START TABLE ATLAS.20 HERE]**

21
 22 **Table Atlas.20:** European reanalysis products [*Table to be moved to Annex on Reanalyses in SOD*]
 23

Name	Provider	Resolution	Domain	Time Range	Reference
EURO4M MESAN		5 km			(Landelius et al., 2016)
COSMO-ENS-REA12	Uni Bonn & Cologne DWD	0.018° × 0.018°	Central Europe	2006–2010	(Bach et al., 2016)
COSMO-REA6	Uni Bonn & Cologne DWD	0.055° × 0.055°	Europe	1995–2015	(Bollmeyer et al., 2015)
COSMO-REA2	Uni Bonn & Cologne DWD	0.11° × 0.11°	Europe	2007–2013	(Wahl et al., 2017)
HIRLAM 3D	SMHI	0.2° × 0.2°	Europe	1979–2013	(Dahlgren and Gustafsson, 2012)
MÉRA	Irish Meteorological Service	2.5 km	Ireland/United Kingdom	1981–2015	(Whelan et al., 2018)

24
 25 **[END TABLE ATLAS.20 HERE]**
 26
 27

28 *Atlas.5.6.2 Assessment of model performance*

29 30 *Atlas.5.6.2.1 Summary of findings from AR5*

31
 32 The ability of models to simulate the climate in this region has improved in many important aspects since
 33 AR4. Particularly relevant for this region are increased model resolution and a better representation of the
 34 land-surface processes in many of the models that participated in the recent CMIP5 experiment.
 35

36 Although climate models have improved fidelity in simulating aspects of regional climates over Europe and
 37 the Mediterranean, the spread in projections is still substantial, partly due to large amounts of natural
 38 variability in this region (particularly NAO and AMO), besides the inherent model deficiencies. Storm track
 39 biases in the North Atlantic have improved slightly, but models still produce a storm track that is too zonal
 40 and underestimate cyclone intensity.

1
2 *Atlas.5.6.2.2 Assessments of modelled climatology of mean annual cycle and extremes in relation to*
3 *observations*

4
5 GCMs are capable of simulating the main features of mid-latitude climate affecting Europe (Cattiaux et al.,
6 2013; McSweeney et al., 2015). In standard-resolution CMIP5 GCMs, however, the Atlantic storm track
7 intensity is too weak and too zonal while the jet is too strong (Zappa et al., 2013). The persistence of weather
8 patterns is typically underestimated (Cattiaux et al., 2013), as well as the frequency of Euro-Atlantic
9 blocking in winter (Anstey et al., 2013; Davini and D’Andrea, 2016; Dunn-Sigouin and Son, 2013; Mori et
10 al., 2014). Higher horizontal resolution typically helps to mitigate these biases (Berckmans et al., 2013).

11
12 Regional climate models driven by reanalysis have been extensively evaluated regarding a range of climate
13 features over Europe and the Mediterranean (Casanueva et al., 2016; Cavicchia et al., 2018; Drobinski, P.,
14 Bastin, S., Arsouze, T., Beranger, K., Flaounas, E., Stefanon, 2018; Fantini et al., 2018; Harzallah et al.,
15 2018; Ivanov et al., 2017; Panthou et al., 2018; Terzago et al., 2017; Vaithinada Ayar et al., 2016). Standard
16 assessments of RCMs confirm that the Euro-CORDEX and Med-CORDEX ensembles are capable of
17 reproducing the salient features of European climate, corresponding to the ENSEMBLES simulations
18 (Kotlarski et al., 2014). They have been shown to be able to represent realistically circulation features such
19 as coastal low-level jet (over Portugal), medicanes (Gaertner et al., 2018), Mediterranean cyclones (Flaounas
20 et al., 2018; Sanchez-Gomez and Somot, 2018) and intensity, direction and inland penetration of the sea
21 breeze (south of France, (Cardoso et al., 2016; Drobinski et al., 2018)). Evaluation of extreme events such as
22 temperature records (Bador et al., 2017), extreme precipitation (Ribes et al., 2019) or other variables – such
23 as surface shortwave and longwave radiation (Nabat et al., 2014, 2015b) –, aerosol optical depth (Nabat et
24 al., 2013), regional winds (Belušić et al., 2018; Dafka et al., 2018; Obermann-Hellhund et al., 2018), SST
25 diurnal cycle (Voltaire et al., 2017), air-sea fluxes (Waldman et al., 2017), and long-term deep -sea
26 temperature and salinity characteristics (Somot et al., 2018a) have also been carried out.

27
28 Systematic errors persist such as cold and wet biases over much of the continent and warm dry biases in the
29 south in summer. Seasonal and regionally -averaged temperature biases generally do not exceed 1.5°C, while
30 precipitation biases are typically ±40% range (Kotlarski et al., 2014). The warm and dry summer bias over
31 southern and south-eastern Europe is reduced compared to the previous ENSEMBLES simulations
32 (Dell’Aquila et al., 2018; Giot et al., 2016; Katragkou et al., 2015; Prein and Gobiet, 2017). In some cases
33 these biases are mitigated by compensating errors further complicating the picture within the Euro-CORDEX
34 ensemble (García-Díez et al., 2015; Katragkou et al., 2015). RCMs are able to reproduce the basic anomaly
35 structure of temperature and precipitation connected to blocking, though misrepresent some aspects.
36 Increased resolution did not improve the representation of these features (Jury et al., 2018). RCMs are able to
37 reproduce the main areas of high cyclone frequency in the Mediterranean Sea, although the frequency of
38 intense cyclones is generally underestimated (Flaounas et al., 2018).

39
40 The formulation of land surface modules in RCMs greatly determines the spread between Euro-CORDEX
41 RCMs in terms of the overall soil-moisture interannual variability and the spatial patterns and annual cycles
42 of surface fluxes for the different European climate zones (Knist et al., 2017). The models reproduce the
43 spatial pattern of weak land-atmosphere coupling in northern Europe and stronger coupling in southern
44 Europe. However, in the transition zone from strong to weak coupling covering large parts of central Europe,
45 many of the RCMs tend to overestimate the coupling strength.

46
47 Bias adjustment, weather generators and statistical downscaling methods have been assessed in the VALUE
48 network (Maraun et al., 2015b) (see also Chapter 10, Section 10.3.3.3 and Box 10.2 “Issues in Bias
49 Adjustment”). Bias adjustment requires as input a climate model that adequately simulates the processes
50 controlling the regional climate of interest (Maraun et al., 2017b). Although the approach in principle adjusts
51 all calibrated aspects well, problems may arise for extreme quantiles (Gutiérrez et al., 2018b; Hertig et al.,
52 2018). For extreme precipitation, non-parametric methods outperform parametric methods over the observed
53 range of values (Hertig et al., 2018). Quantile mapping tends to overestimate interannual variability and to
54 deteriorate historical trends (Maraun et al., 2017a). Univariate bias -adjustment methods inherit temporal and
55 spatial dependence from the driving model, although the adjustment of wet days slightly improves these

1 aspects for precipitation (Maraun et al., 2017a; Widmann, 2019).

2
3 An evaluation of the Euro-CORDEX models has been carried out using the data included in the Interactive
4 Atlas portal (Section Atlas.7). A detailed description of the reference data, metrics and models being
5 evaluated is given in Section Atlas.3.

6
7
8 **[START FIGURE ATLAS.58: HERE]**

9
10 **Figure Atlas.58:** Evaluation of precipitation-based indices for five RCMs driven by ERA-Interim (rows 2-6), in terms
11 of the relative bias with respect to the observational reference (EWEMBI) for the three European
12 subdomains NEU, CEU and MED. For comparison purposes, results are also shown for the driving
13 dataset, ERA-Interim (first row). See Section Atlas.3 for details on the RCMs, observations and
14 indices used.

15
16 **[END FIGURE ATLAS.58: HERE]**

17 18 19 *Atlas.5.6.2.3 Assessments of modelled trends and variability*

20
21 RCMs have been shown to reproduce the recent downward trend in snowfall days over northern Spain (Pons
22 et al., 2016). Inclusion of a realistic description of the past anthropogenic aerosol trend is crucial to avoid
23 underestimation of the observed trend in surface shortwave radiation and surface temperature by RCMs
24 (Bartók et al., 2017; Ceppi et al., 2012; Nabat et al., 2014). Over the Mediterranean, RCMs generally
25 underestimate the observed long-term temperature trend, mostly in summer, even with respect to the driving
26 reanalysis. They show rather limited ability to reproduce decadal variability in temperature and precipitation
27 over the Euro-Mediterranean region (Dell'Aquila et al., 2018), which is strongly related to the considerable
28 natural variability at this time scale (Aalbers et al., 2018). Euro-CORDEX models are generally able to
29 capture historical heatwaves and heatwaves with magnitudes up to the 2003 event in France (Ouzeau et al.,
30 2016).

31
32 When they are well forced at their ocean boundary, coupled Regional Climate System Models (RCSMs) are
33 able to reproduce relatively well the past sea-level variability and trend of the Mediterranean Sea (Adloff et
34 al., 2018). Coupled RCSMs do tend to underestimate observed trends in SST and in marine heatwaves in the
35 Mediterranean Sea as well as latent-heat loss trends (Darmaraki et al., 2019; Nabat et al., 2014; Sevault et al.,
36 2014) and the deep-water mass characteristics (Somot et al., 2018b). The origin of this bias is unclear.

37 38 39 *Atlas.5.6.2.4 Added value of RCMs and convection permitting models (CPMs)*

40
41 RCMs run at 12 km generally show similar area-averaged, seasonal mean features compared to coarser-scale
42 simulations (with GCMs and lower-resolution RCMs). However, higher-resolution simulations do show
43 improved performance in reproducing the spatial patterns and seasonal cycle of mean precipitation over all
44 European regions (Mayer et al., 2015; Soares and Cardoso, 2018), extreme precipitation (Fantini et al., 2018;
45 Prein et al., 2016; Ruti et al., 2016a; Torma et al., 2015), snow-melt driven runoff in the Alps (Coppola et al.,
46 2018), and mountainous zones (Torma, 2019). This is mainly due to the better representation of orography at
47 high resolution (e.g. Dyrddal et al., 2018). Precipitation improvements in summer are attributed to better
48 representation of larger spatial convection structures. Nevertheless, limited added value was noted for
49 heatwaves (Vautard et al., 2013).

50
51 Convection-Permitting RCMs (CPRCM, running at a resolution of typically 1 to 3 km) are better able to
52 capture observed extreme precipitation behaviour than 12-km RCMs (Berthou et al., 2018; Fumière et al.,
53 2019; Kendon et al., 2014; Lind et al., 2016; Prein et al., 2015). Ban et al. (2014) found Clausius-Clapeyron
54 (CC) scaling between temperature and moderate (90th percentile value) hourly precipitation events, while
55 super-CC scaling was noted for the extreme (99th percentile and up) tails of hourly precipitation.

1
2 Over specific geographic features such as mountains, high-resolution CPRCMs are able to modulate strongly
3 the climate change signal simulated by the low-resolution GCMs (Giorgi et al., 2016; Torma and Giorgi,
4 2019). This is especially true for summer precipitation over the Alps where opposite signs of changes in
5 mean and extreme precipitation are generated by the CMIP5 GCM ensemble and the 12-km Med-CORDEX
6 and Euro-CORDEX RCM ensemble (Giorgi et al., 2016). The physical basis of this climate change signal
7 modulation is fairly well understood.
8
9

10 *Atlas.5.6.2.5 Assessment of coupled regional climate system models*

11
12 Coupled RCMs for the Baltic, North Sea and Mediterranean Sea have been further explored since AR5.
13 New, or updated, higher-resolution, coupled atmosphere-ocean-ice model systems have been found to
14 simulate realistically the observed climate with improvement with respect to stand-alone atmosphere model
15 versions in features like the winter SST in the Baltic Sea, the correlation between precipitation and SST,
16 between surface heat-flux components and SST, and for weather events like convective snow bands over the
17 Baltic Sea (e.g. Gröger et al., 2015; Pham et al., 2017; Tian et al., 2013; Van Pham et al., 2014; Wang et al.,
18 2015). Wang et al. (2015), Gröger et al. (2015) and Tian et al. (2013) have shown that coupling makes a
19 significant difference over relatively small areas that include the areas where ocean and atmosphere are
20 coupled. Panthou et al. (2018) also showed that over land differences between atmosphere-only and coupled
21 RCMs are confined to coastal areas that are directly influenced by SST anomalies. In contrast, Van Pham et
22 al. (2014) showed significant differences in seasonal mean temperature across a widespread continental
23 domain.
24

25 Med-CORDEX atmosphere-RCMs and coupled RCSMs including the atmosphere-aerosol-land-river-ocean
26 regional coupling have been assessed for mean climate characteristics with a focus on decadal variability.
27 Coupled RCSMs adequately represent the Mediterranean climate and its extremes, with similar skill as the
28 ENSEMBLES ensemble and the Euro-CORDEX ensemble (Dell'Aquila et al., 2018; Fantini et al., 2018;
29 Gaertner et al., 2018). Sea wind (Akhtar et al., 2018), the turbulent air-sea fluxes (Akhtar et al., 2018;
30 Sevault et al., 2014), and the seasonal cycle of the medicane frequency (Gaertner et al., 2018) have been
31 also shown to be improved in coupled RCSMs.
32

33 The role of aerosol forcing is increasingly analysed as new and more realistic aerosol datasets become
34 available (Nabat et al., 2013; Pavlidis et al.), and as RCMs begin to include interactive aerosols (Drugé et al.;
35 Nabat et al., 2012, 2015a). Explicitly accounting for aerosol effects in RCMs leads to improved
36 representation of the surface shortwave radiation at various scales: long-term means (Gutiérrez et al., 2018a),
37 past trends (Nabat et al., 2014), day-to-day variability (Nabat et al., 2015a) and future climate projections
38 (Boé et al. *in prep.*; Gutiérrez et al. *in prep.*). It is *likely* that including a realistic representation of aerosol in
39 climate models over Europe decreases positive land- and sea-surface temperature trends, with associated
40 reductions in evaporation and precipitation, and increases the deep-water formation rate in the Mediterranean
41 Sea (Nabat et al., 2014). For favourable circulation types, the representation of aerosols affects the simulated
42 heatwave intensity over Europe (Nabat et al., 2015a; Pavlidis et al.).
43

44 The impact of on-line coupling of a city module in a 12-km RCM over France has been assessed by Daniel et
45 al. (2018). In an evaluation run, improving the representation of cities in this RCM led to a regional surface
46 warming extending well beyond the urban areas. The impact on precipitation was shown to be small.
47

48 While the importance of vegetation and land-use change on climate has received a lot of attention of the
49 GCM community, results on regional scales are rather sparse and eventually contradicting (Levis, 2010).
50 Large differences between the implemented land surface models, the vegetation -coupling strategy and the
51 way of implementing maps of land-cover change do play a role (Pitman et al., 2009).
52

53 Wramneby et al. (2010) identified central Europe, the Scandinavian mountains and southern Europe as
54 climate-vegetation hotspots. Specifically for southern Europe they found that increased summer dryness
55 restricts plant growth and survival, causing a positive warming feedback through reduced evapotranspiration.

1 Alo and Anagnostou (2017) found that summer warming in the Mediterranean area is reduced when
2 allowing interactive vegetation responses to altered climate conditions, as a result of counteracting cooling
3 due to an increased albedo, and warming due to a decreased Leaf Area Index (LAI) in response to regional
4 warming. Davin et al. (2019) explored idealized land-use scenarios using the CORDEX-FPS-LUCAS
5 ensemble (Rechid et al.). They concluded that it is difficult to reach consensus on the sign of summer
6 temperature responses to widespread afforestation. A large part of the inter-model spread was attributed to
7 the representation of land processes.

10 *Atlas.5.6.3 Assessment of projections*

12 *Atlas.5.6.3.1 Summary of findings from AR5 and SR1.5*

14 The CMIP5 projections reveal warming in all seasons for the three European subregions, while precipitation
15 projections are more variable across subregions and seasons.

17 A large ensemble of RCM-GCM simulations shows that the temperature response is robust in spite of a
18 considerable uncertainty related to the choice of (GCM/RCM) model combination and sampling (natural
19 variability), even for the 2021–2050 time frame.

21 It is *likely* that in the next decades the frequency of warm days and warm nights will increase in most land
22 regions, while the frequency of cold days and cold nights will decrease. Models also project increases in the
23 duration, intensity and spatial extent of heatwaves and warm spells for the near term. Several studies project
24 that European high-percentile summer temperatures are projected to warm faster than mean temperatures.

26 Studies assessed in SR1.5 have clearly identified a possible amplification of temperature extremes by
27 changes in soil moisture, acting as a mechanism that further magnifies the intensity and frequency of
28 heatwaves related to summer drying conditions. Other studies indicate that European winter variability may
29 be related to sea-ice reductions in the Barents-Kara Sea.

31 In the winter half year, NEU and CEU are projected to have increased mean precipitation associated with
32 increased atmospheric moisture, increased moisture convergence and intensification in extratropical cyclone
33 activity and no change or a moderate reduction in the MED. In the summer half year, NEU and CEU mean
34 precipitation are projected to have only small changes whereas there is a notable reduction in MED. High-
35 resolution projections from the Japanese high-resolution model ensemble and results from coordinated multi-
36 model GCM/RCM experiments (e.g. ENSEMBLES) agree with these findings.

38 A 2°C global warming is associated with a robust increase in seasonal mean precipitation over central and
39 northern Europe in winter and with decreases in mean precipitation in central/southern Europe in summer.
40 These precipitation changes more pronounced than with a 1.5°C global warming.

42 For a 2°C global warming, an increase in runoff is projected for north-eastern Europe while decreases are
43 projected in the Mediterranean region, where runoff differences between 1.5°C and 2°C global warmings
44 will be most prominent. At high latitudes high river flows are expected to be more frequent.

46 From the special report SR1.5 it appears that probabilities associated with increases in drought frequency and
47 magnitude are substantially larger at 2°C than at 1.5°C in the Mediterranean region (*medium confidence*).
48 Drying in the Mediterranean is consistent with projected changes in the Hadley circulation.

50 AR5 WGII, and in particular the European chapter (Chapter 23) therein, provide detailed hazard projections.
51 They report that there is *medium confidence* in extreme -wind increase in central and northern Europe, and
52 *low confidence* of a small decreasing trend in Southern Europe by the end of century. The literature assessed
53 in AR5 shows *high confidence* in an increase in extreme sea level events and a significant increase of storm
54 surge for the North Sea, to the west of United Kingdom and Ireland. The frequency of 100-year return period
55 river-discharge event is expected to increase in continental Europe and decrease in some northern and

1 southern European regions. Increase in extreme discharge is projected in Finland, Denmark, Ireland, the
2 Rhine basin, the Danube basin and France. Snowmelt flood may decrease by the end of the 21st century and
3 peak floods in northern Europe may increase in autumn and winter due to increased rainfall in these seasons.
4 A decline in low flow is projected by 2100 for United Kingdom, Turkey, France and rivers fed by Alpine
5 glaciers.

6
7 In the near term, decadal predictability is likely to be critically dependent on the regional impacts of modes
8 of variability ‘internal’ to the climate system. However, it has been shown that NAO trends do not account
9 for a large fraction of the long-term future change in mean temperature or precipitation, and that large-scale
10 atmospheric circulation changes in CMIP5 models are not the main driver of the warming projected in
11 Europe by the end of the century (2081–2100).

12
13 In Europe adaptation policy has been developed across all levels of government, with some adaptation
14 planning integrated into coastal and water management, into environmental protection and land planning and
15 into disaster risk management.

16 17 18 *Atlas.5.6.3.2 Assessment of regional projections, and the uncertainty cascade for future projections*

19
20 Global warming can lead to systematic changes in regional climate variability via various mechanisms.
21 Thermodynamic responses such as altered lapse rates (Brogi et al., 2019; Kröner et al., 2017) and land-
22 atmosphere feedbacks (Boé and Terray, 2014) modify temporal and spatial variability of temperature and
23 precipitation, including altered seasonal and diurnal cycle and return frequency of extremes. Regional
24 feedbacks with sea surface, land surface, clouds, radiation and other processes modulate the regional
25 response to enhanced warming. Spatial pooling of climate change signals enhances the statistical robustness
26 of the observed and projected trends (Fischer et al., 2013).

27
28 Regional climate change simulations from Euro-CORDEX have been assessed for levels of global warming
29 at 1.5 and 2.0°C (Ruti et al., 2016b; Schaller et al., 2016; Teichmann et al., 2018). The projections indicate
30 enhanced local warming also at relatively low global warming levels, particularly towards the north in
31 winter. At approximately 50°N a divide between a wet (north) and dry (south) trend is projected (Jacob et al.,
32 2018). RCM results can diverge and may both attenuate and amplify the GCM signals (Giorgi et al., 2016).

33
34 Precipitation extremes, particularly on daily and shorter time scales, are projected to increase even for
35 regions where the mean precipitation is projected to decrease (Ban et al., 2015; Rajczak and Schär, 2017;
36 Trambly and Somot, 2018).

37
38 Figure Atlas.59: shows projected changes in maximum and minimum extreme temperature and extreme
39 precipitation, derived from the CMIP5 subset ensemble (see Section Atlas.3 for details on observations and
40 model selection). The [preliminary] results show a consistent meridional gradient of changes in heavy
41 precipitation, with more heavy precipitation days in NEU and a tendency for a reduced frequency in the
42 southern part of MED. The number of warm nights and warm days is increasing throughout Europe, with
43 larger changes in southern Europe and along the North Sea and Atlantic coast (Ouzeau et al. 2016).

44
45
46 **[START FIGURE ATLAS.59: HERE]**

47
48 **Figure Atlas.59:** Projected changes in maximum and minimum temperature and extreme precipitation from CMIP5 for
49 the European region, derived from the Interactive Atlas. (a-c) Daily rainfall amount corresponding to
50 the 95th percentile (P95, in mm/day) defining ‘very wet days’ for (a) the observational reference
51 (EWEMBI) and (b) the CMIP5 subset (ensemble mean), for the reference period 1986–2005. (c)
52 Relative change in frequency of very wet days (days exceeding the P95 threshold) for the future
53 2081–2100 period (RCP8.5). Similar results in (d–f) and (g–i) for absolute daily minimum and
54 maximum temperature corresponding to the 90th percentile (P90, defining ‘warm nights’ and ‘warm
55 days’, respectively) and the corresponding changes in frequency for the 2081–2100 period (RCP8.5).

1 The corresponding results for the EURO-CORDEX dataset, as well as similar analysis for other
2 indices, are available at the Interactive Atlas (<http://ipcc-atlas.ifca.es>).

3
4 **[END FIGURE ATLAS.59: HERE]**

5
6
7 Figure Atlas.60: shows results for the climate change response for land grid points in northern European in
8 winter and in southern European in summer for a number of precipitation indices, for different global mean
9 warming levels. A clear positive precipitation response is visible in winter for northern European at 3°
10 warming levels, both for mean precipitation and the mean wet-day precipitation and extreme precipitation. In
11 southern European in summer, more land area is experiencing reductions of mean precipitation; in particular,
12 the number of wet days is reduced and the number of consecutive dry days increased. [*Placeholder for*
13 *further analysis in the SOD*].

14
15
16 **[START FIGURE ATLAS.60: HERE]**

17
18 **Figure Atlas.60:** [*Placeholder for analysis to be carried out with the climate4R hub*] Probability distribution functions
19 of land fraction experiencing a certain change, compared to the reference period, for some
20 precipitation indices under 1.5°C (black), 2°C (blue), and 3°C (red) of global mean warming,
21 respectively. First column refers to NEU in DJF and second column to SEU in JJA. Results are shown
22 as median (thick lines) and interquartile range (thin lines) of the individual RCMs' probability
23 distribution functions. Units are standard deviation of the 30-year (1981–2010) time series of the
24 index. (From Dosio and Fischer, 2017)

25
26 **[END FIGURE ATLAS.60: HERE]**

27
28
29 For a large part of the European continent, inconsistent climate change signals between GCMs and RCMs is
30 shown for surface shortwave radiation (Bartók et al., 2017; Gutiérrez et al.), surface temperature and
31 precipitation (Boé et al. *in prep.*; Fernández et al., 2018; Sørland et al., 2018). This is especially true for the
32 summer season in which RCM ensembles warm and dry significantly less than their corresponding driving
33 GCM ensemble. It is unclear yet if RCMs or GCMs are the more reliable sources of information for large-
34 scale climate change over Europe. Some authors claim that RCMs are more realistic because having a
35 smaller bias for the present climate (Sørland et al., 2018), or better cloud representation (Bartók et al., 2017).
36 Other authors claim that GCMs are more reliable due to representation of aerosol forcing and air-sea
37 coupling that is missing in many RCMs (Boé et al. *in prep.*; Gutiérrez et al. *in prep.*).

38
39 Multi-model ensembles of ocean-atmosphere coupled RCM-based climate change projections within Med-
40 CORDEX and the Baltic and North Seas now allow climate change assessments for air-sea fluxes and ocean
41 variables there while taking into account various sources of uncertainty. Darmaraki et al. (2019) used an
42 ensemble of five fully coupled RCMs and a total of 11 projections to assess the future evolution of the
43 Mediterranean SST and related marine heatwaves at high resolution. By the end of the 21st century and
44 under RCP8.5, Mediterranean extreme SSTs (99th daily percentile) are expected to rise by 3.6°C,
45 significantly more than the annual mean SST increase (3.1°C). Despite different methodologies and time
46 periods, it is *likely* that Med-CORDEX RCM and CMIP5 GCM results agree well on the Mediterranean
47 SST warming rate (Darmaraki et al., 2019; Mariotti et al., 2015). Similarly, an ensemble with one coupled
48 atmosphere-ocean-ice RCM for the Baltic Sea and the North Sea downscaling five different GCMs show that
49 both seas undergo warming, strong freshening and, for some simulations, changes in the circulation as
50 regional warming continues (Gröger et al., 2015). For the same model ensemble, (Dietrich et al., 2019) found
51 spatially non-uniform changes in air-sea interaction over the North Sea indicating the importance of
52 simulating the coupled system.

53
54 By 2100 and under RCP8.5, RCM simulations project an average annual increase in the frequency, length
55 and intensity of long-lasting marine heatwaves compared to the present-day climatology (Darmaraki et al.,
56 2019). Their evolution is found to be mainly due to an increase in the mean SST but increased daily SST

1 variability also plays a noticeable role.

2
3
4 Many studies have assessed the potential local-to-regional impacts of altered climate conditions over Europe.
5 For instance, increasing precipitation over Norway is projected to lead to increases in local flooding
6 magnitudes (Hanssen-Bauer et al., 2017). Other studies include the assessment of solar power (Gutiérrez et
7 al. *in prep.*), the robustness of temperature and precipitation impacts, increases in the frequency of the low-
8 level jet off the Iberian coast (Cardoso et al., 2016) and drought increases over the Czech Republic. Record
9 future daily temperature are projected to increase over France (Bador et al., 2017) with surface daily
10 maximum temperatures above 50°C. Increased temperature extremes are expected to occur as the world
11 crosses the 1.5 and 2°C thresholds of global mean warming (Jacob et al., 2018; Teichmann et al., 2018;
12 Vautard et al., 2013).

13
14
15 *Atlas.5.6.3.3 New experimental designs, particularly those involving CPMs: time slice simulations,*
16 *surrogate warming experiments*

17
18 Although still in its infancy, climate change modeling at convection-permitting scales holds great promise.
19 The CORDEX Flagship Program is creating a first-of-its-kind ensemble of climate experiments using
20 convection-permitting models for the extended alpine domain (Coppola et al., 2018). Initial indications are
21 that it substantially improves projections, in particular for precipitation on daily and shorter time scales
22 (Kendon et al., 2016). Due to their computational cost, future CPRCM simulations are usually time slice
23 experiments. Approaches to generate representative lateral boundary forcing capturing the spread of GCM
24 projections are under continuous development (Dai et al., 2017). Work is also under way to combine the best
25 of dynamical and statistical approaches (Sun et al., 2015; Walton et al., 2015). A number of techniques exists
26 to produce scenarios of future, unprecedented weather events that may assist in enriching the visualization of
27 climate change characteristics. Attema et al. (2014) and Lenderink et al. (2019) have applied a so-called
28 "surrogate warming experiment" in which a recent episode of weather conditions, captured in a limited-area
29 NWP model, is placed in a warmer world by repeating the NWP simulation with elevated temperatures in the
30 boundary and initial conditions.

31
32
33 *Atlas.5.6.3.4 National climate change scenario's, their method of aggregating climate projections, and the*
34 *fit-for-purpose to assess climate change impacts*

35
36 Many European countries have a national climate change assessments, each with its own method of
37 aggregating and presenting climate projections (Table Atlas.21:). Most national programs utilize global and
38 regional climate model output collected in programs such as CMIP5, PRUDENCE, ENSEMBLES and
39 CORDEX. In some cases, these model results are transferred into quantitative information on regional
40 climate change features, in others they are used to serve as benchmark for a national resource to generate this
41 quantitative information. For example, Klima-i-Norge 2100 in Norway downscales and assesses a 10-
42 member subset of the Euro-CORDEX ensemble (Hanssen-Bauer et al., 2017) while in Sweden a large
43 ensemble of GCM simulations and scenarios downscaled by a single (national) regional climate model are
44 evaluated (Kjellström et al., 2016). For climate change impact studies and work with adaptation to climate
45 change, bias adjustment and further downscaling to high resolution (4 × 4 km) with empirical methods have
46 been employed to tailor model output to the user's needs. The French national climate change assessment
47 (Ouzeau et al. 2016) and related web services – such as the DRIAS service (Lémond et al., 2011) – are based
48 on the 12-km Euro-CORDEX projection simulations available at that time. Similarly, the Spanish National
49 Adaptation Plan (Escenarios-PNACC 2017) is based on the high-resolution Euro-CORDEX dataset, and
50 includes as well statistical downscaled data for hundreds of stations using several downscaling methods
51 (Sánchez et al., 2017). In the Netherlands, van den Hurk et al. (2014) aggregated 245 CMIP5 projections into
52 four discrete storylines with different large-scale climatic drivers, allowing for a comprehensive societal
53 impact assessment of a wide variety of regional climate change features.

54
55 A trans-European evaluation and intercomparison of the different approaches, assumptions, their

1 implications and potential inconsistencies has yet to be performed.

2
3
4 **[START TABLE ATLAS.21 HERE]**

5
6 **Table Atlas.21:** Overview of national climate change assessments

Country	Reference Period	Time Horizons	RCPs or Emissions Scenarios
Austria (2015) ^a	1971-2000	2021–2050, 2071–2100	RCP4.5, RCP8.5
Belgium (2015) ^b	Not defined explicitly	30, 50 and 100 years ahead	Low, medium, high (RCP4.5 and RCP8.5 used)
Denmark (2014) ^c	1986–2005	2046–2065, 2081–2100	RCP2.6, RCP4.5, RCP6.0, RCP8.5
Finland (2016) ^d			
France (2014?) ^e	1976–2005	2021–2050, 2041–2070, 2071–2100	RCP 2.6, RCP4.5, RCP8.5
Germany (2015) ^f	1961–1990	2021–2050, 2071–2100	Range of models (A1B model runs used)
Ireland (2018) ^g	1971–2000	2021–2050, 2071–2100	RCP2.6 and RCP8.5 (also runs for RCP4.5 used)
Netherlands (2014) ^h	1981–2010	Around 2030, 2050, 2085	4 based on range of change of global temperature + circulation (runs for RCP4.5–8.5 used)
Norway (2017) ⁱ	1971–2000	2031–2060, 2071–2100	RCP4.5, RCP8.5
Portugal (2015?) ^j	1971–2000	2011–2040, 2041–2070, 2071–2100	RCP4.5, RCP8.5
Spain (2017) ^k	1971–2000	2011–2040, 2041–2070, 2071–2100	RCP4.5, RCP8.5 (additional scenarios and periods for statistical downscaling)
Sweden (2014) ^l	1971–2000	2011–2040, 2041–2070, 2071–2100	RCP2.6, RCP4.5, RCP8.5 (A1B)
Switzerland (2018) ^m	1981–2010	2020–2049, 2045–2074, 2070–2099	RCP2.6, RCP4.5, RCP8.5
United Kingdom (2018) ⁿ	1981–2010, 1961–1990	2020–2039 to 2080–2099 (subsequent 20-year periods)	RCP2.6, RCP4.5, RCP6.0, RCP8.5

7 Notes:

8 (a) www.bmlfuw.gv.at/umwelt/klimaschutz/klimapolitik_national/anpassungsstrategie/klimaszenarien.html

9 (b) www.kuleuven.be/hydr/cc/CCI-HYDR_rp.htm

10 (c) www.dmi.dk/fileadmin/user_upload/Rapporter/DKC/2014/Klimaforandringer_dmi.pdf

11 (d) www.geophysica.fi/pdf/geophysica_2016_51_1-2_017_ruosteenoja.pdf

12 (e) www.drias-climat.fr/decouverte

13 (f) www.kliwas.de

14 (g) www.epa.ie/pubs/reports/research/climate/Research_Report_244.pdf

15 (h) www.climatescenarios.nl

16 (i) klimaservicesenter.no/faces/desktop/scenarios.xhtml

17 (j) portaldoclima.pt/en

18 (k) escenarios.adaptecca.es, www.aemet.es/es/serviciosclimaticos/cambio_climat

19 (l) www.smhi.se/en/climate/climate-scenarios

20 (m) www.meteoswiss.admin.ch/home/latest-news/news/climate-scenarios-ch2018.html

21 (n) www.metoffice.gov.uk/research/collaboration/ukcp

22
23 **[END TABLE ATLAS.21 HERE]**

1 *Atlas.5.7 North America*

2

3 **Climate of North America**

4

5 The climate of North America is characterized by diverse spatial and temporal scales and variabilities. North
6 America is generally well covered by the observational network and used as a test-bed for varieties of
7 climate model intercomparison projects. However, most of the global climate models do suffer severe biases
8 including simulation of Low-Level Jet, diurnal convection, hurricane, meso-scale convective systems. These
9 model biases have limited our understanding of the mechanisms responsible for climate change and its
10 impact based on global climate models. Therefore, different types of regional climate models have been
11 developed and used for climate change research. In this subsection on North America, the Atlas specifically
12 focuses on reviewing CORDEX and related literature on North America. It builds and expands on to
13 complement the assessment of Chapter 11 on extremes, the assessment of relevant hazards in Chapter 12 and
14 information on observed and other aspects of projected changes in the climate system in other WGI chapters
15 whilst taking into consideration the work of the WGII regional chapter. The Interactive Atlas then presents
16 the different regional information that has been assessed in these chapters and in the CORDEX literature
17 assessed in the Atlas, including the different climate variables and indices, and climate processes and how
18 these are evaluated and analysed.

19

20 In AR5 assessment, regional aspects of North American climate change were reviewed in WGI and WGII. In
21 summary, some of the climate change features over North America have been attributed to anthropogenic
22 causes with *very high or high confidence*, such as severe heat, heavy precipitation, declining snowpack,
23 temperature related stress on ecosystem and crop yields. However, human health impact from extreme
24 climate events have been observed without confirmation on attribution of its cause to climate change related
25 trends.

26

27

28 *Atlas.5.7.1 Observations, trends and attribution*

29

30 It is *likely* that North American has experienced both warming temperature and a general increase in
31 precipitation in the 20th and early 21st century. For example, the annual mean temperature and the annual
32 total rainfall have increased over the contiguous United States of America (USA) (Figure Atlas.61:). At the
33 same time, extreme climate conditions, such as heavy precipitation has increased in the 20th century (Figure
34 Atlas.62: and heat stress during summer season has also increased throughout different reanalyses though
35 areas of significant change (stippled) do vary across these datasets (Figure Atlas.63:). This increase in
36 extreme hot days is accompanied by observed decreases in frost days over much of North America. There
37 are regional contrasts in terms of where these observed changes stand out. For example, the eastern USA and
38 Pacific Northwest have received more rainfall than the rest of North America in the past.

39

40

41 **[START FIGURE ATLAS.61: HERE]**

42

43 **Figure Atlas.61:** (a) Annual averaged temperature for the continental USA. The linear trend for the entire period is
44 0.06°C per decade. The linear trend for the 1950–2006 period is 0.15°C per decade and for the 1970–
45 2006 period is 0.31°C per decade. (b) Annual total precipitation for the continental USA, 1901–2006.
46 The linear trend during the 1901–2006 period is 4.5 mm per decade and is 12.1 mm per decade for the
47 1950–2006 period. The smoothed black lines were generated with a 13-point binomial filter. (Figure 1
48 of Easterling et al. (2007))

49

50 **[END FIGURE ATLAS.61: HERE]**

51

52

53 **[START FIGURE ATLAS.62: HERE]**

54

55 **Figure Atlas.62:** Time series (1895–2008) of national average heavy precipitation event index (HPEI) for the entire
56 year (annual, black) for August through October (ASO, blue), and for heavy events associated with

1 tropical cyclones (TC, red). The HPEI is normalized such that the annual time series averages 1.0. The
2 values for other periods indicate the fractional contribution of that season to the total (Figure 1 of
3 Kunkel et al. (2016))
4

5 **[END FIGURE ATLAS.62: HERE]**

6
7
8 **[START FIGURE ATLAS.63: HERE]**

9
10 **Figure Atlas.63:** Trends (in °C/decade) in reanalyses maximum Heat Index (HI_{max}). (a) Intermediate time period
11 trends for NNRA1 and (b) shorter time period trends for six reanalyses (Figure 7 of Grotjahn and
12 Huynh, 2018)
13

14 **[END FIGURE ATLAS.63: HERE]**

15 16 17 *Atlas.5.7.2 Assessment of model performance*

18
19 North America can be divided into several characteristic climatic regions (Figure Atlas.64:), which can be
20 used in evaluation of regional climate model performance (see Figure Atlas.65:, Martynov et al. (2013)).
21 Regional climate models (RCMs) in CORDEX generally have higher spatial resolution and are expected to
22 resolve the regional climate information better than GCMs.
23

24
25 **[START FIGURE ATLAS.64: HERE]**

26
27 **Figure Atlas.64:** Subdomains used in model evaluation over North America (Figure 6 of Martynov et al., 2013).
28

29 **[END FIGURE ATLAS.64: HERE]**

30
31
32 **[START FIGURE ATLAS.65: HERE]**

33
34 **Figure Atlas.65:** Interannual correlation coefficients between precipitation and 2-m temperature in CRCM5 simulation
35 (black bars) and the reference base of ERA-Interim, CRU TS3.10 and UDel for temperature (red
36 bars), for (a) JJA and (b) DJF. Hollow diamonds show the correlation coefficients between the biases
37 of simulated precipitation and 2-m temperature values from corresponding reference values. (Figure 7
38 of Martynov et al., 2013).
39

40 **[END FIGURE ATLAS.65: HERE]**

41
42
43 High-resolution regional climate modelling is important for areas with complex terrain, such as the
44 Intermountain Region of the western USA between the Cascade-Sierra range and the Rocky Mountains (see
45 Figure Atlas.66:a). Seasonal cycle of precipitation over the Intermountain Region is a combination of the
46 annual and the semiannual cycles. The simulated annual cycles are generally too strong, and the winter
47 precipitation is too large. On the other hand, the semiannual phases are well captured by the regional climate
48 models in the North American Regional Climate Change Assessment Program (NARCCAP) (Figure
49 Atlas.66:).
50

51
52 **[START FIGURE ATLAS.66: HERE]**

53
54 **Figure Atlas.66:** (a) Orography and (b) cold-season rainfall (November–May, from UDEL) of the Intermountain
55 Region. The major mountain ranges are outlined by redlines. (c) to (g) Monthly rainfall histogram of
56 UDEL, averaged from the five regions indicated in (b), superimposed with the corresponding

1 precipitation of the NARR (thick black line) and all RCMs (coloured lines). Note the precipitation
2 scale in (c) is twice of that in (d) to (g). The abbreviations of the RCMs and their designated colours
3 are indicated under (b). (Figure 1 of Wang et al., 2009)
4

5 **[END FIGURE ATLAS.66: HERE]**
6
7

8 Regional climate models also have been used to evaluate for extreme rainfall and temperature. In general, the
9 annual cycle and spatial patterns of extreme temperature are generally better than those of extreme
10 precipitation (Figure Atlas.67: and Figure Atlas.68:, respectively). It has been suggested that differences in
11 physical parameterizations of rainfall could be a contributing factor to such differences in extreme
12 temperature and precipitation (Whan and Zwiers, 2016).
13

14
15 **[START FIGURE ATLAS.67: HERE]**
16

17 **Figure Atlas.67:** Average of annual TXx difference from ANUSPLIN+Livneh in (a) CanRCM4, (b) CanRCM4-022,
18 (c) CanRCM4-noSN, (d) CanRCM4-NCEP2, (e) CRCM5, (f) NARR, (g) ERA-Interim, (h) annual
19 mean in ANUSPLIN + Livneh. Stippling in (a) to (g) indicates pixels where differences are not
20 significant at the 5% significance level from a Student's t-test. (Figure 3 of Whan and Zwiers, 2016)
21

22 **[END FIGURE ATLAS.67: HERE]**
23
24

25 **[START FIGURE ATLAS.68: HERE]**
26

27 **Figure Atlas.68:** Averages of annual Rx5day difference from ANUSPLIN + Livneh in (a) CanRCM4, (b) CanRCM4-
28 022, (c) CanRCM4-noSN, (d) CanRCM4-NCEP2, (e) CRCM5, (f) NARR, (g) ERA-Interim, (h)
29 annual mean in ANUSPLIN + Livneh. Stippling in (a) to (g) indicates pixels where differences are not
30 significant at the 5% significance level from a Student's t-test. (Figure 9 of Whan and Zwiers, 2016)
31

32 **[END FIGURE ATLAS.68: HERE]**
33
34

35 *Atlas.5.7.3 Assessment of projections* 36

37 Figure Atlas.69: shows the projected change in the mean 2-m temperature between periods 2071–2100 and
38 1981–2010, for DJF (a–d) and JJA (e–h), in the CRCM5 simulations (left) and the corresponding CGCM
39 simulations (right). Generally, regional climate modelling simulations with CRCM5 are similar to those with
40 CGCM, i.e. the latter being the dominant factor in the projections. Nevertheless, in terms of precipitation,
41 there still exist differences between regional climate model and global climate model simulations (see Figure
42 Atlas.70:).
43
44

45 **[START FIGURE ATLAS.69: HERE]**
46

47 **Figure Atlas.69:** Changes in the DJF (a–d) and JJA (e–h) average 2-m temperature in the period of 2071–2100
48 compared to 1981–2010, for CRCM-Can (a, e), CanESM2 (b, f), CRCM-MPI (c, g) and MIP-ESM-
49 LR (d, h) (Figure 14 of Šeparović et al., 2013).
50

51 **[END FIGURE ATLAS.69 HERE]**
52
53

54 **[START FIGURE ATLAS.70: HERE]**
55

56 **Figure Atlas.70:** Same as Figure Atlas.69: but for precipitation (Figure 15 of Šeparović et al., 2013)

1
2 **[END FIGURE ATLAS.70 HERE]**
3
4

5 Due to their higher spatial resolution, RCMs are used to provide more complex regional climate projections.
6 One example is the simulation of Rain-On-Snow events (ROS), which have serious impacts on various
7 sectors through hazards such as floods (e.g. Putkonen and Roe (2003)). ROS is *likely* to decrease due to
8 reducing snowfall and snow cover, but to increase due to increasing rainfall days under warmer climate (Il
9 Jeong and Sushama, 2018). Projected changes to the number of ROS days show similar spatial patterns with
10 those of ROS amount. Generally ROS runoff for January–May is projected to decrease due to decreasing
11 Snow Water Equivalent (SWE) in the future. However, the range between the minimum and the maximum
12 indicates uncertainty in projections (see Figure Atlas.71:).
13

14
15 **[START FIGURE ATLAS.71: HERE]**
16

17 **Figure Atlas.71:** Ensemble-averaged values of three ROS characteristics for the January–May months for the current
18 (1976–2005) period (first column) and minimum, mean, and maximum projected changes (%) to the
19 characteristics for the future (2041–2070) period (second–forth columns), based on the three current
20 and six future RCM-GCM simulations, respectively. Zonally averaged values of projected changes to
21 the three characteristics are also shown in fifth column (Figure 8 of Il Jeong and Sushama, 2018).
22

23 **[END FIGURE ATLAS.71 HERE]**
24
25

26 0 shows projected changes in high and low extreme temperature and extreme precipitation, derived from the
27 subset of CMIP5 ensemble (left column) along with the 20th century mean (1986–2005) of the observation
28 and that of the CMIP5 for validation. The [*preliminary*] results show (i) increasing heavy precipitation along
29 coastal regions, (ii) overall increasing number of warm nights and warm days throughout North America,
30 with larger changes in southern and central North America except over mountainous regions.
31

32
33 **[START FIGURE ATLAS.72 HERE]**
34

35 **Figure Atlas.72:** (a–c) Daily rainfall amount corresponding to the 95th percentile (P95, in mm/day) defining ‘very wet
36 days’ for (a) the observational reference (EWEMBI) and (b) the CMIP5 subset (ensemble mean), for
37 the reference period 1986–2005. (c) Change in frequency of very wet days for the future 2081–2100
38 period (RCP8.5) defined as exceeding the historical P95 threshold (results shown as relative change,
39 %). Similar results in (d–f) and (g–i) for absolute daily minimum and maximum temperature amounts
40 corresponding to the 90th percentile (P90, defining ‘warm nights’ and ‘warm days’, respectively) and
41 the corresponding changes in frequency for the future 2081–2100 period (RCP8.5) defined as
42 exceeding the historical P90 threshold (results shown as relative change, %). Similar analysis for other
43 indices and scenarios (including warming levels) are available at the Interactive Atlas ([http://ipcc-
44 atlas.ifca.es](http://ipcc-atlas.ifca.es)).
45

46 **[END FIGURE ATLAS.72 HERE]**
47
48

49 *Atlas.5.8 Small Islands*

50
51 *[Material will be added into this section from identified but not yet active Contributing Authors in the SOD.]*
52

53 *Atlas.5.8.1 Observations, trends and attribution*

54
55 *Atlas.5.8.2 Assessment of model performance*
56

1
2
3
4
5
6
7
8
9
10
11
12
13
14
15
16
17
18
19
20
21
22
23
24
25
26
27
28
29
30
31
32
33
34
35
36
37
38
39
40
41
42
43
44
45
46
47
48
49
50
51
52
53
54

Atlas.5.8.3 Assessment of projections

Atlas.5.9 Oceans

[Material will be added into this section from identified but not yet active Contributing Authors in the SOD.]

Atlas.5.9.1 Observations, trends and attribution

Atlas.5.9.2 Assessment of model performance

Atlas.5.9.3 Assessment of projections

Atlas.5.10 Polar regions

Atlas.5.10.1 Arctic

The Arctic has polar climate which is governed by mid-latitude atmospheric circulation, baroclinicity at the polar front, the planetary wave meanders of the Jetstream and blocking highs. The Arctic temperatures have increased from the mid-1950s to 2017, and in particular during winter (October–May) (Box et al., 2019). The potential for Arctic climate to change due to increased greenhouse gases was established in modelling in the 1980s (Manabe and Stouffer, 1980) and clearly demonstrated in more recent observational studies (Serreze et al., 2000). A number of physical processes contribute to amplified Arctic temperature variations as compared to the global temperature in particular surface albedo feedbacks and sea-ice extent (Screen and Simmonds, 2010).

Atlas.5.10.1.1 Assessment of observations, trends and attribution

The findings of the most recent IPCC reports, AR5 and SR1.5, put current Arctic temperatures in to a millennial context. A recent multi-proxy 2000-year Arctic temperature reconstruction shows that temperatures during the first centuries were comparable or even higher than during the 20th century (Consortium et al., 2013; Hanhijärvi et al., 2013). During the Medieval Climate Anomaly (MCA; around 950AD–1400AD), portions of the Arctic and sub-Arctic experienced periods warmer than any subsequent period, except for the most recent 50 years (Kaufman et al., 2009; Kobashi et al., 2010, 2011; Spielhagen et al., 2011; Vinther et al., 2010). Tingley and Huybers (2013) provided a statistical analysis of northern high-latitude temperature reconstructions back to 1400 and found that recent extreme hot summers are unprecedented over this time span. Marine proxy records indicate anomalously high SSTs north of Iceland and the Norwegian Sea from 900 to 1300, followed by a generally colder period that ended in the early 20th century. Modern SSTs in this region may still be lower than the warmest intervals of the 900–1300 period (Cunningham et al., 2013). Further north, in Fram Strait, modern SSTs from Atlantic Water appear warmer than those reconstructed from foraminifera for any prior period of the last 2000 years. It is therefore assessed that despite the uncertainties, there is *sufficiently strong evidence* that it is *likely* that there has been an anthropogenic contribution to the very substantial warming in Arctic land surface temperatures over the past 50 years.

It appears that recent Arctic changes are in response to a combination of global-scale warming, from warm anomalies from internal climate variability on different time scales, and are amplified from multiple feedbacks. For example, when the 2007 sea ice minimum occurred, Arctic temperatures had been rising and sea ice extent had been decreasing over the previous two decades (Screen and Simmonds, 2010; Stroeve et al., 2007). Further, the Arctic-wide increases of temperature in the last decade contrast with the episodic

1 regional increases in the early 20th century, suggesting that it is *unlikely* that recent increases are due to the
2 same primary climate process as the early 20th century.
3

4 The Arctic has warmed at more than twice the global rate over the past 50 years (Box et al., 2019). The
5 greatest increase of more than 2°C since 1960 occurred during the cold season. However, Chung et al. (2013)
6 estimated that the 1979–2011 domain-average air surface temperature for the 70°N–90°N region showed a
7 clear warming trend, both for annual and seasonal means. On the Arctic scale, Matthes et al. (2015) showed
8 widespread decreases in extreme cold spells, although there are small areas of statistically significant
9 increases in cold spells in Siberia. Changes in extreme warm spells were found to be generally small
10 throughout the Arctic except in Scandinavia, where increases of up to 2.5 days per decade have occurred.
11 Long cold spells (cold events lasting more than 15 days) have almost completely disappeared since 2000
12 (Arctic Monitoring and Assessment Programme, 2017). Further, above 64°N the satellite-observed rate of
13 warming since 1981 was $\sim 0.60 \pm 0.07^\circ\text{C}$ per decade in the Arctic. The trend in temperature over sea ice
14 covered regions was estimated to be 0.47°C per decade (*very likely* between 0.37°C and 0.57°C per decade at
15 90% confidence level), whereas the trend was significantly higher at 0.77°C per decade (*very likely* between
16 0.60°C and 0.94°C per decade) over Greenland (Comiso and Hall, 2014). Graham et al. (2017) estimated a
17 positive trend from 1980 to 2016 in the maximum winter 2-m air temperature of 0.70°C per decade at the
18 North Pole, but smaller than the mean winter trend of 1.27°C per decade. There was a positive trend in the
19 overall duration of winter warming events ($T_{2\text{m}} > -10^\circ\text{C}$) for both the North Pole region (4.25 days per
20 decade) and Pacific Central Arctic (1.16 days per decade), due to an increased number of events of longer
21 duration. In the permafrost region of the Northern Hemisphere annual air temperatures showed trends of
22 0.13°C per decade for 1901–2014, 0.40°C per decade for 1979–2014, and 0.32°C per decade during the
23 period 1998–2014. Winter air temperatures showed the greatest increase during 1901–2014, while autumn
24 air temperatures increased the most during 1979–2014. Regarding trends in cold spells during winter and
25 summer a widespread decrease occurred of up to -4 days per decade (Matthes et al., 2015a). Changes in
26 warm spells are mostly small throughout the Arctic less than ± 1 day per decade and statistically not
27 significant.
28

29 Observational records (1966–2010) from 517 historical Russian surface weather stations over northern
30 Eurasia examined changing precipitation characteristics (Ye et al., 2016) providing numbers and
31 geographical distribution of mean seasonal precipitation total, frequency, and intensity. Higher precipitation
32 intensity but lower frequency and little change in annual precipitation total occurred. Positive trend in
33 precipitation intensity in all seasons, strongest in winter and spring, weakest in summer were observed.
34 Precipitation intensity increased at a rate of about 1–3% per each degree of air temperature increase. Further,
35 precipitation frequency shows predominantly decreasing trend in the majority of stations for all seasons. In
36 the present-day climate, the mean annual precipitation in the Arctic (70°N–90°N) is dominated by snowfall,
37 with $65 \pm 5\%$ of precipitation currently falling in solid form (this model-mean value compares favourably to
38 the $68 \pm 2\%$ as evaluated from the observationally driven JRA-55 reanalysis) (Bintanja and Andry, 2017). A
39 type of extreme event with major impact in the Arctic is freezing rain, or rain-on-snow events. For example,
40 Hansen et al. (2014) examined the recent occurrence of such events in Svalbard and concluded that the
41 frequency of rain-on-snow events is *likely* to increase in the Arctic (Arctic Monitoring and Assessment
42 Programme, 2017). Further, Groisman et al. (2016) provided a long-term climatology of freezing rain and
43 freezing drizzle events for the past four decades, and assessed changes in the frequency and intensity of these
44 events (e.g. by comparing the 2005–2014 period to the previous 30-year baseline period). In North America
45 north of the Arctic Circle, it was found to increase by about 1 day/yr. Over Norway, freezing rain
46 occurrences increased substantially, especially in the Norwegian Arctic. In European Russia and western
47 Siberia, the frequency of freezing rain somewhat increased (except the southernmost steppe regions and the
48 Arctic regions). The contribution of heavy daily precipitation amounts to the total precipitation has increased
49 over Fennoscandia since 1950 (Hartmann et al., 2013).
50

51 52 *Atlas.5.10.1.2 Assessments of model performance*

53
54 HIRHAM5 RCM can generally reproduce the temporal and spatial variation of the temperature, although a
55 systematic cold bias of around -2°C exists in all seasons (Zhou et al., 2019). Further, the model reproduces

1 the observed warming trend over the entire Arctic, which is more obvious in DJF, MAM, and SON. The
2 temporal evolution of the simulated Arctic warming trends (in the 11-year moving windows) are highly
3 consistent with observations. The spatial distributions of trends in all seasons are in good agreement, with
4 most pronounced warming trends detected over the Arctic Ocean. Matthes et al. (2015b) emphasized based
5 on HIRHAM RCM that the winter temperature biases mainly are negative with a maximum of -10°C .
6 Localized positive biases occur over Central and Eastern Siberia, parts of Alaska, and the Scandinavian
7 Coast having a maximum of 7.5°C . During summer, biases range from -7°C to 1°C . Only few single stations
8 show positive biases, where in general, the biases were negative. In addition, the CCLM RCM simulated
9 high spatial and temporal variability of the winter 2-m air temperature increased in the Arctic in agreement
10 with reanalyses (ASR and ERA-I) (Kohnemann et al., 2017). The maximum warming occurs in the Kara and
11 Barents Sea between March 2003 and 2012 and is responsible for up to a 20°C increase. February and March
12 are the months with the highest 2-m air temperature increase of almost 5°C for 2002/2003–2011/2012,
13 averaged over the ocean and sea ice area north of 70°N . Taking only the ocean areas into account, the RMS
14 error is smaller in the down scaling of CMIP5 than in GCMs in all seasons (Koenigk and Berg, 2015). In
15 winter, the RCA bias is smaller over the Arctic Ocean than in the GCMs, which are substantially colder than
16
17 ERA-I. In spring and autumn, RCA has a small positive temperature bias (1°C – 2°C) over the Arctic Ocean,
18 where in summer, both regional and global simulations are about 1°C colder than ERA-I. Over land, RCA is
19 too cold in both spring and summer. On Figure Atlas.73:, for example, the CMIP5 minimum and maximum
20 temperatures are shown together with observations for the reference period. The relative change in warm
21 nights and days illustrating the greatest change in frequency for the future 2081–2100 (RCP8.5) of more than
22 60% around Svalbard and the Barents Sea is also depicted.

23
24
25 **[START FIGURE ATLAS.73 HERE]**

26
27 **Figure Atlas.73:** (a–c) Daily rainfall amount corresponding to the 95th percentile (P95, in mm/day) defining ‘very wet
28 days’ for (a) the observational reference (EWEMBI) and (b) the CMIP5_subset (ensemble mean), for
29 the reference period 1986–2005. (c) Change in frequency of very wet days for the future 2081–2100
30 period (RCP8.5) defined as exceeding the historical P95 threshold (results shown as relative change,
31 %). Similar results in (d–f) and (g–i) for absolute daily minimum and maximum temperature amounts
32 corresponding to the 90th percentile (P90, defining ‘warm nights’ and ‘warm days’, respectively) and
33 the corresponding changes in frequency for the future 2081–2100 period (RCP8.5) defined as
34 exceeding the historical P90 threshold (results shown as relative change, %). Similar analysis for other
35 indices and scenarios (including warming levels) are available at the Interactive Atlas ([http://ipcc-
36 atlas.ifca.es](http://ipcc-atlas.ifca.es)).

37
38 **[END FIGURE ATLAS.73 HERE]**

39
40
41 Simulated annual mean precipitation (1986–2005) agrees well with the observed precipitation maximum
42 over the Greenland Sea and the Norwegian Sea (Kusunoki et al., 2015). The regional average annual
43 precipitation according to the model is 1.1 mm, which is larger than the observed value of 0.88 mm. This
44 positive bias of 22% is partly due to model overestimates of precipitation in the North Pole region, where
45 observations show a local minimum. The spatial correlation coefficient between observations and
46 simulations is as high as 0.84. Excessive precipitation over Alaska and the western Arctic is consistent with
47 the results of Kattsov et al. (2007), but in this later study the bias over the eastern Arctic and the
48 Norwegian/Barents Sea region is opposite to the results of Kattsov et al. (2007). These differences in the bias
49 distribution can be attributed to differences in used models and in the time periods of the analyses. As an
50 example on Figure Atlas.73: to emphasize the variability in precipitation within the Arctic region, the 95th
51 percentile (P95, in mm/day) CMIP5_subset (ensemble mean; 1986–2005) was compared to observed P95
52 intensity, indicating reasonable similarities.

53
54 Intense precipitation (SDII; Simple Daily Precipitation Intensity Index, defined as the total annual
55 precipitation divided by the number of rainy days (precipitation ≥ 1 mm/day)) simulations reproduce the
56 intense precipitation over the Greenland Sea, but underestimates precipitation over other regions. Arctic

1 average SDII from the model is 8% smaller than the observed value, which originates from the overestimate
2 of the number of rainy days, indicating that the model tends to predict too many weak rainfall events. Spatial
3 correlation coefficient between observations and the simulation is as low as 0.68. Further, the model
4 reproduces the observed R5d (maximum 5-day precipitation total) distribution reasonably well but
5 overestimates it around Svalbard. The Arctic averaged R5d from the model shows a positive bias of 17%.
6 The spatial correlation coefficient between observations and the simulation is 0.69. Boisvert et al. (2018)
7 compared precipitation estimates from eight widely used atmospheric reanalyses over the period 2000–2016
8 for the Arctic Ocean finding that the magnitude, frequency, and phase of precipitation vary drastically,
9 although interannual variability is similar.

10
11 CMIP5 models perform well in simulating twentieth-century snowfall, although there is a positive bias in the
12 multi-model ensemble relative to the observed data in many regions (Krasting et al., 2013). Cold bias
13 contributes to the positive snowfall bias. Lack of spatial resolution in the model topography has a serious
14 impact on the simulation of snowfall. The patterns of relative maxima and minima of snowfall, however, are
15 captured reasonably well by the models. The magnitude of annual snowfall is in better agreement over the
16 eastern half of North America (coincides with the relatively flat terrain and a higher density of stations to
17 capture the regional variations of snowfall), while the largest absolute errors are found in the western part of
18 the continent (consistent with the coarse representation of the Rocky Mountains in the models as well as with
19 biases that may be present in the observational data) (Krasting et al., 2013). Over Eurasia, the snowfall
20 maximum in the central plateau of Siberia is significantly over-simulated by the models by as much as 250–
21 300 cm.

22
23 WRF consistently underestimates extreme precipitation amounts compared to the station observation. scales
24 and interannual variability for widespread extreme events are roughly equivalent to the observed scales
25 (Glisan and Gutowski, 2014). With the exception of Canada East, the location of highest average
26 precipitation was always found in the region favoured for widespread extreme events. Moreover, these
27 regions were located over higher topography and thus indicated a significant orographic contribution to the
28 extreme events.

31 *Atlas.5.10.1.3 Assessment of projections*

32
33 Given plausible increases in GHG concentrations over the next two decades assuming no aggressive
34 mitigation action, recent modelling studies suggest that average autumn and winter Arctic temperatures
35 would increase by 4°C by 2040 and 5°C–9°C by late century. Arctic warming exhibits a very pronounced
36 seasonal cycle, however, with exceptionally strong warming in the winter months up to $14.1 \pm 2.9^\circ\text{C}$ in
37 December and only moderate warming during the summer season (Bintanja and Kriken, 2016). Bintanja
38 and Van Der Linden (2013) also estimated an Arctic winter warming over the 21st century to exceed the
39 summer warming by at least a factor of four, irrespective of the magnitude of climate forcing. Arctic summer
40 warming is surprisingly modest, even after summer sea ice has completely disappeared. Overland et al.,
41 (2004) highlighted the difference between the near-term ‘adaptation timescale’ and the long-term ‘mitigation
42 timescale’ for the Arctic-wide warming, averaged over 60°N–90°N relative to northern hemisphere changes
43 for the winter half of the year (November through May). Only in the latter half of the century do the
44 projections from the RCP4.5 and RCP8.5 emission scenarios noticeably separate. By the end of the century
45 the warming is approximately twice as large under the higher-emission RCP8.5 scenario, pointing to the
46 impact of emission reductions with RCP4.5 (Arctic Monitoring and Assessment Programme, 2017). More
47 specifically under the strong forcing scenario, annual mean surface air temperatures in the Arctic (70°N–
48 90°N) suggest an increase by $8.5 \pm 2.1^\circ\text{C}$ (model-mean value and inter-model standard deviation) over the
49 course of the 21st century (Bintanja and Andry, 2017).

50
51 Future changes in precipitation intensity over the Arctic based on three-member ensemble simulations using
52 a global atmospheric model with a high horizontal resolution (60-km grid) for the period 1872–2099 (228
53 years) were estimated (Kusunoki et al., 2015). The annual mean precipitation, the simple daily precipitation
54 intensity index, and the maximum 5-day precipitation total averaged over the Arctic increased monotonically
55 towards the end of the 21st century. Further, on Figure Atlas.73: a change in the frequency of very wet days

1 for the future 2081–2100 period (RCP8.5) is shown, with values of up to 100%.

2
3 CMIP5 models RCP8.5 and RCP4.5 21st century (2006–2100) simulations however showed a decrease in
4 average annual Arctic snowfall (70°N–90°N), despite the strong precipitation increase. While total Arctic
5 precipitation will increase by about 40%, snowfall will actually diminish. According to Krasting et al. (2013)
6 in the higher-latitude regions, such as Greenland, any decreases in snowfall associated with warming
7 (CMIP5 for RCP4.5 for 2006–2100) are largely overwhelmed by increases in snowfall related to
8 precipitation increases. Climate models project that, at the end of the 21st century under strong forcing
9 (RCP8.5), about 60% of Arctic precipitation could consist of rain; hence, rainfall would become the
10 dominant form of Arctic precipitation. The reduction in Arctic snowfall is expected to be most pronounced
11 during summer and autumn when temperatures would be close to the melting point, but also winter rainfall is
12 projected to intensify considerably. Towards the end of the 21st century (2091–2100), Arctic precipitation is
13 projected to increase by 50 to 60%. In central Arctic, the snowfall fraction would barely remain larger than
14 50%, and precipitation would be dominated by rainfall in much of the Arctic. The most dramatic reductions
15 in snowfall fraction are projected to occur over the North Atlantic and especially the Barents Sea.

16 17 18 *Atlas.5.10.2 Antarctic*

19
20 The current climate in Antarctica and the Southern Ocean is influenced by interactions between the inland
21 ice sheet, the sea, sea ice, and the atmosphere, and their responses to climate drivers, past and present. The
22 Southern Hemisphere polar jet entrain low pressure zones that circulate around Antarctica - these transient
23 weather systems are responsible for transporting moisture into the ice sheet and snowfall formation (King
24 and Turner, 1997). Snowfall is the largest positive component of the Antarctic surface mass balance, both
25 exhibiting significant spatial and temporal variability over the ice sheet highlighted by recent observational
26 and modelling studies (Agosta et al., 2019; Palerme et al., 2014) stressing the importance of high-resolution
27 representation and physical parameterizations adapted for Antarctica. There is a large discrepancy in the
28 recent trends of the East (EAIS) and the West Antarctic ice sheet (WAIS) surface mass balance affecting the
29 total mass balance: EAIS demonstrated an increase in the anomalous snowfall events during the recent two
30 decades with relatively ice loss, while precipitation over WAIS was not enough to compensate for the
31 increasing ice mass loss (Boening et al., 2012; King et al., 2012). Rare anomalous snowfall events have an
32 important contribution to the Antarctic surface mass balance and recent two decades showed an increase in
33 the number and intensity of such events (Lenaerts et al., 2013) related to the enhanced anomalous moisture
34 transport and blocking (Gorodetskaya et al., 2014; Schlosser et al., 2010). This is potentially related to the
35 enhancement of the global hydrological cycle during the last 50 years, as well as changes in the polar jet
36 stream favouring occasional strong meridional moisture transport. Overall the Antarctic ice sheet has been
37 losing mass and its contribution to the global sea level has been recently estimated as much as $2,720 \pm 1,390$
38 billion tons of ice between 1992 and 2017, corresponding to an increase in mean sea level of 7.6 ± 3.9 mm
39 (IMBIE team, 2018).

40 41 42 *Atlas.5.10.2.1 Assessment of observations, trends and attribution*

43
44 Assessment of Antarctic wide station data since the early 1950s has demonstrated considerable warming
45 over the Antarctic Peninsula where in the northern and western parts of the Peninsula temperatures have
46 risen by as much as 0.5°C per decade between 1951 and 2006 (Turner et al., 2014). The temperature record
47 at Byrd station, West Antarctica has revealed a linear increase in annual temperature between 1958 and 2010
48 of similar magnitude ($2.4 \pm 1.2^\circ\text{C}$) and confirmed existing reports of rapid statistically significant warming
49 over West Antarctica in recent decades not only in annual and austral winter and spring, but also during
50 austral summer (Bromwich et al., 2012). A continued increase in temperature could lead to more frequent
51 and longer duration episodes of surface melt over the West Antarctic Ice Sheet. However, longer time series
52 of temperature records in the Antarctic Peninsula region have revealed that this significant warming has halted
53 since the late 1990s (see Figure Atlas.74:), which reflects the strong natural internal variability of this region
54 and was attributed to a greater frequency of cyclonic conditions in the Weddell sea, resulting in cold, south-
55 easterly winds (Turner et al., 2016). Nevertheless, based on a reconstruction of Antarctic mean near-surface

1 temperatures spanning 1958–2012, Nicolas and Bromwich (2014) showed that West Antarctica and the
2 Antarctic Peninsula have undergone significant annual warming of $0.22 \pm 0.12^\circ\text{C}$ per decade and $0.33 \pm$
3 0.17°C per decade, respectively (*high confidence*). However, although the annual warming is of similar
4 magnitude over both the Antarctic Peninsula and West Antarctica, the seasonality and spatial patterns of the
5 warming for these two regions differs considerably. Temperature increases are greatest in winter over the
6 western side, and summer over the eastern side. The results also show a particularly strong difference
7 between the east and west sides of the Transantarctic mountains during winter and spring (cooling / weak
8 warming and strong warming, respectively), consistent with the barrier created by the mountains preventing
9 anomalous maritime air that has penetrated over West Antarctica from reaching East Antarctica where no
10 significant temperature change was found in 20th century (Nicolas and Bromwich, 2014). But recent
11 observations from Queen Maud Land, East Antarctica, show that the snowfall increases unprecedented over
12 the last two millennia and trends in both accumulation and air temperature for period 1998-2016 are
13 significant and positive: $5.2 \pm 3.7\%$ per decade and $1.1 \pm 0.7^\circ\text{C}$ per decade, respectively (Medley et al.,
14 2018). In fact, it is the most rapid warming rate in the 21st century in Antarctic (see Figure Atlas.74:).
15

16 Records for the past 300 years from two ice cores drilled in Ellsworth Land, West Antarctica have shown
17 that annual snow accumulation has increased by around 30% since 1900, and that these increases follow a
18 200-year period characterised by relatively stable conditions. The increases are linked to changes in regional
19 and large-scale circulation, particularly a deepening of the Amundsen Sea Low (*medium confidence*)
20 (Thomas et al., 2015).
21

22 The recent study on relationship between snowfall and surface mass balance (SMB) using unique collocated
23 set of ground-based and in situ remote sensing instrumentation (Micro Rain Radar, ceilometer, automatic
24 weather station, among others) in Dronning Maud Land, East Antarctica has showed that snowfall is not
25 always associated with accumulation and during 38% snowfall events snow is entirely ablated, while local
26 accumulation is often associated with freshly fallen snow being transported from the upwind regions
27 (Souverijns et al., 2018). This is in line with the first estimations of SMB from local precipitation in
28 comparison to other SMB components during 2012 (statistically normal accumulation year), when only half
29 of annual snowfall is accumulated with 23% being removed by surface and drifting snow sublimation and
30 30% by wind erosion and the total annual SMB has been determined by rare strong snowfall events
31 (Gorodetskaya et al., 2015).
32

33 In overall, a few anomalous precipitation events in East Antarctica, e.g. recorded in 2009 and 2011 and
34 attributed to atmospheric rivers (long narrow corridors of anomalously high vertically integrated horizontal
35 moisture transport (Gorodetskaya et al., 2014)), have compensated for the overall Antarctic ice sheet mass
36 loss dominated by WAIS (Boening et al., 2012; King et al., 2012). Examination of ice core records showed
37 that anomalies of this magnitude had not occurred in the last 60 or so years, but comparable anomalies of this
38 size have occurred further back in time (Lenaerts et al., 2013).
39

40 The spatial and temporal distribution of SMB was investigated in the first comprehensive study of a set of 76
41 firn cores retrieved by various expeditions during the past three decades in East Antarctica (Altnau et al.,
42 2015). In the second half of the 20th century, the SMB had a negative trend in the ice shelf cores, but
43 increased on the plateau. It was shown that, at the coast, atmospheric dynamic effects are more important
44 than thermodynamics while on the plateau the temporal variations of SMB and temperature occur mostly in
45 parallel, and thus can be explained by thermodynamic effects. The Southern Annular Mode (SAM) has
46 exhibited a positive trend since the mid-1960s, which is assumed to lead to a cooling and drying of East
47 Antarctica. This was not confirmed by the firn core data.
48

49 Investigated precipitation and synoptic regime for the two contrasting, extreme years 2009 and 2010 at
50 Dome C, Antarctica have shown that a strongly zonal flow in 2010 led to precipitation and temperature
51 minima in 2010, whereas strong amplification of Rossby waves with frequent warm air intrusions in 2009
52 caused high precipitation amounts and new high-temperature records, particularly in winter. This was
53 associated with a strongly positive (negative) SAM index and (positive) negative zonal wave-number 3 index
54 in 2010 (2009) (Schlosser et al., 2016).
55

1 Strong surface melt over the Larsen C ice shelf can occur frequently throughout the dark Antarctic winter,
2 which from 2015 to 2017 contributed ~23% of annual melt fluxes. The peak wintertime intensities can
3 exceed summertime values, when the melt energy is mostly provided by solar radiation. The intense winter
4 surface melt is driven by episodes of warm and dry Foehn winds descending down the leeside of the
5 Antarctic Peninsula, resulting in sustained surface melt fluxes in excess of 200 W/m², which are primarily
6 driven by downward turbulent fluxes of sensible heat (Kuipers Munneke et al., 2018).

7
8 Surface melting of the ice shelves and coastal margins of West Antarctica in recent years is increased due to
9 increased intrusions of warm marine air onto the ice sheet caused by Amundsen Sea blocking anticyclones
10 and the negative polarity of the SAM, which are both related to El Nino conditions (Scott et al., 2019).

11
12
13 **[START FIGURE ATLAS.74: HERE]**

14
15 **Figure Atlas.74:** From Medley et al., 2018. Left: Figure S12 with the annual temperature trends for 1998–2016 at 38
16 AWS and surface stations from MET-READER (Turner et al., 2004). Right: Figure S3. Bias corrected
17 MERRA-2 (Bosilovich, 2015) trends based on comparison with the MET-READER database.
18 Coloured circles show the observed AWS trends from the MET-READER database. The region of
19 influence for the Kohlen AWS is outlined in red. This confirms that warming is likely occurring
20 within the red bounds, but that it is likely not as strong as the AWS at Kohlen since the warming is
21 strongest there.

22
23 **[END FIGURE ATLAS.74 HERE]**

24 25 26 *Atlas.5.10.2.2 Assessment of model performance*

27
28 Evaluation of the ability of 41 global climate models from the CMIP5 project to simulate the forcing fields
29 which would have the greatest impact for regional climate models has demonstrated that fewer than ten
30 models show reasonable biases (Agosta et al., 2015). The rates of precipitation accumulation and air
31 temperature change were underestimated by an ensemble of global climate models, suggesting that
32 projections of the contribution of Queen Maud Land to sea level rise are underestimated, as is also the
33 mitigating impact of enhanced snowfall (Medley et al., 2018).

34
35 Regional climate model studies were used to demonstrate that the record high surface temperatures at
36 Esperanza station (located near the northern tip of the Antarctic Peninsula) observed in March 2015
37 (+17.5°C) was related to an atmospheric river that caused an intensification of the Foehn wind and associated
38 local warming. This resulted not only in record high surface temperatures on the eastern flanks of the
39 Antarctic Peninsula, but also major melt pond formation on the ice shelf and sea ice disintegration east of the
40 Antarctic Peninsula (Bozkurt et al., 2018).

41
42 A high-resolution regional climate model used to investigate the influence of regional and large-scale
43 variability on summer air temperatures over ice shelves fringing the Amundsen Sea Embayment has
44 demonstrated that El Nino episodes are associated with the more frequent occurrence of near-surface air
45 temperatures above the melting point over the ice shelves, i.e. enhanced surface melt. By contrast, the
46 polarity of the Southern Annular Mode and the location of the Amundsen Sea Low were shown to have
47 negligible impact on surface melting of West Antarctic ice shelves (Deb et al., 2018).

48
49 The variability of Antarctic precipitation (both mean and extremes) influenced by four large-scale circulation
50 patterns, namely the Southern Annular Mode, the Southern Baroclinic Annular Mode, and two tropical-
51 teleconnection patterns, was captured in general by a regional climate model (Marshall et al., 2017).
52 However, despite the coarse resolution coupled climate models are able to represent these large-scale
53 circulation patterns, they struggle to correctly represent their associated regional impacts on precipitation.

54
55 Investigated precipitation regime of Dome Fuji, Antarctica, with a combination of observational precipitation
56 data and model data from AMPS (Antarctic Mesoscale Prediction system), which basically employed Polar

1 WRF, has showed that only 60% of the annual precipitation was related to synoptic event-type precipitation
2 caused by warm air advection due to strong ridging of the upper-level flow and 40% of the precipitation fell
3 as diamond dust (Dittmann et al., 2016).

4
5 To examine the sensitivity of Antarctic surface mass balance for the period 1979–2015 to perturbations of
6 sea surface conditions the MAR model was applied and showed reasonable results when lower sea-ice
7 concentrations (i.e. warmer conditions) caused increased precipitation, while higher sea-ice concentrations
8 (i.e. colder conditions) lead to decreased precipitation, which in both cases significantly affected the surface
9 mass balance around the coastal regions. Sensitivity experiments with warmer conditions (i.e. consistent with
10 future climate change) showed surface mass balance anomalies integrated over the entire ice sheet of
11 between 5–13% relative to the present climate (Kittel et al., 2018). Furthermore, for the same period 1979–
12 2015, outputs of MAR together with another RCM RACMO2 (both forced by reanalysis products) were
13 analysed for missing or underrepresented processes in both RCMs (Agosta et al., 2019). The results have
14 showed that the estimation of surface mass balance from both models is similar and confirmed the
15 importance of drifting snow transport, which is not included in MAR and underestimated in RACMO2.
16 Additionally, sublimation fluxes were much larger than previous model-based estimates suggested a need to
17 be better constrained in RCMs. In MAR sublimation represented only 16% of the simulated snowfall loaded
18 at the ground for the year 2015.

19
20 An upgrade in the physics package of RACMO2.3 (relative to RACMO2.1) included changes to the cloud
21 scheme and cloud microphysics, as well as radiative and turbulent schemes, was evaluated on the simulated
22 SMB and its components. The upgrade resulted in a considerable improvement of simulated SMB over the
23 interior of Antarctica, resulting in an almost complete alleviation of any biases. Integrated over the entire
24 grounded ice sheet, the SMB simulated by RACMO2.3 increased to 1793 Gt/yr, an increase of 45 Gt/yr
25 compared to RACMO2.1, and due almost entirely to an increase in snowfall. The changes are attributed to
26 improvements in the representation of cloud microphysics and large-scale circulation patterns, which affect
27 topographically forced precipitation (Van Wessem et al., 2014).

28
29 As an example of regional climate models performance, annual precipitation sums calculated by three RCMs
30 forced with two GCMs all participated in the project Polar-CORDEX (Section Atlas.3.4) are shown on
31 Figure Atlas.75:. All individual outputs and ensemble mean are in accordance with the Antarctic climatology
32 with extremely dry interior of the continent and most precipitation around at coastal area and the Antarctic
33 Peninsula region.

34
35
36 **[START FIGURE ATLAS.75: HERE]**

37
38 **Figure Atlas.75:** Climatological mean of annual precipitation for the reference period 1986–2005 from individual
39 RCMs (lower panel) and their ensemble mean (upper map). RCM data from Polar-CORDEX project.
40 Similar analysis for other indices and scenarios (including warming levels) are available at the
41 Interactive Atlas (<http://ipcc-atlas.ifca.es>).

42
43 **[END FIGURE ATLAS.75 HERE]**

44 45 46 *Atlas.5.10.2.3 Assessment of projections*

47
48 Two-meter air temperature in the future climate of the Antarctic Ice Sheet is expected to increase by 1.8°C–
49 3.0°C in 2100 and 2.4°C–5.3°C in 2200 based on the projections of the regional climate model RACMO2
50 forced by two different global climate models (ECHAM5 and HadCM3) and two different emission
51 scenarios (A1B and E1). Increases in rainfall and snowfall over the next two centuries (which together will
52 contribute 60–200 Gt/yr) will be projected to largely determine future changes in surface mass balance, and
53 that the snowfall would remain an order of magnitude greater than sublimation and runoff would remain
54 small (Ligtenberg et al., 2013).

1
2
3 Projections of temperature change show warming over the whole Antarctic continent, but with different rate
4 and intensity regionally. Change in number of Icing Days (ID) per year, when daily minimum temperature is
5 below 0°C, is shown on Figure Atlas.76: as a demonstration of spatial and temporal distribution of warming
6 for RCP8.5 in 2041–2060 over the reference period 1986–2005. Upper panel of the Figure Atlas.76:
7 demonstrates individual RCM projections and shows that the most effect (almost two months less) is
8 expected over Bellingshausen Sea, West Antarctica. Time series of spatially aggregated values over the
9 whole continent confirms warming as well, since the delta of ID is over 20 days less.

10
11
12 **[START FIGURE ATLAS.76 HERE]**

13
14 **Figure Atlas.76:** Climatological mean of change in icing days (ID) for RCP8.5 in 2041–2060 over the reference period
15 1986–2005 from individual RCMs (upper panel) and time series of spatially integrated indexes (lower
16 panel). RCM data from Polar-CORDEX project. Similar analysis for other indices and scenarios
17 (including warming levels) are available at the Interactive Atlas (<http://ipcc-atlas.ifca.es>).

18
19 **[END FIGURE ATLAS.76 HERE]**

20
21
22 Regional climate model projections have showed that East Antarctica is increasingly *likely* to experience
23 snow accumulation anomalies towards the end of the 21st century attributed to anomalously high snowfall of
24 the scale as during the first half of 2009 in Dronning Maud Land, East Antarctica, resulted in a large mass
25 increase of around 160 Gt. Such enhanced snowfall is expected to significantly mitigate 21st century global
26 sea level rise (Lenaerts et al., 2013).

27
28 CMIP5 models project on average that precipitation for the whole Antarctic continent will increase by
29 between 5.5% (scenario RCP 2.6) and 24.5% (scenario RCP 8.5) by the end of the century, which
30 corresponds to a negative contribution to sea level from –19 mm to –71 mm between 2006 and 2099.
31 However, only around one third of the CMIP5 models agree within $\pm 20\%$ of the snowfall rate observed by
32 the CloudSat satellite for the period 1986–2005 (with the remaining models largely overestimating current
33 Antarctic precipitation). If only these models in relatively good agreement with CloudSat observations are
34 analysed, then larger precipitation changes of between 7.4% and 29.3% are projected to occur by the end of
35 the century, with an associated reduction in sea level from –25 mm to –85 mm between 2006 and 2099
36 (Palerme et al., 2016).

37
38 A combination of observations and regional climate model simulations has showed that the relationship
39 between summer air temperatures and surface melting over Antarctic ice shelves was highly non-linear.
40 Subsequently based on regional climate model projections surface melt over Antarctic ice shelves will
41 double by mid-century for both intermediate and high-emission scenarios. However, between mid and end-
42 of-century the surface melting associated with the high-emission scenario greatly exceeds that of the
43 intermediate-scenario, with melt on several ice shelves under the high-emission scenario (such as Larsen C,
44 Wilkins, George VI) approaching or surpassing intensities that were linked with the collapse of Larsen A and
45 B (Trusel et al., 2015).

46
47 The rate of increase of continental-scale accumulation in SMB is approximated as $5 \pm 1\%$ per °C, based on
48 broad agreement in the results from the different approaches of a combination of ice core records, paleo-
49 simulations, projections by a range of global climate models, and one high-resolution regional climate model
50 projection to robustly constrain the dependence of continental-scale accumulation changes over the Antarctic
51 Ice Sheet on temperature changes (Frieler et al., 2015).

52
53 Projections of all RCMs from Polar-CORDEX for total annual precipitation change in the middle of the 21st
54 century for RCP8.5 show precipitation increasing over the most Antarctic continent corresponding to the
55 different rate and intensity of warming (Figure Atlas.77:). Upper panel of Figure Atlas.77: shows three

1 RCMs ensemble mean and standard deviation demonstrating the maximum increase of precipitation in
2 Bellingshausen Sea with good model agreement.

3
4
5 **[START FIGURE ATLAS.77 HERE]**

6
7 **Figure Atlas.77:** Climatological mean of change in annual precipitation PRCPTOT (mm year⁻¹) for RCP8.5 in 2041–
8 2060 over the reference period 1986–2005 from individual RCMs calculation (lower panel) and RCM
9 ensemble mean (left upper panel) with standard deviation (right upper panel). RCM data from Polar-
10 CORDEX project. Similar analysis for other indices and scenarios (including warming levels) are
11 available at the Interactive Atlas (<http://ipcc-atlas.ifca.es>).

12
13 **[END FIGURE ATLAS.77 HERE]**

14
15
16 Time series of spatially integrated over Antarctic annual and austral summer DJF precipitation change over
17 the reference period 1986–2005 for both RCP4.5 and RCP8.5 from individual RCMs and their ensemble
18 mean (Figure Atlas.78:) demonstrate that the precipitation is expected to increase more for RCP8.5 and
19 annual values rather than less aggressive RCP4.5 and only austral summer season.

20
21 **[START FIGURE ATLAS.78: HERE]**

22
23 **Figure Atlas.78:** Time series of spatially integrated over Antarctic annual (lower panel) and austral summer DJF (upper
24 panel) precipitation change (mm/day) for RCP4.5 (upper panel) and RCP8.5 (lower panel) over the
25 reference period 1986–2005 from individual RCMs (dotted line) and RCM ensemble mean (bold blue
26 line). RCM data from Polar-CORDEX project. Similar analysis for other indices and scenarios
27 (including warming levels) are available at the Interactive Atlas (<http://ipcc-atlas.ifca.es>).

28
29 **[END FIGURE ATLAS.78 HERE]**

30 31 32 *Atlas.5.11 Typological Domains*

33
34 From WGII Cross Chapter Papers: *Biodiversity hotspots (land, coasts and oceans), Cities and settlements by*
35 *the sea, Deserts semi-arid areas and desertification, Mediterranean region, Mountains, Polar regions,*
36 *Tropical forests*

37 38 39 *Atlas.5.11.1 Mountains*

40 41 **The Hindu Kush Himalaya (HKH)**

42
43 The Hindu Kush Himalaya (HKH) encompasses over 4.2 million km² area, and together with Tien Shan
44 mountains form the largest area of permanent ice cover outside of the North and South Poles, and is the
45 origin of 10 major river basins (Sharma et al., 2019). The HKH extend from the Hindu Kush valleys in
46 Afghanistan to the hill and mountain systems of Myanmar. The complex terrain between these regions
47 include the arid and semi-arid regions of the Pamir and Karakoram mountains; the high Himalaya of India,
48 Nepal, and Pakistan; the undisturbed ecology of Bhutan; and the Tibetan Plateau of China (see more details
49 in Sharma et al., 2019).

50
51 The climate is mostly alpine over the Himalaya but varies within HKH significantly with elevation from
52 snow-capped higher elevations to tropical/subtropical climates at lower elevations. The HKH climate
53 modulates the global weather patterns by serving as a heat source in summer and heat sink in winter. The
54 HKH and the elevated Tibetan Plateau exert significant influence on the Asian summer monsoon system.
55 The HKH is sensitive to climate change and variability (see more details in Krishnan et al., 2019).

1 *Atlas.5.11.1.1 Observations, trends and attribution*

2
3 A review by Nengker et al (2018) on past studies confirms the consistent increases in temperature over the
4 Himalayas using regional/local observations, the higher rate of warming in the recent decades over
5 Himalayas and Tibetan Plateau, the season specific responses to warming over Himalayas, the dependency
6 of temperature trends on elevation, among others. This study also assessed the uncertainty in temperature
7 observations over the Himalayas using four datasets (APHROTEMP, CRU, University of Delaware, and
8 NCEP reanalyses), and found that APHROTEMP is the most suitable dataset for model evaluation studies in
9 the period 1970–2005.

10
11 The chapter on unravelling the climate change in the Hindu Kush Himalayan mountains (Krishnan et al.,
12 2019) in the recent HIMAP report (Wester et al., 2019) assessed that for the past five to six decades, the
13 HKH have shown a rising trend of extreme warm events; a falling trend of extreme cold events; and a rising
14 trend in extreme values and frequencies of temperature-based indices (both minimum and maximum). The
15 number of cold nights reduced by 1 night per decade and the number of cold days reduced by 0.5 days per
16 decade, while the number of warm nights increased by 1.7 nights per decade and number of warm days
17 increased by 1.2 days per decade. These analyses used the global land surface daily air temperature data set
18 developed by CMA V1.0 for the 55-year period (1961–2015). The linear trends in temperature over HKH
19 was analysed using the monthly mean, maximum and minimum temperature data provided by the CMA
20 GLSAT–V1.0. The 5° x 5° latitude-longitude grid box temperature anomalies in this dataset were calculated
21 by averaging anomalies for the stations within each grid box during the analysis period 1901–2014 (see
22 Annex 1 in Krishnan et al., 2019).

23
24 Ghimire et al. (2018) has provided an overview of the past studies that reported discrepancies between the
25 observed precipitation datasets over the Himalayas. This study compared three precipitation datasets
26 (APHRODITE, GPCC, and CRU), and concluded that the vertical interpolation method included in the
27 APHRODITE data was important for their study of precipitation in complex topography such as Himalayas
28 where there is a sudden increase in the elevation.

29
30 The HIMAP report analysed the observed precipitation changes in HKH using monthly dataset from CMA
31 GLMP-V1.0 for the period 1901–2013. The observed changes in precipitation extremes over HKH was
32 assessed using the Global Land Daily Precipitation data set V1.0 (CMA GLDP–V1.0) for the period 1961-
33 2013 (see Annex 1 in Krishnan et al., 2019).

34
35
36 *Atlas.5.11.1.2 Assessment of model performance*

37
38 Nengker et al. (2018) evaluated the performance of five CORDEX South Asia RCMs for simulating the key
39 features of the present day (1970–2005) near surface air temperature climatology over the Himalayan region.
40 This study found that this RCM ensemble does exceptionally well in capturing the spatial patterns of
41 temperature climatology over Himalayas for the present climate even though the models showed a
42 significant cold bias. In spite of the general intensification of cold bias with increasing elevation, the RCMs
43 showed a greater rate of warming than the observation throughout entire altitudinal stretch of study region.
44 The simulated rate of warming during winter season was found to be relatively higher at high altitudes. This
45 study also found a seasonal response of RCM performance and its spatial variability to elevation. CORDEX
46 RCMs and their driving CMIP5 GCMs feature low fidelity for Indus Basin watersheds (Hasson et al.,
47 2019b).

48
49 Mishra (2015) reported that the four CORDEX South Asia RCMs used in their study showed larger
50 uncertainty (1–3.6°C in temperature and 18–60% in precipitation) than that of the observations in the
51 Himalayan water towers (e.g., Indus, Ganges, and Brahmaputra river basins). This study showed that the
52 RCMs exhibited large cold bias (6–8°C) and were not able to reproduce the observed warming in the
53 Himalayan water towers.

54
55 Sanjay et al. (2017b) using 13 CORDEX South Asia RCM historical experiments showed that the

1 downscaled seasonal mean temperatures have relatively larger cold bias than their driving CMIP5 GCMs
2 over the hilly subregions within the HKH region. It was also shown that the downscaled RCMs and their
3 driving GCMs overestimated the total precipitation in the HKH subregions during the summer monsoon and
4 winter seasons.

5 Ghimire et al. (2018) evaluated the ability of 11 CORDEX South Asia RCMs for simulating the seasonal
6 precipitation during June to September over the Himalayan region. The RCMs indicated large spread in
7 simulating spatial and temporal distributions of the summer season precipitation over the study region. These
8 high-resolution downscaled precipitation simulations showed dry bias along the foothills of the Himalayas,
9 and in general indicated wet bias at higher elevations.

10
11 The recent HIMAP report (Wester et al., 2019) analysed CMIP5 and CORDEX South Asia projections in the
12 Hindu Kush Himalayan mountains, and assessed that the consensus among models for the HKH region is
13 weak; a result of the region's complex topography and the coarse resolution of global climate models
14 (Krishnan et al., 2019).

15 16 17 *Atlas.5.11.1.3 Assessment of projections*

18 19 **Future climate change in HKH using high resolution (50 km) RCMs in the framework of WCRP 20 CORDEX South Asia**

21
22 CORDEX South Asia downscaled CMIP5 experiments project in general wetter/drier conditions in near
23 future for western/eastern Himalayan region, except for a part of the Hindu-Kush area in western Himalayan
24 region which shows drier condition (Choudhary and Dimri, 2018). This scenario gets further intensified in
25 far future. The distribution of trend with elevation presented a very complex picture with lower elevations
26 showing a greater trend in far-future under RCP8.5 scenario when compared with higher elevations.
27 Statistically significant strong rate of warming (0.03–0.09 °C/year) across all the seasons and RCPs have
28 been projected over the Indian Himalayan region (IHR) by the CORDEX South Asia RCMs and their
29 ensemble (Dimri et al., 2018b). A substantial seasonal response to warming with respect to elevation was
30 also found, as December-January season followed by October-November portrays highest rate of warming,
31 specifically at higher elevation sites such as western Himalayas and northern part of central Himalayas.
32 Climate downscaling over the Hindu Kush Himalayan (HKH) region showed that the CORDEX South Asia
33 multi-RCMs provide relatively better confidence than their driving CMIP5 GCMs in projecting the
34 magnitude of seasonal warming for the hilly subregion within the Karakoram and northwestern Himalaya,
35 with higher projected change of 5.4 °C during winter than of 4.9 °C during summer monsoon season by the
36 end of 21st century under the high-end emissions (RCP8.5) scenario (Sanjay et al., 2017b). There is less
37 agreement among these RCMs on the magnitude of the projected warming over the hilly subregions within
38 the central Himalaya and the southeastern Himalaya and Tibetan Plateau. Statistically significant higher
39 warming rate (0.23–0.52 °C/decade) for both minimum and maximum air temperature are projected over the
40 Indian Himalayan region for all the seasons by the CORDEX South Asia RCMs and their ensemble under
41 RCP4.5 and RCP8.5 scenarios (Dimri et al., 2018a). The CORDEX South Asia downscaled multi-RCMs
42 showed good consensus and low RCM uncertainty in projecting that the summer monsoon precipitation will
43 intensify by about 22% in the hilly subregion within the southeastern Himalaya and Tibetan Plateau for the
44 far-future period under the RCP8.5 scenario (Sanjay et al., 2017b). The cold and wet biases of the CORDEX
45 South Asia RCMs and of their driving CMIP5 datasets over the Himalayan watersheds of Indus Basin
46 (Jhelum, Kabul and upper Indus basin) were higher in magnitude than their projected changes under RCP8.5
47 scenario by the end of 21st century, indicating uncertain future climates for the Indus Basin watersheds
48 (Hasson et al., 2019a).

49
50 Similarly, CORDEX-South Asia over Indian Himalayan region under RCP4.5 and RCP8.5 shows higher
51 warming rate (0.23–0.52 °C/decade) for both minimum and maximum air temperature (Tmin and Tmax). The
52 overall trend of Diurnal temperature range (DTR) portrays increasing trend across entire area with highest
53 magnitude under RCP8.5. This higher rate of increase is imparted from the predominant rise of Tmax as
54 compared to Tmin (Dimri et al., 2018a; Soraisam et al., 2018).

1 The IPCC AR5 (2013) recent HIMAP report (2019) highlighted that large gaps in observations exist in the
2 HKH, especially in Afghanistan, Pakistan, Myanmar, Bhutan, and Nepal, and for the north-western part of
3 the Tibetan Plateau. This sparseness of observational data is the major source of uncertainty for the
4 estimation of long-term trends of mean and extreme climatic indices in the HKH (see section 3.5 in Krishnan
5 et al., 2019). The major uncertainty with the estimates of extreme temperature trends is expected from the
6 systematic bias in the historical temperature data series caused by urbanization. The evidence for elevation-
7 dependent warming in the HKH is increasing, but further research is needed to explore the mechanisms
8 underlying this phenomenon involving multiple feedbacks, such as snow–albedo interactions, water vapour–
9 cloud–radiation interactions, aerosol forcing, etc. The precipitation response to climate change over the HKH
10 region is subject to larger uncertainties both in the CMIP and CORDEX models.

13 **Atlas.6 Assessment of communication approaches with case studies/narratives and guidance on how** 14 **to interpret these**

15
16 **Key messages:** Empirical research on the effectiveness of climate information communication shows trade-
17 offs in conveying complicated information whilst ensuring ease of interpretation and use. Communication
18 approaches favoured by users are not always the approaches that achieve greatest accuracy in interpretation.
19 Best-practice guidance is emerging to achieve greater consistency in the understanding and use of climate
20 information.

21
22 The primary purpose of IPCC reports is to provide policymakers at all levels with the scientific information
23 they need to develop climate policies. The term ‘policymaker’ in itself covers a wide range of users with
24 varying societal and cultural perspectives, expertise and specialist scientific knowledge. Aside from feeding
25 into international, national and local climate policy, region-specific information on climate impacts and
26 projected changes under different scenarios contained within the IPCC reports serve a practical purpose and
27 lead to better operational forecasts, spatial planning and early warning systems. The detailed technical
28 findings in IPCC reports also serve as an important benchmark resource for the research community. Finally,
29 growing societal engagement with climate change means IPCC reports are increasingly used directly by
30 businesses, the financial sector, health practitioners, civil society, the media and educators at all levels.
31 While the primary audience, at least traditionally, remains decision makers, the IPCC reports could
32 effectively be considered a tiered set of products with information relevant to a range of audiences.

33
34 Climate change affects many aspects of human civilization. This lifts the communication of scientific
35 findings regarding climate change to a level that goes beyond the dissemination of scientific facts. Any
36 message can be interpreted in many ways, depending on the reputation and (perceived) purpose of the
37 messenger, the framing of the message, the value pattern of the recipient, and the communication strategy
38 that is used.

39
40 Information on observed or projected climate change can be aggregated to different levels across a range of
41 spatial and temporal scales, from global mean long-term climate characteristics to regionalized and tailored
42 records of observed or projected impacts on a specific group of people. The aggregation scale not only
43 affects the (un)certainly level or confidence in the presented findings, but also the perception of the
44 information by recipients. Assessing impacts of climate change does require integration of climate and non-
45 climatic information, which makes communication between inter- and transdisciplinary teams necessary.
46 Although ‘neutral’ communication about climate change is difficult to achieve or define, communication
47 actions aimed at presenting results of an assessment of scientific findings regarding climate change have a
48 different purpose and format than actions that are intended to inform a specific target audience in order to
49 support adaptation or mitigation policies.

50
51 An overview of concepts of climate change communication is given below, including the range of
52 approaches to communicate uncertainty, ethical issues, and the effectiveness of the various communication
53 strategies.

1 *Atlas.6.1 Approaches to communicating uncertainty and confidence*

2
3 Scientists tend to focus on what they do not know before emphasizing points of agreement (National
4 Academies of Sciences and Medicine, 2017). This focus on uncertainty obscures the level of scientific
5 consensus on main climate change features (Lewandowsky et al., 2015). In addition, it can lead to ‘action
6 paralysis’, when a weighting or comparison of available adaptation or mitigation actions is complicated by
7 the large number of unresolved drivers for determining an optimal mix of measures.

8
9 Rather than stressing the inherent uncertainty in the understanding of past phenomena or future pathways, an
10 emphasis on a ‘likely’ or ‘plausible’ range of conditions is being advocated to be an effective approach in
11 climate change communication. A number of approaches and an evaluation of their effectiveness are under
12 development.

13 14 15 *Atlas.6.1.1 Communicating uncertainty information using ensembles of models and scenarios*

16
17 The communication of uncertainty has a profound influence on the perception of information that is
18 exchanged during the communication process. In climate science, uncertainty refers to the inherent inability
19 to quantify the past, current or expected state of (components of) the climate system. It is usually expressed
20 by displaying information with an associated likelihood range, generated by the use of ensembles of data sets
21 or model projections (Slingo and Palmer, 2011). Major sources of uncertainty in (IPCC) climate change
22 assessments include imperfection of observational records, model formulation, natural variability and socio-
23 economic pathways.

24
25 This likelihood range can reflect both reconstructions of past climate variability (where uncertainty tends to
26 increase with the length of the time period due to reduced quality and representability of available
27 observations and proxies) and future climate (where sources of uncertainties vary with the lead time).

28
29 Many climate adaptation and mitigation planning activities utilize past and future climate reconstructions
30 and projections to generate plausible ranges of relevant climate characteristics (van den Hurk et al., 2018).
31 Interactions between the physical and socio-economical elements of the climate system is included in the
32 methodology in choosing scenario assumptions and following driver-effect cascades from the climate
33 response to anthropogenic forcings to regional impacts and risk changes. In this ‘top-down’ mapping
34 approach, uncertainty generally increases with longer time scales and smaller spatial and sectoral domains.
35 Aggregation of the large ensemble of potential futures into a limited subset of discrete scenarios is applied
36 using storylines and narratives [see Section Atlas.6.1.3].

37 38 39 *Atlas.6.1.2 Event attribution*

40
41 “Disasters such as record-breaking heatwaves and extreme rainfall are likely to become more common
42 because the build-up of greenhouse gases is altering the atmosphere. Warmer air contains more water vapour
43 and stores more energy; the increasing temperatures can also change large-scale atmospheric circulation
44 patterns. But extreme weather can also arise from natural cycles, such as the El Niño phenomenon that
45 periodically warms sea surface temperatures in the tropical Pacific Ocean.” (Schiermeier, 2018)

46
47 Various methods exist to detect the contribution of climate change to the probability of a given extreme
48 climate event. Some of these methods use ensembles of climate projections with and without accounting for
49 anthropogenic climate change, in which a difference of the number of occurrences of a particular event
50 (diagnosed by a meteorological indicator such as the cumulative rainfall in a given period and area) is
51 indicative of a change of the likelihood of such an event that can be attributed to climate change. Other
52 methods utilize observed trends of extreme events, and compare return times of these events under current
53 climate conditions to those under climate conditions of the early 20th century. There is now an increasing
54 number of studies on attributing extreme weather events to climate change (see Figure Atlas.79:).

55

1 **[START Figure Atlas.79: HERE]**

2
3 **Figure Atlas.79:** Number of publications on attributing extreme weather events to climate change (Schiermeier, 2018).

4
5 **[END FIGURE ATLAS.79 HERE]**

6
7
8 *Atlas.6.1.3 Narratives and storylines to communicate climate change impacts*

9
10 Communicating the full extent of available information on future climate for a region, including a
11 quantification of uncertainties, can act as a barrier to the uptake and use of such information (Daron et al.,
12 2018; Lemos et al., 2012). To address the need to simplify and increase the relevance of information for
13 specific contexts, recent studies have adopted narrative and storyline approaches (Hazeleger et al., 2015;
14 Shepherd et al., 2018) (see Chapter 1 for definitions, and Chapter 10 for further discussion on these
15 concepts). Narratives and storylines (defined in Section 1.2.4.2 and Section 10.5.3.1) can also be used to help
16 describe relationships between physical climate processes across spatial and temporal scales, and how these
17 influence a region's climate (e.g. Dessai et al., 2018; Zappa et al., 2017) but here their role in communicating
18 future climate information to address societal challenges is emphasized.

19
20 As a communication device, narratives and storylines can bring together multiple sources of information,
21 from model simulations of climatic and socio-economic trends to expert opinion. They can provide rich
22 descriptions of specific climate futures and how they may impact target locations and/or societal sectors. In
23 doing so, they can be used to sample the many possible future climates to span relevant uncertainties (e.g. in
24 projected rainfall changes) or provide illustrations of events put in a future-climate context.

25
26 Some uses of climate narratives also focus on the process of their construction and demonstrate the added
27 value of co-produced narratives to enhance knowledge integration in decision-making contexts, explicitly
28 acknowledging and including climate-impact information (Jack et al., *in prep.*). An IPCC expert meeting on
29 assessing and combining multi-model climate projections (IPCC, 2010) recommended that in cases when
30 quantitative information is limited or missing, regional climate assessments could use narratives in addition
31 or as an alternative. It may now be argued that information need not be missing or limited for narratives to
32 have value, both as a tool to communicate climate information and as a process for knowledge integration.

33
34 *Atlas.6.1.4 Climate services portals and national and regional climate assessments*

35
36 Hewitson et al. (2017) reviewed 42 climate information websites (CIWs) – considered a representative
37 sample of English-based CIWs – and developed a typology illustrating different purposes, levels of content,
38 and interfaces. They highlighted four areas of concern: 1) the ethics of information provision in a context of
39 real-world consequences; 2) interfaces that present barriers to achieving robust solutions; 3) weak capacity of
40 both users and providers to identify information of value from the multi-model and multi-method data; and
41 4) inclusion of data that infer skill.

42
43 An increasing number of national and international climate change assessment programs have been
44 performed, aiming at mapping climate change information relevant for adaptation and mitigation decision
45 support. An overview of such programmes for Europe is discussed in section Atlas.5.6.3.4.

46
47
48 *Atlas.6.2 Effectiveness of climate information communication*

49
50 Communicating climate information to guide policy development and decision-making often requires
51 tailoring of information. In doing so, various approaches are used to summarize and visualize climate
52 information. To improve understanding and inform guidance on best practices, a growing number of
53 empirical studies are assessing the effectiveness of different approaches.

54
55 Budescu et al. (2012) evaluated interpretations of the IPCC likelihood language used in previous assessment

1 reports, finding that target audiences may not understand information in the way it was intended, leading to
2 confusion and misinterpretation.

3
4 There remains a need for more detailed and comprehensive studies evaluating the effectiveness of different
5 climate information communication approaches for use by different target audiences.

6
7 The following section outlines the key principles of effective climate science communication.

8
9 **1. Trust in the source of the science message is important for effective climate science communication.**

10
11 Trust in the messenger acts as a heuristic shortcut, allowing the reader to make decisions about what
12 messages to believe (Slovic et al., 2004). This is especially important when communicating complex
13 scientific information, in the context of a ‘fake news’ media environment. Whilst research shows
14 consistently high levels of trust in scientists in Europe (McCright et al., 2016), no organizations, institutions,
15 or experts are universally trusted on all issues (National Academies of Sciences, 2017). Audiences will have
16 the greatest trust in the messengers who they perceive as sharing their values and identity (Corner et al.,
17 2014). Cues from trusted political leaders and other elite voices have a strong influence on how individuals
18 engage with climate science messages (Feldman and Sol Hart, 2018; Motta, 2018; Zanicco et al., 2018).
19 This work contributes to a growing literature on the value of communicating expert consensus about
20 contested scientific issues (Goldberg et al., 2019).

21
22 **2. Climate science communication should be related to what is tangible and familiar to the audience.**

23
24 Audiences tend to think of climate change as a problem distant from them in time and space (Spence et al.,
25 2012). Relating long-term global processes to impacts more immediate and local to the audience can
26 overcome this psychological distancing (Polk, 2018; Wiest et al., 2015). There is evidence that in some
27 circumstances localised scenarios can trigger defence mechanisms in audiences, who as a result of feeling
28 threatened may seek to deny the messaging (Brügger et al., 2015; McDonald et al., 2015).

29
30 **3. Climate science communication can be made more effective by relating the science to the things that
31 matter to your audience.**

32
33 Highlighting the co-benefits of taking action on climate change can improve engagement with climate
34 science messaging. Audiences appear receptive to climate science communication that addresses the health
35 benefits of cleaner energy (e.g. reduced air and water pollution), though overall the evidence remains mixed
36 (Hathaway and Maibach, 2018). Messages that identify positive outcomes of mitigation efforts (such as
37 improvements in social welfare and creating a society where people are more considerate and caring, or that
38 focus on the economic and technological development that climate policies can bring) seem to be more
39 effective (Bain et al., 2012). There is evidence that politically conservative audiences are more favourable
40 towards scientific messages when these are focused on pollution and the ‘purity’ of the natural environment
41 (Feinberg and Willer, 2013).

42
43 **4. Climate science communication can be made more effective by using a narrative format.**

44
45 A narrative structure can simplify otherwise complex issues and help audiences make decisions in the face of
46 this complexity (Mohan and Topp, 2018). Understanding and engagement with narratives can be made more
47 effective if the scientific information if it is presented in a narrative format congruent with the audiences’
48 values, rather than presented as a list of facts (Harris, 2017; Jones and Song, 2014; Nisbet and Markowitz,
49 2016). On the other hand, many studies suggest that the framing of information is crucial to the way in which
50 it is disseminated or discussed (Berkhout et al., 2013; Lakoff, 2010).

51
52 **5. Effective climate science communication should focus on what is known, not what is uncertain.**

53
54 Uncertainty in climate science communication can lead different audiences to interpret the information in
55 different ways (Corner et al., 2012). Audiences who do not understand science is a debate and an ongoing

1 process of reducing uncertainty are more likely to dismiss scientific messages that highlight uncertainty in
2 the findings (Rabinovich and Morton, 2012). Leading with what is known, rather than what is uncertain,
3 leads to improved engagement with climate science messages (Trenberth, 2012). ‘False balance’ in media
4 reports between scientists and sceptics has skewed how most people think about scientific agreement on
5 climate change (Boykoff, 2011), and makes it difficult for non-expert audiences to critically judge the
6 respective merits of differing interpretations of the climate science. Some research has recommended
7 reframing uncertainty information using the closely related concept of ‘risk’, with which as the language of
8 the insurance, health and national security sectors, most people are more familiar (Pidgeon and Fischhoff,
9 2011). It is also argued that scientists must realize that their engagement in advocacy does not necessarily
10 hurt their credibility (Kotcher et al., 2017).

11 12 **6. Support science communication with an effective visual vocabulary.**

13
14 The visual communication of climate science can take many forms, including graphs, infographics,
15 animations and photographs. Studies have used interviews and online surveys to assess interpretations of
16 visualizations used to communicate climate uncertainties to decision makers (Daron et al., 2015; Lorenz et
17 al., 2015; McMahon et al., 2015; Retchless and Brewer, 2016). They commonly find wide-ranging
18 interpretations of the same information and distorted understanding that can be caused by seemingly
19 arbitrary visualization choices. Taylor et al. (2015) found that preferences for a particular visualization
20 approach does not always align with the approaches that achieve greatest accuracy in interpretation.

21 22 **7. Combat the post--truth society**

23
24 Societal trends have contributed to the emergence of post-truth in recent years (Lewandowsky et al., 2017;
25 Temmerman et al., 2019). The public attention is diverted from the veracity of information by an abundance
26 of information and with it the notions of ‘true facts’ and ‘alternative facts’ which surround climate science
27 communication more generally the democratic discourse. Acceptation of climate science communication
28 messages may be helped by pushing forwards transparency about the communication means (Kovach and
29 Rosenstiel, 2007), sources and affiliation, inoculation strategies that inform and deconstruct ‘fake news’
30 campaigns (Lewandowsky et al., 2017), technological solutions (data mining and visualisation, deep
31 learning, use of social media bots) (Persily, 2017), and the general education of the public.

32
33 With new insights from a range of scientific disciplines, including the cognitive and psychological sciences
34 (Harold et al., 2016), best-practice guidance for communicating and visualizing climate data is emerging.
35 Budescu et al. (2012) showed that using a dual verbal-numerical scale allows for greater consistency in
36 understanding confidence and uncertainty. Kaye et al. (2012) and Retchless and Brewer (2016) provided
37 guidance on the use of colour, masking and other graphical approaches to represent uncertainty. Beyond
38 communication of climate information through papers, reports and web-based platforms, new World
39 Meteorological Organization guidance discusses the value of different user-engagement approaches (WMO,
40 2018) to improve climate information communication, particularly in developing climate services. The
41 guidance provides examples from passive to interactive and focused engagements, showing that deeper and
42 more valuable engagement is best achieved through face-to-face interaction.

43
44 In addition, new evidence is emerging about the potential of photographic imagery to build trust in scientific
45 communication. Photographs which connect people and climate in ways deemed credible and authentic
46 support positive engagement with climate change messaging (Chapman et al., 2016). Effective visual
47 communication needs to connect with the values and identity of its audience (Ballantyne et al., 2018).

48 49 **8. Persons’ values are key determinants of their response to climate science messages.**

50
51 A ‘value’ is a guiding principle in the life of a person and forms the core aspects of a person’s identity
52 (Schwartz, 1992). Values are the ‘bedrock’ on which specific attitudes are founded (Maio, 2017). A
53 programme of research spanning several decades, 44 nations and over 25,000 respondents (Schwartz et al.,
54 2012) has identified that certain types of values cluster together. Research into climate change
55 communication has confirmed that certain clusters of values are consistently associated with positive

1 engagement with climate science messaging (Corner et al., 2014; Kahan, 2012; Zia and Todd, 2010).

4 **Atlas.7 Description of the online “Interactive Atlas”**

6 This section provides a description of the ‘AR6 WGI Interactive Atlas’, a new tool in AR6 allowing for a
7 flexible spatial and temporal analysis of relevant WGI global and regional climate change information
8 (CMIP5 and some CORDEX domains in this version) taking also into account the needs of WGII. It builds
9 on and extends the assessments and methodological recommendations made in WGI chapters (in particular
10 the Atlas regional synthesis assessment in the previous sections), providing a more comprehensive analysis
11 of the information beyond the specific scope and limited space of the chapters.

13 The Interactive Atlas is developed in collaboration with WGI and WGII chapters, focusing on relevant
14 variables, indices and hazard metrics and allowing for a spatial and temporal analysis with a predefined
15 granularity (e.g. flexible seasons and a number of predefined alternatives for subregions and baseline and
16 future periods, including warming levels). The First order Draft (FOD) version presented here includes some
17 basic atmospheric (temperatures and precipitation) and oceanic (sea surface temperature, pH and Oxygen)
18 variables and some illustrative derived indices (used in the Atlas and Chapter 12). In particular, the
19 Interactive Atlas provides global information in the form of interactive maps, for the climate change signal
20 of these variables and indices (for several future periods, both time slices and warming levels) considering a
21 number of alternative reference baselines. It also provides regional analysis for a number of predefined
22 (reference and typological) regions in the form of plumes and scatter plots (e.g. temperature versus
23 precipitation) of aggregated spatial values. This allows for an in-depth comprehensive analysis (and
24 intercomparison) of global and regional datasets.

26 Note that this prototype is still incomplete (e.g. observations are missing), and its main purpose is to start a
27 dialogue with WGI and WGII Chapters on its possibilities and challenges (e.g. the integration of global and
28 regional projections). The goal of this first version has been to develop a functional prototype to test the
29 technology used in terms of performance, real-time usability and scalability and, thus, reduced subsets have
30 been used for this purpose (see below). The Interactive Atlas FOD is available for review at ipcc-atlas.ifca.es
31 (login details and indications are provided upon registration as reviewer).

34 **Atlas.7.1 Why an interactive online Atlas in AR6?**

36 The idea of an interactive online Atlas was first discussed in the IPCC Expert Meeting on Assessing Climate
37 Information for the Regions, ICTP, Trieste, 16–18 May 2018. One of the main limitations of previous static
38 global and regional information (including the AR5 Atlas) was the limited flexibility to explore the products
39 (e.g. global maps) in order to be informative for different regions and impact sectors. For instance, the use of
40 standard seasons limits the assessment in many cases, such as regions affected by monsoons or seasonal
41 rainband migrations or other phenomena driven seasons. The limited number of variables which can be
42 treated on a printed Atlas also prevents the inclusion of relevant indices and hazard metrics. One of the main
43 general concerns raised by this online alternative was the potential danger of having an unmanageable
44 number of final products impossible to assess following the IPCC assessment process. All the
45 recommendations and concerns have been taken into account in the design of the Interactive Atlas,
46 implementing a tool for flexible regional and temporal analysis, but with limited predefined functionality and
47 granularity. Moreover, links have been established with other chapters (e.g. using common tools) in order to
48 support their assessment and adopt their methodological recommendations.

50 In order to facilitate the assessment of the Interactive Atlas, it has been implemented tracking relevant
51 navigation information in the URL, so any product visualized by the Interactive Atlas (as characterized by
52 the particular dataset, region, variable, season, scenario, future and baseline periods, and analysis tool) can
53 be reproduced using the review code provided by the Interactive Atlas for the particular page viewed. This
54 serves as a sort of ID which facilitates the review process of the granular products shown by the Interactive
55 Atlas.

1
2
3 ***Atlas.7.2 Description of the interactive Atlas: Functionalities and datasets***

4
5 The Interactive Atlas FOD described in this section builds on the development done in the framework
6 Spanish National Adaptation Plan (PNACC – AdapteCCa) in order to design a regional scenarios portal to
7 assist the Spanish climate change adaptation community. The basic functionalities initially included in the
8 AR6 WGI Interactive Atlas were based on those already implemented in AdapteCCa and have been
9 extended to cope with the particular requirements of the datasets and functionalities planned for the
10 Interactive Atlas. In particular, the functionalities available in the FOD have been designed to showcase the
11 possibilities that offers interactivity building on four basic products:

- 12 • global maps,
- 13 • temporal plumes,
- 14 • annual cycle plots and
- 15 • two-variable scatter plots (e.g. temperature vs. precipitation).

16
17 The first of these products provides global information for any of the variables and indices and the latter
18 three convey spatially aggregated information for particular region(s) selected by the user from a number of
19 predefined alternatives (currently ‘AR6 WGI reference regions’ for atmospheric variables, and ‘ocean
20 biomes’ for oceanic ones; see Section Atlas.2.2 for more details and plans about regional definitions). Figure
21 Atlas.80: shows a screenshot of the Interactive Atlas (main window) which shows the global map of climate
22 change for the default configuration of dataset, variable, scenario and season (as shown in the tabs at the top
23 of the window).

24
25
26 **[START FIGURE ATLAS.80 HERE]**

27
28 **Figure Atlas.80:** A screenshot illustrating the main window of the AR6 WGI Interactive Atlas, which displays a global
29 map with the annual temperature climate change signal from the CMIP5 dataset for the mid-term
30 future period. The main controls at the top of the window allow selecting the dataset (currently a
31 global CMIP5 subset and regional EURO-, AFRICA- and ANTARCTIC-CORDEX at 0.44°), variable
32 (atmospheric and oceanic variables and indices), scenario (currently RCP4.5 and 8.5 for different time
33 slices and warming levels) and season (annual, standard seasons and user-defined ones). Regional
34 information for a particular region (from a predefined number of options, currently the ‘AR6
35 reference regions’ for atmospheric variables and ‘Ocean biomes’ for oceanic variables) can be
36 obtained interactively by clicking on the map over the region (or using the selector on the top) and
37 pressing the ‘view regional information button’; see Figure Atlas.81:). Note that the full URL for this
38 screen (as copied from the browser) tracks all the information of the default choice: [http://ipcc-
39 atlas.ifca.es/#&model=CMIP5_mmm&variable=tas&scenario=rcp85&temporalFilter=year&layers=A
40 R6&period=medium&anomaly=ANOMALY&zoom=2](http://ipcc-atlas.ifca.es/#&model=CMIP5_mmm&variable=tas&scenario=rcp85&temporalFilter=year&layers=AR6&period=medium&anomaly=ANOMALY&zoom=2)

41
42 **[END FIGURE ATLAS.80 HERE]**

43
44
45 This FOD version includes both atmospheric (daily mean, minimum and maximum temperatures and
46 precipitation) and oceanic (sea surface temperature, pH and oxygen) variables, as well as an illustrative
47 index used in Chapter 12 (days with maximum temperature above 35 deg C, considering both raw and bias
48 corrected data; see Annex VII: Hazard and Extreme Indices for the definition) and some illustrative indices
49 used in the Atlas regional synthesis:

- 50 • ‘warm days’: number of days with daily maximum temperature above the 90th percentile of the
51 baseline period,
- 52 • ‘warm nights’: number of days with daily minimum temperature above the 90th percentile of the
53 baseline period,
- 54 • ‘very wet days’: number of days with daily accumulated precipitation above the 95th percentile of
55 the baseline period,

56

1 Note that we have used a simple definition here, computing the percentiles using all available data in the
2 baseline period, and obtaining the frequency of exceeding these thresholds in the different future periods
3 (either time slices or warming levels). Therefore, note that these indices do not correspond to the standard
4 ETCCDI definitions.

5
6 The global and regional datasets included in the Interactive Atlas are a subset of CMIP5 models (interpolated
7 to a common 2° grid), and three regional datasets from the EURO-, AFRICA- and ANTARCTICA-
8 CORDEX, respectively, at the common resolution of 0.44° (detailed information on these datasets is given in
9 Sections Atlas.3.3 and Atlas.3.4, as well as plans for future integration of new datasets). Data from the
10 historical, RCP45 and RCP85 scenarios is available in all cases, and the user can select the future period of
11 analysis as either a time slice (considering, for consistency with the AR5 Atlas the future periods 2016-2035,
12 2046-2065 and 2081-2100 for near-, mid- and long-terms, respectively), or as a warming level (1.5° and 2°;
13 see Section Atlas.2.1 for full details on the different options and future plans).

14
15 Figure Atlas.80: illustrates the functionality of the Interactive Atlas, which allows to analyse the available
16 information in a flexible but controlled form (only a limited number of possibilities exist). Note that some of
17 the included alternatives are disabled and are only included to illustrate the different possibilities being
18 considered. For instance, regarding the baseline periods, the only active option is the AR5 baseline (1986–
19 2005), whereas the other two alternatives shown (AR5: 1995–2014 and WMO: 1981–2010) will be
20 implemented in the future after discussion with WGII.

21
22 In order to provide some initial measure of uncertainty, this version includes a simple model agreement
23 criterion (in coordination with Chapter 12). In particular, regions where less than 66% of models agree in the
24 sign of the ensemble-mean change are masked out (stippled with grey boxes). Note that this assessment does
25 not take into account whether the individual models' projected changes are significant. This will be modified
26 in future versions when an agreement is made on the adopted form for representing confidence/uncertainty in
27 the results.

28
29 Regional information can be obtained interactively by selecting (clicking on) the region(s) of interest (or
30 using the selector in the upper part) and indicating the type of product from a number of options: temporal
31 series (ensemble plumes), annual cycle plots, or two-variables scatter plots. Figure Atlas.82: and Atlas.82
32 show two examples of regional analysis for the same selection. Note that the dataset, variable, scenario and
33 season can be changed at any time and the regional information (for the currently selected region) will be
34 change accordingly, thus providing high interactivity in the exploration of products. Note that the
35 information displayed in these products will correspond to the aggregated results of the region(s) selected
36 and displays higher granularity since the results of individual models are represented and not only the
37 ensemble mean (or ensemble statistics).

38
39 In the case of the plumes (Figure Atlas.82:), the annual/seasonal time series for the individual models are
40 represented for the whole 2005–2100 period and specific details on the model values can be obtained by
41 hovering over the plume on a particular year. Similarly, the annual cycle panel shows the (monthly) annual
42 cycle, as given by the ensemble and by the different GCMs. Note that the granularity of the final Interactive
43 Atlas will be defined for each of the products based on the assessment and recommendations from other
44 chapters.

45
46 In the case of the scatter plots (Figure Atlas.82:), the application shows the current selection (variable,
47 dataset, scenario and season) on the x-axis, and allows to select a second variable for the y-axis (e.g.
48 temperature vs. precipitation, in this example). The dots represent different GCMs and the different colours
49 indicate the near-, mid- and long-term future periods. Fine granularity is provided by hovering over a
50 particular point.

1 **[START FIGURE ATLAS.81: HERE]**

2
3 **Figure Atlas.81:** Regional information for a selected region (the Mediterranean) in the form of a time series plume for
4 a mid-term time slice (top) and a 2°C warming level (bottom). Note that the corresponding periods are
5 indicated with grey shading (with intensity proportional to the number of models including each
6 particular year for the case of the warming levels). Fine granularity is provided by hovering over a
7 particular point, obtaining information of particular models (top panel).
8

9 **[END FIGURE ATLAS.81 HERE]**

10
11
12 **[START FIGURE ATLAS.82: HERE]**

13
14 **Figure Atlas.82:** Regional information for a selected region (the Mediterranean) in the form of scatter-plot. This
15 product allows to select a second variable to show in the diagram (CMIP5 precipitation in this case, in
16 addition to CMIP5 temperature originally selected) and displays the results for the three near-, mid-
17 and long-term periods in different colours (each point represents a given model).
18

19 **[END FIGURE ATLAS.82 HERE]**

20 21 22 *Atlas.7.3 Accessibility and reproducibility*

23
24 The accessibility and reproducibility of scientific results is nowadays a major concern in all scientific
25 disciplines (Baker, 2016). During the design and development of the Interactive Atlas, special attention has
26 been paid to these problems in order to ensure the transparency of the products feeding the Interactive Atlas
27 (which will be all publicly available). Accessibility will be established in collaboration with the IPCC Data
28 Distribution Centre, since all final products provided by the Atlas will be based on curated IPCC-DDC
29 datasets and will include full provenance information as part of the provided metadata (see Atlas.7.5). The
30 Atlas products are generated using open source frameworks – e.g. the climate4R framework (Iturbide et al.,
31 2019) – based on free software community tools (e.g. R) for data post-processing (re-gridding, aggregation,
32 adjustment, etc.) and evaluation and quality control (when applicable). Full metadata will be generated for all
33 final products, including provenance, post-processing workflow description and code and product-specific
34 information (see Atlas.7.4 for some examples already implemented in the FOD). Moreover, standards will be
35 adopted when available (e.g. RDF for metadata description).
36

37 In summary, a number of actions have been conducted in order to facilitate the open access and
38 reproducibility of results, including:

- 39 • Open access to raw data and derived Atlas products;
- 40 • Provision of full provenance metadata describing the product generation workflow;
- 41 • Free availability of the software and code used. As an example, code for reproducing some of the
42 figures of the Atlas Chapter is already available at github.com/SantanderMetGroup/IPCC-Atlas
- 43 • Use of standards and open-source tools.
44

45 All Atlas products and flexibility options for extended analysis will build on recommendations and
46 assessments made in WGI Chapters. For instance, products based on bias correction or statistical
47 downscaling will be consider according to the assessment and recommendations done by Chapters 10–12.
48 There also is the possibility to include non-climate data when it provides context information. The
49 incorporation of new products in the Atlas expanding the analysis provided in other chapters need to be a
50 collaborative process. A number of requirements are listed:

- 51 • The scripts/code used to generate the dataset supporting a new product would be based on and
52 incorporated into the package used to generate the other interactive Atlas datasets and made publicly
53 available; the Atlas team can collaborate in this process integrating and harmonizing tools;
- 54 • The dataset generated would need to be assessed in the relevant chapter;
- 55 • The Interactive Atlas would provide functionality to select reference periods, emissions, regions,

1 plotting options as agreed with the chapter as being appropriate for the relevant dataset.

2
3 *[Placeholder for a Box with an illustration of a reproducible worked out example from the Atlas]*

6 ***Atlas.7.4 Exporting products (including metadata) in different formats***

7
8 All the products visualized in the Interactive Atlas can be exported in a variety of formats, including PNG
9 files (and also PDF in cases with vector information, e.g. for temporal plumes). Moreover, products with
10 spatial information (only the global maps in the current version) can be downloaded in GIS format
11 (GeoTIFF). These options can be selected in the right-hand side buttons of the main screen (see Figure
12 Atlas.80:) under the zooming options.

13
14 For some test products of the Interactive Atlas (only global maps in this version), a comprehensive
15 provenance metadata description has been generated, including all details needed for reproducibility, from
16 the data sources to the different post-processes applied to obtain the final product (detailed information on
17 the specific metadata provenance model used, METACLIP, is given in next section). In these cases, there is
18 also the possibility to download a PNG file augmented with attached metadata information (in JSON
19 format). This option is available when a the METACLIP icon is shown instead of the PNG at the bottom of
20 the right-hand side panel (see Figure Atlas.80:); by clicking this button the enhanced PNG file will be
21 downloaded. The machine readable metadata embedded in the PNG file and can be accessed and interpreted
22 automatically using specific JSON software/libraries.

23
24 In order to facilitate metadata consultation, the METACLIP framework has an interactive interpreter
25 designed as an interactive provenance visualization tool to navigate through complex data workflows and
26 obtain, for each step, a semantic description of the operations undertaken, thereby allowing for an easy
27 interpretation of the provenance information by users with different levels of expertise. This is a drag-and-
28 drop facility where users can drop the files downloaded from the Interactive Atlas to visually explore the
29 metadata. For example, Figure Atlas.83: shows the metadata for the augmented PNG file corresponding to
30 the default selection of the Interactive Atlas, and obtained by clicking on the METACLIP button. The
31 visualization interface provides provenance description at different levels of granularity, in such a way that
32 the most technical details (e.g. command calls which are only relevant for expert users) remain hidden unless
33 explicitly queried.

34
35
36 **[START FIGURE ATLAS.83: HERE]**

37
38 **Figure Atlas.83:** Screenshot of the METACLIP Interpreter for provenance visualization (metaclip.org), displaying the
39 provenance of a temperature anomaly map downloaded from the Interactive Atlas as a PNG file with
40 attached METACLIP metadata (METACLIP export option). The blow-up shows a specific dataset
41 from the 9-member ensemble used to produce the map. It shows details about the dataset provenance
42 such as its DOI identifying the source of data, the experiment (RCP 8.5), the modelling centre, GCM
43 information, data provider and associated Project (CMIP5). The interface allows the user to expand
44 the detail of information if needed by clicking in each of the nodes and reading the metadata in the left
45 panel. It is also possible zooming in/out, scrolling and saving a user-defined position of the graph.

46
47 **[END FIGURE ATLAS.83 HERE]**

50 ***Atlas.7.5 Provenance for the full chain from the data source to the final product***

51
52 Provenance is defined as a ‘record that describes the people, institutions, entities, and activities involved in
53 producing, influencing, or delivering a piece of data or a thing’. This information can be used to form
54 assessments about their quality, reliability or trustworthiness. In the context of the outcomes of the
55 Interactive Atlas, having an effective way of dealing with data provenance is a necessary condition to ensure
56 not only the reproducibility of results, but also to build trust on the information provided. However, the

1 relative complexity of the data and the post-processing workflows involved may prevent from a proper
2 communication of data provenance with full details for reproducibility. Therefore, a special effort has been
3 made in order to build a comprehensive provenance metadata model for the Interactive Atlas products.
4

5 Provenance frameworks are typically based on RDF (Resource Description Framework), a family of World
6 Wide Web Consortium (W3C) specifications originally designed as a metadata model – RDF Working
7 Group 2014: www.w3.org/RDF (Candan et al., 2001). It is an abstract model that has become a general
8 method for conceptual description of information for the Web, using a variety of syntax notations and
9 serialization formats. Designed to provide a framework that ensures interoperability between metadata
10 frameworks, RDF allows for structured and semi-structured data to be mixed, exposed, and shared across
11 different applications. As a result, RDF has been widely adopted in many different fields. To this aim,
12 specific vocabularies have been written in RDF, containing a conceptual model of a particular – more or less
13 broad – domain of knowledge. Vocabularies list the types of objects, the relationships that connect them and
14 constraints on the ways that objects and relationships can be combined, being used for description,
15 classification and reasoning. METACLIP (Bedia et al., 2019) exploits RDF through specific vocabularies,
16 written in the OWL ontology language, describing different aspects involved in climate product generation,
17 from the data source to the post-processing workflow, extending international standard vocabularies such as
18 PROV-O (Moreau et al., 2015). The METACLIP vocabularies are publicly available in the METACLIP
19 GitHub repository (github.com/metaclip/vocabularies).
20

21 METACLIP makes an emphasis in the delivery of ‘final products’ (understood as any piece of information
22 that is stored in a file, such as a plot or a map) with a full semantic description of its origin and meaning
23 attached to it. On the one hand, a web-based front-end (the METACLIP Interpreter) achieves ‘human
24 readability’ of very detailed and potentially complex provenance information (including the source code
25 generating the product), facilitating its interpretability to users with different levels of expertise thanks to its
26 granularity. On the other hand, METACLIP ensures ‘machine readability’ through the reuse of well-defined,
27 standard metadata vocabularies, providing semantic interoperability and the possibility of developing
28 database engines supporting advanced provenance analytics. Therefore, this framework has been adopted in
29 order to generate provenance information and attach it as metadata to the products generated by the
30 interactive Atlas. A specific vocabulary (IPCC_TERMS) is created alongside the inclusion of new products
31 in the Interactive Atlas. As an example, Figure Atlas.84: shows the semantic vocabularies needed to encode
32 the information Figure Atlas.83: (provenance of the CMIP5 datasets).
33
34

35 **[START FIGURE ATLAS.84: HERE]**

36
37 **Figure Atlas.84:** Illustration of the provenance of an individual ‘dataset’ (corresponding to the blow-up highlighted by
38 the red square in Figure Atlas.83:), describing its source (DOI number), data provider (ESGF),
39 experiment (RCP 8.5), modelling centre (GFDL) and GCM (ESM2M). The metadata model re-uses
40 an existing ontology (PROV-O, prefix ‘prov:’, blue) and creates domain-specific extension for climate
41 products via the METACLIP ontologies DATASOURCE (indicated by prefix ‘ds:’, orange) and
42 IPCC_TERMS (‘ipcc:’, magenta).
43

44 **[END FIGURE ATLAS.84 HERE]**

45 46 47 **Atlas.8 Knowledge gaps**

48
49 *[Preliminary statements]*

50
51 There is the need to increase significantly the standard and comprehensiveness of guidance material on the
52 quality and applicability of accessible regional climate data.
53

54 Some regions are lacking a comprehensive evaluation of downscaled climate data.
55

1 Climate scientists need to increase their skills in engaging with the increasingly broad audience for their
2 findings and this demands new skills of scientists to use and engage with a wider range of communications
3 channels.
4
5 Scientists, policy-makers and practitioners across the whole spectrum of climate change science and its
6 applications need to improve their awareness of the importance of working in multidisciplinary teams and
7 their skills in engaging in them.
8
9 Calculating observed climate changes, evaluation of models and developing bias correction and downscaling
10 is hampered by uneven distribution of observations, monitoring and poor data availability
11
12

1 **Frequently Asked Questions**

2 3 **FAQ ATLAS.1: If results from models are uncertain, how can we trust them?**

4
5 *A model is a simplified representation of something more complicated. Children's play, for instance, often*
6 *involves models of anything from machines to human social systems. For predicting weather and climate,*
7 *models are built which are simplified representations of the complicated physical and chemical interactions*
8 *which take place in the atmosphere, on land and in the oceans. These take the form of computer models*
9 *which solve complex mathematical equations derived from these simplified representations. Clearly it is not*
10 *possible to represent all the detail of the real world in a computer model and so the results it will generate*
11 *will only approximate the real world, i.e. will contain a degree of uncertainty. However, if we compare these*
12 *results with observations then we can quantify this uncertainty which can allow us to say how much trust we*
13 *can have in them. In the case of climate change projections we can use an assessment of how well models*
14 *have been able to reproduce recent climate changes, and the reasons for these, to estimate how much we can*
15 *trust them to predict how the climate will continue to change in the future. In turn, this then allows us to*
16 *explore with reasonable confidence the potential impacts of climate change under various scenarios of world*
17 *evolution and to examine the robustness of a given adaptation option under a wide range of possible futures.*

18
19 Climate models, global or regional, coupled or uncoupled, are numerical simulations of real-world systems;
20 they solve complex mathematical equations based on well-established physical laws defining the behaviour
21 of the weather and climate. It is not possible nevertheless to represent all the detail of the real world in a
22 computer model, so approximations have to be made, such as the choice of the temporal and spatial
23 resolution of the calculations or the processes included in the models. These approximations lead to some
24 inherent uncertainty.

25
26 Since the first climate models with a simplified representation of the atmosphere, our knowledge of the real
27 world has much improved and remarkable advances have been made in computer power. Models have
28 incorporated more of the complexity of the climate system with its many potential interactions and
29 feedbacks. Current state-of-the-art climate models now include fully interactive clouds, oceans, land surfaces
30 and aerosols, with the latest models containing detailed atmospheric chemistry and the climate carbon cycle.
31 Increasing numerical resources have allowed for an ever increasing of the spatial and temporal resolutions at
32 which calculations are made, as well as for the incorporation of more complex parameterisations.

33
34 As a result, far more and far more detailed experiments are run with different versions of the models. We can
35 quantify the uncertainty in our predictions and thereby increase confidence in the results. As models have
36 evolved, the fundamental physical responses of the modelled climate systems have remained consistent with
37 the early simpler models, and the coupling process has not uncovered any major errors in the pre-existing
38 models.

39
40 The uncertainty of the models can be (and is) characterised. Models are tried and tested in a number of ways.
41 They are used to reproduce the climate of the recent past and the present day, having considerable success at
42 this, both in terms of the average and variations in space and time. They are also used to reproduce what we
43 know about ancient climates. They are calibrated and validated using observations from experiments or
44 analogies, and then run using input data representing future climate. This work gives confidence in the
45 results of the models, or if need be, a representation of their weaknesses which can be in turn taken into
46 account when assessing their results.

47
48 While explicitly discussing uncertainty is important for good climate science and the confidence assessment
49 in model results, uncertainty about the future conflicts with individual needs for predictability and control.
50 To address this, scenarios called Representative Concentration Pathways (RCPs) can be used to interpret
51 scientific uncertainty regarding future climate conditions more meaningfully.

52
53 RCPs describe a range of plausible future concentrations of global greenhouse gases and aerosols in the
54 atmosphere, which could come as a result of different combinations of future economic, demographic,
55 policy, institutional and technological conditions. Through climate modelling, these RCPs are translated into

1 projected changes in temperature and precipitation, among other climate variables, revealing a range of
2 possible futures. These enable researchers to explore the potential impacts of climate change, and for
3 decision makers to examine the robustness of a given adaptation option under a wide range of possible
4 futures. Decision-makers should treat projections as indicators of possible future trends (and not absolute
5 values) which can inform their pursuit of climate-resilient development pathways.
6

7 Thus, scientific uncertainty can here be interpreted as the opportunity to explore rigorously a range of
8 possible future scenarios and to chart climate-resilient pathways, rather than as a lack of any reasonable view
9 of what the future might look like.

10
11 *[Placeholder: A schematic of all processes represented in climate models, illustrating the complexity of the*
12 *climate systems and its interaction with humans and nature.]*
13

14
15
16
17

18 *[Other proposed FAQs*

19
20 *Given CMIP5, CMIP6, CORDEX, which model(s) is(are) best for our region?*

21
22 *How do you evaluate models when there is sparse observation?*

23
24 *How can I use the (interactive online) Atlas for mitigation and adaptation studies?*

25
26 *How can I use the (interactive online) Atlas for climate risk assessment?*

27
28 *Specifics FAQs on the Atlas tools regarding the use of the tool in the direction of providing guidance*

- 29
30
31
32
- *Where can I find the information to produce the figure(s)?*
 - *Where are the metadata?]*

1
2
3
4
5
6

[START TABLE ATLAS.22 HERE]

Table Atlas.22: Regional scale summary of climate change projections in South Asia.

S.No.	GCM		RCM	Time period	Relative time	Resolution	Domain	Scenarios		Authors	Results	
											Temperature	Precipitation
1	ECHAM5	MRI	RegCM4	2030s, 2050s and 2080s		30 km	South Asia	IPCC AR4	A2, A1B and B1	(Ahmed and Suphachalasai, 2014)	They concluded steadily progressing warming will be widespread across the region with increases of 4°C to 5°C by the 2080s for the A2 scenario.	Precipitation increases were projected for eastern and north-eastern areas for the monsoon season, becoming an identified signal only toward the end of the century. The drier winter months see smaller projected changes or decreasing trends.
2	CMIP5	20 GCMs		2061-2100	1966-2005		Global	IPCC AR5	RCP8.5	Scoccimarro et al. (2013)		Projected changes in difference between the 90th and 99th percentile daily precipitation. Regions where the projected increases were found to be greatest included India, southern China and Southeast Asia, with the difference increasing by 10 mm/day for 2061-2100 relative to 1966-2005.
3	CMIP3		PRCIS				Indus Basin within India			(Deshpande and Kulkarni, 2015)		1-day duration 5 cm or greater rainstorms covering at least 40,000 km ² of the

												Indus Basin within India, projected future increases in intensity and decreases in frequency.
4	CMIP5	10 GCMs		2050–2099	Pre-industrial		India and South Asia	IPCC AR5	RCP8.5	Jourdain et al. (2013)		Increased summer monsoon rainfall for India and South Asia (for nine out of the ten GCMs) of 5% to 20% increases for 2050-2099 relative to the pre-industrial period. Most of the Indian increase occurs over the Himalayas.
5	CMIP5						Global			Seth et al. (2013)		Increased moisture convergence and precipitation in late summer in all monsoon regions. annual cycle of monsoon region precipitation.
6	CMIP5	20GCMs							RCP8.5	Menon et al. (2013)		Increase in Indian summer monsoon rainfall under the RCP8.5 scenario by the end of the century. They also reported a projected increasing trend in interannual variability.
7	CMIP5	23 GCMs							RCP8.5	(Srivastava and Delsole, 2014)		South Asian summer monsoon precipitation is robustly projected (JJAS mean rainfall) to increase due to

												anthropogenic climate change.
8	CMIP5	30 GCMs							RCP8.5	(Freychet et al., 2015)		With moderate confidence, more intense and frequent extreme precipitation was projected for the Indian region due to changes in atmospheric moisture content and circulation
9	CMIP5	20 GCMs (a subset of four models (BNU-ESM, MPI-ESM-LR, MIROC5 and NorESM1-M) were selected)		2051–2099	1951–1999				RCP8.5	(Sharmila et al., 2015)		All-India summer monsoon rainfall magnitude will increase together with a lengthening of the season due to later monsoon withdrawal. Intensity and frequency of both strong and weak monsoons are projected to increase. Daily variability changes indicate increases in heavy rainfall events (> 40 mm/day) and decreased low rain-rate events (<10 mm/day) and wet day frequencies. Additionally, enhanced propensity for shorter active and longer break spells is projected.
10	CMIP5	GCMs		21 st century						(Mei et al., 2015)		They suggest warmer temperatures increase atmospheric moisture content,

												overwhelming weakening monsoon circulation, thus increasing both moisture convergence and summer monsoon precipitation over South Asia.
11	CMIP5			2021–2015 and 2071–2100	1971–2000				RCP4.5 and RCP8.5	(Palazzi et al., 2015)		All models indicate an increase in summer (i.e. monsoon) precipitation for the Himalaya.
12	CMIP5									Sabeerali et al. (2015)		Find all CMIP5 GCMs investigated produced unrealistic ISMR projections due to excessive convective relative to stratiform precipitation and so recommend improved cloud microphysics formulations are required before projections will be reliable.
13	Two GCMs (ECHAM5 and HadCM3)		Three RCMs (CLM, HadRM3 and REMO)		1970–1999		India.		A1B scenario	(Kumar et al., 2013)	An ensemble mean RCM warming of 1.5°C and 3.9°C by mid and end of century.	Ensemble mean RCM precipitation projections show summer monsoon season increases of 20% to 40% over the peninsular and 10% to 20% over the northeast and Western Gnats by the end of the 21 st century.
14										(Syed et al., 2014b)	Warming of 2.5°C to 5°C, with the largest	

											warming over their northern Pakistan and India subregion, and a 30% increase in summer monsoon precipitation over north eastern India, Bangladesh and Myanmar.	
15	Driven by ECHAM5	Three GCMs	Seven RCMs	2041–2060					A1B	(Niu et al., 2015)		Overall a stronger Indian summer monsoon is projected by most of climate models during 2041–2060.
16			PRECIS RCM				entire Indus river basin		A1B scenario	Rajbhandari et al. (2014)	Warming was greater over the upper than the lower Indus, with greater warming in winter than in the other seasons.	Projections simulated an increase in precipitation over the upper Indus basin and decrease over the lower Indus basin with winter precipitation decreases particularly evident over the southern part of the basin. There was an overall increase in the number of rainy days over the basin, but in the border area between the upper and lower basins (where the rainfall amount is highest) there was a decrease in the number of rainy days accompanied by an increase in rainfall intensity.
17		One GCM	One RCM						RCP4.5	(Dash et al., 2014)		Their results

		(GFDL-ESM2M)	(RegCM4)						and RCP8.5			projected decrease in JJAS rainfall under the RCP8.5 scenario over the central, eastern, and peninsular India by the end of the century is in the range of 30–40% of their mean reference period values. Under the RCP4.5 scenario, similar decreasing estimates lie in the range of 15–25 %, also significant at 95% level.
18		Stretched-grid variable-resolution GCM (Krishnan et al., 2013)	Land-surface model			35 km	South Asian monsoon region and tropical Indian Ocean		RCP4.5	(Ramarao et al., 2015)		Continuation of summer monsoon rainfall declines with corresponding soil moisture decreases until the end of the 21 st century. evapotranspiration (ET) reduction accompanying the soil moisture drying has an elasticity factor of approximately two (i.e. a 1% decrease in soil moisture results in a 2% decrease in ET).
19	CMIP5	AOGCMs	Multi-RCMs	(2036–2065) and (2066–2095)		50 km	Hindu Kush Himalayan (HKH)-CORDEX_SA		RCP4.5 and RCP8.5	(Sanjay et al., 2017b)	Seasonal warming for the hilly subregion within the Karakoram and north-western Himalaya, with higher projected change of 5.4°C during winter than of	Summer monsoon precipitation will intensify by about 22% in the hilly subregion within the south-eastern Himalaya and Tibetan Plateau for the far-

											4.9°C during summer monsoon season by the end of 21 st century under the high-end emissions (RCP8.5) scenario.	future period under the RCP8.5 scenario.
20		AGCM		(2010–2039), (2040–2069) and (2070–2100)		40 km	South and East Asia	IPCC AR5	RCP4.5 and RCP8.5	(Woo et al., 2018)		Correlation coefficients (CCs) pattern of precipitation over South Asia shows an in-phase relationship with North China and an out-of-phase relationship with Korea–Japan, while precipitation variations over Korea–Japan and Southern China exhibit an out-of-phase relationship with South Asia. The CCs analysis between the two Asian blocks during different time slices shows the strongest CCs during the near and far future with the RCP8.5 scenario.
21	CMIP5			1860–2099	1961–1990		India	IPCC AR5	RCP2.6, RCP4.5, RCP6.0 and RCP8.5	Chaturvedi et al. (2012)	Under the business-as-usual (between RCP6 and RCP8.5) scenario, mean warming in India is likely to be in the range 1.7°C–2°C by 2030s and 3.3°C–4.8°C by 2080s relative to pre-industrial times.	All-India precipitation under the business-as-usual scenario is projected to increase from 4 to 5% by 2030s and from 6 to 14% towards the end of the century (2080s). Consistent positive trend in frequency of extreme precipitation

												days (e.g. > 40 mm/day) for decades 2060s and beyond.
22		GCM	High-resolution zooming				South Asia			(Sabin and Mujumdar, 2016)		Persistent decrease of monsoonal rains and prolongation of soil drying.
23	CMIP5	GCM							Transient warming scenario	(Lee et al., 2018)		Half a degree additional warming would bring more frequent and stronger heavy precipitation events, exerting devastating impacts on the human and natural system over the Asian monsoon region.
24				2020–2049	1960–1989					(Hamman et al., 2016)	The cooling trend over the Asian continent is likely to make it even more severe in its impact than 1960–1989.	The epoch 2020–2049 is likely to be another dry one.
25		CGCM3.1 by Canadian Center for Climate Modeling and Analysis version 3.1	Statistical Downscaling Model (SDSM)				River basins in South Asia—the Ganges and the Brahmaputra		A1B and A2	(Pervez and Henebry, 2014b)		Precipitation during and after the monsoon is likely to increase in both basins. Peak monsoon precipitation is likely to shift from July to August, and may impact the livelihoods of large rural populations linked to subsistence agriculture in the basins.
26	CMIP5	45 GCMs		2046–2075	1976–2005	0.5° grids	South Asia		RCP8.5	Zheng et al. (2018)		The modelling results indicate that future runoff will increase throughout most of

												the region except in the far northeast and far northwest. The median projection shows increases in mean annual runoff of 20–30% in the Indian subcontinent.
27	CMIP5	CanESM2, CNRM-CM5, GFDL-ESM2M, MIROC5 and MPI-ESM-LR		2080–2099	1986–2005				RCP 4.5	Sudeepkuma et al. (2018)		The ensemble mean of models projects a strengthening of the wind speed towards north (north of 15°N) and weakening to the southern region (especially south of 12°N). In the case of active-break conditions, the active spells are found to be strengthening over northern India and weakening over the peninsular India, the break spells intensify over southern tip of peninsular India indicating intense breaks. which facilitates wetting of northern Indian regions and drying of southern peninsular regions
28			CORDEX-SA_RCM				Indian Himalayan region-CORDEX-South Asia		RCP4.5 and RCP8.5	Dimri et al. (2018)	Higher warming rate (0.23°C–0.52°C per decade) for both minimum and maximum air temperature (Tmin and Tmax) is observed for all the seasons under both	

											RCPs. The overall trend of Diurnal temperature range (DTR) portrays increasing trend across entire area with highest magnitude under RCP8.5. This higher rate of increase is imparted from the predominant rise of Tmax as compared to Tmin.	
29	CMIP5			2006–2050	1961–2005				RCP4.5 and RCP8.5	(Sarhi et al., 2015)		Future projected change of JJAS wind shows anticyclonic circulation over Arabian Sea at 850 hPa and cyclonic circulation around 40°N,70°E–90°E at 200 hPa which may be a possible cause of changes in JJAS rainfall over Indian regions.
30			CORDEX-South-Asia data	2011–2060	1970–2005		Northeast-India		RCP4.5	(Soraisam et al., 2018)	Increasing trend for both seasonal maximum and minimum temperature over the northeast India. The frequency of extreme monthly maximum and minimum temperature are projected to increase.	Decreasing insignificant trend in seasonal precipitation.
31	CMIP5								RCP8.5	(Mukherjee et al., 2018)		The frequency of precipitation extremes is projected to rise more

												prominently in southern and central India in the mid and end of the 21 st century.
32		GCM20	RegCM4.3	2008–2025 and 2080–2098	1980–1998		Pakistan		A1B under AR4 for GCM20 and RCP8.5 under AR5 for RegCM4.3	Ahmad and Hussain (2017)	Under A1B scenario GCM20 mean DJF temperature change in 2008–2025 projection period suggests an up to 5°C rise in the north–most region of the country. RegCM4.3 under RCP8.5 scenario suggests an up to 11°C rise in the mean temperature projection of 2008–2025 DJF season over the northern region of the country.	GCM20 JJAS precipitation rate of change under A1B scenario in the 2008–2025 projection period suggests a relative decrease of up to 20 mm/day over the central parts of the country. RegCM4.3 under RCP8.5 suggests a mean JJAS precipitation decrease of up to 0.5 mm/day in 2008–2025 projection over south–eastern region of the country.
33		GCM20	RegCM4.3	2008–2025 and 2080–2098	1980–1998	GCM20=20 Km and RegCM4.3=25km	Pakistan		A1B under AR4 for GCM20 and RCP8.5 under AR5 for RegCM4.3	Ahmad and Hussain (2019)	The GCM20 (RegCM4.3) has shown a 2.1°C (4.7°C) warm shift in the 90th percentile of DJF daily mean temperature in 2008–2016 projection period relative to 1990–1998 baseline period.	GCM20 (RegCM4.3) suggests a substantial JJAS mean precipitation increase of 9.0 mm/day (29.2 mm/day) in the 90th percentile for the 2008–2016 projection period.
34		AOGCMs		2011–2030, 2046–2065, and 2080–2099	1976–2011		Pakistan		IPCC AR4	(Nabeel and Athar, 2018)		The AOGCM projections display a gradual increase in annual precipitation in AJK, KPK, and Punjab, whereas an increase and then

												decrease in Balochistan and Sindh. In humid and semi-arid climate areas, there is an increase in annual precipitation in all three projected periods.
35		22 AOGCMs		2025–2049, 2050–2074, and 2075–2099	1975–1999				A2, A1B, and B1	(Saeed and Athar, 2018)	The projected robust changes in the temperature by the end of 21 st century are in the range of 3°C to 4°C during the winter season and on an annual basis, in the central and western regions of Punjab province, especially in A2 and A1B emission scenarios. Changes in both precipitation and temperature are larger in the summer season (JAS) as compared to the winter season in the coming decades, relative to the baseline period.	The winter season (from December to March), 66% of the models display robust projected increase of winter precipitation by about 10% relative to the baseline period, irrespective of emission scenario and projection period, in the upper northern subregion of Pakistan (latitude > 35°N).
	Crop model			2020s and 2050s	2008 and 2009					Nasim et al. (2016)	Grain yield of sunflower could reduce by up to 15% by the 2020s with an average increase in temperature of +1°C, and by up to 25% if temperatures increased by up to 2°C for the 2050s. Adaptation strategies showed that, if the	

											crop were sown between 14 days (for 2020) and 21 days (for 2050) earlier than the current date (last week in February), yield losses could potentially be reduced.	
--	--	--	--	--	--	--	--	--	--	--	--	--

1
2
3

[END TABLE ATLAS.22 HERE]

1 **References**

- 2
- 3 A.K. Srivastava, D. R. K. and M. N. R. (2017). “Variability and Long-Term Changes in Surface Air Temperatures Over
4 the Indian Subcontinent,” in *Observed Climate Variability and Change over the Indian Region* (Springer India).
5 doi:10.1007/978-981-10-2531-0_2.
- 6 Aalbers, E. E., Lenderink, G., van Meijgaard, E., and van den Hurk, B. J. J. M. (2018). Local-scale changes in mean
7 and heavy precipitation in Western Europe, climate change or internal variability? *Clim. Dyn.* 50.
8 doi:10.1007/s00382-017-3901-9.
- 9 Aalto, J., Kämäräinen, M., Shodmonov, M., Rajabov, N., and Venäläinen, A. (2017). Features of Tajikistan’s past and
10 future climate. *Int. J. Climatol.* 37, 4949–4961. doi:10.1002/joc.5135.
- 11 Abadi, A. M., Oglesby, R., Rowe, C., and Mawalagedara, R. (2018). Evaluation of GCMs historical simulations of
12 monthly and seasonal climatology over Bolivia. *Clim. Dyn.* 51, 733–754. doi:10.1007/s00382-017-3952-y.
- 13 Adloff, F., Jordà, G., Somot, S., Sevault, F., Arsouze, T., Meyssignac, B., et al. (2018). Improving sea level simulation
14 in Mediterranean regional climate models. *Clim. Dyn.* 51, 1167–1178. doi:10.1007/s00382-017-3842-3.
- 15 Agosta, C., Amory, C., Kittel, C., Orsi, A., Favier, V., Gallée, H., et al. (2019). Estimation of the Antarctic surface mass
16 balance using the regional climate model MAR (1979–2015) and identification of dominant processes. *Cryosph.*
17 13, 281–296. doi:10.5194/tc-13-281-2019.
- 18 Agosta, C., Fettweis, X., and Datta, R. (2015). Evaluation of the CMIP5 models in the aim of regional modelling of the
19 Antarctic surface mass balance. *Cryosph.* 9, 2311–2321. doi:10.5194/tc-9-2311-2015.
- 20 Ahmad, I., Tang, D., Wang, T., Wang, M., and Wagan, B. (2015). Precipitation Trends over Time Using Mann-Kendall
21 and Spearman’s rho Tests in Swat River Basin, Pakistan. *Adv. Meteorol.* 2015, 1–15. doi:10.1155/2015/431860.
- 22 Ahmed, M., and Suphachalasai, S. (2014). *Assessing the Costs of Climate Change and Adaptation in South Asia*.
23 Available at: [http://www.adb.org/sites/default/files/pub/2014/assessing-costs-climate-change-and-adaptation-](http://www.adb.org/sites/default/files/pub/2014/assessing-costs-climate-change-and-adaptation-south-asia.pdf)
24 [south-asia.pdf](http://www.adb.org/sites/default/files/pub/2014/assessing-costs-climate-change-and-adaptation-south-asia.pdf).
- 25 Akhtar, N., Brauch, J., and Ahrens, B. (2018). Climate modeling over the Mediterranean Sea: impact of resolution and
26 ocean coupling. *Clim. Dyn.* 51, 933–948. doi:10.1007/s00382-017-3570-8.
- 27 Ali, M. M., Nagamani, P. V., Sharma, N., Venu Gopal, R. T., Rajeevan, M., Goni, G. J., et al. (2015). Relationship
28 between ocean mean temperatures and Indian summer monsoon rainfall. *Atmos. Sci. Lett.* 16, 408–413.
29 doi:10.1002/asl2.576.
- 30 Allaberdıyev, G. (2010). Изменение климата и Туркменистан. Available at: <https://www.undpcc.org/docs/National>
31 [issues papers/Climate Change/29_Turkmenistan NIP_Climate Change.pdf](https://www.undpcc.org/docs/National) [Accessed April 3, 2019].
- 32 Almeida, C. T., Oliveira-Júnior, J. F., Delgado, R. C., Cubo, P., and Ramos, M. C. (2017). Spatiotemporal rainfall and
33 temperature trends throughout the Brazilian Legal Amazon, 1973–2013. *Int. J. Climatol.* doi:10.1002/joc.4831.
- 34 Alo, C. A., and Anagnostou, E. N. (2017). A sensitivity study of the impact of dynamic vegetation on simulated future
35 climate change over Southern Europe and the Mediterranean. *Int. J. Climatol.* 37, 2037–2050.
36 doi:10.1002/joc.4833.
- 37 Altnau, S., Schlosser, E., Isaksson, E., and Divine, D. (2015). Climatic signals from 76 shallow firn cores in Dronning
38 Maud Land, East Antarctica. *Cryosph.* 9, 925–944. doi:10.5194/tc-9-925-2015.
- 39 Alves, L. (2016). Análise estatística da sazonalidade e tendências das estações chuvosas e seca na Amazônia: Clima
40 presente e projeções futuras. Available at: <http://urlib.net/8JMKD3MGP3W34P/3L9KTPH>.
- 41 Alves, L. M., Cavalcanti, I. F. A., Silveira, V. P., and Marengo, J. A. (2013). “Classificação de anos secos na estação
42 chuvosa e seca na Amazônia,” in *Secas na Amazônia: causas e consequências*, eds. L. S. Borma and C. A. Nobre
43 (São Paulo: Oficina Textos), 49–77. Available at: [https://www.ofitexto.com.br/livro/secas-na-amazonia-causas-e-](https://www.ofitexto.com.br/livro/secas-na-amazonia-causas-e-consequencias/)
44 [consequencias/](https://www.ofitexto.com.br/livro/secas-na-amazonia-causas-e-consequencias/).
- 45 Amador, J. (1998). A climatic feature of the tropical Americas: The trade wind easterly jet. *Top. Meteor. Ocean.* 5, 91–
46 102.
- 47 Ambrizzi, T., Reboita, M. S., da Rocha, R. P., and Llopart, M. (2019). The state of the art and fundamental aspects of
48 regional climate modeling in South America. *Ann. N. Y. Acad. Sci.* 1436, 98–120. doi:10.1111/nyas.13932.
- 49 Angeles-Malaspina, M., González-Cruz, J. E., and Ramírez-Beltrán, N. (2018). Projections of Heat Waves Events in the
50 Intra-Americas Region Using Multimodel Ensemble. *Adv. Meteorol.* 2018, 1–16. doi:10.1155/2018/7827984.
- 51 Angeles, M. E., Gonzalez, J. E., Erickson, D. J., and Hernández, J. L. (2007). Predictions of future climate change in the
52 caribbean region using global general circulation models. *Int. J. Climatol.* 27, 555–569. doi:10.1002/joc.1416.
- 53 Angeles, M. E., González, J. E., Ramírez-Beltrán, N. D., Tepley, C. A., and Comarazamy, D. E. (2010). Origins of the
54 Caribbean Rainfall Bimodal Behavior. *J. Geophys. Res. Atmos.* 115. doi:10.1029/2009JD012990.
- 55 Anstey, J. A., Davini, P., Gray, L. J., Woollings, T. J., Butchart, N., Cagnazzo, C., et al. (2013). Multi-model analysis of
56 Northern Hemisphere winter blocking: Model biases and the role of resolution. *J. Geophys. Res. Atmos.* 118,
57 3956–3971. doi:10.1002/jgrd.50231.
- 58 Arctic Monitoring and Assessment Programme (2017). *Snow, Water, Ice and Permafrost in the Arctic (SWIPA) 2017*.
- 59 Attema, J. J., Loriaux, J. M., and Lenderink, G. (2014). Extreme precipitation response to climate perturbations in an
60 atmospheric mesoscale model. *Environ. Res. Lett.*, 14003. doi:10.1088/1748-9326/9/1/014003.

- 1 Awange, J. L., Mpelasoka, F., and Goncalves, R. M. (2016). When every drop counts: Analysis of Droughts in Brazil
2 for the 1901–2013 period. *Sci. Total Environ.* 566–567, 1472–1488. doi:10.1016/j.scitotenv.2016.06.031.
- 3 Bach, L., Schraff, C., Keller, J. D., and Hense, A. (2016). Towards a probabilistic regional reanalysis system for
4 Europe: Evaluation of precipitation from experiments. *Tellus, Ser. A Dyn. Meteorol. Oceanogr.* 68.
5 doi:10.3402/tellusa.v68.32209.
- 6 Bador, M., Terray, L., Boé, J., Somot, S., Alias, A., Gibelin, A.-L., et al. (2017). Future summer mega-heatwave and
7 record-breaking temperatures in a warmer France climate. *Environ. Res. Lett.* 12, 074025. doi:10.1088/1748-
8 9326/aa751c.
- 9 Bain, P. G., Hornsey, M. J., Bongiorno, R., and Jeffries, C. (2012). Promoting pro-environmental action in climate
10 change deniers. *Nat. Clim. Chang.* 2, 600–603. doi:10.1038/nclimate1532.
- 11 Baker, M. (2016). 1,500 scientists lift the lid on reproducibility. *Nature.* doi:10.1038/533452a.
- 12 Ballantyne, A. G., Glaas, E., Neset, T.-S., and Wibeck, V. (2018). Localizing Climate Change: Nordic Homeowners’
13 Interpretations of Visual Representations for Climate Adaptation. *Environ. Commun.* 12, 638–652.
14 doi:10.1080/17524032.2017.1412997.
- 15 Ban, N., Schmidli, J., and Schär, C. (2014). Evaluation of the convection-resolving regional climate modeling approach
16 in decade-long simulations. *J. Geophys. Res. Atmos.* 119, 7889–7907. doi:10.1002/2014JD021478.
- 17 Ban, N., Schmidli, J., and Schär, C. (2015). Heavy precipitation in a changing climate: Does short-term summer
18 precipitation increase faster? *Geophys. Res. Lett.* 42, 2014GL062588. doi:10.1002/2014GL062588.
- 19 Barreiro, M. (2010). Influence of ENSO and the South Atlantic Ocean on climate predictability over Southeastern
20 South America. *Clim. Dyn.* 35, 1493–1508. doi:10.1007/s00382-009-0666-9.
- 21 Barros, V. R., Boninsegna, J. A., Camilloni, I. A., Chidiak, M., Magrín, G. O., and Rusticucci, M. (2015). Climate
22 change in Argentina: trends, projections, impacts and adaptation. *Wiley Interdiscip. Rev. Clim. Chang.* 6, 151–
23 169. doi:10.1002/wcc.316.
- 24 Bartók, B., Wild, M., Folini, D., Lüthi, D., Kotlarski, S., Schär, C., et al. (2017). Projected changes in surface solar
25 radiation in CMIP5 global climate models and in EURO-CORDEX regional climate models for Europe. *Clim.*
26 *Dyn.* 49, 2665–2683. doi:10.1007/s00382-016-3471-2.
- 27 Batista, R. J. R., Gonçalves, F. L. T., and da Rocha, R. P. (2016). Present climate and future projections of the thermal
28 comfort index for the metropolitan region of São Paulo, Brazil. *Clim. Change* 137, 439–454. doi:10.1007/s10584-
29 016-1690-5.
- 30 Beck, H. E., Vergopolan, N., Pan, M., Levizzani, V., Van Dijk, A. I. J. M., Weedon, G. P., et al. (2017). Global-scale
31 evaluation of 22 precipitation datasets using gauge observations and hydrological modeling. *Hydrol. Earth Syst.*
32 *Sci.* doi:10.5194/hess-21-6201-2017.
- 33 Bedia, J., San-Martín, D., Iturbide, M., Herrera, S., Manzanar, R., and Gutiérrez, J. M. (2019). METACLIP : A
34 semantic provenance framework for climate products. *Environ. Model. Softw.*
- 35 Bell, G. D., and Chelliah, M. (2006). Leading Tropical Modes Associated with Interannual and Multidecadal
36 Fluctuations in North Atlantic Hurricane Activity. *J. Clim.* 19, 590–612. doi:10.1175/JCLI3659.1.
- 37 Bellprat, O., and Doblas-Reyes, F. (2016). Attribution of extreme weather and climate events overestimated by
38 unreliable climate simulations. *Geophys. Res. Lett.* 43, 2158–2164. doi:10.1002/2015GL067189.
- 39 Belušić, A., Prtenjak, M. T., Güttler, I., Ban, N., Leutwyler, D., and Schär, C. (2018). Near-surface wind variability
40 over the broader Adriatic region: insights from an ensemble of regional climate models. *Clim. Dyn.* 50, 4455–
41 4480. doi:10.1007/s00382-017-3885-5.
- 42 Bender, M. A., Knutson, T. R., Tuleya, R. E., Sirutis, J. J., Vecchi, G. A., Garner, S. T., et al. (2010). Modeled Impact
43 of Anthropogenic Warming on the Frequency of Intense Atlantic Hurricanes. *Science (80-.).* 327, 454–458.
44 doi:10.1126/science.1180568.
- 45 Berckmans, J., Woollings, T., Demory, M.-E., Vidale, P.-L., and Roberts, M. (2013). Atmospheric blocking in a high
46 resolution climate model: influences of mean state, orography and eddy forcing. *Atmos. Sci. Lett.* 14, 34–40.
47 doi:10.1002/asl2.412.
- 48 Berg, P., Norin, L., and Olsson, J. (2016). Creation of a high resolution precipitation data set by merging gridded gauge
49 data and radar observations for Sweden. *J. Hydrol.* 541, 6–13. doi:10.1016/J.JHYDROL.2015.11.031.
- 50 Berkhout, F., van den Hurk, B., Bessembinder, J., de Boer, J., Bregman, B., and van Drunen, M. (2013). Framing
51 climate uncertainty: socio-economic and climate scenarios in vulnerability and adaptation assessments. *Reg.*
52 *Environ. Chang.* 14, 879–893. doi:10.1007/s10113-013-0519-2.
- 53 Berthou, S., Kendon, E. J., Chan, S. C., Ban, N., Leutwyler, D., Schär, C., et al. (2018). Pan-European climate at
54 convection-permitting scale: a model intercomparison study. *Clim. Dyn.* doi:10.1007/s00382-018-4114-6.
- 55 Biasutti, M., Sobel, A. H., Camargo, S. J., and Creyts, T. T. (2012). Projected changes in the physical climate of the
56 Gulf Coast and Caribbean. *Clim. Change* 112, 819–845. doi:10.1007/s10584-011-0254-y.
- 57 Bintanja, R., and Andry, O. (2017). Towards a rain-dominated Arctic. *Nat. Clim. Chang.* 7, 263–267.
58 doi:10.1038/nclimate3240.
- 59 Bintanja, R., and Krikken, F. (2016). Magnitude and pattern of Arctic warming governed by the seasonality of radiative
60 forcing. *Sci. Rep.* 6, 1–7. doi:10.1038/srep38287.
- 61 Bintanja, R., and Van Der Linden, E. C. (2013). The changing seasonal climate in the Arctic. *Sci. Rep.* 3, 1–8.

- 1 doi:10.1038/srep01556.
- 2 Bitencourt, D. P., Fuentes, M. V., Maia, P. A., and Amorim, F. T. (2016). Frequência, Duração, Abrangência Espacial e
3 Intensidadedas Ondas de Calor no Brasil. *Rev. Bras. Meteorol.* 31, 506–517. doi:10.1590/0102-
4 778631231420150077.
- 5 Blanchet, J., Molinié, G., and Touati, J. (2018). Spatial analysis of trend in extreme daily rainfall in southern France.
6 *Clim. Dyn.* 51, 799–812. doi:10.1007/s00382-016-3122-7.
- 7 Blázquez, J., and Nuñez, M. N. (2013). Performance of a high resolution global model over southern South America.
8 *Int. J. Climatol.* 33, 904–919. doi:10.1002/joc.3478.
- 9 Boé, J., Somot, S., and Corre, L. Large differences in Summer climate change over Europe as projected by global and
10 regional climate models : causes and consequences. *prep.*
- 11 Boé, J., Somot, S., and Corre, L. Large differences in Summer climate change over Europe as projected by global and
12 regional climate models: causes and consequences. *prep.*
- 13 Boé, J., and Terray, L. (2014). Land–sea contrast, soil-atmosphere and cloud-temperature interactions: interplays and
14 roles in future summer European climate change. *Clim. Dyn.* 42, 683–699. doi:10.1007/s00382-013-1868-8.
- 15 Boening, C., Lebsack, M., Landerer, F., and Stephens, G. (2012). Snowfall-driven mass change on the East Antarctic
16 ice sheet. *Geophys. Res. Lett.* doi:10.1029/2012GL053316.
- 17 Boers, R., Brandsma, T., and Siebesma, A. P. (2017). Impact of aerosols and clouds on decadal trends in all-sky solar
18 radiation over the Netherlands (1966–2015). *Atmos. Chem. Phys.* 17, 8081–8100. doi:10.5194/acp-17-8081-2017.
- 19 Boisvert, L. N., Webster, M. A., Petty, A. A., Markus, T., Bromwich, D. H., and Cullather, R. I. (2018).
20 Intercomparison of precipitation estimates over the Arctic ocean and its peripheral seas from reanalyses. *J. Clim.*
21 31, 8441–8462. doi:10.1175/JCLI-D-18-0125.1.
- 22 Bollmeyer, C., Keller, J. D., Ohlwein, C., Wahl, S., Crewell, S., Friederichs, P., et al. (2015). Towards a high-resolution
23 regional reanalysis for the European CORDEX domain. *Q. J. R. Meteorol. Soc.* 141, 1–15. doi:10.1002/qj.2486.
- 24 Bosilovich, M. G. (2015). MERRA-2 : initial evaluation of the climate. Available at:
25 <https://searchworks.stanford.edu/view/12280665> [Accessed April 4, 2019].
- 26 Box, J. E., Colgan, W. T., Christensen, T. R., Schmidt, N. M., Lund, M., Parmentier, F.-J. W., et al. (2019). Key
27 indicators of Arctic climate change: 1971–2017. *Environ. Res. Lett.* 14, 045010. doi:10.1088/1748-9326/aafc1b.
- 28 Boykoff, M. T. (2011). *Who speaks for the climate? Making sense of media reporting on climate change*. Cambridge:
29 Cambridge University Press doi:10.1017/CBO9780511978586.
- 30 Bozkurt, D., Rondanelli, R., Marín, J. C., and Garreaud, R. (2018). Foehn Event Triggered by an Atmospheric River
31 Underlies Record-Setting Temperature Along Continental Antarctica. *J. Geophys. Res. Atmos.* 123, 3871–3892.
32 doi:10.1002/2017JD027796.
- 33 Brogli, R., Kröner, N., Sørland, S. L., Lüthi, D., Schär, C., Brogli, R., et al. (2019). The Role of Hadley Circulation and
34 Lapse-Rate Changes for the Future European Summer Climate. *J. Clim.* 32, 385–404. doi:10.1175/JCLI-D-18-
35 0431.1.
- 36 Bromwich, D. H., Nicolas, J. P., Monaghan, A. J., Lazzara, M. A., Keller, L. M., Weidner, G. A., et al. (2012). Central
37 West Antarctica among the most rapidly warming regions on Earth. *Nat. Geosci.* 6, 139. Available at:
38 <https://doi.org/10.1038/ngeo1671>.
- 39 Brügger, A., Dessai, S., Devine-Wright, P., Morton, T. A., and Pidgeon, N. F. (2015). Psychological responses to the
40 proximity of climate change. *Nat. Clim. Chang.* 5, 1031–1037. doi:10.1038/nclimate2760.
- 41 Budescu, D. V., Por, H.-H., and Broomell, S. B. (2012). Effective communication of uncertainty in the IPCC reports.
42 *Clim. Change* 113, 181–200. doi:10.1007/s10584-011-0330-3.
- 43 Burger, F., Brock, B., and Montecinos, A. (2018). Seasonal and elevational contrasts in temperature trends in Central
44 Chile between 1979 and 2015. *Glob. Planet. Change* 162, 136–147. doi:10.1016/j.gloplacha.2018.01.005.
- 45 Cabos, W., Sein, D. V., Durán-Quesada, A., Liguori, G., Koldunov, N. V, Martínez-López, B., et al. (2018). Dynamical
46 downscaling of historical climate over CORDEX Central America domain with a regionally coupled atmosphere-
47 -ocean model. *Clim. Dyn.* doi:10.1007/s00382-018-4381-2.
- 48 Cabré, M. F., Solman, S., and Núñez, M. (2016). Regional climate change scenarios over southern South America for
49 future climate (2080-2099) using the MM5 Model. Mean, interannual variability and uncertainties. *Atmosfera* 29,
50 35–60. doi:10.20937/ATM.2016.29.01.04.
- 51 Caesar, J., Alexander, L., and Vose, R. (2006). Large-scale changes in observed daily maximum and minimum
52 temperatures: Creation and analysis of a new gridded data set. *J. Geophys. Res.* 111, D05101.
53 doi:10.1029/2005JD006280.
- 54 Camilo, J. A., Andrade, C. L. T., Amaral, T. A., Tigges, C. H. P., Melo, M. L. A., Chou, S. C., et al. (2018). Impact of
55 climate change on maize grown in the Brazilian cerrado. in *2018 Detroit, Michigan July 29 - August 1, 2018* (St.
56 Joseph, MI: American Society of Agricultural and Biological Engineers). doi:10.13031/aim.201800967.
- 57 Campbell, J. D., Taylor, M. A., Stephenson, T. S., Watson, R. A., and Whyte, F. S. (2011). Future climate of the
58 Caribbean from a regional climate model. *Int. J. Climatol.* 31, 1866–1878. doi:10.1002/joc.2200.
- 59 Candan, K. S., Liu, H., and Suvarna, R. (2001). Resource Description Framework : Metadata and Its Applications.
60 *SIGKDD Explor.* doi:10.1145/507533.507536.
- 61 Cantet, P., Déqué, M., Palany, P., and Maridet, J.-L. (2014). The importance of using a high-resolution model to study

- 1 the climate change on small islands: the Lesser Antilles case. *Tellus A Dyn. Meteorol. Oceanogr.* 66, 24065.
2 doi:10.3402/tellusa.v66.24065.
- 3 Cardil, A., Molina, D. M., and Kobziar, L. N. (2014). Extreme temperature days and their potential impacts on southern
4 Europe. *Nat. Hazards Earth Syst. Sci.* 14, 3005–3014. doi:10.5194/nhess-14-3005-2014.
- 5 Cardoso, R. M., Soares, P. M. M., Lima, D. C. A., and Semedo, A. (2016). The impact of climate change on the Iberian
6 low-level wind jet: EURO-CORDEX regional climate simulation. *Tellus A Dyn. Meteorol. Oceanogr.* 68, 29005.
7 doi:10.3402/tellusa.v68.29005.
- 8 Casanueva, A., Kotlarski, S., Herrera, S., Fernández, J., Gutiérrez, J. M., Boberg, F., et al. (2016). Daily precipitation
9 statistics in a EURO-CORDEX RCM ensemble: added value of raw and bias-corrected high-resolution
10 simulations. *Clim. Dyn.* 47, 719–737. doi:10.1007/s00382-015-2865-x.
- 11 Casanueva, A., Rodríguez-Puebla, C., Frías, M. D., and González-Reviriego, N. (2014). Variability of extreme
12 precipitation over Europe and its relationships with teleconnection patterns. *Hydrol. Earth Syst. Sci.* 18, 709–725.
13 doi:https://doi.org/10.5194/hess-18-709-2014.
- 14 Cassou, C., Terray, L., and Phillips, A. S. (2005). Tropical Atlantic influence on European heat waves. *J. Clim.*
15 doi:10.1175/JCLI3506.1.
- 16 Cattiaux, J., Douville, H., and Peings, Y. (2013). European temperatures in CMIP5: origins of present-day biases and
17 future uncertainties. *Clim. Dyn.* 41, 2889–2907. doi:10.1007/s00382-013-1731-y.
- 18 Cavalcanti, I. F. A., Carril, A. F., Penalba, O. C., Grimm, A. M., Menéndez, C. G., Sanchez, E., et al. (2015).
19 Precipitation extremes over La Plata Basin – Review and new results from observations and climate simulations.
20 *J. Hydrol.* 523, 211–230. doi:10.1016/j.jhydrol.2015.01.028.
- 21 Cavazos, T., and Arriaga-Ramírez, S. (2012). Downscaled Climate Change Scenarios for Baja California and the North
22 American Monsoon during the Twenty-First Century. *J. Clim.* 25, 5904–5915. doi:10.1175/JCLI-D-11-00425.1.
- 23 Cavazos, T., Luz-Nino, R., Cerezo-Mota, R., Fuentes-Franco, R., Mendez, M., and L.F., P.-M. (2019). Intercomparison
24 of regional Climate models and climatic trends in the Cordex CAM (Central America Caribbean and Mexico)
25 domain. *Submitted*.
- 26 Cavicchia, L., Scoccimarro, E., Gualdi, S., Marson, P., Ahrens, B., Berthou, S., et al. (2018). Mediterranean extreme
27 precipitation: a multi-model assessment. *Clim. Dyn.* 51, 901–913. doi:10.1007/s00382-016-3245-x.
- 28 Ceccherini, G., Russo, S., Ametztoy, I., Romero, C. P., and Carmona-Moreno, C. (2016). Magnitude and frequency of
29 heat and cold waves in recent decades: the case of South America. *Nat. Hazards Earth Syst. Sci.* 16, 821–831.
30 doi:10.5194/nhess-16-821-2016.
- 31 Centella-Artola, A., Taylor, M. A., Bezanilla-Morlot, A., Martínez-Castro, D., Campbell, J. D., Stephenson, T. S., et al.
32 (2015). Assessing the effect of domain size over the Caribbean region using the PRECIS regional climate model.
33 *Clim. Dyn.* 44, 1901–1918. doi:10.1007/s00382-014-2272-8.
- 34 Ceppi, P., Scherrer, S. C., Fischer, A. M., and Appenzeller, C. (2012). Revisiting Swiss temperature trends 1959–2008.
35 *Int. J. Climatol.* 32, 203–213. doi:10.1002/joc.2260.
- 36 Cerezo-Mota, R., Cavazos, T., Arriaga, R., Torres-Alavez, A., Sieck, K., Nikulin, G., et al. (2015). CORDEX-NA:
37 Factors inducing dry/wet years on the North American Monsoon region. *Int. J. Climatol.* 36.
38 doi:10.1002/joc.4385.
- 39 Chapman, D. A., Corner, A., Webster, R., and Markowitz, E. M. (2016). Climate visuals: A mixed methods
40 investigation of public perceptions of climate images in three countries. *Glob. Environ. Chang.* 41, 172–182.
41 doi:10.1016/j.gloenvcha.2016.10.003.
- 42 Cheong, W. K., Timbal, B., Golding, N., Sirabaha, S., Kwan, K. F., Cinco, T. A., et al. (2018). Observed and modelled
43 temperature and precipitation extremes over Southeast Asia from 1972 to 2010. *Int. J. Climatol.* 38, 3013–3027.
44 doi:10.1002/joc.5479.
- 45 Chou, S. C., Lyra, A., Mourão, C., Dereczynski, C., Pilotto, I., Gomes, J., et al. (2014a). Assessment of Climate Change
46 over South America under RCP 4.5 and 8.5 Downscaling Scenarios. *Am. J. Clim. Chang.* 03, 512–527.
47 doi:10.4236/ajcc.2014.35043.
- 48 Chou, S. C., Lyra, A., Mourão, C., Dereczynski, C., Pilotto, I., Gomes, J., et al. (2014b). Assessment of Climate Change
49 over South America under RCP 4.5 and 8.5 Downscaling Scenarios. *Am. J. Clim. Chang.* 03, 512–527.
50 doi:10.4236/ajcc.2014.35043.
- 51 Choudhary, A., and Dimri, A. P. (2018). Assessment of CORDEX-South Asia experiments for monsoonal precipitation
52 over Himalayan region for future climate. *Clim. Dyn.* 50, 3009–3030. doi:10.1007/s00382-017-3789-4.
- 53 Christensen, J. H., Kumar, K. K., Aldria, E., An, S.-I., Cavalcanti, I. F. A., Castro, M. de, et al. (2013). “Climate
54 Phenomena and their Relevance for Future Regional Climate Change Supplementary Material,” in *Climate
55 Change 2013: The Physical Science Basis. Contribution of Working Group I to the Fifth Assessment Report of the
56 Intergovernmental Panel on Climate Change*, 62. doi:10.1017/CBO9781107415324.028.
- 57 Christidis, N., Stott, P. A., Christidis, N., and Stott, P. A. (2015). Extreme Rainfall in the United Kingdom During
58 Winter 2013/14: The Role of Atmospheric Circulation and Climate Change. *Bull. Am. Meteorol. Soc.* 96, S46–
59 S50. doi:10.1175/BAMS-D-15-00094.1.
- 60 Chung, C. E., Cha, H., Vihma, T., Räisänen, P., and Decremmer, D. (2013). On the possibilities to use atmospheric
61 reanalyses to evaluate the warming structure in the Arctic. *Atmos. Chem. Phys.* 13, 11209–11219.

- 1 doi:10.5194/acp-13-11209-2013.
- 2 Chung, J. X., Juneng, L., Tangang, F., and Jamaluddin, A. F. (2018). Performances of BATS and CLM land-surface
3 schemes in RegCM4 in simulating precipitation over CORDEX Southeast Asia domain. *Int. J. Climatol.* 38, 794–
4 810. doi:10.1002/joc.5211.
- 5 Cinco, T. A., de Guzman, R. G., Hilario, F. D., and Wilson, D. M. (2014). Long-term trends and extremes in observed
6 daily precipitation and near surface air temperature in the Philippines for the period 1951–2010. *Atmos. Res.* 145–
7 146, 12–26. doi:10.1016/J.ATMOSRES.2014.03.025.
- 8 Collins, M., Knutti, R., Arblaster, J., Dufresne, J.-L., Fichet, T., Friedlingstein, P., et al. (2013). “Chapter 12 - Long-
9 term climate change: Projections, commitments and irreversibility,” in *Climate Change 2013: The Physical
10 Science Basis. IPCC Working Group I Contribution to AR5*, ed. IPCC (Cambridge: Cambridge University Press).
11 Available at: <http://pure.iiasa.ac.at/id/eprint/10551/>.
- 12 Colorado-Ruiz, G., Cavazos, T., Salinas, J. A., De Grau, P., and Ayala, R. (2018). Climate change projections from
13 Coupled Model Intercomparison Project phase 5 multi-model weighted ensembles for Mexico, the North
14 American monsoon, and the mid-summer drought region. *Int. J. Climatol.* 38, 5699–5716. doi:10.1002/joc.5773.
- 15 Comiso, J. C., and Hall, D. K. (2014). Climate trends in the Arctic as observed from space. *Wiley Interdiscip. Rev.*
16 *Clim. Chang.* 5, 389–409. doi:10.1002/wcc.277.
- 17 Consortium, P. 2k, Ahmed, M., Anchukaitis, K. J., Asrat, A., Borgaonkar, H. P., Braida, M., et al. (2013). Continental-
18 scale temperature variability during the past two millennia. *Nat. Geosci.* 6, 339–346. doi:10.1038/ngeo1797.
- 19 Coppola, E., Giorgi, F., Raffaele, F., Fuentes-Franco, R., Giuliani, G., Llopart-Pereira, M., et al. (2014a). Present and
20 future climatologies in the phase I CREMA experiment. *Clim. Change* 125, 23–38. doi:10.1007/s10584-014-
21 1137-9.
- 22 Coppola, E., Giorgi, F., Raffaele, F., Fuentes-Franco, R., Giuliani, G., Llopart-Pereira, M., et al. (2014b). Present and
23 future climatologies in the phase I CREMA experiment. *Clim. Change* 125, 23–38. doi:10.1007/s10584-014-
24 1137-9.
- 25 Coppola, E., Sobolowski, S., Pichelli, E., Raffaele, F., Ahrens, B., Anders, I., et al. (2018). A first-of-its-kind multi-
26 model convection permitting ensemble for investigating convective phenomena over Europe and the
27 Mediterranean. *Clim. Dyn.* doi:10.1007/s00382-018-4521-8.
- 28 Corner, A., Markowitz, E., and Pidgeon, N. (2014). Public engagement with climate change: the role of human values.
29 *Wiley Interdiscip. Rev. Clim. Chang.* 5, 411–422. doi:10.1002/wcc.269.
- 30 Corner, A., Whitmarsh, L., and Xenias, D. (2012). Uncertainty, scepticism and attitudes towards climate change: biased
31 assimilation and attitude polarisation. *Clim. Change* 114, 463–478. doi:10.1007/s10584-012-0424-6.
- 32 Coumou, D., and Rahmstorf, S. (2012). A decade of weather extremes. *Nat. Clim. Chang.* 2, 491–496.
33 doi:10.1038/nclimate1452.
- 34 Cruz, F. T., Narisma, G. T., Dado, J. B., Singhruck, P., Tangang, F., Linarka, U. A., et al. (2017). Sensitivity of
35 temperature to physical parameterization schemes of RegCM4 over the CORDEX-Southeast Asia region. *Int. J.*
36 *Climatol.* 37, 5139–5153. doi:10.1002/joc.5151.
- 37 Cruz, F. T., Narisma, G. T., Villafuerte, M. Q., Cheng Chua, K. U., and Olaguera, L. M. (2013). A climatological
38 analysis of the southwest monsoon rainfall in the Philippines. *Atmos. Res.* 122, 609–616.
39 doi:10.1016/J.ATMOSRES.2012.06.010.
- 40 Cruz, F. T., and Sasaki, H. (2017). Simulation of Present Climate over Southeast Asia Using the Non-Hydrostatic
41 Regional Climate Model. *SOLA* 13, 13–18. doi:10.2151/sola.2017-003.
- 42 Cueto, O. R. G., Soto, N. S., Núñez, M. Q., Benítez, S. O., and Limón, N. V. (2013). Extreme temperature scenarios in
43 Mexicali, Mexico under climate change conditions. *Atmósfera* 26, 509–520. doi:https://doi.org/10.1016/S0187-
44 6236(13)71092-0.
- 45 Cueto, R. O. G., Martínez, A. T., and Ostos, E. J. (2010). Heat waves and heat days in an arid city in the northwest of
46 México: current trends and in climate change scenarios. *Int. J. Biometeorol.* 54, 335–345. doi:10.1007/s00484-
47 009-0283-7.
- 48 Cunningham, L. K., Austin, W. E., Knudsen, K. L., Eiriksson, J., Scourse, J. D., Wanamaker, A. D., et al. (2013).
49 Reconstructions of surface ocean conditions from the northeast Atlantic and Nordic seas during the last
50 millennium. *Holocene*. doi:10.1177/0959683613479677.
- 51 da Rocha, R. P., Reboita, M. S., Dutra, L. M. M., Llopart, M. P., and Coppola, E. (2014). Interannual variability
52 associated with ENSO: present and future climate projections of RegCM4 for South America-CORDEX domain.
53 *Clim. Change* 125, 95–109. doi:10.1007/s10584-014-1119-y.
- 54 Dafka, S., Toreti, A., Luterbacher, J., Zanis, P., Tyrlis, E., and Xoplaki, E. (2018). On the ability of RCMs to capture
55 the circulation pattern of Etesians. *Clim. Dyn.* 51, 1687–1706. doi:10.1007/s00382-017-3977-2.
- 56 Dahlgren, P., and Gustafsson, N. (2012). Assimilating host model information into a limited area model. *Tellus, Ser. A*
57 *Dyn. Meteorol. Oceanogr.* 64. doi:10.3402/tellusa.v64i0.15836.
- 58 Dahlgren, P., Landelius, T., Kållberg, P., and Gollvik, S. (2016). A high-resolution regional reanalysis for Europe. Part
59 1: Three-dimensional reanalysis with the regional High-Resolution Limited-Area Model (HIRLAM). *Q. J. R.*
60 *Meteorol. Soc.* 142, 2119–2131. doi:10.1002/qj.2807.
- 61 Dai, A. (2011). Drought under global warming: A review. *Wiley Interdiscip. Rev. Clim. Chang.* doi:10.1002/wcc.81.

- 1 Dai, A., Rasmussen, R. M., Ikeda, K., and Liu, C. (2017). A new approach to construct representative future forcing
2 data for dynamic downscaling. *Clim. Dyn.*, 1–9. doi:10.1007/s00382-017-3708-8.
- 3 Daniel, M., Lemonsu, A., Déqué, M., Somot, S., Alias, A., and Masson, V. (2018). Benefits of explicit urban
4 parameterization in regional climate modeling to study climate and city interactions. *Clim. Dyn.*
5 doi:10.1007/s00382-018-4289-x.
- 6 Darmaraki S., Somot S., Sevault F., N. P. (2019). Past variability of Mediterranean Marine Heat Waves. *Submitted*.
- 7 Darmaraki, S., Somot, S., Sevault, F., Nabat, P., Cabos Narvaez, W. D., Cavicchia, L., et al. (2019). Future evolution of
8 Marine Heatwaves in the Mediterranean Sea. *Clim. Dyn.* doi:10.1007/s00382-019-04661-z.
- 9 Daron, J. (2014a). Regional Climate Messages: West Africa. *Sci. Rep. from CARIIA Adapt. Scale Semi-Arid Reg. Proj.*
- 10 Daron, J. D. (2014b). Regional Climate Messages for East Africa. *Cariia Assar*.
- 11 Daron, J. D., Lorenz, S., Wolski, P., Blamey, R. C., and Jack, C. (2015). Interpreting climate data visualisations to
12 inform adaptation decisions. *Clim. Risk Manag.* 10, 17–26. doi:10.1016/J.CRM.2015.06.007.
- 13 Daron, J., Macadam, I., Kanamaru, H., Cinco, T., Katzfey, J., Scannell, C., et al. (2018). Providing future climate
14 projections using multiple models and methods: insights from the Philippines. *Clim. Change* 148, 187–203.
15 doi:10.1007/s10584-018-2183-5.
- 16 Dash, S. K., Mishra, S. K., and Pattnayak, K. C. (2014). Projected seasonal mean summer monsoon over India and
17 adjoining regions for the twenty-first century. doi:10.1007/s00704-014-1310-0.
- 18 Dash, S. K., Mishra, S. K., Pattnayak, K. C., Mamgain, A., Mariotti, L., Coppola, E., et al. (2015a). Projected seasonal
19 mean summer monsoon over India and adjoining regions for the twenty-first century. *Theor. Appl. Climatol.* 122,
20 581–593. doi:10.1007/s00704-014-1310-0.
- 21 Dash, S. K., Pattnayak, K. C., Panda, S. K., Vaddi, D., and Mamgain, A. (2015b). Impact of domain size on the
22 simulation of Indian summer monsoon in RegCM4 using mixed convection scheme and driven by HadGEM2:
23 Impact of domain size on ISM simulations. *Clim. Dyn.* 44, 961–975. doi:10.1007/s00382-014-2420-1.
- 24 Davin, E. L., Rechid, D., Breil, M., Cardoso, R. M., Coppola, E., Hoffmann, P., et al. (2019). Biogeophysical impacts
25 of forestation in Europe: First results from the LUCAS Regional Climate Model intercomparison. *Earth Syst.*
26 *Dyn. Discuss.*, 1–31. doi:10.5194/esd-2019-4.
- 27 Davini, P., and D’Andrea, F. (2016). Northern Hemisphere Atmospheric Blocking Representation in Global Climate
28 Models: Twenty Years of Improvements? *J. Clim.* 29, 8823–8840. doi:10.1175/JCLI-D-16-0242.1.
- 29 de Abreu, R. C., Cunningham, C., Rudorff, C. M., Rudorff, N., Abatan, A. A., Tett, S. F. B., et al. (2019). Contribution
30 of Anthropogenic Climate Change to April–May 2017 Heavy Precipitation over the Uruguay River Basin. *Bull.*
31 *Am. Meteorol. Soc.* 100, S37–S41. doi:10.1175/BAMS-D-18-0102.1.
- 32 de Barros Soares, D., Lee, H., Loikith, P. C., Barkhordarian, A., and Mechoso, C. R. (2017). Can significant trends be
33 detected in surface air temperature and precipitation over South America in recent decades? *Int. J. Climatol.* 37,
34 1483–1493. doi:10.1002/joc.4792.
- 35 de Carvalho, L. M. V., and Cavalcanti, I. F. A. (2016). “The South American Monsoon System (SAMS),” in *The*
36 *Monsoons and Climate Change: Observations and Modeling*, eds. L. M. V. de Carvalho and C. Jones (Cham:
37 Springer International Publishing), 121–148. doi:10.1007/978-3-319-21650-8_6.
- 38 de Jesus, E., da Rocha, R., Reboita, M., Llopart, M., Mosso Dutra, L., and Remedio, A. (2016). Contribution of cold
39 fronts to seasonal rainfall in simulations over the southern La Plata Basin. *Clim. Res.* 68, 243–255.
40 doi:10.3354/cr01358.
- 41 Deb, P., Orr, A., Bromwich, D. H., Nicolas, J. P., Turner, J., and Hosking, J. S. (2018). Summer Drivers of
42 Atmospheric Variability Affecting Ice Shelf Thinning in the Amundsen Sea Embayment, West Antarctica.
43 *Geophys. Res. Lett.* 45, 4124–4133. doi:10.1029/2018GL077092.
- 44 Dell’Aquila, A., Mariotti, A., Bastin, S., Calmanti, S., Cavicchia, L., Deque, M., et al. (2018). Evaluation of simulated
45 decadal variations over the Euro-Mediterranean region from ENSEMBLES to Med-CORDEX. *Clim. Dyn.* 51,
46 857–876. doi:10.1007/s00382-016-3143-2.
- 47 Déqué, M., and Somot, S. (2008). Analysis of heavy precipitation for France using high resolution ALADIN RCM
48 simulations. *Időjárás Quaterly J. Hungarian Meteorol. Serv.* 112, PP. 179-190. Available at: [https://hal-](https://hal-meteofrance.archives-ouvertes.fr/meteo-00370705/)
49 [meteofrance.archives-ouvertes.fr/meteo-00370705/](https://hal-meteofrance.archives-ouvertes.fr/meteo-00370705/) [Accessed March 22, 2019].
- 50 Deshpande, N. R., and Kulkarni, B. D. (2015). Changing pattern of heavy rainstorms in the Indus basin of India under
51 global warming scenarios. *J. Earth Syst. Sci.* 124, 829–841. doi:10.1007/s12040-015-0570-0.
- 52 Dessai, S., Bhawe, A., Birch, C., Conway, D., Garcia-Carreras, L., Gosling, J. P., et al. (2018). Building narratives to
53 characterise uncertainty in regional climate change through expert elicitation. *Environ. Res. Lett.* 13, 074005.
54 doi:10.1088/1748-9326/aabccd.
- 55 Diedhiou, A., Bichet, A., Wartenburger, R., Seneviratne, S. I., Rowell, D. P., Sylla, M. B., et al. (2018). Changes in
56 climate extremes over West and Central Africa at 1.5 and 2 degree C global warming. *Environ. Res. Lett.* 13,
57 65020. doi:10.1088/1748-9326/aac3e5.
- 58 Dietrich, C., Wang, S., Schimanke, S., Gröger, M., Klein, B., Hordoir, B., et al. (2019). Surface Heat Budget over the
59 North Sea in Climate Change Simulations. *Submitted*.
- 60 Dileepkumar, R., AchutaRao, K., and Arulalan, T. (2018). Human influence on sub-regional surface air temperature
61 change over India. *Sci. Rep.* 8, 8967. doi:10.1038/s41598-018-27185-8.

- 1 Dimri, A. P., Kumar, D., Choudhary, A., and Maharana, P. (2018a). Future changes over the Himalayas : Maximum and
2 minimum temperature. *Glob. Planet. Change* 162, 212–234. doi:10.1016/j.gloplacha.2018.01.015.
- 3 Dimri, A. P., Kumar, D., Choudhary, A., and Maharana, P. (2018b). Future changes over the Himalayas: Mean
4 temperature. *Glob. Planet. Change* 162, 235–251. doi:10.1016/J.GLOPLACHA.2018.01.014.
- 5 Diro, G., Rauscher, S. A., Giorgi, F., and M. Tompkins, A. (2012a). Sensitivity of seasonal climate and diurnal
6 precipitation over Central America to land and sea surface schemes in RegCM4. *Clim. Res.* 52, 31–48.
7 doi:10.3354/cr01049.
- 8 Diro, G. T., Giorgi, F., Fuentes-Franco, R., Walsh, K. J. E., Giuliani, G., and Coppola, E. (2014). Tropical cyclones in a
9 regional climate change projection with RegCM4 over the CORDEX Central America domain. *Clim. Change*
10 125, 79–94. doi:10.1007/s10584-014-1155-7.
- 11 Diro, G. T., Tompkins, A. M., and Bi, X. (2012b). Dynamical downscaling of ECMWF Ensemble seasonal forecasts
12 over East Africa with RegCM3. *J. Geophys. Res. Atmos.* 117. doi:10.1029/2011JD016997.
- 13 Dittmann, A., Schlosser, E., Masson-Delmotte, V., Powers, J. G., Manning, K. W., Werner, M., et al. (2016).
14 Precipitation regime and stable isotopes at Dome Fuji, East Antarctica. *Atmos. Chem. Phys.* 16, 6883–6900.
15 doi:10.5194/acp-16-6883-2016.
- 16 Donat, M. G., Alexander, L. V., Yang, H., Durre, I., Vose, R., Dunn, R. J. H., et al. (2013). Updated analyses of
17 temperature and precipitation extreme indices since the beginning of the twentieth century: The HadEX2 dataset.
18 *J. Geophys. Res. Atmos.* 118, 2098–2118. doi:10.1002/jgrd.50150.
- 19 Dosio, A., and Fischer, E. M. (2017). Will Half a Degree Make a Difference? Robust Projections of Indices of Mean
20 and Extreme Climate in Europe Under 1.5°C, 2°C, and 3°C Global Warming. *Geophys. Res. Lett.* 45, 935–944.
21 doi:10.1002/2017GL076222.
- 22 Dosio, A., and Panitz, H. J. (2016). Climate change projections for CORDEX-Africa with COSMO-CLM regional
23 climate model and differences with the driving global climate models. *Clim. Dyn.* 46. doi:10.1007/s00382-015-
24 2664-4.
- 25 Drobinski, P., Bastin, S., Arsouze, T., Beranger, K., Flaounas, E., Stefanon, M. (2018). North-western Mediterranean
26 sea-breeze circulation in a regional climate system model. *Clim. Dyn.* 51, 1077–1093. doi:10.1007/s00382-017-
27 3595-z.
- 28 Drobinski, P., Silva, N. Da, Panthou, G., Bastin, S., Muller, C., Ahrens, B., et al. (2018). Scaling precipitation extremes
29 with temperature in the Mediterranean: past climate assessment and projection in anthropogenic scenarios. *Clim.*
30 *Dyn.* 51, 1237–1257. doi:10.1007/s00382-016-3083-x.
- 31 Drugé, T., Nabat, P., Mallet, M., and Somot, S. Model simulation of ammonium and nitrate aerosols distribution in the
32 Euro-Mediterranean region and their radiative and climatic effects over 1979-2016. doi:10.5194/acp-2018-1101.
- 33 Dunn-Sigouin, E., and Son, S.-W. (2013). Northern Hemisphere blocking frequency and duration in the CMIP5 models.
34 *J. Geophys. Res. Atmos.* 118, 1179–1188. doi:10.1002/jgrd.50143.
- 35 Dyrrdal, A. V., Stordal, F., and Lussana, C. (2018). Evaluation of summer precipitation from EURO-CORDEX fine-
36 scale RCM simulations over Norway. *Int. J. Climatol.* 38, 1661–1677. doi:10.1002/joc.5287.
- 37 Easterling, D. R., Wallis, T. W. R., Lawrimore, J. H., and Heim Jr., R. R. (2007). Effects of temperature and
38 precipitation trends on U.S. drought. *Geophys. Res. Lett.* 34. doi:10.1029/2007GL031541.
- 39 Emanuel, K. A. (1995). Sensitivity of Tropical Cyclones to Surface Exchange Coefficients and a Revised Steady-State
40 Model incorporating Eye Dynamics. *J. Atmos. Sci.* 52, 3969–3976.
- 41 Endris, H. S., Lennard, C., Hewitson, B., Dosio, A., Nikulin, G., and Panitz, H. J. (2016). Teleconnection responses in
42 multi-GCM driven CORDEX RCMs over Eastern Africa. *Clim. Dyn.* doi:10.1007/s00382-015-2734-7.
- 43 Endris, H. S., Omondi, P., Jain, S., Lennard, C., Hewitson, B., Chang’a, L., et al. (2013). Assessment of the
44 performance of CORDEX regional climate models in simulating East African rainfall. *J. Clim.* doi:10.1175/JCLI-
45 D-12-00708.1.
- 46 Enfield, D. B., Mestas-Núñez, A. M., and Trimble, P. J. (2001). The Atlantic Multidecadal Oscillation and its relation
47 to rainfall and river flows in the continental U.S. *Geophys. Res. Lett.* 28, 2077–2080.
48 doi:10.1029/2000GL012745.
- 49 Engelbrecht, F., Adegoke, J., Bopape, M. J., Naidoo, M., Garland, R., Thatcher, M., et al. (2015). Projections of rapidly
50 rising surface temperatures over Africa under low mitigation. *Environ. Res. Lett.* doi:10.1088/1748-
51 9326/10/8/085004.
- 52 Espinoza, J. C., Ronchail, J., Frappart, F., Lavado, W., Santini, W., and Guyot, J. L. (2013). The Major Floods in the
53 Amazonas River and Tributaries (Western Amazon Basin) during the 1970–2012 Period: A Focus on the 2012
54 Flood*. *J. Hydrometeorol.* 14, 1000–1008. doi:10.1175/JHM-D-12-0100.1.
- 55 Fantini, A., Raffaele, F., Torma, C., Bacer, S., Coppola, E., Giorgi, F., et al. (2018). Assessment of multiple daily
56 precipitation statistics in ERA-Interim driven Med-CORDEX and EURO-CORDEX experiments against high
57 resolution observations. *Clim. Dyn.* 51, 877–900. doi:10.1007/s00382-016-3453-4.
- 58 Feinberg, M., and Willer, R. (2013). The Moral Roots of Environmental Attitudes. *Psychol. Sci.* 24, 56–62.
59 doi:10.1177/0956797612449177.
- 60 Feldman, L., and Sol Hart, P. (2018). Climate change as a polarizing cue: Framing effects on public support for low-
61 carbon energy policies. *Glob. Environ. Chang.* 51, 54–66. doi:10.1016/j.gloenvcha.2018.05.004.

- 1 Fernandes, K., Giannini, A., Verchot, L., Baethgen, W., and Pinedo-Vasquez, M. (2015). Decadal covariability of
2 Atlantic SSTs and western Amazon dry-season hydroclimate in observations and CMIP5 simulations. *Geophys.*
3 *Res. Lett.* 42, 6793–6801. doi:10.1002/2015GL063911.
- 4 Fernández, J., Frías, M. D., Cabos, W. D., Cofiño, A. S., Domínguez, M., Fita, L., et al. (2018). Consistency of climate
5 change projections from multiple global and regional model intercomparison projects. *Clim. Dyn.*
6 doi:10.1007/s00382-018-4181-8.
- 7 Fernandez, J. P. R., Franchito, S. H., Rao, V. B., and Llopart, M. (2017). Changes in Koppen-Trewartha climate
8 classification over South America from RegCM4 projections. *Atmos. Sci. Lett.* 18, 427–434. doi:10.1002/asl.785.
- 9 Fischer, E. M., Beyerle, U., and Knutti, R. (2013). Robust spatially aggregated projections of climate extremes. *Nat.*
10 *Clim. Chang.* 3, 1033. Available at: <http://dx.doi.org/10.1038/nclimate2051>.
- 11 Fischer, E. M., and Knutti, R. (2015a). Anthropogenic contribution to global occurrence of heavy-precipitation and
12 high-temperature extremes. *Nat. Clim. Chang.* 5, 560–564. doi:10.1038/nclimate2617.
- 13 Fischer, E. M., and Knutti, R. (2015b). Anthropogenic contribution to global occurrence of heavy-precipitation and
14 high-temperature extremes. *Nat. Clim. Chang.* 5, 560–564. doi:10.1038/nclimate2617.
- 15 Flaounas, E., Kelemen, F. D., Wernli, H., Gaertner, M. A., Reale, M., Sanchez-Gomez, E., et al. (2018). Assessment of
16 an ensemble of ocean–atmosphere coupled and uncoupled regional climate models to reproduce the climatology
17 of Mediterranean cyclones. *Clim. Dyn.* 51, 1023–1040. doi:10.1007/s00382-016-3398-7.
- 18 Flato, G., Marotzke, J., Abiodun, B., Braconnot, P., Chou, S. C., Collins, W., et al. (2013). IPCC 2013 AR5 - Chapter 9:
19 Evaluation of Climate Models. *Clim. Chang. 2013 Phys. Sci. Basis. Contrib. Work. Gr. I to Fifth Assess. Rep.*
20 *Intergov. Panel Clim. Chang.*, 741–866. doi:10.1017/CBO9781107415324.
- 21 Fleig, A. K., Tallaksen, L. M., James, P., Hisdal, H., and Stahl, K. (2015). Attribution of European precipitation and
22 temperature trends to changes in synoptic circulation. *Hydrol. Earth Syst. Sci.* 19, 3093–3107.
23 doi:<https://doi.org/10.5194/hess-19-3093-2015>.
- 24 Fontrodona Bach, A., Schrier, G., Melsen, L. A., Klein Tank, A. M. G., and Teuling, A. J. (2018). Widespread and
25 Accelerated Decrease of Observed Mean and Extreme Snow Depth Over Europe. *Geophys. Res. Lett.* 45, 12,312–
26 12,319. doi:10.1029/2018GL079799.
- 27 Freychet, N., Hsu, H. H., Chou, C., and Wu, C. H. (2015). Asian summer monsoon in CMIP5 projections: A link
28 between the change in extreme precipitation and monsoon dynamics. *J. Clim.* 28, 1477–1493. doi:10.1175/JCLI-
29 D-14-00449.1.
- 30 Frieler, K., Clark, P. U., He, F., Buizert, C., Reese, R., Ligtenberg, S. R. M., et al. (2015). Consistent evidence of
31 increasing Antarctic accumulation with warming. *Nat. Clim. Chang.* 5, 348. Available at:
32 <https://doi.org/10.1038/nclimate2574>.
- 33 Frolov, A. V., Blinov, V. G., Golitsyn, G., Dymnikov, V. P., Izrael, Y. A., and Alekseev, G. V. (2014). *The Second*
34 *Roshydromet Assessment Report on Climate Change and its Consequences in the Russian Federation*.
- 35 Fu, R., Yin, L., Li, W., Arias, P. A., Dickinson, R. E., Huang, L., et al. (2013). Increased dry-season length over
36 southern Amazonia in recent decades and its implication for future climate projection. *Proc. Natl. Acad. Sci.* 110,
37 18110–18115. doi:10.1073/pnas.1302584110.
- 38 Fuentes-Franco, R., Coppola, E., Giorgi, F., Graef, F., and Pavia, E. G. (2014). Assessment of RegCM4 simulated inter-
39 annual variability and daily-scale statistics of temperature and precipitation over Mexico. *Clim. Dyn.* 42, 629–
40 647. doi:10.1007/s00382-013-1686-z.
- 41 Fuentes-Franco, R., Coppola, E., Giorgi, F., Pavia, E. G., Diro, G. T., and Graef, F. (2015). Inter-annual variability of
42 precipitation over Southern Mexico and Central America and its relationship to sea surface temperature from a set
43 of future projections from CMIP5 GCMs and RegCM4 CORDEX simulations. *Clim. Dyn.* 45, 425–440.
44 doi:10.1007/s00382-014-2258-6.
- 45 Fuentes-Franco, R., Giorgi, F., Coppola, E., and Zimmermann, K. (2017). Sensitivity of tropical cyclones to resolution,
46 convection scheme and ocean flux parameterization over Eastern Tropical Pacific and Tropical North Atlantic
47 Oceans in the RegCM4 model. *Clim. Dyn.* 49, 547–561. doi:10.1007/s00382-016-3357-3.
- 48 Fumière, Q., Déqué, M., Nuissier, O., Somot, S., Alias, A., Caillaud, C., et al. (2019). Extreme rainfall in
49 Mediterranean France during autumn: added-value of the AROME-Climate Convection-Permitting Regional
50 Climate Model. *Submitted*.
- 51 Gaertner, M. Á., González-Alemán, J. J., Romera, R., Domínguez, M., Gil, V., Sánchez, E., et al. (2018). Simulation of
52 medicanes over the Mediterranean Sea in a regional climate model ensemble: impact of ocean–atmosphere
53 coupling and increased resolution. *Clim. Dyn.* 51, 1041–1057. doi:10.1007/s00382-016-3456-1.
- 54 Gamble, D. W., and Curtis, S. (2008). Caribbean precipitation: review, model and prospect. *Prog. Phys. Geogr. Earth*
55 *Environ.* 32, 265–276. doi:10.1177/0309133308096027.
- 56 García-Díez, M., Fernández, J., and Vautard, R. (2015). An RCM multi-physics ensemble over Europe: multi-variable
57 evaluation to avoid error compensation. *Clim. Dyn.* 45, 3141–3156. doi:10.1007/s00382-015-2529-x.
- 58 Gbobaniyi, E., Sarr, A., Sylla, M. B. M. B., Diallo, I., Lennard, C., Dosio, A., et al. (2014). Climatology, annual cycle
59 and interannual variability of precipitation and temperature in CORDEX simulations over West Africa. *Int. J.*
60 *Climatol.* 34. doi:10.1002/joc.3834.
- 61 Ge, F., Zhu, S., Peng, T., Zhao, Y., Sielmann, F., Fraedrich, K., et al. (2019). Risks of precipitation extremes over

- 1 Southeast Asia: does 1.5 or 2 degrees global warming make a difference? *Environ. Res. Lett.* doi:10.1088/1748-
2 9326/aaff7e.
- 3 Georgia's Third National Communication to the UNFCCC (2015). Available at:
4 <https://unfccc.int/resource/docs/natc/geonc3.pdf> [Accessed April 2, 2019].
- 5 Gevorgyan, A. (2014). Surface and tropospheric temperature trends in Armenia. *Int. J. Climatol.* 34, 3559–3573.
6 doi:10.1002/joc.3928.
- 7 Gevorgyan, A., Melkonyan, H., Aleksanyan, T., Iritsyan, A., and Khalatyan, Y. (2016). An assessment of observed and
8 projected temperature changes in Armenia. *Arab. J. Geosci.* 9, 27. doi:10.1007/s12517-015-2167-y.
- 9 Ghimire, S., Choudhary, A., and Dimri, A. P. (2018). Assessment of the performance of CORDEX-South Asia
10 experiments for monsoonal precipitation over the Himalayan region during present climate: part I. *Clim. Dyn.* 50,
11 2311–2334. doi:10.1007/s00382-015-2747-2.
- 12 Giorgi, F., Coppola, E., Raffaele, F., Diro, G. T., Fuentes-Franco, R., Giuliani, G., et al. (2014). Changes in extremes
13 and hydroclimatic regimes in the CREMA ensemble projections. *Clim. Change* 125, 39–51. doi:10.1007/s10584-
14 014-1117-0.
- 15 Giorgi, F., Coppola, E., Solmon, F., Mariotti, L., Sylla, M. B., Bi, X., et al. (2012). RegCM4: Model description and
16 preliminary tests over multiple CORDEX domains. *Clim. Res.* doi:10.3354/cr01018.
- 17 Giorgi, F., Torma, C., Coppola, E., Ban, N., Schär, C., and Somot, S. (2016). Enhanced summer convective rainfall at
18 Alpine high elevations in response to climate warming. *Nat. Geosci.* 9, 584–589. doi:10.1038/ngeo2761.
- 19 Giot, O., Termonia, P., Degrauwe, D., De Troch, R., Caluwaerts, S., Smet, G., et al. (2016). Validation of the ALARO-
20 0 model within the EURO-CORDEX framework. *Geosci. Model Dev.* 9, 1143–1152. doi:10.5194/gmd-9-1143-
21 2016.
- 22 Glisan, J. M., and Gutowski, W. J. (2014). WRF winter extreme daily precipitation over the North American CORDEX
23 Arctic. *J. Geophys. Res.* 119, 10.738-10.748. doi:10.1002/2014JD021676.
- 24 Gloor, M., Barichivich, J., Ziv, G., Brienen, R., Schöngart, J., Peylin, P., et al. (2015). Recent Amazon climate as
25 background for possible ongoing and future changes of Amazon humid forests. *Global Biogeochem. Cycles* 29,
26 1384–1399. doi:10.1002/2014GB005080.
- 27 Goldberg, M. H., Linden, S., Ballew, M. T., Rosenthal, S. A., and Leiserowitz, A. (2019). The role of anchoring in
28 judgments about expert consensus. *J. Appl. Soc. Psychol.* 49, 192–200. doi:10.1111/jasp.12576.
- 29 Gong, D. Y., and Ho, C. H. (2002a). The Siberian High and climate change over middle to high latitude Asia. *Theor.*
30 *Appl. Climatol.* 72, 1–9. doi:10.1007/s007040200008.
- 31 Gong, D. Y., and Ho, C. H. (2002b). The Siberian High and climate change over middle to high latitude Asia. *Theor.*
32 *Appl. Climatol.* 72, 1–9. doi:10.1007/s007040200008.
- 33 Gorodetskaya, I. V., Kneifel, S., Maahn, M., Van Tricht, K., Thiery, W., Schween, J. H., et al. (2015). Cloud and
34 precipitation properties from ground-based remote-sensing instruments in East Antarctica. *Cryosph.* 9, 285–304.
35 doi:10.5194/tc-9-285-2015.
- 36 Gorodetskaya, I. V., Tsukernik, M., Claes, K., Ralph, M. F., Neff, W. D., and Van Lipzig, N. P. M. (2014). The role of
37 atmospheric rivers in anomalous snow accumulation in East Antarctica. *Geophys. Res. Lett.* 41, 6199–6206.
38 doi:10.1002/2014GL060881.
- 39 Goswami, B. N., Venugopal, V., Sengupta, D., Madhusoodanan, M. S., and Xavier, P. K. (2006). Increasing Trend of
40 Extreme Rain Events Over India in a Warming Environment. *Science (80-.)*. 314, 1442–1445.
41 doi:10.1126/science.1132027.
- 42 Graham, R. M., Cohen, L., Petty, A. A., Boisvert, L. N., Rinke, A., Hudson, S. R., et al. (2017). Increasing frequency
43 and duration of Arctic winter warming events. *Geophys. Res. Lett.* 44, 6974–6983. doi:10.1002/2017GL073395.
- 44 Gregersen, I. B., Madsen, H., Rosbjerg, D., and Arnbjerg-Nielsen, K. (2015). Long term variations of extreme rainfall
45 in Denmark and southern Sweden. *Clim. Dyn.* 44, 3155–3169. doi:10.1007/s00382-014-2276-4.
- 46 Gröger, M., Dieterich, C., Meier, M. H. E., and Schimanke, S. (2015). Thermal air–sea coupling in hindcast simulations
47 for the North Sea and Baltic Sea on the NW European shelf. *Tellus A Dyn. Meteorol. Oceanogr.* 67, 26911.
48 doi:10.3402/tellusa.v67.26911.
- 49 Groisman, P. Y., Bulygina, O. N., Yin, X., Vose, R. S., Gulev, S. K., Hanssen-Bauer, I., et al. (2016). Recent changes in
50 the frequency of freezing precipitation in North America and Northern Eurasia. *Environ. Res. Lett.* 11.
51 doi:10.1088/1748-9326/11/4/045007.
- 52 Grotjahn, R., and Huynh, J. (2018). Contiguous US summer maximum temperature and heat stress trends in CRU and
53 NOAA Climate Division data plus comparisons to reanalyses. *Sci. Rep.* 8, 11146. doi:10.1038/s41598-018-
54 29286-w.
- 55 Gu, H., Wang, G., Yu, Z., and Mei, R. (2012). Assessing future climate changes and extreme indicators in east and
56 south Asia using the RegCM4 regional climate model. *Clim. Change* 114, 301–317. doi:10.1007/s10584-012-
57 0411-y.
- 58 Gu, H., Yu, Z., Yang, C., and Ju, Q. (2018). Projected Changes in Hydrological Extremes in the Yangtze River Basin
59 with an Ensemble of Regional Climate Simulations. *Water* 10, 1279. doi:10.3390/w10091279.
- 60 Gudmundsson, L., and Seneviratne, S. I. (2015). European drought trends. in *Extreme Hydrological Events - IAHS-*
61 *IACS-IAG Joint Symposium JHI, 26th General Assembly of the International Union of Geodesy and Geophysics,*

- 1 *Prague, Czech Republic, 22 June–2 July 2015* (Copernicus GmbH), 75–79.
2 doi:<https://doi.org/10.5194/piahs-369-75-2015>.
- 3 Guhathakurta, P., and Rajeevan, M. (2008). Trends in the rainfall pattern over India. *Int. J. Climatol.* 28, 1453–1469.
4 doi:10.1002/joc.1640.
- 5 Gulizia, C., and Camilloni, I. (2015). Comparative analysis of the ability of a set of CMIP3 and CMIP5 global climate
6 models to represent precipitation in South America. *Int. J. Climatol.* 35, 583–595. doi:10.1002/joc.4005.
- 7 Gulizia, C., Camilloni, I., and Doyle, M. (2013). Identification of the principal patterns of summer moisture transport in
8 South America and their representation by WCRP/CMIP3 global climate models. *Theor. Appl. Climatol.* 112,
9 227–241. doi:10.1007/s00704-012-0729-4.
- 10 Guo, D.-L., Sun, J.-Q., and Yu, E.-T. (2018). Evaluation of CORDEX regional climate models in simulating
11 temperature and precipitation over the Tibetan Plateau. *Atmos. Ocean. Sci. Lett.* 11, 219–227.
12 doi:10.1080/16742834.2018.1451725.
- 13 Guo, H., Bao, A., Liu, T., Ndayisaba, F., He, D., Kurban, A., et al. (2017). Meteorological drought analysis in the
14 Lower Mekong Basin using satellite-based long-term CHIRPS product. *Sustain.* 9. doi:10.3390/su9060901.
- 15 Guo, H., Xu, M., and Hu, Q. (2011). Changes in near-surface wind speed in China: 1969–2005. *Int. J. Climatol.* 31,
16 349–358. doi:10.1002/joc.2091.
- 17 Gutiérrez-Ruacho, O. G., Brito-Castillo, L., and Díaz-Castro, S. C. (2010). Trends in rainfall and extreme temperatures
18 in northwestern Mexico. *Clim. Res.* 42, 133–142.
- 19 Gutiérrez, C., Somot, S., Nabat, P., Mallet, M., Gaertner, M. A., and Perpiñán, O. Impact of aerosol evolution in future
20 photovoltaic potential. *prep*.
- 21 Gutiérrez, C., Somot, S., Nabat, P., Mallet, M., Gaertner, M. Á., and Perpiñán, O. (2018a). Impact of aerosols on the
22 spatiotemporal variability of photovoltaic energy production in the Euro-Mediterranean area. *Sol. Energy* 174,
23 1142–1152. doi:10.1016/J.SOLENER.2018.09.085.
- 24 Gutiérrez, J. M., Maraun, D., Widmann, M., Huth, R., Hertig, E., Benestad, R., et al. (2018b). An intercomparison of a
25 large ensemble of statistical downscaling methods over Europe: Results from the VALUE perfect predictor cross-
26 validation experiment. *Int. J. Climatol.* doi:10.1002/joc.5462.
- 27 Gutowski, J. W., Giorgi, F., Timbal, B., Frigon, A., Jacob, D., Kang, H. S., et al. (2016). WCRP COordinated Regional
28 Downscaling EXperiment (CORDEX): A diagnostic MIP for CMIP6. *Geosci. Model Dev.* doi:10.5194/gmd-9-
29 4087-2016.
- 30 Haapala, J. J., Ronkainen, I., Schmelzer, N., and Sztobryn, M. (2015). “Recent Change—Sea Ice,” in (Springer, Cham),
31 145–153. doi:10.1007/978-3-319-16006-1_8.
- 32 Hamman, J., Nijssen, B., Brunke, M., Cassano, J., Craig, A., DuVivier, A., et al. (2016). Land surface climate in the
33 regional Arctic system model. *J. Clim.* 29, 6543–6562. doi:10.1175/JCLI-D-15-0415.1.
- 34 Hamon, M., Beuvier, J., Somot, S., Lellouche, J.-M., Greiner, E., Jordà, G., et al. (2016). Design and validation of
35 MEDRYS, a Mediterranean Sea reanalysis over the period 1992–2013. *Ocean Sci.* 12. doi:10.5194/os-12-577-
36 2016.
- 37 Hanhijärvi, S., Tingley, M. P., and Korhola, A. (2013). Pairwise comparisons to reconstruct mean temperature in the
38 Arctic Atlantic Region over the last 2,000 years. *Clim. Dyn.* 41, 2039–2060. doi:10.1007/s00382-013-1701-4.
- 39 Hannart, A., Vera, C., Cerne, B., and Otto, F. E. L. (2015). Causal Influence of Anthropogenic Forcings on the
40 Argentinian Heat Wave of December 2013. *Bull. Am. Meteorol. Soc.* 96, S41–S45. doi:10.1175/BAMS-D-15-
41 00137.1.
- 42 Hansen, B. B., Isaksen, K., Benestad, R. E., Kohler, J., Pedersen, Å., Loe, L. E., et al. (2014). Warmer and wetter
43 winters: Characteristics and implications of an extreme weather event in the High Arctic. *Environ. Res. Lett.* 9.
44 doi:10.1088/1748-9326/9/11/114021.
- 45 Hanssen-Bauer, I., Førland, E., Haddeland, I., Hisdal, H., Lawrence, D., Mayer, S., et al. (2017). Climate in Norway
46 2100 – A knowledge base for climate adaptation. Norwegian Centre for Climate Services Available at:
47 https://cms.met.no/site/2/klimaservicesenteret/klima-i-norge-2100/_attachment/11592?_ts=15c10419731.
- 48 Harold, J., Lorenzoni, I., Shipley, T. F., and Coventry, K. R. (2016). Cognitive and psychological science insights to
49 improve climate change data visualization. *Nat. Clim. Chang.* 6, 1080–1089. doi:10.1038/nclimate3162.
- 50 Harris, D. M. (2017). Telling the story of climate change: Geologic imagination, praxis, and policy. *Energy Res. Soc.*
51 *Sci.* 31, 179–183. doi:10.1016/J.ERSS.2017.05.027.
- 52 Hartmann, D. L., Tank, A. M. G. K., and Rusticucci, M. (2013). IPCC Fifth Assessment Report, Climate Change 2013:
53 The Physical Science Basis. *IPCC AR5*, 31–39.
- 54 Harzallah, A., Jordà, G., Dubois, C., Sannino, G., Carillo, A., Li, L., et al. (2018). Long term evolution of heat budget in
55 the Mediterranean Sea from Med-CORDEX forced and coupled simulations. *Clim. Dyn.* 51, 1145–1165.
56 doi:10.1007/s00382-016-3363-5.
- 57 Hasson, S. ul, Böhner, J., and Chishtie, F. (2019a). Low fidelity of CORDEX and their driving experiments indicates
58 future climatic uncertainty over Himalayan watersheds of Indus basin. *Clim. Dyn.* 52, 777–798.
59 doi:10.1007/s00382-018-4160-0.
- 60 Hasson, S. ul, Böhner, J., and Chishtie, F. (2019b). Low fidelity of CORDEX and their driving experiments indicates
61 future climatic uncertainty over Himalayan watersheds of Indus basin. *Clim. Dyn.* 52, 777–798.

- 1 doi:10.1007/s00382-018-4160-0.
- 2 Hathaway, J., and Maibach, E. W. (2018). Health Implications of Climate Change: a Review of the Literature About the
3 Perception of the Public and Health Professionals. *Curr. Environ. Heal. Reports* 5, 197–204. doi:10.1007/s40572-
4 018-0190-3.
- 5 Hawkins, E., and Sutton, R. (2016). Connecting Climate Model Projections of Global Temperature Change with the
6 Real World. *Bull. Am. Meteorol. Soc.* 97, 963–980. doi:10.1175/BAMS-D-14-00154.1.
- 7 Hazeleger, W., Van Den Hurk, B. J. J. M., Min, E., Van Oldenborgh, G. J., Petersen, A. C., Stainforth, D. A., et al.
8 (2015). Tales of future weather. *Nat. Clim. Chang.* 5. doi:10.1038/nclimate2450.
- 9 Henderson, G. R., and Leathers, D. J. (2009). European snow cover extent variability and associations with atmospheric
10 forcings. *Int. J. Climatol.* 30, n/a-n/a. doi:10.1002/joc.1990.
- 11 Herrera, S., Fernández, J., and Gutiérrez, J. M. (2016). Update of the Spain02 gridded observational dataset for EURO-
12 CORDEX evaluation: assessing the effect of the interpolation methodology. *Int. J. Climatol.* 36, 900–908.
13 doi:10.1002/joc.4391.
- 14 Hertig, E., Maraun, D., Bartholy, J., Pongracz, R., Vrac, M., Mares, I., et al. (2018). Comparison of statistical
15 downscaling methods with respect to extreme events over Europe: Validation results from the perfect predictor
16 experiment of the COST Action VALUE. *Int. J. Climatol.* doi:10.1002/joc.5469.
- 17 Hewitson, B., Waagsaether, K., Wohland, J., Kloppers, K., and Kara, T. (2017). Climate information websites: an
18 evolving landscape. *Wiley Interdiscip. Rev. Clim. Chang.* 8, e470. doi:10.1002/wcc.470.
- 19 Hewitt, H. T., Copsey, D., Culverwell, I. D., Harris, C. M., Hill, R. S. R., Keen, A. B., et al. (2011). Design and
20 implementation of the infrastructure of HadGEM3: the next-generation Met Office climate modelling system.
21 *Geosci. Model Dev.* 4, 223–253. doi:10.5194/gmd-4-223-2011.
- 22 Hidalgo, H., Durán-Quesada, A., Amador, J., and Alfaro, E. (2015). The Caribbean Low-Level Jet, the Inter-Tropical
23 Convergence Zone and Precipitation Patterns in the Intra-Americas Sea: A Proposed Dynamical Mechanism.
24 *Geogr. Ann. Ser. A, Phys. Geogr.* 97. doi:10.1111/geoa.12085.
- 25 Hijioaka, Y., E. Lin, J.J. Pereira, R.T. Corlett, X. Cui, G.E. Insarov, R.D. Lasco, E. Lindgren, and A. Surjan, 2014
26 (2014). “No Title,” in *Asia. In: Climate Change 2014: Impacts, Adaptation, and Vulnerability. Part B: Regional*
27 *Aspects. Contribution of Working Group II to the Fifth Assessment Report of the Intergovernmental Panel on*
28 *Climate Change*, eds. K. L. E. Barros, V.R., C.B. Field, D.J. Dokken, M.D. Mastrandrea, K.J. Mach, T.E. Bilir,
29 M. Chatterjee and L. L. W. Y.O. Estrada, R.C. Genova, B. Girma, E.S. Kissel, A.N. Levy, S. MacCracken,
30 P.R. Mastrandrea (Cambridge University Press, Cambridge, United Kingdom and New York, NY, USA), 1327–
31 1370.
- 32 Hobgood, J. (2005). “Tropical Cyclones,” in *Encyclopedia of World Climatology*, ed. J. E. Oliver (Dordrecht: Springer
33 Netherlands), 750–755. doi:10.1007/1-4020-3266-8_213.
- 34 Hoerling, M., Hurrell, J., Eischeid, J., and Phillips, A. (2006). Detection and attribution of twentieth-century northern
35 and southern African rainfall change. *J. Clim.* doi:10.1175/JCLI3842.1.
- 36 Holland, G. J., and Webster, P. J. (2007). Heightened tropical cyclone activity in the North Atlantic: natural variability
37 or climate trend? *Philos. Trans. R. Soc. A Math. Phys. Eng. Sci.* 365, 2695–2716. doi:10.1098/rsta.2007.2083.
- 38 Hori, M., Nohara, D., and Tanaka, H. (2008). Influence of Arctic Oscillation towards the Northern Hemisphere Surface
39 Temperature Variability under the Global Warming Scenario. *J. Meteorol. Soc. Japan* 85, 847–859.
40 doi:10.2151/jmsj.85.847.
- 41 Hoyos, C. D., Agudelo, P. A., Webster, P. J., and Curry, J. A. (2006). Deconvolution of the Factors Contributing to the
42 Increase in Global Hurricane Intensity. *Science* (80-). 312, 94–97. Available at:
43 <http://www.jstor.org/stable/3845986>.
- 44 Hsu, P. C., Li, T., and Wang, B. (2011). Trends in global monsoon area and precipitation over the past 30 years.
45 *Geophys. Res. Lett.* 38, n/a-n/a. doi:10.1029/2011GL046893.
- 46 Hu, Z. Z. (1997). Interdecadal variability of summer climate over East Asia and its association with 500 hPa height and
47 global sea surface temperature. *J. Geophys. Res. Atmos.* 102, 19403–19412. doi:10.1029/97jd01052.
- 48 Huang, A., Zhou, Y., Zhang, Y., Huang, D., Zhao, Y., and Wu, H. (2014). Changes of the annual precipitation over
49 central Asia in the twenty-first century projected by multimodels of CMIP5. *J. Clim.* 27, 6627–6646.
50 doi:10.1175/JCLI-D-14-00070.1.
- 51 Hurd, C. L., Lenton, A., Tilbrook, B., and Boyd, P. W. (2018). Current understanding and challenges for oceans in a
52 higher-CO2 world. *Nat. Clim. Chang.* 8, 686–694. doi:10.1038/s41558-018-0211-0.
- 53 Hurrell, J. W., Kushnir, Y., Visbeck, M., and Ottersen, G. (2003). An overview of the North Atlantic Oscillation.
54 *Geophys. Monogr. Ser.*
- 55 Hussain, A. (2017). Evaluation of Past and Projected Climate Change in Pakistan Region Based on GCM20 and
56 RegCM4 . 3 Outputs. 13, 63–86.
- 57 Il Jeong, D., and Sushama, L. (2018). Rain-on-snow events over North America based on two Canadian regional
58 climate models. *Clim. Dyn.* 50, 303–316. doi:10.1007/s00382-017-3609-x.
- 59 IMBIE team (2018). Mass balance of the Antarctic Ice Sheet from 1992 to 2017. *Nature* 558, 219–222.
60 doi:10.1038/s41586-018-0179-y.
- 61 Indasi, V. (2019). Genealogy of Gridded Precipitation Datasets over Southern Africa. *prep*.

- 1 IPCC (2010). *Meeting Report of the Intergovernmental Panel on Climate Change Expert Meeting on Assessing and*
2 *Combining Multi Model Climate Projections.*, eds. T. F. Stocker, D. Qin, G.-K. Plattner, M. Tignor, and P. M.
3 Midgley IPCC Working Group I Technical Support Unit, University of Bern, Bern, Switzerland Available at:
4 <https://naturalsciences.ch/service/publications/75800-assessing-and-combining-multi-model-climate-projections>
5 [Accessed April 2, 2019].
- 6 IPCC (2018a). Global Warming of 1.5°C. An IPCC Special Report on the impacts of global warming of 1.5°C above
7 pre-industrial levels and related global greenhouse gas emission pathways, in the context of strengthening the
8 global response to the threat of climate change., eds. V. Masson-Delmotte, P. Zhai, H.-O. Pörtner, D. Roberts, J.
9 Skea, P. R. Shukla, et al. In Press.
- 10 IPCC (2018b). *Special report on 1.5 degree Global Warming.* Available at:
11 http://report.ipcc.ch/sr15/pdf/sr15_spm_final.pdf.
- 12 Iran's third National Communication to UNFCCC (2017).
- 13 Irannezhad, M., Chen, D., Kløve, B., and Moradkhani, H. (2017). Analysing the variability and trends of precipitation
14 extremes in Finland and their connection to atmospheric circulation patterns. *Int. J. Climatol.* 37, 1053–1066.
15 doi:10.1002/joc.5059.
- 16 Isotta, F. A., Vogel, R., and Frei, C. (2015). Evaluation of European regional reanalyses and downscalings for
17 precipitation in the Alpine region. *Meteorol. Zeitschrift* 24, 15–37. doi:10.1127/metz/2014/0584.
- 18 Iturbide, M., Bedia, J., Herrera, S., Baño-Medina, J., Fernández, J., Frías, M. D., et al. (2019). The R-based climate4R
19 open framework for reproducible climate data access and post-processing. *Environ. Model. Softw.* 111, 42–54.
20 doi:10.1016/j.envsoft.2018.09.009.
- 21 Ivanov, M., Warrach-Sagi, K., and Wulfmeyer, V. (2017). Field significance of performance measures in the context of
22 regional climate model evaluation. Part 1: temperature. *Theor. Appl. Climatol.*, 1–19. doi:10.1007/s00704-017-
23 2100-2.
- 24 Ivušić S., Somot S., Güttler I., H. K. Assessment of regional climate model mean and extreme daily precipitation
25 statistics over Croatia. *prep.*
- 26 Jacob, D. (2001). A note to the simulation of the annual and inter-annual variability of the water budget over the Baltic
27 Sea drainage basin. *Meteorol Atmos Phys* 77, 61–73. doi:<https://doi.org/10.1007/s007030170017>.
- 28 Jacob, D., Kotova, L., Teichmann, C., Sobolowski, S. P., Vautard, R., Donnelly, C., et al. (2018). Climate Impacts in
29 Europe Under +1.5°C Global Warming. *Earth's Futur.* doi:10.1002/2017EF000710.
- 30 Jézéquel, A., Yiou, P., Radanovics, S., Vautard, R., Jézéquel, A., Yiou, P., et al. (2018). Analysis of the Exceptionally
31 Warm December 2015 in France Using Flow Analogues. *Bull. Am. Meteorol. Soc.* 99, S76–S79.
32 doi:10.1175/BAMS-D-17-0103.1.
- 33 Jiang, Y., Luo, Y., Zhao, Z., and Tao, S. (2010). Changes in wind speed over China during 1956-2004. *Theor. Appl.*
34 *Climatol.* 99, 421–430. doi:10.1007/s00704-009-0152-7.
- 35 Jin, C.-S., Cha, D. H., Lee, D. K., Suh, M. S., Hong, S. Y., Kang, H. S., et al. (2016). Evaluation of climatological
36 tropical cyclone activity over the western North Pacific in the CORDEX-East Asia multi-RCM simulations. *Clim.*
37 *Dyn.* 47, 765–778. doi:10.1007/s00382-015-2869-6.
- 38 Jin, Q., and Wang, C. (2017). A revival of Indian summer monsoon rainfall since 2002. *Nat. Clim. Chang.* 7, 587.
39 Available at: <https://doi.org/10.1038/nclimate3348>.
- 40 Joetzjer, E., Douville, H., Delire, C., and Ciais, P. (2013). Present-day and future Amazonian precipitation in global
41 climate models: CMIP5 versus CMIP3. *Clim. Dyn.* 41, 2921–2936. doi:10.1007/s00382-012-1644-1.
- 42 Jones, C., and Carvalho, L. M. V. (2013). Climate Change in the South American Monsoon System: Present Climate
43 and CMIP5 Projections. *J. Clim.* 26, 6660–6678. doi:10.1175/JCLI-D-12-00412.1.
- 44 Jones, M. D., and Song, G. (2014). Making Sense of Climate Change: How Story Frames Shape Cognition. *Polit.*
45 *Psychol.* 35, 447–476. doi:10.1111/pops.12057.
- 46 Jones, P. D., Lister, D. H., Osborn, T. J., Harpham, C., Salmon, M., and Morice, C. P. (2012). Hemispheric and large-
47 scale land-surface air temperature variations: An extensive revision and an update to 2010. *J. Geophys. Res.*
48 *Atmos.* 117, n/a-n/a. doi:10.1029/2011JD017139.
- 49 Jones, P., Harpham, C., Burton, A., and Goodess, C. (2016). Downscaling regional climate model outputs for the
50 Caribbean using a weather generator. *Int. J. Climatol.* 36, n/a-n/a. doi:10.1002/joc.4624.
- 51 Juneng, L., Tangang, F., Chung, J., Ngai, S., Tay, T., Narisma, G., et al. (2016a). Sensitivity of Southeast Asia rainfall
52 simulations to cumulus and air-sea flux parameterizations in RegCM4. *Clim. Res.* 69, 59–77.
53 doi:10.3354/cr01386.
- 54 Juneng, L., Tangang, F., Chung, J. X., Ngai, S. T., Tay, T. W., Narisma, G., et al. (2016b). Sensitivity of Southeast Asia
55 rainfall simulations to cumulus and air-sea flux parameterizations in RegCM4. *Clim. Res.* doi:10.3354/cr01386.
- 56 Jury, M. R. (2013). Climate trends in southern Africa. *S. Afr. J. Sci.* doi:10.1590/sajs.2013/980.
- 57 Jury, M. W., Herrera, S., Gutiérrez, J. M., and Barriopedro, D. (2018). Blocking representation in the ERA-Interim
58 driven EURO-CORDEX RCMs. *Clim. Dyn.* doi:10.1007/s00382-018-4335-8.
- 59 Kahan, D. (2012). Why we are poles apart on climate change. *Nature* 488, 255–255. doi:10.1038/488255a.
- 60 Kang, S., Im, E.-S., and Eltahir, E. A. B. (2019). Future climate change enhances rainfall seasonality in a regional
61 model of western Maritime Continent. *Clim. Dyn.* 52, 747–764. doi:10.1007/s00382-018-4164-9.

- 1 Karmalkar, A. V., Taylor, M. A., Campbell, J., Stephenson, T., New, M., Centella, A., et al. (2013). A review of
2 observed and projected changes in climate for the islands in the Caribbean. *Atmósfera* 26, 283–309.
3 doi:10.1016/S0187-6236(13)71076-2.
- 4 Karmalkar, A. V., Bradley, R. S., and Diaz, H. F. (2011). Climate change in Central America and Mexico: regional
5 climate model validation and climate change projections. *Clim. Dyn.* 37, 605–629. doi:10.1007/s00382-011-1099-
6 9.
- 7 Karlsruhas, K. B., and Busalacchi, A. J. (2009). The Role of SST in the East Pacific Warm Pool in the Interannual
8 Variability of Central American Rainfall. *J. Clim.* 22, 2605–2623. doi:10.1175/2008JCLI2468.1.
- 9 Karlsruhas, K. B., Seager, R., Giannini, A., and Busalacchi, A. J. (2013). A simple mechanism for the climatological
10 midsummer drought along the Pacific coast of Central America. *Atmósfera* 26, 261–281. doi:10.1016/S0187-
11 6236(13)71075-0.
- 12 Katragkou, E., García-Díez, M., Vautard, R., Sobolowski, S., Zanis, P., Alexandri, G., et al. (2015). Regional climate
13 hindcast simulations within EURO-CORDEX: evaluation of a WRF multi-physics ensemble. *Geosci. Model Dev.*
14 8, 603–618. doi:10.5194/gmd-8-603-2015.
- 15 Kattsov, V. M., Walsh, J. E., Chapman, W. L., Govorkova, V. A., Pavlova, T. V., and Zhang, X. (2007). Simulation and
16 Projection of Arctic Freshwater Budget Components by the IPCC AR4 Global Climate Models. *J.*
17 *Hydrometeorol.* 8, 571–589. doi:10.1175/jhm575.1.
- 18 Katzfey, J., Nguyen, K., McGregor, J., Hoffmann, P., Ramasamy, S., Nguyen, H. Van, et al. (2016). High-resolution
19 simulations for Vietnam - methodology and evaluation of current climate. *Asia-Pacific J. Atmos. Sci.* 52, 91–106.
20 doi:10.1007/s13143-016-0011-2.
- 21 Kaufman, D. S., Schneider, D. P., McKay, N. P., Ammann, C. M., Bradley, R. S., Briffa, K. R., et al. (2009). Recent
22 warming reverses long-term arctic cooling. *Science (80-)*. doi:10.1126/science.1173983.
- 23 Kaye, N. R., Hartley, A., and Hemming, D. (2012). Mapping the climate: guidance on appropriate techniques to map
24 climate variables and their uncertainty. *Geosci. Model Dev.* 5, 245–256. doi:10.5194/gmd-5-245-2012.
- 25 Kendon, E. J., Ban, N., Roberts, N. M., Fowler, H. J., Roberts, M. J., Chan, S. C., et al. (2016). Do Convection-
26 Permitting Regional Climate Models Improve Projections of Future Precipitation Change? *Bull. Am. Meteorol.*
27 *Soc.* 98, 79–93. doi:10.1175/BAMS-D-15-0004.1.
- 28 Kendon, E. J., Roberts, N. M., Fowler, H. J., Roberts, M. J., Chan, S. C., and Senior, C. A. (2014). Heavier summer
29 downpours with climate change revealed by weather forecast resolution model. *Nat. Clim. Chang.* 4, 570–576.
30 doi:10.1038/nclimate2258.
- 31 Kennedy, J. J., Rayner, N. A., Smith, R. O., Parker, D. E., and Saunby, M. (2011a). Reassessing biases and other
32 uncertainties in sea surface temperature observations measured in situ since 1850: 1. Measurement and sampling
33 uncertainties. *J. Geophys. Res. Atmos.* 116. doi:10.1029/2010JD015218.
- 34 Kennedy, J. J., Rayner, N. A., Smith, R. O., Parker, D. E., and Saunby, M. (2011b). Reassessing biases and other
35 uncertainties in sea surface temperature observations measured in situ since 1850: 2. Biases and homogenization.
36 *J. Geophys. Res. Atmos.* 116. doi:10.1029/2010JD015220.
- 37 Kew, S. f., Philip, S. Y., Jan van Oldenborgh, G., van der Schrier, G., Otto, F. E. L., Vautard, R., et al. (2019). The
38 Exceptional Summer Heat Wave in Southern Europe 2017. *Bull. Am. Meteorol. Soc.* 100, S49–S53.
39 doi:10.1175/BAMS-D-18-0109.1.
- 40 Kieu-Thi, X., Vu-Thanh, H., Nguyen-Minh, T., Le, D., Nguyen-Manh, L., Takayabi, I., et al. (2016). Rainfall and
41 Tropical Cyclone Activity over Vietnam Simulated and Projected by the Non-Hydrostatic Regional Climate
42 Model - NHRCM. *J. Meteorol. Soc. Japan. Ser. II* 94A, 135–150. doi:10.2151/jmsj.2015-057.
- 43 Kim, I. W., Oh, J., Woo, S., and Kripalani, R. H. (2018). Evaluation of precipitation extremes over the Asian domain:
44 observation and modelling studies. *Clim. Dyn.* 52, 1–26. doi:10.1007/s00382-018-4193-4.
- 45 King, J. C. (John C., and Turner, J. (John) (1997). *Antarctic meteorology and climatology*. Cambridge University Press.
- 46 King, M. A., Bingham, R. J., Moore, P., Whitehouse, P. L., Bentley, M. J., and Milne, G. A. (2012). Lower satellite-
47 gravimetry estimates of Antarctic sea-level contribution. *Nature*. doi:10.1038/nature11621.
- 48 Kirono, D. G., Butler, J. R., McGregor, J. L., Ripaldi, A., Katzfey, J., and Nguyen, K. (2015). Historical and future
49 seasonal rainfall variability in Nusa Tenggara Barat Province, Indonesia: Implications for the agriculture and
50 water sectors. *Clim. Risk Manag.* 12, 45–58. doi:10.1016/j.crm.2015.12.002.
- 51 Kitembe, J., Favre, A., Dosio, A., Lennard, C., Sabiiti, G., and Nimusiima, A. (2018). Evaluation of rainfall simulations
52 over Uganda in CORDEX regional climate models. *Theor. Appl. Climatol.* doi:10.1007/s00704-018-2643-x.
- 53 Kittel, C., Amory, C., Agosta, C., Delhasse, A., Doutreloup, S., Huot, P.-V., et al. (2018). Sensitivity of the current
54 Antarctic surface mass balance to sea surface conditions using MAR. *Cryosph.* 12, 3827–3839. doi:10.5194/tc-
55 12-3827-2018.
- 56 Kjellström, E., Bärring, L., Nikulin, G., Nilsson, C., Persson, G., and Strandberg, G. (2016). Production and use of
57 regional climate model projections – A Swedish perspective on building climate services. *Clim. Serv.* 2–3, 15–29.
58 doi:10.1016/j.cliser.2016.06.004.
- 59 Kjellström, E., Engström, E., Koenigk, T., Matei, D., Moberg, A., Tyrlis, E., et al. The exceptional warm and dry
60 Swedish summer 2018. *prep*.
- 61 Klotzbach, P. J. (2011). El Niño–Southern Oscillation’s Impact on Atlantic Basin Hurricanes and U.S. Landfalls. *J.*

- 1 *Clim.* 24, 1252–1263. doi:10.1175/2010JCLI3799.1.
- 2 Klutse, N. A. B., Ajayi, V. O., Gbobaniyi, E. O., Egbebiyi, T. S., Kouadio, K., Nkrumah, F., et al. (2018). Potential
3 impact of 1.5 °C and 2 °C global warming on consecutive dry and wet days over West Africa. *Environ. Res. Lett.*
4 doi:10.1088/1748-9326/aab37b.
- 5 Klutse, N. A. B., Gibba, P., Kebe, I., Nikiema, P. M. P. M., Sylla, M. B. M. B., Nikiema, P. M. P. M., et al. (2016).
6 “Climate Change over West Africa: Recent Trends and Future Projections,” in *Adaptation to Climate Change and*
7 *Variability in Rural West Africa* doi:10.1007/978-3-319-31499-0_3.
- 8 Knist, S., Goergen, K., Buonomo, E., Christensen, O. B., Colette, A., Cardoso, R. M., et al. (2017). Land-atmosphere
9 coupling in EURO-CORDEX evaluation experiments. *J. Geophys. Res. Atmos.* 122, 2016JD025476.
10 doi:10.1002/2016JD025476.
- 11 Knutson, T. R., Sirutis, J. J., Garner, S. T., Vecchi, G. A., and Held, I. M. (2008). Simulated reduction in Atlantic
12 hurricane frequency under twenty-first-century warming conditions. *Nat. Geosci.* 1, 359. Available at:
13 <https://doi.org/10.1038/ngeo202>.
- 14 Kobashi, T., Kawamura, K., Severinghaus, J. P., Barnola, J. M., Nakaegawa, T., Vinther, B. M., et al. (2011). High
15 variability of Greenland surface temperature over the past 4000 years estimated from trapped air in an ice core.
16 *Geophys. Res. Lett.* doi:10.1029/2011GL049444.
- 17 Kobashi, T., Severinghaus, J. P., Barnola, J. M., Kawamura, K., Carter, T., and Nakaegawa, T. (2010). Persistent multi-
18 decadal Greenland temperature fluctuation through the last millennium. *Clim. Change.* doi:10.1007/s10584-009-
19 9689-9.
- 20 Koenigk, T., and Berg, P. (2015). Arctic climate change in an ensemble of future scenario simulations with the regional
21 atmosphere model RCA. 1, 1–19. doi:10.3402/polar.v34.24603.
- 22 Kohnemann, S. H. E., Heinemann, G., Bromwich, D. H., and Gutjahr, O. (2017). Extreme Warming in the Kara Sea and
23 Barents Sea during the Winter Period 2000–16. *J. Clim.* 30, 8913–8927. doi:10.1175/JCLI-D-16-0693.1.
- 24 Koster, R. D., Dirmeyer, P. A., Hahmann, A. N., Ijpelaar, R., Tyahla, L., Cox, P., et al. (2002). Comparing the Degree
25 of Land–Atmosphere Interaction in Four Atmospheric General Circulation Models. *J. Hydrometeorol.* 3, 363–
26 375. doi:10.1175/1525-7541(2002)003<0363:CTDOLA>2.0.CO;2.
- 27 Koster, R. D., Suarez, M. J., and Heiser, M. (2000). Variance and Predictability of Precipitation at Seasonal-to-
28 Interannual Timescales. *J. Hydrometeorol.* 1, 26–46. doi:10.1175/1525-
29 7541(2000)001<0026:VAPOPA>2.0.CO;2.
- 30 Kotcher, J. E., Myers, T. A., Vraga, E. K., Stenhouse, N., and Maibach, E. W. (2017). Does Engagement in Advocacy
31 Hurt the Credibility of Scientists? Results from a Randomized National Survey Experiment. *Environ. Commun.*
32 11, 415–429. doi:10.1080/17524032.2016.1275736.
- 33 Kotlarski, S., Keuler, K., Christensen, O. B., Colette, A., Déqué, M., Gobiet, A., et al. (2014). Regional climate
34 modeling on European scales: a joint standard evaluation of the EURO-CORDEX RCM ensemble. *Geosci. Model*
35 *Dev.* 7, 1297–1333. doi:10.5194/gmd-7-1297-2014.
- 36 Kotlarski, S., Szabó, P., Herrera, S., Räty, O., Keuler, K., Soares, P. M., et al. (2017). Observational uncertainty and
37 regional climate model evaluation: A pan-European perspective. *Int. J. Climatol.*, 1–20. doi:10.1002/joc.5249.
- 38 Kovach, B., and Rosenstiel, T. (2007). *The Elements of Journalism. What Newspeople Should Know and the Public*
39 *Should Expect*. Three Rivers Press; Revised, Updated edition (April 24, 2007).
- 40 Krasting, J. P., Broccoli, A. J., Dixon, K. W., and Lanzante, J. R. (2013). Future changes in northern hemisphere
41 snowfall. *J. Clim.* 26, 7813–7828. doi:10.1175/JCLI-D-12-00832.1.
- 42 Kripalani, R. H., Kulkarni, A., Sabade, S. S., and Khandekar, M. L. (2003). Indian Monsoon Variability in a Global
43 Warming Scenario. *Nat. Hazards* 29, 189–206. doi:10.1023/A:1023695326825.
- 44 Krishnan, R., Sabin, T. P., Vellore, R., Mujumdar, M., Sanjay, J., Goswami, B. N., et al. (2016). Deciphering the
45 desiccation trend of the South Asian monsoon hydroclimate in a warming world. *Clim. Dyn.* 47, 1007–1027.
46 doi:10.1007/s00382-015-2886-5.
- 47 Krishnan, R., Shrestha, A. B., Ren, G., Rajbhandari, R., Saeed, S., Sanjay, J., et al. (2019). “Unravelling Climate
48 Change in the Hindu Kush Himalaya: Rapid Warming in the Mountains and Increasing Extremes,” in *The Hindu*
49 *Kush Himalaya Assessment* (Cham: Springer International Publishing), 57–97. doi:10.1007/978-3-319-92288-
50 1_3.
- 51 Krishnan, T. P. S. R., Ghattas, J., Dufresne, S. D. J., Hourdin, F., and Pascal, T. (2013). High resolution simulation of
52 the South Asian monsoon using a variable resolution global climate model. 173–194. doi:10.1007/s00382-012-
53 1658-8.
- 54 Kröner, N., Kotlarski, S., Fischer, E., Lüthi, D., Zubler, E., and Schär, C. (2017). Separating climate change signals into
55 thermodynamic, lapse-rate and circulation effects: theory and application to the European summer climate. *Clim.*
56 *Dyn.* 48, 3425–3440. doi:10.1007/s00382-016-3276-3.
- 57 Kruger, A. C., and Sekele, S. S. (2013). Trends in extreme temperature indices in South Africa: 1962–2009. *Int. J.*
58 *Climatol.* doi:10.1002/joc.3455.
- 59 Kuipers Munneke, P., Luckman, A. J., Bevan, S. L., Smeets, C. J. P. P., Gilbert, E., van den Broeke, M. R., et al.
60 (2018). Intense Winter Surface Melt on an Antarctic Ice Shelf. *Geophys. Res. Lett.* 45, 7615–7623.
61 doi:10.1029/2018GL077899.

- 1 Kumar, P., Wiltshire, A., Mathison, C., Asharaf, S., Ahrens, B., Lucas-Picher, P., et al. (2013). Downscaled climate
2 change projections with uncertainty assessment over India using a high resolution multi-model approach. *Sci.*
3 *Total Environ.* 468–469, S18–S30. doi:10.1016/j.scitotenv.2013.01.051.
- 4 Kumi, N., and Abiodun, B. J. (2018). Potential impacts of 1.5 °c and 2 °c global warming on rainfall onset, cessation
5 and length of rainy season in West Africa. *Environ. Res. Lett.* doi:10.1088/1748-9326/aab89e.
- 6 Kunkel, K. E., Robinson, D. A., Champion, S., Yin, X., Estilow, T., and Frankson, R. M. (2016). Trends and Extremes
7 in Northern Hemisphere Snow Characteristics. *Curr. Clim. Chang. Reports* 2, 65–73. doi:10.1007/s40641-016-
8 0036-8.
- 9 Kusunoki, S., Mizuta, R., and Hosaka, M. (2015). Future changes in precipitation intensity over the Arctic projected by
10 a global atmospheric model with a 60-km grid size. *Polar Sci.* 9, 277–292.
11 doi:https://doi.org/10.1016/j.polar.2015.08.001.
- 12 Kwan, M. S., Tangang, F. T., and Juneng, L. (2014). Present-day regional climate simulation over Malaysia and
13 western Maritime Continent region using PRECIS forced with ERA40 reanalysis. *Theor. Appl. Climatol.* 115, 1–
14 14. doi:10.1007/s00704-013-0873-5.
- 15 Lakoff, G. (2010). Why it Matters How We Frame the Environment. *Environ. Commun.* 4, 70–81.
16 doi:10.1080/17524030903529749.
- 17 Landelius, T., Dahlgren, P., Gollvik, S., Jansson, A., and Olsson, E. (2016). A high-resolution regional reanalysis for
18 Europe. Part 2: 2D analysis of surface temperature, precipitation and wind. *Q. J. R. Meteorol. Soc.* 142, 2132–
19 2142. doi:10.1002/qj.2813.
- 20 Landsea, C. (2007). Counting Atlantic tropical cyclones back to 1900. *Eos, Trans. Am. Geophys. Union* 88, 197–202.
21 doi:10.1029/2007EO180001.
- 22 Latif, M., Semenov, V. A., and Park, W. (2015). Super El Niños in response to global warming in a climate model.
23 *Clim. Change* 132, 489–500. doi:10.1007/s10584-015-1439-6.
- 24 Latif, M., Syed, F. S., and Hannachi, A. (2017). Rainfall trends in the South Asian summer monsoon and its related
25 large-scale dynamics with focus over Pakistan. *Clim. Dyn.* 48, 3565–3581. doi:10.1007/s00382-016-3284-3.
- 26 Lee, D., Min, S. K., Fischer, E., Shiogama, H., Bethke, I., Lierhammer, L., et al. (2018). Impacts of half a degree
27 additional warming on the Asian summer monsoon rainfall characteristics. *Environ. Res. Lett.* 13, 044033.
28 doi:10.1088/1748-9326/aab55d.
- 29 Lémond, J., Dandin, P., Planton, S., Vautard, R., Pagé, C., Déqué, M., et al. (2011). DRIAS: a step toward Climate
30 Services in France. *Adv. Sci. Res.* 6, 179–186. doi:10.5194/asr-6-179-2011.
- 31 Lemos, M. C., Kirchoff, C. J., and Ramprasad, V. (2012). Narrowing the climate information usability gap. *Nat. Clim.*
32 *Chang.* 2, 789–794. doi:10.1038/nclimate1614.
- 33 Lenaerts, J. T. M., van Meijgaard, E., van den Broeke, M. R., Ligtenberg, S. R. M., Horwath, M., and Isaksson, E.
34 (2013). Recent snowfall anomalies in Dronning Maud Land, East Antarctica, in a historical and future climate
35 perspective. *Geophys. Res. Lett.* 40, 2684–2688. doi:10.1002/grl.50559.
- 36 Lenderink, G., Belusic, D., Fowler, H. J., Kjellström, E., Lind, P., van Meijgaard, E., et al. (2019). Systematic
37 thermodynamic responses of hourly precipitation extremes in a warming experiment with a convection-permitting
38 climate model. *Submitted*.
- 39 Lennard, C., Nikulin, G., Dosio, A., and Moufouma-Okia, W. (2018). On the need for regional climate information over
40 Africa under varying levels of global warming. *Environ. Res. Lett.* doi:10.1088/1748-9326/aab2b4.
- 41 Levis, S. (2010). Modeling vegetation and land use in models of the Earth System. *Wiley Interdiscip. Rev. Clim. Chang.*
42 1, 840–856. doi:10.1002/wcc.83.
- 43 Lewandowsky, S., Ecker, U. K. H., and Cook, J. (2017). Beyond Misinformation: Understanding and Coping with the
44 “Post-Truth” Era. *J. Appl. Res. Mem. Cogn.* 6, 353–369. doi:10.1016/J.JARMAC.2017.07.008.
- 45 Lewandowsky, S., Oreskes, N., Risbey, J. S., Newell, B. R., and Smithson, M. (2015). Seepage: The effect of climate
46 denial on the scientific community. *Glob. Environ. Chang.* 33, 1–13. doi:10.1016/j.gloenvcha.2015.02.013.
- 47 Li, H., Dai, A., Zhou, T., and Lu, J. (2010a). Responses of East Asian summer monsoon to historical SST and
48 atmospheric forcing during 1950–2000. *Clim. Dyn.* 34, 501–514. doi:10.1007/s00382-008-0482-7.
- 49 Li, H., Dai, A., Zhou, T., and Lu, J. (2010b). Responses of East Asian summer monsoon to historical SST and
50 atmospheric forcing during 1950–2000. *Clim. Dyn.* 34, 501–514. doi:10.1007/s00382-008-0482-7.
- 51 Li, J., Yu, R., Yuan, W., Chen, H., Sun, W., and Zhang, Y. (2015). Precipitation over East Asia simulated by NCAR
52 CAM5 at different horizontal resolutions. *J. Adv. Model. Earth Syst.* 7, 774–790. doi:10.1002/2014MS000414.
- 53 Li, Z., Cao, L., Zhu, Y., and Yan, Z. (2016). Comparison of two homogenized datasets of daily
54 maximum/mean/minimum temperature in China during 1960–2013. *J. Meteorol. Res.* 30, 53–66.
55 doi:10.1007/s13351-016-5054-x.
- 56 Ligtenberg, S., Berg, W. J., Van den Broeke, M., Rae, J., and van Meijgaard, E. (2013). *Future surface mass balance of*
57 *the Antarctic ice sheet and its influence on sea level change, simulated by a regional atmospheric climate model.*
58 doi:10.1007/s00382-013-1749-1.
- 59 Limjikanan, S., and Limsakul, A. (2012). Observed Trends in Surface Air Temperatures and Their Extremes in Thailand
60 from 1970 to 2009. *J. Meteorol. Soc. Japan. Ser. II* 90, 647–662. doi:10.2151/jmsj.2012-505.
- 61 Limsakul, A., and Singhruck, P. (2016). Long-term trends and variability of total and extreme precipitation in Thailand.

- 1 *Atmos. Res.* 169, 301–317. doi:10.1016/J.ATMOSRES.2015.10.015.
- 2 Lind, P., Lindstedt, D., Kjellström, E., Jones, C., Lind, P., Lindstedt, D., et al. (2016). Spatial and Temporal
3 Characteristics of Summer Precipitation over Central Europe in a Suite of High-Resolution Climate Models. *J.*
4 *Clim.* 29, 3501–3518. doi:10.1175/JCLI-D-15-0463.1.
- 5 Liu, H. W., Zhou, T. J., Zhu, Y. X., and Lin, Y. H. (2012). The strengthening East Asia summer monsoon since the
6 early 1990s. *Chinese Sci. Bull.* 57, 1553–1558. doi:10.1007/s11434-012-4991-8.
- 7 Llopart, M., Coppola, E., Giorgi, F., da Rocha, R. P., and Cuadra, S. V. (2014). Climate change impact on precipitation
8 for the Amazon and La Plata basins. *Clim. Change* 125, 111–125. doi:10.1007/s10584-014-1140-1.
- 9 Llopart, M., Reboita, M., and da Rocha, R. (2019). Multimodel climate projections over South America CORDEX
10 domain. *Submitted*.
- 11 Loh, J. Le, Tangang, F., Juneng, L., Hein, D., and Lee, D.-I. (2016). Projected rainfall and temperature changes over
12 Malaysia at the end of the 21st century based on PRECIS modelling system. *Asia-Pacific J. Atmos. Sci.* 52, 191–
13 208. doi:10.1007/s13143-016-0019-7.
- 14 López-Franca, N., Zaninelli, P., Carril, A., Menéndez, C., and Sánchez, E. (2016). Changes in temperature extremes for
15 21st century scenarios over South America derived from a multi-model ensemble of regional climate models.
16 *Clim. Res.* 68, 151–167. doi:10.3354/cr01393.
- 17 Lorenz, S., Dessai, S., Forster, P. M., and Paavola, J. (2015). Tailoring the visual communication of climate projections
18 for local adaptation practitioners in Germany and the UK. *Philos. Trans. R. Soc. A Math. Phys. Eng. Sci.* 373,
19 20140457. doi:10.1098/rsta.2014.0457.
- 20 Loupian, E., Burtsev, M. A., Bartalev, S. A., and Kashnitskii, A. (2015). IKI center for collective use of satellite data
21 archiving , processing and analysis systems aimed at solving the problems of environmental study and
22 monitoring. *Curr. Probl. Remote Sens. Earth From Sp.* 12, 263–284.
- 23 Lucas-Picher, P., Christensen, J. H., Saeed, F., Kumar, P., Asharaf, S., Ahrens, B., et al. (2011). Can Regional Climate
24 Models Represent the Indian Monsoon? *J. Hydrometeorol.* 12, 849–868. doi:10.1175/2011jhm1327.1.
- 25 Lussana, C., Saloranta, T., Skaugen, T., Magnusson, J., Tveito, O. E., and Andersen, J. (2018). seNorge2 daily
26 precipitation, an observational gridded dataset over Norway from 1957 to the present day. *Earth Syst. Sci. Data;*
27 *Katlenburg-Lindau* 10, 235–249. doi:http://dx.doi.org/10.5194/essd-10-235-2018.
- 28 Luterbacher, J., Werner, J. P., Smerdon, J. E., Fernández-Donado, L., González-Rouco, F. J., Barriopedro, D., et al.
29 (2016). European summer temperatures since Roman times. *Environ. Res. Lett.* 11, 024001. doi:10.1088/1748-
30 9326/11/2/024001.
- 31 Lyon, B. (2014). Seasonal drought in the Greater Horn of Africa and its recent increase during the March-May long
32 rains. *J. Clim.* doi:10.1175/JCLI-D-13-00459.1.
- 33 Lyon, B., and Dewitt, D. G. (2012). A recent and abrupt decline in the East African long rains. *Geophys. Res. Lett.*
34 doi:10.1029/2011GL050337.
- 35 LYRA, A. de A., CHOU, S. C., and SAMPAIO, G. de O. (2016). Sensitivity of the Amazon biome to high resolution
36 climate change projections. *Acta Amaz.* 46, 175–188. doi:10.1590/1809-4392201502225.
- 37 Ma, L., Zhang, T., Frauenfeld, O. W., Ye, B., Yang, D., and Qin, D. (2009). Evaluation of precipitation from the ERA-
38 40, NCEP-1, and NCEP-2 reanalyses and CMAP-1, CMAP-2, and GPCP-2 with ground-based measurements in
39 China. *J. Geophys. Res. Atmos.* 114. doi:10.1029/2008JD011178.
- 40 MacKellar, N., New, M., and Jack, C. (2014). Observed and modelled trends in rainfall and temperature for South
41 Africa: 1960-2010. *S. Afr. J. Sci.* doi:10.1590/sajs.2014/20130353.
- 42 Madsen, H., Lawrence, D., Lang, M., Martinkova, M., and Kjeldsen, T. R. (2014). Review of trend analysis and climate
43 change projections of extreme precipitation and floods in Europe. *J. Hydrol.* 519, 3634–3650.
44 doi:10.1016/j.jhydrol.2014.11.003.
- 45 Magaña, V., Amador, J. A., and Medina, S. (1999). The Midsummer Drought over Mexico and Central America. *J.*
46 *Clim.* 12, 1577–1588. doi:10.1175/1520-0442(1999)012<1577:TMDOMA>2.0.CO;2.
- 47 Maio, G. R. (2017). *The psychology of human values*. Routledge.
- 48 Manabe, S., and Stouffer, R. J. (1980). Sensitivity of a global climate model to an increase of CO₂ concentration in the
49 atmosphere. *J. Geophys. Res.* 85, 5529. doi:10.1029/JC085iC10p05529.
- 50 Mann, M. E., Emanuel, K. A., Holland, G. J., and Webster, P. J. (2007). Atlantic tropical cyclones revisited. *Eos, Trans.*
51 *Am. Geophys. Union* 88, 349–350. doi:10.1029/2007EO360002.
- 52 Manomaiphiboon, K., Octaviani, M., Torsri, K., and Towprayoon, S. (2013). Projected changes in means and extremes
53 of temperature and precipitation over Thailand under three future emissions scenarios. *Clim. Res.* 58, 97–115.
54 doi:10.3354/cr01188.
- 55 Manzanas, R., Amekudzi, L. K., Preko, K., Herrera, S., and Gutiérrez, J. M. (2014). Precipitation variability and trends
56 in Ghana: An intercomparison of observational and reanalysis products. *Clim. Change*. doi:10.1007/s10584-014-
57 1100-9.
- 58 Manzanas, R., Brands, S., San-Martín, D., Lucero, A., Limbo, C., and Gutiérrez, J. M. (2015). Statistical downscaling
59 in the tropics can be sensitive to reanalysis choice: A case study for precipitation in the Philippines. *J. Clim.* 28,
60 4171–4184. doi:10.1175/JCLI-D-14-00331.1.
- 61 Maraun, D., Huth, R., Gutiérrez, J. M., Martín, D. S., Dubrovsky, M., Fischer, A., et al. (2017a). The VALUE perfect

- 1 predictor experiment: evaluation of temporal variability. *Int. J. Climatol.* doi:10.1002/joc.5222.
- 2 Maraun, D., Shepherd, T. G., Widmann, M., Zappa, G., Walton, D., Gutiérrez, J. M., et al. (2017b). Towards process-
3 informed bias correction of climate change simulations. *Nat. Clim. Chang.* 7, 664–773.
4 doi:10.1038/nclimate3418.
- 5 Maraun, D., Widmann, M., and Gutiérrez, J. M. (2018). Statistical downscaling skill under present climate conditions:
6 A synthesis of the VALUE perfect predictor experiment. *Int. J. Climatol.* doi:10.1002/joc.5877.
- 7 Maraun, D., Widmann, M., Gutiérrez, J. M., Kotlarski, S., Chandler, R. E., Hertig, E., et al. (2015a). VALUE: A
8 framework to validate downscaling approaches for climate change studies. *Earth's Futur.* 3, 1–14.
9 doi:10.1002/2014EF000259.
- 10 Maraun, D., Widmann, M., Gutiérrez, J. M., Kotlarski, S., Chandler, R. E., Hertig, E., et al. (2015b). VALUE: A
11 framework to validate downscaling approaches for climate change studies. *Earth's Futur.* 3, 1–14.
12 doi:10.1002/2014EF000259.
- 13 Marengo, J. A., and Espinoza, J. C. (2016). Extreme seasonal droughts and floods in Amazonia: causes, trends and
14 impacts. *Int. J. Climatol.* 36, 1033–1050. doi:10.1002/joc.4420.
- 15 Marengo, J. A., Souza, C. M., Thonicke, K., Burton, C., Halladay, K., Betts, R. A., et al. (2018). Changes in Climate
16 and Land Use Over the Amazon Region: Current and Future Variability and Trends. *Front. Earth Sci.* 6.
17 doi:10.3389/feart.2018.00228.
- 18 Marengo, J. A., Torres, R. R., and Alves, L. M. (2017). Drought in Northeast Brazil—past, present, and future. *Theor.*
19 *Appl. Climatol.* 129, 1189–1200. doi:10.1007/s00704-016-1840-8.
- 20 Marengo, J., Alves, L., and Torres, R. (2016). Regional climate change scenarios in the Brazilian Pantanal watershed.
21 *Clim. Res.* 68, 201–213. doi:10.3354/cr01324.
- 22 Mariotti, A., Pan, Y., Zeng, N., and Alessandri, A. (2015). Long-term climate change in the Mediterranean region in the
23 midst of decadal variability. *Clim. Dyn.* 44, 1437–1456. doi:10.1007/s00382-015-2487-3.
- 24 Marshall, G. J., Thompson, D. W. J., and van den Broeke, M. R. (2017). The Signature of Southern Hemisphere
25 Atmospheric Circulation Patterns in Antarctic Precipitation. *Geophys. Res. Lett.* 44, 11,580–11,589.
26 doi:10.1002/2017GL075998.
- 27 Martin, E. R., and Schumacher, C. (2011). The Caribbean Low-Level Jet and Its Relationship with Precipitation in
28 IPCC AR4 Models. *J. Clim.* 24, 5935–5950. doi:10.1175/JCLI-D-11-00134.1.
- 29 Martínez-Austria, P. F., and Bandala, E. R. (2017). Temperature and Heat-Related Mortality Trends in the Sonoran and
30 Mojave Desert Region. *Atmosphere (Basel)*. 8. doi:10.3390/atmos8030053.
- 31 Martínez-Austria, P. F., Bandala, E. R., and Patiño-Gómez, C. (2016). Temperature and heat wave trends in northwest
32 Mexico. *Phys. Chem. Earth, Parts A/B/C* 91, 20–26. doi:10.1016/j.pce.2015.07.005.
- 33 Martínez-Castro, D., Porfirio da Rocha, R., Bezanilla-Morlot, A., Alvarez-Escudero, L., Reyes-Fernández, J. P., Silva-
34 Vidal, Y., et al. (2006). Sensitivity studies of the RegCM3 simulation of summer precipitation, temperature and
35 local wind field in the Caribbean Region. *Theor. Appl. Climatol.* doi:10.1007/s00704-005-0201-9.
- 36 Martínez-Castro, D., Vichot-Llano, A., Bezanilla-Morlot, A., Centella-Artola, A., Campbell, J., Giorgi, F., et al. (2018).
37 The performance of RegCM4 over the Central America and Caribbean region using different cumulus
38 parameterizations. *Clim. Dyn.* 50, 4103–4126. doi:10.1007/s00382-017-3863-y.
- 39 Martínez-Castro, D., Vichot-Llano, A., Bezanilla-Morlot, A., Centella-Artola, A., Campbell, J., and Vilorio-Holguin, C.
40 (2016). Performance of RegCM-4.3 over the Caribbean region using different configurations of the Tiedtke
41 convective parameterization scheme. *Rev. Climatol.* 16, 77–98.
- 42 Martínez-Castro, D., Vichot Llano, A., Bezanilla, A., Centella-Artola, A., Campbell, J., Giorgi, F., et al. (2017). The
43 performance of RegCM4 over the Central America and Caribbean region using different cumulus
44 parameterizations. *Clim. Dyn.*, 1–24. doi:10.1007/s00382-017-3863-y.
- 45 Martínez Sanchez, J. N., and Cavazos, T. (2014). Eastern Tropical Pacific hurricane variability and landfalls on
46 Mexican coasts. *Clim. Res.* 58, 221–234. doi:10.3354/cr01192.
- 47 Martynov, A., Laprise, R., Sushama, L., Winger, K., Šeparović, L., and Dugas, B. (2013). Reanalysis-driven climate
48 simulation over CORDEX North America domain using the Canadian Regional Climate Model, version 5: model
49 performance evaluation. *Clim. Dyn.* 41, 2973–3005. doi:10.1007/s00382-013-1778-9.
- 50 Matthes, H., Rinke, A., and Dethloff, K. (2015a). Recent changes in Arctic temperature extremes: Warm and cold spells
51 during winter and summer. *Environ. Res. Lett.* 10, 114020. doi:10.1088/1748-9326/10/11/114020.
- 52 Matthes, H., Rinke, A., and Dethloff, K. (2015b). Recent changes in Arctic temperature extremes: Warm and cold spells
53 during winter and summer. *Environ. Res. Lett.* 10, 114020. doi:10.1088/1748-9326/10/11/114020.
- 54 Maure, G., Pinto, I., Ndebele-Murisa, M., Muthige, M., Lennard, C., Nikulin, G., et al. (2018). The southern African
55 climate under 1.5 °C and 2 °C of global warming as simulated by CORDEX regional climate models. *Environ.*
56 *Res. Lett.* doi:10.1088/1748-9326/aab190.
- 57 Mayer, S., Fox Maule, C., Sobolowski, S., Bøssing Christensen, O., Danielsen Sørup, H. J., Antonia Sunyer, M., et al.
58 (2015). Identifying added value in high-resolution climate simulations over Scandinavia. *Tellus A Dyn. Meteorol.*
59 *Oceanogr.* 67, 24941. doi:10.3402/tellusa.v67.24941.
- 60 Mayowa, O. O., Pour, S. H., Shahid, S., Mohsenipour, M., Harun, S. Bin, Heryansyah, A., et al. (2015). Trends in
61 rainfall and rainfall-related extremes in the east coast of peninsular Malaysia. *J. Earth Syst. Sci.* 124, 1609–1622.

- 1 doi:10.1007/s12040-015-0639-9.
- 2 Mba, W. P., Longandjo, G.-N. T., Moufouma-Okia, W., Bell, J.-P., James, R., Vondou, D. A., et al. (2018).
3 Consequences of 1.5 °C and 2 °C global warming levels for temperature and precipitation changes over Central
4 Africa. *Environ. Res. Lett.* 13, 055011. doi:10.1088/1748-9326/aab048.
- 5 McCright, A. M., Dunlap, R. E., and Marquart-Pyatt, S. T. (2016). Political ideology and views about climate change in
6 the European Union. *Env. Polit.* 25, 338–358. doi:10.1080/09644016.2015.1090371.
- 7 McDonald, R. I., Chai, H. Y., and Newell, B. R. (2015). Personal experience and the ‘psychological distance’ of climate
8 change: An integrative review. *J. Environ. Psychol.* 44, 109–118. doi:10.1016/j.jenvp.2015.10.003.
- 9 McLean, N. M., Stephenson, T. S., Taylor, M. A., and Campbell, J. D. (2015). Characterization of Future Caribbean
10 Rainfall and Temperature Extremes across Rainfall Zones. *Adv. Meteorol.* 2015, 1–18. doi:10.1155/2015/425987.
- 11 McMahan, R., Stauffacher, M., and Knutti, R. (2015). The unseen uncertainties in climate change: reviewing
12 comprehension of an IPCC scenario graph. *Clim. Change* 133, 141–154. doi:10.1007/s10584-015-1473-4.
- 13 McSweeney, C. F., Jones, R. G., Lee, R. W., and Rowell, D. P. (2015). Selecting CMIP5 GCMs for downscaling over
14 multiple regions. *Clim. Dyn.* 44, 3237–3260. doi:10.1007/s00382-014-2418-8.
- 15 Medley, B., McConnell, J. R., Neumann, T. A., Reijmer, C. H., Chellman, N., Sigl, M., et al. (2018). Temperature and
16 Snowfall in Western Queen Maud Land Increasing Faster Than Climate Model Projections. *Geophys. Res. Lett.*
17 45, 1472–1480. doi:10.1002/2017GL075992.
- 18 Mei, R., Ashfaq, M., Rastogi, D., Leung, L. R., and Dominguez, F. (2015). Dominating controls for wetter South Asian
19 summer monsoon in the twenty-first century. *J. Clim.* 28, 3400–3419. doi:10.1175/JCLI-D-14-00355.1.
- 20 Méndez, M., and Magaña, V. (2010). Regional Aspects of Prolonged Meteorological Droughts over Mexico and
21 Central America. *J. Clim.* 23, 1175–1188. doi:10.1175/2009JCLI3080.1.
- 22 Menéndez, C., Zaninelli, P., Carril, A., and Sánchez, E. (2016). Hydrological cycle, temperature, and land surface-
23 atmosphere interaction in the La Plata Basin during summer: response to climate change. *Clim. Res.* 68, 231–241.
24 doi:10.3354/cr01373.
- 25 Meque, A., and Abiodun, B. J. (2015). Simulating the link between ENSO and summer drought in Southern Africa
26 using regional climate models. *Clim. Dyn.* doi:10.1007/s00382-014-2143-3.
- 27 Michelangeli, P.-A., Vautard, R., and Legras, B. (1995). Weather Regimes: Recurrence and Quasi Stationarity. *J.*
28 *Atmos. Sci.* 52, 1237–1256. doi:10.1175/1520-0469(1995)052<1237:WRRAS>2.0.CO;2.
- 29 Mishra, V. (2015). Climatic uncertainty in Himalayan water towers. *J. Geophys. Res.* 120, 2689–2705.
30 doi:10.1002/2014JD022650.
- 31 Mohan, A., and Topp, K. (2018). India’s energy future: Contested narratives of change. *Energy Res. Soc. Sci.* 44, 75–
32 82. doi:10.1016/j.erss.2018.04.040.
- 33 Mooley, D. A., and Parthasarathy, B. (1984). Fluctuations in All-India summer monsoon rainfall during 1871–1978.
34 *Clim. Change* 6, 287–301. doi:10.1007/BF00142477.
- 35 Moreau, L., Groth, P., Cheney, J., Lebo, T., and Miles, S. (2015). The rationale of PROV. *J. Web Semant.*
36 doi:10.1016/j.websem.2015.04.001.
- 37 Mori, M., Watanabe, M., Shiogama, H., Inoue, J., and Kimoto, M. (2014). Robust Arctic sea-ice influence on the
38 frequent Eurasian cold winters in past decades. *Nat. Geosci.* 7, 869–873. doi:10.1038/ngeo2277.
- 39 Motta, M. (2018). The enduring effect of scientific interest on trust in climate scientists in the United States. *Nat. Clim.*
40 *Chang.* 8, 485–488. doi:10.1038/s41558-018-0126-9.
- 41 Mouhamed, L., Traore, S. B., Alhassane, A., and Sarr, B. (2013). Evolution of some observed climate extremes in the
42 West African Sahel. *Weather Clim. Extrem.* doi:10.1016/j.wace.2013.07.005.
- 43 Mourão, C., Chou, S. C., and Marengo, J. (2016). Downscaling Climate Projections over La Plata Basin. *Atmos. Clim.*
44 *Sci.* 06, 1–12. doi:10.4236/acs.2016.61001.
- 45 Mukherjee, S., Aadhar, S., Stone, D., and Mishra, V. (2018). Increase in extreme precipitation events under
46 anthropogenic warming in India. *Weather Clim. Extrem.* 20, 45–53. doi:10.1016/j.wace.2018.03.005.
- 47 Nabat, P., Solmon, F., Mallet, M., Kok, J. F., and Somot, S. (2012). Dust emission size distribution impact on aerosol
48 budget and radiative forcing over the Mediterranean region: a regional climate model approach. *Atmos. Chem.*
49 *Phys.* 12, 10545–10567. doi:10.5194/acp-12-10545-2012.
- 50 Nabat, P., Somot, S., Mallet, M., Chiapello, I., Morcrette, J. J., Solmon, F., et al. (2013). A 4-D climatology
51 (1979–2009) of the monthly tropospheric aerosol optical depth distribution over the
52 Mediterranean region from a comparative evaluation and blending of remote sensing and model products. *Atmos.*
53 *Meas. Tech.* 6, 1287–1314. doi:10.5194/amt-6-1287-2013.
- 54 Nabat, P., Somot, S., Mallet, M., Michou, M., Sevault, F., Driouech, F., et al. (2015a). Dust aerosol radiative effects
55 during summer 2012 simulated with a coupled regional aerosol-atmosphere-ocean model over the Mediterranean.
56 *Atmos. Chem. Phys.* 15. doi:10.5194/acp-15-3303-2015.
- 57 Nabat, P., Somot, S., Mallet, M., Sanchez-Lorenzo, A., and Wild, M. (2014). Contribution of anthropogenic sulfate
58 aerosols to the changing Euro-Mediterranean climate since 1980. *Geophys. Res. Lett.* 41, 5605–5611.
59 doi:10.1002/2014GL060798.
- 60 Nabat, P., Somot, S., Mallet, M., Sevault, F., Chiacchio, M., and Wild, M. (2015b). Direct and semi-direct aerosol
61 radiative effect on the Mediterranean climate variability using a coupled regional climate system model. *Clim.*

- 1 *Dyn.* 44, 1127–1155. doi:10.1007/s00382-014-2205-6.
- 2 Nabeel, A., and Athar, H. (2018). Observed , stochastically simulated , and projected precipitation variability in
3 Pakistan.
- 4 Naranjo-Diaz, L. R., and Centella, A. (1998). Recent trends in the climate of Cuba. *Weather* 53, 78–85.
5 doi:10.1002/j.1477-8696.1998.tb03964.x.
- 6 National Academies of Sciences and Medicine, E. (2017). *Communicating Science Effectively: A Research Agenda*.
7 Washington, DC: The National Academies Press doi:10.17226/23674.
- 8 National Academies of Sciences, E. and M. (2017). *Communicating Science Effectively*. Washington, D.C.: National
9 Academies Press doi:10.17226/23674.
- 10 Navarro-Estupiñan, J., Robles-Morua, A., Vivoni, E. R., Zepeda, J. E., Montoya, J. A., and Verduzco, V. S. (2018).
11 Observed trends and future projections of extreme heat events in Sonora, Mexico. *Int. J. Climatol.* 38, 5168–
12 5181. doi:10.1002/joc.5719.
- 13 Nengker, T., Choudhary, A., and Dimri, A. P. (2018). Assessment of the performance of CORDEX-SA experiments in
14 simulating seasonal mean temperature over the Himalayan region for the present climate: Part I. *Clim. Dyn.* 50,
15 2411–2441. doi:10.1007/s00382-017-3597-x.
- 16 Neukom, R., Luterbacher, J., Villalba, R., Küttel, M., Frank, D., Jones, P. D., et al. (2010). Multi-centennial summer
17 and winter precipitation variability in southern South America. *Geophys. Res. Lett.* 37, n/a-n/a.
18 doi:10.1029/2010GL043680.
- 19 Ngo-Duc, T., Kieu, C., Thatcher, M., Nguyen-Le, D., and Phan-Van, T. (2014). Climate projections for Vietnam based
20 on regional climate models. *Clim. Res.* 60, 199–213. doi:10.3354/cr01234.
- 21 Ngo-Duc, T., Tangang, F. T., Santisirisomboon, J., Cruz, F., Trinh-Tuan, L., Nguyen-Xuan, T., et al. (2017).
22 Performance evaluation of RegCM4 in simulating extreme rainfall and temperature indices over the CORDEX-
23 Southeast Asia region. *Int. J. Climatol.* 37, 1634–1647. doi:10.1002/joc.4803.
- 24 Nguyen-Xuan, T., Ngo-Duc, T., Kamimera, H., Trinh-Tuan, L., Matsumoto, J., Inoue, T., et al. (2016). The Vietnam
25 Gridded Precipitation (VnGP) Dataset: Construction and Validation. *SOLA* 12, 291–296. doi:10.2151/sola.2016-
26 057.
- 27 Nguyen, K. C. and K. J. W. (2001). Interannual, Decadal, and Transient Greenhouse Simulation of Tropical Cyclone-
28 like Vortices in a Regional Climate Model of the South Pacific. *J. Clim.* 14, 3043–3054.
- 29 Niang, I., Ruppel, O. C., Abdrabo, M. A., Essel, A., Lennard, C., Padgham, J., et al. (2014). Chapter 22 - Africa. *Clim.*
30 *Chang. 2014 Impacts, Adapt. Vulnerability - Contrib. Work. Gr. II to Fifth Assess. Rep. Intergov. Panel Clim.*
31 *Chang.* doi:10.1017/CBO9781107415386.002.
- 32 Nicolas, J. P., and Bromwich, D. H. (2014). New Reconstruction of Antarctic Near-Surface Temperatures: Multidecadal
33 Trends and Reliability of Global Reanalyses. *J. Clim.* 27, 8070–8093. doi:10.1175/JCLI-D-13-00733.1.
- 34 Nikulin, G., Lennard, C., Dosio, A., Kjellström, E., Chen, Y., Hansler, A., et al. (2018). The effects of 1.5 and 2 degrees
35 of global warming on Africa in the CORDEX ensemble. *Environ. Res. Lett.* doi:10.1088/1748-9326/aab1b1.
- 36 Nisbet, M. C., and Markowitz, E. (2016). *Strategic science communication on environmental issues*. American
37 Association for the Advancement of Science Available at: [https://mcmprodaaas.s3.amazonaws.com/s3fs-](https://mcmprodaaas.s3.amazonaws.com/s3fs-public/content_files/NisbetMarkowitz_StrategicSciCommOnEnvironmentalIssues_WhitePaper.pdf)
38 [public/content_files/NisbetMarkowitz_StrategicSciCommOnEnvironmentalIssues_WhitePaper.pdf](https://mcmprodaaas.s3.amazonaws.com/s3fs-public/content_files/NisbetMarkowitz_StrategicSciCommOnEnvironmentalIssues_WhitePaper.pdf).
- 39 Niu, X., Wang, S., Tang, J., Lee, D., Gutowski, W., Dairaku, K., et al. (2015). Projection of Indian summer monsoon
40 climate in 2041–2060 by multiregional and global climate models. doi:10.1002/2014JD022620.Received.
- 41 Nobre, C. A., Sampaio, G., Borma, L. S., Castilla-Rubio, J. C., Silva, J. S., and Cardoso, M. (2016). Land-use and
42 climate change risks in the Amazon and the need of a novel sustainable development paradigm. *Proc. Natl. Acad.*
43 *Sci.* 113, 10759 LP – 10768. Available at: <http://www.pnas.org/content/113/39/10759.abstract>.
- 44 Noël, B., Van De Berg, W. J., Van Meijgaard, E., Kuipers Munneke, P., Van De Wal, R. S. W., and Van Den Broeke,
45 M. R. (2015). Evaluation of the updated regional climate model RACMO2.3: Summer snowfall impact on the
46 Greenland Ice Sheet. *Cryosphere* 9, 1831–1844. doi:10.5194/tc-9-1831-2015.
- 47 Obermann-Hellhund, A., Conte, D., Somot, S., Torma, C. Z., and Ahrens, B. (2018). Mistral and Tramontane wind
48 systems in climate simulations from 1950 to 2100. *Clim. Dyn.* 50. doi:10.1007/s00382-017-3635-8.
- 49 Osborn, T. J., Wallace, C. J., Harris, I. C., and Melvin, T. M. (2016). Pattern scaling using ClimGen: monthly-
50 resolution future climate scenarios including changes in the variability of precipitation. *Clim. Change* 134, 353–
51 369. doi:10.1007/s10584-015-1509-9.
- 52 Osima, S., Indasi, V. S., Zaroug, M., Endris, H. S., Gudoshava, M., Misiani, H. O., et al. (2018). Projected climate over
53 the Greater Horn of Africa under 1.5 °c and 2 °c global warming. *Environ. Res. Lett.* doi:10.1088/1748-
54 9326/aaba1b.
- 55 Otto, F. E. L., Hausteine, K., Uhe, P., Coelho, C. A. S., Aravequia, J. A., Almeida, W., et al. (2015). Factors Other Than
56 Climate Change, Main Drivers of 2014/15 Water Shortage in Southeast Brazil. *Bull. Am. Meteorol. Soc.* 96, S35–
57 S40. doi:10.1175/BAMS-D-15-00120.1.
- 58 Ouzeau, G., Déqué, M., Jouini, M., Planton, S., and Vautard, R. (2014). “Scénarios régionalisés : édition 2014 pour la
59 métropole et les régions d’outre-mer,” in *Le climat de la France au XXI e siècle* Volume 4. (France: Ministère de
60 l’Écologie, du Développement durable et de l’Énergie (sous la direction de Jean Jouzel)), 1–64. Available at:
61 https://www.ecologique-solidaire.gouv.fr/sites/default/files/ONERC_Climat_France_XXI_Volume_4_VF.pdf

- 1 [Accessed March 29, 2019].
- 2 Ouzeau, G., Soubeyroux, J.-M., Schneider, M., Vautard, R., and Planton, S. (2016). Heat waves analysis over France in
3 present and future climate: Application of a new method on the EURO-CORDEX ensemble. *Clim. Serv.* 4, 1–12.
4 doi:10.1016/J.CLISER.2016.09.002.
- 5 Overland, J. E., Spillane, M. C., and Soreide, N. N. (2004). Integrated analysis of physical and biological pan-arctic
6 change. *Clim. Change*. doi:10.1023/B:CLIM.0000018512.40506.d2.
- 7 Pai, D. S., Sridhar, L., Badwaik, M. R., and Rajeevan, M. (2015). Analysis of the daily rainfall events over India using a
8 new long period (1901–2010) high resolution (0.25^o × 0.25^o) gridded rainfall
9 data set. *Clim. Dyn.* 45, 755–776. doi:10.1007/s00382-014-2307-1.
- 10 Paiva, A. R. De, Jr, J. H., and Orville, R. E. (2016). Journal of Geophysical Research : Atmospheres from high-speed
11 videos. 8493–8505. doi:10.1002/2016JD025137.Received.
- 12 Pal, J. S., Giorgi, F., Bi, X., Elguindi, N., Solmon, F., Gao, X., et al. (2007). Regional climate modeling for the
13 developing world: The ICTP RegCM3 and RegCM3. *Bull. Am. Meteorol. Soc.* 88, 1395–1409.
14 doi:10.1175/BAMS-88-9-1395.
- 15 Palazzi, E., Hardenberg, J. Von, and Terzago, S. (2015). Precipitation in the Karakoram-Himalaya : a CMIP5 view.
16 *Clim. Dyn.*, 21–45. doi:10.1007/s00382-014-2341-z.
- 17 Palerme, C., Genthon, C., Claud, C., Kay, J., Wood, N., and Lecuyer, T. (2016). Evaluation of current and
18 projected Antarctic precipitation in CMIP 5 models. in.
- 19 Palerme, C., Kay, J. E., Genthon, C., and Lecuyer, T., Wood, N. B., and Claud, C. (2014). How much snow
20 falls on the Antarctic ice sheet? *Cryosph.* 8, 1577–1587. doi:10.5194/tc-8-1577-2014.
- 21 Panthou, G., Vrac, M., Drobinski, P., Bastin, S., and Li, L. (2018). Impact of model resolution and Mediterranean sea
22 coupling on hydrometeorological extremes in RCMs in the frame of HyMeX and MED-CORDEX. *Clim. Dyn.* 51,
23 915–932. doi:10.1007/s00382-016-3374-2.
- 24 Park, C., Min, S. K., Lee, D., Cha, D. H., Suh, M. S., Kang, H. S., et al. (2016). Evaluation of multiple regional climate
25 models for summer climate extremes over East Asia. *Clim. Dyn.* 46, 2469–2486. doi:10.1007/s00382-015-2713-z.
- 26 Pavia, E. G., Graef, F., and Reyes, J. (2006). PDO–ENSO Effects in the Climate of Mexico. *J. Clim.* 19, 6433–6438.
27 doi:10.1175/JCLI4045.1.
- 28 Pavlidis, V., Katragkou, E., Prein, A., Georgoulas, A., Kartsios, S., Zanis, P., et al. Investigating the impact of aerosol
29 climatologies in regional climate mode simulations over Europe. *prep*.
- 30 Peel, M. C., Finlayson, B. L., and McMahon, T. A. (2007). Hydrology and Earth System Sciences Updated world map
31 of the Köppen-Geiger climate classification. Available at: www.hydrol-earth-syst-sci.net/11/1633/2007/.
- 32 Penalba, O. C., and Robledo, F. A. (2010). Spatial and temporal variability of the frequency of extreme daily rainfall
33 regime in the La Plata Basin during the 20th century. *Clim. Change*. doi:10.1007/s10584-009-9744-6.
- 34 Persily, N. (2017). The 2016 U.S. Election: Can Democracy Survive the Internet? | Journal of Democracy. *J. Democr.*
35 28, 63–76. Available at: [https://www.journalofdemocracy.org/articles/the-2016-u-s-election-can-democracy-](https://www.journalofdemocracy.org/articles/the-2016-u-s-election-can-democracy-survive-the-internet/)
36 [survive-the-internet/](https://www.journalofdemocracy.org/articles/the-2016-u-s-election-can-democracy-survive-the-internet/) [Accessed March 29, 2019].
- 37 Pervez, M. S., and Henebry, G. M. (2014a). Projections of the Ganges-Brahmaputra precipitation-Downscaled from
38 GCM predictors. *J. Hydrol.* 517, 120–134. doi:10.1016/j.jhydrol.2014.05.016.
- 39 Pervez, S., and Henebry, G. M. (2014b). Projections of the Ganges – Brahmaputra precipitation — Downscaled from
40 GCM predictors. 517, 120–134. doi:10.1016/j.jhydrol.2014.05.016.
- 41 Peterson, T. C., Taylor, M. A., Demeritte, R., Duncombe, D. L., Burton, S., Thompson, F., et al. (2002). Recent
42 changes in climate extremes in the Caribbean region. *J. Geophys. Res. Atmos.* 107, ACL 16-1-ACL 16-9.
43 doi:10.1029/2002JD002251.
- 44 Pham, T. Van, Brauch, J., Früh, B., and Ahrens, B. (2017). Simulation of snowbands in the Baltic Sea area with the
45 coupled atmosphere-ocean-ice model COSMO-CLM/NEMO. *Meteorol. Zeitschrift* 26, 71–82.
46 doi:10.1127/metz/2016/0775.
- 47 Pidgeon, N., and Fischhoff, B. (2011). The role of social and decision sciences in communicating uncertain climate
48 risks. *Nat. Clim. Chang.* 1, 35–41. doi:10.1038/nclimate1080.
- 49 Pielke, R. A., Landsea, C., Mayfield, M., Layer, J., and Pasch, R. (2005). Hurricanes and Global Warming. *Bull. Am.*
50 *Meteorol. Soc.* 86, 1571–1576. doi:10.1175/BAMS-86-11-1571.
- 51 Pinto, I., Lennard, C., Tadross, M., Hewitson, B., Dosio, A., Nikulin, G., et al. (2016). Evaluation and projections of
52 extreme precipitation over southern Africa from two CORDEX models. *Clim. Change*. doi:10.1007/s10584-015-
53 1573-1.
- 54 Pitman, A. J., De Noblet-Ducoudré, N., Cruz, F. T., Davin, E. L., Bonan, G. B., Brovkin, V., et al. (2009). Uncertainties
55 in climate responses to past land cover change: First results from the LUCID intercomparison study. *Geophys.*
56 *Res. Lett.* 36, 1–6. doi:10.1029/2009GL039076.
- 57 Polk, E. (2018). “Communicating Climate Change: Where Did We Go Wrong, How Can We Do Better?,” in *Handbook*
58 *of Communication for Development and Social Change* (Singapore: Springer Singapore), 1–19. doi:10.1007/978-
59 981-10-7035-8_26-1.
- 60 Pons, M. R., Herrera, S., and Gutiérrez, J. M. (2016). Future trends of snowfall days in northern Spain from
61 ENSEMBLES regional climate projections. *Clim. Dyn.* 46, 3645–3655. doi:10.1007/s00382-015-2793-9.

- 1 Prakash, S. (2019). Performance assessment of CHIRPS, MSWEP, SM2RAIN-CCI, and TMPA precipitation products
2 across India. *J. Hydrol.* doi:10.1016/j.jhydrol.2019.01.036.
- 3 Prakash, S., Mitra, A. K., Momin, I. M., Pai, D. S., Rajagopal, E. N., and Basu, S. (2014). Comparison of TMPA-3B42
4 Versions 6 and 7 Precipitation Products with Gauge-Based Data over India for the Southwest Monsoon Period. *J.*
5 *Hydrometeorol.* 16, 346–362. doi:10.1175/jhm-d-14-0024.1.
- 6 Prein, A. F., and Gobiet, A. (2017). Impacts of uncertainties in European gridded precipitation observations on regional
7 climate analysis. *Int. J. Climatol.* 37, 305–327. doi:10.1002/joc.4706.
- 8 Prein, A. F., Gobiet, A., Truhetz, H., Keuler, K., Goergen, K., Teichmann, C., et al. (2016). Precipitation in the EURO-
9 CORDEX 0.11° and 0.44° simulations: high resolution, high benefits? *Clim. Dyn.* 46, 383–412.
10 doi:10.1007/s00382-015-2589-y.
- 11 Prein, A. F., Langhans, W., Fossier, G., Ferrone, A., Ban, N., Goergen, K., et al. (2015). A review on regional
12 convection-permitting climate modeling: Demonstrations, prospects, and challenges. *Rev. Geophys.* 53, 323–361.
13 doi:10.1002/2014RG000475.
- 14 Pulak Guhathakurta and Jayashree V Revadekar (2017). “Observed Variability and Long-Term Trends of Rainfall Over
15 India,” in *Observed Climate Variability and Change over the Indian Region* (Singapore: Springer, Singapore).
- 16 Putkonen, J., and Roe, G. (2003). Rain-on-snow events impact soil temperatures and affect ungulate survival. *Geophys.*
17 *Res. Lett.* 30. doi:10.1029/2002GL016326.
- 18 Rabinovich, A., and Morton, T. A. (2012). Unquestioned Answers or Unanswered Questions: Beliefs About Science
19 Guide Responses to Uncertainty in Climate Change Risk Communication. *Risk Anal.* 32, 992–1002.
20 doi:10.1111/j.1539-6924.2012.01771.x.
- 21 Raghavan, S. V., Hur, J., and Liong, S. Y. (2018a). Evaluations of NASA NEX-GDDP data over Southeast Asia:
22 present and future climates. *Clim. Change* 148, 503–518. doi:10.1007/s10584-018-2213-3.
- 23 Raghavan, S. V., Vu, M. T., and Liong, S. Y. (2016). Regional climate simulations over Vietnam using the WRF
24 model. *Theor. Appl. Climatol.* 126, 161–182. doi:10.1007/s00704-015-1557-0.
- 25 Raghavan, S. V., Liu, J., Nguyen, N. S., Vu, M. T., and Liong, S.-Y. (2018b). Assessment of CMIP5 historical
26 simulations of rainfall over Southeast Asia. *Theor. Appl. Climatol.* 132, 989–1002. doi:10.1007/s00704-017-
27 2111-z.
- 28 Rahmawati, N., and Lubczynski, M. W. (2018). Validation of satellite daily rainfall estimates in complex terrain of Bali
29 Island, Indonesia. *Theor. Appl. Climatol.* 134, 513–532. doi:10.1007/s00704-017-2290-7.
- 30 Rajbhandari, R., Shrestha, A. B., Kulkarni, A., Patwardhan, S. K., and Bajracharya, S. R. (2015). Projected changes in
31 climate over the Indus river basin using a high resolution regional climate model (PRECIS). 339–357.
32 doi:10.1007/s00382-014-2183-8.
- 33 Rajczak, J., and Schär, C. (2017). Projections of Future Precipitation Extremes Over Europe: A Multimodel Assessment
34 of Climate Simulations. *J. Geophys. Res. Atmos.* 122, 10,773–10,800. doi:10.1002/2017JD027176.
- 35 Rajeevan, M., Bhatte, J., and Jaswal, A. K. (2008). Analysis of variability and trends of extreme rainfall events over
36 India using 104 years of gridded daily rainfall data. *Geophys. Res. Lett.* 35. doi:10.1029/2008GL035143.
- 37 Ramarao, M. V. S., Krishnan, R., Sanjay, J., and Sabin, T. P. (2015). Understanding land surface response to changing
38 South Asian monsoon in a warming climate. 943–977. doi:10.5194/esdd-6-943-2015.
- 39 Ramarao, M. V. S., Sanjay, J., Krishnan, R., Mujumdar, M., Bazaz, A., and Revi, A. (2018). On observed aridity
40 changes over the semiarid regions of India in a warming climate. *Theor. Appl. Climatol.*, 1–10.
41 doi:10.1007/s00704-018-2513-6.
- 42 Rao, V. B., Franchito, S. H., Santo, C. M. E., and Gan, M. A. (2016). An update on the rainfall characteristics of Brazil:
43 seasonal variations and trends in 1979–2011. *Int. J. Climatol.* 36, 291–302. doi:10.1002/joc.4345.
- 44 Ratna, S., Ratnam, J., Behera, S., Tangang, F., and Yamagata, T. (2017). Validation of the WRF regional climate model
45 over the subregions of Southeast Asia: climatology and interannual variability. *Clim. Res.* 71, 263–280.
46 doi:10.3354/cr01445.
- 47 Ratnam, J. V., Behera, S. K., Ratna, S. B., Rajeevan, M., and Yamagata, T. (2016). Anatomy of Indian heatwaves. *Sci.*
48 *Rep.* 6, 24395. Available at: <https://doi.org/10.1038/srep24395>.
- 49 Rauthe, M., Steiner, H., Riediger, U., Mazurkiewicz, A., and Gratzki, A. (2013). A Central European precipitation
50 climatology – Part I: Generation and validation of a high-resolution gridded daily data set (HYRAS). *Meteorol.*
51 *Zeitschrift* 22, 235–256. doi:10.1127/0941-2948/2013/0436.
- 52 Reboita, M., Dutra, L., and Dias, C. (2016). Diurnal cycle of precipitation simulated by RegCM4 over South America:
53 present and future scenarios. *Clim. Res.* 70, 39–55. doi:10.3354/cr01416.
- 54 Reboita, M. S., da Rocha, R. P., de Souza, M. R., and Llopart, M. (2018). Extratropical cyclones over the southwestern
55 South Atlantic Ocean: HadGEM2-ES and RegCM4 projections. *Int. J. Climatol.* 38, 2866–2879.
56 doi:10.1002/joc.5468.
- 57 Reboita, M. S., da Rocha, R. P., Dias, C. G., and Ynoue, R. Y. (2014a). Climate Projections for South America:
58 RegCM3 Driven by HadCM3 and ECHAM5. *Adv. Meteorol.* 2014, 1–17. doi:10.1155/2014/376738.
- 59 Reboita, M. S., da Rocha, R. P., Dias, C. G., and Ynoue, R. Y. (2014b). Climate Projections for South America:
60 RegCM3 Driven by HadCM3 and ECHAM5. *Adv. Meteorol.* 2014, 1–17. doi:10.1155/2014/376738.
- 61 Rechid, D., Davin, E. L., de Noblet-Ducoudré, N., and Katragkou, E. The CORDEX Flagship Pilot Study LUCAS:

- 1 Impact of land use changes on climate in Europe across spatial and temporal scales. *prep.*
- 2 Retchless, D. P., and Brewer, C. A. (2016). Guidance for representing uncertainty on global temperature change maps.
- 3 *Int. J. Climatol.* 36, 1143–1159. doi:10.1002/joc.4408.
- 4 Ribes, A., Thao, S., Vautard, R., Dubuisson, B., Somot, S., Colin, J., et al. (2019). Observed increase in extreme daily
- 5 rainfall in the French Mediterranean. *Clim. Dyn.* 52, 1095–1114. doi:10.1007/s00382-018-4179-2.
- 6 Richard, Y., Fauchereau, N., Pocard, I., Rouault, M., and Trzaska, S. (2001). 20th century droughts in southern Africa:
- 7 Spatial and temporal variability, teleconnections with oceanic and atmospheric conditions. *Int. J. Climatol.* 21,
- 8 873–885. doi:10.1002/joc.656.
- 9 Rohini, P., Rajeevan, M., and Srivastava, A. K. (2016). On the Variability and Increasing Trends of Heat Waves over
- 10 India. *Sci. Rep.* 6, 26153. Available at: <https://doi.org/10.1038/srep26153>.
- 11 Roxy, M. K., Ritika, K., Terray, P., Murtugudde, R., Ashok, K., and Goswami, B. N. (2015). Drying of Indian
- 12 subcontinent by rapid Indian Ocean warming and a weakening land-sea thermal gradient. *Nat. Commun.* 6, 7423.
- 13 Available at: <https://doi.org/10.1038/ncomms8423>.
- 14 Rupa Kumar, K., Sahai, A. K., Krishna Kumar, K., Patwardhan, S. K., Mishra, P. K., Revadekar, J. V., et al. (2006).
- 15 High-resolution climate change scenarios for India for the 21st century. *Curr. Sci.* 90, 334–345.
- 16 doi:10.1029/2002JD002670.
- 17 Ruscica, R. C., Menéndez, C. G., and Sörensson, A. A. (2016a). Land surface-atmosphere interaction in future South
- 18 American climate using a multi-model ensemble. *Atmos. Sci. Lett.* 17, 141–147. doi:10.1002/asl.635.
- 19 Ruscica, R. C., Menéndez, C. G., and Sörensson, A. A. (2016b). Land surface-atmosphere interaction in future South
- 20 American climate using a multi-model ensemble. *Atmos. Sci. Lett.* 17, 141–147. doi:10.1002/asl.635.
- 21 Rusticucci, M., Kyselý, J., Almeida, G., and Lhotka, O. (2016). Long-term variability of heat waves in Argentina and
- 22 recurrence probability of the severe 2008 heat wave in Buenos Aires. *Theor. Appl. Climatol.* 124, 679–689.
- 23 doi:10.1007/s00704-015-1445-7.
- 24 Rutgersson, A., Jaagus, J., Schenk, F., Stendel, M., Barring, L., Briede, A., et al. (2015). “Recent Change—
- 25 Atmosphere,” in (Springer, Cham), 69–97. doi:10.1007/978-3-319-16006-1_4.
- 26 Ruti, P. M., Somot, S., Giorgi, F., Dubois, C., Flaounas, E., Obermann, A., et al. (2016a). Med-CORDEX initiative for
- 27 Mediterranean climate studies. *Bull. Am. Meteorol. Soc.* 97. doi:10.1175/BAMS-D-14-00176.1.
- 28 Ruti, P. M., Somot, S., Giorgi, F., Dubois, C., Flaounas, E., Obermann, A., et al. (2016b). Med-CORDEX Initiative for
- 29 Mediterranean Climate Studies. *Bull. Am. Meteorol. Soc.* 97, 1187–1208. doi:10.1175/BAMS-D-14-00176.1.
- 30 Sa’adi, Z., Shahid, S., Ismail, T., Chung, E.-S., and Wang, X.-J. (2017). Trends analysis of rainfall and rainfall extremes
- 31 in Sarawak, Malaysia using modified Mann–Kendall test. *Meteorol. Atmos. Phys.*, 1–15. doi:10.1007/s00703-
- 32 017-0564-3.
- 33 Sabin, R. K. T. P., and Mujumdar, R. V. M. (2016). Deciphering the desiccation trend of the South Asian monsoon
- 34 hydroclimate in a warming world. *Clim. Dyn.* 47, 1007–1027. doi:10.1007/s00382-015-2886-5.
- 35 Saeed, F., Almazroui, M., Islam, N., and Khan, M. S. (2017). Intensification of future heat waves in Pakistan: a study
- 36 using CORDEX regional climate models ensemble. *Nat. Hazards* 87, 1635–1647. doi:10.1007/s11069-017-2837-
- 37 z.
- 38 Saeed, F., and Athar, H. (2018). Assessment of simulated and projected climate change in Pakistan using IPCC AR4-
- 39 based AOGCMs. 967–980.
- 40 Salio, P., Hobouchian, M. P., García Skabar, Y., and Vila, D. (2015). Evaluation of high-resolution satellite
- 41 precipitation estimates over southern South America using a dense rain gauge network. *Atmos. Res.*
- 42 doi:10.1016/j.atmosres.2014.11.017.
- 43 Salman, S. A., Shahid, S., Ismail, T., Ahmed, K., and Wang, X.-J. (2018). Selection of climate models for projection of
- 44 spatiotemporal changes in temperature of Iraq with uncertainties. *Atmos. Res.* 213, 509–522.
- 45 doi:10.1016/J.ATMOSRES.2018.07.008.
- 46 SAMUELSSON, P., JONES, C. G., WILLÉN, U., ULLERSTIG, A., GOLLVIK, S., HANSSON, U. L. F., et al. (2011).
- 47 The Rossby Centre Regional Climate model RCA3: model description and performance. *Tellus A* 63, 4–23.
- 48 doi:10.1111/j.1600-0870.2010.00478.x.
- 49 Sanchez-Gomez, E., and Somot, S. (2018). Impact of the internal variability on the cyclone tracks simulated by a
- 50 regional climate model over the Med-CORDEX domain. *Clim. Dyn.* 51. doi:10.1007/s00382-016-3394-y.
- 51 Sanchez-Lorenzo, A., Wild, M., Brunetti, M., Guijarro, J. A., Hakuba, M. Z., Calbó, J., et al. (2015). Reassessment and
- 52 update of long-term trends in downward surface shortwave radiation over Europe (1939–2012). *J. Geophys. Res.*
- 53 *Atmos.* 120, 9555–9569. doi:10.1002/2015JD023321.
- 54 Sánchez, E., Rodríguez-Fonseca, B., Bladé, I., Brunet, M., Aznar, R., Cacho, I., et al. (2017). Progress in Detection and
- 55 Projection of Climate Change in Spain since the 2010 CLIVAR-Spain regional climate change assessment report.
- 56 *CLIVAR Exch.*
- 57 Sánchez, E., Solman, S., Remedio, A. R. C., Berbery, H., Samuelsson, P., Da Rocha, R. P., et al. (2015a). Regional
- 58 climate modelling in CLARIS-LPB: a concerted approach towards twentyfirst century projections of regional
- 59 temperature and precipitation over South America. *Clim. Dyn.* 45, 2193–2212. doi:10.1007/s00382-014-2466-0.
- 60 Sánchez, E., Solman, S., Remedio, A. R. C., Berbery, H., Samuelsson, P., Da Rocha, R. P., et al. (2015b). Regional
- 61 climate modelling in CLARIS-LPB: a concerted approach towards twentyfirst century projections of regional

- 1 temperature and precipitation over South America. *Clim. Dyn.* 45, 2193–2212. doi:10.1007/s00382-014-2466-0.
- 2 Sanjay, J., Krishnan, R., Shrestha, A. B., Rajbhandari, R., and Ren, G.-Y. (2017a). Downscaled climate change
3 projections for the Hindu Kush Himalayan region using CORDEX South Asia regional climate models. *Adv.*
4 *Clim. Chang. Res.* 8, 185–198. doi:10.1016/J.ACCRE.2017.08.003.
- 5 Sanjay, J., Krishnan, R., Shrestha, A. B., Rajbhandari, R., and Ren, G. Y. (2017b). Downscaled climate change
6 projections for the Hindu Kush Himalayan region using CORDEX South Asia regional climate models. *Adv.*
7 *Clim. Chang. Res.* 8, 185–198. doi:10.1016/j.accre.2017.08.003.
- 8 Sarthi, P. P., Ghosh, S., and Kumar, P. (2015). Possible future projection of Indian Summer Monsoon Rainfall (ISMR)
9 with the evaluation of model performance in Coupled Model Inter-comparison Project Phase 5 (CMIP5). *Glob.*
10 *Planet. Change* 129, 92–106. doi:10.1016/j.gloplacha.2015.03.005.
- 11 Satgé, F., Ruelland, D., Bonnet, M.-P., Molina, J., and Pillco, R. (2019). Consistency of satellite-based precipitation
12 products in space and over time compared with gauge observations and snow- hydrological modelling in the Lake
13 Titicaca region. *Hydrol. Earth Syst. Sci.* 23, 595–619. doi:10.5194/hess-23-595-2019.
- 14 Satyamurty, P., Mattos, L. F., Nobre, C. A., and Silva Dias, P. L. (1998). “Tropics - South America,” in *Meteorology of*
15 *the Southern Hemisphere*, eds. D. J. Kauly and D. G. Vincent (Boston: Meteorological Monograph. American
16 Meteorological Society), 119–139.
- 17 Saurral, R. I., Camilloni, I. A., and Barros, V. R. (2017). Low-frequency variability and trends in centennial
18 precipitation stations in southern South America. *Int. J. Climatol.* 37, 1774–1793. doi:10.1002/joc.4810.
- 19 Schaller, N., Kay, A. L., Lamb, R., Massey, N. R., van Oldenborgh, G. J., Otto, F. E. L., et al. (2016). Human influence
20 on climate in the 2014 southern England winter floods and their impacts. *Nat. Clim. Chang.* 6, 627–634.
21 doi:10.1038/nclimate2927.
- 22 Scherrer, S. C., Fischer, E. M., Posselt, R., Liniger, M. A., Croci-Maspoli, M., and Knutti, R. (2016). Emerging trends
23 in heavy precipitation and hot temperature extremes in Switzerland. *J. Geophys. Res. Atmos.* 121, 2626–2637.
24 doi:10.1002/2015JD024634.
- 25 Schiermeier, Q. (2018). Droughts, heatwaves and floods: How to tell when climate change is to blame. *Nature* 560, 20–
26 22. doi:10.1038/d41586-018-05849-9.
- 27 Schleussner, C.-F., Lissner, T. K., Fischer, E. M., Wohland, J., Perrette, M., Golly, A., et al. (2016). Differential climate
28 impacts for policy-relevant limits to global warming: the case of 1.5 °C and 2 °C.
29 *Earth Syst. Dyn.* 7, 327–351. doi:10.5194/esd-7-327-2016.
- 30 Schlosser, E., Manning, K. W., Powers, J. G., Duda, M. G., Birnbaum, G., and Fujita, K. (2010). Characteristics of
31 high-precipitation events in Dronning Maud Land, Antarctica. *J. Geophys. Res.* 115, D14107.
32 doi:10.1029/2009JD013410.
- 33 Schlosser, E., Stenni, B., Valt, M., Cagnati, A., Powers, J. G., Manning, K. W., et al. (2016). Precipitation and synoptic
34 regime in two extreme years 2009 and 2010 at Dome C, Antarctica – implications for ice core interpretation.
35 *Atmos. Chem. Phys.* 16, 4757–4770. doi:10.5194/acp-16-4757-2016.
- 36 Schwartz, S. H. (1992). Universals in the Content and Structure of Values: Theoretical Advances and Empirical Tests in
37 20 Countries. *Adv. Exp. Soc. Psychol.* 25, 1–65. doi:10.1016/S0065-2601(08)60281-6.
- 38 Schwartz, S. H., Cieciuch, J., Vecchione, M., Davidov, E., Fischer, R., Beierlein, C., et al. (2012). Refining the theory
39 of basic individual values. *J. Pers. Soc. Psychol.* 103, 663–688. doi:10.1037/a0029393.
- 40 Scian, B., and Pierini, J. (2013). Variability and trends of extreme dry and wet seasonal precipitation in Argentina. A
41 retrospective analysis. *Atmósfera* 26, 3–26. doi:10.1016/S0187-6236(13)71059-2.
- 42 Scott, R. C., Nicolas, J. P., Bromwich, D. H., Norris, J. R., Lubin, D., Scott, R. C., et al. (2019). Meteorological Drivers
43 and Large-Scale Climate Forcing of West Antarctic Surface Melt. *J. Clim.* 32, 665–684. doi:10.1175/JCLI-D-18-
44 0233.1.
- 45 Screen, J. A., and Simmonds, I. (2010). Increasing fall-winter energy loss from the Arctic Ocean and its role in Arctic
46 temperature amplification. *Geophys. Res. Lett.* doi:10.1029/2010GL044136.
- 47 Sein, D. V., Mikolajewicz, U., Gröger, M., Fast, I., Cabos, W., Pinto, J. G., et al. (2015). Regionally coupled
48 atmosphere-ocean- sea ice-marine biogeochemistry model ROM: 1. Description and validation. *J. Adv. Model.*
49 *Earth Syst.* doi:https://doi.org/10.1002/2014MS000357.
- 50 Šeparović, L., Alexandru, A., Laprise, R., Martynov, A., Sushama, L., Winger, K., et al. (2013). Present climate and
51 climate change over North America as simulated by the fifth-generation Canadian regional climate model. *Clim.*
52 *Dyn.* 41, 3167–3201. doi:10.1007/s00382-013-1737-5.
- 53 Serreze, M. C., Walsh, J. E., Cja[om III, F. S., Osterkamp, T., Dyurgerov, M., Romanovsky, V., et al. (2000).
54 Observational evidence of recent change in the northern-high-latitude environment. *Clim. Chang.*
55 doi:10.1126/science.1155121.
- 56 Sevault, F., Somot, S., Alias, A., Dubois, C., Lebeaupin-Brossier, C., Nabat, P., et al. (2014). A fully coupled
57 Mediterranean regional climate system model: design and evaluation of the ocean component for the 1980–2012
58 period. *Tellus A Dyn. Meteorol. Oceanogr.* 66, 23967. doi:10.3402/tellusa.v66.23967.
- 59 Sharma, D., and Babel, M. S. (2014). Trends in extreme rainfall and temperature indices in the western Thailand. *Int. J.*
60 *Climatol.* 34, 2393–2407. doi:10.1002/joc.3846.
- 61 Sharma, E., Molden, D., Rahman, A., Khatiwada, Y. R., Zhang, L., Singh, S. P., et al. (2019). “Introduction to the
Do Not Cite, Quote or Distribute Atlas-151 Total pages: 242

- 1 Hindu Kush Himalaya Assessment,” in *The Hindu Kush Himalaya Assessment* (Cham: Springer International
2 Publishing), 1–16. doi:10.1007/978-3-319-92288-1_1.
- 3 Sharmila, S., Joseph, S., Sahai, A. K., Abhilash, S., and Chattopadhyay, R. (2015). Future projection of Indian summer
4 monsoon variability under climate change scenario : An assessment from CMIP5 climate models. *Glob. Planet.
5 Change* 124, 62–78. doi:10.1016/j.gloplacha.2014.11.004.
- 6 Shepherd, T. G., Boyd, E., Calel, R. A., Chapman, S. C., Dessai, S., Dima-West, I. M., et al. (2018). Storylines: an
7 alternative approach to representing uncertainty in physical aspects of climate change. *Clim. Change* 151, 555–
8 571. doi:10.1007/s10584-018-2317-9.
- 9 Shongwe, M. E., Lennard, C., Liebmann, B., Kalognomou, E.-A., Ntsangwane, L., Pinto, I., et al. (2015). An evaluation
10 of CORDEX regional climate models in simulating precipitation over Southern Africa. *Atmos. Sci. Lett.*
11 doi:10.1002/asl2.538.
- 12 Siew, J. H., Tangang, F. T., and Juneng, L. (2013). Evaluation of CMIP5 coupled atmosphere-ocean general circulation
13 models and projection of the Southeast Asian winter monsoon in the 21st century. *Int. J. Climatol.* 34, n/a-n/a.
14 doi:10.1002/joc.3880.
- 15 Sillmann, J., Kharin, V. V., Zhang, X., Zwiers, F. W., and Bronaugh, D. (2013a). Climate extremes indices in the
16 CMIP5 multimodel ensemble: Part 1. Model evaluation in the present climate. *J. Geophys. Res. Atmos.* 118,
17 1716–1733. doi:10.1002/jgrd.50203.
- 18 Sillmann, J., Kharin, V. V., Zwiers, F. W., Zhang, X., and Bronaugh, D. (2013b). Climate extremes indices in the
19 CMIP5 multimodel ensemble: Part 2. Future climate projections. *J. Geophys. Res. Atmos.* 118, 2473–2493.
20 doi:10.1002/jgrd.50188.
- 21 Silva, W. L., Dereczynski, C., Chou, S. C., and Cavalcanti, I. (2014). Future Changes in Temperature and Precipitation
22 Extremes in the State of Rio de Janeiro (Brazil). *Am. J. Clim. Chang.* 03, 353–365. doi:10.4236/ajcc.2014.34031.
- 23 Singh Swati A4 - Ghosh, Subimal A4 - Sahana, A. S. A4 - Vittal, H. A4 - Karmakar, Subhankar, S. A.-S. (2017). Do
24 dynamic regional models add value to the global model projections of Indian monsoon? *Clim. Dyn.* v. 48, 1375-
25 1397–2017 v.48 nos.3–4. doi:10.1007/s00382-016-3147-y.
- 26 Singh, D., Tsiang, M., Rajaratnam, B., and Diffenbaugh, N. S. (2014). Observed changes in extreme wet and dry spells
27 during the South Asian summer monsoon season. *Nat. Clim. Chang.* 4, 456. Available at:
28 <https://doi.org/10.1038/nclimate2208>.
- 29 Siswanto, S., van Oldenborgh, G. J., van der Schrier, G., Jilderda, R., and van den Hurk, B. (2016). Temperature,
30 extreme precipitation, and diurnal rainfall changes in the urbanized Jakarta city during the past 130 years. *Int. J.
31 Climatol.* 36, 3207–3225. doi:10.1002/joc.4548.
- 32 Skansi, M. de los M., Brunet, M., Sigró, J., Aguilar, E., Arevalo Groening, J. A., Bentancur, O. J., et al. (2013).
33 Warming and wetting signals emerging from analysis of changes in climate extreme indices over South America.
34 *Glob. Planet. Change* 100, 295–307. doi:10.1016/j.gloplacha.2012.11.004.
- 35 Slingo, J., and Palmer, T. (2011). Uncertainty in weather and climate prediction. *Philos. Trans. R. Soc. A Math. Phys.*
36 *Eng. Sci.* 369, 4751–4767. doi:10.1098/rsta.2011.0161.
- 37 Slovic, P., Finucane, M. L., Peters, E., and MacGregor, D. G. (2004). Risk as Analysis and Risk as Feelings: Some
38 Thoughts about Affect, Reason, Risk, and Rationality. *Risk Anal.* 24, 311–322. doi:10.1111/j.0272-
39 4332.2004.00433.x.
- 40 Small, R. J. O., de Szoeko, S. P., and Xie, S.-P. (2007). The Central American Midsummer Drought: Regional Aspects
41 and Large-Scale Forcing. *J. Clim.* 20, 4853–4873. doi:10.1175/JCLI4261.1.
- 42 Soares, P. M. M., and Cardoso, R. M. (2018). A simple method to assess the added value using high-resolution climate
43 distributions: application to the EURO-CORDEX daily precipitation. *Int. J. Climatol.* 38, 1484–1498.
44 doi:10.1002/joc.5261.
- 45 Solman, S. (2016). Systematic temperature and precipitation biases in the CLARIS-LPB ensemble simulations over
46 South America and possible implications for climate projections. *Clim. Res.* 68, 117–136. doi:10.3354/cr01362.
- 47 Solman, S. A. (2013a). Regional Climate Modeling over South America: A Review. *Adv. Meteorol.* 2013, 1–13.
48 doi:10.1155/2013/504357.
- 49 Solman, S. A. (2013b). Regional Climate Modeling over South America: A Review. *Adv. Meteorol.* 2013, 1–13.
50 doi:10.1155/2013/504357.
- 51 Solman, S. A., Nuñez, M. N., and Cabré, M. F. (2008). Regional climate change experiments over southern South
52 America. I: present climate. *Clim. Dyn.* 30, 533–552. doi:10.1007/s00382-007-0304-3.
- 53 Solman, S. A., Sanchez, E., Samuelsson, P., da Rocha, R. P., Li, L., Marengo, J., et al. (2013). Evaluation of an
54 ensemble of regional climate model simulations over South America driven by the ERA-Interim reanalysis:
55 model performance and uncertainties. *Clim. Dyn.* 41, 1139–1157. doi:10.1007/s00382-013-1667-2.
- 56 Somot, S., Houpert, L., Sevault, F., Testor, P., Bosse, A., Taupier-Letage, I., et al. (2018a). Characterizing, modelling
57 and understanding the climate variability of the deep water formation in the North-Western Mediterranean Sea.
58 *Clim. Dyn.* 51, 1179–1210. doi:10.1007/s00382-016-3295-0.
- 59 Somot, S., Houpert, L., Sevault, F., Testor, P., Bosse, A., Taupier-Letage, I., et al. (2018b). Characterizing, modelling
60 and understanding the climate variability of the deep water formation in the North-Western Mediterranean Sea.
61 *Clim. Dyn.* 51, 1179–1210.

- 1 Sonali, P., and RS, N. (2018). Detection and attribution of climate change signals in South India maximum and
2 minimum temperatures . *Clim. Res.* 76, 145–160. Available at: [https://www.int-res.com/abstracts/cr/v76/n2/p145-](https://www.int-res.com/abstracts/cr/v76/n2/p145-160/)
3 160/.
- 4 Soraisam, B., Karumuri, A., and D.S., P. (2018). Uncertainties in observations and climate projections for the North
5 East India. *Glob. Planet. Change* 160, 96–108. doi:10.1016/j.gloplacha.2017.11.010.
- 6 Sörensson, A. A., and Ruscica, R. C. (2018). Intercomparison and Uncertainty Assessment of Nine Evapotranspiration
7 Estimates Over South America. *Water Resour. Res.* 54, 2891–2908. doi:10.1002/2017WR021682.
- 8 Sørland, S. L., Schär, C., Lüthi, D., and Kjellström, E. (2018). Bias patterns and climate change signals in GCM-RCM
9 model chains. *Environ. Res. Lett.* 13, 074017. doi:10.1088/1748-9326/aacc77.
- 10 Souverijns, N., Gossart, A., Gorodetskaya, I. V., Lhermitte, S., Mangold, A., Laffineur, Q., et al. (2018). How does the
11 ice sheet surface mass balance relate to snowfall? Insights from a ground-based precipitation radar in East
12 Antarctica. *Cryosph.* 12, 1987–2003. doi:10.5194/tc-12-1987-2018.
- 13 Sparrow, S., Su, Q., Tian, F., Li, S., Chen, Y., Chen, W., et al. (2018). Attributing human influence on the July 2017
14 Chinese heatwave: The influence of sea-surface temperatures. *Environ. Res. Lett.* 13. doi:10.1088/1748-
15 9326/aae356.
- 16 Spence, A., Poortinga, W., and Pidgeon, N. (2012). The Psychological Distance of Climate Change. *Risk Anal.* 32, 957–
17 972. doi:10.1111/j.1539-6924.2011.01695.x.
- 18 Sperber, K. R., Annamalai, H., Kang, I. S., Kitoh, A., Moise, A., Turner, A., et al. (2013). The Asian summer monsoon:
19 An intercomparison of CMIP5 vs. CMIP3 simulations of the late 20th century. *Clim. Dyn.* 41, 2711–2744.
20 doi:10.1007/s00382-012-1607-6.
- 21 Spielhagen, R. F., Werner, K., Sørensen, S. A., Zamelczyk, K., Kandiano, E., Budeus, G., et al. (2011). Enhanced
22 modern heat transfer to the arctic by warm atlantic water. *Science (80-)*. doi:10.1126/science.1197397.
- 23 Srivastava, A. K., and Delsole, T. (2014). Robust forced response in South Asian summer monsoon in a future climate.
24 *J. Clim.* 27, 7849–7860. doi:10.1175/JCLI-D-13-00599.1.
- 25 Stennett-Brown, R., Jones, J. J., Stephenson, T., and Taylor, M. (2017). Future Caribbean temperature and rainfall
26 extremes from statistical downscaling: STATISTICAL DOWNSCALING OF CARIBBEAN TEMPERATURE
27 AND RAINFALL. *Int. J. Climatol.* 37. doi:10.1002/joc.5126.
- 28 Stephenson, T. S., Vincent, L. A., Allen, T., Van Meerbeeck, C. J., McLean, N., Peterson, T. C., et al. (2014). Changes
29 in extreme temperature and precipitation in the Caribbean region, 1961–2010. *Int. J. Climatol.* 34, 2957–2971.
30 doi:10.1002/joc.3889.
- 31 Steptoe, H., Jones, S. E. O., and Fox, H. (2018). Correlations Between Extreme Atmospheric Hazards and Global
32 Teleconnections: Implications for Multihazard Resilience. *Rev. Geophys.* 56, 50–78.
33 doi:10.1002/2017RG000567.
- 34 Stott, P. (2016). How climate change affects extreme weather events. *Science (80-)*. 352, 1517–1518.
35 doi:10.1126/science.aaf7271.
- 36 Stroeve, J., Holland, M. M., Meier, W., Scambos, T., and Serreze, M. (2007). Arctic sea ice decline: Faster than
37 forecast. *Geophys. Res. Lett.* doi:10.1029/2007GL029703.
- 38 Sudeepkumar, B. L., Babu, C. A., and Varikoden, H. (2018). Future projections of active-break spells of Indian summer
39 monsoon in a climate change perspective. *Glob. Planet. Change* 161, 222–230.
40 doi:10.1016/j.gloplacha.2017.12.020.
- 41 Sun, L., Deser, C., and Tomas, R. A. (2015). Mechanisms of Stratospheric and Tropospheric Circulation Response to
42 Projected Arctic Sea Ice Loss. *J. Clim.* 28, 7824–7845. doi:10.1175/JCLI-D-15-0169.1.
- 43 Sun, Q., Miao, C., Duan, Q., Ashouri, H., Sorooshian, S., and Hsu, K. L. (2018). A Review of Global Precipitation Data
44 Sets: Data Sources, Estimation, and Intercomparisons. *Rev. Geophys.* doi:10.1002/2017RG000574.
- 45 Supari, Tangang, F., Juneng, L., and Aldrian, E. (2017). Observed changes in extreme temperature and precipitation
46 over Indonesia. *Int. J. Climatol.* 37, 1979–1997. doi:10.1002/joc.4829.
- 47 Suryachandra, C. T. S., and Dhakate, A. R. A. R. (2015). Why ensemble mean projection of south Asian monsoon
48 rainfall by CMIP5 models is not reliable? *Clim. Dyn.*, 161–174. doi:10.1007/s00382-014-2269-3.
- 49 Syafrina, A. H., Zalina, M. D., and Juneng, L. (2015). Historical trend of hourly extreme rainfall in Peninsular
50 Malaysia. *Theor. Appl. Climatol.* 120, 259–285. doi:10.1007/s00704-014-1145-8.
- 51 Syed, F. S., Iqbal, W., Syed, A. A. B., and Rasul, G. (2014a). Uncertainties in the regional climate models simulations
52 of South-Asian summer monsoon and climate change. *Clim. Dyn.* 42, 2079–2097. doi:10.1007/s00382-013-1963-
53 x.
- 54 Syed, F. S., Iqbal, W., Syed, A. A. B., and Rasul, G. (2014b). Uncertainties in the regional climate models simulations
55 of South-Asian summer monsoon and climate change. *Clim. Dyn.* 42, 2079–2097. doi:10.1007/s00382-013-1963-
56 x.
- 57 Sylla, M. B., Giorgi, F., Coppola, E., and Mariotti, L. (2013). Uncertainties in daily rainfall over Africa: Assessment of
58 gridded observation products and evaluation of a regional climate model simulation. *Int. J. Climatol.* 33, 1805–
59 1817. doi:10.1002/joc.3551.
- 60 Sylla, M. B., Nikiema, P. M., Gibba, P., Kebe, I., and Klutse, N. A. B. (2016). *Climate change over West Africa: Recent*
61 *trends and future projections*. doi:10.1007/978-3-319-31499-0_3.

- 1 Sylla, M. B., Pal, J. S., Faye, A., Dimobe, K., and Kunstmann, H. (2018). Climate change to severely impact West
2 African basin scale irrigation in 2 °C and 1.5 °C global warming scenarios. *Sci. Rep.* doi:10.1038/s41598-018-
3 32736-0.
- 4 Tabary, P., Dupuy, P., Gueguen, C., Moulin, L., Laurantin, O., Merlier, C., et al. (2011). A 10-year (1997-2006)
5 reanalysis of Quantitative Precipitation Estimation over France: methodology and first results. IAHS Publ
6 Available at: <http://web13.extendcp.co.uk/iahs.info/uploads/dms/15900.351> Abstracts 53.pdf [Accessed March
7 22, 2019].
- 8 Takayabu, I., Hibino, K., Sasaki, H., Shiogama, H., Mori, N., Shibutani, Y., et al. (2015). Erratum: Climate change
9 effects on the worst-case storm surge: A case study of Typhoon Haiyan (Environmental Research Letters (2015)
10 10 (064011)). *Environ. Res. Lett.* doi:10.1088/1748-9326/10/8/089502.
- 11 Tan, J., Jakob, C., Rossow, W. B., and Tselioudis, G. (2015). Increases in tropical rainfall driven by changes in
12 frequency of organized deep convection. *Nature* 519, 451–454. doi:10.1038/nature14339.
- 13 Tangang, F., Santisirisomboon, J., Juneng, L., Salimun, E., Chung, J., Supari, et al. Projected future changes in mean
14 precipitation over Thailand based on multi-model regional climate simulations of CORDEX Southeast Asia. *Int.*
15 *J. Climatol.*
- 16 Tangang, F., Supari, S., Chung, J. X., Cruz, F., Salimun, E., Ngai, S. T., et al. (2018). Future changes in annual
17 precipitation extremes over Southeast Asia under global warming of 2°C. *APN Sci. Bull.* 8.
18 doi:10.30852/sb.2018.436.
- 19 Taylor, A. L., Dessai, S., and de Bruin, W. B. (2015). Communicating uncertainty in seasonal and interannual climate
20 forecasts in Europe. *Philos. Trans. R. Soc. A Math. Phys. Eng. Sci.* 373, 20140454. doi:10.1098/rsta.2014.0454.
- 21 Taylor, C. M., Belusic, D., Guichard, F., Parker, D. J., Vischel, T., Bock, O., et al. (2017). Frequency of extreme
22 Sahelian storms tripled since 1982 in satellite observations. *Nature*. doi:10.1038/nature22069.
- 23 Taylor, M. A., and Alfaro, E. J. (2005). “Central America and the Caribbean, Climate of.” in *Encyclopedia of World*
24 *Climatology*, ed. J. E. Oliver (Dordrecht: Springer Netherlands), 183–189. doi:10.1007/1-4020-3266-8_37.
- 25 Taylor, M. A., Centella, A., Charlery, J., Bezanilla, A., Campbell, J., Borrajerro, I., et al. (2013a). The Precip Caribbean
26 Story: Lessons and Legacies. *Bull. Am. Meteorol. Soc.* 94, 1065–1073. doi:10.1175/BAMS-D-11-00235.1.
- 27 Taylor, M. A., Clarke, L. A., Centella, A., Bezanilla, A., Stephenson, T. S., Jones, J. J., et al. (2018). Future Caribbean
28 Climates in a World of Rising Temperatures: The 1.5 vs 2.0 Dilemma. *J. Clim.* 31, 2907–2926.
29 doi:10.1175/JCLI-D-17-0074.1.
- 30 Taylor, M., Whyte, F., Stephenson, T., and Campbell, J. (2013b). Why dry? Investigating the future evolution of the
31 Caribbean Low Level Jet to explain projected Caribbean drying. *Int. J. Climatol.* 33, 784–792.
32 doi:10.1002/joc.3461.
- 33 Teichmann, C., Bülow, K., Otto, J., Pfeifer, S., Rechid, D., Sieck, K., et al. (2018). Avoiding Extremes: Benefits of
34 Staying below +1.5 °C Compared to +2.0 °C and +3.0 °C Global Warming. *Atmosphere (Basel)*. 9, 115.
35 doi:10.3390/atmos9040115.
- 36 Temmerman, M., Moernaut, R., Coesemans, R., and Mast, J. (2019). Post-truth and the political: Constructions and
37 distortions in representing political facts. *Discourse, Context Media* 27, 1–6. doi:10.1016/J.DCM.2018.10.002.
- 38 Terzago, S., von Hardenberg, J., Palazzi, E., and Provenzale, A. (2017). Snow water equivalent in the Alps as seen by
39 gridded data sets, CMIP5 and CORDEX climate models. *Cryosph.* 11, 1625–1645. doi:10.5194/tc-11-1625-2017.
- 40 Thirumalai, K., DiNezio, P. N., Okumura, Y., and Deser, C. (2017). Extreme temperatures in Southeast Asia caused by
41 El Niño and worsened by global warming. *Nat. Commun.* 8, 15531. doi:10.1038/ncomms15531.
- 42 Thomas, E. R., Hosking, J. S., Tuckwell, R. R., Warren, R. A., and Ludlow, E. C. (2015). Twentieth century increase in
43 snowfall in coastal West Antarctica. *Geophys. Res. Lett.* 42, 9387–9393. doi:10.1002/2015GL065750.
- 44 Thorne, P. W., Parker, D. E., Tett, S. F. B., Jones, P. D., McCarthy, M., Coleman, H., et al. (2005). Revisiting
45 radiosonde upper air temperatures from 1958 to 2002. *J. Geophys. Res.* 110, D18105.
46 doi:10.1029/2004JD005753.
- 47 Tian, T., Boberg, F., Bøssing Christensen, O., Hesselbjerg Christensen, J., She, J., and Vihma, T. (2013). Resolved
48 complex coastlines and land–sea contrasts in a high-resolution regional climate model: a comparative study using
49 prescribed and modelled SSTs. *Tellus A Dyn. Meteorol. Oceanogr.* 65, 19951. doi:10.3402/tellusa.v65i0.19951.
- 50 Tingley, M. P., and Huybers, P. (2013). Recent temperature extremes at high northern latitudes unprecedented in the
51 past 600 years. *Nature*. doi:10.1038/nature11969.
- 52 Torma, C. (2019). Evaluation of EURO-CORDEX and Med-CORDEX regional climate model ensembles over the
53 Carpathian Region using the high resolution gridded observational database: CARPATCLIM. *Idojárás*.
- 54 Torma, C., and Giorgi, F. (2019). On the evidence of orographical modulation of regional fine scale precipitation
55 change signals: The Carpathians. *Submitted*.
- 56 Torma, C., Giorgi, F., and Coppola, E. (2015). Added value of regional climate modeling over areas characterized by
57 complex terrain-Precipitation over the Alps. *J. Geophys. Res. Atmos.* 120, 3957–3972.
58 doi:10.1002/2014JD022781.
- 59 Torres, R. R., and Marengo, J. A. (2013). Uncertainty assessments of climate change projections over South America.
60 *Theor. Appl. Climatol.* 112, 253–272. doi:10.1007/s00704-012-0718-7.
- 61 Trambly, Y., and Somot, S. (2018). Future evolution of extreme precipitation in the Mediterranean. *Clim. Change* 151,
Do Not Cite, Quote or Distribute Atlas-154 Total pages: 242

- 1 289–302. doi:10.1007/s10584-018-2300-5.
- 2 Trenberth, K. E. (2012). Framing the way to relate climate extremes to climate change. *Clim. Change* 115, 283–290.
- 3 doi:10.1007/s10584-012-0441-5.
- 4 Trenberth, K. E., and Josey, S. A. (2007). Observations: surface and atmospheric climate change. *Changes* 164, 235–
- 5 336. doi:10.5194/cp-6-379-2010.
- 6 Trinh-Tuan, L., Matsumoto, J., Tangang, F. T., Juneng, L., Cruz, F., Narisma, G., et al. (2018). Application of Quantile
- 7 Mapping Bias Correction for Mid-future Precipitation Projections over Vietnam. *Sci. Online Lett. Atmos.* 15, 1–6.
- 8 doi:10.2151/sola.
- 9 Trusel, L. D., Frey, K. E., Das, S. B., Karnauskas, K. B., Kuipers Munneke, P., van Meijgaard, E., et al. (2015).
- 10 Divergent trajectories of Antarctic surface melt under two twenty-first-century climate scenarios. *Nat. Geosci.* 8,
- 11 927–932. doi:10.1038/ngeo2563.
- 12 Turner, J., Barrand, N. E., Bracegirdle, T. J., Convey, P., Hodgson, D. A., Jarvis, M., et al. (2014). Antarctic climate
- 13 change and the environment: an update. *Polar Rec. (Gr. Brit.)* 50, 237–259. doi:10.1017/S0032247413000296.
- 14 Turner, J., Colwell, S. R., Marshall, G. J., Lachlan-Cope, T. A., Carleton, A. M., Jones, P. D., et al. (2004). The SCAR
- 15 READER Project: Toward a High-Quality Database of Mean Antarctic Meteorological Observations. *J. Clim.* 17,
- 16 2890–2898. doi:10.1175/1520-0442(2004)017<2890:TSRPTA>2.0.CO;2.
- 17 Turner, J., Lu, H., White, I., King, J. C., Phillips, T., Hosking, J. S., et al. (2016). Absence of 21st century warming on
- 18 Antarctic Peninsula consistent with natural variability. *Nature* 535, 411. Available at:
- 19 <https://doi.org/10.1038/nature18645>.
- 20 Um, M. J., Kim, Y., and Kim, J. (2017). Evaluating historical drought characteristics simulated in CORDEX East Asia
- 21 against observations. *Int. J. Climatol.* 37, 4643–4655. doi:10.1002/joc.5112.
- 22 Vaittinada Ayar, P., Vrac, M., Bastin, S., Carreau, J., Déqué, M., and Gallardo, C. (2016). Intercomparison of statistical
- 23 and dynamical downscaling models under the EURO- and MED-CORDEX initiative framework: present climate
- 24 evaluations. *Clim. Dyn.* 46, 1301–1329. doi:10.1007/s00382-015-2647-5.
- 25 Valdés-Pineda, R., Valdés, J. B., Diaz, H. F., and Pizarro-Tapia, R. (2016). Analysis of spatio-temporal changes in
- 26 annual and seasonal precipitation variability in South America-Chile and related ocean–atmosphere circulation
- 27 patterns. *Int. J. Climatol.* doi:10.1002/joc.4532.
- 28 Valverde, M. C., and Marengo, J. A. (2014). Extreme Rainfall Indices in the Hydrographic Basins of Brazil. *Open J.*
- 29 *Mod. Hydrol.* 04, 10–26. doi:10.4236/ojmh.2014.41002.
- 30 van den Besselaar, E. J. M., van der Schrier, G., Cornes, R. C., Iqbal, A. S., Klein Tank, A. M. G., Besselaar, E. J. M.
- 31 van den, et al. (2017). SA-OBS: A Daily Gridded Surface Temperature and Precipitation Dataset for Southeast
- 32 Asia. *J. Clim.* 30, 5151–5165. doi:10.1175/JCLI-D-16-0575.1.
- 33 van den Hurk, B., Hewitt, C., Jacob, D., Bessembinder, J., Doblus-Reyes, F., and Döscher, R. (2018). The match
- 34 between climate services demands and Earth System Models supplies. *Clim. Serv.* 12, 59–63.
- 35 doi:10.1016/J.CLISER.2018.11.002.
- 36 van den Hurk, B., van Oldenborgh, G. J., Lenderink, G., Hazeleger, W., Haarsma, R., and de Vries, H. (2014). Drivers
- 37 of mean climate change around the Netherlands derived from CMIP5. *Clim. Dyn.* 42. doi:10.1007/s00382-013-
- 38 1707-y.
- 39 Van Khiem, M., Redmond, G., McSweeney, C., and Thuc, T. (2014). Evaluation of dynamically downscaled ensemble
- 40 climate simulations for Vietnam. *Int. J. Climatol.* 34, 2450–2463. doi:10.1002/joc.3851.
- 41 Van Pham, T., Brauch, J., Dieterich, C., Frueh, B., and Ahrens, B. (2014). New coupled atmosphere-ocean-ice system
- 42 COSMO-CLM/NEMO: assessing air temperature sensitivity over the North and Baltic Seas. *Oceanologia* 56,
- 43 167–189. doi:10.5697/OC.56-2.167.
- 44 Van Wessem, J. M., Reijmer, C. H., Morlighem, M., Mouginot, J., Rignot, E., Medley, B., et al. (2014). Improved
- 45 representation of East Antarctic surface mass balance in a regional atmospheric climate model. *J. Glaciol.* 60,
- 46 761–770. doi:10.3189/2014JoG14J051.
- 47 Vautard, R., Cattiaux, J., Yiou, P., Thépaut, J. N., and Ciais, P. (2010). Northern Hemisphere atmospheric stalling partly
- 48 attributed to an increase in surface roughness. *Nat. Geosci.* 3, 756–761. doi:10.1038/ngeo979.
- 49 Vautard, R., Gobiet, A., Jacob, D., Belda, M., Colette, A., Déqué, M., et al. (2013). The simulation of European heat
- 50 waves from an ensemble of regional climate models within the EURO-CORDEX project. *Clim. Dyn.* 41, 2555–
- 51 2575. doi:10.1007/s00382-013-1714-z.
- 52 Vautard, R., Yiou, P., van Oldenborgh, G.-J., Lenderink, G., Thao, S., Ribes, A., et al. (2015). Extreme Fall 2014
- 53 Precipitation in the Cévennes Mountains. *Bull. Am. Meteorol. Soc.* 96, S56–S60. doi:10.1175/BAMS-D-15-
- 54 00088.1.
- 55 Vermishev, M., and Moir, S. eds. (2015). *Armenia's Third National Communication on Climate Change*. Yerevan:
- 56 “Lusabats” Publishing House Available at: www.nature-ic.am [Accessed April 2, 2019].
- 57 Vicente-Serrano, S. M., Lopez-Moreno, J.-I., Beguería, S., Lorenzo-Lacruz, J., Sanchez-Lorenzo, A., García-Ruiz, J.
- 58 M., et al. (2014). Evidence of increasing drought severity caused by temperature rise in southern Europe. *Environ.*
- 59 *Res. Lett.* 9, 044001. doi:10.1088/1748-9326/9/4/044001.
- 60 Vicente-Serrano, S. M., López-Moreno, J. I., Correa, K., Avalos, G., Bazo, J., Azorin-Molina, C., et al. (2018). Recent
- 61 changes in monthly surface air temperature over Peru, 1964–2014. *Int. J. Climatol.* 38, 283–306.

- 1 doi:10.1002/joc.5176.
- 2 Vichot-Llano, A. . M.-C. (2017). Estado actual de las representación de los principales factores del clima del Caribe por
3 modelos climáticos regionales. Estudios de sensibilidad y validación. *Rev. Cuba. Meteorol.* 23, 232–261.
- 4 Vichot-Llano, A., Bezanilla-Morlot, A., Martínez-Castro, D., and Centella-Artola, A. (2019). Present situation of the
5 application of downscaling methods to the climate change pr ojections in Central America and the Caribbean.
6 *Rev. Cuba. Meteorol.* 25.
- 7 Vichot-Llano, A., Martínez-Castro, D., Centella-Artola, A., and Bezanilla-Morlot, A. (2014). Sensibilidad al cambio de
8 dominio y resolución de tres configuraciones del modelo climático regional RegCM 4.3 para la región de
9 América Central y el Caribe. *Rev. Climatol.* 14, 45–62. Available at:
10 <http://webs.ono.com/reclim11/reclim14e.pdf>.
- 11 Vidal, J.-P., Martin, E., Franchistéguy, L., Baillon, M., and Soubeyroux, J.-M. (2010). A 50-year high-resolution
12 atmospheric reanalysis over France with the Safran system. *Int. J. Climatol.* 30, 1627–1644.
13 doi:10.1002/joc.2003.
- 14 Villafuerte, M. Q., and Matsumoto, J. (2015). Significant influences of global mean temperature and ENSO on extreme
15 rainfall in Southeast Asia. *J. Clim.* 28, 1905–1919. doi:10.1175/JCLI-D-14-00531.1.
- 16 Villafuerte, M. Q., Matsumoto, J., Akasaka, I., Takahashi, H. G., Kubota, H., and Cinco, T. A. (2014). Long-term
17 trends and variability of rainfall extremes in the Philippines. *Atmos. Res.* 137, 1–13.
18 doi:10.1016/j.atmosres.2013.09.021.
- 19 Villarini, G., and Vecchi, G. A. (2013). Projected Increases in North Atlantic Tropical Cyclone Intensity from CMIP5
20 Models. *J. Clim.* 26, 3231–3240. doi:10.1175/JCLI-D-12-00441.1.
- 21 Vinther, B. M., Jones, P. D., Briffa, K. R., Clausen, H. B., Andersen, K. K., Dahl-Jensen, D., et al. (2010). Climatic
22 signals in multiple highly resolved stable isotope records from Greenland. *Quat. Sci. Rev.*
23 doi:10.1016/j.quascirev.2009.11.002.
- 24 Voldoire, A., Decharme, B., Pianezze, J., Lebeauupin Brossier, C., Sevault, F., Seyfried, L., et al. (2017). SURFEX v8.0
25 interface with OASIS3-MCT to couple atmosphere with hydrology, ocean, waves and sea-ice models, from
26 coastal to global scales. *Geosci. Model Dev.* 10, 4207–4227. doi:10.5194/gmd-10-4207-2017.
- 27 Vuille, M., Franquist, E., Garreaud, R., Lavado Casimiro, W. S., and Cáceres, B. (2015). Impact of the global warming
28 hiatus on Andean temperature. *J. Geophys. Res. Atmos.* 120, 3745–3757. doi:10.1002/2015JD023126.
- 29 Wahl, S., Bollmeyer, C., Crewell, S., Figura, C., Friederichs, P., Hense, A., et al. (2017). A novel convective-scale
30 regional reanalysis COSMO-REA2: Improving the representation of precipitation. *Meteorol. Zeitschrift* 26, 345–
31 361. doi:10.1127/metz/2017/0824.
- 32 Waldman, R., Somot, S., Herrmann, M., Bosse, A., Caniaux, G., Estournel, C., et al. (2017). Modeling the intense
33 2012–2013 dense water formation event in the northwestern Mediterranean Sea: Evaluation with an ensemble
34 simulation approach. *J. Geophys. Res. Ocean.* 122, 1297–1324. doi:10.1002/2016JC012437.
- 35 Walsh, K. ~J. ~E., Nguyen, K.-C., and McGregor, J. ~L. (2004). Fine-resolution regional climate model simulations of
36 the impact of climate change on tropical cyclones near Australia. *Clim. Dyn.* 22, 47–56. doi:10.1007/s00382-003-
37 0362-0.
- 38 Walsh, K. J. E., Fiorino, M., Landsea, C. W., and McInnes, K. L. (2007). Objectively Determined Resolution-
39 Dependent Threshold Criteria for the Detection of Tropical Cyclones in Climate Models and Reanalyses. *J. Clim.*
40 20, 2307–2314. doi:10.1175/JCLI4074.1.
- 41 Walton, D. B., Sun, F., Hall, A., and Capps, S. (2015). A Hybrid Dynamical–Statistical Downscaling Technique. Part I:
42 Development and Validation of the Technique. *J. Clim.* 28, 4597–4617. doi:10.1175/JCLI-D-14-00196.1.
- 43 Wang, B., and An, S. I. (2001). Why the properties of El Niño changed during the late 1970s. *Geophys. Res. Lett.* 28,
44 3709–3712. doi:10.1029/2001GL012862.
- 45 Wang, B., Ding, Q., and Jhun, J. G. (2006). Trends in Seoul (1778–2004) summer precipitation. *Geophys. Res. Lett.* 33,
46 L15803. doi:10.1029/2006GL026418.
- 47 Wang, C., Zhang, L., Lee, S. K., Wu, L., and Mechoso, C. R. (2014). A global perspective on CMIP5 climate model
48 biases. *Nat. Clim. Chang.* doi:10.1038/nclimate2118.
- 49 Wang, L., and Chen, W. (2010). How well do existing indices measure the strength of the East Asian winter monsoon?
50 *Adv. Atmos. Sci.* 27, 855–870. doi:10.1007/s00376-009-9094-3.
- 51 Wang, L., Huang, R., Gu, L., Chen, W., and Kang, L. (2009a). Interdecadal variations of the East Asian winter
52 monsoon and their association with Quasi-stationary planetary wave activity. *J. Clim.* 22, 4860–4872.
53 doi:10.1175/2009JCLI2973.1.
- 54 Wang, P., Tang, J., Sun, X., Liu, J., and Juan, F. (2018). Spatiotemporal characteristics of heat waves over China in
55 regional climate simulations within the CORDEX-EA project. *Clim. Dyn.* 0, 1–20. doi:10.1007/s00382-018-4167-
56 6.
- 57 Wang, S.-Y., Gillies, R. R., Takle, E. S., and Gutowski Jr., W. J. (2009b). Evaluation of precipitation in the
58 Intermountain Region as simulated by the NARCCAP regional climate models. *Geophys. Res. Lett.* 36.
59 doi:10.1029/2009GL037930.
- 60 Wang, S., Dieterich, C., Döscher, R., Höglund, A., Hordoir, R., Meier, H. E. M., et al. (2015). Development and
61 evaluation of a new regional coupled atmosphere–ocean model in the North Sea and Baltic Sea. *Tellus A Dyn.*

- 1 *Meteorol. Oceanogr.* 67, 24284. doi:10.3402/tellusa.v67.24284.
- 2 Wang, Y. (2009). How Do Outer Spiral Rainbands Affect Tropical Cyclone Structure and Intensity? *J. Atmos. Sci.* 66,
3 1250–1273. doi:10.1175/2008JAS2737.1.
- 4 Webster, P. J., Holland, G. J., Curry, J. A., and Chang, H.-R. (2005). Changes in Tropical Cyclone Number, Duration,
5 and Intensity in a Warming Environment. *Science* (80-.). 309, 1844–1846. doi:10.1126/science.1116448.
- 6 Wester, P., Mishra, A., Mukherji, A., and Shrestha, A. B. (2019). *The Hindu Kush Himalaya Assessment*. , eds. P.
7 Wester, A. Mishra, A. Mukherji, and A. B. Shrestha Cham: Springer International Publishing doi:10.1007/978-3-
8 319-92288-1.
- 9 Whan, K., and Zwiers, F. (2016). Evaluation of extreme rainfall and temperature over North America in CanRCM4 and
10 CRCM5. *Clim. Dyn.* 46, 3821–3843. doi:10.1007/s00382-015-2807-7.
- 11 Whelan, E., Gleeson, E., and Hanley, J. (2018). An evaluation of MéRA, a high-resolution mesoscale regional
12 reanalysis. *J. Appl. Meteorol. Climatol.* 57, 2179–2196. doi:10.1175/JAMC-D-17-0354.1.
- 13 Whyte, F. S., Taylor, M. A., Stephenson, T. S., and Campbell, J. D. (2008). Features of the Caribbean low level jet. *Int.*
14 *J. Climatol.* 28, 119–128. doi:10.1002/joc.1510.
- 15 Widmann, M. (2019). Validation of spatial variability in downscaling results from the VALUE perfect predictor
16 experiment. *Int. J. Climatol.* doi:10.1002/joc.6024.
- 17 Wiest, S. L., Raymond, L., and Clawson, R. A. (2015). Framing, partisan predispositions, and public opinion on climate
18 change. *Glob. Environ. Chang.* 31, 187–198. doi:10.1016/J.GLOENVCHA.2014.12.006.
- 19 Williams, A. P., and Funk, C. (2011). A westward extension of the warm pool leads to a westward extension of the
20 Walker circulation, drying eastern Africa. *Clim. Dyn.* doi:10.1007/s00382-010-0984-y.
- 21 WMO (2017). *WMO Guidelines on the Calculation of Climate Normals (WMO-No. 1203)*. WMO. , ed. World
22 Meteorological Organization (WMO) Geneva: World Meteorological Organization (WMO) Available at:
23 https://library.wmo.int/doc_num.php?explnum_id=4166.
- 24 WMO (2018). *Guidance on Good Practices for Climate Services User Engagement: Expert Team on User Interface for*
25 *Climate Services*. World Meteorological Organization, WMO-No. 1214 Available at:
26 https://library.wmo.int/index.php?lvl=notice_display&id=20254#.XKX5raBKhaQ.
- 27 Woo, S., Singh, G. P., Oh, J. H., and Lee, K. M. (2018). Possible teleconnections between East and South Asian
28 summer monsoon precipitation in projected future climate change. *Meteorol. Atmos. Phys.*, 1–13.
29 doi:10.1007/s00703-017-0573-2.
- 30 World Bank Climate Change Knowledge Portal Available at:
31 <https://climateknowledgeportal.worldbank.org/country/bahrain/climate-data-projections> [Accessed April 5, 2019].
- 32 Wramneby, A., Smith, B., and Samuelsson, P. (2010). Hot spots of vegetation-climate feedbacks under future
33 greenhouse forcing in Europe. *J. Geophys. Res.* 115, D21119. doi:10.1029/2010JD014307.
- 34 Wu, Y., and Polvani, L. M. (2017). Recent Trends in Extreme Precipitation and Temperature over Southeastern South
35 America: The Dominant Role of Stratospheric Ozone Depletion in the CESM Large Ensemble. *J. Clim.* 30, 6433–
36 6441. doi:10.1175/JCLI-D-17-0124.1.
- 37 Xie, P., Arkin, P. A., and Janowiak, J. E. (2007). “CMAP: The CPC merged analysis of precipitation,” in *Advances in*
38 *Global Change Research* (Dordrecht: Springer Netherlands), 319–328. doi:10.1007/978-1-4020-5835-6_25.
- 39 Xu, K., Milliman, J. D., and Xu, H. (2010). Temporal trend of precipitation and runoff in major Chinese Rivers since
40 1951. *Glob. Planet. Change* 73, 219–232. doi:10.1016/j.gloplacha.2010.07.002.
- 41 Yang, B., Wang, Y., and Wang, B. (2007). The Effect of Internally Generated Inner-Core Asymmetries on Tropical
42 Cyclone Potential Intensity. *J. Atmos. Sci.* 64, 1165–1188. doi:10.1175/JAS3971.1.
- 43 Yang, W., Seager, R., Cane, M. A., and Lyon, B. (2015). The rainfall annual cycle bias over East Africa in CMIP5
44 coupled climate models. *J. Clim.* doi:10.1175/JCLI-D-15-0323.1.
- 45 Ye, H., Fetzer, E. J., Behrangi, A., Wong, S., Lambriksen, B. H., Wang, C. Y., et al. (2016). Increasing daily
46 precipitation intensity associated with warmer air temperatures over northern Eurasia. *J. Clim.* 29, 623–636.
47 doi:10.1175/JCLI-D-14-00771.1.
- 48 Yin, L., Fu, R., Shevliakova, E., and Dickinson, R. E. (2013). How well can CMIP5 simulate precipitation and its
49 controlling processes over tropical South America? *Clim. Dyn.* 41, 3127–3143. doi:10.1007/s00382-012-1582-y.
- 50 Yoon, J.-H. (2016). Multi-model analysis of the Atlantic influence on Southern Amazon rainfall. *Atmos. Sci. Lett.* 17,
51 122–127. doi:10.1002/asl.600.
- 52 Yu, R., Wang, B., and Zhou, T. (2004). Tropospheric cooling and summer monsoon weakening trend over East Asia.
53 *Geophys. Res. Lett.* 31, 1–4. doi:10.1029/2004GL021270.
- 54 Zahid, M., and Rasul, G. (2012). Changing trends of thermal extremes in Pakistan. *Clim. Change* 113, 883–896.
55 doi:10.1007/s10584-011-0390-4.
- 56 Zaninelli, P. G., Menéndez, C. G., Falco, M., López-Franca, N., and Carril, A. F. (2019). Future hydroclimatological
57 changes in South America based on an ensemble of regional climate models. *Clim. Dyn.* 52, 819–830.
58 doi:10.1007/s00382-018-4225-0.
- 59 Zanolco, C., Boudet, H., Nilson, R., Satein, H., Whitley, H., and Flora, J. (2018). Place, proximity, and perceived harm:
60 extreme weather events and views about climate change. *Clim. Change* 149, 349–365. doi:10.1007/s10584-018-
61 2251-x.

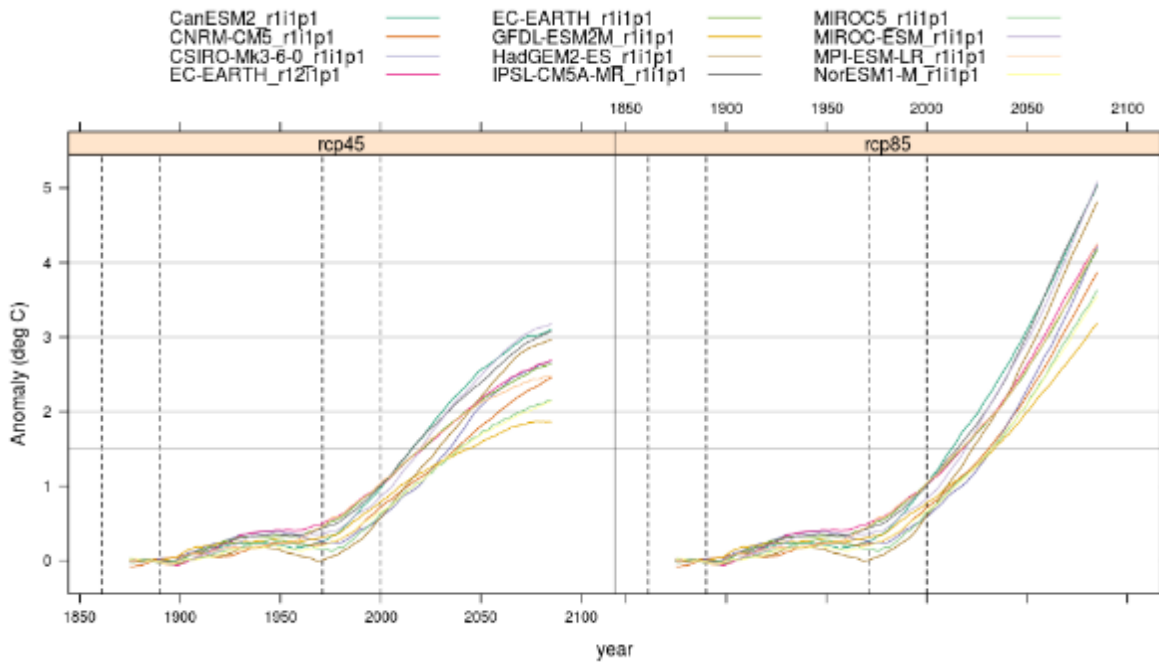
- 1 Zappa, G., Shaffrey, L. C., and Hodges, K. I. (2013). The Ability of CMIP5 Models to Simulate North Atlantic
2 Extratropical Cyclones*. *J. Clim.* 26, 5379–5396. doi:10.1175/JCLI-D-12-00501.1.
- 3 Zappa, G., Shepherd, T. G., Zappa, G., and Shepherd, T. G. (2017). Storylines of Atmospheric Circulation Change for
4 European Regional Climate Impact Assessment. *J. Clim.* 30, 6561–6577. doi:10.1175/JCLI-D-16-0807.1.
- 5 Zazulie, N., Rusticucci, M., and Raga, G. B. (2017). Regional climate of the subtropical central Andes using high-
6 resolution CMIP5 models—part I: past performance (1980–2005). *Clim. Dyn.* 49, 3937–3957.
7 doi:10.1007/s00382-017-3560-x.
- 8 Zhang, L., and Zhou, T. (2011). An assessment of monsoon precipitation changes during 1901–2001. *Clim. Dyn.* 37,
9 279–296. doi:10.1007/s00382-011-0993-5.
- 10 Zheng, H., Chiew, F. H. S., Charles, S., and Podger, G. (2018). Future climate and runoff projections across South Asia
11 from CMIP5 global climate models and hydrological modelling. *J. Hydrol. Reg. Stud.* 18, 92–109.
12 doi:10.1016/J.EJRH.2018.06.004.
- 13 Zhou, T., Gong, D., Li, J., and Li, B. (2009a). Detecting and understanding the multi-decadal variability of the East
14 Asian Summer Monsoon - Recent progress and state of affairs. *Meteorol. Zeitschrift* 18, 455–467.
15 doi:10.1127/0941-2948/2009/0396.
- 16 Zhou, T., Yu, R., Zhang, J., Drange, H., Cassou, C., Deser, C., et al. (2009b). Why the Western Pacific Subtropical
17 High Has Extended Westward since the Late 1970s. *J. Clim.* 22, 2199–2215. doi:10.1175/2008JCLI2527.1.
- 18 Zhou, T., and Zou, L. (2010). Understanding the predictability of East Asian summer monsoon from the reproduction of
19 land-sea thermal contrast change in AMIP-type simulation. *J. Clim.* 23, 6009–6026.
20 doi:10.1175/2010JCLI3546.1.
- 21 Zhou, W., Tang, J., Wang, X., Wang, S., Niu, X., and Wang, Y. (2016a). Evaluation of regional climate simulations
22 over the CORDEX-EA-II domain using the COSMO-CLM model. *Asia-Pacific J. Atmos. Sci.* 52, 107–127.
23 doi:10.1007/s13143-016-0013-0.
- 24 Zhou, W., Tang, J., Wang, X., Wang, S., Niu, X., and Wang, Y. (2016b). Evaluation of regional climate simulations
25 over the CORDEX-EA-II domain using the COSMO-CLM model. *Asia-Pacific J. Atmos. Sci.* 52, 107–127.
26 doi:10.1007/s13143-016-0013-0.
- 27 Zhou, X., Matthes, H., Rinke, A., Huang, B., Yang, K., and Dethlo, K. (2019). Simulating Arctic 2-m air temperature
28 and its linear trends using the HIRHAM5 regional climate model. 217, 137–149.
29 doi:10.1016/j.atmosres.2018.10.022.
- 30 Zhu, C., Wang, B., Qian, W., and Zhang, B. (2012). Recent weakening of northern East Asian summer monsoon: A
31 possible response to global warming. *Geophys. Res. Lett.* 39, n/a-n/a. doi:10.1029/2012GL051155.
- 32 Zhu, J., Huang, G., Wang, X., Cheng, G., and Wu, Y. (2018). High-resolution projections of mean and extreme
33 precipitations over China through PRECIS under RCPs. *Clim. Dyn.* 50, 4037–4060. doi:10.1007/s00382-017-
34 3860-1.
- 35 Zia, A., and Todd, A. M. (2010). Evaluating the effects of ideology on public understanding of climate change science:
36 How to improve communication across ideological divides? *Public Underst. Sci.* 19, 743–761.
37 doi:10.1177/0963662509357871.
- 38 Zou, L., and Zhou, T. (2016). Future summer precipitation changes over CORDEX-East Asia domain downscaled by a
39 regional ocean-atmosphere coupled model: A comparison to the stand-alone RCM. *J. Geophys. Res.* 121, 2691–
40 2704. doi:10.1002/2015JD024519.
- 41 Zou, L., Zhou, T., and Peng, D. (2016). Dynamical downscaling of historical climate over CORDEX East Asia domain:
42 A comparison of regional ocean-atmosphere coupled model to stand-alone RCM simulations. *J. Geophys. Res.*
43 121, 1442–1458. doi:10.1002/2015JD023912.
- 44 Булыгина, О. Н., Коршунова, Н. Н., and Разуваев, В. Н. (2014). Специализированные массивы данных для
45 климатических исследований. *Труды ВНИИГМИ-МЦД*, 136–148. Available at:
46 [http://meteo.ru/publications/125-trudy-vniigmi/trudy-vniigmi-mtsd-vypusk-177-2014-g/518-spetsializirovannyye-](http://meteo.ru/publications/125-trudy-vniigmi/trudy-vniigmi-mtsd-vypusk-177-2014-g/518-spetsializirovannyye-massivy-dannykh-dlya-klimaticheskikh-issledovaniy)
47 [massivy-dannykh-dlya-klimaticheskikh-issledovaniy](http://meteo.ru/publications/125-trudy-vniigmi/trudy-vniigmi-mtsd-vypusk-177-2014-g/518-spetsializirovannyye-massivy-dannykh-dlya-klimaticheskikh-issledovaniy) [Accessed April 1, 2019].
- 48 Ильясов, Ш., Забенко, О., Гайдамак, Н., Кириленко, А., Мырсадиев, Н., Шевченко, В., et al. (2013).
49 *Климатический профиль Кыргызской Республики*.
- 50 Кожаметов, П. Ж., and Никифорова, Л. Н. (2016). *Погодные стихии в Казахстане в условиях глобального*
51 *изменения климата*. Астана Available at: [https://new.kazhydromet.kz/upload/pagefiles/nits/УКИ НИЦ/Climate](https://new.kazhydromet.kz/upload/pagefiles/nits/УКИ НИЦ/Climate Change_09-2017_RUS_Light.pdf)
52 [Change_09-2017_RUS_Light.pdf](https://new.kazhydromet.kz/upload/pagefiles/nits/УКИ НИЦ/Climate Change_09-2017_RUS_Light.pdf) [Accessed April 3, 2019].
53
54

1 **Figures**

2

3

4



5

6 **Figure Atlas.1:** Global mean temperature (30-year running mean) for the selected CMIP5 ensemble, considering
7 RCPs 4.5 and 8.5. The reference GWLs are indicated by the horizontal grey lines. Preindustrial (1861–1890) and
8 reference (1971–2000) periods are also delimited by the dashed vertical lines.

9

10

1

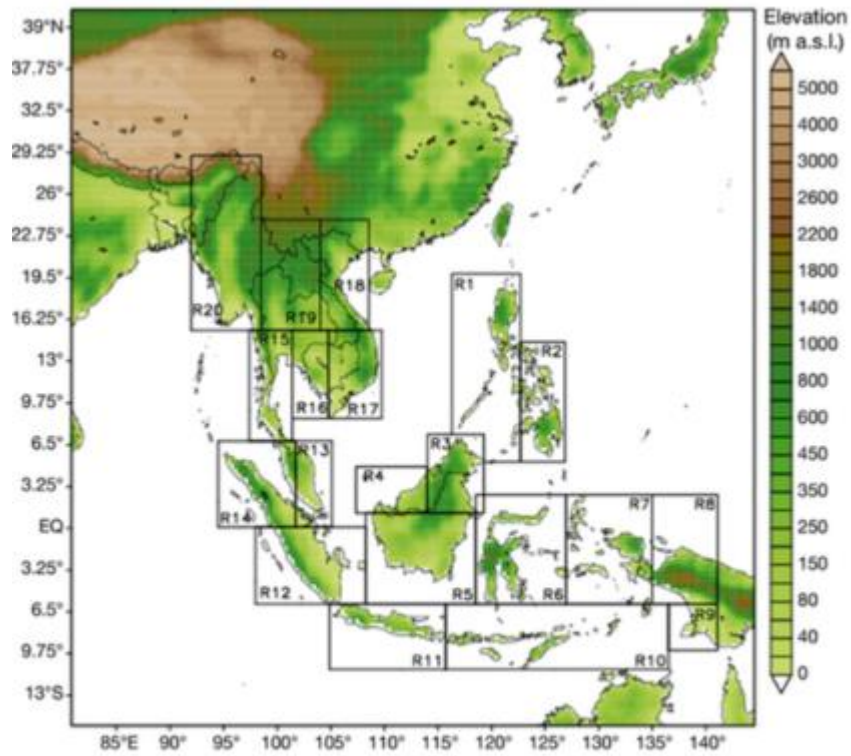
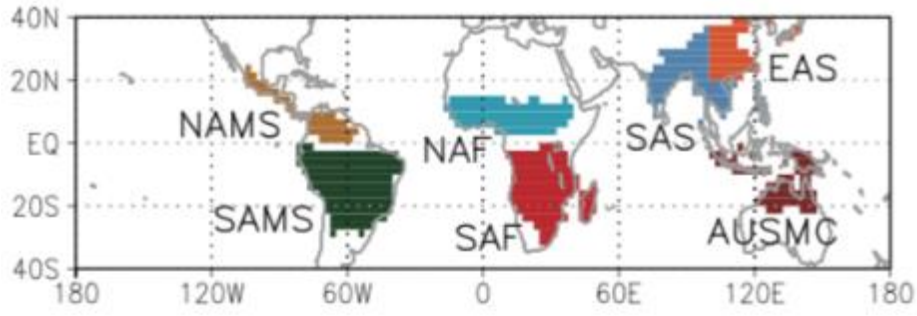


Fig. 1. Simulation domain and topography for the SEACLID/CORDEX-SEA sensitivity test experiments. The boxes indicate the 20 sub-regions used for further regional model performance assessment

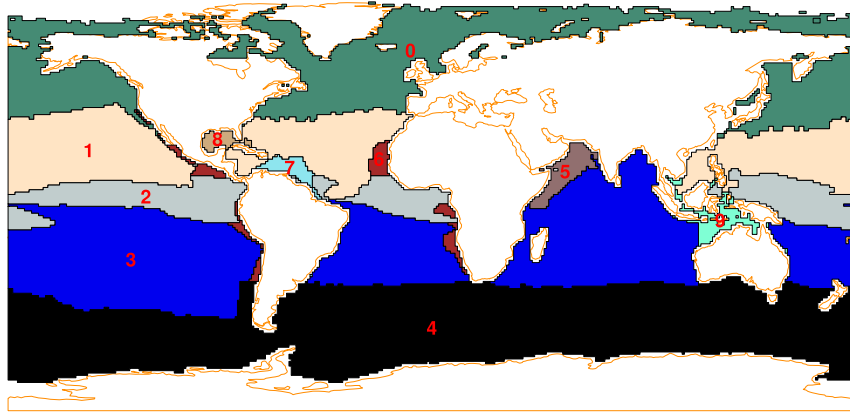
2
3
4
5
6
7

Figure Atlas.3: CORDEX-SEA subregions based on historical rainfall climatology and variability (Juneng et al., 2016)

1



2



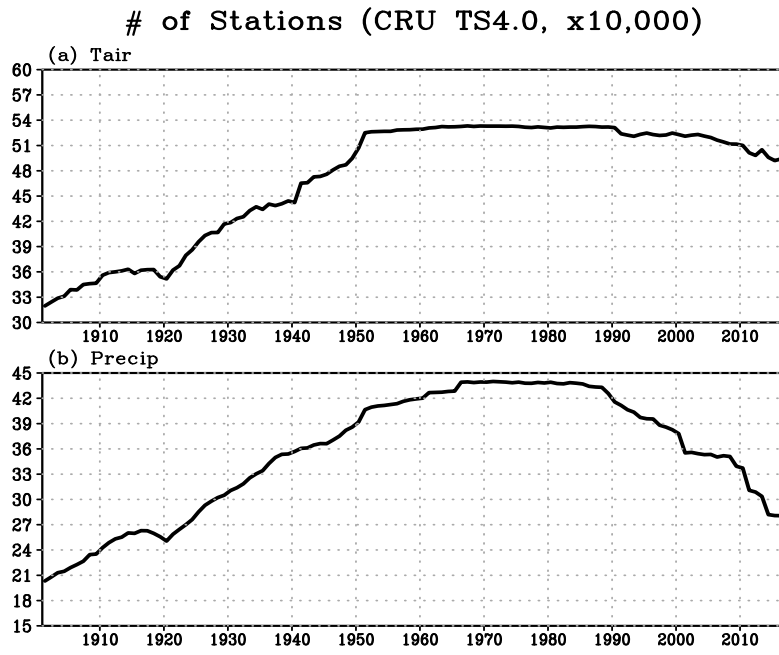
3

4

Figure Atlas.4: Land monsoon regions (top) and ocean biomes (bottom).

5

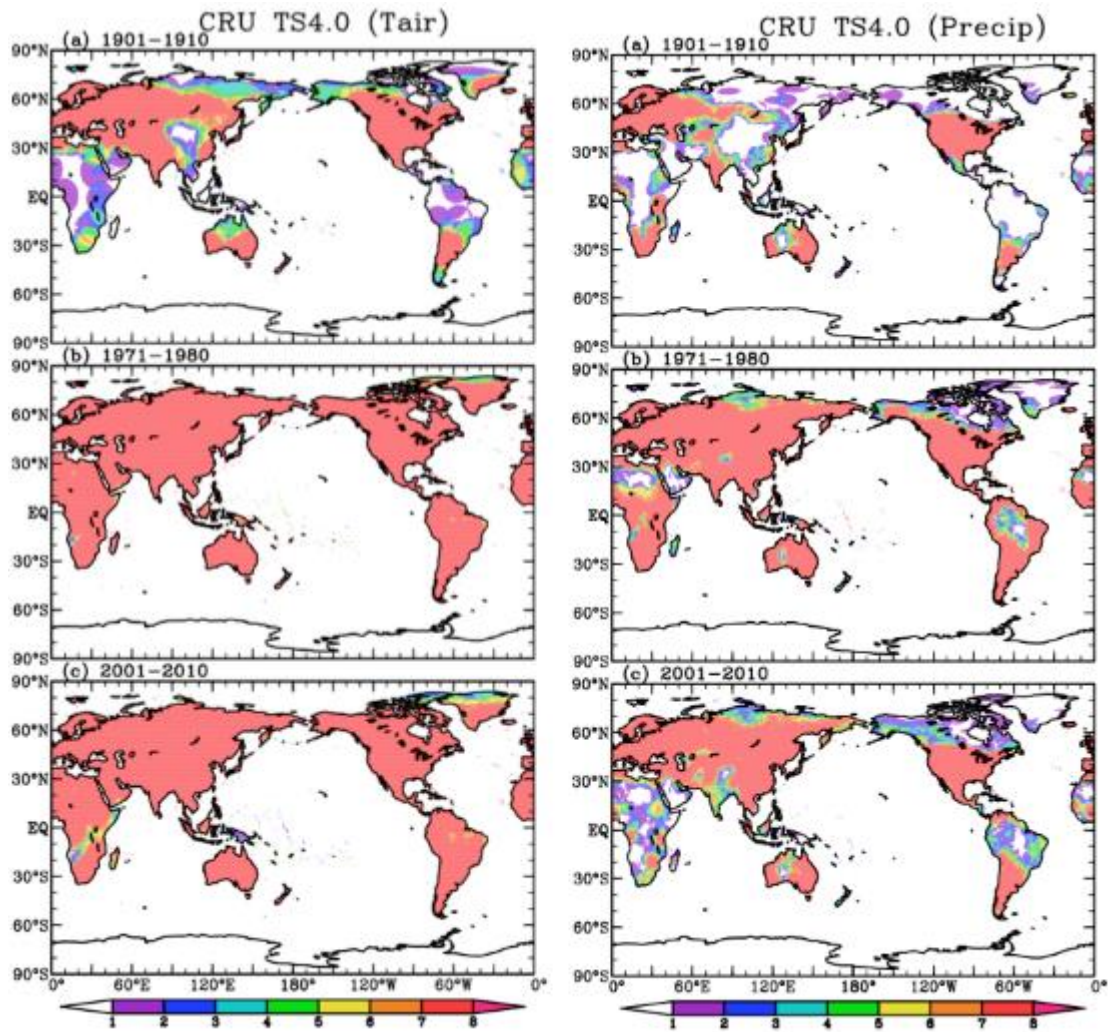
1



2
3
4
5
6
7

Figure Atlas.5: Number of stations reported over the entire globe for surface air temperature (above) and precipitation (below) for CRU TS4.0 dataset.

1

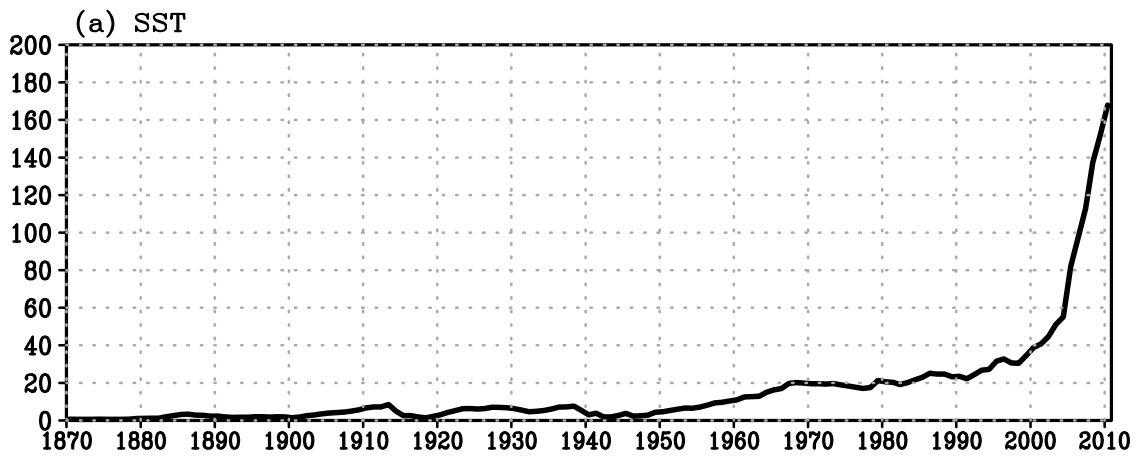


2
3
4
5
6
7

Figure Atlas.6: Number of stations per 0.5 x 0.5 grid cell reported over the period of 1901–1910, 1971–1980, and 2001–2010 for surface air temperature for CRU TS4.0 dataset.

1

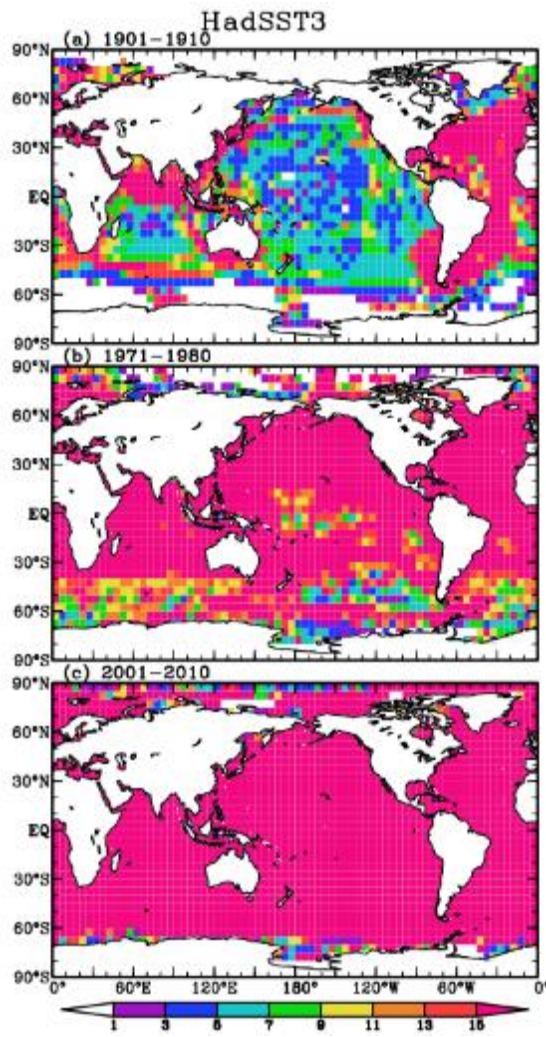
of observations (HadSST3, x10,000)



2
3
4
5
6

Figure Atlas.7: Same as Figure Atlas.5:, but for number of observations in the HadSST3 dataset.

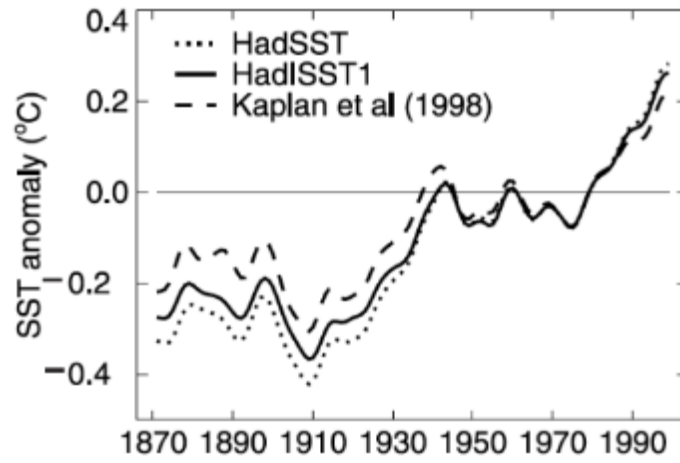
1



2
3
4
5
6

Figure Atlas.8: Same as Figure Atlas.6:, but for number of observations in the HadSST3 dataset.

1



2
3
4
5
6
7

Figure Atlas.9: Global (excluding the Southern Ocean) annual average SST anomaly (relative to 1971–1990), for the period 1871–2000. Annual averages smoothed using a 21-pt binomial filter (from Rayner et al., 2003).

1

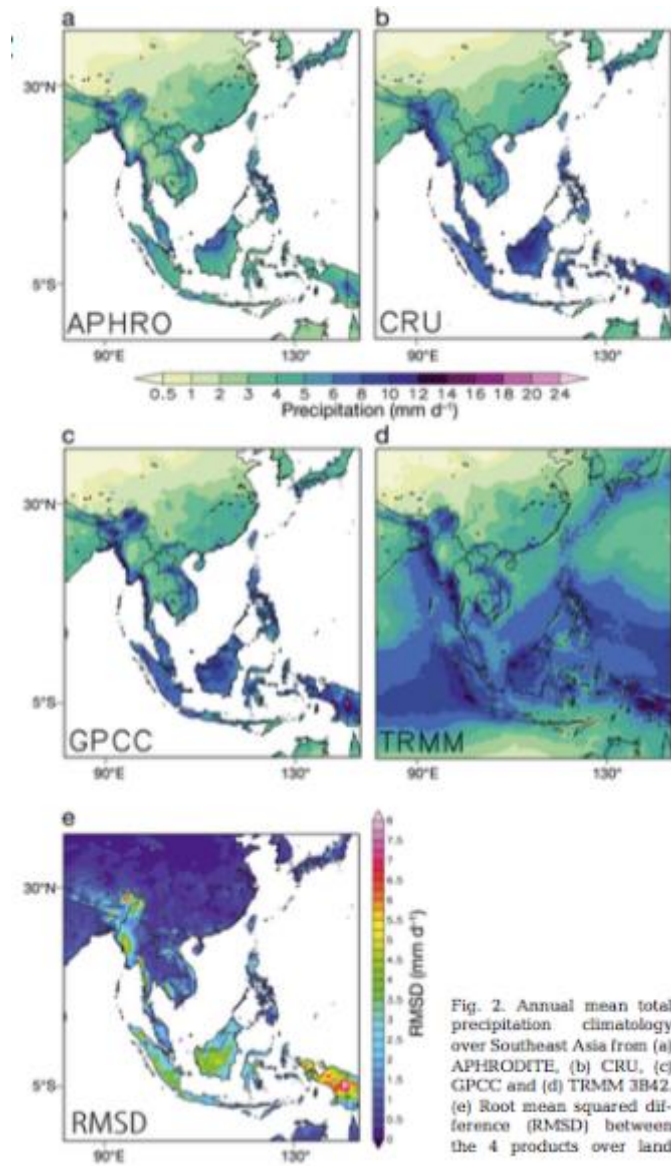
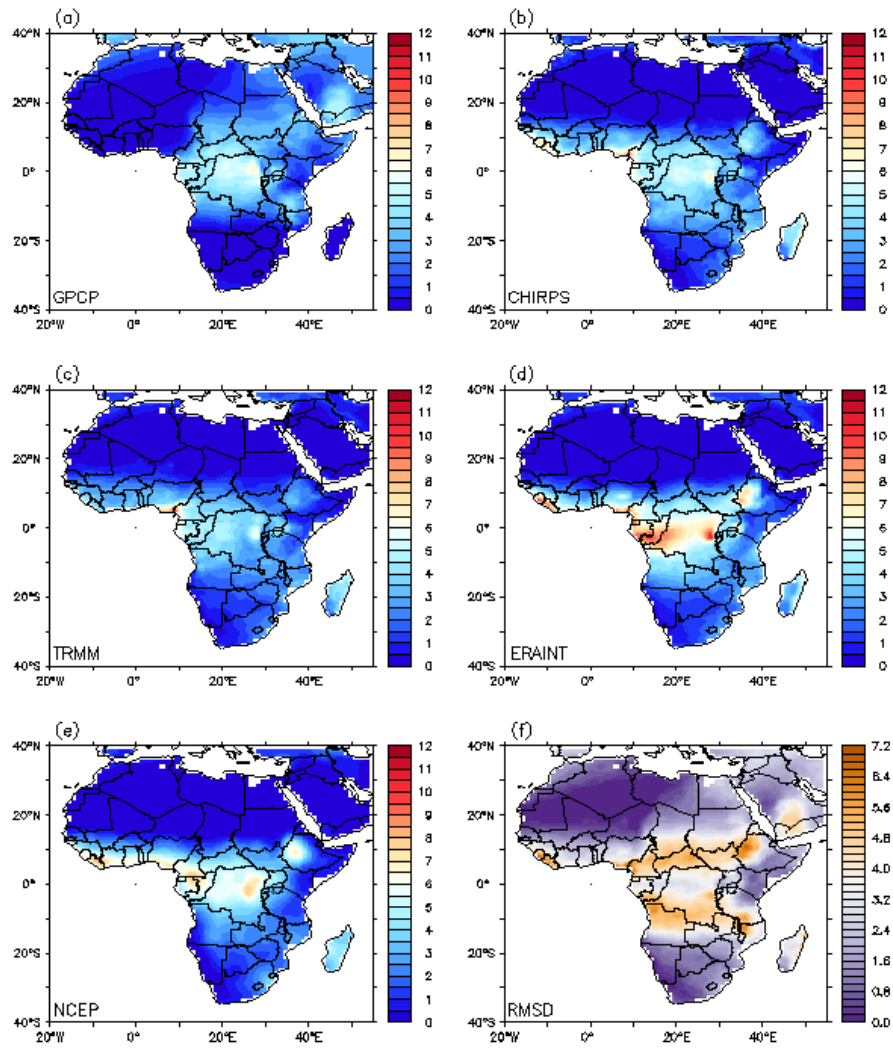


Fig. 2. Annual mean total precipitation climatology over Southeast Asia from (a) APHRODITE, (b) CRU, (c) GPCC and (d) TRMM 3B42. (e) Root mean squared difference (RMSD) between the 4 products over land

2
3
4
5

Figure Atlas.11: Differences in precipitation values in the different observation datasets in Southeast Asia (from Juneng et al., 2016)

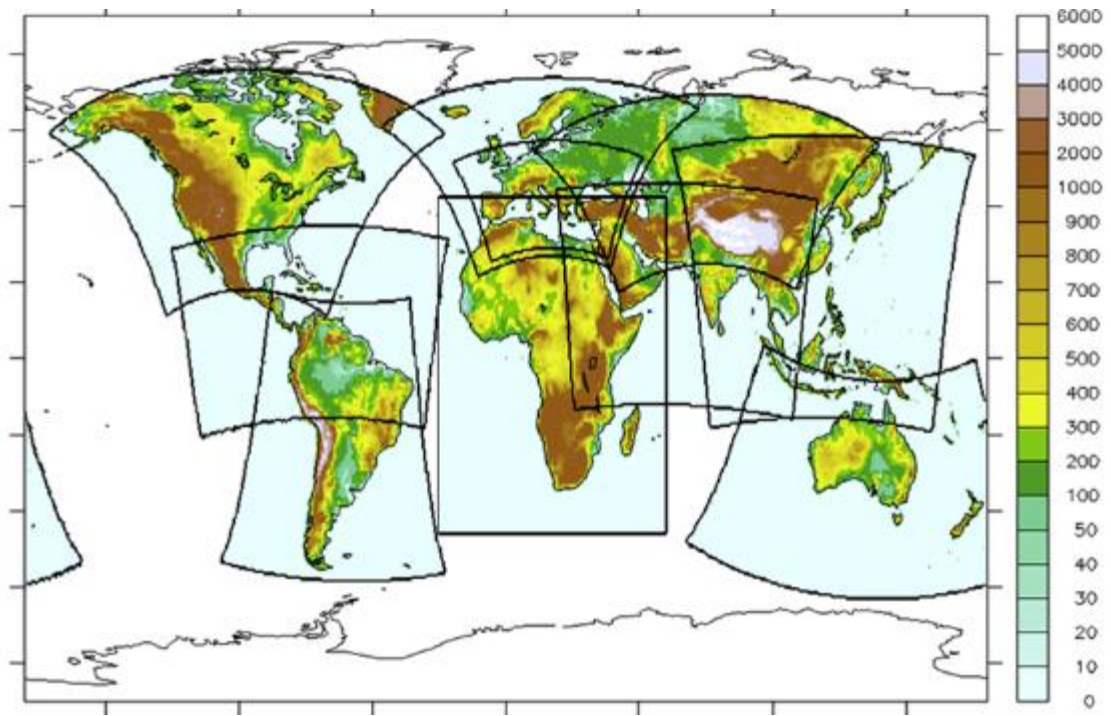
1



2
3
4

Figure Atlas.12: Similar to Figure Atlas.11 but for Africa.

1



2

3

4

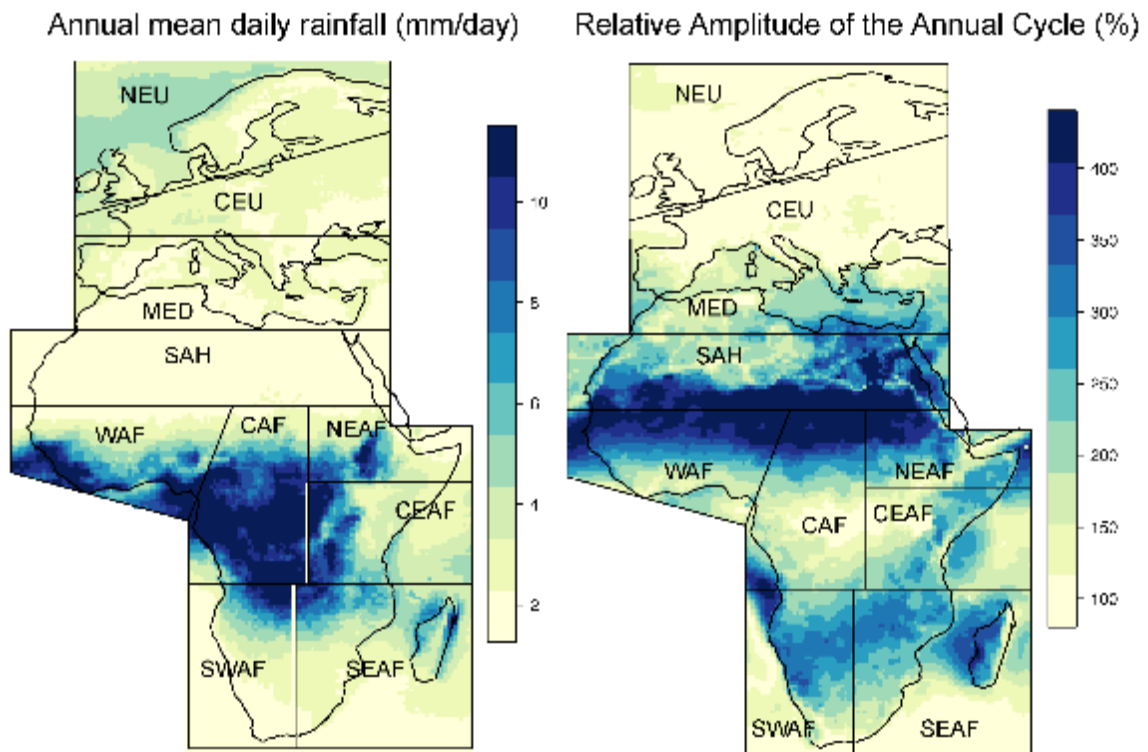
5

6

7

Figure Atlas.13: Major non-polar CORDEX domains and topography. [This figure includes incomplete information. To be updated.]

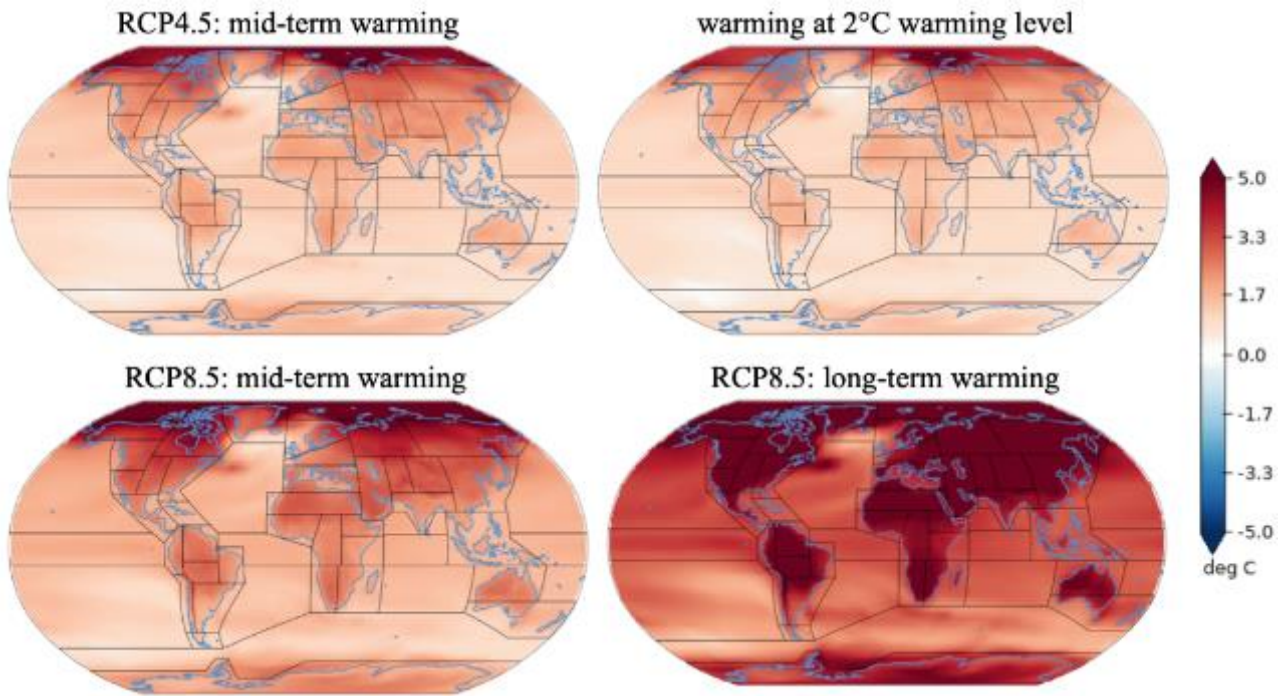
1



2
3
4
5
6
7
8
9
10
11

Figure Atlas.14: (Left) Annual mean daily precipitation (mm/day) for the observational reference EWEMBI for the different AR6 WGI reference regions over Europe and Africa used for spatial aggregation of regional information in the Interactive Atlas (see Section Atlas.2 for more details). (Right) Relative Amplitude of the Annual Cycle, defined as the difference between maximum and minimum value (30-day moving window over calendar days), relative to the mean of these two values.

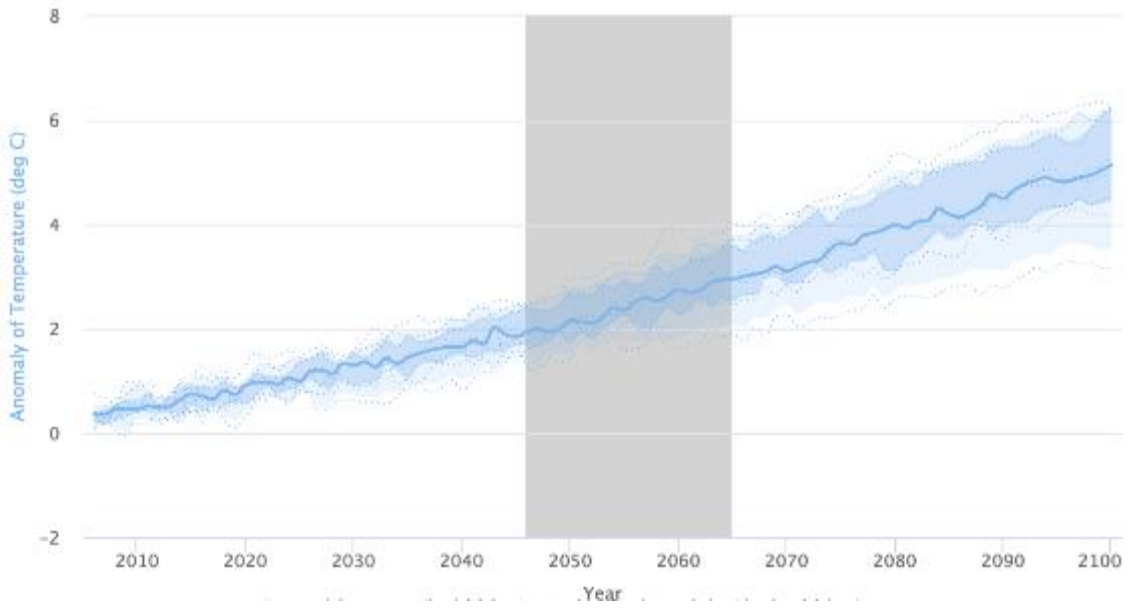
1



2
3
4
5
6
7
8
9
10
11

Figure Atlas.15: Global temperature changes projected for mid-century (left column) under RCP4.5 (top) and 8.5 (bottom) compared to, in the right column, a global mean warming levels of 2°C (top) and at the end of the century under RCP8.5 emissions (bottom) from an ensemble of nine CMIP5 GCMs. Note that the future period warmings are calculated against a baseline period of 1986–2005 whereas the global mean warming level is defined with respect to a ‘pre-industrial’ baseline of 1861–1890. Thus, the other three maps would show greater warmings with respect to this earlier baseline.

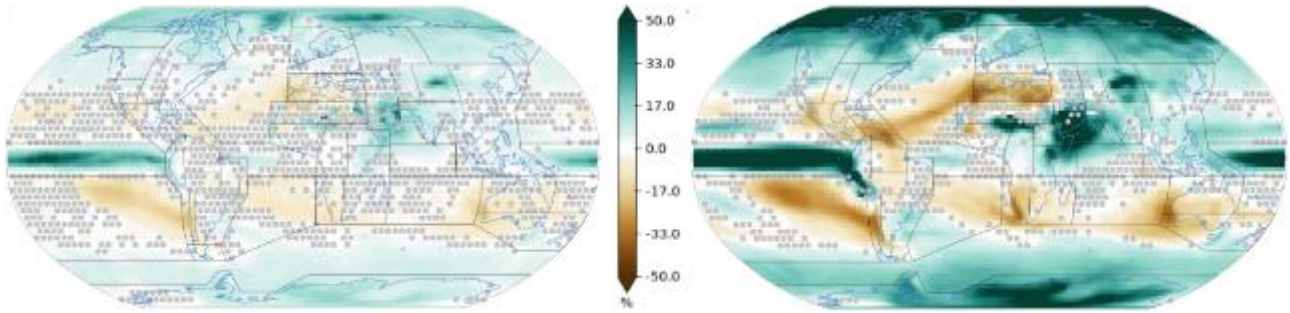
1



2
3
4
5
6

Figure Atlas.16: Global average surface air temperature increases projected by nine CMIP5 models under the RCP8.5 emissions scenario from 2005 to 2100 relative to a 1986–2005 baseline.

1



2

3

4

5

6

7

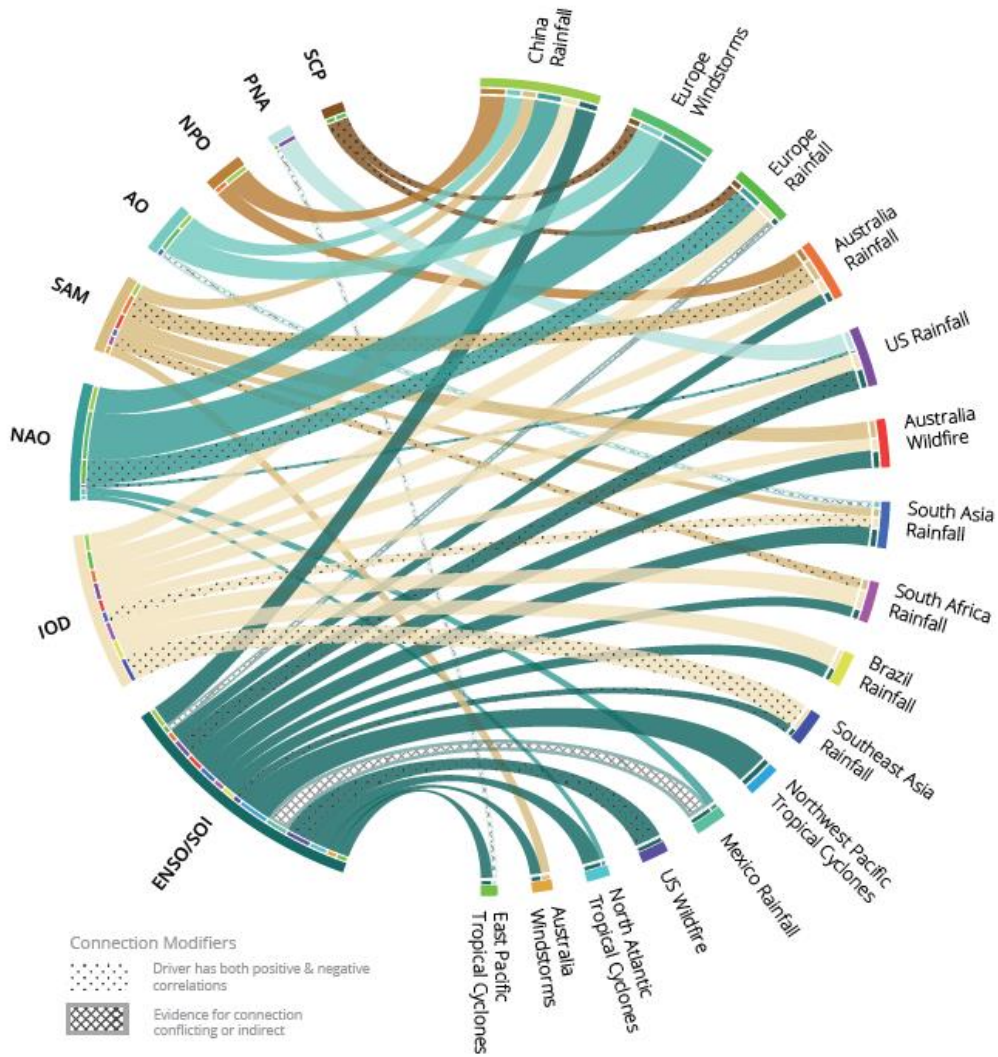
8

9

10

Figure Atlas.17: Global precipitation changes projected at 2°C global mean warming compared to pre-industrial levels (left) and for 2081-2100 under RCP8.5 emissions compared to the 1986-2005 (right) from an ensemble of nine CMIP5 GCMs. Regions are stippled where less than six out of the nine models do not agree on the sign of the change (noting that this assessment does not take into account whether the individual models’ projected changes are significant).

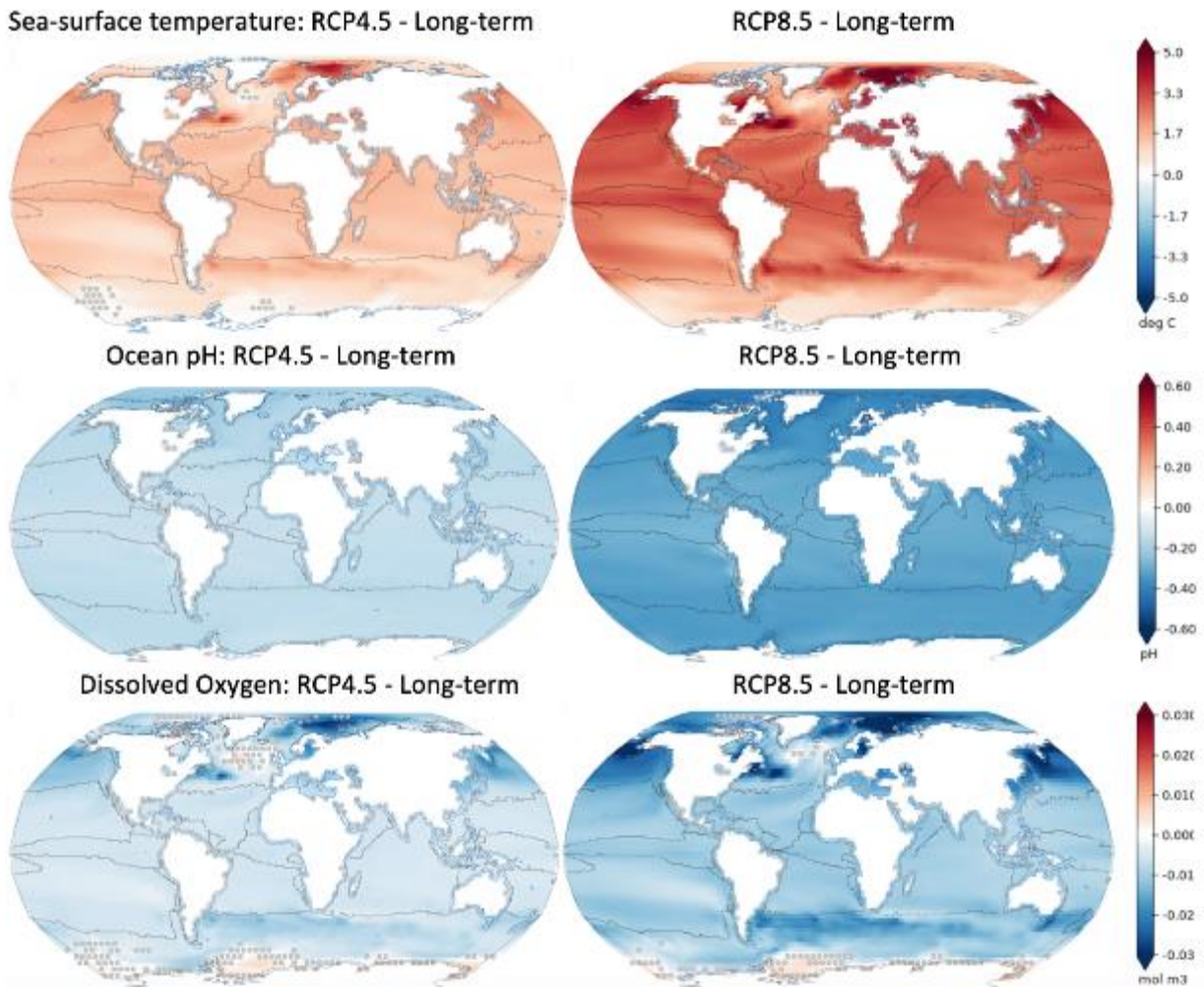
1



2
3
4
5
6
7
8

Figure Atlas.18: Influence of major modes of variability on regional extreme events relevant to assessing multi-hazard resilience (Stephoe et al., 2018). Ribbon colours define the driver from which they originate and their width is proportional to the correlation. Hatching represent where there is conflicting evidence for a correlation or where the driver is not directly related to the hazard and dots represent drivers that have both a positive and negative correlation with the hazard.

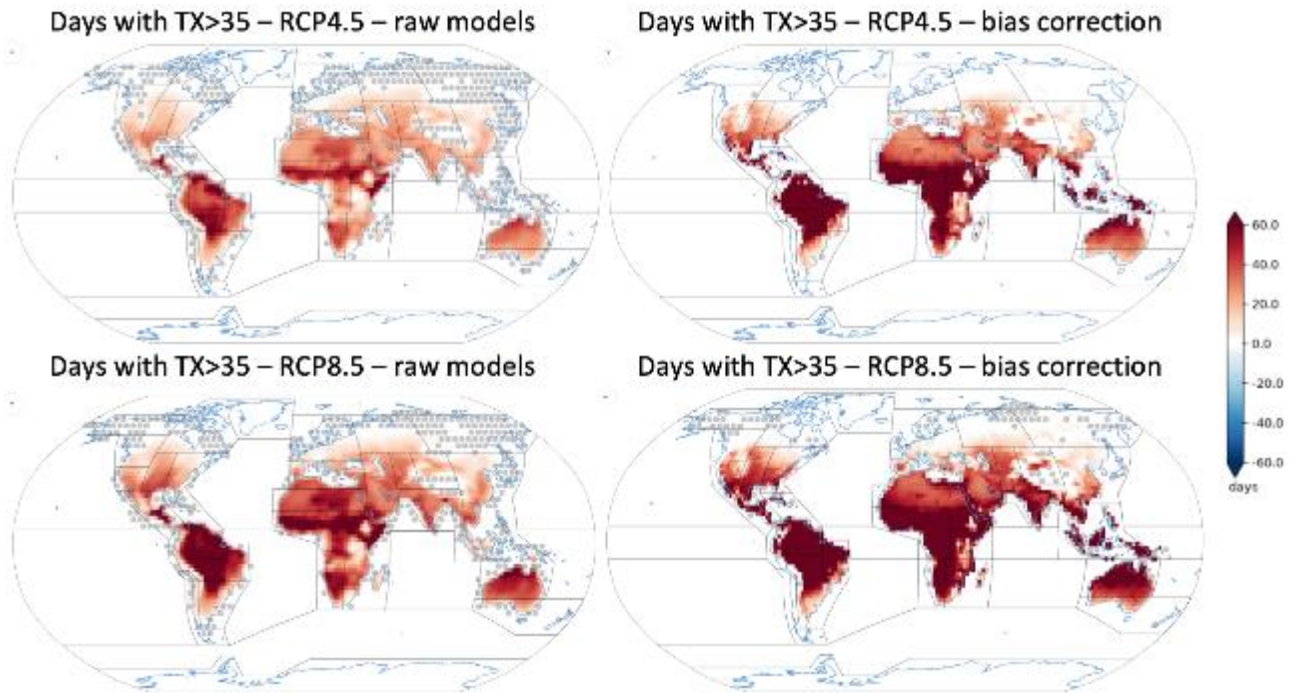
1



2
3
4
5
6
7
8
9
10

Figure Atlas.19: Projected changes in sea-surface temperature (top), ocean pH (middle) and dissolved oxygen (bottom) for 2081-2100 under the RCP4.5 (left column) and 8.5 (right column) emissions compared to a 1986–2005 baseline period from an ensemble of nine CMIP5 GCMs. Regions are stippled where less than six out of the nine models do not agree on the sign of the change (noting that this assessment does not take into account whether the individual models’ projected changes are significant)

1

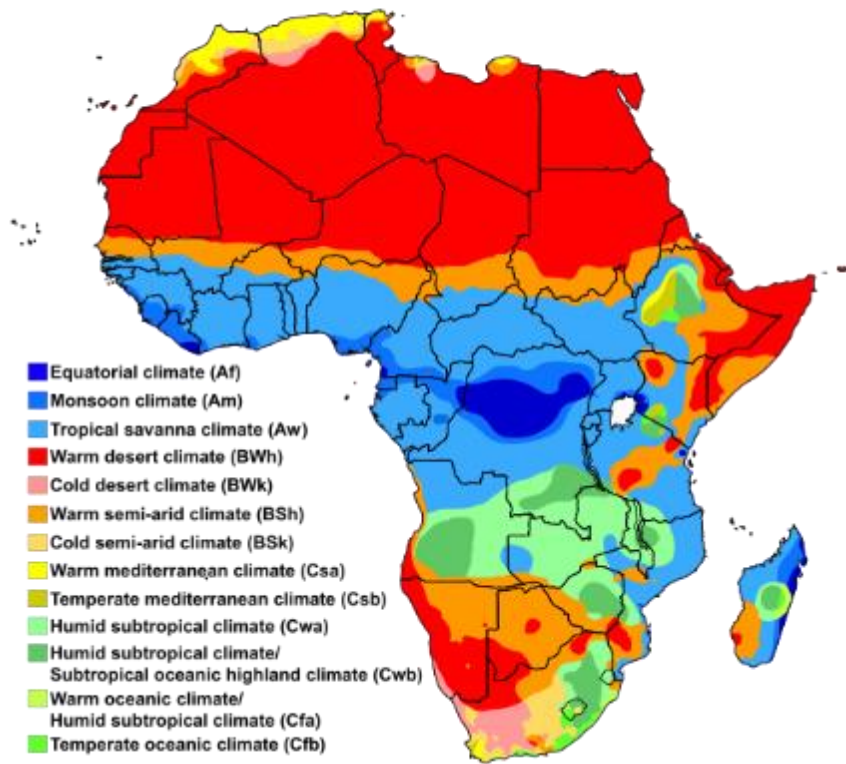


2
3
4
5
6
7
8
9
10
11
12
13

Figure Atlas.20: Projected changes in the number of days per year in which the maximum temperature exceeds 35°C from an ensemble of nine CMIP5 GCMs (the ensemble mean is considered in all cases). The top/bottom rows correspond to a future mid-term period 2046–2065 (compared to 1986–2005) under the RCP4.5/8.5 emissions scenarios respectively considering the raw model data (left column) and bias corrected (EQM method) data (right column). Regions are stippled where less than six out of the nine models do not agree on the sign of the change (noting that this assessment does not take into account whether the individual models’ projected changes are significant). [The Interactive Atlas shows the results for two alternative bias correction methods; see Annex VII for more details.]

1

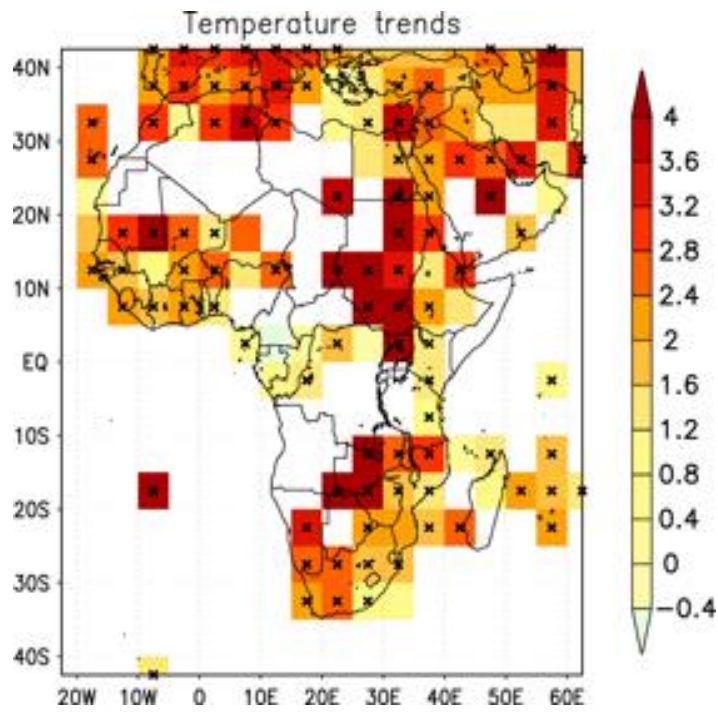
Africa map of Köppen climate classification



2
3
4
5

Figure Atlas.21: Köppen-Geiger climate type map of Africa (Peel et al., 2007).

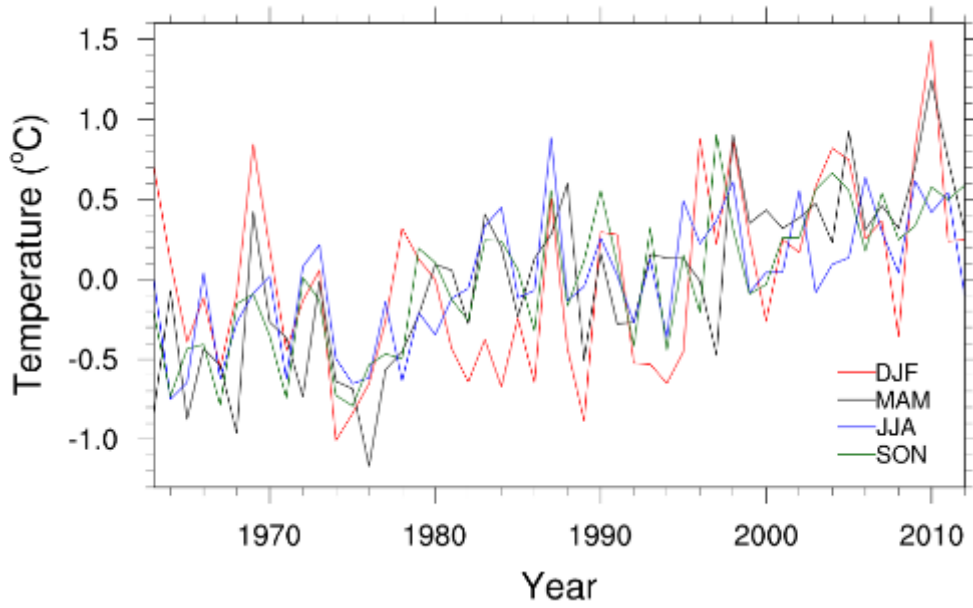
1



2
3
4
5
6
7
8
9

Figure Atlas.22: Observed trends in annual-average near-surface temperatures ($^{\circ}\text{C}/\text{century}$) over Africa for the period 1961–2010, calculated using the method of pairwise-slopes applied to the 5° longitude \times 5° latitude gridded CRUTEM4v data of CRU. The grid boxes where the trends are statistically significant according to the Spearman rank correlation test are indicated by crosses (Engelbrecht et al., 2015)

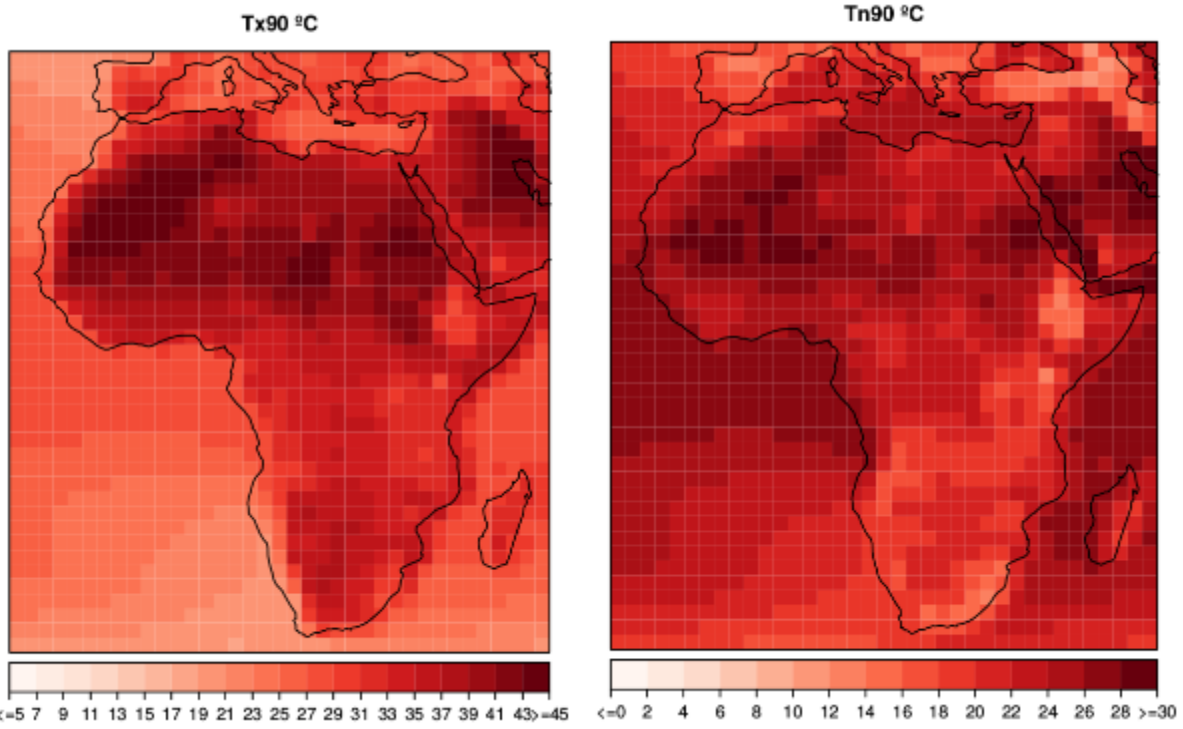
1



2
3
4
5
6

Figure Atlas.23: Time series of West Africa land area averaged seasonal temperature anomalies between 1963 and 2012. Data taken from CRU TS3.22 dataset (Daron, 2014a)

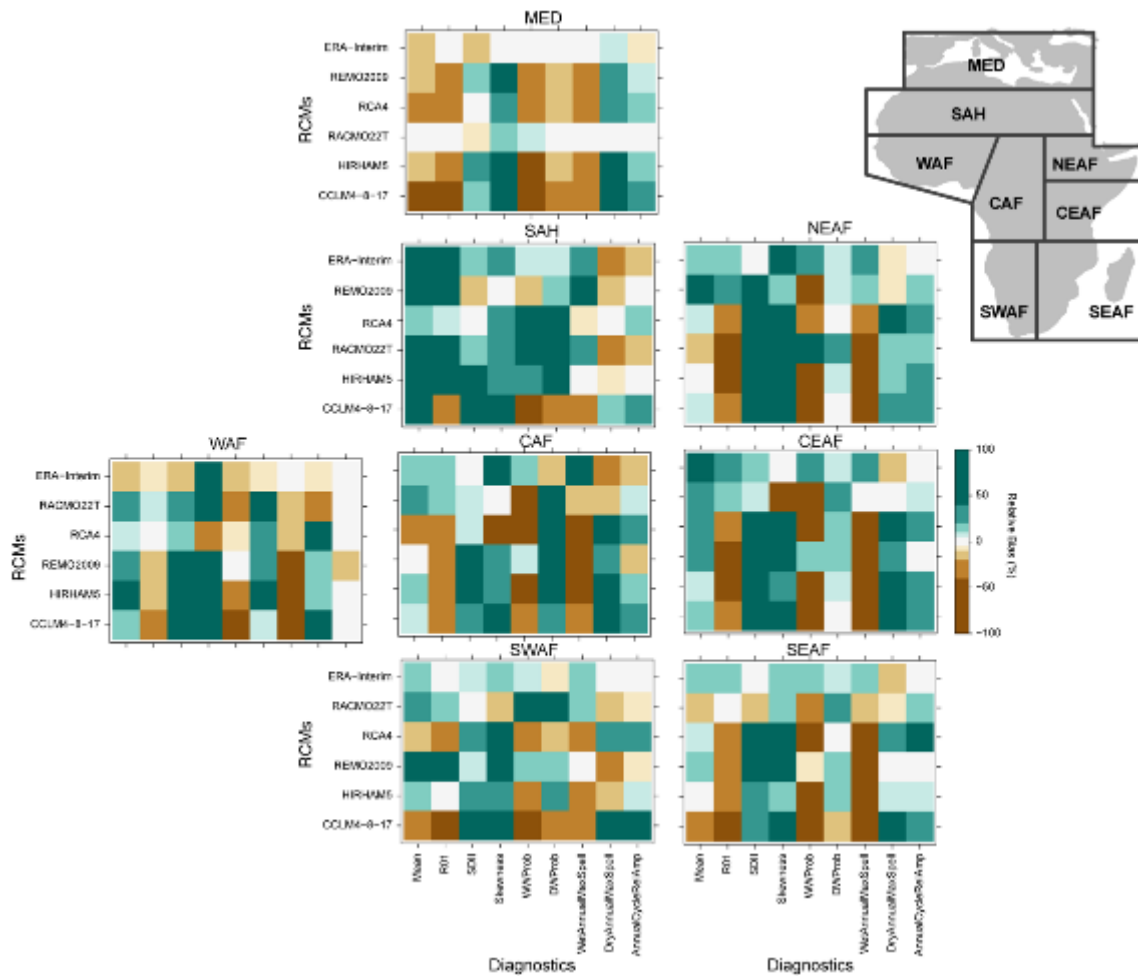
1



2
3
4
5
6

Figure Atlas.24: 90th percentiles for maximum and minimum temperatures during 1986-2005 from EWEMBI, the reference dataset for ISI-MIP, which is a calibrated version of ERA-Interim (Engelbrecht et al., 2015)

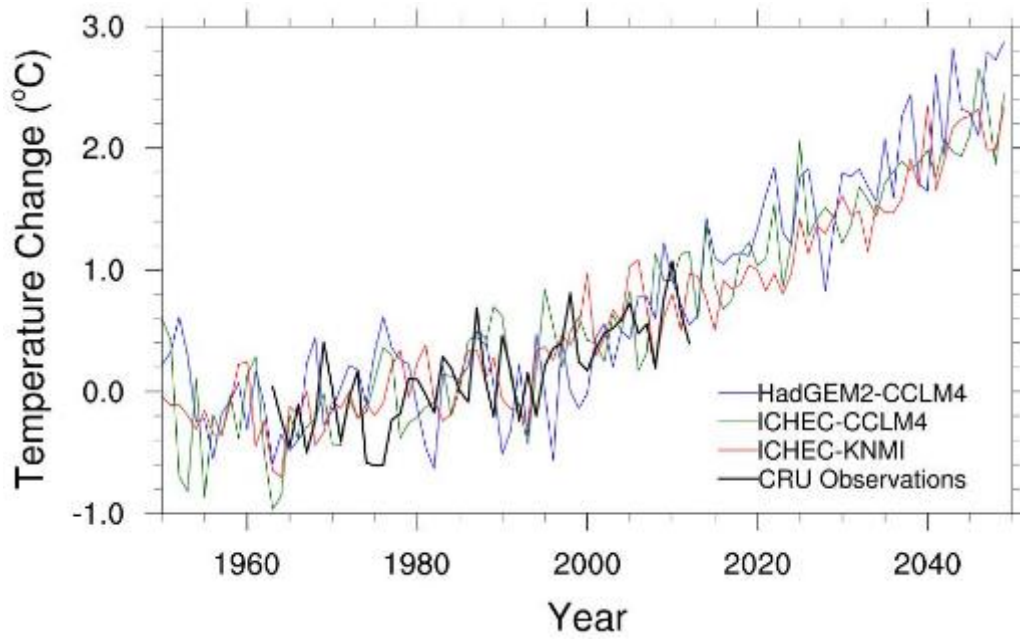
1



2
3
4
5
6
7
8
9

Figure Atlas.25: Evaluation of precipitation-based indices for five RCMs driven by ERA-Interim (rows 2-6), in terms of relative bias with respect to the observational reference (EWEMBI) over the eight AR6 African regions. For comparison purposes, results are also shown for the driving dataset, ERA-Interim (first row). Section **Atlas.3.4** provides details about the RCMs, observations and indices used.

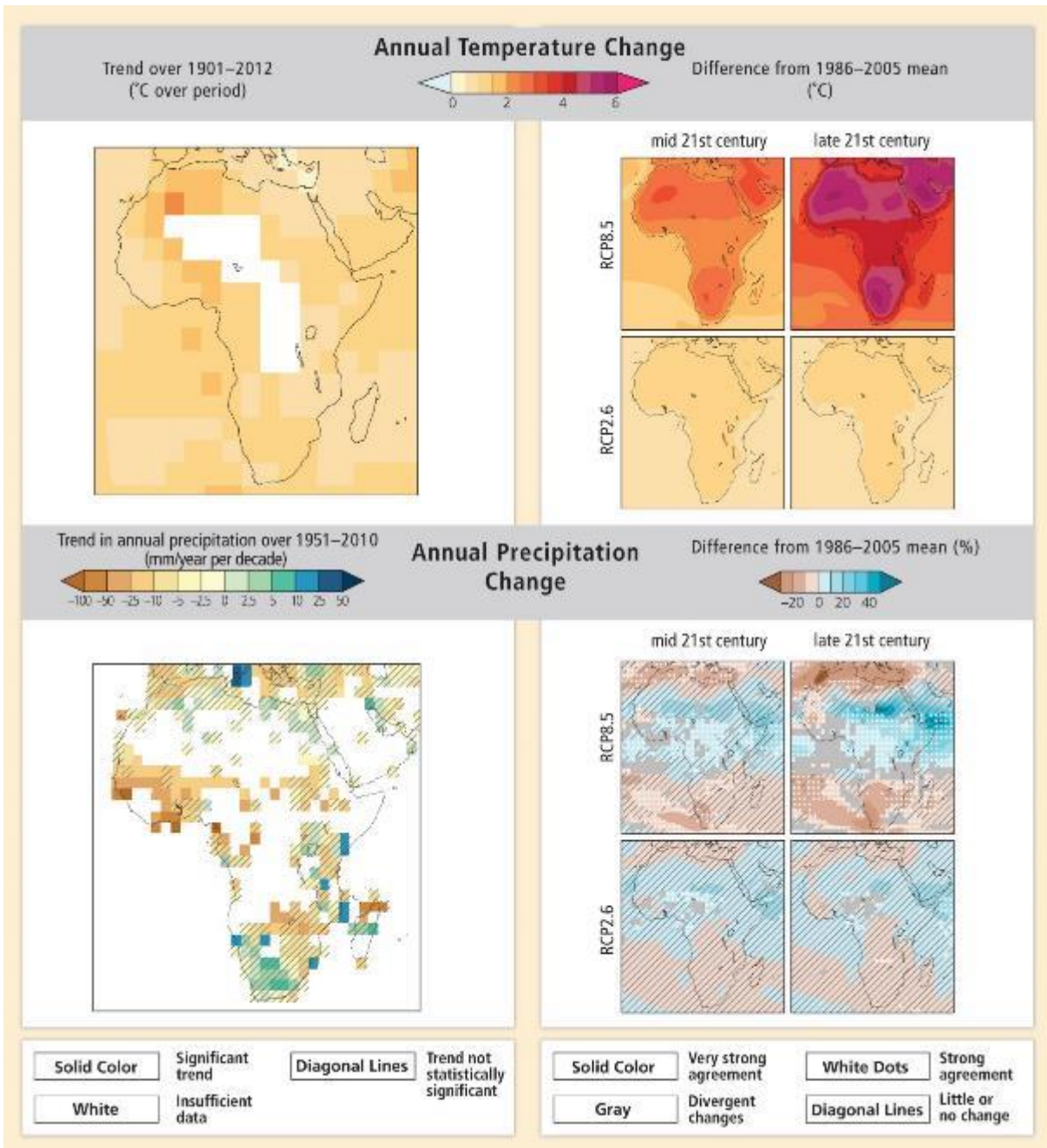
1



2
3
4
5
6
7
8
9

Figure Atlas.26: Time series of the change in West Africa annual average temperatures from three CORDEX models analysed (see the legend). The model changes are relative to the average of the models from 1963 to 2000, while the CRU TS3.22 observational data (from 1963 to 2012) are relative to the observed 1963 to 2000 average (Daron, 2014a)

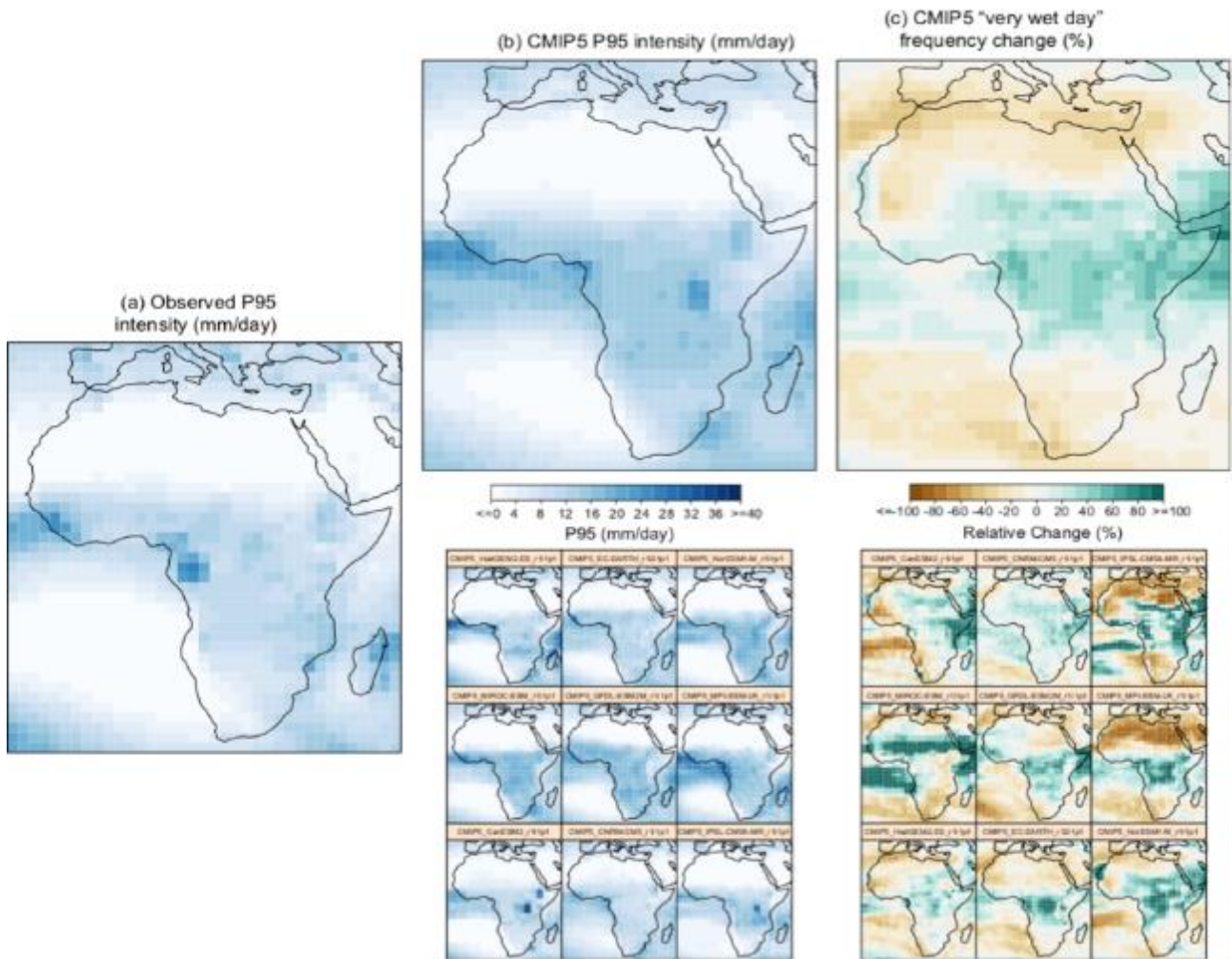
1



2
3
4
5
6
7
8

Figure Atlas.27: Observed and projected temperature and precipitation change in Africa (from the AR5 WGII Chapter 22 (Africa, Figure 22-1))

1



2
3
4
5
6
7
8
9
10

Figure Atlas.28: Daily rainfall amount corresponding to the 95th percentile (P95, in mm/day) defining ‘very wet days’ for (a) the observational reference (EWEMBI) and (b) the CMIP5_subset of nine GCMs, for the reference period 1986–2005. (c) Change in frequency of very wet days for the future 2081–2100 period (RCP8.5) defined as exceeding the historical P95 threshold (results shown as relative change, %). Results are shown model by model in the bottom panels, with the ensemble means shown in the upper panels.

1

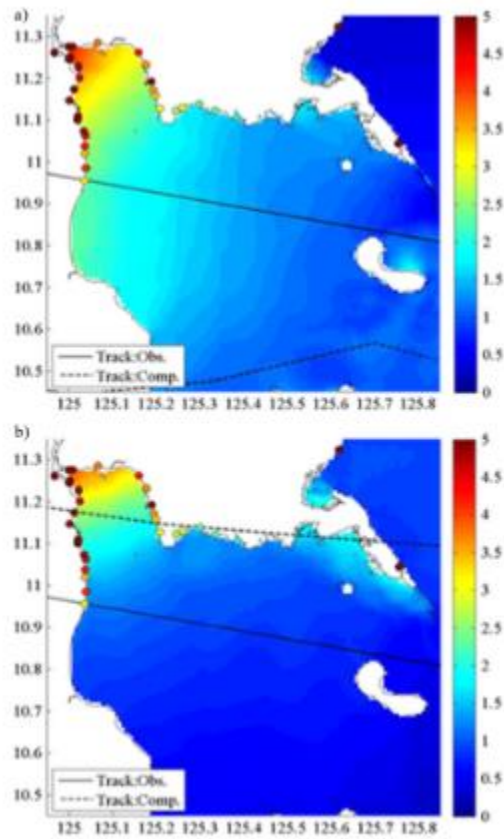
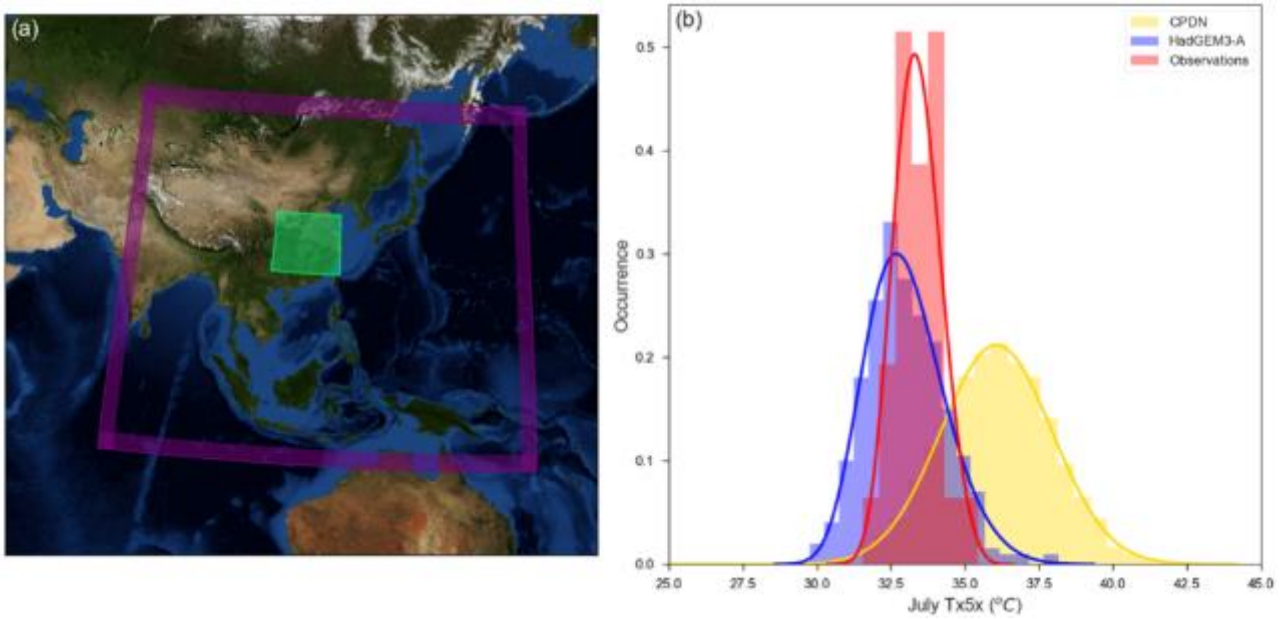


Figure 6. Maximum water surface elevation predicted by using the SuWAT model (domain D3). Results of experiment m02 (1001) in (a) ALL and (b) NAT. The coloured dots around the coastline show inundation data obtained by a field survey.

2
3
4
5
6
7

Figure Atlas.29: Maximum surface water elevation from storm surge simulations driven by Supertyphoon Haiyan in a hypothetical natural climate without anthropogenic influence (top) compared to in the current climate (bottom). The coloured dots show inundation data collected by a field study. (Takayabu et al., 2015).

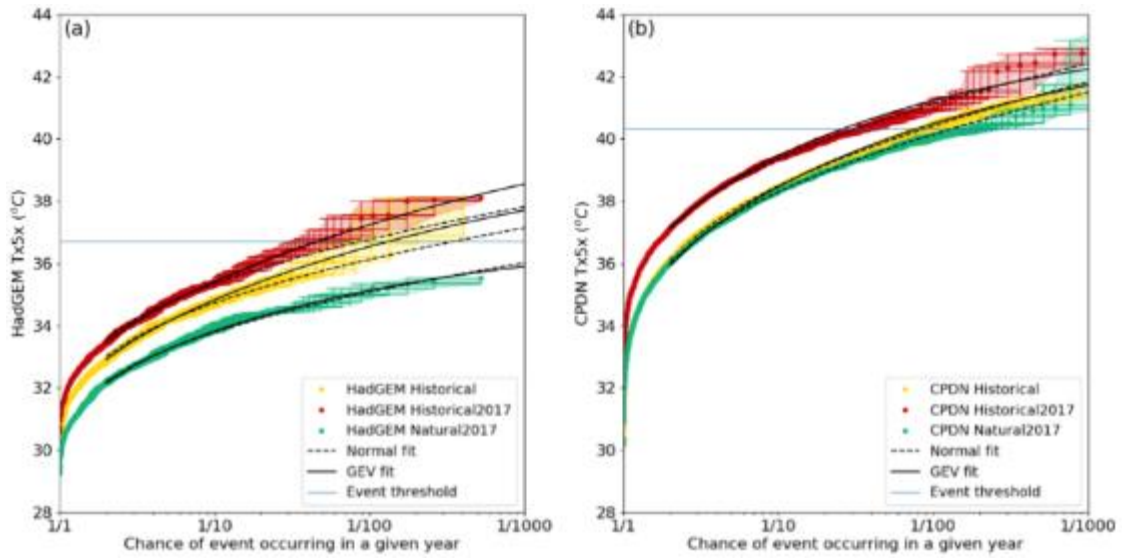
1



2
3
4
5
6
7
8
9
10

Figure Atlas.30: (a) Weather@home East Asia 50-km regional boundary (purple, with shading indicating the regional model sponge layer). The study area for the analysis is shown in green. (b) Distributions of the fractional occurrence of July Tx5x for 1987–2013 from the station data observations (Li et al., 2016) (red), HadGEM3-GA6 (blue) and weather@home (yellow). For the observations and HadGEM3-GA6 a GEV fit is shown. For weather@home a normal fit is shown

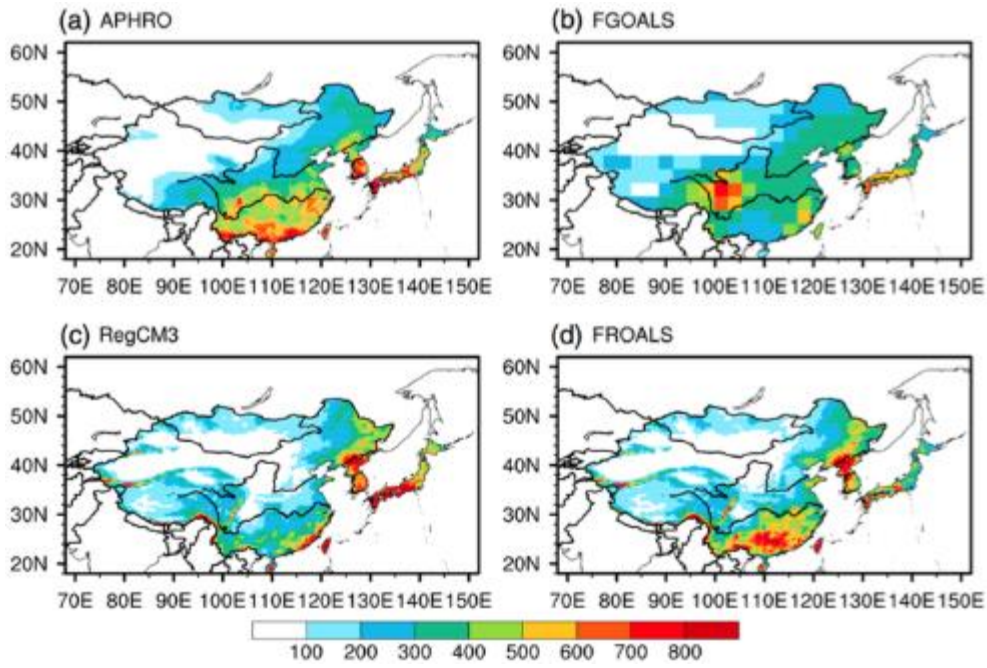
1



2
3
4
5
6
7
8
9

Figure Atlas.31: Return times from Historical (yellow), Historical2017 (red) and Natural2017 (green) simulations for Tx5x from (a) HadGEM3-GA6 and (b) CPDN weather@home ensemble. Both normal (dashed black) and GEV (solid black) fits are shown with the exception of ‘CPDN Historical’ where the GEV fit is poor and thus omitted from the figure.

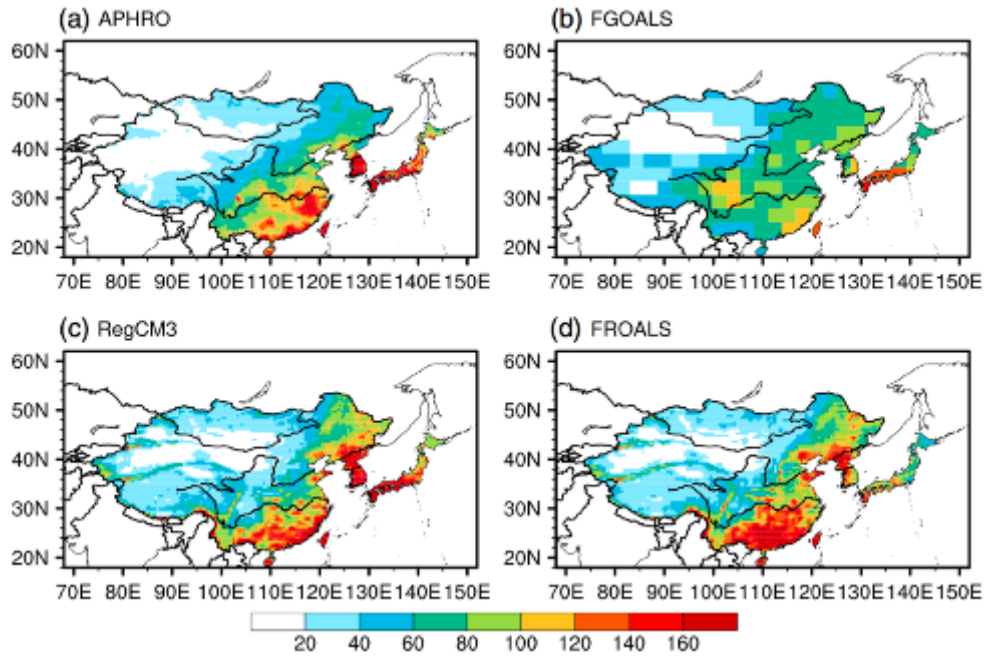
1



2
3
4
5
6
7
8

Figure Atlas.32: The spatial distribution of the JJA total rainfall (shading) averaged over 1981–2005 derived from (a) the APHRO data set, (b) the FGOALS model (GCM), (c) the RegCM3, and (d) the FROALS model. Figure from Zou et al. (2016).

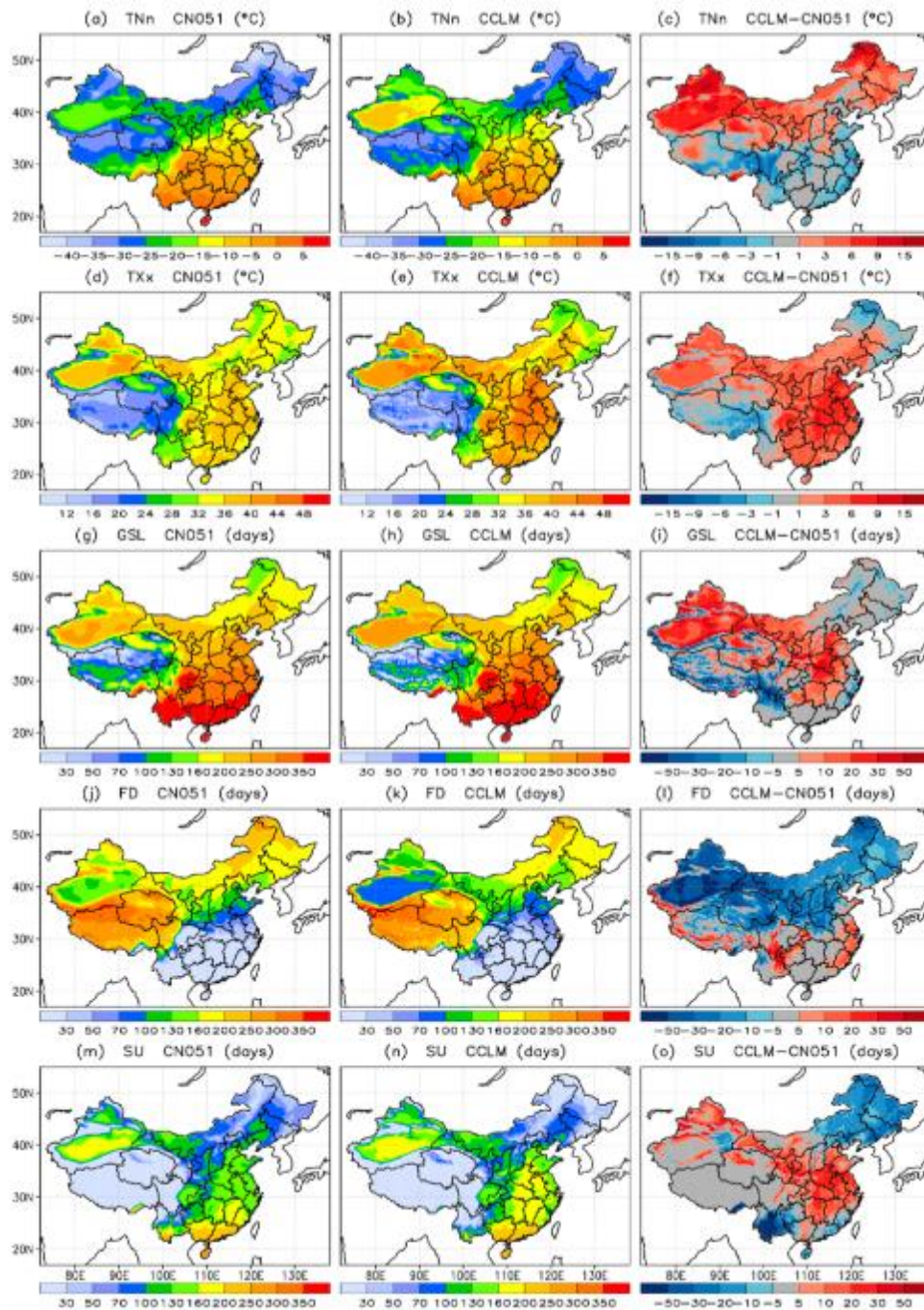
1



2
3
4
5
6

Figure Atlas.33: As in Figure Atlas.32: but for the maximum consecutive 5-day precipitation (R5d). Figure from Zou et al. (2016).

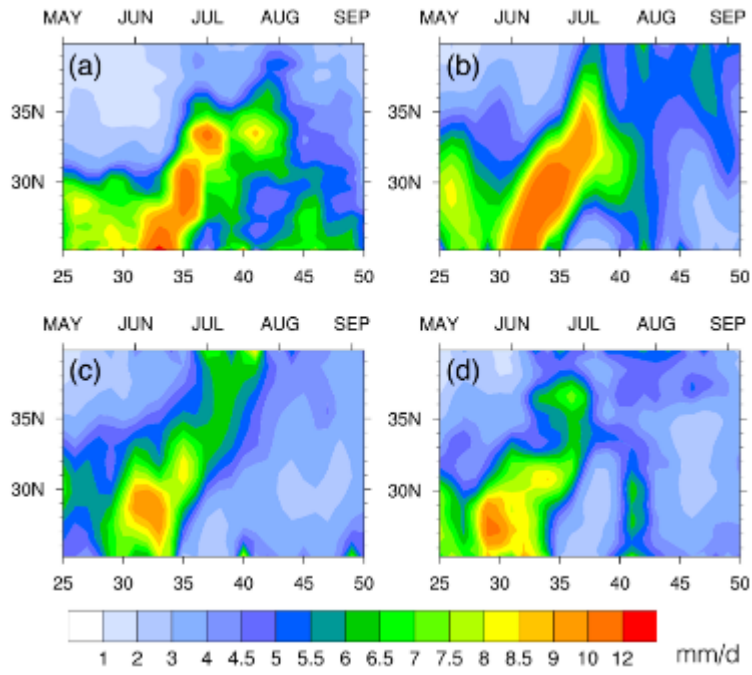
1



2
3
4
5
6
7
8
9
10

Figure Atlas.34: Extreme temperature indices for the period 1989–2010, as given by the CN051 observations (left column), the CCLM RCM (middle column), and the corresponding (CCLM-CN051) biases (right column): Tn (minimum daily Tmin), Tx (maximum daily Tmax), GSL (annual count between first span of mean temperature > 5°C and first span after < 5°C), FD (annual count when the daily minimum temperature < 0°C), and SU (annual count when daily maximum temperature > 25°C) from top to bottom rows. Figure from Zhou et al. (2016b)

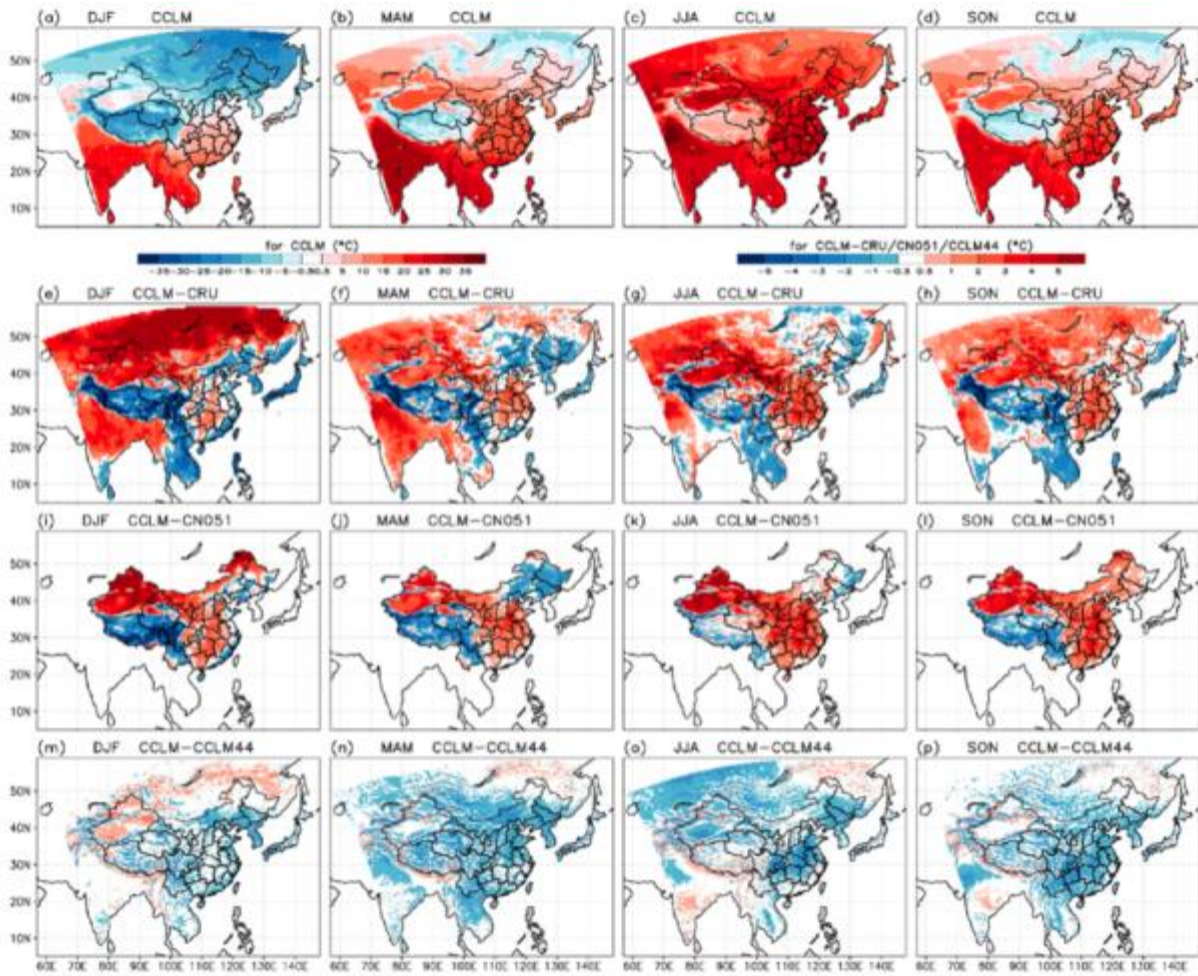
1



2
3
4
5
6
7
8

Figure Atlas.35: Time-latitude cross section of precipitation averaged between 110°E and 120°E from (a) TRMM observed estimates and simulated by CAM5 at (b) T42, (c) T106, and (d) T266. The bottom x axis represents the pentad number. Figure from Li et al. (2015).

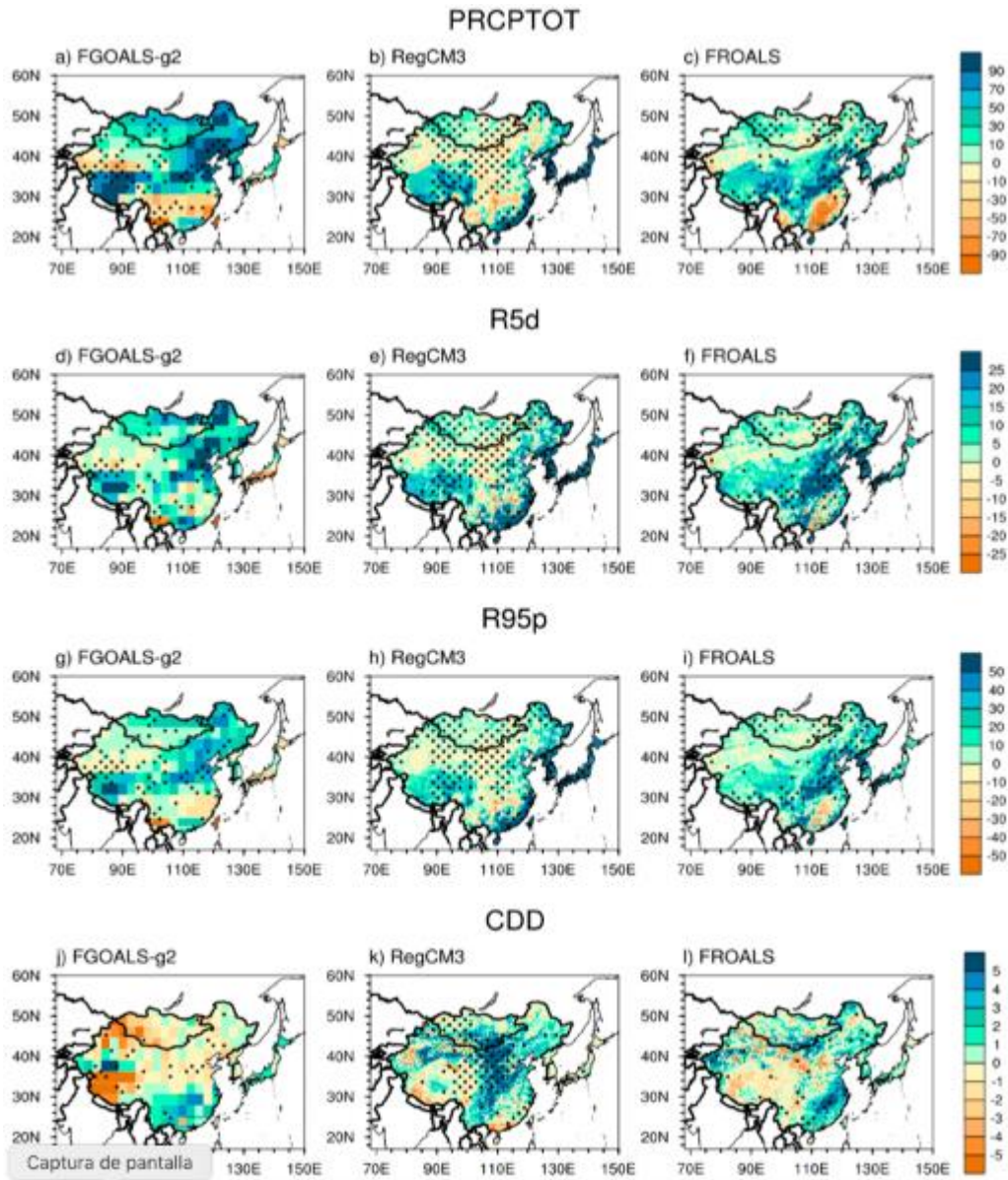
1



2
3
4
5
6
7
8
9
10

Figure Atlas.36: Observed and simulated seasonal mean 2-m temperatures for the period 1989–2010, for 0.22 CCLM simulations (CCLM, top row), CCLM bias against CRU (CCLM-CRU, second row), CCLM bias against CN051 (CCLM-CN051, third row) and 0.22 CCLM simulations difference against 0.44 CCLM simulations (CCLM-CCLM44, bottom row). The columns from left to right are for winter (DJF), spring (MAM), summer (JJA), and autumn (SON). Figure from Zhou et al. (2016b).

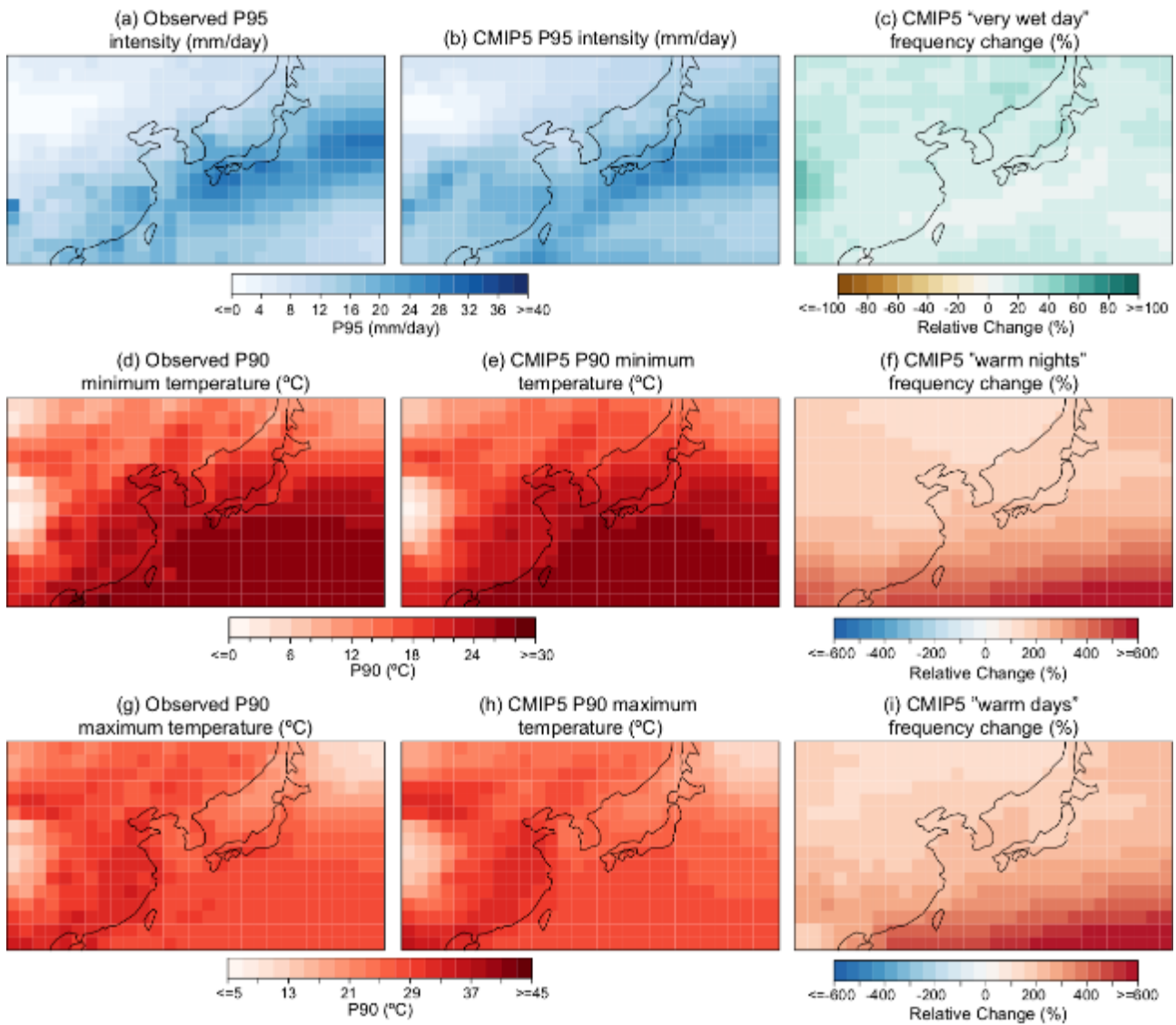
1



2
3
4
5
6
7
8
9
10
11

Figure Atlas.37: Spatial distributions of the projected changes to the June-July-August (JJA) mean total rainfall (PRCPTOT, mm), extreme rainfall amount indices (R5d and R95p, mm) and maximum number of consecutive dry days (CDDs, day) for the period of 2051–2070 under the RCP 8.5 scenario relative to the period of 1986–2005. Results for FGOALS-g2, RegCM3 and FROALS are shown in the left, middle and right column, respectively. Dotted areas are statistically significant at the 5% level, according to Student's t test. Figure from Zou and Zhou (2016)

1



2

3

Figure Atlas.38: (a-c) Daily rainfall amount corresponding to the 95th percentile (P95, in mm/day) defining 'very wet days' for (a) the observational reference (EWEMBI) and (b) the CMIP5_subset (ensemble mean of nine GCMs), for the reference period 1986–2005. (c) Change in frequency of very wet days for the future 2081–2100 period (RCP8.5) defined as exceeding the historical P95 threshold (results shown as relative change, %). Similar results in (d–f) and (g–i) for absolute daily minimum and maximum temperature amounts corresponding to the 90th percentile (P90, defining 'warm nights' and 'warm days', respectively) and the corresponding changes in frequency for the future 2081–2100 period (RCP8.5) defined as exceeding the historical P90 threshold (results shown as relative change, %). Similar analysis for other indices and scenarios (including warming levels) are available at the Interactive Atlas (<http://ipcc-atlas.ifca.es>)

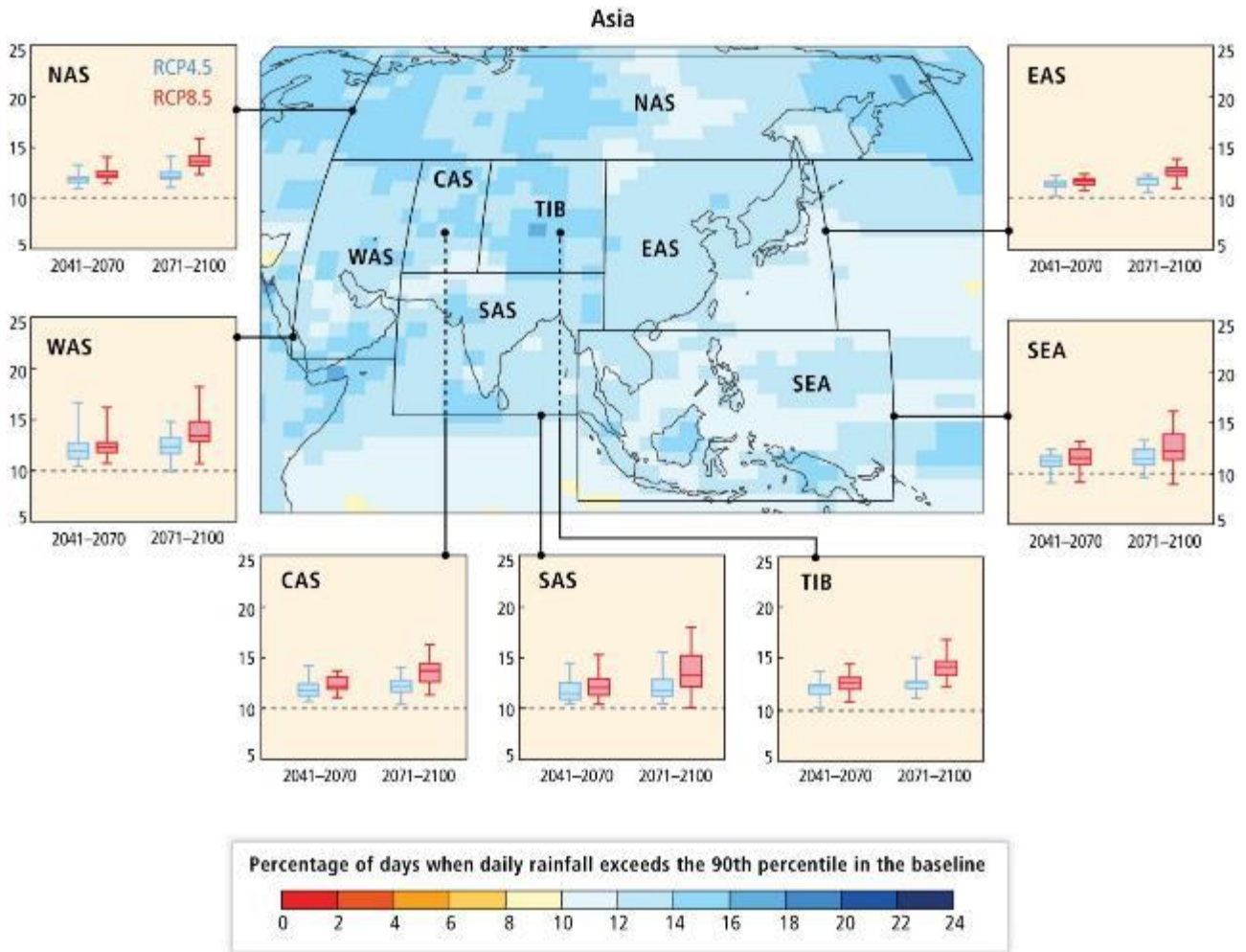
11

12

13

14

1



2
3
4
5
6
7
8

Figure Atlas.39: Projected changes in heavy rainfall days (defined as events above the 90% percentile of daily rainfall in the model baseline simulation) in the CMIP5 ensemble for two future time periods and two emissions scenarios (RCP4.5 and 8.5) relative to a 1961–1990 baseline (Figure 21-8 in the AR5 WGII Chapter 21 Regional Context)

1

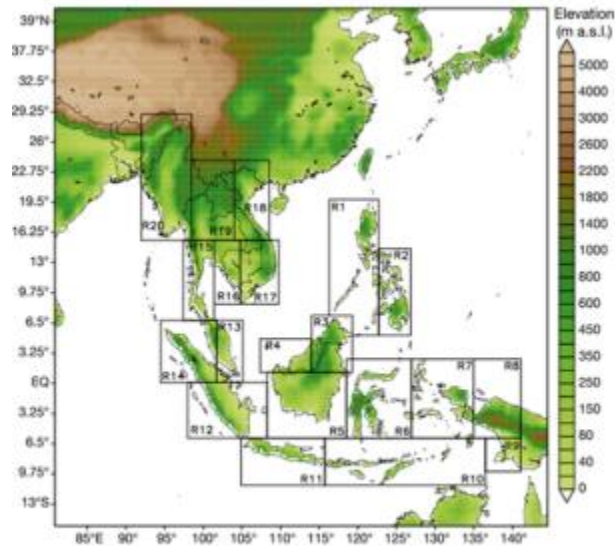
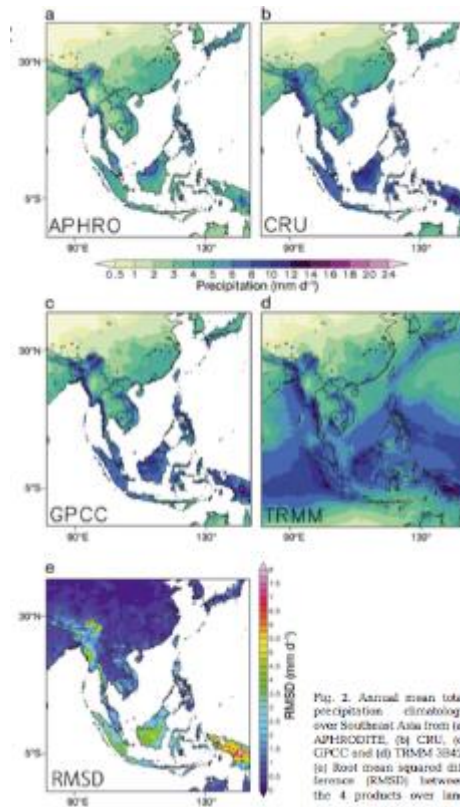


Fig. 1. Simulation domain and topography for the SEACLID/CORDEX-SEA sensitivity test experiments. The boxes indicate the 20 sub-regions used for further regional model performance assessment.

2
3
4
5
6
7

Figure Atlas.41: CORDEX-SEA subregions based on historical rainfall climatology and variability (Juneng et al., 2016)

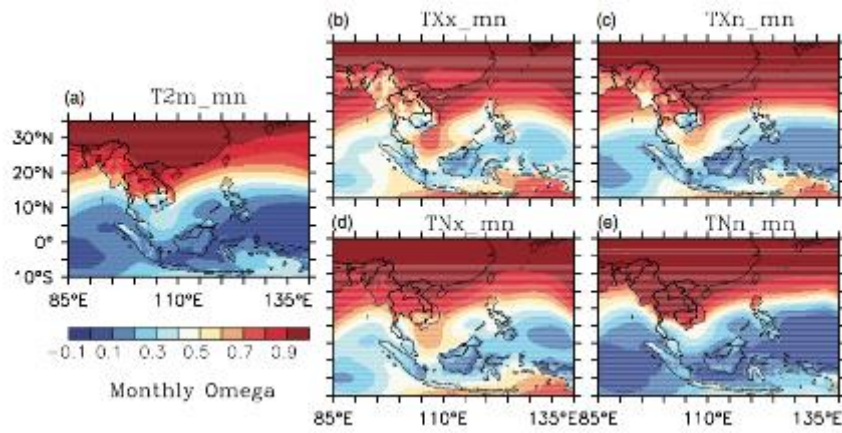
1
2



3
4
5
6
7
8

Figure Atlas.42: [Placeholder: Differences in the precipitation values of the various observation datasets available for Southeast Asia from Juneng et al. (2016). (Note that differences in density, and temporal coverage will also be shown).]

1



2

3

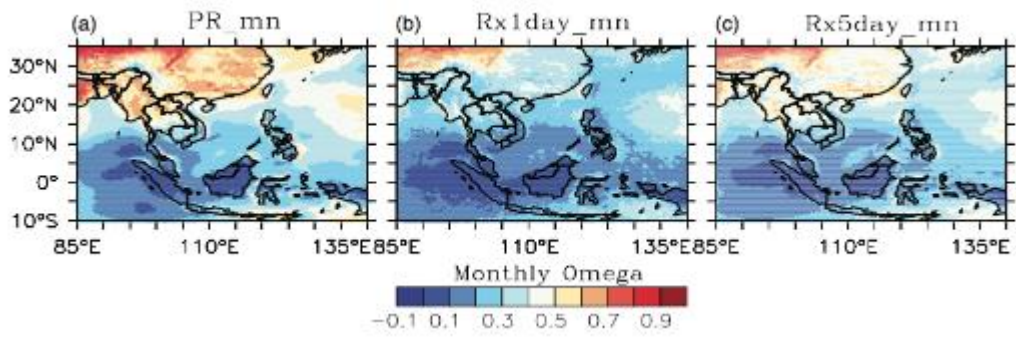
4

Figure Atlas.43: Similarity index omega between the different CORDEX-SEA historical simulations for different temperature-based extreme indices (from Ngo-Duc et al., 2017)

5

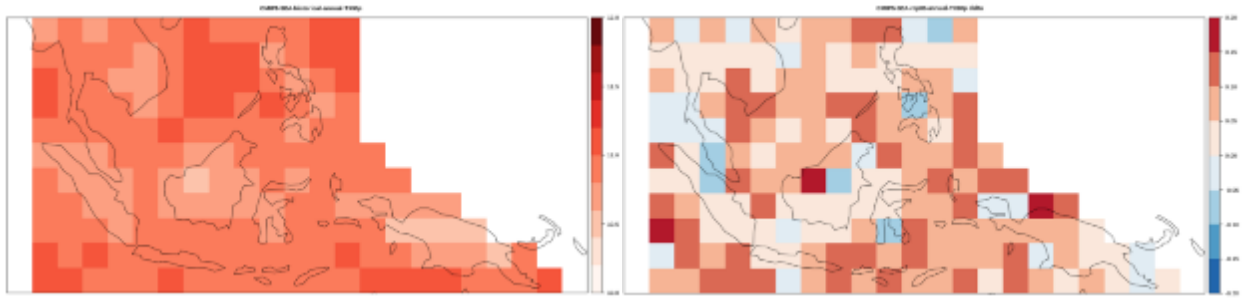
6

7



1
2 **Figure Atlas.44:** The same as Figure Atlas.43: but for precipitation (from Ngo-Duc et al., 2017)
3
4

1



2

3

4

Figure Atlas.45: An ensemble average of the CMIP5 models (available in the Interactive Atlas) for (a) the simulation of the percentage of days when the maximum temperature exceeds 90th percentile values (TX90p) for the historical baseline period (1986–2005) and (b) the projected mid-future (2041–2060) changes, under RCP85, compared to the baseline values. Similar analysis for other indices and scenarios (including warming levels) are available at the Interactive Atlas (<http://ipcc-atlas.ifca.es>).

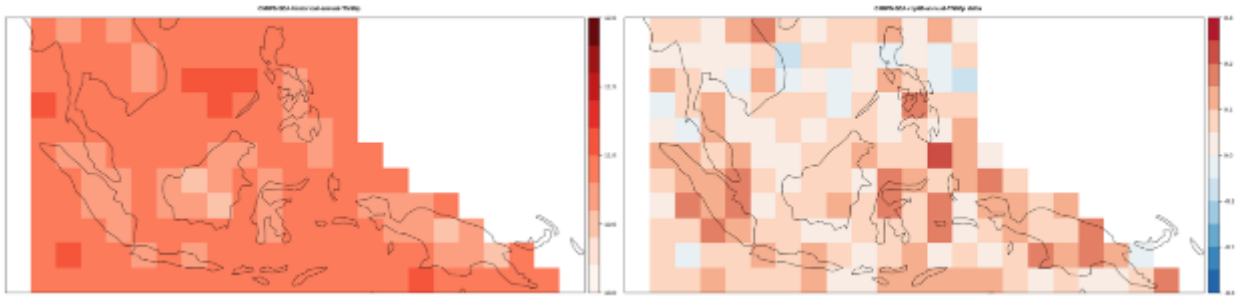
7

8

9

10

1



2

3

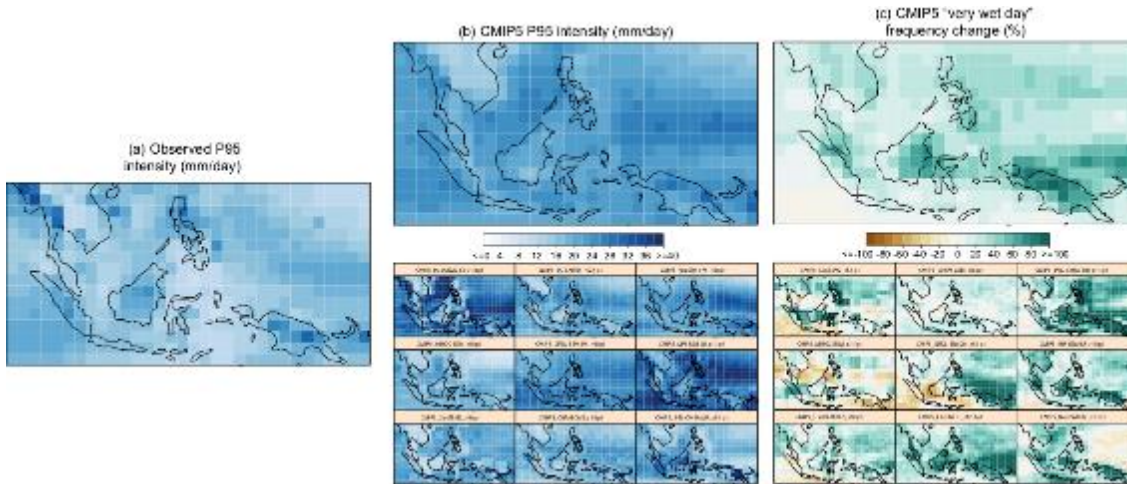
4

5

6

Figure Atlas.46: The same as Figure Atlas.45: but for minimum temperature (TN90p).

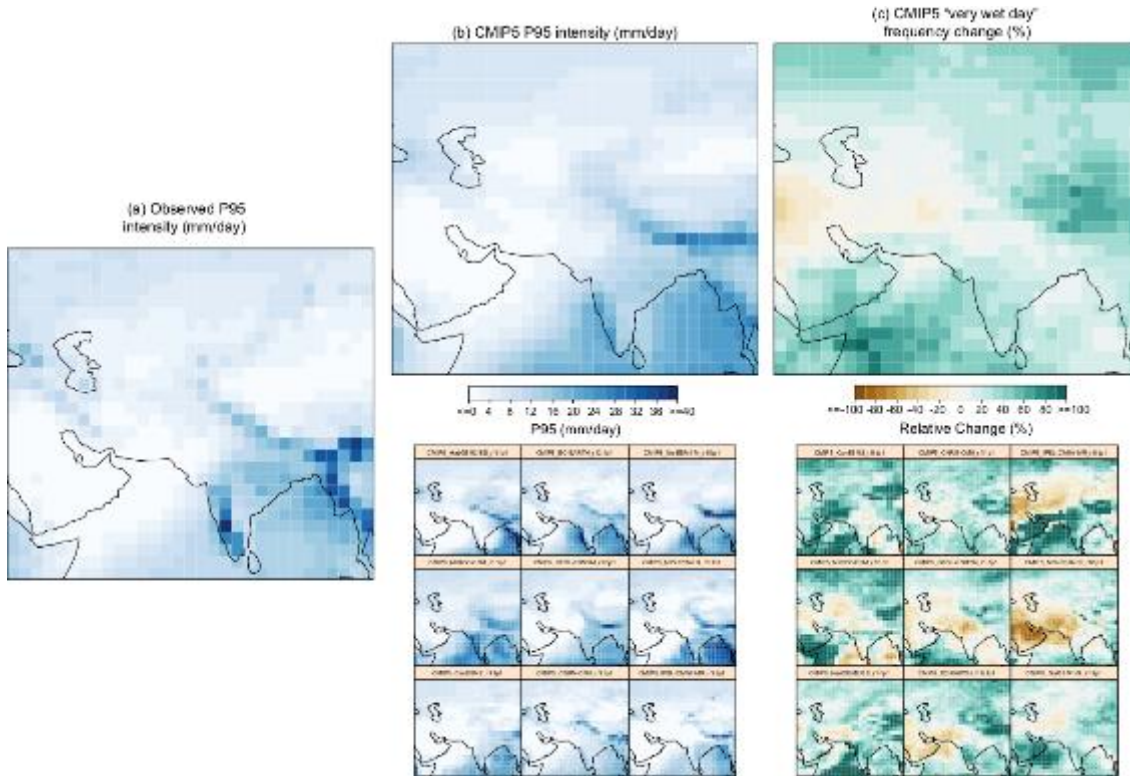
1



2
3
4
5
6
7
8
9
10
11

Figure Atlas.47: Daily rainfall amount corresponding to the 95th percentile (P95, in mm/day) defining “very wet days” for (a) the observational reference (EWEMBI) and (b) the CMIP5_subset, for the reference period 1986–2005. (c) Change in frequency of very wet days for the future 2081–2100 period (RCP8.5) defined as exceeding the historical P95 threshold (results shown as relative change, %). Results are shown model by model in the bottom panels, with the ensemble means shown in the upper panels. Similar analysis for other indices and scenarios (including warming levels) are available at the Interactive Atlas (<http://ipcc-atlas.ifca.es>).

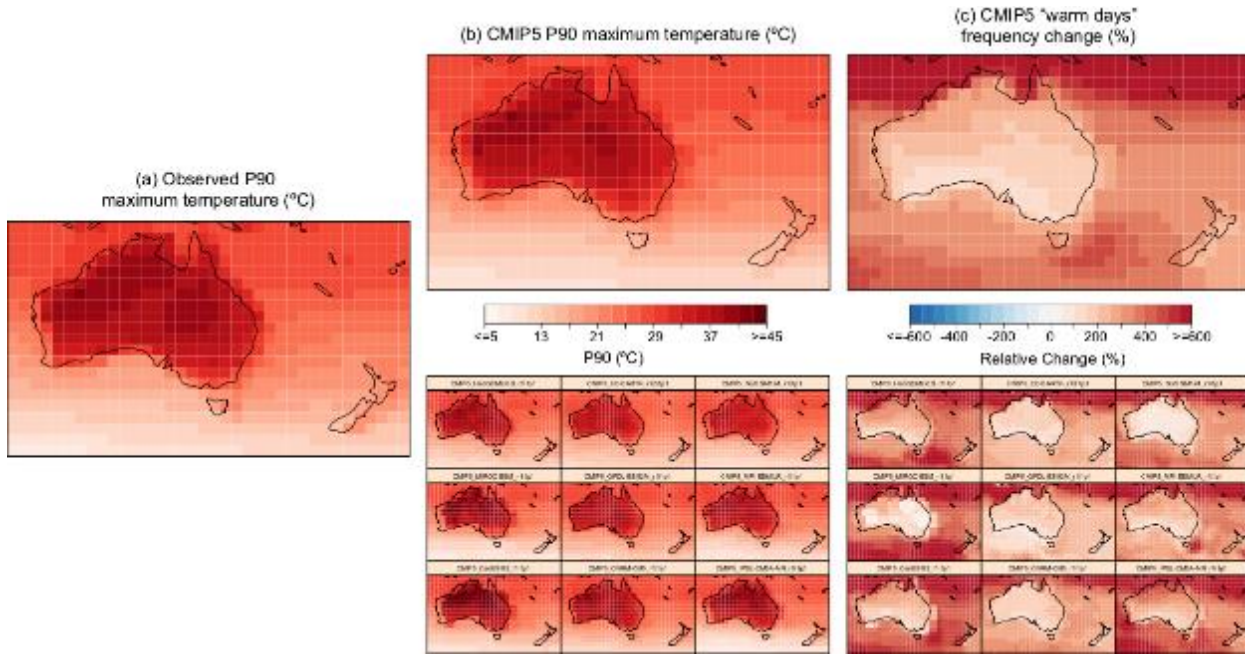
1



2
3
4
5
6
7
8
9
10

Figure Atlas.48: Daily rainfall amount corresponding to the 95th percentile (P95, in mm/day) defining “very wet days” for (a) the observational reference (EWEMBI) and (b) the CMIP5_subset, for the reference period 1986–2005. (c) Change in frequency of very wet days for the future 2081–2100 period (RCP8.5) defined as exceeding the historical P95 threshold (results shown as relative change, %). Results are shown model by model in the bottom panels, with the ensemble means shown in the upper panels. Similar analysis for other indices and scenarios (including warming levels) are available at the Interactive Atlas (<http://ipcc-atlas.ifca.es>)

1



2

3

4

Figure Atlas.49: Absolute daily maximum temperature amount corresponding to the 90th percentile (P90, in °C) defining ‘warm days’ for (a) the observational reference (EWEMBI) and (b) the CMIP5_subset, for the reference period 1986–2005. (c) Change in frequency of warm days for the future 2081–2100 period (RCP8.5) defined as exceeding the historical P90 threshold (results shown as relative change, %). Results are shown model by model in the bottom panels, with the ensemble means shown in the upper panels. Similar analysis for other indices and scenarios (including warming levels) are available at the Interactive Atlas (<http://ipcc-atlas.ifca.es>).

5

6

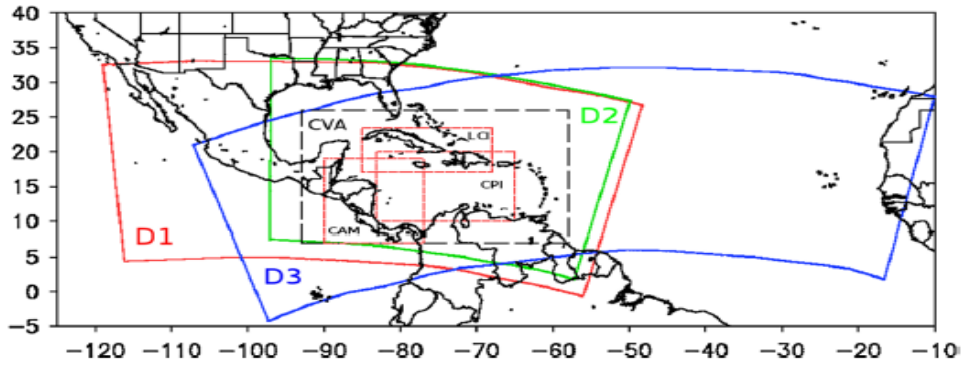
7

8

9

10

1



2

3

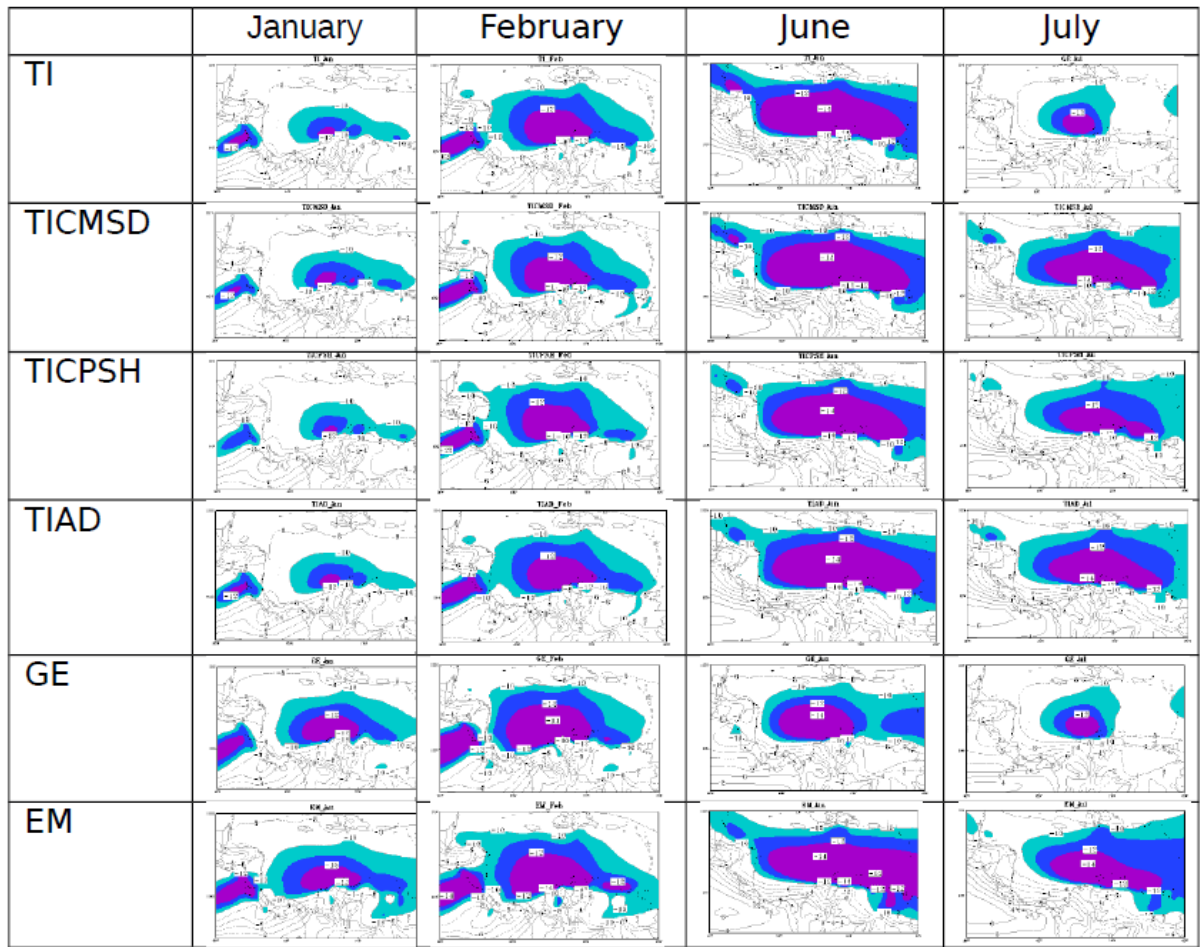
4

5

6

Figure Atlas.50: Domains D1 (red), D2 (green) and D3 (blue), defined in the work of Centella-Artola et al. (2015) excluding the buffer zones.

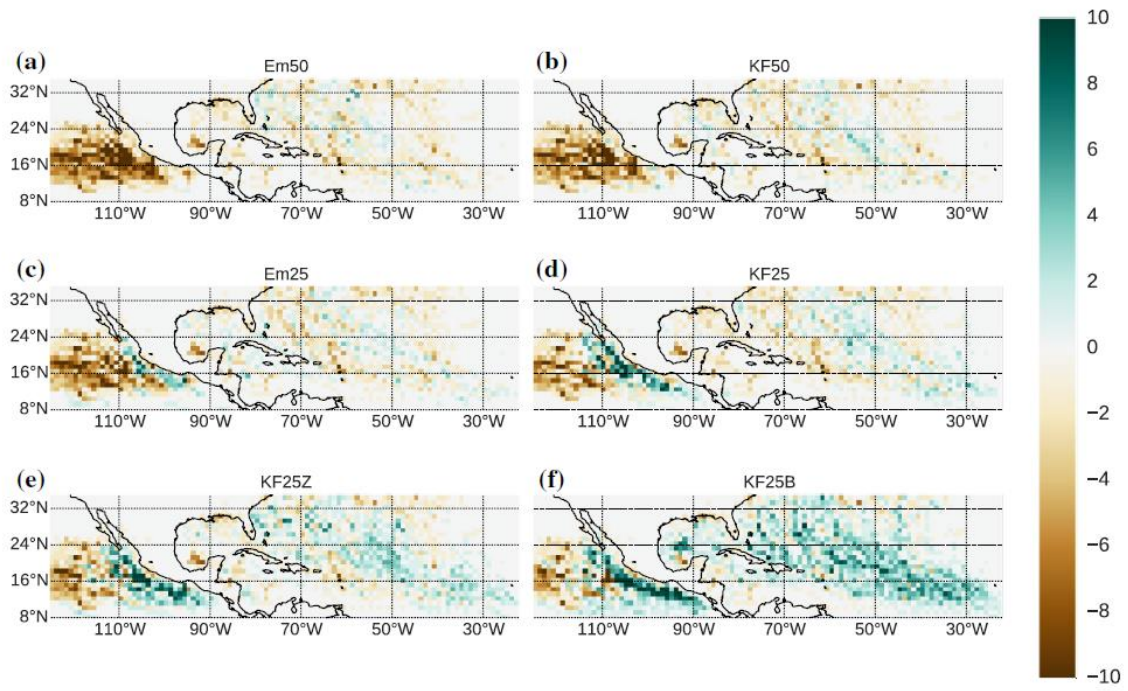
1



2
3
4
5
6
7
8

Figure Atlas.51: Averaged winds for January, February, June and July (in columns) for the different configurations of the model tested in Martínez-Castro et al. (2016) (in rows) for the central region of the Caribbean where the Caribbean low level jet is located. The isotach intervals with more than 10 m/s are shown shaded.

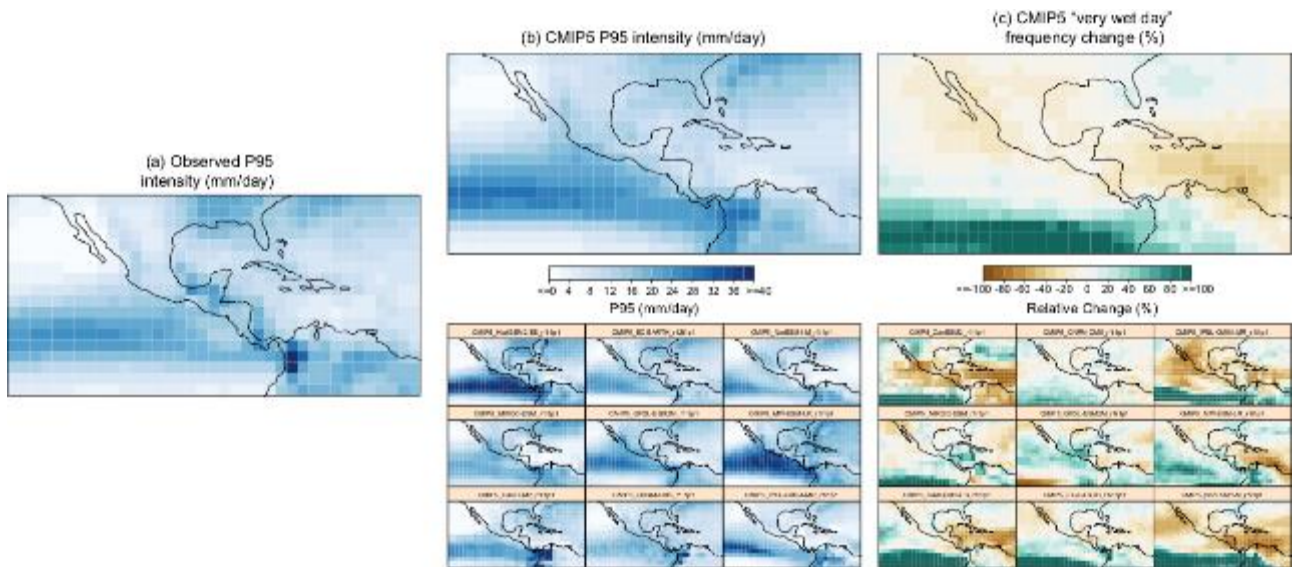
1



2
3
4
5
6

Figure Atlas.52: Biases of the density of trajectories by grid points for the different model configurations used by Fuentes-Franco et al. (2017)

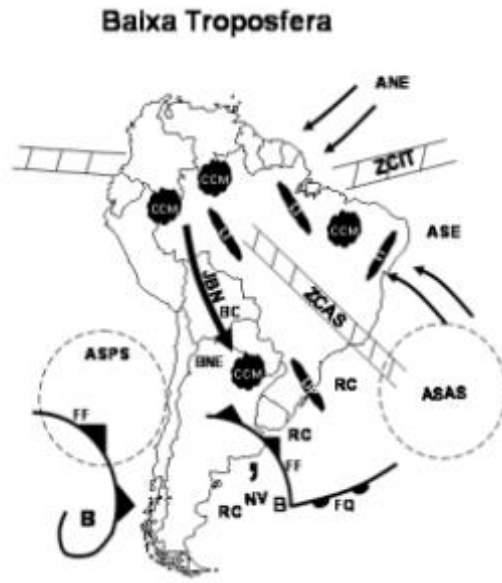
1



2
3
4
5
6
7
8
9
10
11

Figure Atlas.53: Daily rainfall amount corresponding to the 95th percentile (P95, in mm/day) defining ‘very wet days’ for (a) the observational reference (EWEMBI) and (b) the CMIP5 subset, for the reference period 1986–2005. (c) Change in frequency of very wet days for the future 2081–2100 period (RCP8.5) defined as exceeding the historical P95 threshold (results shown as relative change, %). Results are shown model by model in the bottom panels, with the ensemble means shown in the upper panels. Similar analysis for other indices and scenarios (including warming levels) are available at the Interactive Atlas (<http://ipcc-atlas.ifca.es>).

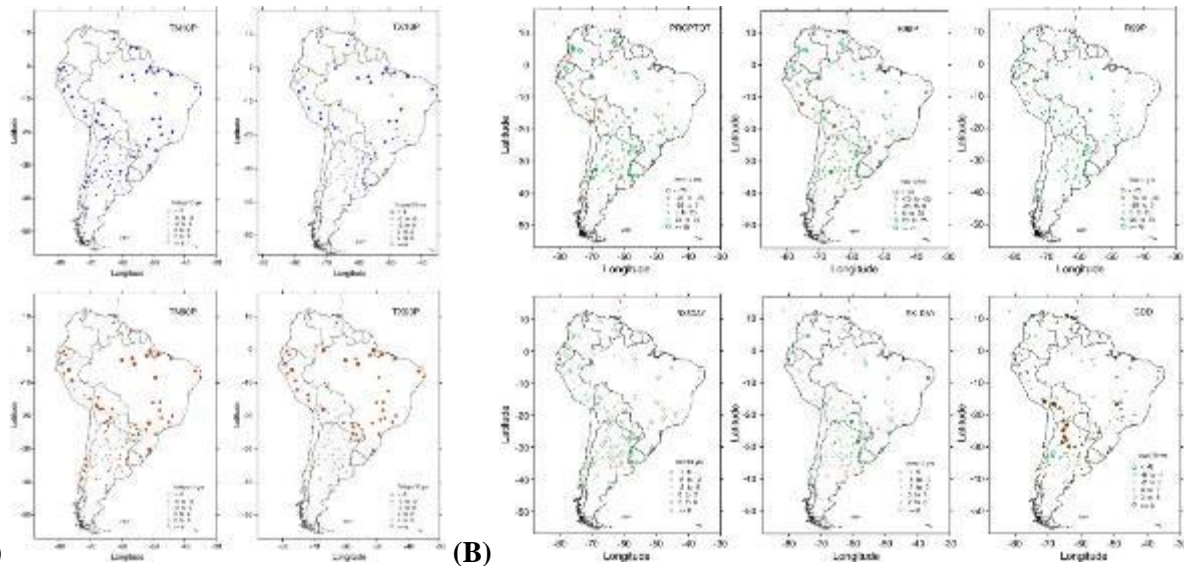
1



2
3
4
5

Figure Atlas.54: Schematic of lower tropospheric systems over South America (Satyamurty et al., 1998).

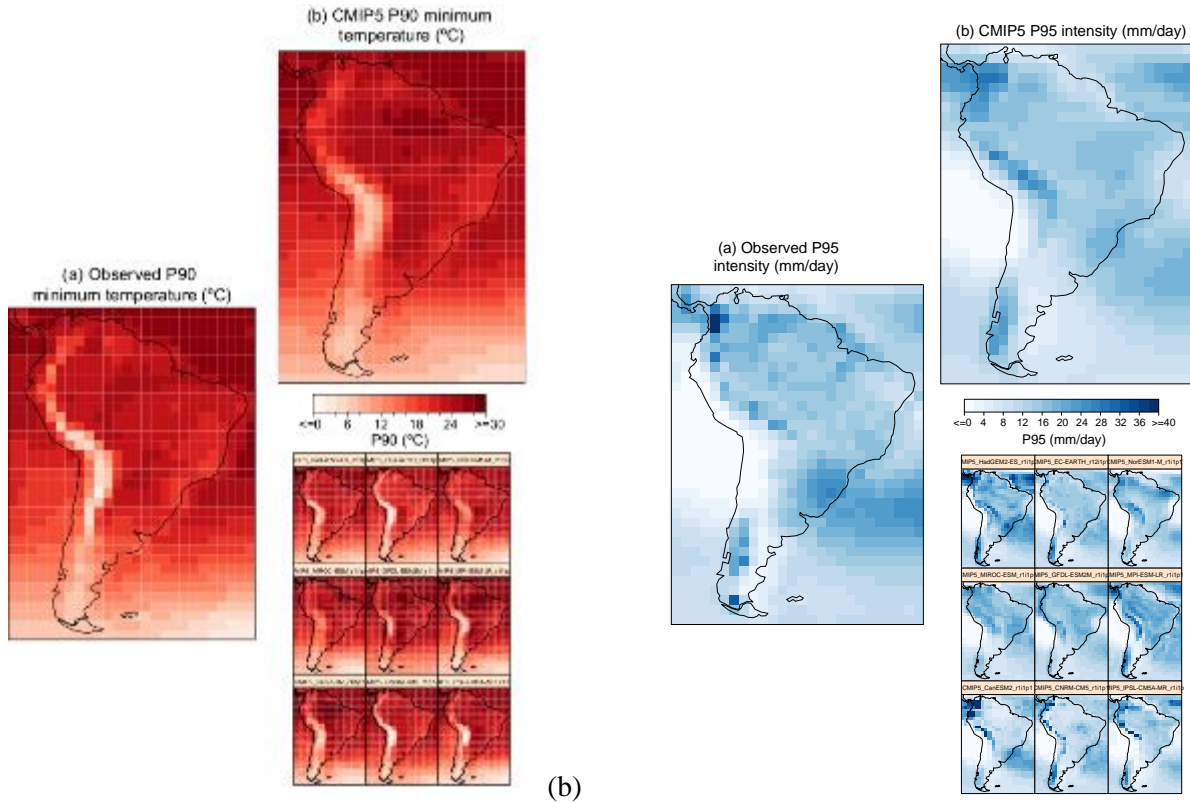
1



2
3
4
5
6
7
8
9
10
11
12

(A) **(B)**
Figure Atlas.55: Local robust trends estimated annually for the 1969–2009 period for (a) cold nights (upper left plot), cold days (upper right panel), warm nights (bottom left panel) and warm days (bottom right panel), all showing warming and (b) for annual total rainfall (upper left panel), very wet days (upper central panel), extremely wet days (upper right panel), annual maximum consecutive 5-day precipitation (bottom left panel), annual maximum 1-day precipitation (bottom central panel) and consecutive dry days (bottom right panel). [Note, here placeholder figure taken from Skansi et al. (2013). To be updated to observational reference dataset (e.g. EWEMBI or other that will be used in the Atlas).]

1



2
3
4
5
6
7
8
9
10
11
12

Figure Atlas.56: (a) Absolute daily minimum temperature amount corresponding to the 90th percentile (P90, in °C) defining ‘warm nights’ for the observational reference (EWEMBI) and the CMIP5_subset, for the reference period 1986–2005; (b) Daily rainfall amount corresponding to the 95th percentile (P95, in mm/day) defining ‘very wet days’ for the observational reference (EWEMBI) and the CMIP5_subset, for the reference period 1986–2005. Results are shown model by model in the bottom panels, with the ensemble means shown in the upper panels. Similar analysis for other indices and scenarios (including warming levels) are available at the Interactive Atlas (<http://ipcc-atlas.ifca.es>)

1

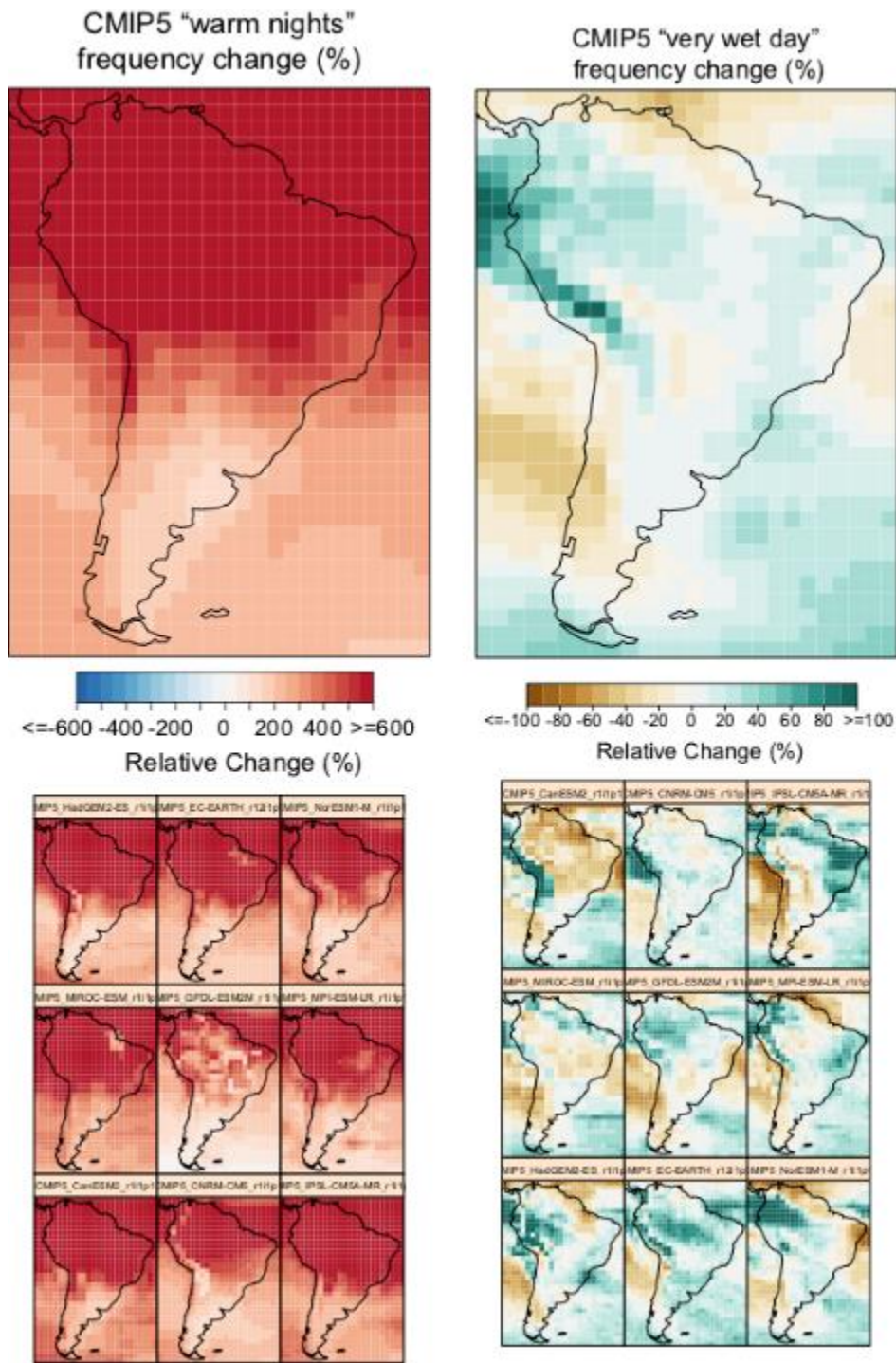
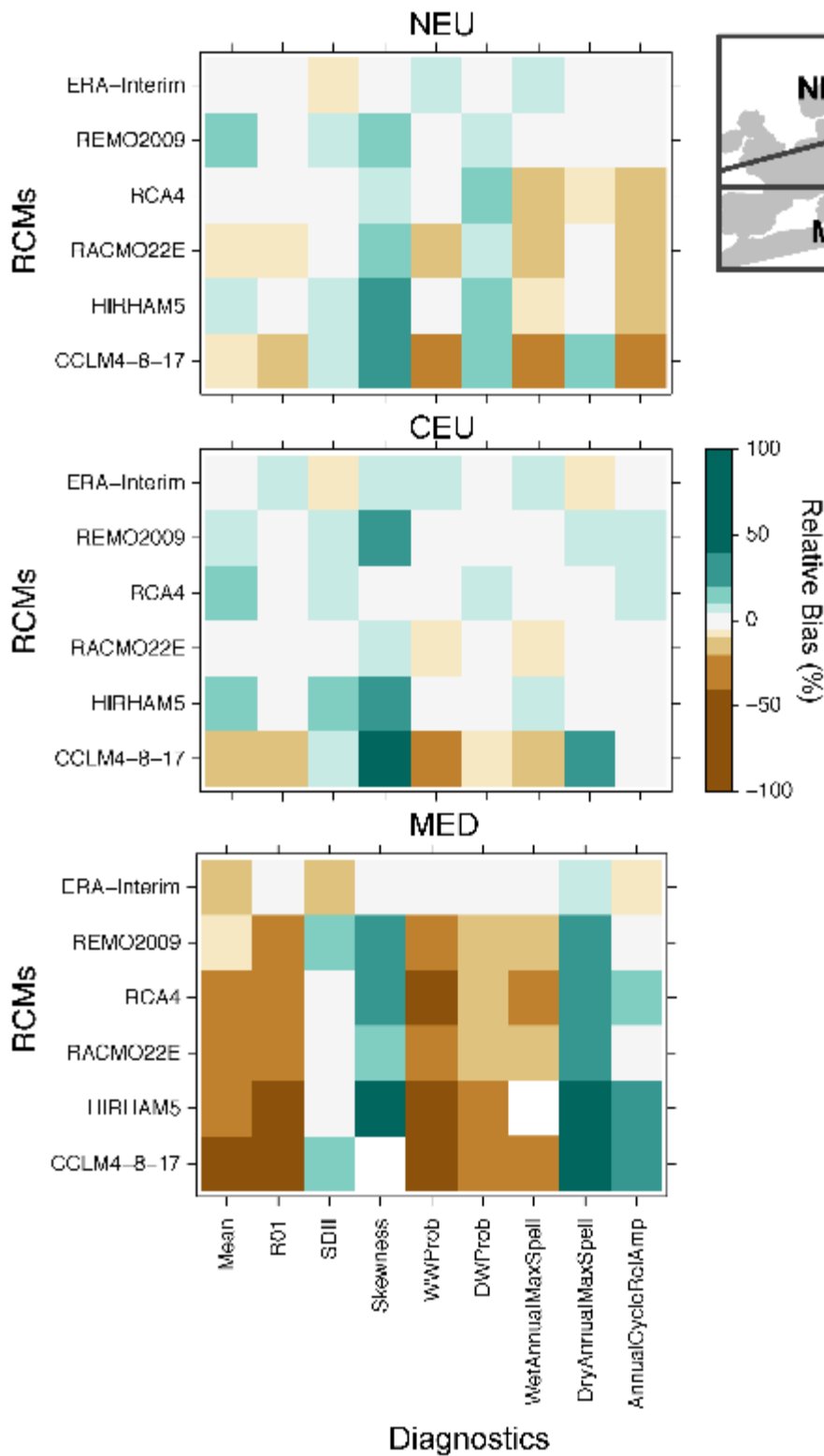


Figure Atlas.57: (Left) Change in frequency of warm nights for the future 2081-2100 period (RCP8.5) defined as exceeding the historical P90 threshold (results shown as relative change, %); (right) Change in frequency of very wet days for the future 2081-2100 period (RCP8.5) defined as exceeding the historical P95 threshold (results shown as relative change, %). Results are shown model by model in the bottom panels, with the ensemble means shown in the upper panels. Similar analysis for other indices and scenarios (including warming levels) are available at the Interactive Atlas (<http://ipcc-atlas.ifca.es>).

2
3
4
5
6
7
8
9
10
11

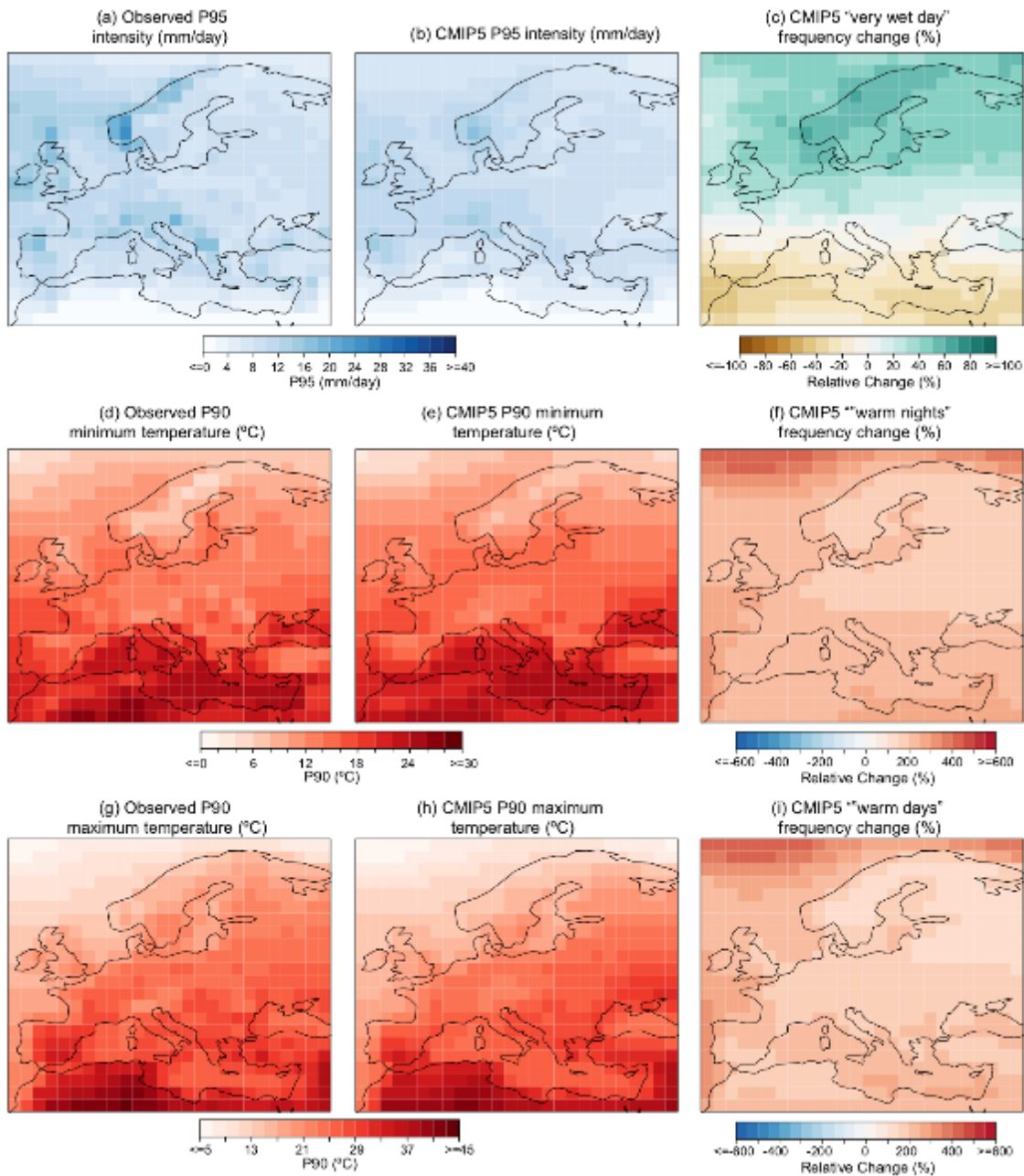
1



2
3
4
5
6
7
8
9

Figure Atlas.58: Evaluation of precipitation-based indices for five RCMs driven by ERA-Interim (rows 2-6), in terms of the relative bias with respect to the observational reference (EWEMBI) for the three European subdomains NEU, CEU and MED. For comparison purposes, results are also shown for the driving dataset, ERA-Interim (first row). See Section Atlas.3 for details on the RCMs, observations and indices used.

1



2
3
4
5
6
7
8
9
10
11
12
13
14
15

Figure Atlas.59: Projected changes in maximum and minimum temperature and extreme precipitation from CMIP5 for the European region, derived from the Interactive Atlas. (a-c) Daily rainfall amount corresponding to the 95th percentile (P95, in mm/day) defining 'very wet days' for (a) the observational reference (EWEMBI) and (b) the CMIP5 subset (ensemble mean), for the reference period 1986–2005. (c) Relative change in frequency of very wet days (days exceeding the P95 threshold) for the future 2081–2100 period (RCP8.5). Similar results in (d–f) and (g–i) for absolute daily minimum and maximum temperature corresponding to the 90th percentile (P90, defining 'warm nights' and 'warm days', respectively) and the corresponding changes in frequency for the 2081–2100 period (RCP8.5). The corresponding results for the EURO-CORDEX dataset, as well as similar analysis for other indices, are available at the Interactive Atlas (<http://ipcc-atlas.ifca.es>).

1

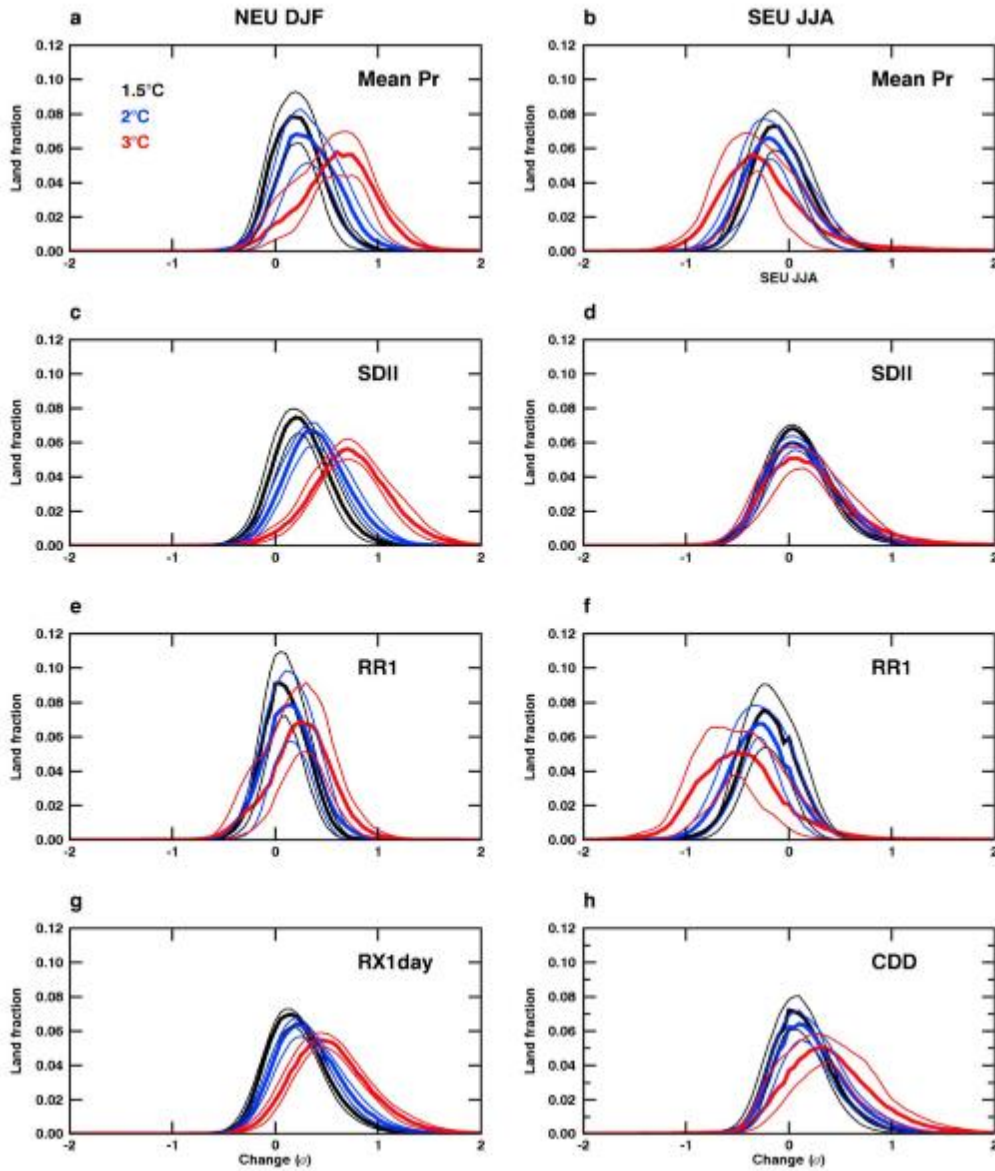
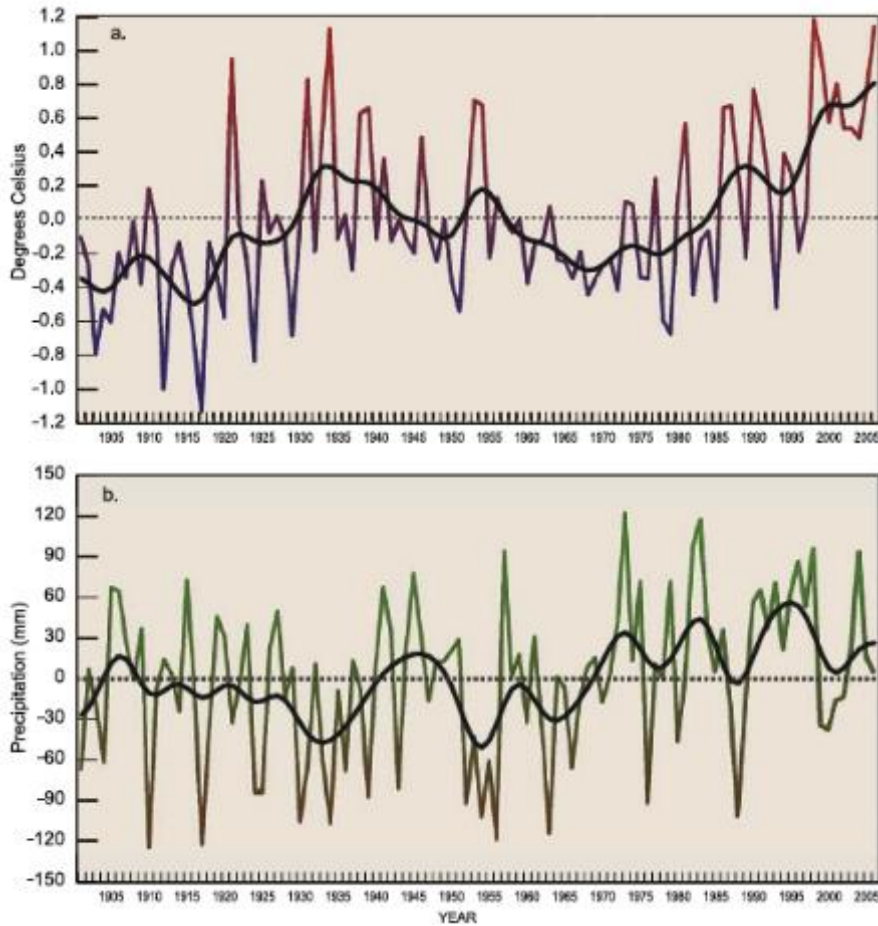


Figure Atlas.60: [Placeholder for analysis to be carried out with the climate4R hub] Probability distribution functions of land fraction experiencing a certain change, compared to the reference period, for some precipitation indices under 1.5°C (black), 2°C (blue), and 3°C (red) of global mean warming, respectively. First column refers to NEU in DJF and second column to SEU in JJA. Results are shown as median (thick lines) and interquartile range (thin lines) of the individual RCMs' probability distribution functions. Units are standard deviation of the 30-year (1981–2010) time series of the index. (From Dosio and Fischer, 2017)

2
3
4
5
6
7
8
9
10

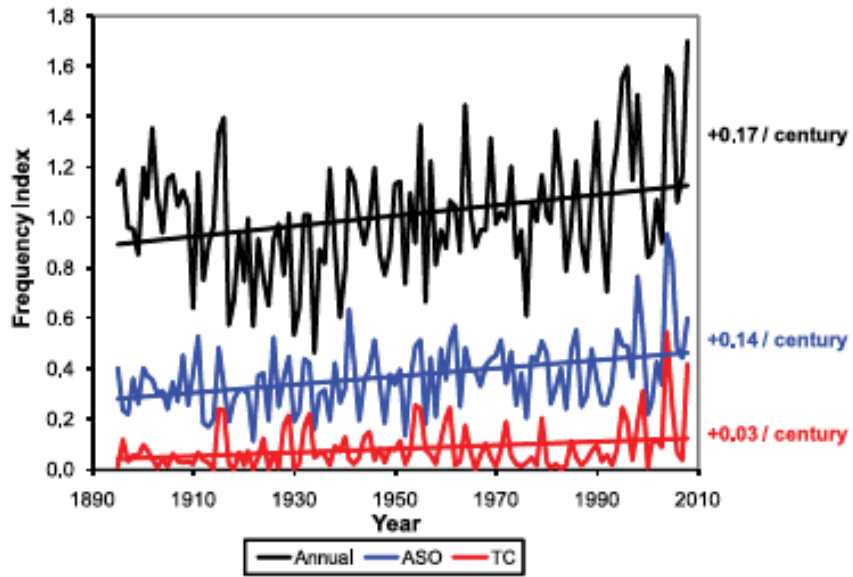
1



2
3
4
5
6
7
8
9

Figure Atlas.61: (a) Annual averaged temperature for the continental USA. The linear trend for the entire period is 0.06°C per decade. The linear trend for the 1950–2006 period is 0.15°C per decade and for the 1970–2006 period is 0.31°C per decade. (b) Annual total precipitation for the continental USA, 1901–2006. The linear trend during the 1901–2006 period is 4.5 mm per decade and is 12.1 mm per decade for the 1950–2006 period. The smoothed black lines were generated with a 13-point binomial filter. (Figure 1 of Easterling et al. (2007))

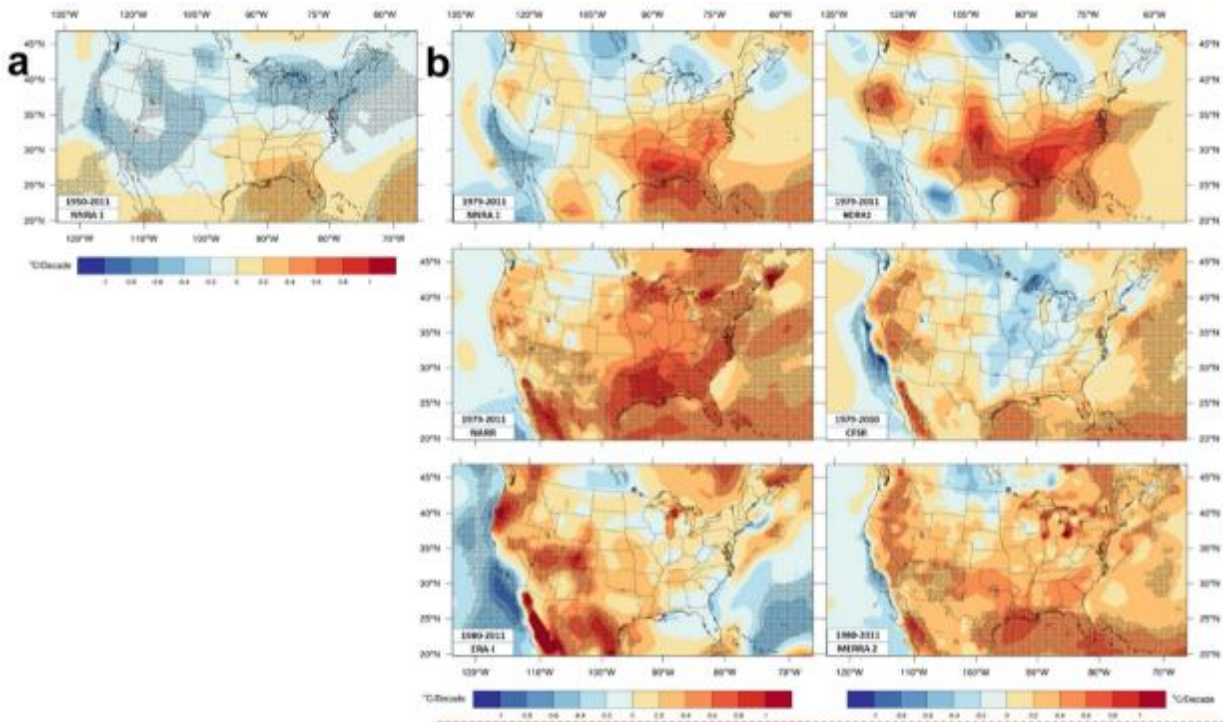
1



2
3
4
5
6
7
8

Figure Atlas.62: Time series (1895–2008) of national average heavy precipitation event index (HPEI) for the entire year (annual, black) for August through October (ASO, blue), and for heavy events associated with tropical cyclones (TC, red). The HPEI is normalized such that the annual time series averages 1.0. The values for other periods indicate the fractional contribution of that season to the total (Figure 1 of Kunkel et al. (2016))

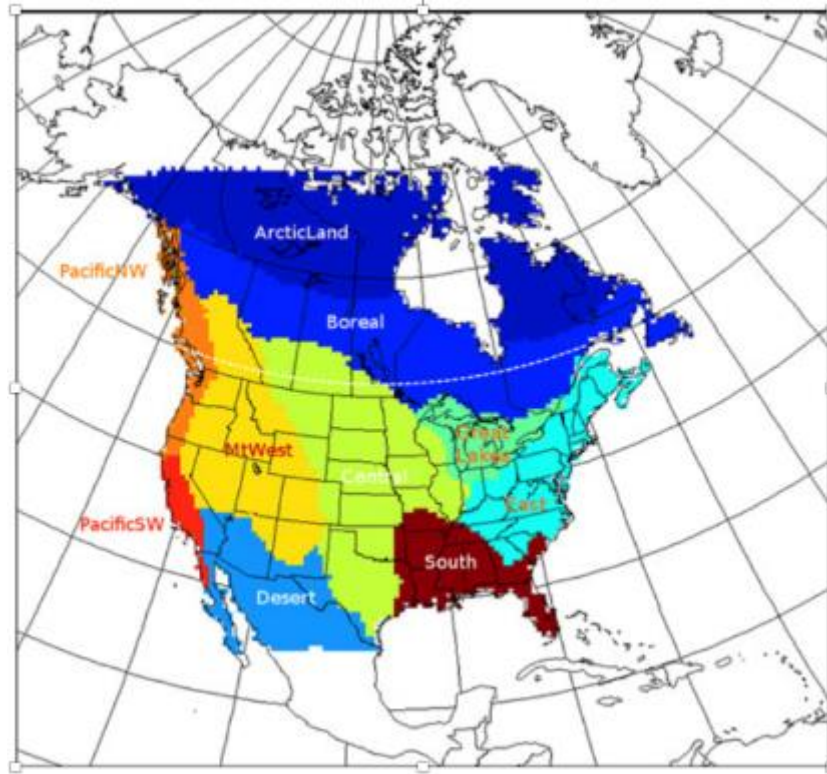
1



2
3
4
5
6
7

Figure Atlas.63: Trends (in °C/decade) in reanalyses maximum Heat Index (HI_{max}). (a) Intermediate time period trends for NNRA1 and (b) shorter time period trends for six reanalyses (Figure 7 of Grotjahn and Huynh, 2018)

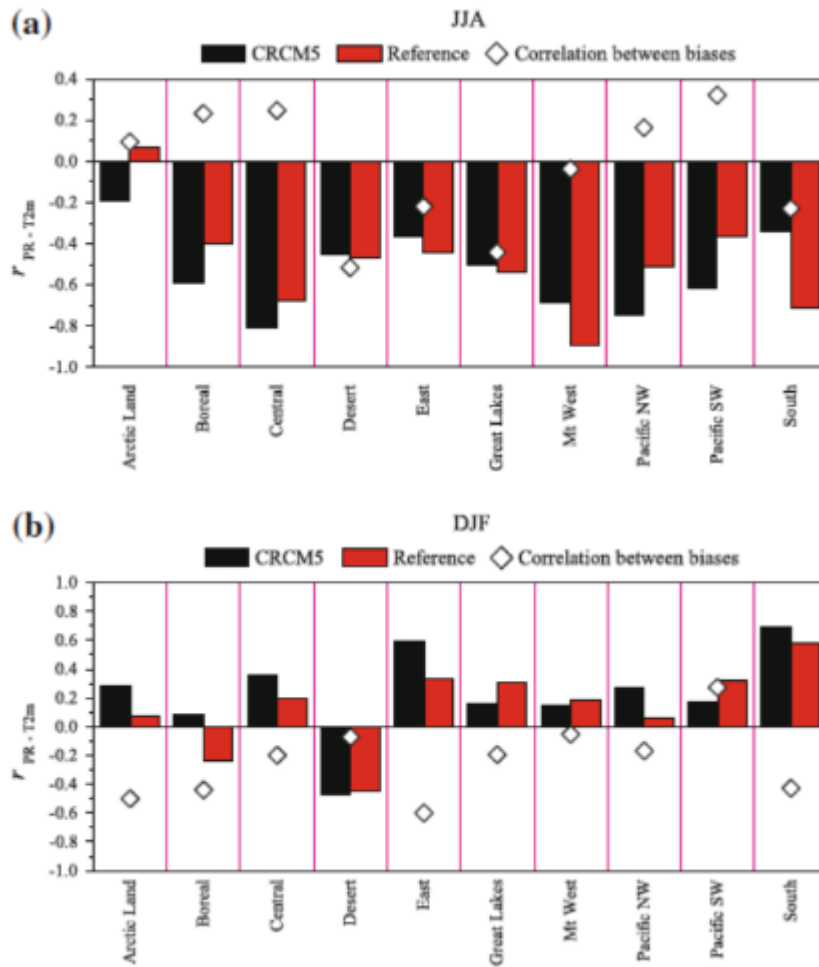
1



2
3
4
5
6

Figure Atlas.64: Subdomains used in model evaluation over North America (Figure 6 of Martynov et al., 2013).

1



2
3
4
5
6
7
8
9

Figure Atlas.65: Interannual correlation coefficients between precipitation and 2-m temperature in CRCM5 simulation (black bars) and the reference base of ERA-Interim, CRU TS3.10 and UDel for temperature (red bars), for (a) JJA and (b) DJF. Hollow diamonds show the correlation coefficients between the biases of simulated precipitation and 2-m temperature values from corresponding reference values. (Figure 7 of Martynov et al., 2013)

1

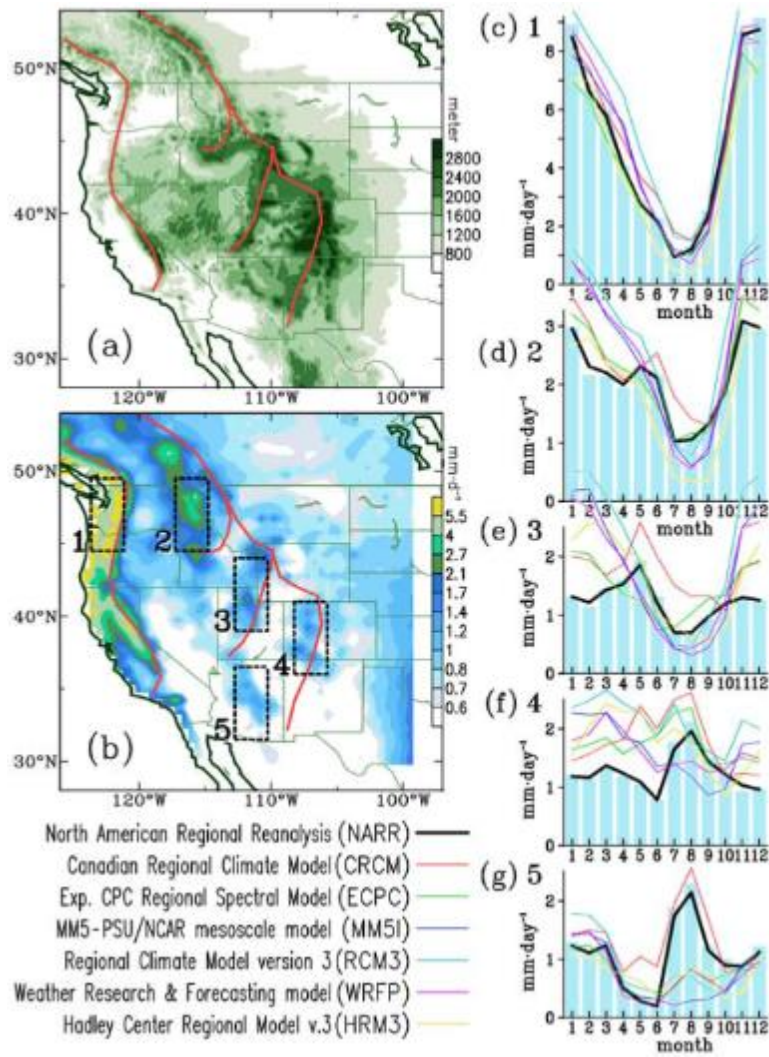
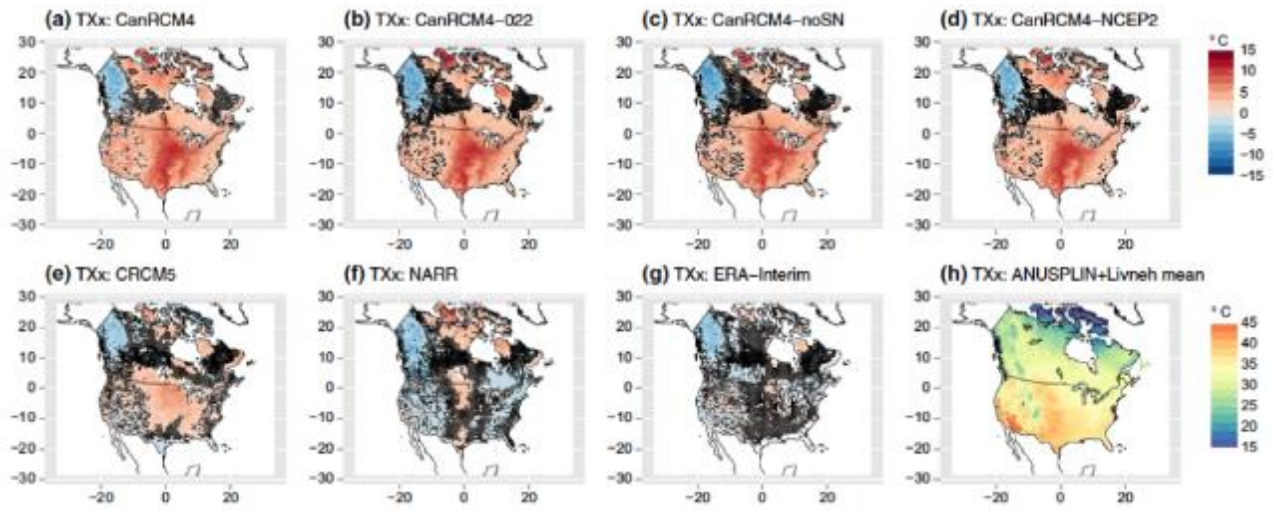


Figure Atlas.66: (a) Orography and (b) cold-season rainfall (November–May, from UDEL) of the Intermountain Region. The major mountain ranges are outlined by redlines. (c) to (g) Monthly rainfall histogram of UDEL, averaged from the five regions indicated in (b), superimposed with the corresponding precipitation of the NARR (thick black line) and all RCMs (coloured lines). Note the precipitation scale in (c) is twice of that in (d) to (g). The abbreviations of the RCMs and their designated colours are indicated under (b). (Figure 1 of Wang et al., 2009)

2
3
4
5
6
7
8
9
10

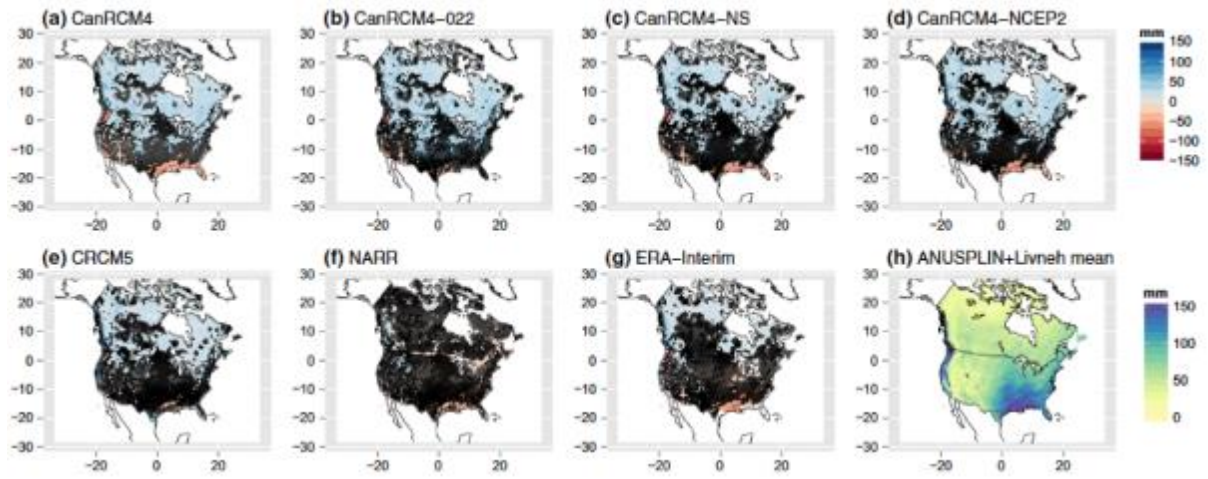
1



2
3
4
5
6
7
8
9

Figure Atlas.67: Average of annual TXx difference from ANUSPLIN+Livneh in (a) CanRCM4, (b) CanRCM4-022, (c) CanRCM4-noSN, (d) CanRCM4-NCEP2, (e) CRCM5, (f) NARR, (g) ERA-Interim, (h) annual mean in ANUSPLIN + Livneh. Stippling in (a) to (g) indicates pixels where differences are not significant at the 5% significance level from a Student’s t-test. (Figure 3 of Whan and Zwiers, 2016)

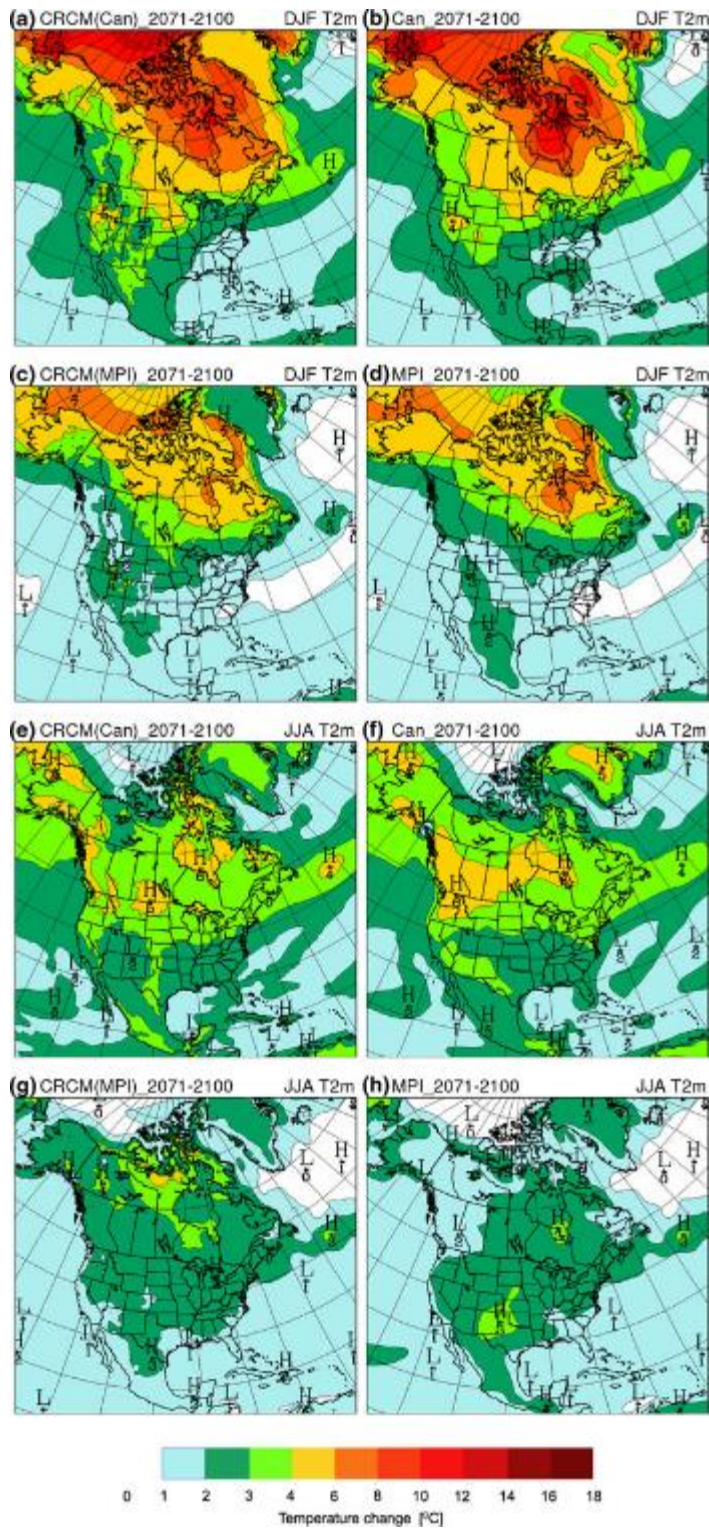
1



2
3
4
5
6
7
8
9

Figure Atlas.68: Averages of annual Rx5day difference from ANUSPLIN + Livneh in (a) CanRCM4, (b) CanRCM4-022, (c) CanRCM4-noSN, (d) CanRCM4-NCEP2, (e) CRCM5, (f) NARR, (g) ERA-Interim, (h) annual mean in ANUSPLIN + Livneh. Stippling in (a) to (g) indicates pixels where differences are not significant at the 5% significance level from a Student’s t-test. (Figure 9 of Whan and Zwiers, 2016)

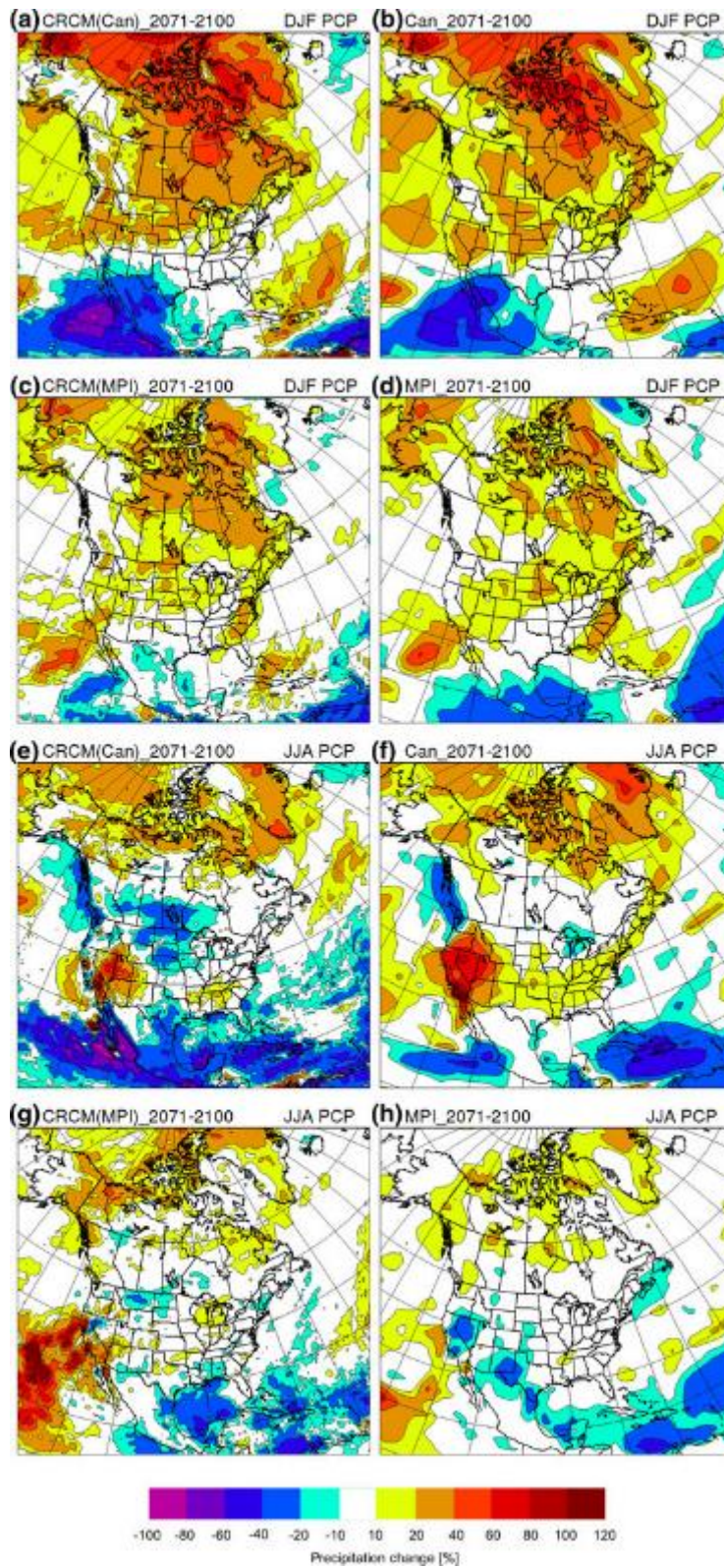
1



2
3
4
5
6
7
8

Figure Atlas.69: Changes in the DJF (a–d) and JJA (e–h) average 2-m temperature in the period of 2071–2100 compared to 1981–2010, for CRCM-Can (a, e), CanESM2 (b, f), CRCM-MPI (c, g) and MIP-ESM-LR (d, h) (Figure 14 of Šeparović et al., 2013)

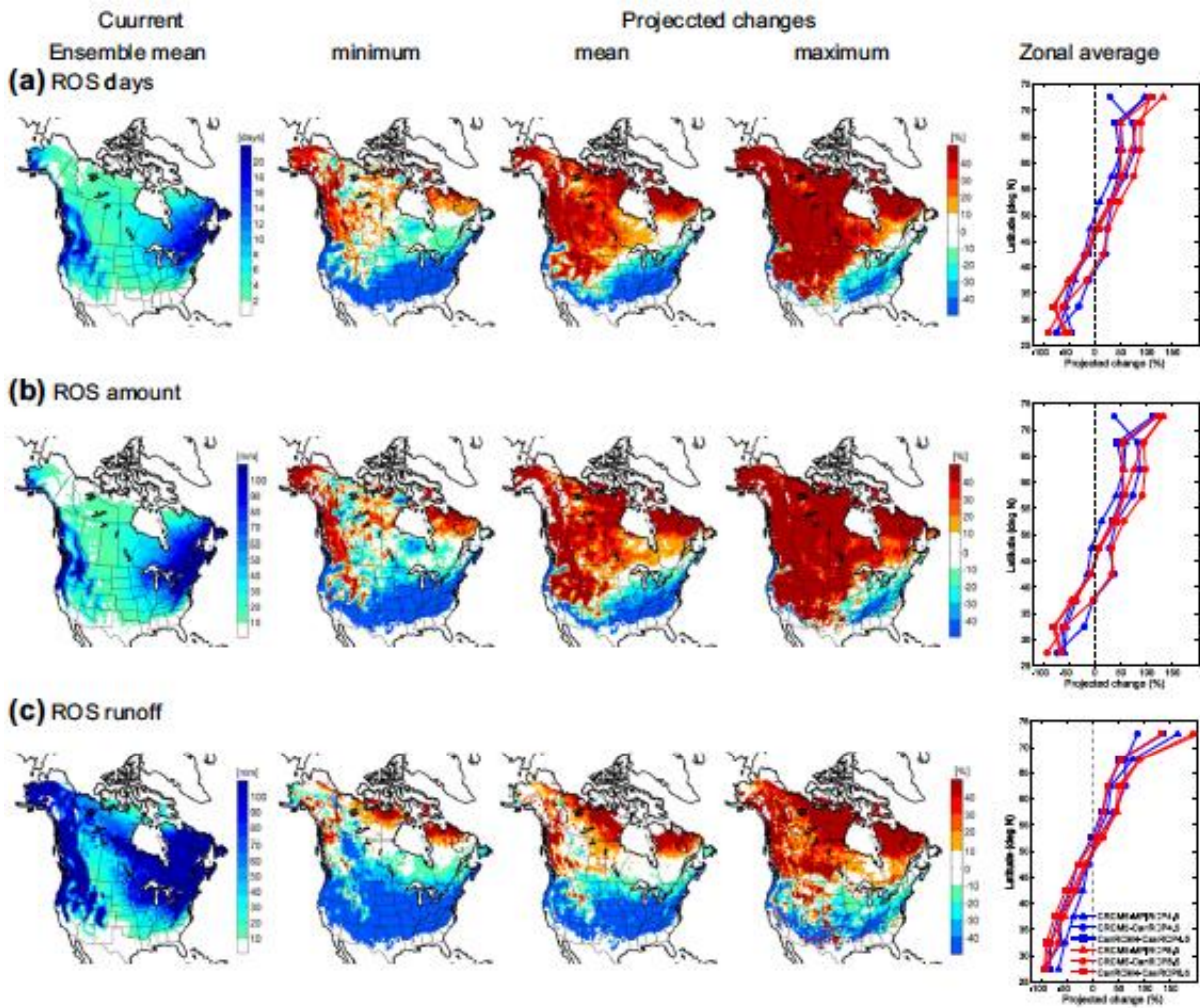
1



2
3
4
5
6

Figure Atlas.70: Same as Figure Atlas.69: but for precipitation (Figure 15 of Šeparović et al., 2013)

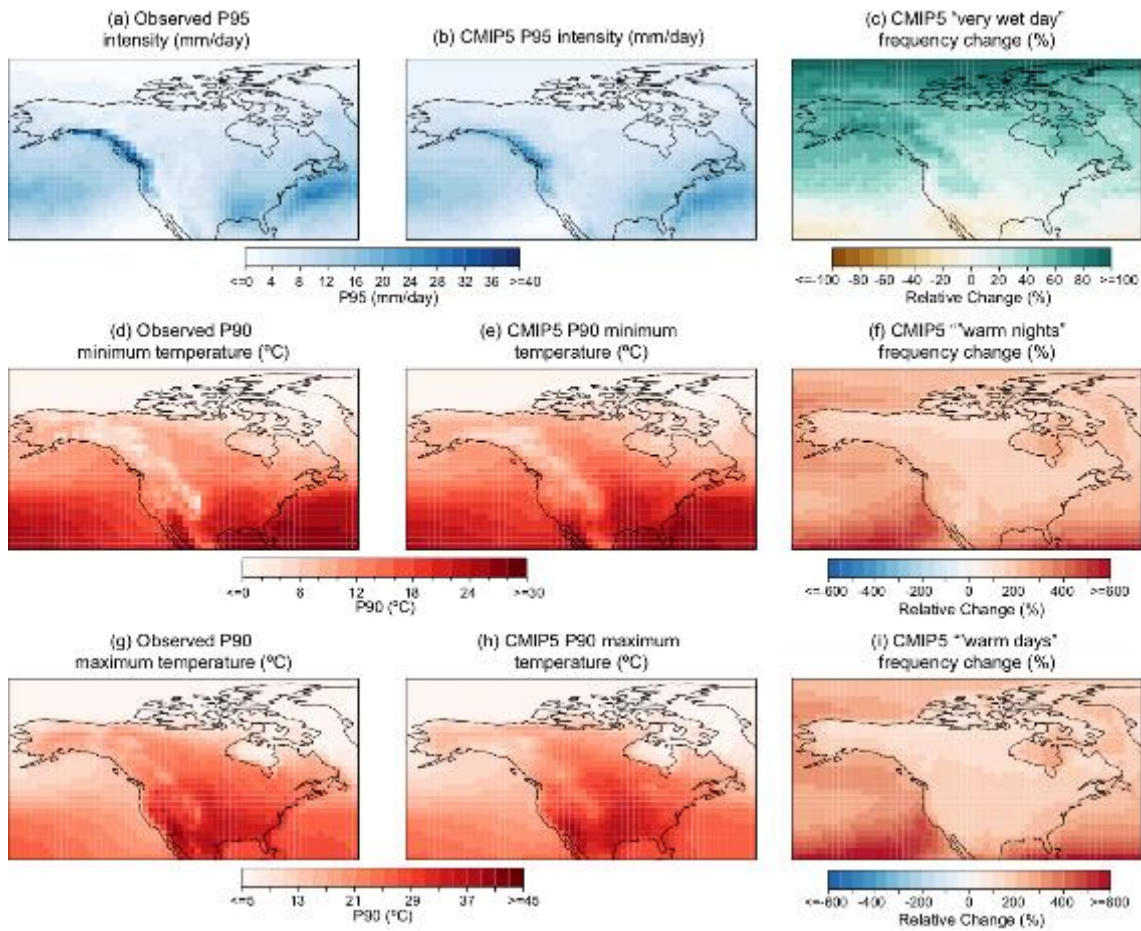
1



2
3
4
5
6
7
8
9
10

Figure Atlas.71: Ensemble-averaged values of three ROS characteristics for the January–May months for the current (1976–2005) period (first column) and minimum, mean, and maximum projected changes (%) to the characteristics for the future (2041–2070) period (second–forth columns), based on the three current and six future RCM-GCM simulations, respectively. Zonally averaged values of projected changes to the three characteristics are also shown in fifth column (Figure 8 of Il Jeong and Sushama, 2018)

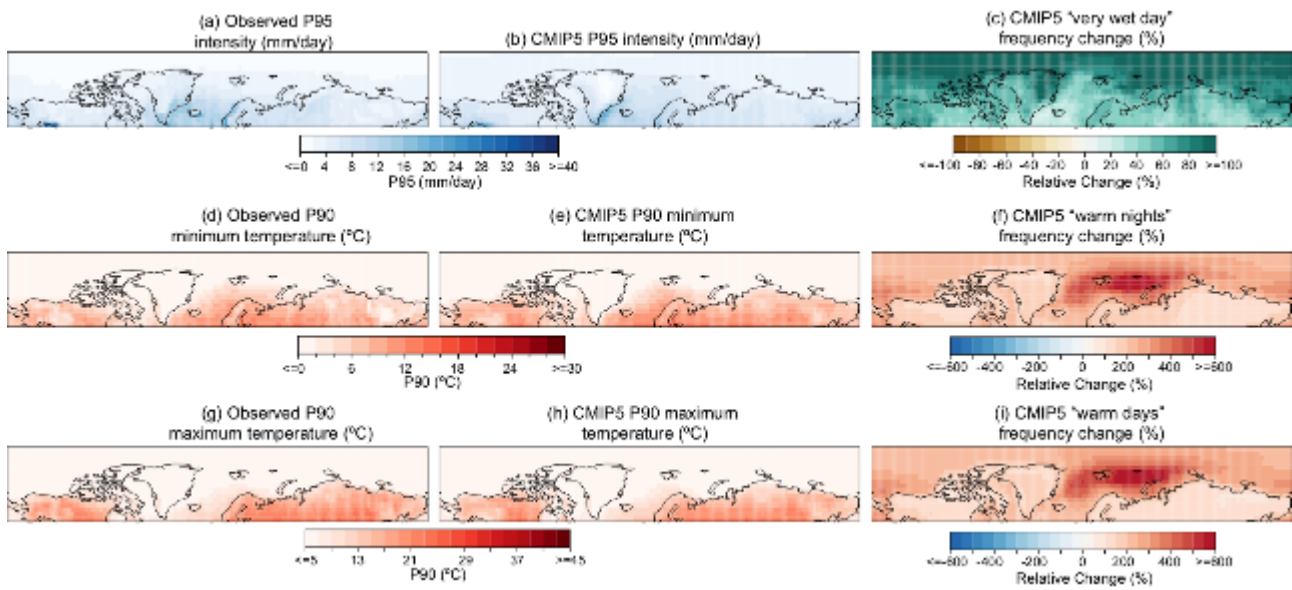
1



2
3
4
5
6
7
8
9
10
11
12
13
14

Figure Atlas.72: (a–c) Daily rainfall amount corresponding to the 95th percentile (P95, in mm/day) defining ‘very wet days’ for (a) the observational reference (EWEMBI) and (b) the CMIP5 subset (ensemble mean), for the reference period 1986–2005. (c) Change in frequency of very wet days for the future 2081–2100 period (RCP8.5) defined as exceeding the historical P95 threshold (results shown as relative change, %). Similar results in (d–f) and (g–i) for absolute daily minimum and maximum temperature amounts corresponding to the 90th percentile (P90, defining ‘warm nights’ and ‘warm days’, respectively) and the corresponding changes in frequency for the future 2081–2100 period (RCP8.5) defined as exceeding the historical P90 threshold (results shown as relative change, %). Similar analysis for other indices and scenarios (including warming levels) are available at the Interactive Atlas (<http://ipcc-atlas.ifca.es>).

1



2
3
4
5
6
7
8
9
10
11
12
13
14
15

Figure Atlas.73: (a–c) Daily rainfall amount corresponding to the 95th percentile (P95, in mm/day) defining ‘very wet days’ for (a) the observational reference (EWEMBI) and (b) the CMIP5_subset (ensemble mean), for the reference period 1986–2005. (c) Change in frequency of very wet days for the future 2081–2100 period (RCP8.5) defined as exceeding the historical P95 threshold (results shown as relative change, %). Similar results in (d–f) and (g–i) for absolute daily minimum and maximum temperature amounts corresponding to the 90th percentile (P90, defining ‘warm nights’ and ‘warm days’, respectively) and the corresponding changes in frequency for the future 2081–2100 period (RCP8.5) defined as exceeding the historical P90 threshold (results shown as relative change, %). Similar analysis for other indices and scenarios (including warming levels) are available at the Interactive Atlas (<http://ipcc-atlas.ifca.es>).

1

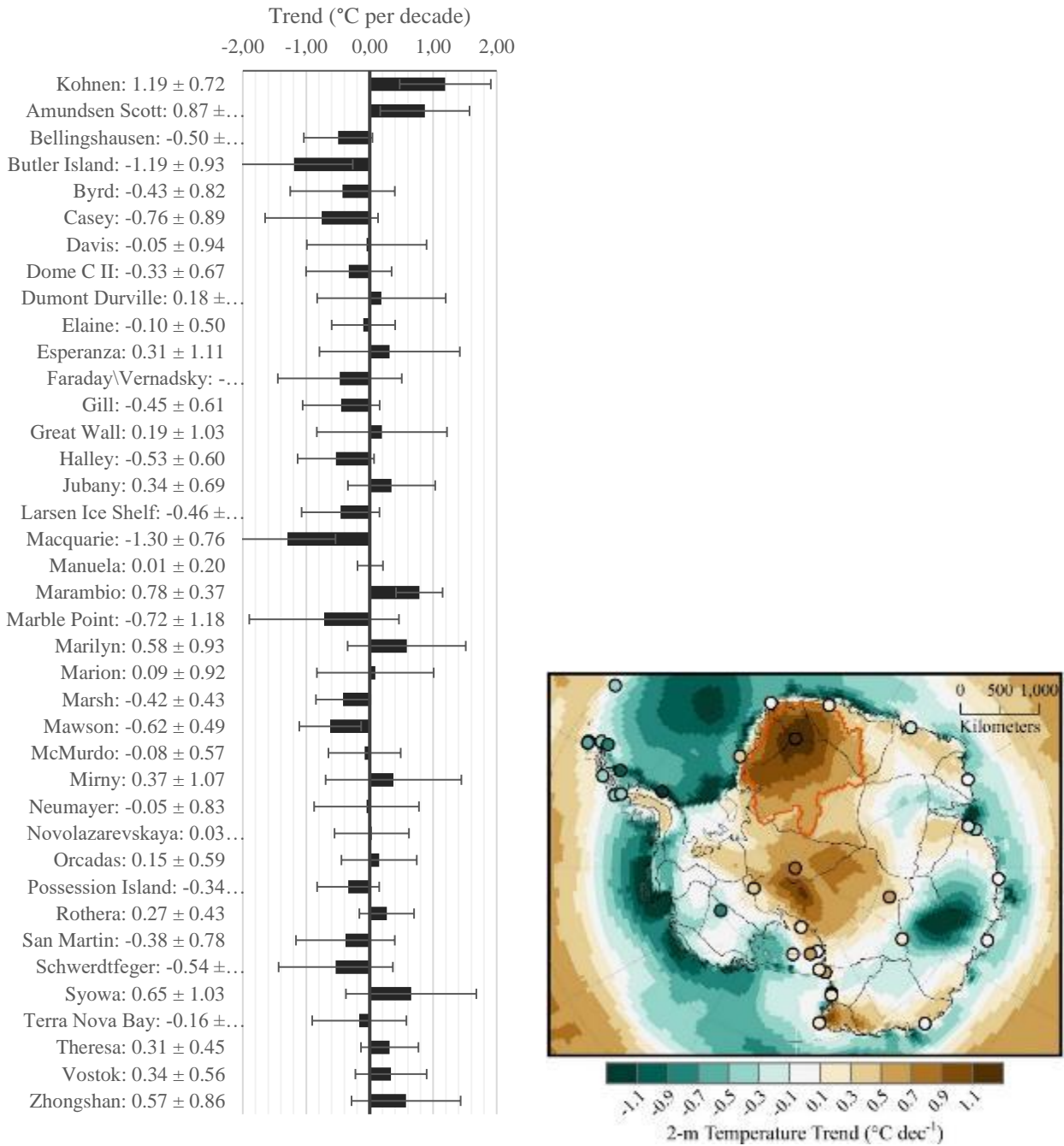
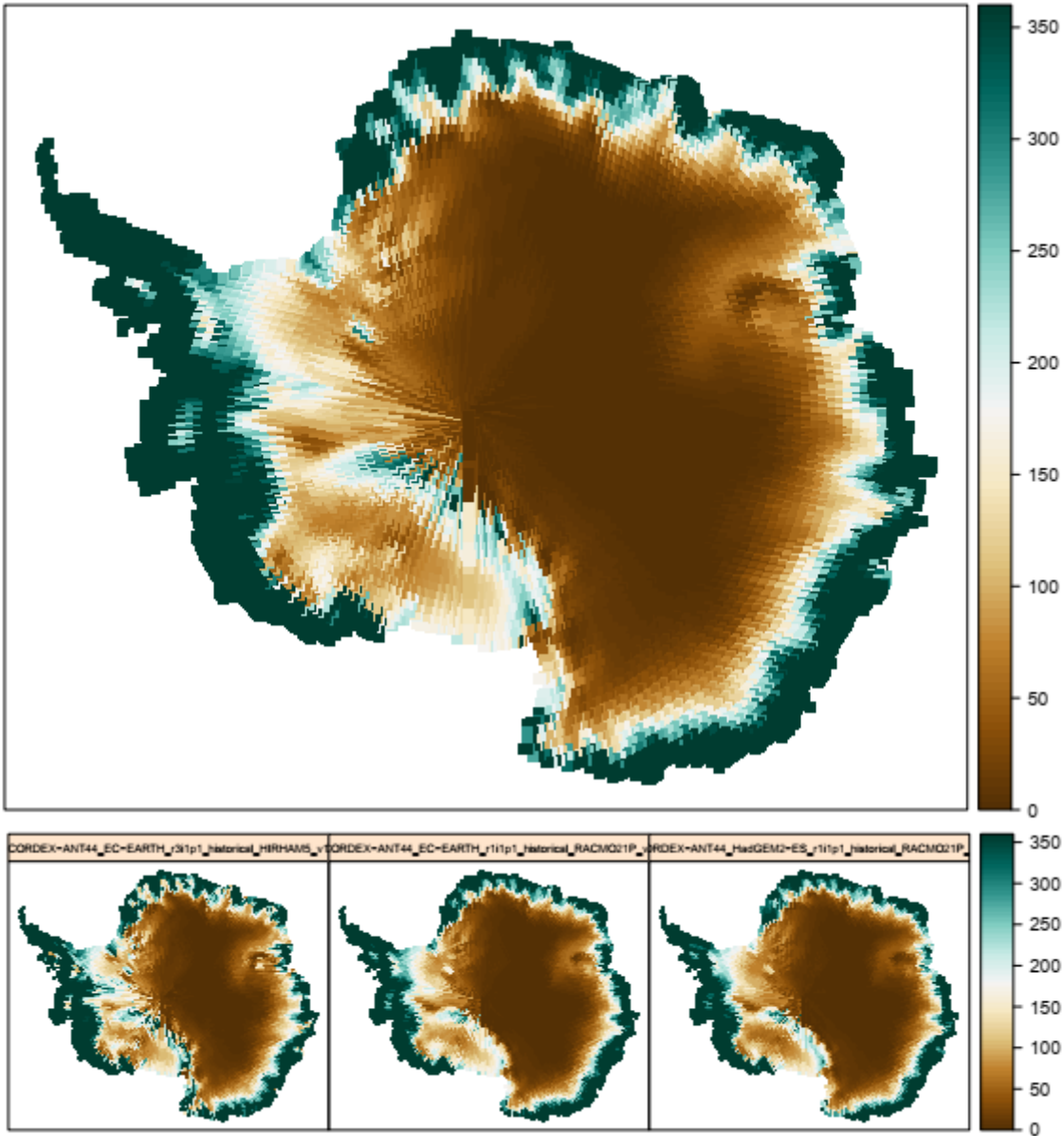


Figure Atlas.74: From Medley et al., 2018. Left: Figure S12 with the annual temperature trends for 1998–2016 at 38 AWS and surface stations from MET-READER (Turner et al., 2004). Right: Figure S3. Bias corrected MERRA-2 (Bosilovich, 2015) trends based on comparison with the MET-READER database. Coloured circles show the observed AWS trends from the MET-READER database. The region of influence for the Kohnen AWS is outlined in red. This confirms that warming is likely occurring within the red bounds, but that it is likely not as strong as the AWS at Kohnen since the warming is strongest there.

2
3
4
5
6
7
8
9
10
11

1

ANT44-ANT-historical-annual-PRCPTOT



2

3

4

5

6

7

8

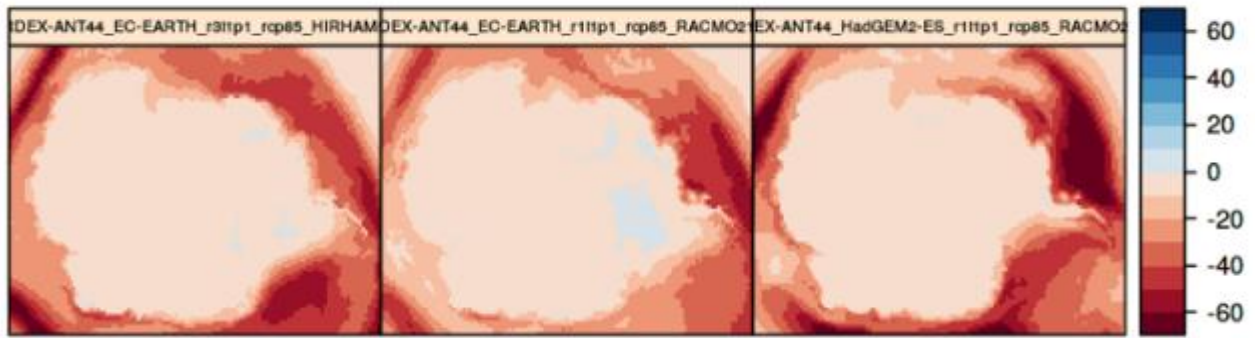
9

10

Figure Atlas.75: Climatological mean of annual precipitation for the reference period 1986–2005 from individual RCMs (lower panel) and their ensemble mean (upper map). RCM data from Polar-CORDEX project. Similar analysis for other indices and scenarios (including warming levels) are available at the Interactive Atlas (<http://ipcc-atlas.ifca.es>)

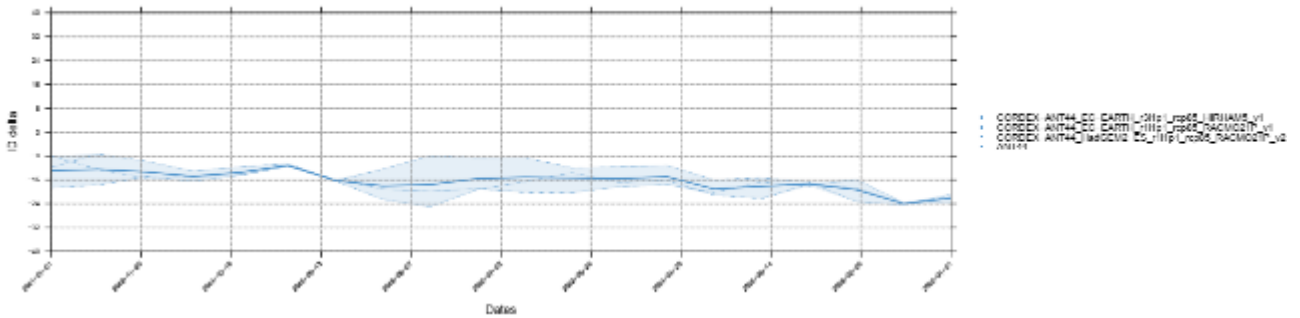
1

ANT44-ANT-rcp85-annual-ID delta



2

ANT44-ANT-rcp85-annual-ID



3

4

Figure Atlas.76: Climatological mean of change in icing days (ID) for RCP8.5 in 2041–2060 over the reference period 1986–2005 from individual RCMs (upper panel) and time series of spatially integrated indexes (lower panel). RCM data from Polar-CORDEX project. Similar analysis for other indices and scenarios (including warming levels) are available at the Interactive Atlas (<http://ipcc-atlas.ifca.es>)

5

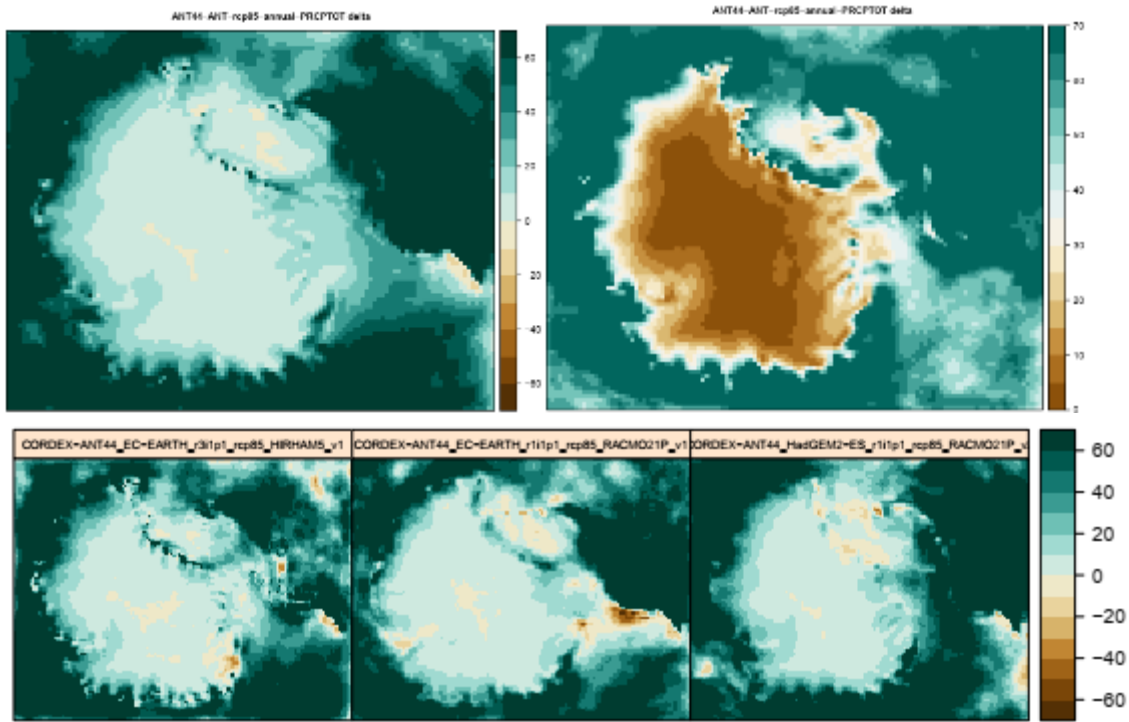
6

7

8

9

1



2

3

4

5

6

7

8

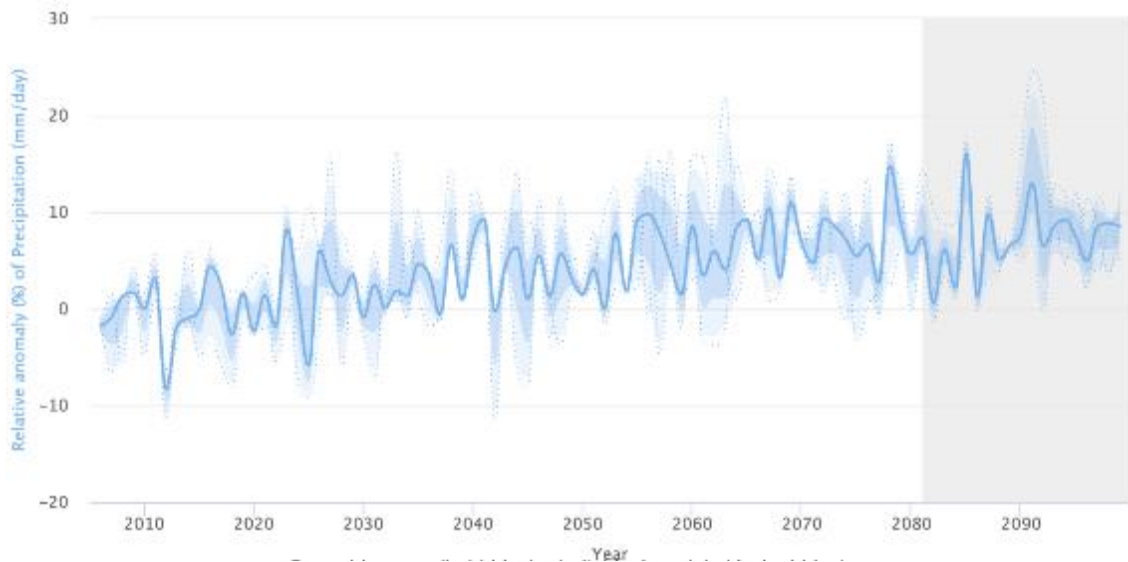
9

10

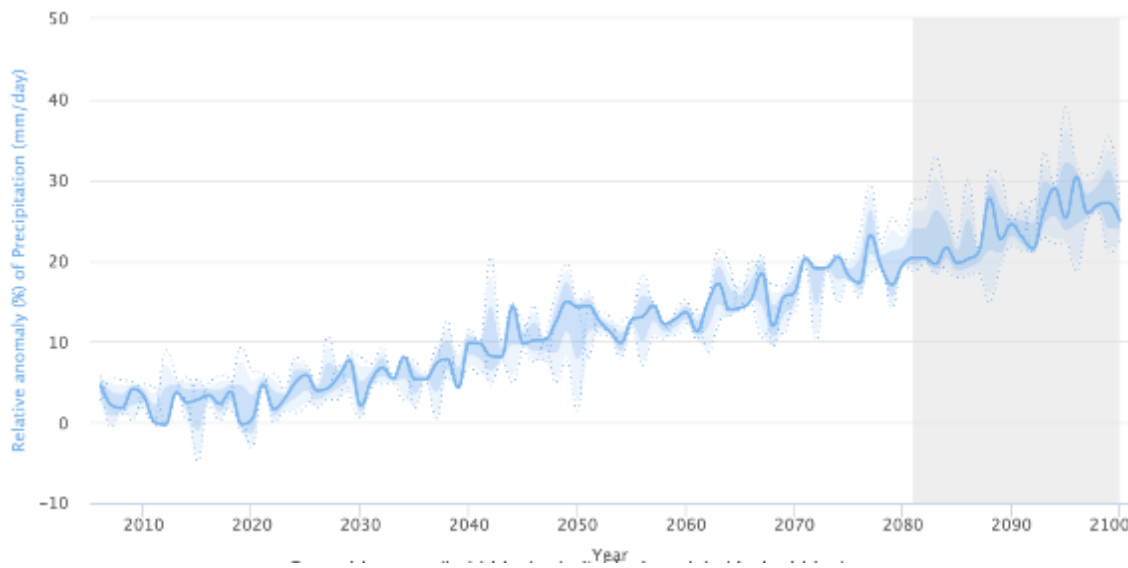
11

Figure Atlas.77: Climatological mean of change in annual precipitation PRCPTOT (mm year⁻¹) for RCP8.5 in 2041–2060 over the reference period 1986–2005 from individual RCMs calculation (lower panel) and RCM ensemble mean (left upper panel) with standard deviation (right upper panel). RCM data from Polar-CORDEX project. Similar analysis for other indices and scenarios (including warming levels) are available at the Interactive Atlas (<http://ipcc-atlas.ifca.es>)

1



2



3

4

Figure Atlas.78: Time series of spatially integrated over Antarctic annual (lower panel) and austral summer DJF (upper panel) precipitation change (mm/day) for RCP4.5 (upper panel) and RCP8.5 (lower panel) over the reference period 1986–2005 from individual RCMs (dotted line) and RCM ensemble mean (bold blue line). RCM data from Polar-CORDEX project. Similar analysis for other indices and scenarios (including warming levels) are available at the Interactive Atlas (<http://ipcc-atlas.ifca.es>)

10

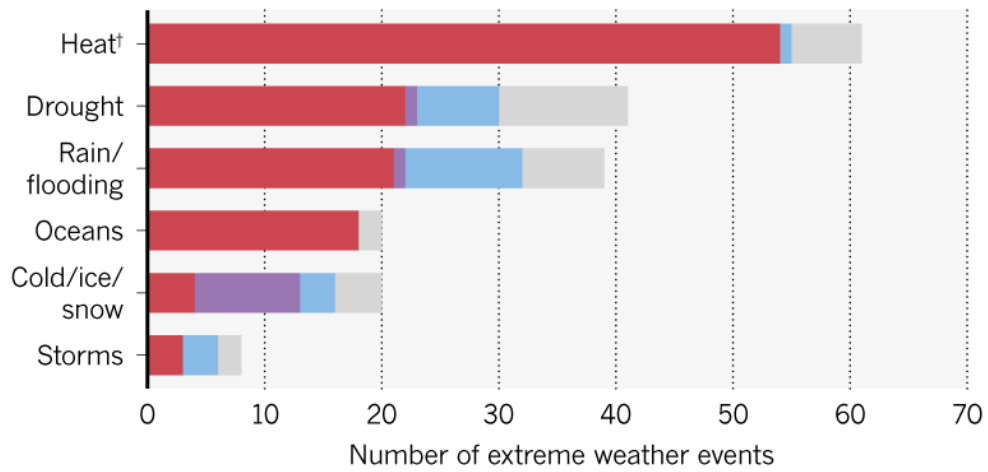
11

1

Attribution science

Researchers have published more than 170 studies* examining the role of human-induced climate change in 190 extreme weather events.

■ More severe or more likely to occur
 ■ Less severe or likely to occur
 ■ No discernible human influence
 ■ Insufficient data/inconclusive



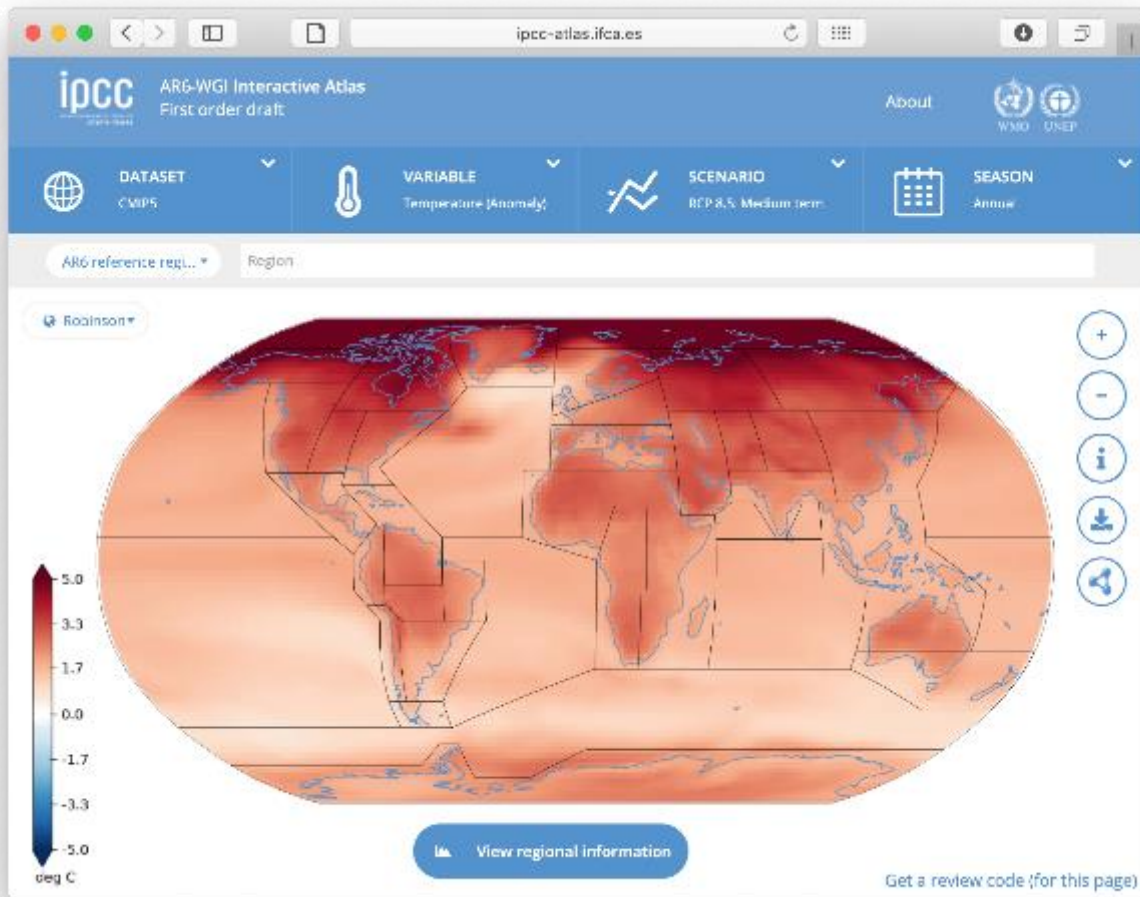
©nature

*Studies from 2004–18 collated by *Nature* and CarbonBrief. †Heat includes heatwaves and wildfires; Oceans includes studies on marine heat, coral bleaching and marine-ecosystem disruption.

2
3
4
5

Figure Atlas.79: Number of publications on attributing extreme weather events to climate change (Schiermeier, 2018).

1



2
3
4
5
6
7
8
9
10
11
12
13
14
15
16
17

Figure Atlas.80: A screenshot illustrating the main window of the AR6 WGI Interactive Atlas, which displays a global map with the annual temperature climate change signal from the CMIP5 dataset for the mid-term future period. The main controls at the top of the window allow selecting the dataset (currently a global CMIP5 subset and regional EURO-, AFRICA- and ANTARCTIC-CORDEX at 0.44°), variable (atmospheric and oceanic variables and indices), scenario (currently RCP4.5 and 8.5 for different time slices and warming levels) and season (annual, standard seasons and user-defined ones). Regional information for a particular region (from a predefined number of options, currently the ‘AR6 reference regions’ for atmospheric variables and ‘Ocean biomes’ for oceanic variables) can be obtained interactively by clicking on the map over the region (or using the selector on the top) and pressing the ‘view regional information button’; see **Figure Atlas.81:**). Note that the full URL for this screen (as copied from the browser) tracks all the information of the default choice: http://ipcc-atlas.ifca.es/#&model=CMIP5_mmm&variable=tas&scenario=rcp85&temporalFilter=year&layers=AR6&period=medium&anomaly=ANOMALY&zoom=2

1



2
3
4
5
6
7
8

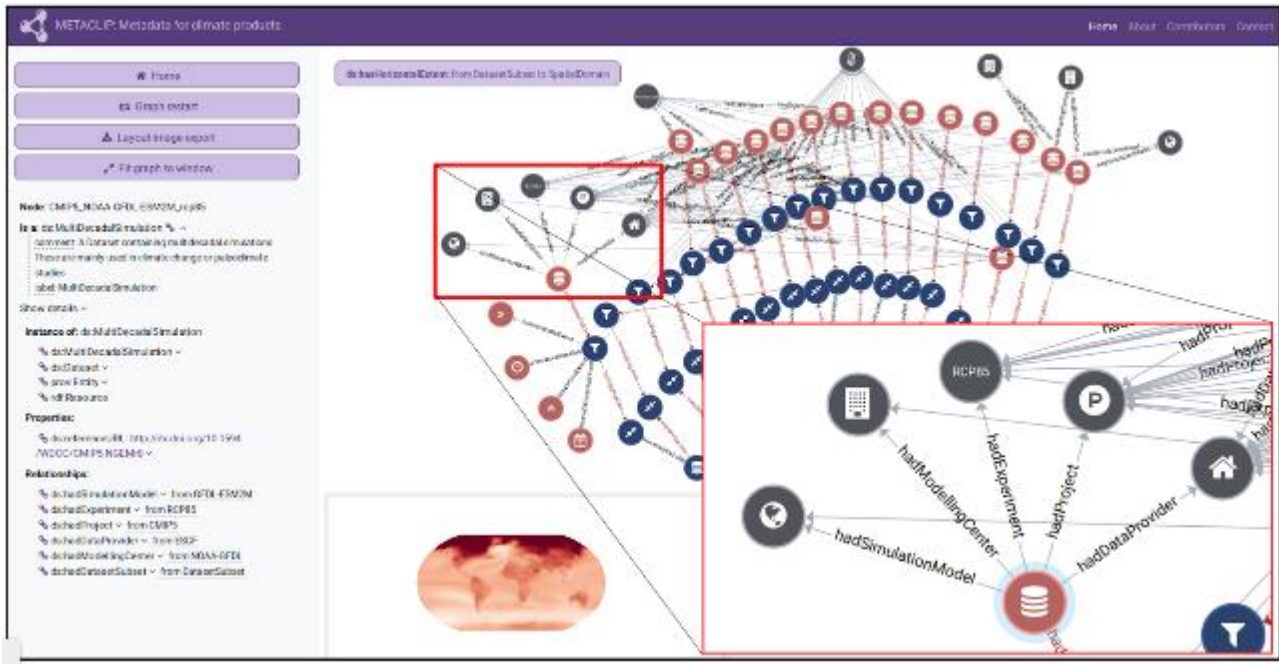
Figure Atlas.81: Regional information for a selected region (the Mediterranean) in the form of a time series plume for a mid-term time slice (top) and a 2°C warming level (bottom). Note that the corresponding periods are indicated with grey shading (with intensity proportional to the number of models including each particular year for the case of the warming levels). Fine granularity is provided by hovering over a particular point, obtaining information of particular models (top panel).



1
2
3
4
5
6
7

Figure Atlas.82: Regional information for a selected region (the Mediterranean) in the form of scatter-plot. This product allows to select a second variable to show in the diagram (CMIP5 precipitation in this case, in addition to CMIP5 temperature originally selected) and displays the results for the three near-, mid- and long-term periods in different colours (each point represents a given model)..

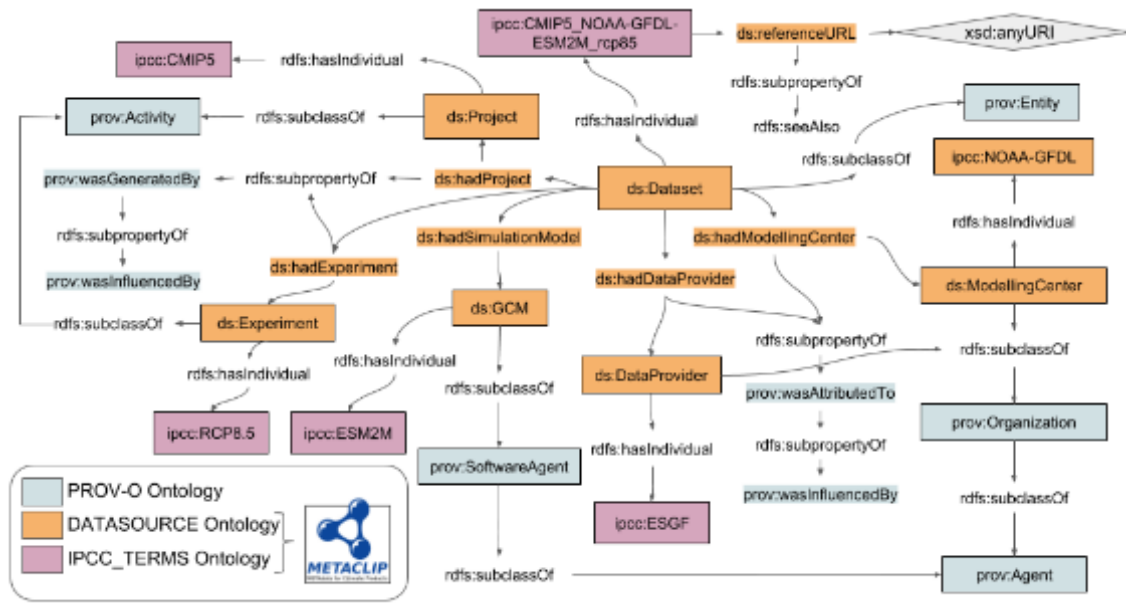
1



2
3
4
5
6
7
8
9
10
11
12
13

Figure Atlas.83: Screenshot of the METACLIP Interpreter for provenance visualization (metaclip.org), displaying the provenance of a temperature anomaly map downloaded from the Interactive Atlas as a PNG file with attached METACLIP metadata (METACLIP export option). The blow-up shows a specific dataset from the 9-member ensemble used to produce the map. It shows details about the dataset provenance such as its DOI identifying the source of data, the experiment (RCP 8.5), the modelling centre, GCM information, data provider and associated Project (CMIP5). The interface allows the user to expand the detail of information if needed by clicking in each of the nodes and reading the metadata in the left panel. It is also possible zooming in/out, scrolling and saving a user-defined position of the graph.

1



2
3
4
5
6
7
8
9
10
11

Figure Atlas.84: Illustration of the provenance of an individual ‘dataset’ (corresponding to the blow-up highlighted by the red square in Figure Atlas.83:), describing its source (DOI number), data provider (ESGF), experiment (RCP 8.5), modelling centre (GFDL) and GCM (ESM2M). The metadata model re-uses an existing ontology (PROV-O, prefix ‘prov:’, blue) and creates domain-specific extension for climate products via the METACLIP ontologies DATASOURCE (indicated by prefix ‘ds:’, orange) and IPCC_TERMS (‘ipcc:’, magenta).